UNIVERSIDAD COMPLUTENSE DE MADRID
FACULTAD DE CIENCIAS QUÍMICAS

TESIS DOCTORAL

Monitorización de biomarcadores de envejecimiento en muestras clínicas con inmunosensores electroquímicos

MEMORIA PARA OPTAR AL GRADO DE DOCTOR

PRESENTADA POR

Esther Sánchez Tirado

DIRECTORES

Araceli González Cortés
Paloma Yáñez-Sedeño Orive
José Manuel Pingarrón Carrazón

© Esther Sánchez Tirado. 2020

UNIVERSIDAD COMPLUTENSE DE MADRID
FACULTAD DE CIENCIAS QUÍMICAS
DEPARTAMENTO DE QUÍMICA ANALÍTICA

MONITORIZACIÓN DE BIOMARCADORES DE ENVEJECIMIENTO EN MUESTRAS CLÍNICAS CON INMUNOSENSORES ELECTROQUÍMICOS

Directores:

Dra. Araceli González Cortés

Profesora Titular de Universidad

Dra. Paloma Yáñez-Sedeño Orive

Catedrática de Universidad

Dr. José Manuel Pingarrón Carrazón

Catedrático de Universidad

MEMORIA PARA OPTAR AL GRADO DE DOCTOR PRESENTADA POR:

ESTHER SÁNCHEZ TIRADO

Madrid, 2020

Índice

1

Summary

MONITORING OF AGEING BIOMARKERS IN CLINICAL SAMPLES USING ELECTROCHEMICAL IMMUNOSENSORS

1.1. INTRODUCTION

Ageing is a time-dependent physiological functional decline, which appears to be driven by the progressive accumulation through the life of a variety of random molecular defects that build up within cells and tissues.

During ageing, a chronic, sterile and low-grade inflammation, called *"inflammageing*", is developed as the long-term result of a chronic physiological stimulation of the innate immune system, which can become damaging in the elderly, contributing to the pathogenesis of age-related diseases.

Likewise, this stage results in an inflammatory profile, which is confirmed by the high levels of pro-inflammatory cytokines and the low concentration of anti-inflammatory ones. This change mainly may be attributed to the alterations in the immune system.

1.2. AIMS OF THIS WORK

The main objective of this Doctoral Thesis is the design, preparation and application of different electrochemical immunosensing platforms with improved analytical characteristics for individual or multiple determination of ageing biomarkers in clinical samples.

For this purpose, several configurations were developed using electrochemical grafting, poly(pyrrolepropionic) acid and different carbon nanomaterials for electrode modification, as well as novel immobilization strategies, and poly-HRP-Strept and carbon nanotubes-modified hybrids as carrier nanotags for signal amplification.

All the immunosensor designed were applied to the determination of different scarcely studied *"inflammageing"* biomarkers for which there were no similar configurations or, when existing, the analytical characteristics of the methodology were significantly improved.

All this research work was carried out by application of the usual methodology of bioelectroanalysis, which involves the design of the immunosensor and the recognition strategy, optimization of the experimental variables, characterization studies, construction of the calibration plot and establishment of the analytical characteristics, followed by the studies of repeatability, reproducibility and selectivity of the method.

In all cases, the analytical usefulness of the configurations designed was demonstrated by applying them to the determination of physiological concentrations of these species in clinical samples, such as certified biological reference material, serum and/or saliva.

Finally, the results were compared with those obtained by the respective commercial ELISA immunoassays, with no significant differences between the results provided by both methods, which shows the usefulness of the configurations developed.

1.3. RESEARCH RESULTS

First, the employment of a carboxylic-functionalized conducting polymer poly(pyrrolepropionic) acid allowed the preparation of an immunosensor for the determination of endoglin in serum.

Besides, the first immunosensor for the determination of the prostaglandin-like compound 8-isoprostane has been developed using an electrochemical platform consisting of a disposable screen-printed carbon electrode modified with carboxylated carbon nanohorns for the covalent immobilization of specific capture antibody.

For the first time, the reduced graphene oxide-carboxymethylcellulose hybrid was used for the development of a novel electrochemical immunosensor for the determination of adiponectin in serum.

Moreover, an electrochemical immunosensor for the determination of transforming growth factor beta 1 has been prepared using azide functionalized multi-walled carbon nanotubes and alkyne-immunoglobulin G by means of copper(I) catalyzed azide-alkyne cycloaddition, *"click chemistry"*, as an efficient strategy for the covalent immobilization of immunoreagents without altering their configurations and preserving their biological activity.

Furthermore, an electrochemical platform prepared by grafting of diazonium salt of *p*-aminobenzoic acid onto a screen-printed carbon electrode was used to prepare an immunosensor for interferon gamma determination in certified biological reference material and saliva.

As well, a dual screen-printed carbon electrode modified with *4*-carboxyphenyl-functionalized double-walled carbon nanotubes have been used as platform for the preparation of electrochemical immunosensors for the simultaneous determination of the cytokines interleukin 1 beta and tumor necrosis factor alpha in serum samples.

In addition, an aminoviologen-carbon nanotube conjugate functionalized with detection antibody and peroxidase was used as signal amplification strategy in the preparation of an immunosensor for the determination of transforming growth factor beta 1 in saliva samples.

Finally, the development and performance of an electrochemical immunosensor using magnetic multi-walled carbon nanotubes as nanocarrier tags for the determination of human fetuin A in saliva samples were also described.

1.4. MILESTONES

As a result of the research work described in this Doctoral Thesis, the followings scientific articles have been published:

1. C.B. Arenas, E. Sánchez-Tirado, I. Ojeda, C.A. Gómez-Suárez, A. González-Cortés, R. Villalonga, P. Yáñez-Sedeño, J.M. Pingarrón, An electrochemical immunosensor for adiponectin using reduced graphene oxide-carboxymethylcellulose hybrid as electrode scaffold, *Sens. Actuators B Chem.* 223 (2016) 89–94.

2. E. Sánchez-Tirado, A. González-Cortés, P. Yáñez-Sedeño, J.M. Pingarrón, Carbon nanotubes functionalized by click chemistry as scaffolds for the preparation of electrochemical immunosensors. Application to the determination of TGF-beta 1 cytokine, *Analyst* 141 (2016) 5730–5737.

3. E. Sánchez-Tirado, A. González-Cortés, M. Yudasaka, S. Iijima, F. Langa, P. Yáñez-Sedeño, J.M. Pingarrón, Electrochemical immunosensor for the determination of 8-isoprostane aging biomarker using carbon nanohorns-modified disposable electrodes, *J. Electroanal. Chem.* 793 (2017) 197–202.

4. E. Sánchez-Tirado, C. Salvo, A. González-Cortés, P. Yáñez-Sedeño, F. Langa, J.M. Pingarrón, Electrochemical immunosensor for simultaneous determination of interleukin-1 beta and tumor necrosis factor alpha in serum and saliva using dual screen printed electrodes modified with functionalized double-walled carbon nanotubes, *Anal. Chim. Acta* 959 (2017) 66–73.

5. E. Sánchez-Tirado, L.M. Arellano, A. González-Cortés, P. Yáñez-Sedeño, F. Langa, J.M. Pingarrón, Viologen-functionalized single-walled carbon nanotubes as carrier nanotags for electrochemical immunosensing.

Application to TGF-β1 cytokine, *Biosens. Bioelectron.* 98 (2017) 240–247.

6. E. Sánchez-Tirado, A. González-Cortés, P. Yáñez-Sedeño, J.M. Pingarrón, Magnetic multiwalled carbon nanotubes as nanocarrier tags for sensitive determination of fetuin in saliva, *Biosens. Bioelectron.* 113 (2018) 88–94.

7. E. Martínez-Periñán, E. Sánchez-Tirado, A. González-Cortés, R. Barderas, J.M. Sánchez-Puelles, L. Martínez-Santamaría, S. Campuzano, P. Yáñez-Sedeño, J.M. Pingarrón, Amperometric determination of endoglin in human serum using disposable immunosensors constructed with poly(pyrrolepropionic) acid-modified electrodes, *Electrochim. Acta* 292 (2018) 887–894.

8. E. Sánchez-Tirado, A. González-Cortés, P. Yáñez-Sedeño, J.M. Pingarrón, Electrochemical immunosensor for the determination of the cytokine interferon gamma (IFN-γ) in saliva, *Talanta* 211 (2020) 120761.

2

Resumen

MONITORIZACIÓN DE BIOMARCADORES DE ENVEJECIMIENTO EN MUESTRAS CLÍNICAS CON INMUNOSENSORES ELECTROQUÍMICOS

2.1. INTRODUCCIÓN

El envejecimiento es un deterioro funcional fisiológico dependiente del tiempo, que parece ser impulsado por la acumulación progresiva de defectos moleculares aleatorios en células y tejidos a lo largo de la vida.

Durante el envejecimiento, se desarrolla un perfil inflamatorio crónico, estéril y de bajo grado, denominado *"inflammageing"*, que se confirma por el aumento de los niveles de citoquinas pro-inflamatorias y la disminución de los niveles de citoquinas anti-inflamatorias, siendo el resultado, a largo plazo, de una estimulación fisiológica crónica del sistema inmune innato, que puede ser perjudicial en la edad adulta, contribuyendo a la patogénesis de enfermedades relacionadas con la edad.

2.2. OBJETIVOS DEL TRABAJO

El objetivo principal de esta Tesis Doctoral es el diseño, preparación y aplicación de diferentes plataformas electroquímicas inmunosensoras con características analíticas mejoradas para la determinación individual o múltiple de biomarcadores de envejecimiento en muestras clínicas.

Con este propósito, se desarrollaron varias configuraciones utilizando la técnica del *grafting* o injertado electroquímico, ácido poli(pirrolpropiónico) y diferentes nanomateriales de carbono para la modificación de los electrodos, así como nuevas estrategias de inmovilización, y poli-HRP-Strept y nanotubos de carbono híbridos como estrategia electroactiva de amplificación de la señal.

Todos los inmunosensores desarrollados se aplicaron a la determinación de diferentes biomarcadores de envejecimiento escasamente estudiados para los que no

existían configuraciones similares o, cuando existían, las características analíticas de las metodologías previas se mejoraron significativamente.

Todo este trabajo de investigación se llevó a cabo mediante la aplicación de la metodología habitual seguida para el diseño de inmunosensores, la elección de la estrategia de reconocimiento, la optimización de las variables experimentales, los estudios de caracterización, la construcción de la curva de calibrado y la obtención de las características analíticas y los estudios de repetibilidad, reproducibilidad y selectividad.

En todos los casos, la utilidad analítica de las configuraciones desarrolladas se demostró mediante su aplicación a la determinación de estos biomarcadores en muestras clínicas, tales como un material de referencia certificado, suero o saliva.

Finalmente, los resultados obtenidos empleando los inmunosensores desarrollados se compararon con los proporcionados por los respectivos inmunoensayos ELISA comerciales, no obteniéndose diferencias significativas entre los resultados proporcionados por ambos métodos, lo que demuestra la utilidad de las configuraciones desarrolladas.

2.3. RESULTADOS

En primer lugar, el empleo de un ácido poli(pirrolpropiónico) de polímero conductor carboxifuncionalizado permitió la preparación de un inmunosensor para la determinación de endoglina en suero.

Además, se desarrolló el primer inmunosensor para la determinación de 8-isoprostano, utilizando una plataforma electroquímica consistente en un electrodo serigrafiado de carbono desechable modificado con nanocuernos de carbono carboxilados como base para la inmovilización covalente del anticuerpo de captura específico.

Del mismo modo, se utilizó por primera vez un híbrido de óxido de grafeno reducido y carboximetilcelulosa como base para el desarrollo de un inmunosensor electroquímico para la determinación de adiponectina en suero.

También, se preparó un novedoso inmunosensor electroquímico para la determinación de factor de crecimiento transformante beta 1 utilizando nanotubos de carbono de pared múltiple funcionalizados por medio de una cicloadición azida-alquino catalizada por cobre (I), *"química click"*, como estrategia eficiente para la inmovilización covalente de inmunorreactivos, preservando su actividad biológica.

Asimismo, se utilizó la técnica del *grafting* o injertado electroquímico, donde la sal de diazonio del ácido *p*-aminobenzoico se usó como base para generar grupos carboxílicos sobre la superficie de un electrodo serigrafiado de carbono y preparar un inmunosensor electroquímico para la determinación de interferón gamma en un material de referencia certificado y saliva.

De la misma forma, se empleó un electrodo serigrafiado de carbono dual modificado con nanotubos de carbono de pared doble funcionalizados con grupos *4*-carboxifenilo como plataforma para la preparación de un inmunosensor electroquímico para la determinación simultánea de las citoquinas interleucina 1 beta y factor de necrosis tumoral alfa en suero.

Por otro lado, se utilizó un conjugado aminoviológeno-nanotubos de carbono funcionalizado con anticuerpo de detección y peroxidasa como estrategia de amplificación de la señal en la preparación de un inmunosensor para la determinación de factor de crecimiento transformante beta 1.

Finalmente, también se describió la preparación de un inmunosensor electroquímico utilizando nanotubos de carbono magnéticos como etiquetas de nanoportadores para la determinación de fetuina A humana en saliva.

2.4. LOGROS

Como resultado del trabajo de investigación contenido en esta Tesis Doctoral, se han publicado los siguientes artículos científicos:

1. C.B. Arenas, E. Sánchez-Tirado, I. Ojeda, C.A. Gómez-Suárez, A. González-Cortés, R. Villalonga, P. Yáñez-Sedeño, J.M. Pingarrón, An electrochemical immunosensor for adiponectin using reduced graphene oxide-carboxymethylcellulose hybrid as electrode scaffold, *Sens. Actuators B Chem.* 223 (2016) 89–94.

2. E. Sánchez-Tirado, A. González-Cortés, P. Yáñez-Sedeño, J.M. Pingarrón, Carbon nanotubes functionalized by click chemistry as scaffolds for the preparation of electrochemical immunosensors. Application to the determination of TGF-beta 1 cytokine, *Analyst* 141 (2016) 5730–5737.

3. E. Sánchez-Tirado, A. González-Cortés, M. Yudasaka, S. Iijima, F. Langa, P. Yáñez-Sedeño, J.M. Pingarrón, Electrochemical immunosensor for the determination of 8-isoprostane aging biomarker using carbon nanohorns-modified disposable electrodes, *J. Electroanal. Chem.* 793 (2017) 197–202.

4. E. Sánchez-Tirado, C. Salvo, A. González-Cortés, P. Yáñez-Sedeño, F. Langa, J.M. Pingarrón, Electrochemical immunosensor for simultaneous determination of interleukin-1 beta and tumor necrosis factor alpha in serum and saliva using dual screen printed electrodes modified with functionalized double-walled carbon nanotubes, *Anal. Chim. Acta* 959 (2017) 66–73.

5. E. Sánchez-Tirado, L.M. Arellano, A. González-Cortés, P. Yáñez-Sedeño, F. Langa, J.M. Pingarrón, Viologen-functionalized single-walled carbon nanotubes as carrier nanotags for electrochemical immunosensing.

Application to TGF-β1 cytokine, *Biosens. Bioelectron.* 98 (2017) 240–247.

6. E. Sánchez-Tirado, A. González-Cortés, P. Yáñez-Sedeño, J.M. Pingarrón, Magnetic multiwalled carbon nanotubes as nanocarrier tags for sensitive determination of fetuin in saliva, *Biosens. Bioelectron.* 113 (2018) 88–94.

7. E. Martínez-Periñán, E. Sánchez-Tirado, A. González-Cortés, R. Barderas, J.M. Sánchez-Puelles, L. Martínez-Santamaría, S. Campuzano, P. Yáñez-Sedeño, J.M. Pingarrón, Amperometric determination of endoglin in human serum using disposable immunosensors constructed with poly(pyrrolepropionic) acid-modified electrodes, *Electrochim. Acta* 292 (2018) 887–894.

8. E. Sánchez-Tirado, A. González-Cortés, P. Yáñez-Sedeño, J.M. Pingarrón, Electrochemical immunosensor for the determination of the cytokine interferon gamma (IFN-γ) in saliva, *Talanta* 211 (2020) 120761.

3

Introduction

Ageing is evidenced by a progressive, generalized impairment of biological functions resulting in an increased vulnerability to environmental challenge and a higher risk of disease and death. Despite its enormous complexity, one key mechanism explaining this process is the development of a chronic, low grade inflammatory status called "*inflammageing*", which is related to oxidative stress, and plays a leading role in the pathogenesis of geriatric diseases.

Population ageing is nowadays a major demographic trend worldwide due to improved longevity requiring quality of life and to the great impact that it produces on health-care systems. Understanding of the key biological processes involved in healthy ageing makes necessary the discovery of new ageing biomarkers and methodologies for their detection and monitoring.

In this Doctoral Thesis, an attempt has been made to contribute to this knowledge by developing novel methods based on electrochemical biosensors and immunoassay strategies for the early detection of some biomolecules involved in these processes.

3.1. AIMS AND WORK PLAN

The experimental work presented in this Doctoral Thesis has been carried out in the laboratories of the Electroanalysis and Electrochemical (Bio)Sensors Group of the Faculty of Chemistry at the Complutense University of Madrid and fits into the objectives of the Project CTQ2015-70023-R financed by the Spanish Ministry of Economy and Competitiveness entitled "*Ageing biomarkers: electrochemical monitoring in clinical samples using immunosensors based on novel immobilization and amplification strategies*".

The specific objective of this research is the design and preparation of new electrochemical platforms for the development of immunosensors applied to the individual or multiple determination of ageing biomarkers. The configurations proposed, which involve latest-generation nanomaterials as well as novel strategies for immobilizing the immunoreagents, have been applied to some of these scarcely studied biomarkers in clinical samples such as human serum and saliva.

The relevance of this purpose lies mainly in the growing interest of the proposed biomarkers for which electrochemical biosensors had not been described and the challenges come from the need to improve the analytical performance of conventional immunoassay methods that are based on the use of expensive and time-consuming Enzyme-Linked ImmunoSorbent Assays (ELISA) techniques. Faced with these, the immunosensors developed in this work offer noticeable advantages such as shorter assay times, higher precision and lower reagents and sample consumption. In addition, all these improvements are linked to the special characteristics of electrochemical transduction, in particular its high sensitivity, selectivity, low cost and miniaturization capacity.

As it is known, the key aspects to take into account in the design of an electrochemical immunosensor are the surface architecture connecting the biological element with the electrode and the immobilization strategy. In this work, highly conductive immunosensing platforms also rich in linking positions were constructed,

where stable and oriented immobilization schemes could be implemented. Once reached, these goals where complemented with the establishment of immunoassay strategies suitable for sensitive, reliable and real-time detection of physiological concentrations of proteins that are important marker parameters of ageing and related diseases.

With these perspectives and the objective of adding a high degree of innovation further improving the performance characteristics of monitoring, the lines of work followed included: a) the design of new nanostructured electrode surfaces involving uncommon nanomaterials; b) the use of simple strategies for bioreagents immobilization on different electrode platforms including covalent attachment, "*click chemistry"* or grafting methods with diazonium salts and c) the design of detection methods with signal amplification by means of multienzyme or nanohybrid materials.

All the experimental work presented in this Thesis has been accomplished by applying the usual methodology in the electroanalytical research, which involves the following steps:

1. Design of the immunosensor configuration and recognition strategy.
2. Optimization of the experimental variables involved in the preparation of the immunosensor and the electrochemical detection.
3. Characterization studies.
4. Establishment of calibration plots and analytical characteristics of the method.
5. Selectivity and stability studies.
6. Application to the analysis of samples.

3.2. RELATIONSHIP BETWEEN AGEING, OXIDATIVE STRESS AND INFLAMMATION

Ageing is a time-dependent physiological functional decline affecting living organisms, which is underpinned by alterations within molecular pathways, and is the most profound risk factor for many non-communicable diseases [Xia, 2017]. Likewise, ageing appears to be driven by the progressive accumulation through the life of a variety of random molecular defects that build up within cells and tissues. These defects start to arise very early in life, probably in utero, but in the early years, both the fraction of affected cells and the average burden of damage per affected cell are low. However, over time the faults increase, resulting eventually in age-related functional impairment of tissues and organs. This concept makes clear the life-course nature of the underlying mechanisms. Thus, ageing is a continuous process, starting early and developing gradually, instead of being a distinct phase that begins in middle to late life. Since there are multiple kinds of molecular and cellular damage and a corresponding variety of mechanisms to protect against and repair them, ageing is a highly complex process involving diverse mechanisms at different levels [Kirkwood, 2009].

It is worth mentioning that related to the ageing of the immune system, an apparent paradox seems to occur. Despite a decrease in immune responsiveness to infection and vaccination and even a reduction in infection-associated immunopathology, the elderly individual experiences an increase in systemic inflammation, which can aggravate degenerative diseases, and is at increased risk of autoimmune disease [Cavanagh, 2012]. In that way, during the ageing an inflammatory profile is being developed ("*inflammageing*"), which is confirmed by the high levels of pro-inflammatory and the low level of anti-inflammatory cytokines in the elderly. This change occurs mainly because of the alterations in the immune system. In the bone marrow, the stromal cells are less efficient to produce the cytokines that are appropriate for the production and maturation of the

hematopoietic stem cells. Furthermore, thymus atrophies and in the peripheral lymphoid tissues changes are observed which are possible to influence the maturation of progenital B cells and the capability of immune system for antigenic presentation. Moreover, as for cells of innate immunity, it has been shown that in the monocytes some members of the Toll-like receptors family are underexpressed and are functionally impaired. In addition, neutrophils have impaired phagocytosis and chemotaxis and the number of natural killer cells (NK cells) is increased with upregulated cytotoxic activities [Fragoulis, 2008].

Inflammation can be beneficial as an acute, transient immune response to harmful conditions such as traumatic tissue injury or an invading pathogen. This response also facilitates the repair, turnover and adaptation of many tissues. However, acute inflammatory responses to pathogen associated molecular patterns may be damaged during ageing, leading to increased susceptibility to infection. Chronic inflammation has many features of acute inflammation but is usually of low grade and persistent, resulting in responses that lead to tissue degeneration. There are several possible mechanisms of chronic inflammation such as: a) continuous production of reactive molecules by infiltrating leukocytes designed to kill pathogens, which eventually damages the structural and cellular elements of tissues, or b) impaired non-immune cells and activated immune cells leading to the production of cytokines that amplify or modulate the inflammatory response and alter the phenotypes of nearby cells, often in detriment of normal tissue function. Many aged tissues are probably in a chronically inflamed state, although without signs of infection [Franceschi, 2014].

In this way, the term "*inflammageing*" describes the low-grade, chronic, systemic inflammation in ageing, in the absence of overt infection, and is a highly significant risk factor for both morbidity and mortality in the elderly people [Franceschi, 2014; Woods, 2012].

Oxidative stress has been defined as a disturbance in the balance between the production of reactive oxygen species (free radicals) and antioxidant defenses, which may lead to tissue injury and represents a common if not universal denominator of toxicity [Betteridge, 2000; Gagné, 2014]. Free radicals are formed in large amounts as an unavoidable by-product of many biochemical processes and, in some instances, deliberately, as in activated neutrophils. In addition, these reactive oxygen species may be generated in the body in response to electromagnetic radiation from the environment and acquired directly as oxidizing pollutants such as ozone and nitrogen dioxide. If antioxidant defenses are deficient then damage may occur in a variety of tissues [Betteridge, 2000]. During respiration, the release of uncoupled high-energy electrons by mitochondria and chloroplasts represents one of the major sources of reactive oxygen species in cells. Many xenobiotics have the potential to uncouple electron transport in mitochondria, which could lead to important leakage of electrons in the intracellular environment and cause oxidative damage. Oxidative stress is intimately related to inflammation. It has been demonstrated that the production of reactive oxygen species could also result from inflammation reactions, in which nitric oxide and hydrogen peroxide are produced, and during oxidative metabolism of xenobiotics. Besides, a molecular inflammatory theory of ageing postulates that the activation of redox-sensitive transcription factors by age-related oxidative stress up-regulates the expression of pro-inflammatory genes. Furthermore, it has been stated that there is an association between these processes and age-related disorders such as hypoxia [de Gonzalo-Calvo, 2010].

Summarizing, it can be said that oxidative stress occurs when an excess of oxygen radicals are produced in cells, crushing the normal antioxidant capacity. It could result from the presence of xenobiotics, the activation of the immune system in response to invading microorganisms (inflammation) or radiation [Gagné, 2014]. The antioxidant system neutralize free radicals functioning at the cellular, membrane and extracellular levels by means of the endogenous enzyme families: catalase, peroxidase, superoxide dismutase, as well as tocopherols, the glutathione system

and additional antioxidants such as vitamins A, C and E. When the concentration of reactive species is not controlled by internal defense mechanisms, oxidative damage occurs to proteins, lipids and DNA, which could lead to cytotoxicity, genotoxicity and even carcinogenesis when impaired (mutated) cells proliferate.

3.3. AGEING BIOMARKERS AND THEIR BIOLOGICAL SIGNIFICANCE

As mentioned above, ageing is a ubiquitous complex phenomenon that results from environmental, stochastic, genetic and epigenetic events in different cell types and tissues and their interactions throughout life [Franceschi, 2014]. In order to point out the biomarkers involved in the ageing process, first the biomarker definition given by the World Health Organization (WHO) will be reminded. Such definition considers as biomarker any substance, structure or process that can be measured in the body or its products and influence or predict the incidence of outcome or disease [Frijhoff, 2015]. By following such definition, a panel of biomolecules used to predict the physiological age and, furthermore, the life span or to explain the biological process behind ageing or ageing-related diseases, could be considered ageing biomarkers. Nevertheless, the concept of biomarkers of ageing and age-related disease began to appear in the gerontologic and geriatric literature in the early 1980s when the interest was in eliminating the confounding influence of disease from research on ageing so that biomarkers of underlying processes of ageing could be developed [Ludwig, 1980; Reff, 1982; Sprott, 1985]. The question of what was ageing and what was disease was at the core of the development of scientific legitimacy for the young science of ageing. Otherwise, an ageing biomarker must predict the rate of ageing, monitor a basic process that underlies the ageing process, not the effects of disease, and be able to be tested repeatedly without harming the patient [Xia, 2017]. Additionally, it must be something that works in humans an in laboratory animals, so that it can be tested in them before validated in humans.

Figure 3.1 shows in an illustrative way the comments expressed above, also noting some biomarkers of ageing, which have been considered analytical objectives of this work. The properties of these biomolecules and the interest of their determination are described below.

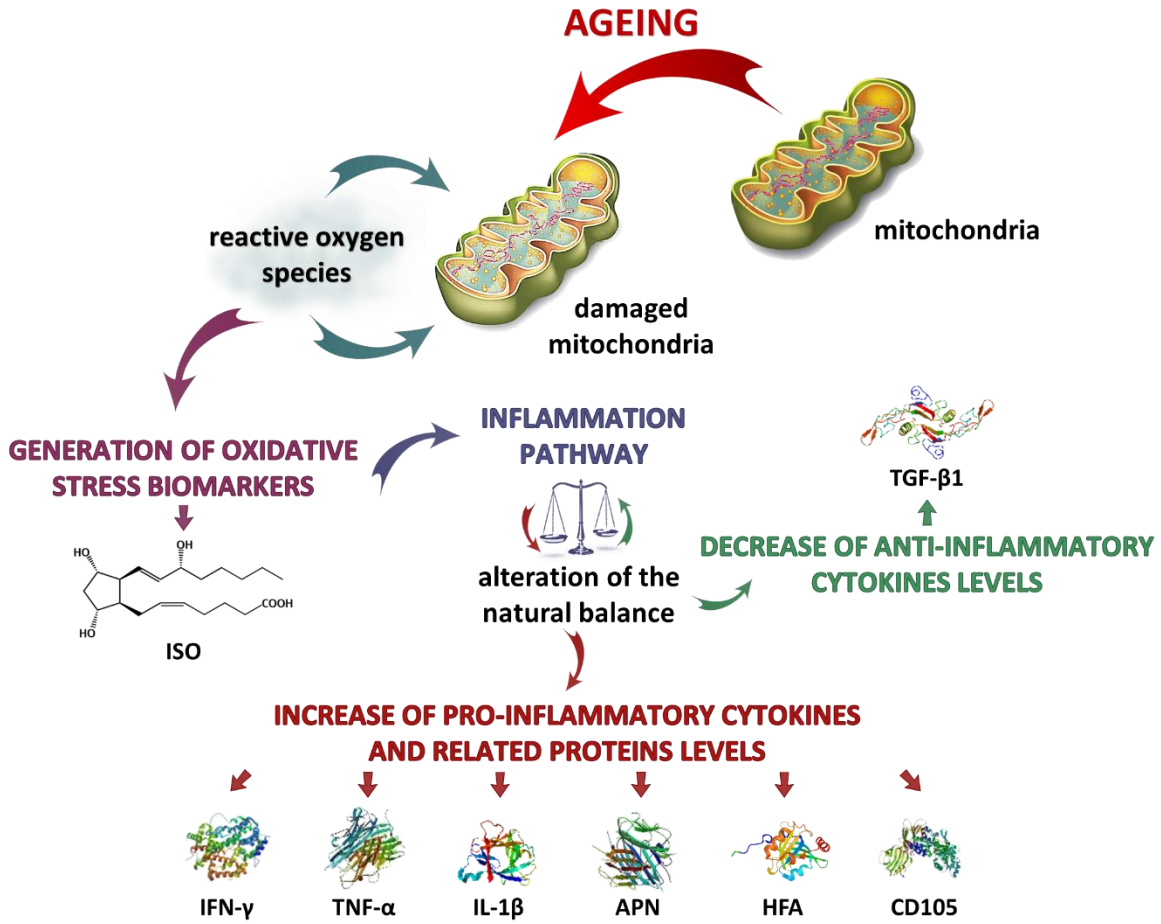

Figure 3.1. Mitochondrial reactive oxygen species activation of inflammation pathway and effect of this alteration on the analytes studied [Rea, 2018]

3.3.1. Biomarkers related to oxidative stress

As described above, oxidative stress constitute an alteration in the balance between the production of reactive oxygen species and the antioxidant defense system in place to counter them [Halliwell, 1994]. The great importance of free radical oxidation of cellular components is well known and the species involved, coming from many sources including the environment and a variety of bioprocesses, have long been regarded as a class of ageing biomarkers, and are classified according

to the type of damage they produce in the organism in: a) DNA or RNA injury, b) protein oxidation or nitration and c) lipid peroxidation [Xia, 2017].

This last process has a great importance, since lipids are a major component of living organisms and probably the first easy target of free radicals once they are produced [Praticò, 2002]. The susceptibility of lipids to oxidation is due to their molecular structure abundant with reactive double bonds [Ho, 2013]. Indeed, lipids are readily attacked by free radicals, resulting in the formation of a number of peroxidation products. Lipid peroxides are unstable indicators of oxidative stress in cells that decompose to form more complex and reactive compounds such as isoprostanes [Milne, 2011], which are one of the most studied compound families and used to quantify oxidative stress *in vivo* [Ho, 2013; Montuschi, 1999]. In this work, we have studied a specific isoprostane, the 8-isoprostane (ISO), which is the product of oxidative damage to phospholipids (Figure 3.2).

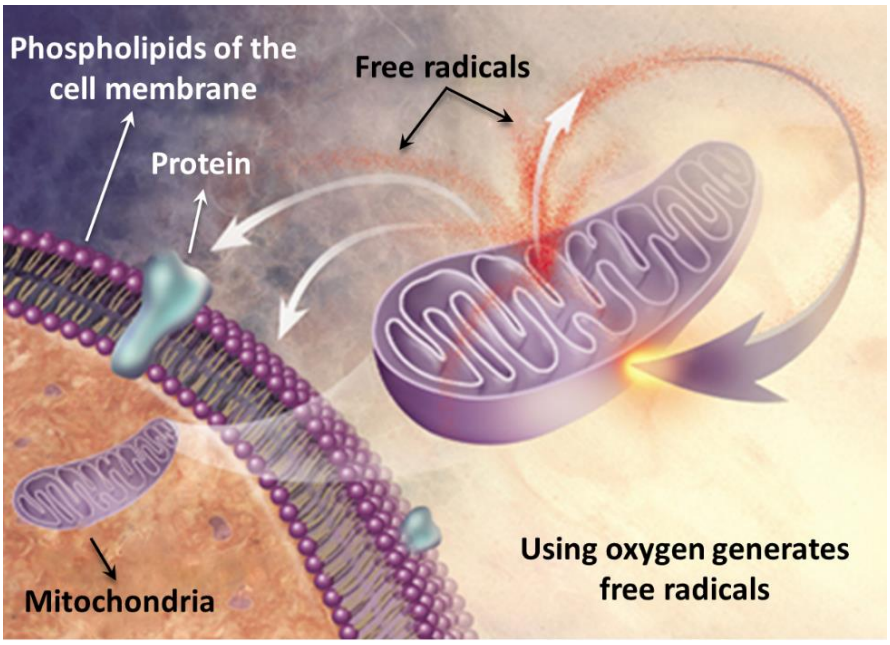

Figure 3.2. Mitochondria damaged by oxidative stress indicating the movement of free radicals to other parts of the cell [Garzón, 2009]

It has been shown that lipid peroxidation might play an important role in initiating and/or mediating some aspects of ageing, being widely demonstrated that there is an age-associated increase in the concentrations of lipid peroxidation products. However, establishing the involvement of this phenomenon in the

pathogenesis of the ageing process is not an easy task. The recent development of more reliable techniques to measure lipid peroxidation should be of great help in future studies in this field.

3.3.1.1. 8-isoprostane

Isoprostanes are a unique series of eicosanoids prostaglandin-like compounds formed *in vivo* via non-enzymatic mechanism involving the random free radical-initiated peroxidation of the arachidonic acid of tissue phospholipids (Figure 3.3).

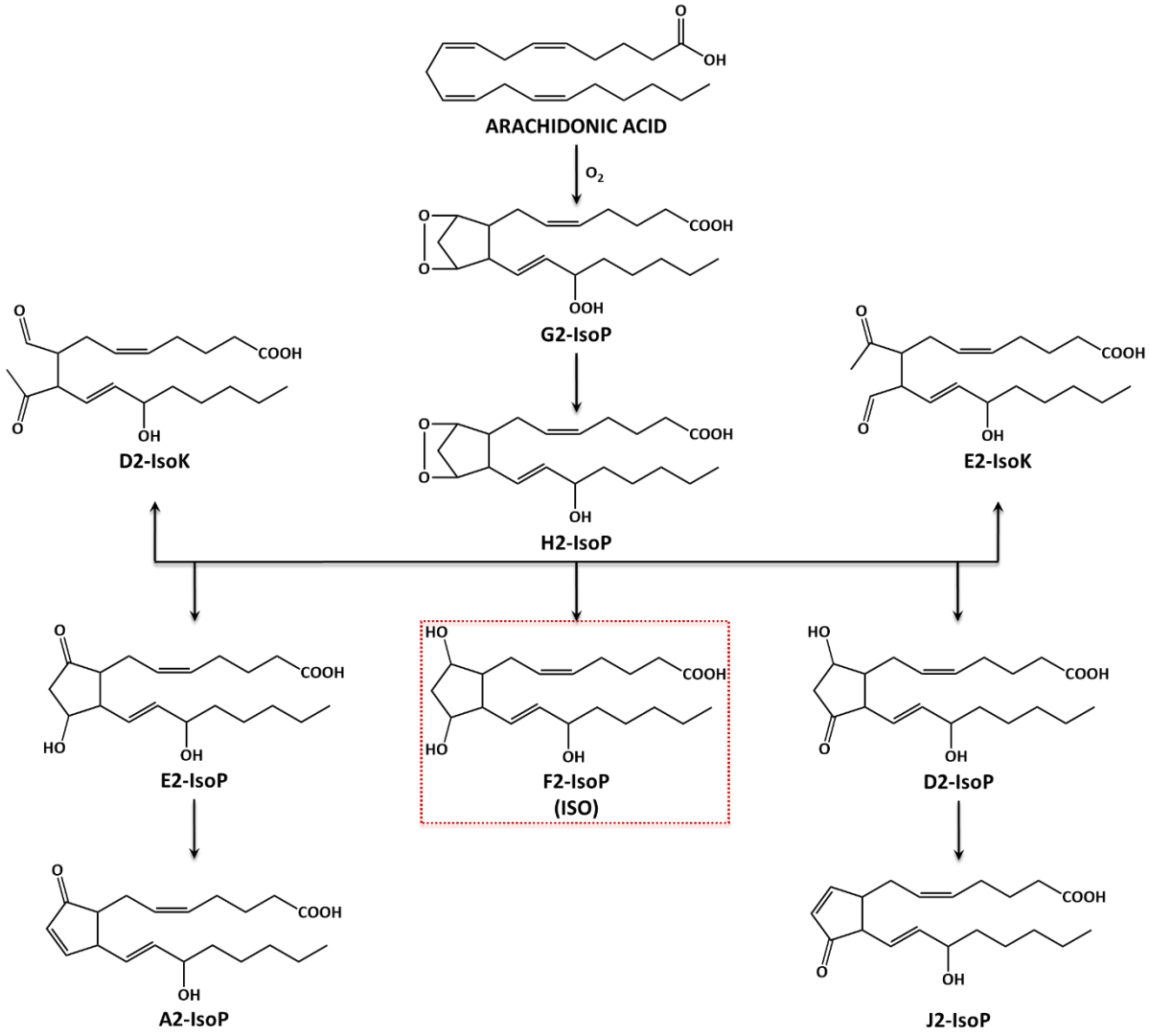

Figure 3.3. Oxidation of arachidonic acid via free radical-catalyzed peroxidation can yield a number of isoprostanes with varying ring structures [Milne, 2011]

They appear as artifacts in tissue and plasma samples, which have undergone oxidative degradation during prolonged or improper storage, as well as in urine under normal conditions, and are elevated by oxidative stress [Banerjee, 1992; Milne, 2011]. Since the discovery of these molecules over 30 years ago by Morrow *et al.* [Morrow, 1990], the quantification of one class of isoprostane has emerged as one of the most accurate approaches for evaluating the oxidant injury *in vivo*. In fact, in the Biomarkers of Oxidative Stress Study (BOSS) sponsored by the National Institute of Health (NIH) of the United States of America, isoprostanes were shown to be the most accurate biomarkers to assess *in vivo* oxidant stress status when compared with other well-known biomarkers [Liu, 2009].

One of the compounds that can be produced in abundance by the mechanism illustrated in Figure 3.3 is 8-isoprostane (ISO), also called 8-epi-PGF2, 8-isoprostaglandin F2α or 8-iso-PGF2α (Figure 3.4). This prostaglandin (PG)-F2-like compound belongs to the F2 isoprostane class and is formed *in vivo* by the free radical-catalyzed peroxidation of arachidonic acid produced *in situ* in cell-membrane phospholipids, from which they are cleaved by phospholipase A2 [Montuschi, 1999; Wang, 1995]. This isoprostane is stable and could be detectable in all human tissues and biological fluids, including plasma, urine, bronchoalveolar lavage, cerebrospinal fluids and bile. However, its quantification in urine and plasma is most convenient and least invasive [Wang, 1995].

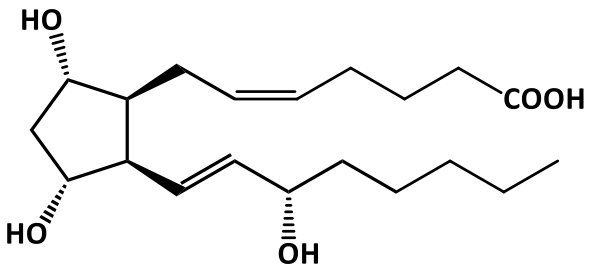

Figure 3.4. Structure of 8-isoprostane [Mizuno, 2015]

ISO has been shown to have intense biological activity. It is a potent pulmonary and renal vasoconstrictor involved as a causative mediator of hepatorenal syndrome and pulmonary oxygen toxicity. High concentrations of ISO in human fluids

and tissues have been found in a diverse array of human disorders. For instance, 8-isoprostane levels in plasma and urine are increased in smokers and in patients with acute paracetamol intoxication and scleroderma, all of these being pathophysiological conditions in which oxidative stress is increased. In addition, high level of ISO was observed in the bronchoalveolar lavage fluid of patients with interstitial lung diseases [Montuschi, 1999].

3.3.2. Biomarkers related to inflammation

Inflammation is the body's reaction to both endogenous and exogenous harmful stimuli and the initiation of the healing process. It can be classified into two types: acute and chronic. Chronic inflammation has cellular side effects, including production of free radicals that can result in oxidative damage and depletion of antioxidants [Hold, 2008]. Macrophages, one of the main components of the inflammatory response, produce reactive oxygen species (ROS) in the form of superoxide, hydrogen peroxide, hydroxyl radical, nitric oxide, hydrochlorous acid and peroxynitrite [Fialkow, 2007; Maeda, 1998]. Production of ROS by the immune system results in release of pro-inflammatory cytokines and chemokines [Costa, 2008; Ryan, 2004].

3.3.2.1. Cytokines

The immune function depends on the biological activities of numerous small glycoprotein messengers called cytokines [McInnes, 2017]. These are signaling proteins, usually with less than 80 kDa in size, which regulate a wide range of biological functions in the organism including innate and acquired immunity, hematopoiesis, inflammation and repair and proliferation through mostly extracellular signaling. Examples of cytokines are tumor necrosis factor (TNF), interleukins (ILs), chemokines, transforming growth factors (TGFs) and interferons (IFNs) [Zhang, 2007]. They are secreted by many cell types, including immune cells like macrophages, B-lymphocytes or T-lymphocytes, among others. Cytokines are

involved in cell-to-cell interactions; they have an effect on closely adjacent cells and therefore function in a predominantly paracrine fashion. These proteins may also act at a distance by secretion of soluble products into the circulation (endocrine or systemic effect) and may have effects on the cell of origin itself (autocrine effect) [Chung, 2009].

The net effect of an inflammatory response is determined by the balance between pro-inflammatory and anti-inflammatory cytokines [Sultani, 2012]. Pro-inflammatory cytokines are produced predominantly by activated macrophages and are involved in the up-regulation of inflammatory reactions. Interleukin 1 beta (IL-1β) and tumor necrosis factor alpha (TNF-α), both studied in this work, are the typical pro-inflammatory cytokines [Zhang, 2007]. On the other hand, anti-inflammatory cytokines are a series of immunoregulatory molecules that control the pro-inflammatory cytokines response. Cytokines act in concert with specific cytokine inhibitors and soluble cytokine receptors to regulate the human immune response. Their physiological role in inflammation and pathological role in systemic inflammatory states are increasingly recognized. Major anti-inflammatory cytokines include transforming growth factor beta family (TGF-β), which is categorized as either anti-inflammatory or pro-inflammatory cytokine under various circumstances. In this way, the regulation of inflammation by these cytokines and cytokine inhibitors is complicated by the fact that the immune system has redundant pathways with multiple elements having similar physiologic effects [Opal, 2000].

The properties of the different cytokines studied in this work are reviewed below.

3.3.2.1.1. Interferon gamma

Interferon gamma (IFN-γ), also known as immune interferon, is a 45 KDa homodimeric cytokine (Figure 3.5) mainly produced by activated T lymphocytes and natural killer cells. It is the unique member of the type II class of interferons family, which also includes fibroblast-derived interferon alpha (IFN-α) and leukocyte-derived

interferon beta (IFN-β) with a very limited structural homology to IFN-γ [Ijzermans, 1989; Markey, 2017; Ryffel, 1993].

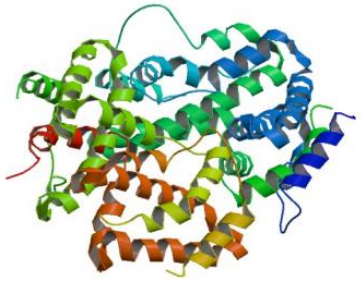

Figure 3.5. Structure of interferon gamma [Ealick, 1991]

IFN-γ is a pleotropic cytokine that induces antiviral, antiproliferative and immunomodulatory effects on numerous target cells [Walter, 2010]. Regarding to ageing, it is also a major pro-inflammatory cytokine, critical to both innate and adaptive immunity, which leads to effective clearance of pathogens through enhanced phagocytosis, pro-inflammatory responses and lymphocyte recruitment [Kak, 2018; Prosnitz, 2018]. Like all interferons, IFN-γ has antiviral activity, but also regulatory functions for macrophages, playing a role as its primary activator in addition to stimulating natural killer cells and neutrophils. It participates in the production of pro-inflammatory cytokines such as IL-1, IL-6 and TNF-α in macrophages and acts as an autocrine or paracrine growth factor in T-lymphocytes [Prosnitz, 2018; Ryffel, 1993]. IFN-γ has also a key role in the production of multiple proteins involved in the antigen-presenting pathways, apoptotic mechanisms, reactive oxygen species (ROS) and reactive nitrogen species (RNS), thus having important regulatory functions [Eley, 2009; Kak, 2018]. Finally, its importance in the immune response against mycobacteria has been confirmed by the demonstration of increased susceptibility, disease severity and poor outcome in individuals with genetic or acquired defects/deficiencies of IFN-γ [Eley, 2009].

3.3.2.1.2. Tumor necrosis factor alpha

Tumor necrosis factor alpha (TNF-α) cytokine, also called cachectin, macrophage cytotoxic factor or differentiation induction factor, is a 26 kDa

transmembrane protein (Figure 3.6) that undergoes cleavage by a metalloproteinase to be released into the circulation as a 17-kDa soluble protein [Musi, 2014]. It is produced by a variety of cells including macrophages, monocytes, endothelial cells or neutrophils. Among the relevant functions, TNF-α mediates expression of genes for growth factors, other cytokines, transcription factors and receptors [Ravussin, 2016]. Besides, it also plays a role in angiogenesis and wound healing. Several studies have identified TNF-α as a predictive marker for the development of septic complications in burn patients [El Ayadi, 2018].

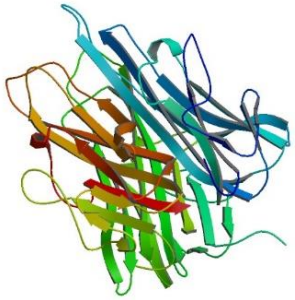

Figure 3.6. Structure of tumor necrosis factor alpha [Reed, 1999]

Some studies design TNF-α as an adipostat because its expression in adipose issue is in some extent proportional to the degree of adiposity. Clinically, elevated plasma levels of TNF-α are associated with insulin resistance and higher body mass index, as well as higher concentrations of both fasting glucose and LDL-cholesterol. In addition, obesity, dyslipidemia and TNF-α are the principal explanatory variables for the various components of the metabolic syndrome. Furthermore, TNF-α increases 11β-HSD1 (11β-hydroxysteroid dehydrogenase) mRNA and enzyme activity and, therefore, local cortisol production in human adipocytes, thus potentially linking TNF-α to visceral adiposity [Musi, 2014; Ravussin, 2016]. Among other biological effects, TNF-α is also involved in the induction of apoptosis, tumor cell cytotoxicity and increased parasiticidal and bactericidal activity of macrophages by inducing the pathways of superoxide and nitric oxide. Finally, TNF-α is the pathophysiological to be secreted in large amounts in acute and chronic diseases, chronic infections, chronic inflammation and cancer effects [Ramírez, 2012].

3.3.2.1.3. Interleukin 1 beta

The IL-1 family, comprising 11 cytokines, is closely linked to innate inflammatory and immune responses. This is because the cytoplasmic segment of all members of these receptors contains the Toll IL-1 receptor (TIR) domain, which is highly homologous to the cytoplasmic domains of all Toll-like receptors (TLR). Although all these proteins are widely studied since they initiate and regulate pro-inflammatory reactions, however, interleukin 1 beta (IL-1β) is the most interesting, due to its role in mediating auto-inflammatory disease [Dinarello, 2013; Lacy, 2017]. IL-1β (Figure 3.7) is also called human leukocytic pyrogen, leukocytic endogenous mediator, mononuclear cell factor or lymphocyte-activating factor. It is largely produced by macrophages and monocytes, but it can also be secreted by other cell types, such as neutrophils, B and T cells. This cytokine is first produced as an inactive 31 kDa pro-form, that is cleaved by caspase 1 to yield the bioactive, functional, mature cytokine and this is then secreted [Lopez-Castejon, 2011; Peral de Castro, 2015; Shen, 2014]. Together with TNF-α, IL-1β initiates further synthesis and release of cytokines and mediators and up-regulates the expression of adhesion molecules on endothelial cells [Oettgen, 2012]. Moreover, IL-1β may also play an important role in angiogenesis and invasiveness of tumor cells [Shen, 2014]. Besides, IL-1β signaling is essential to activate apoptosis and hypertrophy [Barrouin, 2015].

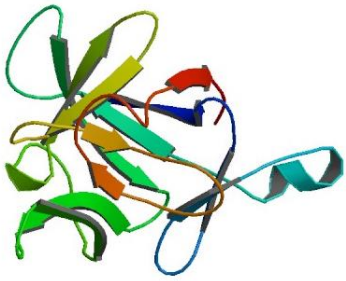

Figure 3.7. Structure of interleukin 1 beta [Yu, 1999]

Talking about the immune function, this cytokine is involved in promoting inflammatory responses, fever, vasodilatation, hypotension, sepsis and also in

allergic diseases, including atopic dermatitis and bronchial asthma. Further, IL-1β has been shown to support T cell survival and increase antibody production from B cells, thus being considered as an important therapeutic target for treatment of allergic inflammation. Additionally, IL-1β is also able to increase the expression of chemokines and adhesion molecules, which promotes the infiltration of inflammatory and immunocompetent cells from the circulation into the tissues [Dinarello, 2009; Lacy, 2017; Peral de Castro, 2015].

3.3.2.1.4. Transforming growth factor beta 1

TGF-β superfamily has important regulatory roles in a number of cellular functions, including proliferation, differentiation and tumor suppression. Although skeletal cells express transforming growth factors beta 1, 2 and 3, however TGF-β1 is the most abundant [De Paula, 2016; Mak, 2006]. It is produced primarily by hematopoietic cells, including activated T, B and NK cells, among others, being synthesized as pro-protein whose signal sequences are cleaved to yield small monomers. [Mak, 2006; Merrill, 1993]. TGF-β1 (Figure 3.8) is a disulphide-linked 28 kDa dimer of two 112-amino acid peptides ubiquitously distributed throughout different tissues and synthesized by many different cells [Kropf, 1997]. This cytokine acts as a potent anti-inflammatory protein that inhibits T-cell activation [Coplan, 2009; Peralta-Zaragoza, 2001] and growth of various types of cells. Moreover, TGF-β can antagonize many immune responses, including T cell and macrophage activation. Therefore, it is a potent negative regulator of immune responses. In addition, transforming growth factor is also known as a key fibrogenic cytokine in stimulating synthesis of regulator of extracellular matrix and inhibiting matrix degradation process [Merrill, 1993; Wu, 2012].

Finally, TGF-β1 has profound effects on skeletal tissues, being involved in joint degenerative diseases such as osteoarthritis, rheumatoid arthritis and genetically inherited disorders. In addition, TGF-β1 is a key mediator of cancer-bone cell

interactions in cancers that metastasize to bone, such as breast and prostate cancers [Dallas, 2008; Grainger, 1995].

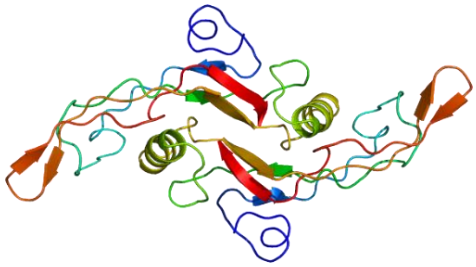

Figure 3.8. Structure of transforming growth factor beta 1 [Hinck, 1996]

3.3.2.1.5. Adiponectin

As it is known, adipose tissue is an active metabolic organ secreting adipocytokines, which are involved in the energy homeostasis and regulation of glucose and lipid metabolism. Ageing is associated with fat redistribution characterized by loss of peripheral subcutaneous fat and accumulation of visceral fat and also in the changes in the function, proliferation, size and number of adipose cells which leads to alterations in the secretion, synthesis and function of the adipocytokines. These are a group of hormones and cytokines with both pro- and anti-inflammatory effects involved also in insulin sensitivity, satiety and reproduction.

Adiponectin (APN), also called Acrp30, adiponectin 30, AdipoQ, apM1 or GBP28, is a prominent member of this family [Mesiano, 2019; Stansfield, 2014; Vaughan 2017] since is the most abundant secretory protein expressed specifically and abundantly in the adipoctyes of adipose tissues. This cytokine is a 244-amino acid hormone (Figure 3.9), which contains four differentiable domains: an amino-terminal signal sequence, a variable region, a collagenous domain and a carboxy-terminal globular domain.

APN promotes fatty acid combustion and originates insulin sensitivity by activating adenosine monophosphate-activated protein kinase (AMPK). In contrast to other secretory products of adipocytes, plasma concentrations of APN are decreased

in obesity, coronary artery disease, type-2 diabetes and insulin resistance. There is a close association between hypoadiponectinemia, insulin resistance and hyperinsulinemia. Conversely, APN expression increases with improved insulin sensitivity and weight loss, data suggesting that decreased plasma levels of APN contribute to some of the metabolic complications associated with obesity [Doehner, 2011; Hirako, 2016; Messini, 2013; Klein, 2016]. Clinical studies also revealed that low levels of plasma APN were associated with decreased serum HDL-cholesterol level, reduced lipoprotein lipase enzyme activity and smaller LDL size [Sharma, 2016]. Furthermore, centarians have higher APN levels associated with longevity. However, in less older individuals dysregulation of APN may be produced by a loss of function of circulating adiponectin or a response to increased inflammatory process [Gulcelik, 2013]. Since adiponectin naturally decreases with age and obesity accelerates the decline in adiponectin levels, one may speculate that obesity alters the ageing process through adiponectin regulation [Jura, 2016].

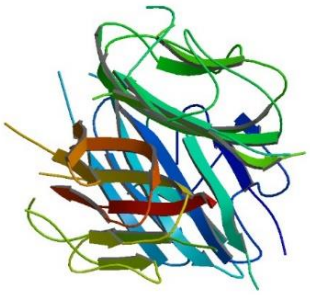

Figure 3.9. Structure of adiponectin [Shapiro, 1998]

3.3.2.2. Other proteins

Apart from the above described, several other proteins have been identified as related to the ageing process. Examples that were considered as targets in this work are human fetuin A and endoglin, whose properties are described below.

3.3.2.2.1. Human fetuin A

Human fetuin A (HFA), also known as α2-Heremans-Schmid glycoprotein or AHSG, is encoded by a single mRNA transcript. Plasmatic HFA is a 59 kDa disulfide

bond-linked two chain polypeptide (Figure 3.10) consisting of two *N*-terminal cystatin domains and a smaller *C*-terminal domain. The A chain is made up of 282 amino acid residues and the B chain is made up of 27 amino acid residues. HFA has three carbohydrate units, which are present on a peptide chain linked with threonine and serine. The gene for fetuin A is localized on chromosome 3q27 in humans [Dziegielewska, 1990; Singh, 2012]. As an acute-phase glycoprotein, HFA is synthesized in the liver and secreted as a liver-derived protein into the blood stream, where is involved in diverse functions including bone resorption, regulation of insulin activity and hepatocyte growth factor (HGF) activity, response to inflammation and inhibition of ectopic mineralization [Kalabay, 2002; Lebreton, 1979; Vaidya, 2010].

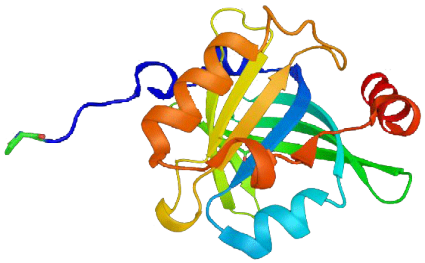

Figure 3.10. Structure of human fetuin A [Jahnen-Dechent, 2011]

HFA is commonly present in the cortical plate of the immature cerebral cortex and the hemopoietic matrix of bone marrow. Low levels of this protein may indicate cardiovascular risks at an early stage [Stefan, 2013] as occur in patients on dialysis [Liang, 2014], hypothyroidism [Bakiner, 2014] and atherosclerosis [Lim, 2007]. Under physiological conditions, HFA counteracts the production of pro-inflammatory cytokines and acts as an inhibitor of soft tissue calcification [Wang, 2012]. It constitutes a major component of mineralo-organic particles that are likely responsible for inflammation and calcification [Wu, 2013]. In addition, inflammatory conditions, such as diet induced obesity and type-2 diabetes, have been proposed to be related to HFA and fatty acid supported signaling via Toll-like receptor 4 [Pal, 2012]. Furthermore, low concentrations of HFA in plasma could be linked to insulin resistance and metabolic syndrome [Huddam, 2013], since HFA exhibits high binding affinity to insulin receptors that specifically inhibit the tyrosine kinase activity

[Goustin, 2011]. Besides, this glycoprotein inhibits APN that indirectly unregulates the secretion of inflammatory cytokines from macrophages, increasing the risk of cardiovascular-associated problems [Reynolds, 2005].

Related to ageing, it has been shown that HFA may also be impacted by this natural process with levels decreasing with age. Epidemiological evidence indicates that older adults with the lowest HFA levels have less risk for type-2 diabetes. Furthermore, this protein has been suggested to be a marker of cognitive decline [Robinson, 2016], since studies have demonstrated that HFA serve an important role in preserving the cognitive abilities of older adults, the higher levels being related to better performance of tasks designed to assess attention, calculation, orientation, language and recall. Besides, significantly lower HFA levels have been observed in individuals with Alzheimer´s disease.

3.3.2.2.2 Endoglin

Endoglin, also known as CD105, is a 180-kDa homodimeric covalently disulphide-linked transmembrane glycosylated protein (Figure 3.11). Structurally, endoglin belongs to the named zona pellucida family of proteins that share a domain of ≈260 amino acid residues at their extracellular region [Rossi, 2012]. It acts as a co-receptor for TGF-β cytokines and can mediate or inhibit TGF-β family signaling [Kramer, 2016; Maring, 2012]. This protein also plays a significant role in angiogenesis, process of crucial importance involved in several physiological and pathological conditions such as cancer [Duff, 2003; Nassiri, 2011]. Indeed, the formation of new blood vessels from pre-existing ones (angiogenesis) is essential for tumor growth and, thereby, increasing levels of endoglin found in biological fluids from affected patients may be used as an indicator for disease progression and risk of metastasis [Martins, 2015; Quintanilla, 2003].

Figure 3.11. Structure of the orphan region of human endoglin [Saito, 2017]

Specifically related to ageing processes, it is worth mentioning that increased CD105 levels are also detected in inflamed tissues. Apart from the endothelium, the protein is expressed in fibroblasts where it modulates TGF-β induced production of the extracellular matrix [Rossi, 2013]. Thus, this glycoprotein is also involved in the development and progression of other important diseases related to angiogenesis, such as rheumatoid arthritis [Koch, 2000], with TGF-β1 and certain epitopes of endoglin up-regulated on myeloid elements [Szekanecz, 1995].

3.4. IMMUNOASSAYS AND IMMUNOSENSORS

Immunoassay is a well-known highly selective bioanalytical method that detects the presence and/or determines the concentration of target compounds in a solution using an antibody or an antigen as a biorecognition agent. The analytical basis of immunoassay lies in the specificity of antibody-antigen immunoreaction and the coupling to appropriate transducers for producing a measurable signal [Ju, 2017].

Antibodies are proteins (immunoglobulins) produced by B-lymphocytes in response to stimulation by an antigen to which they show practical specificity and high binding constants [Azam, 2014; Ju, 2017]. Figure 3.12 shows the common representation of an antibody by a Y-shaped figure consisting of four polypeptide units, two of them identified and known as the heavy chains and the other two sequences as light chains. The two double-ended segments of the Y are denoted as Fab fragments and are the sites at which antibody binds with antigen. The variable

and hypervariable regions of Fab create an active portion that recognizes a specific area of the antigen. The singular segment at the other end of the Y shape is known as the Fc fragment, which cannot bind with the antigen but has the ability to affix to the cell surface and to pass through the placenta [Ju, 2017].

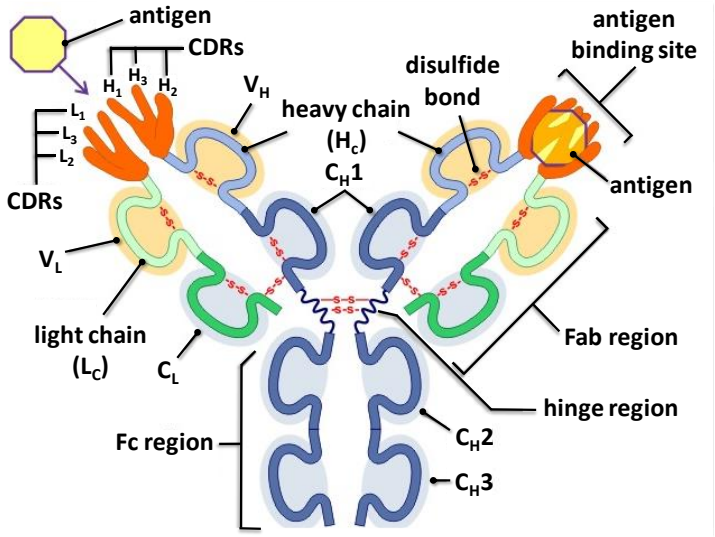

Figure 3.12. Schematic representation of an immunoglobulin G (IgG) [Cohen, 1975]

Immunoassays come in many different formats and schemes, including labeling and labeling-free configurations [Ju, 2017]. The labeling format needs to use some signal molecules conjugated to immunoreagents (antigen or antibody) for producing detectable analytical signals on the immunoreaction, whereas, labeling-free formats directly originate the observable detection signal with no need for additional molecules. Regarding to the different immunoassay schemes, competitive and sandwich-type are the most popular. Both strategies require the use of labels for quantifying the antigen-antibody reaction. Figure 3.13 shows various immunoassay schemes. As it can be observed, in a typical direct competitive immunoassay (Figure 3.13a), the labeled (Ag*) and sample (Ag) antigens compete for the antibody binding sites. In the case of indirect competitive immunoassay (Figure 3.13b), a known amount of antigen (Ag) is firstly immobilized. Separately, a mixture of labeled antibody (Ab*) and the sample antigen (Ag) is prepared and added to the immobilized Ag so that unbound Ab* complex the immobilized Ag.

As it is known, both competitive schemes provide responses inversely proportional to the concentration of antigens in the sample.

In a sandwich immunoassay (Figure 3.13c), the antigen (Ag) is captured by the immobilized antibodies (capture antibodies, cAb) and further complexed by the labeled antibodies (detection or secondary antibodies, dAb*). This scheme provide a signal directly proportional to the concentration of targets. Furthermore, the use of two different antibodies often imparts greater selectivity [Ju, 2017].

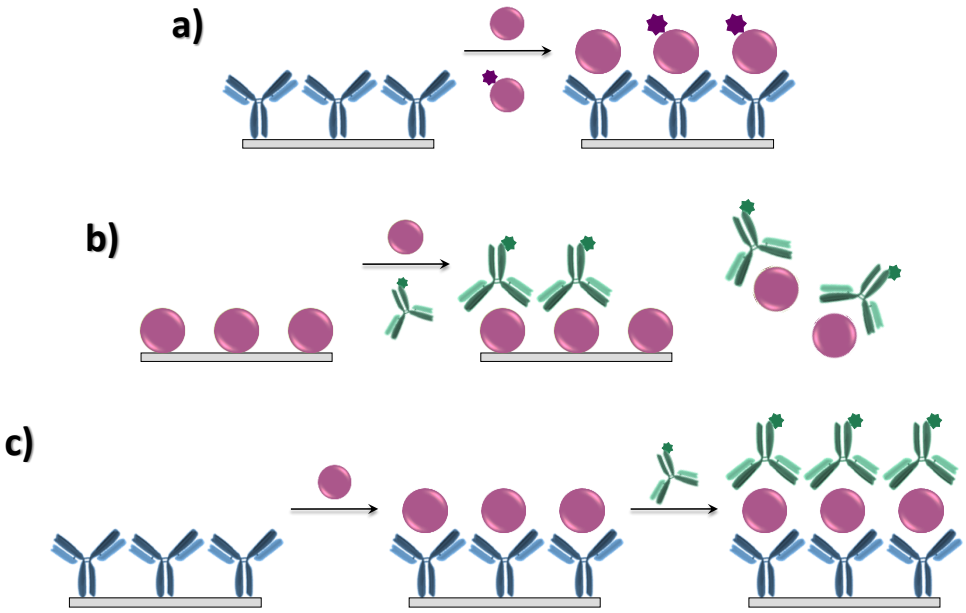

Figure 3.13. Schematic illustration of: a) direct competitive immunoassay, b) indirect competitive immunoassay and c) sandwich immunoassay [Ju, 2017]

Regarding immunosensors, they consist of compact analytical devices where the immunological recognition elements are intimately connected to or integrated within the signal transducer (Figure 3.14). Either antigens or antibodies are immobilized on the surface of a solid substrate and participate in the specific binding allowing recognition of the target analyte [Ju, 2017]. Physicochemical changes resulting from the immunoreaction between immuno-recognition elements and target molecules are then converted to a detectable signal response that is collected and amplified.

As occur with other types of biosensors, the signal transduction using immunosensors is a key process for quantitative measurements. In the case of electrochemical transduction, the event of immunocomplex formation is measured in the form of an electrical signal mainly related to a change in current and/or potential, which can be related to the concentration of analyte [Piro, 2017].

3.5. ELECTROCHEMICAL PLATFORMS

Figure 3.14 shows a scheme of the different platforms prepared for fabricating the immunosensors developed in this Thesis. As it can be seen, a variety of materials and strategies has been used with the objective of obtain the best analytical characteristics for the determination of the selected analytes in clinical samples.

As will be seen in the *Experimental Section*, all configurations proposed were prepared onto screen-printed carbon electrodes (SPCEs), in some cases employing highly conductive carbon nanomaterials as electrode surface modifiers for enhancing the electrochemical responses and also to be used as substrates for biomolecules immobilization or as carrier tags for signal amplification. These nanomaterials were single- double- and multi-walled carbon nanotubes (SWCNTs, DWCNTs and MWCNTs, respectively), graphene oxide (GO) and carbon nanohorns (CNHs). Furthermore, the immobilization strategies followed have taken advantage of the carboxylic groups present as diverse functionalities in materials such as grafted aryl-azo radicals, oxidized carbon nanomaterials or an electronic conductive polymer (poly(pyrrolepropionic) acid, pPPA). As mentioned, in some cases, nanomaterials have been used as means for signal amplification and, in addition, a streptavidin-peroxidase polymer (poly-Strept-HRP) has also been used for this purpose.

In the following sections, the materials and strategies used are described in detail.

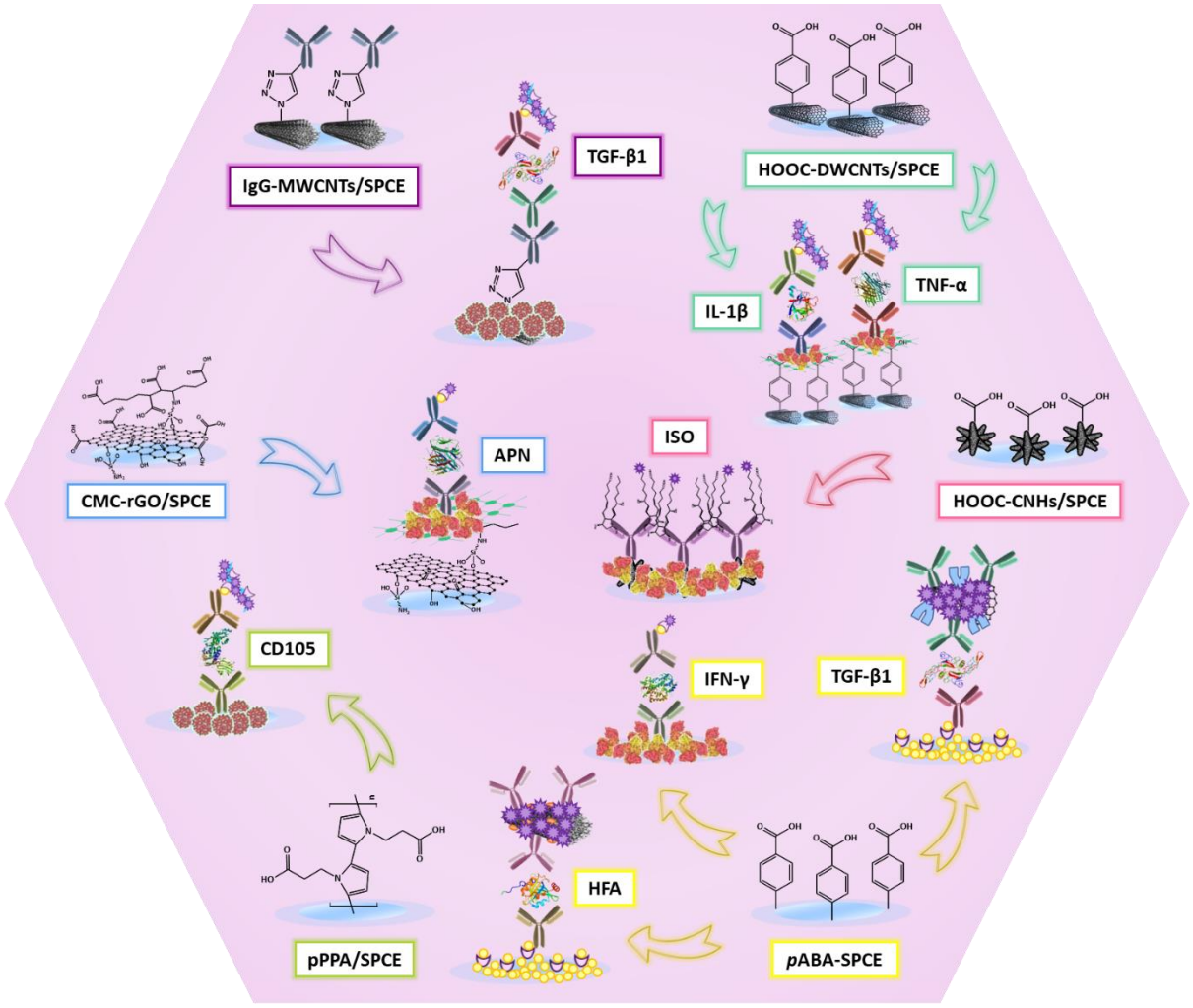

Figure 3.14. Schematic representation of the electrochemical platforms and immunosensors developed

3.5.1. Carbon nanomaterials

It is well known that nanostructuration of working electrodes with nanosized carbon modifiers provides attractive features, such as fast electron transfer kinetics due to the high conductivity of these nanomaterials, elevated surface area, which enhances adsorption of biomolecules, high selectivity and electrocatalysis, due to the unique electronic structure and tunable surface chemistry towards the direction of the assembly for particular capture probe or analyte species [Yáñez-Sedeño, 2017]. In addition, their excellent biological compatibility, ease of preparation and organic functionalization make carbon-based nanomaterials excellent carriers for loading numerous signal elements, such as enzymes, oligonucleotides, antibodies, redox

molecules and inorganic nanomaterials, to greatly amplify the transduction signals of recognition events in electrochemical bioassays.

Among the variety of carbon nanomaterials, carbon nanotubes (CNTs) and graphene have been extensively used as electrode modifiers in the preparation of electrochemical immunosensors. Electrode nanostructuration with these materials allows preparing scaffolds with improved conductivity and selectivity and with enhanced ability for the immobilization of antibodies or antigens [Yáñez-Sedeño, 2016]. In addition, the resulting nanostructured surfaces can be used to design suitable strategies for signal amplification thus leading to significant improvements in sensitivity. More recently, apart from the common single- or multi-walled carbon nanotubes or graphene, other carbon nanoforms have emerged as novel nanostructuration tools suitable to be employed also in the preparation of bioelectrochemical devices achieving improved analytical performance. Double-walled carbon nanotubes and carbon nanohorns are two examples of these most recent applied nanomaterials, whose particular characteristics make them appropriate for the construction of relevant designs of electrochemical immunosensors.

3.5.1.1. Carbon nanotubes

As it is well known, carbon nanotubes (CNTs) are graphene sheets rolled into a seamless cylinder that can be open ended or capped, with diameters as small as 1nm and a length of several micrometers [Porwal, 2017]. Carbons are sp^2 hybridized with three neighbouring atoms resembling a graphitic structure [Karak, 2012]. Despite CNTs are relatively inert, non-immunogenic and highly stable particulate systems [Karandikar, 2017], various constraints have been made on their applications for (bio)sensor preparation due to the lack of solubility in aqueous medium and common solvents as well as their toxicity. These limitations can be overcome by functionalization. To do this, the most common procedure consists in CNTs oxidation by treatment with nitric and/or sulfuric acids, which results in the incorporation of

hydroxyl or carboxyl groups, and the opening of nanotube end caps [Porwal, 2017]. Furthermore, on the basis of functionalization, the oxygen moieties can be used for immobilizing biomolecules and the physical, chemical or biological properties of carbon nanotubes can be modulated [Ahmed, 2018], which make them very attractive materials in a range of applications [He, 2017].

Electrode surfaces modified with carbon nanotubes exhibit improved advantages such as: 1) small size with large surface area, 2) high sensitivity, 3) fast response time, 4) enhanced electron transfer, 5) easy protein immobilization with retention of activity and 6) alleviating surface fouling effects.

Depending on the number of sheets rolled into concentric cylinders, CNTs can be divided into three broad categories (Figure 3.15): SWCNTs, which may be formed by rolling up a single sheet of graphene, DWCNTs, with two sheets, and MWCNTs, which may be formed by rolling up multiple sheets of graphene [Holban, 2016; Porwal, 2017]. These nanotubes have attracted a lot of interest because they are essentially one-dimensional periodic structures with electronic properties (metallic or semiconducting) depending upon their diameter and chirality [McEnaney, 1999].

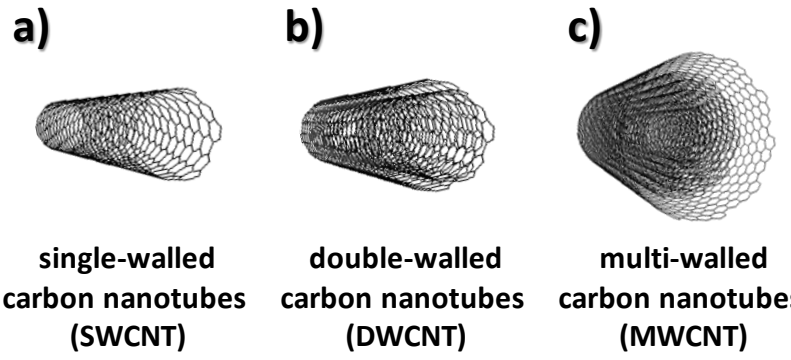

Figure 3.15. Schematic illustration of the structure of three types of carbon nanotubes [Jackson, 2013]

SWCNTs can be considered as a long wrapped graphene sheet by rolling it in certain directions upon which, as well as the diameter, the properties of nanotubes are mainly dictated. For instance, SWCNTs can act as metals or semiconductors, the electronic properties being dependent on the chiral vector in which the graphene was rolled up to form the nanocylinder [Dawidczyk, 2013]. The use of SWCNTs for

the preparation of electrochemical biosensors has provided for a long time many advantages such as enhancing the electrochemical reactivity of important biomolecules and the promotion of electron-transfer reactions of proteins.

DWCNTs are the simplest configuration of the multi-walled counterpart and combine the outstanding properties of this material with those from SWCNTs. The particular structural and electronic properties of DWCNTs have attracted interest for their use in fabricating molecular electronic devices [Wu, 2012b]. It has been found that DWCNTs-modified electrodes exhibit better electrochemical behavior than those modified with SWCNTs, providing fast electron transfer with significant overpotential reduction for various species [Pumera, 2007]. A higher reactivity has also been claimed for DWCNTs, which is probably due to the larger number of lattice defects with respect to SWCNTs. Furthermore, compared with MWCNTs, several beneficial properties have been claimed such as the higher stability under aggressive chemical, mechanical and thermal treatments [Green, 2011]. As it was reported, upon chemical modification of DWCNTs, the outer cylinder acts as a protective sheath that preserves the electronic properties of the inner tube [Brozena, 2010]. Therefore, covalent sidewall chemistry can be performed onto DWCNTs without loss of the intrinsic properties [Punbusayakul, 2013]. Despite their excellent electrochemical properties and the special performance after functionalization, only few examples of sensors and biosensors involving DWCNTs can be found in the literature.

MWCNTs are comprised of various layers of graphite wrapped around one another in a tube-shaped structure with an interlayer dispersing of 3.4 Å, diameters ranging from 10 to 200 nm and lengths upon hundreds of microns. Among the different materials for the electrode modification, it can be said that MWCNTs represent the most famous carbon based nanomaterial in electroanalysis. Functionalized MWCNTs with carboxyl groups have been used during years for the

preparation of electrochemical biosensors by covalent immobilization of biomolecules.

3.5.1.2. Carbon nanohorns

Single-walled carbon nanohorns or, simply, carbon nanohorns (CNHs) are a relatively new type of carbon allotrope. One single CNH consists of a unique horn-shaped graphene sheet with a length of 40 – 50 nm and a diameter ranging between 2 and 5 nm (Figure 3.16) [Zhu, 2014]. CNHs are prepared by vaporizing pure graphite rods via CO_2 laser ablation without using any metal catalysts. Thus, an important advantage of this materials over carbon nanotubes is that CNHs are essentially metal-free [Shi, 2009; Miyawaki, 2008] and can be used directly without purification post-treatment. Typically, CNHs assembles to form nanostructures similar to dahlia flowers composed of several units with a diameter near from 100 nm [Tanaka, 2004; Ajima, 2005]. The distinct structure of carbon nanohorns with conical shape with a particularly sharp apical angle [Liu, 2010] conduces to novel mechanical and electronic properties, which have attracted considerable attention. Furthermore, the special properties of CNHs derive from the high conductivity, the large surface area, the high number of defects and the amount of inner nanospaces. Oxidative treatment of CNHs leads to the production of a large number of exposed oxygen functionalities on the thousands of cone-shaped tips present onto spherical aggregates [Zhang, 2010]. These functionalities can be further exploited for the covalent immobilization of the immunoreagents.

The unique conical structure of CNHs has a great influence on their properties, such as excellent capability for charge transfer, variable porosity resulting in large specific surface area and good adsorption [Karousis, 2016; Zhang, 2007b]. However, their applications have evolved at a much slower pace than CNTs, because of their aggregation into spherical cluster, which makes dispersion and surface modification difficult [Villarreal, 2017].

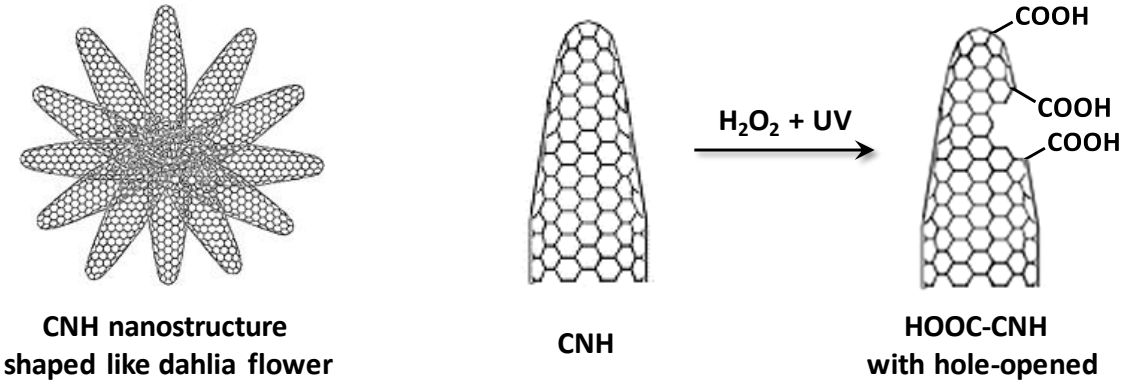

Figure 3.16. Schematic illustration of CNH and light assisted oxidation [Zhang, 2007]

3.5.1.3. Graphene and derivatives

Graphene is currently one of the most used nanomaterials in electrochemical (bio)sensing applications. It is described as a one-atom-thick planar sheet of sp^2 hybridized C–C bonding densely packed in a honeycomb crystal lattice (Figure 3.17a) [Novoselov, 2008]. Each atom in the lattice has a π orbital that contributes to a delocalized network of electrons similar to conduction bands in metals. Importantly, the physical properties of graphene exploited in electrochemical applications are the extreme large surface area, good electrical conductivity, wide potential window, low resistance to charge transfer and high electrocatalitical activity [Alwarappan, 2009].

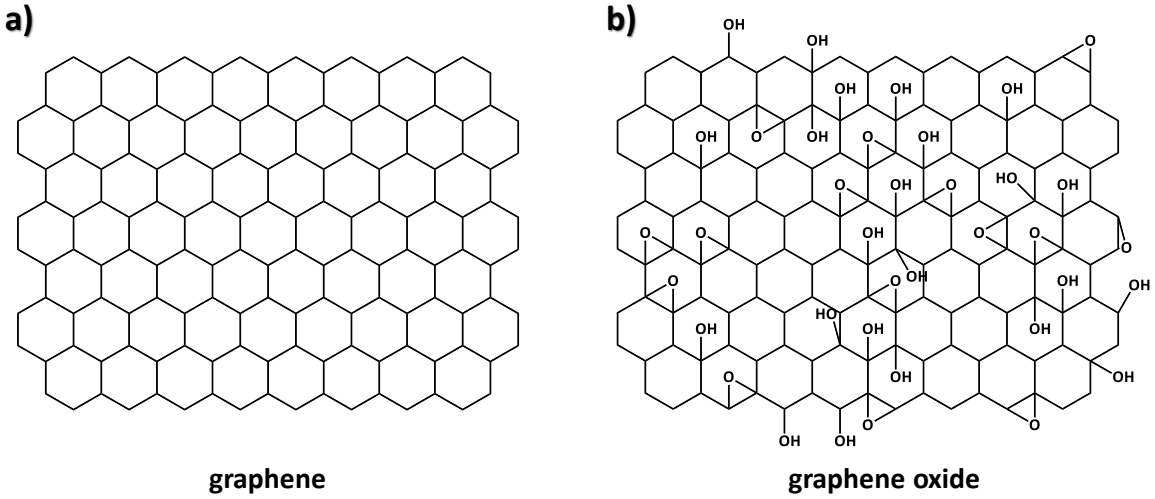

Figure 3.17. a) Graphene and b) graphene oxide (GO) [Pei, 2012]

However, despite these advantages, from the practical point of view, the use of graphene in the construction of biosensors is limited by the low solubility in polar

and non-polar solvents, as well as the absence of groups able to achieve an effective immobilization of biomolecules. These problems can be partially solved by chemical modification as, for example, applying oxidative treatments. The chemical functionalization of graphene is a particularly attractive target because it can improve the solubility and processability as well as enhance the interactions with different class of molecules [Park, 2011].

Graphene oxide (GO) can be synthesized by oxidation of graphite mainly using the Hummers method [Hummers, 1958] followed by step-wise exfoliation applying sonication and stirring to give aqueous colloidal suspensions of GO. The resulting product is a unique material that can be viewed as a single monomolecular layer of graphite with various oxygen-containing functionalities such as epoxy, carbonyl, carboxyl and hydroxyl groups (Figure 3.17b) [Ray, 2015]. These oxygenated groups diminish the interaction between graphite layers and increase the hydrophilic character of the material. The main problem is the formation of structural defects and vacancies that interrupt the sp^2 bonding network thus get worse the electronic properties. It can be said that both graphite oxide and GO are electrically insulating materials. However, all these disadvantages can be solved by GO reduction in order to partially remove oxygen functionalities (epoxy, carboxyl and hydroxyl groups) and recover electrical conductivity by restoring the π-network [Gao, 2015]. The reduction of GO reinstates a large part of the conductivity even though some defects are not eliminated, thus minimizing the drawbacks of low reactivity of graphene. Reduced GO (rGO) combines both graphene and GO characteristics.

A variety of reducing agents has been used to obtain rGO, the most common being hydrazine, sodium borohydride and hydroquinone [Chen, 2010]. Ascorbic acid, as a less toxic and greener reagent [Zhang, 2010b], and electrochemical reduction have also been used.

3.5.2. Conducting polymers

Polymers have expanded their applications as useful materials for the preparation of biosensors. Among them, conducting polymers (CPs) have largely demonstrated their suitability as substrates for biomolecule immobilization because of the different ways of interaction and the fast electron transfer [Teles, 2008]. Indeed, CPs show unusual electrochemical properties like high electrical conductivity, low ionization potential and high electronic affinities which derive from the existing conjugated π electron backbones [Ahuja, 2007]. Particularly, enzyme biosensors have taken advantage of the properties of CPs since a simple approach for their preparation consisted of bioreagents entrapment in the polymer network can be used. However, in the case of affinity biosensors, this strategy is not recommended because the affinity reaction can be strongly hindered. Thus, methods for allowing the ordered immobilization of bioreagents without losing the conductive properties of polymer should be applied. Effective alternatives are CPs containing functional groups for covalent binding of biomolecules. In this work, poly(pyrrolepropionic) acid (pPPA) (Figure 3.18) was used.

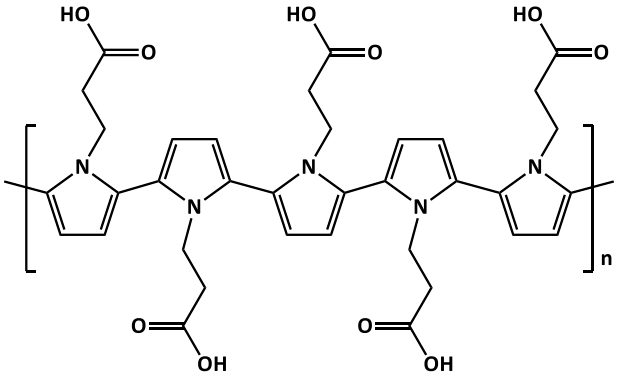

Figure 3.18. Structure of poly(pyrrolepropionic) acid

This polymer belongs to the poly(pyrrole) (pPy) family, being a conducting polymer with abundance of carboxyl groups that can be used for covalent attachment of bioreagents. Although these carboxylic groups decrease the conductivity of this polymer compared to other pPy, its porous structure and hydrophilic property of the films electrodeposited, allow electroactive species to

permeate through the polymer film and generate sensitive electrochemical responses on the electrode surface [Dong, 2006].

3.6. STRATEGIES USED FOR THE IMMOBILIZATION OF BIOMOLECULES

The standard immobilization method, which furnishes reproducible results and could be used for evaluating new methods do not exist. This is because there is no single standard surface on which immobilize and, moreover, because the surface density of immobilized biomolecules depends highly on their own nature, origin and history [Tedeschi, 2003]. The immobilization technique used for a particular application should allow a stable bound between the sensing surface and the bioreceptor without interfering with the biological activity of the system. Furthermore, high sensitivity and an adequate operating range are also essential requisites for development of a biosensor for diagnostic applications and, in principle, these can be met by ensuring a high density of active biomolecules in the sensing surface. Likewise, suitable bioconjugation strategies and stabilization of biomolecules on electrodes are essential for the development of novel and commercially viable biosensors [Liébana, 2016].

Covalent immobilization of biorecognition elements offers important advantages. However, binding of biomolecules requires the presence of reactive functional groups in both the biomolecules and the surface to be modified. Proteins have abundant amino groups, which may react with oxygen moieties such as carboxyl groups to form amide type bonds. This scheme is usually followed in the preparation of electrochemical immunosensors employing electrode surfaces containing a high amount of oxygenated binding functionalities. In this work, this strategy was applied for the preparation of the different immunosensing platforms using SPCEs modified with the following oxygen-containing coatings: pPPA, oxidized CNHs, rGO hybridized with carboxymethyl cellulose, grafted *p*-aminobenzoic acid

(*p*-ABA) and grafted *p*-ABA-DWCNTs. Moreover, carboxylated-SWCNTs or MWCNTs were also used as substrates for covalent immobilization of antibodies and their application as nanocarrier tags for signal amplification. In addition to covalent binding, another much less explored strategy, such as the one based on the copper (I) catalyzed cycloaddition reaction between an azide group and an alkyne *("click chemistry"*, CuAAC) was also used.

3.6.1. Covalent binding

Covalent immobilization of proteins onto electrode surfaces brings very attractive advantages for the preparation of electrochemical biosensors because it provides a good stability of the biomolecules with minimal loss of activity. Generally, the covalent bond is established through the numerous amino groups existing, both at the ends of the polypeptide chains that shape the protein and in the *ε*-amino groups of the lysine residues. These *ε*-amino groups, which are positively charged under slightly acidic or neutral pH conditions, are generally arranged on the outer surface of proteins, being accessible for binding to the electrode surface without denaturation of quaternary protein structure [Hernández, 2011]. However, one of the main drawbacks of this type of immobilization is, in the case of immunosensors, the random and non-oriented nature of bond, which sometimes difficult the access to the antigenic recognition area of antibodies [Yuanyuan, 2006].

Very few chemical groups are known to provide specific and practical conjugation to carboxylic acids (–COOH). Carbodiimide compounds afford the most popular and versatile method for labeling or crosslinking proteins and many other biomolecules to these functions by means of activating carboxyl groups for direct reaction with primary amines via amide bond formation. Because no portion of their chemical structure becomes part of the final bond between conjugated molecules, carbodiimides are considered zero-length carboxyl-to-amine crosslinkers. The most readily available and commonly used carbodiimides are the water-insoluble

N,*N*'-dicyclohexyl carbodiimide (DCC) for non-aqueous organic synthesis methods and the water-soluble *1*-ethyl-*3*-(-*3*-dimethylaminopropyl) carbodiimide (EDC) for aqueous crosslinking (Figure 3.19).

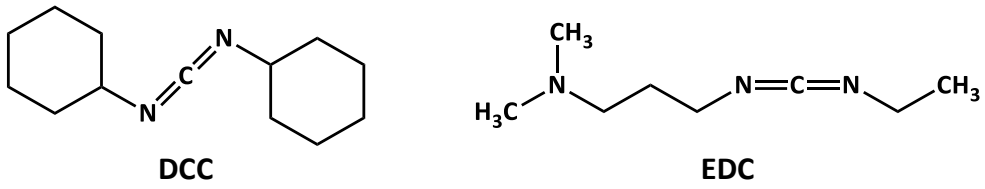

Figure 3.19. Chemical structure of DCC and EDC

EDC reacts with carboxylic acid groups to form an active *O*-acylisourea intermediate that is easily displaced by nucleophilic attack from primary amino groups in the reaction mixture. The primary amine forms an amide bond with the original carboxyl group and an EDC by-product is released as a soluble urea derivative. The *O*-acylisourea intermediate is unstable in aqueous solutions. As the scheme represented in Figure 3.20 shows, other reagent, *N*-hydroxysuccinimide (NHS) or its water-soluble analog *N*-hydroxysulfosuccinimide (NHSS), is often included in EDC coupling protocols in order to improve efficiency or to create dry-stable (amine-reactive) intermediates. EDC couples NHSS to carboxyls, forming an NHSS ester that is considerably more stable than the *O*-acylisourea intermediate while allowing for efficient conjugation to primary amines at physiological pH.

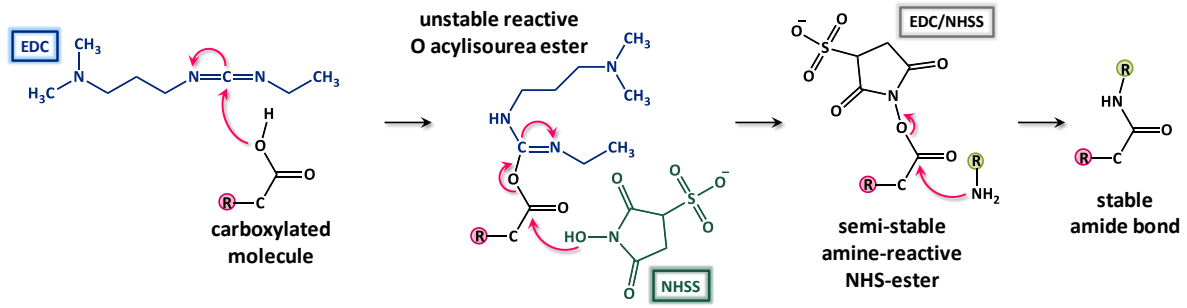

Figure 3.20. EDC plus NHSS crosslinking reaction scheme

The reaction is most efficient in acidic (pH 4.5) conditions and must be performed in buffers devoid of extraneous carboxyls and amines. For example, MES buffer (*2*-(*N*-morpholino)ethanesulfonic acid) is a suitable carbodiimide reaction buffer. Phosphate buffers and neutral pH (up to 7.2) conditions are also compatible

with the reaction, although with lower efficiency. In this case, increasing the amount of EDC in a reaction solution can compensate for the reduced efficiency.

Additionally, terephthalic acid has also been used as carbonyl-terminated linker for covalently immobilization of amino groups, by adding a previous carboxyl group, where a protein can be attached (Figure 3.21) [Rahim Ruslinda, 2013].

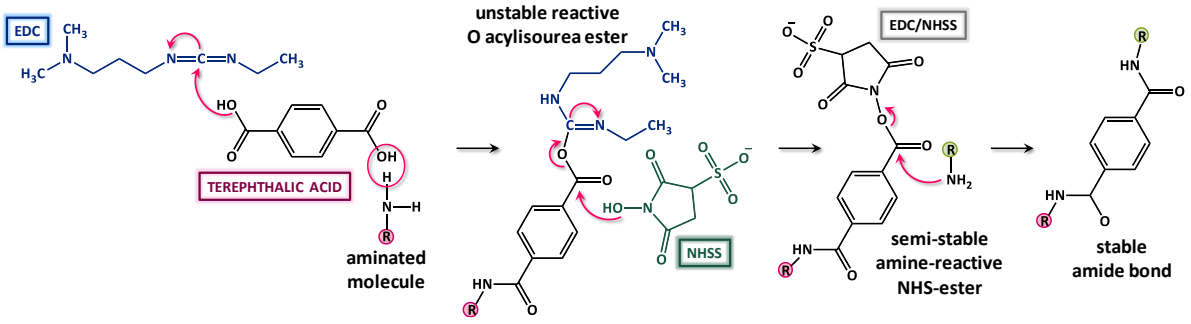

Figure 3.21. EDC plus NHSS crosslinking reaction scheme in the presence of terephthalic acid

Likewise, a novel binding material for covalent immobilization of proteins was developed consisting of a polymer of chromium (III)-based metal complexes, which enables the activation of a variety of substrates for subsequent incorporation of biomolecules [Muir, 2007]. This commercially available product named Mix&Go™ (Anteo Diagnostics), forms multivalent interactions with almost any surface containing electron-donating groups including carboxylate anions [Vukovic, 2014]. The resulting activated surface increases by less than 1 nm thickness the underlying substrate and is storable dry or immersed in aqueous buffer. However, once any proteins are added, the activated surface rapidly forms very strong but gentle binding interactions. Thereby, Mix&Go™ acts like a molecular glue, binding biomolecules to synthetic surfaces. Each metal ion (Cr(III) and others) can form coordinate bonds with electron donating groups present on the vast majority of synthetic surfaces and use the remaining unoccupied coordination sites for proteins binding [Ooi, 2014].

The use of Mix&Go™ offers various advantages over existing methods for activation such as that based on EDC/NHSS chemistry or those involving epoxy, tosyl or hydrophobic interactions. Among these, it is worth highlighting the ease of use

and simplicity of the required procedure, which is able to bind proteins to virtually any surface in minutes [Vukovic, 2014]. In addition, Mix&Go™ can provide a certain degree of orientation for immobilized antibodies since the metal polymer binds preferentially to the Fc region, therefore allowing them to interact properly therefore leaving free the Fab antigen-binding region (Figure 3.22). Acting in this way it can be said that the metal polymer creates antibody-binding domains mimicking binding domains from proteins A and G, comprising two different small ligands and extending as two adjacent side-chains from the polymer backbone. This behavior represents a great advantage with respect to other methods for immobilization that tend to facilitate the attachment on antibodies in a random orientation resulting in a large portion of damaged and/or non-functional antibodies [Abernethy, 2012; Wu, 2008].

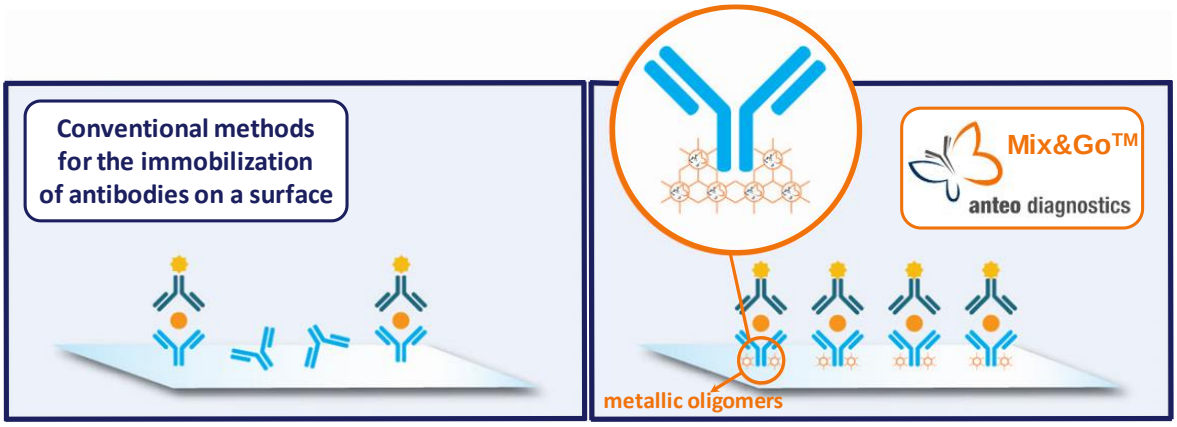

Figure 3.22. Schematic representation of antibodies immobilization using Mix&Go™

3.6.2. Functionalization of the electrode surface

As it was indicated, SPCEs modified with different coatings for immunoreagents immobilization were used as platforms for the development of immunosensors. Among the strategies used for incorporate functionalities to the electrode surface, in the following sub-sections, two general procedures selected for their importance in the context of this work are described.

3.6.2.1. Electrochemical grafting

This name refers to a method for modifying electrode surfaces consisting of an electrochemical reaction that permits organic layers to be attached to solid conducting substrates [Bélanger, 2011]. The reaction usually involves the transfer of an electron between the organic compound and the electrode through a mechanism described in 1992 by Pinson et al. for the modification of carbon electrodes by electrochemical reduction of aryldiazonium salts [Delamar, 1992].

As Figure 3.23 shows with the example of *p*-aminobenzoic acid (*p*-ABA), once the aryl diazonium salt is *in situ* generated in the presence of sodium nitrite, it is electrochemically attached to the electrode surface through a single-step electrografting process by performing successive cyclic voltammetric potential scans.

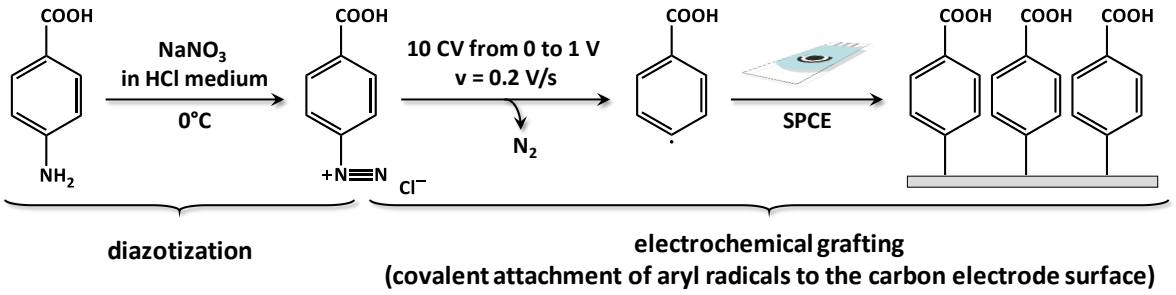

Figure 3.23. Steps involved in the electrochemical grafting by reduction of diazonium salts

The electrografting method has demonstrated to be an efficient way to introduce many types of functional groups onto a variety of materials, mainly carbon and metals requiring short reaction times [Bélanger, 2011]. Moreover, it conduces to the creation of compact and stable monolayers whose density can be controlled by a careful selection of the electrografting protocol [Liu, 2000].

Besides this, there is another method for modifying the electrode surface by electrografting based on the electrochemical oxidation of amine-containing compounds by cyclic voltammetry in the presence of lithium perchlorate in ethanol leading to amine cation radicals and the subsequent linking to the substrate [Liu, 2000] (Figure 3.24).

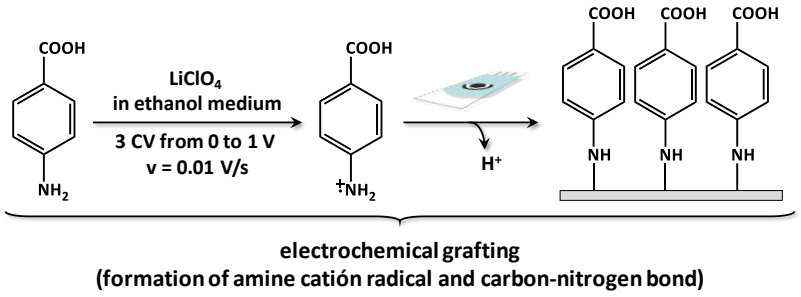

Figure 3.24. Steps involved in the electrochemical grafting by oxidation of aryl-amines

3.6.2.2. Copper (I) catalyzed azide-alkyne cycloaddition

This reaction, designed by CuAAC, belongs to the group of reactions conceived with a similar concept known as *"click chemistry"*. Although it was discovered by Huisgen in the 1950's, it was Sharpless who coined this term to describe highly efficient synthetic reactions that were tolerant of various functional groups and occurred under mild synthetic conditions [Zhang, 2012]. These reactions are used to *"click"* two organic compounds via a heteroatom link (C–X–C) [Gebert, 2017]. Among the number of reactions that fulfill the criteria, the Huisgen *1,3*-dipolar cycloaddition catalyzed by copper (I) between azides and terminal alkynes (CuAAC) (Figure 3.25) has emerged as the frontrunner, being a very convenient and simple method of synthesis of *1,2,3*-triazoles. It has found applications in a wide variety of research areas, including immunosensor development [Hein, 2008; Pospieszny, 2015].

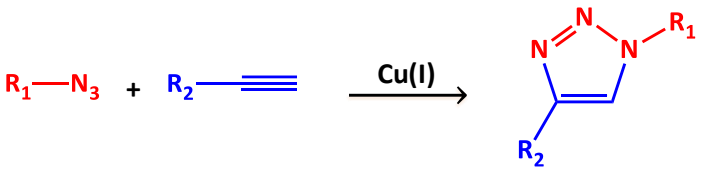

Figure 3.25. Copper (I) catalyzed 1,3-dipolar cycloaddition of azides and terminal alkynes [Haldón, 2015]

Although initially developed as a tool for organic synthesis, currently *"click chemistry"* is one of the most useful ways to incorporate functionalities on different materials. The reasons of its popularity can be found in the interesting characteristics of the *"click reactions"*, as they provide high yields, generate few by-products, are

stereospecific, require mild conditions, use readily available reagents and preferably employ water as a solvent. All these are very useful advantages for the application of this strategy in the preparation of electrochemical biosensors.

Among the different reactions taking part of this set, CuAAC the best known and that usually refers to when talking about *"click chemistry"*. It is compatible with a wide range of pHs, solvents and temperatures and has already been used successfully for the immobilization of biomolecules. It works at room temperature using cuprous ion as the catalyst that can be synthesized by different ways including electrochemically. Moreover, there is a wide variety of possibilities of using this reaction for the construction of electrochemical biosensors in the scheme designed for this work, the starting material were MWCNTs functionalized with azide groups. These were obtained from carboxylated nanotubes to which a long chain linear azido-amine was covalently attached (Figure 3.26). Subsequently, an ethynylated auxiliary antibody (alkyne-IgG) was linked by CuAAC. By this way, once immobilized the resulting conjugate (IgG-MWCNTs) onto the SPCE, a modified electrode surface suitable for use as a platform for the construction of the immunosensor was obtained.

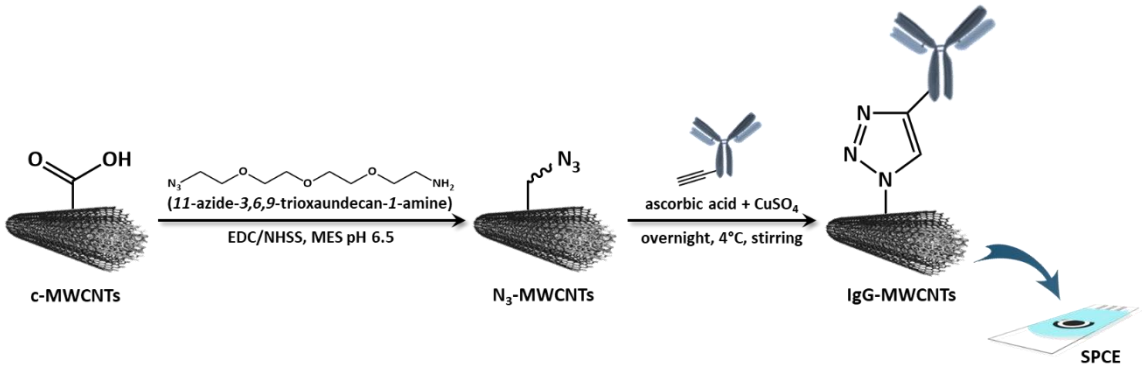

Figure 3.26. Steps involved in the preparation of IgG-MWCNTs/SPCE

3.7. METHODS INVOLVING AFFINITY REACTIONS FOR AGEING BIOMARKERS DETERMINATION

In this section, the methods reported in the literature involving affinity reactions with immunoreagents or nucleic acids applied to the determination of the different biomarkers selected as analytical objectives in this Thesis are revised. As it can be seen, Tables 3.1 to 3.8 summarize the type of configurations used and the analytical characteristics of each method, including those based on some available commercial ELISA kits.

3.7.1. Interferon gamma

Table 3.1 shows the most relevant aspects of the methods described in the literature for the determination of IFN-γ based on electrochemical affinity biosensors as well as those using ELISA kits. As it can be seen, the immunosensors developed so far are based on configurations without and with enzymatic marker. Among the former, those based on electrochemical impedance spectroscopy (EIS) directly measure changes in charge transfer resistance (ΔR_{CT}) related to analyte concentration using electrodes modified with different materials for immobilization of the capture antibody. The detection limits range between tenths and units of pg/mL [Wang, 2017; Ruecha, 2019]. Sandwich-type configurations using CdSNPs as label tags and stripping voltammetry of dissolved nanoparticles [Wang, 2016; Huang, 2015] have also been reported.

Other configurations use horseradish peroxidase (HRP) as the enzyme label with linear calibration plots in the pg/mL range have been applied to the analysis of serum samples. For example, Zhang *et al.* used diallyldimethylammonium chloride (PDDA) and gold nanoparticles (AuNP) composite combined with horseradish peroxidase (HRP)-labeled antibody-conjugated gold nanoparticles (HRP-anti-IFN-AuNPs) bioconjugates as a novel signal tag. In this case, the large amounts of enzyme molecules on the signal tag can catalyze the oxidation of hydroquinone (HQ) by

hydrogen peroxide, which can induce an amplified reductive current, with a detection limit of 0.048 pg/mL [Zhang, 2016].

In addition, immunosensors for the determination of IFN-γ using differential pulse voltammetry (DPV), square wave anodic stripping voltammetry (SWASV) or electrochimioluminescence (ECL) as detection method are also described in the literature. Thus, Zhang *et al.* developed a multilayer screen-printing indium tin oxide (ITO) detector modified with a self-assembled graphene/chitosan (Gr-Chit) composite film followed by glutathione modified gold nanoparticles (GSH-AuNPs). Under optimum conditions, the relative increased differential pulse voltammetry (DPV) peak current values are proportional to the logarithmic value of IFN-γ concentrations in a wide range from 5 to 4000 pg/mL with a detection limit of 0.5 pg/mL [Zhang, 2015].

In their work, Moschou *et al.* adapted an enzyme-linked immunosorbent assay (ELISA) onto a commercial printed circuit board (PCB) electrochemical biosensing platform in order to quantify IFN-γ by the detection of the enzyme product TMB/H_2O_2 using amperometry [Moschou, 2016].

Lastly, Zhu *et al.* developed a sensitive electrochemiluminescent (ECL) immunosensor for real-time and dynamic evaluation of the concentration of interferon gamma secreted by peripheral blood mononuclear cells. The immunosensor was fabricated by attaching gold nanoparticle-coated magnetic beads (AuNP@MB) on a nanofiber prepared from graphene oxide and polyaniline (GO-PANI-NF) for the immobilization of anti-IFN. In this way, the assay is based on a sandwich-type immunoreaction in which the secondary antibody labeled with cadmium sulphide quantum dots (CdSQDs) is used to generate electrochemiluminescence with a wide linear range between 0.1 and 500 pg/mL and a low detection limit (0.03 pg/mL) [Zhu, 2016].

Aptasensors with different detection strategies have also been proposed [Liu, 2010b; Zhang, 2012; Xia, 2015]. They exhibit linear calibration plots in the ng/mL

range [Chen, 2014; Ding, 2017], with limits of detection between few pg/mL [Liu, 2015] and ng/mL [Liu, 2010b; Zhang, 2012]. These were also applied to serum [Chen, 2014; Liu 2015] and cell culture [Xia, 2015; Yan, 2013].

An example is the label-free electrochemical impedance spectroscopy aptasensor based on the use of ternary surface monolayers that selectively capture and detect IFN-γ on gold interdigitated electrodes (AuIDEs) developed by Ding *et al.* [Ding, 2017]. Liu *et al.* used a DNA hairpin containing IFN-γ-binding aptamer thiolated conjugated with methylene blue (MB) as redox tag and immobilized on a gold electrode. Binding of IFN-γ caused the aptamer hairpin to unfold, pushing MB redox molecules away from the electrode and decreasing electron-transfer efficiency. The change in redox current was quantified using square wave voltammetry (SWV) [Liu, 2010b].

Min *et al.* immobilized the *5'*-thiol-modified aptamer probe onto the gold electrode and the interaction with the antigen was recorded using electrochemical impedance spectroscopy and quartz crystal microbalance (QCM) with high sensitivity [Min, 2008].

Table 3.1 also summarizes some of the most representative colorimetric ELISA immunoassays. As can be seen, all of them involve sandwich-type methods using anti-IFN as the capture antibody, a biotinylated secondary antibody (Biotin-anti-IFN) and HRP-streptavidin or HRP-avidin with hydrogen peroxide and TMB for the colorimetric detection. Logaritmic calibration plots with linear ranges between tens and thousands pg/mL IFN-γ and minimum detectable dose (MDD), calculated as the concentration corresponding to the mean response of the zero standard +2*s*, of various units of pg/mL, are claimed. An important drawback of ELISA methods is the long time required for the immunoassay, extending from 3 to 4 hours 30 minutes.

Table 3.1. Electrochemical affinity biosensors for the determination of IFN-γ

BIOSENSOR	TECHNIQUE	LOD, pg/mL	LR, pg/mL	ASSAY TIME	SAMPLE	REFERENCE
IFN-γ-anti-IFN/PANI-G/SPPE	EIS	3.4	5 – 1000	1 h 30 min	spiked serum	Ruecha 2019
IFN-γ-anti-IFN-ZnONPs/GCE	EIS	0.12	0.1 – 100	12 h 30 min	spiked serum	Wang, 2017
IFN-γ-anti-IFN-TiO_2NPs/GCE	EIS	0.74	1 – 200	12 h 50 min	–	Chu, 2017
AuNP-oligo-CdSNP-anti-IFN-IFN-γ-anti-IFN-PANI-MNP/SPCE	SWASV	0.4	0.4 – 40	3 h 30 min	–	Wang, 2016
HRP-AuNPs-anti-IFN-IFN-γ-anti-IFN-AuNPs/PDDA/ITO	DPV	0.048	0.1 – 10000	> 16 h	serum	Zhang, 2016
IFN-γ-anti-IFN-GSH-AuNPs-Gr-Chit/ITO	SWV	0.5	5 – 4000	> 15 h	serum	Zhang, 2015
HRP-Strept-Biotin-anti-IFN-IFN-γ-anti-IFN/GE	amperometry	126.75	126.75 – 1207	5 h 40 min	spiked serum	Moschou,2016
CdSQDs-anti-IFN-IFN-γ-anti-IFN-AuNP@MB/GO-PANI-NF/GCE	ECL	0.03	0.1 – 500	15 h 40 min	cell culture extracts	Zhu, 2016
IFN-γ-ACP-SAM/AuIDE	EIS	520	1000 – 5000	> 15 h	–	Ding, 2017
MB-IFN-γ-DNA-aptamer-SAM/GE	SWV	1000	5000 – 160000	> 17 h	spiked serum	Liu, 2010b
IFN-γ-RNA or DNA-aptamer-SAM/GE	QCM, EIS	2.1 or 21	–	3 h 30 min	spiked FBS	Min, 2008

AC, acetylcysteine; **ACP**, aptamer capture probe; **AuIDE**, gold interdigitated electrode; **AuNP@MB**, gold nanoparticle-coated magnetic beads; **AuNP-oligo-CdSNP**, gold nanoparticle-coated oligonucleotide cadmium sulphide nanoparticle; **AuW**, gold wire; **CdSQDs**, cadmium sulphide quantum dots; **DNA**, deoxyribonucleic acid probe; **DPV**, differential pulse voltammetry; **ECL**, electrochimioluminescence; **EIS**, electrochemical impedance spectroscopy; **FBS**, fetal bovine serum; **GCE**, glassy carbon electrode; **GE**, gold electrode; **GO-PANI-NF**, polyaniline-graphene oxide nanofiber; **Gr-Chit**, graphene/chitosan composite; **GSH-AuNPs**, glutathione-coated gold nanoparticles; **HRP**, horseradish peroxidase; **ITO**, multilayer screen-printing indium tin oxide; **MB**, methylene blue; **PANI-G**, polyaniline-graphene; **PANI-MNP**, polyaniline-magnetic nanoparticle; **PDDA**, polydiallyldimethylammonium; **QCM**, quartz crystal microbalance; **RNA**, ribonucleic acid probe; **SAM**, self-assembled monolayer; **SPCE**, screen-printed carbon electrode; **SPPE**, screen-printed paper electrode; **SWASV**, square wave anodic stripping voltammetry; **SWV**, square wave voltammetry; **TiO_2NPs**, titanium dioxide-modified nanoparticles; **ZnONPs**, zinc oxide nanoparticles

Table 3.1. (Cont.). Commercial ELISA kits for the determination of IFN-γ

SUPPLIER COMPANY	METHODOLOGY	LOD, pg/mL	LR, pg/mL	ASSAY TIME	SAMPLE
ABCAM Ref. ab46025	sandwich assay with Ab, Biotin-Ab and HRP-Strept detection with TMB and H_2O_2	5	12.5 – 400	2 h 40 min	cell culture extracts, plasma, serum
Biolegend Ref. 430104	sandwich assay with Ab, Biotin-Ab and HRP-Av detection with TMB and H_2O_2	7.8	7.8 – 500	22 h 50 min	cell culture extracts, plasma, serum
Biomatik Ref. EKA51839	sandwich assay with Ab, Biotin-Ab and HRP-Strept detection with TMB and H_2O_2	46	46 – 3000	4 h30 min	plasma, serum
Elabscience Ref. E-EL-H0108	sandwich assay with Ab, Biotin-Ab and HRP-Strept detection with TMB and H_2O_2	9.38	15.63 – 1000	3 h 30 min	plasma, serum
LSBio Ref. LS-F567	sandwich assay with Ab, Biotin-Ab and HRP-Strept detection with TMB and H_2O_2	46	46 – 3000	5 h	cell lysate, plasma, serum
Novus Biologicals Ref. NBP1-91174	sandwich assay with Ab, Biotin-Ab and HRP-Strept detection with TMB and H_2O_2	0.99	1.6 – 100	3 h 30 min	cell culture extracts, plasma, serum
RayBiotech Ref. ELH-IFNg-1	sandwich assay with Ab, Biotin-Ab and HRP-Strept detection with TMB and H_2O_2	15	15 – 15000	4 h 45 min	cell culture extracts, plasma, serum
R&D Systems Ref. DIF50	sandwich assay with Ab, Biotin-Ab and HRP-Strept detection with TMB and H_2O_2	8	15.6 – 1000	4 h 30 min	cell culture extracts, plasma, serum
ThermoFisher Ref. EHIFNG	sandwich assay with Ab, Biotin-Ab and HRP-Strept detection with TMB and H_2O_2	2	25.6 – 1000	3 h	cell culture extracts, plasma, serum

3.7.2. 8-isoprostane

Despite the importance of ISO as a biomarker of oxidative stress, the methods existing for its determination are scarce. No examples of affinity biosensors have been found in the literature. However, various colorimetric ELISA kits have been developed for application to human urine using a direct competitive immunoassay with HRP- or AChE-labeled antigen.

Regarding current colorimetric ELISA-type immunoassays for the determination of 8-isoprostane, in Table 3.2 are summarized some of the most representative commercial ELISA kits available.

Table 3.2. Commercial ELISA kits for the determination of ISO

SUPPLIER COMPANY	METHODOLOGY	LOD, pg/mL	LR, pg/mL	ASSAY TIME	SAMPLE
ABCAM Ref. ab175819	direct competitive assay between Ag and HRP-Ag detection with TMB and H_2O_2	1	5 – 5000	2 h 30 min	cell culture extracts, plasma, serum, tissue lysate, urine
Antibodies Online Ref. ABIN2944828	direct competitive assay between Ag and HRP-Ag detection with TMB and H_2O_2	47	78 – 5000	2 h 30 min	plasma, serum
Cayman Chemical Ref. 516351	direct competitive assay between Ag and AChE-Ag detection with DTNB and ACh	2.7	0.8 – 500	20 h	culture medium, lavage fluids and aspirates, plasma, tissue lysate, urine
Cell Biolabs Inc Ref. STA-337	direct competitive assay between Ag and HRP-Ag detection with TMB and H_2O_2	5	5 – 400000	2 h 30 min	plasma, serum, tissue lysate, urine
Creative Diagnostics Ref. DEIA5014	direct competitive assay between Ag and AChE-Ag detection with DTNB and ACh	10	2.5 – 1500	3 h 30 min	plasma, urine
Detroit R&D Ref. 8iso1	direct competitive assay between Ag and HRP-Ag detection with TMB and H_2O_2	10	10 – 5000	2 h 30 min	cell culture extracts, plasma, serum, tissue lysate, urine
Eagle Bioscience Ref. 8IS39-K01 0	direct competitive assay between Ag and AChE-Ag detection with DTNB and ACh	10	10 – 5000	2 h 30 min	cell culture extracts, plasma, serum, tissue lysate, urine
EIAab Ref. E0701h	direct competitive assay between Ag and HRP-Ag detection with TMB and H_2O_2	1	1.56 – 100	4 h 30 min	cell culture extracts, plasma, serum, tissue lysate, urine
Enzo Ref. ADI-900-091	direct competitive assay between Ag and HRP-Ag detection with TMB and H_2O_2	40	160 – 100000	3 h	cell culture extracts, plasma, serum, tissue lysate, urine

As can be seen, all of them are based on direct competitive-type immunoassay in which isoprostane and isoprostane labeled with horseradish peroxidase (HRP-ISO) or acetylcholinesterase (AChE-ISO), compete for the binding sites of the immobilized antibody (anti-ISO). The colorimetric detection of immunocomplexes is carried out using, in the first case, hydrogen peroxide and *3,3',5,5'*-tetramethyl-benzidine (TMB) and, in the second, acetylthiocholine and *5,5'*-dithiobis(*2*-nitrobenzoic acid) (DTNB), also called Ellman's reagent.

The dynamic concentration range obtained with these colorimetric ELISA kits is between a small amount of pg/mL up to several thousand, with a minimum detectable concentration of a few pg/mL. Furthermore, the required analysis time varies from 2 hours 30 minutes to 20 hours from the moment when the immobilization of the capture antibody occurred. It should also be considered that, in some cases, the capture antibody and the blocking agent are already immobilized in the ELISA plates, which means that, at the time of the assay, only the competition between 8-isoprostane and 8-isoprostane labeled with the enzyme and the spectrophotometric detection steps are considered.

In addition, these colorimetric ELISA kits are only worth to determine free 8-isoprostane, so it is necessary to hydrolyze the lipoprotein or phospholipid coupled 8-isoprostane to measure both free and esterified isoprostane.

3.7.3. Tumor necrosis factor alpha

Several electrochemical immunosensors have been found in the literature for the determination of this cytokine. Some of the most representative reported methods for the determination of TNF-α, as well as their analytical characteristics, including information about the methodology used and the type of sample analyzed, are summarized in Table 3.3. Likewise, the immunoassay strategies described for the determination of tumor necrosis factor alpha are based on sandwich-type configurations with peroxidase-labeled or biotinylated antibody as detection

antibodies. Additionally, some label-free TNF-α impedimetric configurations, which are based on the increase or decrease on the voltammetric response of the redox probe after the antigen-antibody interaction, were also found.

The first immunosensor described uses a streptavidin-modified carbon-screened electrode to immobilize the biotinylated capture antibody, as well as silica nanoparticles functionalized with polyguanine and avidin to immobilize the biotinylated detection antibody. The addition of mediator $Ru(bpy)_3^{2+}$ facilitates the electronic transfer reaction between the guanine and the electrode surface [Wang, 2006].

Another immunosensor, developed by Yin *et al.*, is based on the electropolymerization of polyaniline doped with poly (acrylic acid) on a vitrified carbon electrode for the subsequent immobilization of the antibody. The sandwich-type immunosensor is developed by immobilizing the secondary antibody on a conjugate of nanobeads of polystyrene and acrylic acid (PSA) conjugated with gold nanoparticles and alkaline phosphatase [Yin, 2011].

In another example, the capture antibody is immobilized on carbon nanotubes modified with gold nanoparticles and the detection antibody on cerium nanoparticles functionalized with Prussian Blue by crosslinking with glutaraldehyde. This design provides a wide linear range and a low detection limit [Li, 2012].

Qureshi *et al.* carried out the simultaneous detection of CRP, TNF-α and IL-6 using gold interdigitated electrodes modified with mercaptopropionic acid for the immobilization of capture antibodies. The formation of the antigen-antibody complex is detected by changes in the capacitance, obtaining linear intervals between 25 pg/mL and 25 ng/mL for the three antigens [Qureshi, 2010].

Pui *et al.* developed an impedimetric immunosensor for the detection of TNF-α integrated in a platform enabled to detect the toxicity caused by inflammatory responses in cell cultures. Immobilization of the capture antibody is performed on

interdigitated gold microelectrodes functionalized with a monolayer of dithiobis(succinimidyl propionate) (DSP) by the covalent bond formed between the amino group of the antibody and the succinimidyl group of the monolayer. As usual, it is necessary to include a blocking step with ethanolamine to avoid nonspecific adsorption. This device was applied to the analysis of TNF-α released by Jurkat cells by the addition of lipopolysaccharide (LPS), a bacterial endotoxin that activates macrophages to release cytokines. The detection is visualized by a change in the value of the load transfer resistance using a 5 mM ferri/ferrocyanide solution as a redox system [Pui, 2013].

These same authors developed a strategy that allows the determination of TNF-α in undiluted serum. It should be mentioned that there are not many immunosensors found for TNF-α applied to their determination in samples of clinical interest, probably due to problems related to the complexity of the matrix. First, the sample is incubated in a suspension of magnetic particles conjugated with albumin and other antibodies to eliminate the background signal of the serum sample. The magnetic particles are then separated from the rest of the serum solution and the TNF-α contained in the supernatant is captured by the immobilized antibody on the magnetic particles. Finally, TNF-α is separated from said particles by incubating them in 40 µL of 2% sodium dodecylsulfate (SDS) in Tris buffer pH 7.0 for 10 minutes at 63°C. For the impedimetric detection, 40 µL of the previous solution is added to an array of gold microelectrodes followed by the addition of an equal volume of a 5 mM ferri/ferrocyanide solution in phosphate buffer pH 7.4. In this way, a detection limit of 1 pg/mL can be reached in undiluted serum samples [Kongsuphol, 2014].

Hou *et al.* developed an immunosensor for the determination of TNF-α based on the modification of a vitrified carbon electrode with a hydrogel prepared from ferrocene functionalized with phenylalanine and chitosan, to stabilize the gel. Subsequently, the gold nanoparticles on which the capture antibody is immobilized are incorporated. After blocking with BSA, the sandwich-type immunoassay is

established between TNF-α and the detection antibody conjugated with polystyrene spheres labeled with alkaline phosphatase. The enzyme catalyzes the hydrolysis of ascorbic *2*-phosphate acid to ascorbic acid. As expected, the addition of the enzyme substrate in the absence of antigen, does not lead to the formation of ascorbic acid and the ferrocene of the hydrogel is reduced at the electrode. In the presence of the antigen, the addition of the alkaline phosphatase substrate leads to the formation of ascorbic acid, which reduces the ferrocene of the hydrogel causing a decrease in the electrochemical response. Using this strategy, a linear range between 1 pg/mL and 10 ng/mL is obtained, with a limit of detection of 0.5 pg/mL [Hou, 2013].

Sun *et al.* modified a vitrified carbon electrode with peptide nanowires functionalized with ferrocenecarboxylic acid and with gold nanoparticles for the immobilization of the capture antibody. Next, the sandwich immunoassay is established between the TNF-α antigen and a secondary antibody immobilized on gold nanowires modified with glucose oxidase. A wide linear range from 0.005 to 10 ng/mL of TNF-α was obtained [Sun, 2013].

Another publication reported a vitrified carbon electrode is modified with ferricyanide and chitosan by crosslinking with glutaraldehyde. It is then coated with Nafion® to immobilize the capture antibody. As expected, the voltammetric signal decreases as the concentration of TNF-α increases, obtaining a linear interval between 0.02 and 34 ng/mL and a detection limit of 10 ng/mL [Weng, 2013].

Eletxigerra *et al.* employed magnetic microparticles functionalized with carboxyl groups for the immobilization of the capture antibody. For the performance of the sandwich immunoassay, a biotinylated antibody and streptavidin conjugated with the enzyme peroxidase is used. After the deposition of the conjugate of magnetic particles on a disposable carbon electrode, the amperometric detection of the quinone formed after addition of hydroquinone and hydrogen peroxide at –0.2 V is carried out [Eletxigerra, 2014].

Other configurations found in the literature employ disposable carbon electrodes modified with polyanthranilic acid for the immobilization of the capture antibody [Mazloum-Ardakani, 2014] or the antibody is entrapped in a composite nanomaterial formed by fullerene functionalized with multiple wall carbon nanotubes and the ionic liquid *1*-butyl-*3*-methylimidazolium bis(trifluoromethyl-sulfonyl)imide. This material presents an excellent electrocatalytic behavior for the oxidation of catechol. The immunosensor of label-free TNF-α is based on the decrease in the voltammetric response of the redox probe after the antigen-antibody interaction [Mazloum-Ardakani, 2015]. Finally, the same authors develop a composite material consisting of gold nanoparticles, carbon nanotubes and the same ionic liquid in chitosan, which is characterized by its high stability and bioactivity, which is why it was used to immobilize the capture antibody. The sandwich-type configuration was applied to the determination of TNF-α in serum samples [Mazloum-Ardakani, 2015b].

In addition, Table 3.3 includes some of the most representative commercial ELISA kits available for the determination of tumor necrosis factor alpha. All of them are based on sandwich-type immunoassay configurations using a capture antibody and a biotinylated or acetylcholinesterase labeled detection antibody. In the first case, horseradish peroxidase-labeled streptavidin (HRP-Strept) is added and the colorimetric detection of the formation of the immunocomplexes using hydrogen peroxide and TMB is carried out. In the second, Ellman's reagent, which contains acetylcholinesterase substrate, is added for colorimetric detection. These assays allow the determination of tumor necrosis factor alpha in concentration ranges up to 6000 pg/mL, with minimum detectable concentrations varying from 1 to 30 pg/mL. Besides, the required analysis times are quite long, between 3 hours 30 minutes to 4 hours 45 minutes, although some assays require more than 20 hours and overnight incubation. Moreover, in some cases, this analysis time only includes the incubation of the antigen, the detection antibody and the spectrophotometric detection steps.

Table 3.3. Electrochemical immunosensors for the determination of TNF-α

IMMUNOSENSOR	TECHNIQUE	LOD, pg/mL	LR, pg/mL	ASSAY TIME	SAMPLE	REFERENCE
poly[G]NPs-Av-Biotin-anti-TNF-TNF-α-Biotin-anti-TNF-Av/SPCE	SWV	50	100 – 1000000	4 h 45 min	–	Wang, 2006
AuNPs/PSA-AP-anti-TNF-TNF-α-anti-TNF/PANI/PAA/GCE	DPV	10	20 – 20000	2 h 50 min	spiked serum	Yin, 2011
PB-CeO_2-anti-TNF-TNF-α-anti-TNF-AuNPs/CNTs/GCE	amperometry	2	5 – 5000	2 h 30 min	spiked serum	Li, 2012
anti-TNF-MPA/GID	capacitance	25	25 – 25000	31 h	–	Qureshi, 2010
TNF-α-anti-TNF-DSP-Au micro-array	EIS	1	15.6 – 1000	1 h 15 min	cell culture supernates	Pui, 2013
TNF-α-anti-TNF-MBs-COOH/CSGM	EIS	1	1 – 1000	1 h 25 min	spiked serum	Kongsuphol, 2014
AP/PS-anti-TNF-TNF-α-anti-TNF-AuNPs/hydrogel+chitosan/GCE	SWV	0.5	1 – 10000	2 h 30 min	spiked serum	Hou, 2013
GOx/GNR-anti-TNF-TNF-α-anti-TNF-AuNPs/Fc-FF/PDDA/GCE	SWV	5	5 – 10000	2 h 30 min	spiked serum	Sun, 2013
TNF-α-anti-TNF-Nafion/chitosan-GA/GCE	CV	10	20 – 34000	1 h	spiked serum	Weng, 2013
HRP-Strept-Biotin-anti-TNF-TNF-α-anti-TNF-MBs-COOH/SPCE	amperometry	2	5 – 500000	3 h 10 min	spiked serum	Eletxigerra, 2014
TNF-α-anti-TNF-poly(*o*-ABA)/SPCE	EIS	5	5 – 100	2 h	spiked serum	Mazloum-Ardakani, 2014
HRP-anti-TNF-TNF-α-anti-TNF-poly(AntA)/SPCE	DPV	3.2	3.2 – 50	3 h	spiked serum	Mazloum-Ardakani, 2014
TNF-α-anti-TNF-C_{60}-CNTs-IL/SPCE	CV	2	5 – 75	16 h 30 min	spiked serum	Mazloum-Ardakani, 2015
HRP-anti-TNF-TNF-α-anti-TNF-MWCNTs-AuNPs/AuNPs/IL-Chitosan/GCE	DPV	2	6 – 100	17 h 30 min	serum	Mazloum-Ardakani, 2015b

AntA, anthranilic acid; **AP**, alkaline phosphatase; **AuNPs**, gold nanoparticles; **Av**, avidin; **C_{60}**, fullerene; **CNTs**, carbon nanotubes; **CSGM**, comb structured gold microelectrode array; **CV**, cyclic voltammetry; **DPV**, differential pulse voltammetry; **DSP**, dithiobis-succinimidylpropionate; **EIS**, electrochemical impedance spectroscopy; **Fc**, ferrocene; **FF**, diphenylalanine; **GCE**, glassy carbon electrode; **GID**, gold interdigitated electrode; **GNR**, gold nanorod; **GOx**, glucose oxidase; **GSH-AuNPs**, glutathione-coated gold nanoparticles; **HRP**, horseradish peroxidase, **IL**, ionic liquid; **K-Chit-GA**, $K_3[Fe(CN)_6]$-chitosan-glutaraldehyde; **MBs**, magnetic beads; **MPA**, β-mercaptopropionic acid; **MWCNTs**, multi-walled carbon nanotubes; **PAA**, poly(acrylic acid); **PDDA**, polydiallyldimethylammonium; **PANI**, polyaniline; **PB**, Prussian Blue; **poly[G]NPs**, polyguanine nanoparticles; **PS**, polyethylene sphere; **PSA**, poly(styrene-coacrylic acid); **SPCE**, screen-printed carbon electrode; **Strept**, streptavidin; **SWV**, square wave voltammetry

Table 3.3. (Cont.). Commercial ELISA kits for the determination of TNF-α

SUPPLIER COMPANY	METHODOLOGY	LOD, pg/mL	LR, pg/mL	ASSAY TIME	SAMPLE
ABCAM Ref. ab46087	sandwich assay with Ab, Biotin-Ab and HRP-Strept detection with TMB and H_2O_2	10	25 – 800	3 h 40 min	cell culture supernates, plasma, serum, standard solutions
Biovision Ref. K4779-100	sandwich assay with Ab, Biotin-Ab and HRP-Strept detection with TMB and H_2O_2	30	30 – 6000	4 h 45 min	cell culture supernates, plasma, serum, urine
Boster Ref. EK0525	sandwich assay with Ab, Biotin-Ab and HRP-Strept detection with TMB and H_2O_2	1	15.6 – 1000	24 h	cell culture supernates, plasma, serum
Cayman Chemical Ref. 589201	sandwich assay with Ab and AChE-Ab detection with DTNB and ACh	3.9	3.9 – 250	20 h	plasma, serum
eBioscience Ref. 88-7346	sandwich assay with Ab, Biotin-Ab and HRP-Strept detection with TMB and H_2O_2	4	4 – 500	24 h	cell culture supernates, plasma, serum
Enzo Ref. ADI-900-099	sandwich assay with Ab and HRP-Ab detection with TMB and H_2O_2	8.4	15.7 – 1000	4 h	cell culture supernates, plasma, serum
Hycult Biotech Ref. HK307-01	sandwich assay with Ab, Biotin-Ab and HRP-Strept detection with TMB and H_2O_2	10	8 – 2000	3 h 30 min	cell culture supernates, plasma, serum
Novus Biologicals Ref. NBP1-83741	sandwich assay with Ab, Biotin-Ab and HRP-Strept detection with TMB and H_2O_2	5	23 – 1500	4 h 30 min	cell culture supernates, plasma, serum
RayBiotech Ref. ELH-TNFa	sandwich assay with Ab, Biotin-Ab and HRP-Strept detection with TMB and H_2O_2	30	300 – 6000	4 h 45 min	cell culture supernates, plasma, serum

3.7.4. Interleukin 1 beta

Very few electrochemical immunosensors for the determination of interleukin 1 beta, which are summarized in Table 3.4, have been found in the literature.

Baraket *et al.* developed a fully integrated BioMEMS for the simultaneous determination of various interleukins (IL-1β, IL-6 and IL-10) in a concentration range of 1 to 15 pg/mL, which is the window where acute inflammations were observed, using electrochemical impedance to monitor the interaction between the cytokines and the corresponding antibodies [Baraket, 2014].

Moreover, Krause *et al.* described a microfluidic array for the determination of several pro-inflammatory cytokines (TNF-α, IL-6 and IL-1β) and C-reactive protein. In this work, the analytes were captured from serum in a capture chamber by 1-µm magnetic beads coated with antibodies and enzyme labels. Beads are then transported downstream to a detection chamber containing an eight-sensor array coated with glutathione-coated gold nanoparticles (GSH-AuNPs) and a second set of antibodies to capture the beads with analyte proteins [Krause, 2015].

Aydin *et al.* performed an impedimetric immunosensor for the determination of IL-1β by using semi-conductive poly(*2*-thiophen-*3*-yl-malonic acid) (P3-TMA) as an immobilization matrix material and anti-IL a biorecognition element. The polymer P3-TMA bound onto hydroxylated ITO surface via ester bond to form a polymer interface including active carboxyl groups, which bound to anti-IL. In this way, IL-1β was monitored by electrochemical impedance spectroscopy. Under optimized conditions, the relative change in impedance was proportional to the IL-1β concentration between 0.01 and 3 pg/mL with a detection limit of 3 fg/mL [Aydin, 2018].

A label-free biosensing method for determining interleukin 1β in synovial fluids was reported by Chiang *et al.*. The biosensing technique, fiber-optic particle plasmon resonance (FOPPR), is based on gold nanoparticles-modified optical fiber

where the AuNPs surface has been modified by a mixed self-assembled monolayer for further conjugation of anti-IL. Upon binding of IL-1β to anti-IL, the absorbance of AuNPs layer on the optical fiber changes and this signal change is enhanced through multiple total internal reflections along the optical fiber [Chiang, 2010].

Several colorimetric ELISA immunoassays for the determination of interleukin 1 beta in biological samples are commercially available. Table 3.4 summarizes the analytical characteristics of some of the most representative configurations.

The typical methodology is based on sandwich-type immunoassay configuration using a capture antibody, a biotinylated labeled antibody and horseradish peroxidase-labeled streptavidin (HRP-Strept), using hydrogen peroxide and TMB to carry out the detection. Other common strategy is based on the use of an acetylcholinesterase labeled detection antibody, adding Ellman's reagent, which contains acetylcholinesterase substrate for colorimetric detection.

These assays allow the determination of interleukin 1 beta in concentration ranges up to 1000 pg/mL, with minimum detectable concentrations varying from 0.15 to 5.64 pg/mL. Moreover, the required analysis times are, between 2 hours 30 minutes to more than 20 hours.

Table 3.4. Electrochemical immunosensors for the determination of IL-1β

IMMUNOSENSOR	TECHNIQUE	LOD, pg/mL	LR, pg/mL	ASSAY TIME	SAMPLE	REFERENCE
IL-1β-anti-IL-CMA/Au microelectrode (BioMEMS)	EIS	0.3	1 – 15	1 h 15 min	–	Baraket, 2014
HRP-MBs-anti-IL-IL-1β-anti-IL-GSH-AuNPs/PDDA/SPCE	amperometry	0.04	0.04 – 22	2 h 22 min	spiked serum	Krause, 2015
IL-1β-anti-IL-P3-TMA-ITO	EIS	0.003	0.01 – 3	45 min	serum	Aydin, 2018
IL-1β-anti-IL-SAM/AuNPs/FOPPR	SPR	21	0.05 – 10	10 min	synovial fluid	Chiang, 2010

Au microelectrode, gold microelectrode; **AuNPs**, gold nanoparticles; **CMA**, *4*-carboxymethyl aryl diazonium; **EIS**, electrochemical impedance spectroscopy; **FOPPR**, fiber-optic particle plasmon resonance; **GSH-AuNPs**, glutathione-coated gold nanoparticles; **HRP**, horseradish peroxidase; **ITO**, indium tin oxide polymer; **MBs**, magnetic beads; **P3-TMA**, poly(*2*-thiophen-*3*-yl-malonic acid) polymer; **PDDA**, polydiallyldimethylammonium; **SAM**, self-assembled monolayer; **SPCE**, screen-printed carbon electrode; **SWV**, square wave voltammetry; **SPR**, surface plasmon resonance

Table 3.4. (Cont.). Commercial ELISA kits for the determination of IL-1β

SUPPLIER COMPANY	METHODOLOGY	LOD, pg/mL	LR, pg/mL	ASSAY TIME	SAMPLE
ABCAM Ref. ab214025	sandwich assay with Ab, Biotin-Ab and HRP-Strept detection with TMB and H_2O_2	5.64	14.06 – 900	2 h 30 min	cell culture supernates, plasma, serum
Biogems Ref. BGK01584	sandwich assay with Ab, Biotin-Ab and HRP-Strept detection with TMB and H_2O_2	0.15	3.9 – 250	5 h 30 min	cell culture supernates, plasma, serum
BioLegend Ref. 437004	sandwich assay with Ab, Biotin-Ab and HRP-Av detection with TMB and H_2O_2	0.5	2 – 125	20 h 30 min	cell culture supernates, plasma, serum
Boster Ref. EK0392	sandwich assay with Ab, Biotin-Ab and HRP-Av detection with TMB and H_2O_2	0.15	3.9 – 250	5 h	cell culture supernates, plasma, serum
Enzo Ref. ADI-900-130A	sandwich assay with Ab and HRP-Ab detection with TMB and H_2O_2	1	3.9 – 250	2 h 55 min	cell culture supernates, plasma, serum
Invitrogen Ref. BMS224-2	sandwich assay with Ab, Biotin-Ab and HRP-Strept detection with TMB and H_2O_2	0.3	3.9 – 250	3 h 10 min	cell culture supernates, plasma, serum
RayBiotech Ref. ELH-IL1b	sandwich assay with Ab, Biotin-Ab and HRP-Strept detection with TMB and H_2O_2	0.3	0.3 – 100	4 h 45 min	cell culture supernates, plasma, serum
R&D Systems Ref. DLB50	sandwich assay with Ab, Biotin-Ab and HRP-Strept detection with TMB and H_2O_2	1	3.9 – 250	3 h 30 min	cell culture supernates, plasma, serum
Stemcell Technologies Ref. #02004	sandwich assay with Ab, Biotin-Ab and HRP-Strept detection with TMB and H_2O_2	4	10 – 1000	4 h 15 min	cell culture supernates, plasma, serum

3.7.5. Adiponectin

The first methods used to determine plasma levels of adiponectin were chromatographic. A few years ago, many authors used sodium dodecyl sulfate polyacrylamide gel electrophoresis (SDS-PAGE) or Western blot and densitometry for band analysis. Other authors performed gel filtration chromatographic separation and analyzed eluted fractions with SDS-PAGE. Later, Arita *et al.* developed the first enzyme-linked immunosorbent assay (ELISA) and a large number of them are now available commercially [Arita, 1999]. Table 3.5 summarizes the analytical characteristics of some of the most representative commercial ELISA kits available used. Except in one case, immunocomplex formation is detected colorimetrically with TMB and H_2O_2.

There is also great variability in the analytical characteristics of methods based on these systems. The dynamic range of the calibrations extends to concentrations that reach maximum values of 1 µg/mL and the detection limits can reach 234 pg/mL. With regard to the test times, in all cases they are very long, requiring, the shortest, at least two hours and fifteen minutes for it realization.

Most of the ELISA immunoassays are suitable for the determination of total adiponectin. A special case is the enzyme immunoassay with chemiluminescent detection developed by Hayama *et al.* for the determination of high molecular weight adiponectin (HWM) in plasma and serum samples. They use ferrite particles conjugated with an adiponectin monoclonal antibody and the same alkaline phosphatase labeled monoclonal antibody as the detection antibody. In this way, only the high molecular weight adiponectin consisting of 4 or 6 trimers of adiponectin is detected [Hayama, 2010].

With regard to the use of immunosensors, only one configuration for this protein has been found in the literature.

In the first work, an electrochemical immunosensor for adiponectin using screen-printed carbon electrodes modified with functionalized double-walled carbon nanotubes as platforms for immobilization of anti-APN is reported. The oriented binding of specific antibodies toward adiponectin was accomplished by using the metallic-complex chelating polymer Mix&Go™. Under the optimized conditions, a calibration plot for APN was constructed showing a range of linearity extending between 0.05 and 10.0 μg/mL, which is adequate for the determination of the cytokine in serum samples [Ojeda, 2015].

Besides, Sobrova *et al.* studied the electrochemical behaviour of adiponectin on a carbon paste electrode based on the electroactivity of the amino acids tyrosine and tryptophan, which give oxidation signals at 0.78 and 0.92 V, respectively. The strong adsorption of adiponectin on the electrode surface allows its determination by adsorptive transfer stripping wave voltammetry, obtaining a linear calibration between 0.5 and 50 ng/mL and a detection limit of 50 pg/mL. Despite the low detection limit, the high peak potential of the voltammetric signal does not allow the selective determination of adiponectin, so this method has not been applied to the analysis of real samples of clinical interest such as serum, saliva or urine [Sobrova, 2012].

Table 3.5. Electrochemical affinity biosensors for the determination of APN

BIOSENSOR	TECHNIQUE	LOD, ng/mL	LR, ng/mL	ASSAY TIME	SAMPLE	REFERENCE
HRP-Strept-Biotin-anti-APN-APN-anti-APN-Phe-DWCNTs/SPCE	amperometry	14.5	50 – 10000	1 h 30 min	serum	Ojeda, 2015
APN/CPE	AdTS SWV	0.05	0.5 – 50	–	–	Sobrova, 2012

AdTS SWV, adsorptive transfer stripping square wave voltammetry; **CPE**, carbon paste electrode; **HRP**, horseradish peroxidase; **Phe-DWCNTs**, grafted-DWCNTs; **SPCE**, screen-printed carbon electrode; **Strept**, streptavidin

Table 3.5. (Cont.). Commercial ELISA kits for the determination of APN

SUPPLIER COMPANY	METHODOLOGY	LOD, ng/mL	LR, ng/mL	ASSAY TIME	SAMPLE
ABCAM Ref. ab99968	sandwich assay with Ab, Biotin-Ab and HRP-Strept detection with TMB and H_2O_2	< 0.025	0.025 – 18	4 h 45 min	cell culture supernates, plasma, saliva, serum, urine
Abnova Ref. KA0017	sandwich assay with Ab and HRP-Ab detection with TMB and H_2O_2	0.47	1 – 150	2 h 30 min	cell culture supernates, cerebrospinal fluid, plasma, serum, urine
B-Bridge Ref. K1001-1	sandwich assay with Ab, Ab and HRP-IgG detection with TMB and H_2O_2	0.0234	0.375 – 12	3 h 30 min	cell culture supernates, plasma, serum
BioVendor Ref. RD191023100	sandwich assay with Ab and HRP-Ab detection with TMB and H_2O_2	0.47	1 – 150	2 h 10 min	cerebrospinal fluid, plasma, serum, urine
Enzo Ref. ALX-850-337-KI01	sandwich assay with Ab and HRP-Ab detection with TMB and H_2O_2	0.47	1 – 150	3 h	cerebrospinal fluid, plasma, serum, urine
Invitrogen Ref. KHP0041	sandwich assay with Ab, Biotin-Ab and HRP-Strept detection with TMB and H_2O_2	0.1	0.5 – 32	3 h 20 min	cell culture supernates, plasma, serum
Mercodia Ref. 10-1193-01	sandwich assay with Ab HRP-Ab detection with TMB and H_2O_2	1.25	5 – 300	2 h 15 min	plasma, serum
Perkin Elmer Ref. AL209C	sandwich assay with AlphaLISA acceptor beads-Ab, Biotin-Ab and Strept-donor beads detection with TMB and H_2O_2	0.045	0.045 – 1000	3 h 30 min	cell culture supernates, plasma, serum
Phoenix Pharmaceuticals Ref. EK-ADI-01	sandwich assay with Ab, Biotin-Ab and HRP-Strept light emission detection at 615 nm	0.15	0.15 – 10	5 h 25 min	cerebrospinal fluid, homogenized tissues, plasma

3.7.6. Transforming growth factor beta 1

With regard to immunosensors, only four configurations have been found in the literature, two of them developed by our research group (Table 3.6). The first case is an aptasensor that involves the immobilization of the thiolate aptamer labeled with methylene blue on the surface of a gold electrode integrated in a microfluidic system. Thus, it was possible to determine TGF-β1 up to a concentration of 250 ng/mL, with a detection limit of 1 ng/mL. The aptasensor developed was applied to the determination of TGF-β1 released by hepatic cells [Matharu, 2014]. More recently, an immunosensor has been developed for the determination of TGF-β1 in human serum. In this case, the antibody is immobilized on gold electrodes interdigitated by a polyethylene glycol monolayer previously activated using the carbodiimide system (EDC/NHS). The linear range reached was between 1 to 1000 ng/mL and the detection limit was 0.57 ng/mL [Yao, 2016].

In the configuration developed in our research group, the first amperometric immunosensor for the quantification of TGF-β1 was described. This disposable immunosensor uses magnetic particles (MBs) supported on screen-printed carbon electrodes and involves the covalent immobilization of anti-TGF antibodies on MBs functionalized with carboxylic acid, followed by the establishment of the sandwich-type immunoassay using poly-HRP-Strept conjugates for signal amplification purposes. This immunoassay was applied for the determination of low concentrations of TGF-β1 in urine samples, by interpolation of amperometric responses of the samples after a suitable dilution on the calibration line of standards due to the absence of matrix effect. This method achieves a detection limit of 10 pg/mL [Sánchez-Tirado, 2017].

On the other hand, Guerrero *et al.* employed screen-printed gold electrodes modified with grafted *p*-aminobezoic acid to provide scaffolds with high loading of surface confined carboxyl groups used to construct an electrochemical immunosensors for the determination of human plasma samples. The capture

antibody (anti-TGF) was covalently immobilized on the surface of the prepared disposable scaffold and a sandwich-type immunoassay was implemented with biotinylated detector antibody and alkaline phosphatase-labeled streptavidin (AP-Strept). Once the experimental variables have been optimized, a linear range extending between 0.05 and 3.0 ng/mL was obtained [Guerrero, 2018].

In the configuration developed by Honkanen *et al.*, a sandwich-type ELISA immunoassay is developed. In it, the determination of TGF-β1 in urine in patients with membranous glumerulonephritis is carried out using antibodies labeled with alkaline phosphatase and *p*-nitrophenylphosphate as enzymatic substrate in a diethanolamine/$MgCl_2$ medium. This method achieves a detection limit of 10 ng/L [Honkanen, 1997].

The methods used for the determination of TGF-β1 are usually based on ELISA immunoassays available as commercial kits. Table 3.6 also summarizes some of the most representative, including information about the methodology used, detection limit, concentration range, test time and type of sample. Most of them are sandwich-type immunoassays, using an anti-TGF capture antibody and a biotinylated detection antibody, hydrogen peroxide and TMB to perform spectrophotometric detection.

As can be seen, there is great variability in the analytical characteristics of these commercial ELISA kits. Thus, the dynamic range of the calibrations is extended to concentrations that reach maximum values of 60 ng/mL. Moreover, the lowest detection limit is found around 1 pg/mL. In adittion, the test times are, in all cases too long, requiring the shortest 3 hours and 20 minutes to perform the assay.

Table 3.6. Electrochemical affinity biosensors for the determination of TGF-β1

BIOSENSOR	TECHNIQUE	LOD, pg/mL	LR, ng/mL	ASSAY TIME	SAMPLE	REFERENCE
TGF-β1-MB-aptamer-SAM-Au	SWV	1000	1 – 250	2 d	hepatic stellate cells	Matharu, 2014
TGF-β1-anti-TGF-HOOC-PEG-SAM-Au	EIS	586	1 – 1000	1 h 15 min	serum	Yao,2016
poly-HRP-Strept-Biotin-anti-TGF-TGF-β1-anti-TGF-HOOC-MBs/SPCE	amperometry	10	0.015 – 3	2 h 20 min	urine	Sánchez-Tirado, 2017
AP-Strept-Biotin-anti-TGF-TGF-β1-anti-TGF-HOOC-Phe/SPAuE	DPV	10	0.05 – 3	3 h	plasma	Guerrero, 2018

AP, alkaline phosphatase; **Au**, gold electrode; **DPV**, differential pulse voltammetry; **MB**, methylene blue; **MBs**, magnetic-beads; **PEG**, polyethylene glycol; **poly-HRP-Strept**, streptavidin and horseradish peroxidase polymer; **SAM**, self-assembled monolayer; **SPAuE**, screen-printed gold electrode

Table 3.6. (Cont.). Commercial ELISA kits for the determination of TGF-β1

SUPPLIER COMPANY	METHODOLOGY	LOD, ng/mL	LR, ng/mL	ASSAY TIME	SAMPLE
ABCAM Ref. ab100647	sandwich assay with Ab, Biotin-Ab and HRP-Strept detection with TMB and H_2O_2	< 80	82 – 60000	4 h 45 min	cell culture supernates, plasma, serum
Biolegend Ref. 437707	sandwich assay with Ab, Biotin-Ab and HRP-Av detection with TMB and H_2O_2	2.3	7.8 – 500	4 h 15 min	cell culture supernates, plasma, serum
Enzo Ref. ADI-900-155	sandwich assay with Ab, Biotin-Ab and HRP-Strept detection with TMB and H_2O_2	3.3	31.25 – 1000	4 h	cell culture supernates, plasma, serum
Invitrogen Ref. BMS249-4	sandwich assay with Ab, Biotin-Ab and HRP-Strept detection with TMB and H_2O_2	8.6	31 – 2000	4 h 30 min	cell culture supernates, plasma, serum
Invitrogen Ref. BMS2065TEN	sandwich assay with Ab, Biotin-Ab and HRP-Strept detection with TMB and H_2O_2	0.098	0.16 – 10	3 h 30 min	cell culture supernates, plasma, serum
LSBio Ref. LS-F2548	sandwich assay with Ab, Biotin-Ab and HRP-Strept detection with TMB and H_2O_2	1	15.6 – 1000	3 h 20 min	cell culture supernates, plasma, serum, urine
RayBiotech Ref. ELH-TGF-b1-1	sandwich assay with Ab, Biotin-Ab and HRP-Strept detection with TMB and H_2O_2	80	80 – 60000	4 h 45 min	cell culture supernates, plasma, serum
R&D Systems Ref. DB100B	sandwich assay with Ab and HRP-Ab detection with TMB and H_2O_2	4.61	31.2 – 2000	4 h 30 min	cell culture supernates, plasma, serum, urine
USBiological Ref. 028519	sandwich assay with Ab, Biotin-Ab and HRP-Strept detection with TMB and H_2O_2	11.8	31.2 – 2000	3 h 55 min	cell culture supernates, homogenized tissues, plasma, serum, urine

3.7.7. Human fetuin A

Fetuin A is a glycoprotein that has been studied as a potential new biomarker for various types of cancer and tested in tumor cell metastases [Sakwe, 2010; Yi, 2009]. HFA acts as an extracellular adhesive protein that together with adnexa induces cell adhesion and growth [Drake, 2006; Rho, 2009].

Despite its importance as a biomarker, there are few electrochemical methods for its determination. Vashist *et al.* have developed an ELISA-based immunoassay, consisting of the incubation of the wells in NaOH to provide superficial OH groups for subsequent immobilization of the anti-HFA antibody by the addition of a solution containing a mixture of the antibody activated with EDC and *3*-aminopropyltriethoxysilane (APTES). The sandwich immunoassay is established by adding the blood or serum sample, supplemented with the fetuin antigen, and a biotinylated detection antibody conjugated with HRP-streptavidin. The colorimetric detection was carried out by addition of TMB. This configuration allows the determination of HFA in a dynamic range of concentrations between 3 and 243 ng/mL, with a limit of detection of 0.3 ng/mL [Vashit, 2015].

A similar to the previous configuration has been developed by the same working group for the determination of fetuin in the same samples. To do so, the capture antibody was immobilized on a gold chip using the same procedure, carrying out the detection, in this case, by surface plasmon resonance [Vashit, 2014]. It is also interesting a previous study carried out by these authors using different procedures of immobilization of the capture antibody on a gold chip [Vashit, 2011].

Likewise, as HFA is a glycoprotein, its affinity for different lectins has been investigated by several authors. Bertók *et al.* [Bertók, 2013] developed a biosensor using *sambucus nigra lectin* to determine fetuin, allowing quantitative detection of changes in the amount of sialic acid in fetuin. Moreover, Oliveira *et al.* used the

strong interaction between *cratylia mollis* lectin and fetuin to develop an impedimetric immunosensor [Oliveira, 2018].

Nagaraj *et al.* developed another lectin-based biosensor for the label-free detection of HFA. They used a silicon chip with a row of gold electrodes and relied on the impedance variations upon HFA binding to lectins [Nagaraj, 2010].

Silva *et al.* carried out the electrodeposition of poly-*L*-lysine on a glassy carbon electrode. Then the electrode was modified with carboxylated carbon nanotubes by electrostatic attraction to subsequently immobilize the carbohydrate. The lectin-fetuin interaction is detected by decreasing the ferri/ferrocyanide pair signal as a consequence of the progressive increase in charge transfer resistance in the presence of increasingly high concentrations of HFA [Silva, 2016].

Very recently, a fullerene-PAMAM composite was used for the preparation of a chronoimpedimetric immunosensor for HFA with a detection limit of 1.44 ng/mL [Uygun, 2018].

Table 3.7 also shows various commercial ELISA kits based on sandwich-type strategies for HFA determination using anti-HFA as capture antibody and biotinylated detection antibody are available. In all cases, the immunocomplex formation is colorimetrically detected with HRP and TMB at 450 nm, except in one case, which also uses 550 nm.

There is also great variability in the analytical characteristics of these methods. The dynamic range of the calibrations is extended to concentrations that reach maximum values of 500 ng/mL, with the lowest detection limit being less than 0.01 ng/mL. As for the test times, in all cases they are very long, requiring the shortest, two hours and fifty minutes. It is important to note that each well of the microtiter plate supplied has been pre-coated with a specific capture antibody and, therefore, this stage is not included in the indicated test time.

Table 3.7. Electrochemical affinity biosensors for the determination of HFA

IMMUNOSENSOR	TECHNIQUE	LOD, ng/mL	LR, ng/mL	ASSAY TIME	SAMPLE	REFERENCE
HRP-Strept-Biotin-anti-HFA-HFA-anti-HFA-APTES/MTP	colorimetric	0.3	3 – 243	> 1 h 15 min	blood, serum	Vashit, 2015
HFA-anti-HFA-APTES/Au	SPR	0.7	0.3 – 20	> 1 h	blood, serum	Vashit, 2014
HFA-anti-HFA-APTES/Au	SPR	–	0.6 – 20	> 1 h	–	Vashit, 2011
HFA-Lectin-Biotin-Strept-DSP-AuE	EIS	0.001	0.001 – 10	1 h	cell culture supernates	Nagaraj, 2010
HFA-Cramoll-HOOC-CNTs/PLL/GCE	CV	1.7	500 – 25000	4 h 20 min	serum	Silva, 2016
HFA-anti-HFA-GA/PAMAN-NH_2/C_{60}/4-ATP/AuSPE	EIS	1.44	5 – 400	> 5 h 30 min	blood	Uygun, 2018

4-ATP, *4*-aminothiophenol; **APTES**, (*3*-aminopropyl)triethoxysilane; **Au**, gold electrode; **AuE**, gold electrode; **AuSPE**, gold screen printed electrodes; **C_{60}**, fullerene; **CNT**, carbon nanotubes; **Cramoll**, *cratylia mollis* lectin; **CV**, cyclic voltammetry; **DSP**, dithiobis(succinimidyl propionate); **EIS**, electrochemical impedance spectroscopy; **GA**, glutaraldehyde; **GCE**, glassy carbon electrode; **HRP**, horseradish peroxidase; **MTP**, microtiter plate; **PAMAM**, polyamidoamine; **PLL**, poly-*L*-lysine; **SPR**, surface plasmon resonance; **Strept**, streptavidin

Table 3.7. (Cont.). Commercial ELISA kits for the determination of HFA

SUPPLIER COMPANY	METHODOLOGY	LOD, ng/mL	LR, ng/mL	ASSAY TIME	SAMPLE
ABCAM Ref. ab108855	sandwich assay with Ab, Biotin-Ab and HRP-Strept detection with TMB and H_2O_2	> 3	3.13 – 200	4 h	cell culture supernates, cerebrospinal fluid, milk, plasma, serum, urine
Biomatik Ref. EKA52040	sandwich assay with Ab, Biotin-Ab and HRP-Strept detection with TMB and H_2O_2	< 0.032	0.032 – 2	4 h 30 min	cell culture supernates, plasma, serum
BioVendor Ref. RD191037100	sandwich assay with Ab, Biotin-Ab and HRP-Strept detection with TMB and H_2O_2	0.1	2 – 100	< 3 h	cell culture supernates, cerebrospinal fluid, plasma, serum
Eagle Biosciences Ref. FET39-K01	sandwich assay with Ab, Biotin-Ab and HRP-Strept detection with TMB and H_2O_2	5	12.5 – 370	3 h	homogenized tissues, plasma, serum, urine
Epitope Diagnostics Ref. KT-800	sandwich assay with Ab, Biotin-Ab and HRP-Strept detection with TMB and H_2O_2	5	0 – 370	3 h 50 min	cell culture supernates, homogenized tissues, plasma, serum, urine
LSBio Ref. LS-F2668	sandwich assay with Ab, Biotin-Ab and HRP-Strept detection with TMB and H_2O_2	0.273	0.625 – 40	4 h 30 min	plasma, serum
Origene Ref. EA100480	sandwich assay with Ab, Biotin-Ab and HRP-Strept detection with TMB and H_2O_2	< 0.01	0.312 – 20	3 h 30 min	cell culture supernates, plasma, serum
R&D Systems Ref. DFTA00	sandwich assay with Ab, Biotin-Ab and HRP-Strept detection with TMB and H_2O_2	1.74	7.8 – 500	4 h 30 min	cell culture supernates, plasma, serum
ThermoFisher Ref. EHAHSG	sandwich assay with Ab, Biotin-Ab and HRP-Strept detection with TMB and H_2O_2	0.2	0.2 – 50	5 h	cell culture supernates, plasma, serum

3.7.8. Endoglin

Endoglin has been suggested as an appropriate marker for tumor related angiogenesis and neovascularization and its concentration is considered as a valuable diagnostic feature for the prognosis of cancer and for early monitoring of metastasis and cancer relapse. Thus, sensitive methods for the estimation of soluble endoglin concentration have a wide range of applications in fundamental and clinical research [Smirnov, 2016].

Regarding electrochemical methods, only two configurations have been proposed. One of them is a sandwich immunoassay based on the adsorption of the capture antibody on AuNPs and using a second antibody chemically linked to thionin, used as electron mediator, which was then adsorbed onto platinum nanoparticles. A linear range of 1.3 to 200 ng/mL and a detection limit of 0.9 ng/mL were reported [Zeng, 2012] and the second one involves a sandwich magnetoimmunoassay with amperometric detection at disposable screen-printed carbon electrodes with a linear relationship between 0.8 and 10 ng/mL and a limit of detection of 0.2 ng/mL [Torrente-Rodríguez, 2016].

Some examples of commercial enzyme-linked immunosorbent assays for the detection of CD105 that are commercially available are also shown in Table 3.8.

.

Table 3.8. Electrochemical immunosensors for the determination of CD105

IMMUNOSENSOR	TECHNIQUE	LOD, ng/mL	LR, ng/mL	ASSAY TIME	SAMPLE	REFERENCE
PtNP-THI-anti-CD105-CD105-anti-CD105-SN-AuNP/GE	CVc	0.9	1.3 – 200	> 2 d	–	Zeng, 2012
HRP-anti-CD105-CD105-anti-CD105-MBs/SPCE	amperometry	0.2	0.8 – 10	> 1 h	serum	Torrente-Rodríguez, 2016

AuNP, gold nanoparticle; **CV**, cyclic voltammetry; **GE**, gold electrode; **HRP**, horseradish peroxidase; **MB**, carboxylated magnetic beads; **PtNP**; platinum nanoparticle; **SN**, mercaptoethylamine; **SPCE**, screen-printed carbon electrode; **THI**, thionin acetate

Table 3.8. (Cont.). Commercial ELISA kits for the determination of CD105

SUPPLIER COMPANY	METHODOLOGY	LOD, pg/mL	LR, pg/mL	ASSAY TIME	SAMPLE
ABCAM Ref. ab100507	sandwich assay with Ab, Biotin-Ab and HRP-Strept detection with TMB and H_2O_2	< 10	12.35 – 3000	4 h 45 min	cell culture supernates, plasma, serum
Aviva Systems Biology Ref. OKAG00159	sandwich assay with Ab, Biotin-Ab and HRP-Strept detection with TMB and H_2O_2	125	125– 8000	5 h	cell culture supernates, plasma, serum
Biomatik Ref. EKA51975	sandwich assay with Ab, Biotin-Ab and HRP-Strept detection with TMB and H_2O_2	125	125 – 8000	4 h 30 min	cell culture supernates, plasma, serum
Boster Ref. FEK0644	sandwich assay with Ab, Biotin-Ab and HRP-Strept detection with TMB and H_2O_2	< 15	156 – 10000	4 h 30 min	cell culture supernates, plasma, serum
Cusabio Ref. CSB-E10030h	sandwich assay with Ab, Biotin-Ab and HRP-Strept detection with TMB and H_2O_2	47	156 – 10000	5 h	homogenized tissues, plasma, serum
MyBioSource Ref. MBS703511	sandwich assay with Ab, Biotin-Ab and HRP-Strept detection with TMB and H_2O_2	156	156 – 10000	4 h 30 min	homogenized tissues, plasma, serum
RayBiotech Ref. ELH-Endoglin-1	sandwich assay with Ab, Biotin-Ab and HRP-Strept detection with TMB and H_2O_2	10	10 – 3000	4 h 45 min	cell culture supernates, plasma, serum
R&D Systems Ref. DNDG00	sandwich assay with Ab, Biotin-Ab and HRP-Strept detection with TMB and H_2O_2	30	200 – 10000	4 h 30 min	cell culture supernates, plasma, serum
ThermoFisher Ref. EHENG	sandwich assay with Ab, Biotin-Ab and HRP-Strept detection with TMB and H_2O_2	10	12.35 – 3000	4 h 45 min	cell culture supernates, plasma, serum

4

Parte Experimental

4.1. INSTRUMENTACIÓN

4.1.1. Aparatos

Las medidas amperométricas se han llevado a cabo empleando un potenciostato portátil de INBEA Biosensores (Figura 4.1), equipado con el software IbGraph y un potenciostato CHI 1030B de Chemical Instruments, equipado con el software CHI 1030B (Figura 4.2).

Figura 4.1. Potenciostato portátil de uno o dos canales de INBEA Biosensores

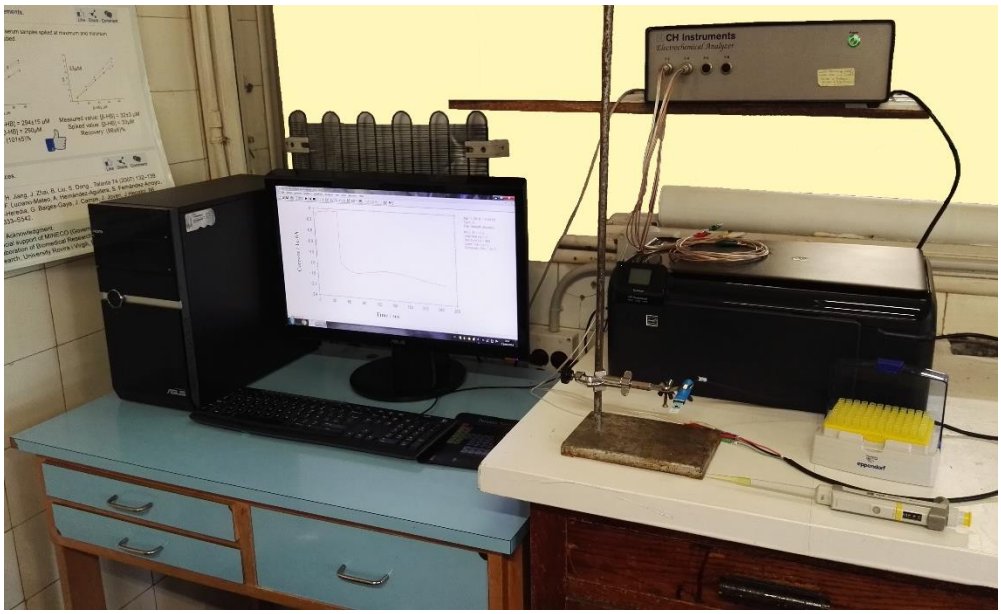

Figura 4.2. Potenciostato de un canal de Chemical Instruments

También se ha empleado un potenciostato Autolab PGSTAT12 (Figura 4.3), equipado con el software GPES 4.7 (General Purpose Electrochemical System) (Ecochemie).

Figura 4.3. Potenciostato Autolab PGSTAT12

Por otro lado, las medidas voltamperométricas se han realizado utilizando un potenciostato Autolab PGSTAT101 (Figura 4.4), equipado con el software Nova 1.6 (Ecochemie).

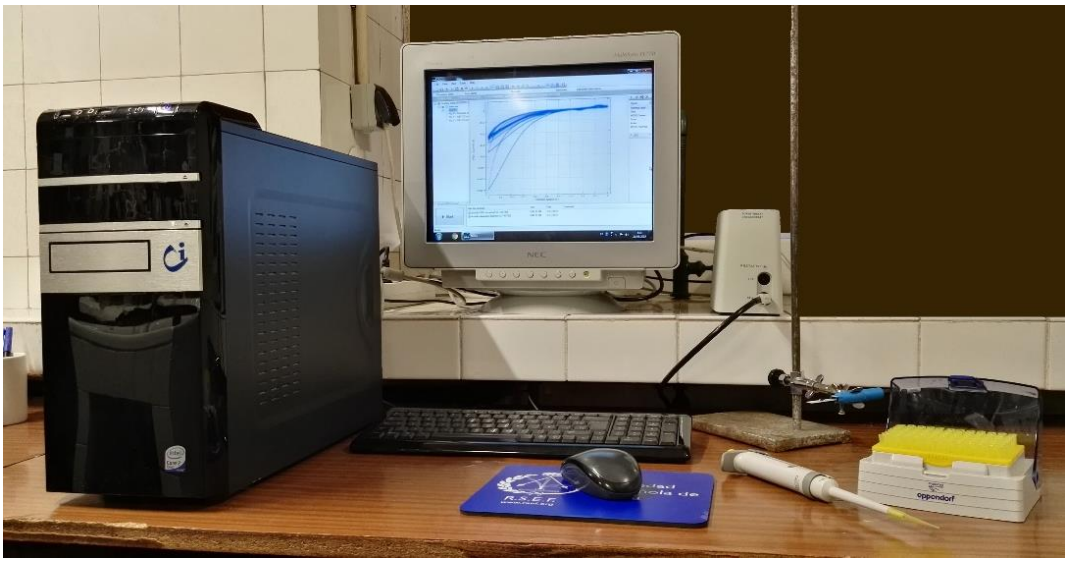

Figura 4.4. Potenciostato Autolab PGSTAT101

Las etapas implicadas en la modificación de la superficie electródica se han monitorizado mediante espectroscopia de impedancia electroquímica y voltamperometría cíclica empleando un potenciostato µAutolab tipo III (Figura 4.5),

controlado por los softwares FRA2 (Frequency Response Analyzer) y GPES 4.7 (General Purpose Electrochemical System) (Ecochemie).

Figura 4.5. Potenciostato µAutolab tipo III

Para la realización de los espectros de resonancia magnética nuclear de protón (^{1}H RMN) se ha empleado un espectrómetro Bruker AVIII 300 MHz (Figura 4.6a) equipado con un inyector automático (B-ACS60) (Figura 4.6b).

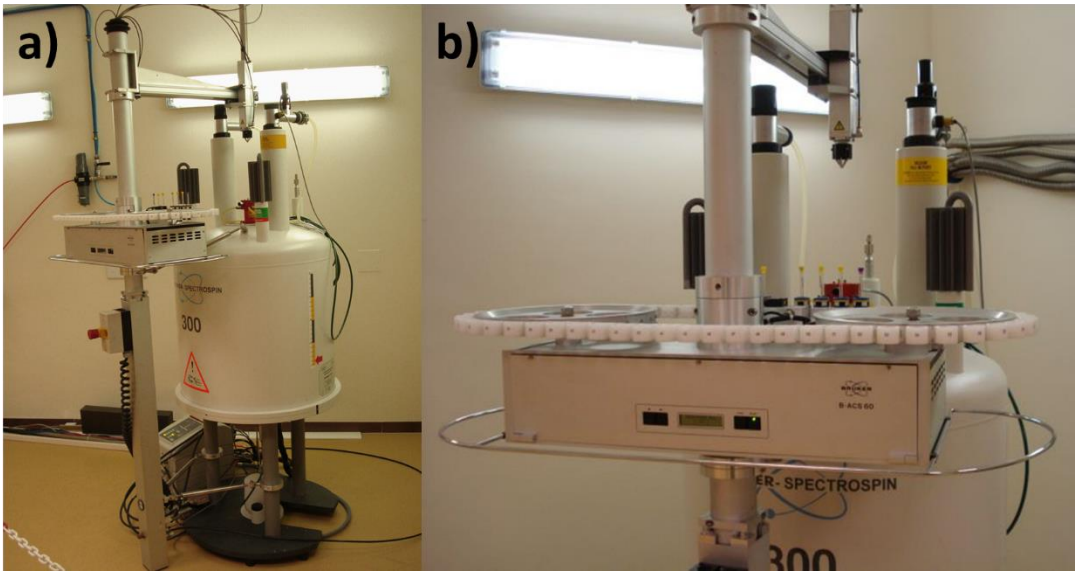

Figura 4.6. a) Espectrómetro Bruker AVIII 300 MHz equipado con b) inyector automático B-ACS60

También se ha utilizado un espectrómetro Bruker Innova 400 MHz (Figura 4.7) para la obtención de los espectros de resonancia magnética nuclear de protón y de carbono 13 (^{1}H y ^{13}C RMN, respectivamente).

Figura 4.7. Espectrómetro Bruker Innova 400 MHz

Los espectros de infrarrojo por Transformada de Fourier (FTIR) se han obtenido con un espectrómetro FTIR Nicolet Magna 750 Serie II (Figura 4.8a), que cuenta con una resolución de 0.5 cm^{-1}, así como de un espectrómetro FTIR Avatar 370 Thermo Nicolet (Figura 4.8b), con una resolución de 0.9 cm^{-1}.

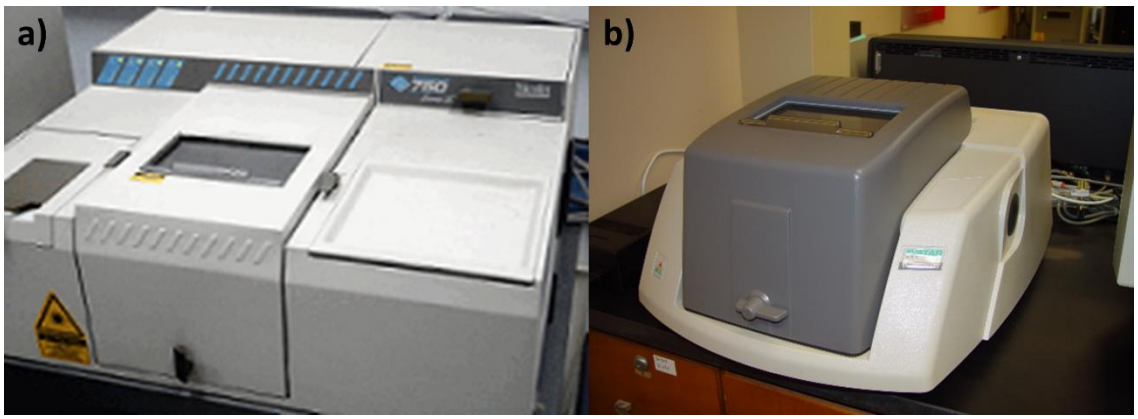

Figura 4.8. Espectrofotómetro a) FTIR Nicolet Magna 750 Serie II y b) FTIR Avatar 370

Los espectros Raman se han obtenido a temperatura ambiente, empleando un microscopio Raman Renishaw inVia Reflex Confocal (Figura 4.9), con un láser de longitud de onda de excitación de 785 nm. Asimismo, se empleó una cámara CCD refrigerada Peltier para recoger los resultados.

Figura 4.9. Microscopio Raman Renishaw inVia Reflex Confocal

Para la realización de los espectros de absorción UV-vis se ha utilizado un espectrofotómetro Shimadzu UV-3600 Plus (Figura 4.10).

Figura 4.10. Espectrofotómetro Shimadzu UV-3600 Plus

Los análisis termogravimétricos se han llevado a cabo en un analizador Mettler Toledo TGA/DSC Linea Excellence (Figura 4.11), bajo atmósfera inerte de nitrógeno con una tasa de 10°C/min, registrándose los cambios de masa en función de la temperatura.

Figura 4.11. Analizador Mettler Toledo TGA/DSC Linea Excellence

Para la caracterización de los nanomateriales sintetizados se ha empleado un microscopio electrónico de barrido de emisión de campo (FESEM), modelo JEOL JSM 7600F (Figura 4.12).

Figura 4.12. Microscopio electrónico de barrido en emisión de campo JEOL JSM 7600F

Asimismo, también se ha utilizado un microscopio electrónico de transmisión (TEM), modelo JEOL JEM 1400 (Figura 4.13), acoplado a un sistema de análisis de composición por fluorescencia de rayos X por energía dispersiva (XEDS).

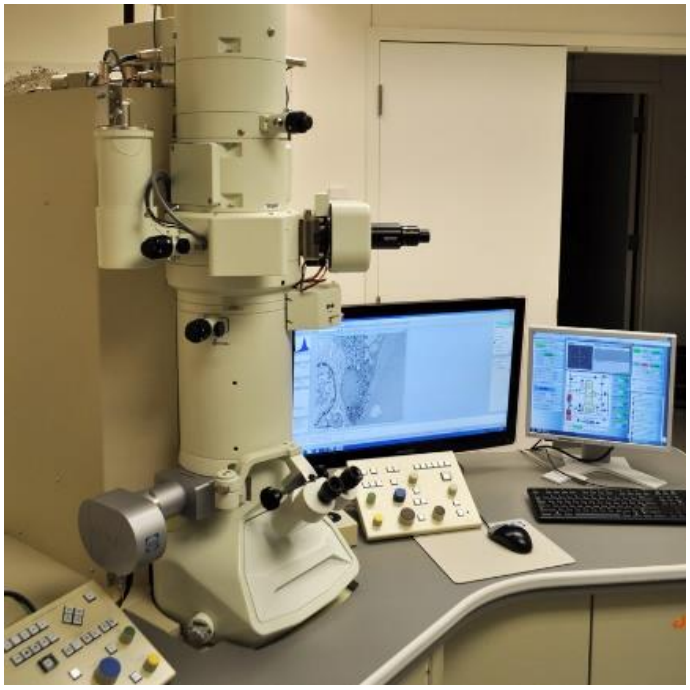

Figura 4.13. Microscopio electrónico de transmisión JEOL JEM 1400

Por último, para obtener los espectros de difracción de rayos X, se ha empleado un difractómetro multi-propósito PANalytical X'Pert MPD (Figura 4.14).

Figura 4.14. Difractómetro multi-propósito PANalytical X'Pert MPD

Las medidas de coercitividad de los nanotubos de carbono de pared múltiple funcionalizados con micropartículas magnéticas se llevaron a cabo empleando el espectrómetro de coercitividad J-Meter (Figura 4.15).

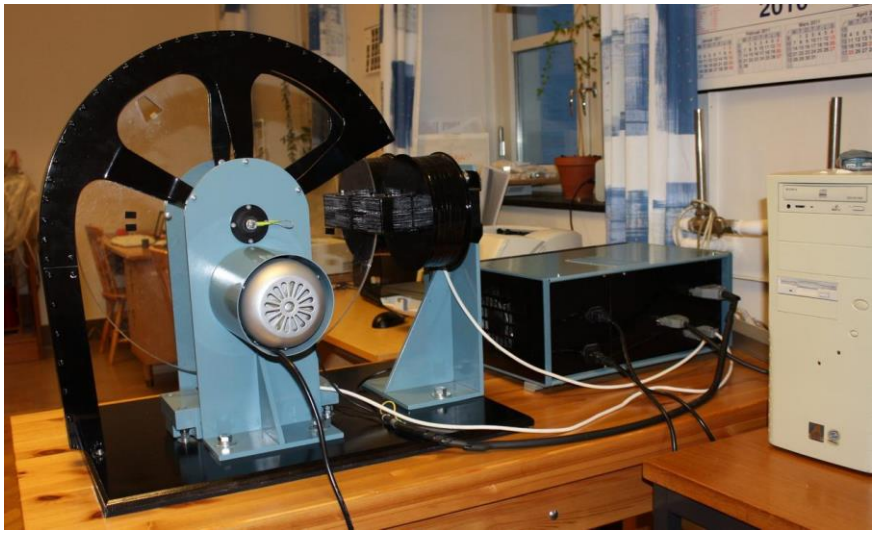

Figura 4.15. Espectrómetro de coercitividad J-Meter

Finalmente, la lectura de las medidas de absorbancia de las placas ELISA comerciales, utilizadas para la validación de los procedimientos desarrollados, se ha llevado a cabo empleando un lector de absorbancias Sunrise™ Absorbance Reader de Tecan (Figura 4.16), equipado con el software Magellan.

Figura 4.16. Lector de absorbancias Sunrise™ Absorbance Reader

4.1.2. Electrodos

Las medidas electroquímicas se han realizado a temperatura ambiente empleando electrodos serigrafiados de carbono (SPCEs) de Metrohm DropSens (Oviedo, España), referencia DRP-110 (Figura 4.17a), que incluyen un electrodo de trabajo de carbono (A = 12.56 mm^2; ϕ = 4 mm), un contraelectrodo de carbono y un

electrodo de pseudo-referencia de plata, así como electrodos duales de la misma marca, referencia DRP-C1110 (Figura 4.17b), con dos superficies elípticas de carbono (A = 5.6 mm^2; ϕ = 4 mm), un contraelectrodo de carbono y un electrodo de pseudo-referencia de plata.

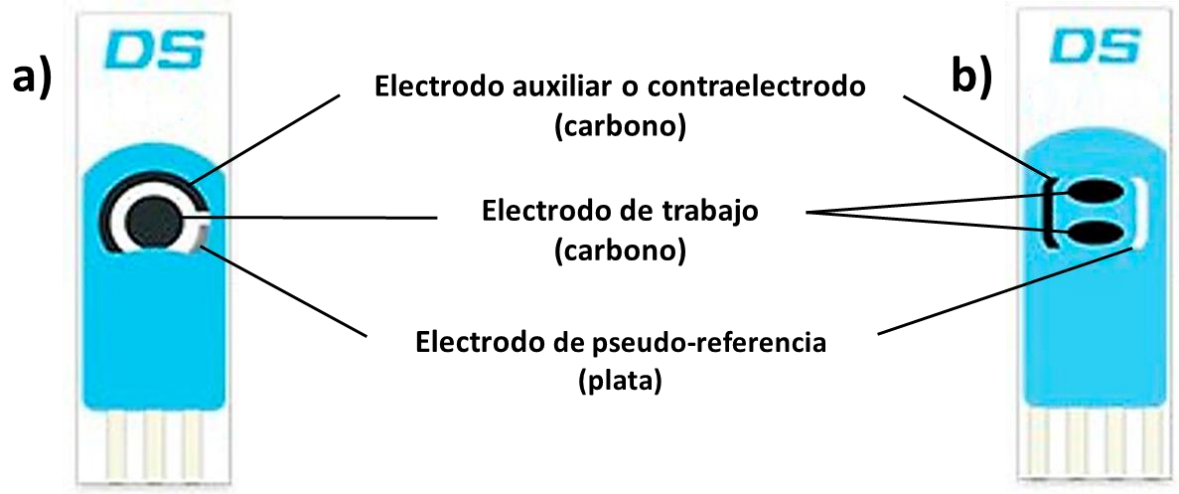

Figura 4.17. Electrodos serigrafiados de carbono comerciales: a) sencillo y b) dual

4.1.3. Otros materiales

Para las medidas de pH se ha empleado un pH-metro de precisión Crison Basic 20+ (Figura 4.18), calibrado de acuerdo con el protocolo establecido por el fabricante con disoluciones reguladoras de pH 4.01, 7.00 y 9.21 a 25.0 ± 0.5°C.

Figura 4.18. pH-metro de precisión Crison Basic 20+

También se ha utilizado una balanza analítica Basic BA-61 (Sartorius), un baño de ultrasonidos Elmasonic S-60 (Elma), una centrifugadora MPW-65R

(MPW Med Instruments) y GZ-416 (GYROZEN), un agitador vórtex (Heidolph y Velp Scientifica),un agitador orbital (ELMI Skyline), un imán de neodimio (AIMAN GZ), un agitador magnético (Velp Scientifica), una estufa Incubat (P–Selecta), un incubador Optic Ivymen System provisto de agitación y sistema de control de temperatura (Comecta S.A.), un rotavapor R-200 (Büchi) y una membrana PTFE de 0.1 µm de tamaño de poro (Millipore), así como diverso material de vidrio.

Para la recolección de muestras de saliva se ha empleado el dispositivo Salivette® (Sarstedt), que se muestra en la Figura 4.19.

Figura 4.19. Dispositivo de recolección de muestras de saliva Salivette®

Por otro lado, para la preparación de la inmunoglobulina etinilada se han utilizado filtros de centrífuga Amicon® Ultra 10 K de 0.5 mL (Merck Millipore) (Figura 4.20).

Figura 4.20. Filtros de centrífuga Amicon® Ultra 10 K de 0.5 mL

4.2. REACTIVOS

4.2.1. Inmunosensor para la determinación de endoglina

El anticuerpo de captura utilizado es un anticuerpo de ratón (anti-CD105), reconstituido hasta una concentración de 720 µg/mL con 1 mL de disolución reguladora PBS de pH 7.4, mientras que el anticuerpo de detección es un anticuerpo de cabra biotinilado (Biotin-anti-CD105), reconstituido hasta una concentración de 36 µg/mL con 1 mL de disolución reguladora PBS de pH 7.4 + 1% BSA (p/v). Ambos anticuerpos, así como la proteína CD105 humana, se incluyen en el DuoSet® ELISA Development System (DY1097) de R&D Systems.

Además, disoluciones de ácido ascórbico (AA), ácido úrico (UA), hemoglobina (HB) e inmunoglobulina G humana (hIgG) de Sigma, albúmina de suero bovino (BSA) de Gerbu, E-cadherina (E-Cad), factor de crecimiento transformante beta 1 (TGF-β1), interleucina 1 beta (IL-1β), receptor de cadherina-17 (Cad17R) y receptor de factor de crecimiento de fibroblastos 4 (FGFR4) de R&D Systems, interleucina 6 (IL-6) e interleucina 8 (IL-8) de Abcam, proteína recombinante ErbB2 humana (ErbB2) de Sino Biological y proteína recombinante p53 humana de longitud completa (p53) de EMD Milipore Corporation se probaron como posibles interferentes.

4.2.2. Inmunosensor para la determinación de 8-isoprostano

Como anticuerpo de captura se ha empleado un anticuerpo de conejo (anti-ISO), diluido hasta la concentración de trabajo empleando disolución reguladora MES 25 mM de pH 5.0. El antígeno (ISO) y el antígeno marcado (HRP-ISO) se han diluido hasta las concentraciones de trabajo empleando disolución reguladora Sample Diluent. Tanto el anticuerpo como los antígenos se incluyen en el kit ELISA OxiSelect™ (STA–337) de Cell Biolabs, Inc.

Para los estudios de selectividad se emplearon disoluciones de adiponectina (APN), ceruloplasmina (Cp), interleucina 6 (IL-6) e interleucina 8 (IL-8) de Abcam, albúmina de suero bovino (BSA) de Gerbu, colesterol (Chol) y hemoglobina (HB) de Sigma, factor de crecimiento transformante beta 1 (TGF-β1) y factor de necrosis tumoral alfa (TNF-α) de R&D Systems.

4.2.3. Inmunosensor para la determinación de adiponectina

Como anticuerpo de captura se ha empleado un anticuerpo de ratón (anti-APN) (H00009370-A01) de Abnova, diluido hasta la concentración de trabajo empleando disolución reguladora MES 25 mM de pH 5.0. El anticuerpo de detección utilizado fue un anticuerpo de conejo biotinilado (Biotin-anti-APN) (ab51420), reconstituido hasta una concentración de 50 µg/mL con disolución reguladora PB 100 mM de pH 7.4 + 0.5% BSA (p/v), al igual que la adiponectina humana (ab190961), ambos de Abcam.

Para evaluar la selectividad de la configuración desarrollada se emplearon disoluciones de albúmina de suero bovino (BSA) de Gerbu, ceruloplasmina (Cp) y grelina (GHRL) de Anaspec, factor de necrosis tumoral alfa (TNF-α) de R&D Systems y proteína C reactiva (CRP) de Fitzgerald.

4.2.4. Inmunosensor para la determinación de factor de crecimiento transformante beta 1

Como anticuerpo de captura primario se ha utilizado un anticuerpo IgG Fc específico de ratón (anti-mouse-IgG) (SAB3700848) de Sigma de 2 mg/mL. El anticuerpo de captura empleado es un anticuerpo de ratón (anti-TGF), reconstituido hasta una concentración de 240 µg/mL con 500 µL de disolución reguladora PBS de pH 7.4, mientras que el anticuerpo de detección es un anticuerpo de pollo biotinilado (Biotin-anti-TGF), reconstituido hasta una concentración de 18 µg/mL con

1 mL de disolución reguladora Reagent Diluent 1. Ambos anticuerpos, así como la proteína TGF-β1 humana, se incluyen en el DuoSet® ELISA Development System (DY240–05) de R&D Systems.

La especificidad de la plataforma inmunosensora desarrollada se evaluó empleando disoluciones de adiponectina (APN), ceruloplasmina (Cp), interleucina 6 (IL-6) e interleucina 8 (IL 8) de Abcam, albúmina de suero bovino (BSA) de Gerbu, bilirrubina (BIL) de Aldrich, colesterol (Chol) y hemoglobina (HB) de Sigma, factor de necrosis tumoral alfa (TNF-α) de R&D Systems, grelina (GHRL) de Anaspec y proteína C reactiva (CRP) de Fitzgerald.

4.2.5. Inmunosensor para la determinación de interferón gamma

El anticuerpo de captura empleado es un anticuerpo de ratón (anti-IFN), reconstituido con 250 µL de disolución reguladora PBS de pH 7.4 para obtener una concentración de 240 µg/mL, mientras que el anticuerpo de detección utilizado es un anticuerpo de ratón biotinilado (Biotin-anti-IFN), reconstituido hasta una concentración de 15 µg/mL con 500 µL de disolución reguladora PBS de pH 7.4 + 1% BSA (p/v). Ambos anticuerpos, así como la proteína IFN-γ humana, se incluyen en el DuoSet® ELISA Development System (DY285B–05) de R&D Systems.

Para los estudios de selectividad se utilizaron los siguientes compuestos: ácido ascórbico (AA), ácido úrico (UA), hemoglobina (HB) e inmunoglobulina G humana (hIgG) de Sigma, albúmina de suero bovino (BSA) de Gerbu, factor de crecimiento transformante beta 1 (TGF-β1), factor de necrosis tumoral alfa (TNF-α), interleucina 1 beta (IL-1β) y ligando de receptor activador para el factor nuclear kappaB (RANKL) de R&D Systems, glucosa (Glu) de Panreac, interleucina 6 (IL-6) e interleucina 8 (IL-8) de Abcam.

4.2.6. Inmunosensor dual para la determinación simultánea de factor de necrosis tumoral alfa e interleucina 1 beta

Para la construcción del inmunosensor para la determinación de factor de necrosis tumoral alfa (TNF-α) se ha empleado un anticuerpo de captura de ratón (anti-TNF), reconstituido hasta una concentración de 240 µg/mL con 500 µL de disolución reguladora PBS de pH 7.4, empleando disolución reguladora MES 25 mM de pH 5.0 para preparar las disoluciones de trabajo. Como anticuerpo de detección se ha utilizado un anticuerpo de cabra biotinilado (Biotin-anti-TNF), reconstituido hasta una concentración de 18 µg/mL con 1 mL de disolución reguladora PBS de pH 7.4 + 1% BSA (p/v). Tanto los anticuerpos como la proteína TNF-α humana se incluyen en el DuoSet® ELISA Development System (DY210–05) de R&D Systems.

Por otro lado, para la preparación del inmunosensor para la determinación de interleucina 1 beta (IL-1β) el anticuerpo de captura utilizado fue un anticuerpo de ratón (anti–IL), reconstituido hasta una concentración de 240 µg/mL con 500 µL de disolución reguladora PBS de pH 7.4. Las disoluciones de trabajo se preparan a partir de la anterior en disolución reguladora MES 25 mM de pH 5.0. El anticuerpo de detección de cabra biotinilado (Biotin-anti-IL) empleado se reconstituye hasta una concentración de 12 µg/mL con 1 mL de disolución reguladora PBS de pH 7.4 + 1% BSA (p/v). Estos anticuerpos, así como la proteína IL-1β humana, están incluidos en el DuoSet® ELISA Development System (DY201–05) de R&D Systems.

Como posibles interferentes se estudiaron disoluciones de adiponectina (APN), ceruloplasmina (Cp), interleucina 6 (IL-6) e interleucina 8 (IL-8) de Abcam, albúmina de suero bovino (BSA) de Gerbu, bilirrubina (BIL) de Aldrich, colesterol (Chol) y hemoglobina (HB) de Sigma, factor de crecimiento transformante beta 1 (TGF-β1), factor de necrosis tumoral alfa (TNF-α) y leptina (Lep) de R&D Systems, grelina (GHRL) de Anaspec y proteína C reactiva (CRP) de Fitzgerald.

4.2.7. Inmunosensor para la determinación de factor de crecimiento transformante beta 1 empleando nanotubos de carbono modificados con aminoviológeno

Los inmunorreactivos empleados para la preparación de esta plataforma sensora se han descrito en el *Apartado 4.2.4*. de este capítulo, siendo el anticuerpo de captura el anticuerpo de pollo biotinilado (Biotin-anti-TGF) y el anticuerpo de detección unido a los V-Phe-SWCNTs un anticuerpo de ratón sin marcaje (anti-TGF), respectivamente.

La especificidad de la configuración desarrollada se evaluó utilizando disoluciones de ácido ascórbico (AA), ácido úrico (UA), cortisol (CL) e inmunoglobulina G humana (hIgG) de Sigma, adiponectina (APN), interleucina 6 (IL-6) e interleucina 8 (IL-8) de Abcam, albúmina de suero bovino (BSA) de Gerbu ,factor de necrosis tumoral alfa (TNF-α) e interleucina 1 beta (IL-1β) de R&D Systems.

4.2.8. Inmunosensor para la determinación de fetuina A humana

El anticuerpo de captura empleado fue un anticuerpo de cabra biotinilado (Biotin-anti-HFA), reconstituido hasta una concentración de 36 µg/mL con 1 mL de disolución reguladora PBS de pH 7.4, mientras que el anticuerpo de detección utilizado fue un anticuerpo de ratón sin marcaje (anti-HFA), reconstituido hasta una concentración de 720 µg/mL con 1 mL disolución reguladora PBS de pH 7.4. Tanto los anticuerpos como la proteína HFA humana se incluyen en el DuoSet® ELISA Development System (DY1184) de R&D Systems.

Para evaluar la selectividad de la configuración desarrollada se utilizaron disoluciones de ácido ascórbico (AA), ácido úrico (UA), creatinina (CR), cortisol (CL), estradiol (E2) e inmunoglobulina G humana (hIgG) de Sigma, albúmina de suero bovino (BSA) de Gerbu, factor de crecimiento transformante beta 1 (TGF-β1), factor de

necrosis tumoral alfa (TNF-α) e interleucina 1 beta (IL-1β) de R&D Systems, interleucina 6 (IL-6) e interleucina 8 (IL-8) de Abcam.

4.3. DISOLUCIONES

Todos los productos utilizados, tanto reactivos como disolventes, fueron de calidad analítica. El agua desionizada (18.2 MΩ·cm a 25°C) se obtuvo empleando un sistema de purificación Millipore Milli-Q.

4.3.1. Disoluciones reguladoras de pH

- **Disolución reguladora AcOH/AcO^- 100 mM de pH 5.5**: se prepara disolviendo 0.410 g de AcONa en 5 mL de agua, ajustándose el pH a 5.5.
- **Disolución reguladora CB 250 mM de pH 9.0**: se prepara disolviendo 0.32 g de Na_2CO_3 (Sigma) y 5 g de $NaHCO_3$ (Scharlau) en 250 mL de agua, ajustándose el pH a 9.0.
- **Disolución reguladora MES 25 mM de pH 5.0**: se prepara disolviendo 1.22 g de ácido *2*-(*N*-morfolino)etanosulfónico (Gerbu) en 250 mL de agua, ajustándose el pH a 5.0.
- **Disolución reguladora MES 25 mM de pH 6.5**: se prepara disolviendo 1.22 g de ácido *2*-(*N*-morfolino)etanosulfónico (Gerbu) en 250 mL de agua, ajustándose el pH a 6.5.
- **Disolución reguladora PB 50 mM de pH 6.0**: se prepara disolviendo 0.03 g de K_2HPO_4 (Merck) y 6.78 g de KH_2PO_4 (Labkem) en 250 mL de agua, ajustándose el pH a 6.0.

- **Disolución reguladora PB 100 mM de pH 6.0**: se prepara disolviendo 0.6743 g de Na_2HPO_4 (Panreac) y 2.4236 g de NaH_2PO_4 (Scharlau) en 250 mL de agua, ajustándose el pH a 6.0.
- **Disolución reguladora PB 10 mM de pH 7.0**: se prepara disolviendo 0.0549 g de Na_2HPO_4 (Panreac) y 0.0846 g de NaH_2PO_4 (Scharlau) en 100 mL de agua, ajustándose el pH a 7.0.
- **Disolución reguladora PB 100 mM de pH 7.4**: se prepara disolviendo 2.172 g de Na_2HPO_4 (Panreac) y 1.1646 g de NaH_2PO_4 (Scharlau) en 250 mL de agua, ajustándose el pH a 7.4.
- **Disolución reguladora PB 100 mM de pH 7.4 + 0.5% BSA (p/v):** se prepara disolviendo 25 mg de albúmina de suero bovino (Gerbu) en 5 mL de disolución reguladora PB 100 mM de pH 7.4.
- **Disolución reguladora PBS 10 mM de pH 7.0**: se prepara disolviendo 0.0286 g de Na_2HPO_4 (Panreac), 0.0074 g de NaH_2PO_4 (Scharlau), 0.0005 g de KCl (Panreac) y 0.2300 g de NaCl (Labkem) en 25 mL de agua, ajustándose el pH a 7.0.
- **Disolución reguladora PBS' 10 mM de pH 7.0**: se prepara disolviendo 0.0710 g de Na_2HPO_4 (Panreac), 0.0600 g de NaH_2PO_4 (Scharlau), 0.0101 g de KCl (Panreac) y 0.4500 g de NaCl (Labkem) en 50 mL de agua, ajustándose el pH a 7.0.
- **Disolución reguladora PBS 100 mM de pH 7.0**: se prepara disolviendo 0.2870 g de Na_2HPO_4 (Panreac), 0.0.074 g de NaH_2PO_4 (Scharlau), 0.0005 g de KCl (Panreac) y 0.2300 g de NaCl (Labkem) en 25 mL de agua, ajustándose el pH a 7.0.
- **Disolución reguladora PBS' 100 mM de pH 7.0**: se prepara disolviendo 0.7098 g de Na_2HPO_4 (Panreac), 0.5999 g de NaH_2PO_4

(Scharlau), 0.0101 g de KCl (Panreac) y 0.2250 g de NaCl (Labkem) en 25 mL de agua, ajustándose el pH a 7.0.

- **Disolución reguladora PBS 100 mM de pH 7.2**: se prepara disolviendo 0.0710 g de Na_2HPO_4 (Panreac), 0.0690 g de NaH_2PO_4 (Scharlau) y 0.0876 g de NaCl (Labkem) en 10 mL de agua, ajustándose el pH a 7.2.

- **Disolución reguladora PBS de pH 7.4**: disolución comercial de concentración NaCl 137 mM, KCl 2.7 mM, Na_2PO_4 8.1 mM, KH_2PO_4 1.5 mM (componente 896036 del DuoSet® Ancillary Reagent Kit 1 de R&D Systems).

- **Disolución reguladora PBS de pH 7.4 + 1% BSA (p/v)**: se prepara disolviendo 50 mg de albúmina de suero bovino (Gerbu) en 5 mL de disolución reguladora PBS de pH 7.4.

- **Disolución reguladora PBST 100 mM de pH 7.0**: se prepara añadiendo 5 µL de Tween® 20 a 10 mL de disolución reguladora PBS 100 mM de pH 7.0.

- **Disolución reguladora PBST' 100 mM de pH 7.0**: se prepara añadiendo 5 µL de Tween® 20 a 10 mL de disolución reguladora PBS' 100 mM de pH 7.0.

- **Disolución reguladora poli-Strept-HRP Stabilizer 85R-112**: disolución comercial que contiene *5*-bromo-*5*-nitro-*1,3*-dioxano como preservante y se encuentra libre de biotina (Fitzgerald).

- **Disolución reguladora Reagent Diluent 1**: se prepara disolviendo 1.4 mL de Reagent Diluent Concentrate 1 (componente 840149 del DuoSet® Ancillary Reagent Kit 1 de R&D Systems) en 98.6 mL de Wash Buffer.

- **Disolución reguladora Sample Diluent**: disolución de 50 mL de pH 7.0 preparada para su uso (componente 233702 del OxiSelect™ 8-iso-Prostaglandin F2α ELISA Kit de Cell Biolabs, Inc.).

4.3.2. Disoluciones para la modificación de la superficie del electrodo de trabajo

- **Disolución de $NaNO_2$ 2 mM**: se prepara disolviendo 1.4 mg de $NaNO_2$ (Panreac) en 10 mL de agua.
- **Disolución de *p*-ABA 7 mM**: se prepara disolviendo 20 mg de ácido *p*-aminobenzoico (Acros) en 2 mL de HCl 1 M.
- **Disolución de *p*-ABA 3 mM + $LiClO_4$ 100 mM**: se prepara disolviendo 4.4 mg de ácido *p*-aminobenzoico (Acros) y 0.1060 g de $LiClO_4$ (Aldrich) en 10 mL de etanol absoluto.
- **Disolución de PPA 5 mM + KCl 0.5 M:** se prepara disolviendo 0.0070 g del monómero ácido *1H*-pirrol-*1*-propiónico (Sigma) y 0.3728 g de KCl (Panreac) en 10 mL de agua.
- **Suspensión de azida-MWCNTs 0.5 mg/mL**: se prepara suspendiendo 1 mg de azida-MWCNTs en 2 mL de agua y se mantiene en un baño de ultrasonidos durante 60 minutos.
- **Suspensión de CMC-rGO 10 µg/mL**: se prepara suspendiendo 1 mg de CMC-rGO en 1 mL de agua y se mantiene en un baño de ultrasonidos durante 60 minutos. Posteriormente, en el momento de depositar la disolución sobre el electrodo, se realiza una dilución 1/100 en el mismo medio, que se mantiene en un baño de ultrasonidos durante 30 minutos.

- **Suspensión de HOOC-Phe-DWCNTs 0.5 mg/mL**: se prepara suspendiendo 1 mg de HOOC-Phe-DWCNTs en 2 mL de agua, se añaden 27.4 µL de Tween® 20 y se mantiene en un baño de ultrasonidos durante 60 minutos.
- **Suspensión de HOOC-CNHs 0.5 mg/mL**: se prepara suspendiendo 1 mg de HOOC-CNHs en 2 mL de agua y se mantiene en un baño de ultrasonidos durante 60 minutos.

4.3.3. Disoluciones para la amplificación de la señal

- **Suspensión de HOOC-mMWCNTs 1.5 mg/mL**: se prepara suspendiendo 1.5 mg de HOOC-mMWCNTs en 1 mL de disolución reguladora PBS' 100 mM de pH 7.0 y se mantiene en un baño de ultrasonidos durante 30 minutos.
- **Suspensión de V-Phe-SWCNTs 0.5 mg/mL**: se prepara suspendiendo 1 mg de V-Phe-SWCNTs en 2 mL de agua y se mantiene en un baño de ultrasonidos durante 90 minutos.

4.3.4. Disoluciones para la modificación de nanomateriales de carbono

- **Disolución de ácido ascórbico 5 mM**: se prepara disolviendo 9 mg de ácido ascórbico (Fluka) en 10 mL de disolución reguladora PB 10 mM de pH 7.0.
- **Disolución de ácido propargílico 185 mM + NHS 185 mM**: se prepara disolviendo 0.39 g de ácido propargílico y 0.64 g de *N*-hidroxisuccinimida en 30 mL de acetato de etilo.

- **Disolución de ácido tereftálico 4 mg/mL**: se prepara disolviendo 4 mg de ácido tereftálico en 1 mL de disolución reguladora PB de pH 8.0.
- **Disolución de APTES al 10% (v/v)**: se prepara añadiendo 5 mL de (*3*-aminopropil) trietoxisilano sobre 45 mL de etanol.
- **Disolución de $CuSO_4$ 5 mM**: se prepara disolviendo 8 mg de $CuSO_4$ (Sigma) en 10 mL de disolución reguladora PB 10 mM de pH 7.0.
- **Disolución de DCC 550 mM**: se prepara disolviendo 1.14 g de *N,N'*-diciclohexilcarbodiimida en 10 mL de acetato de etilo.

4.3.5. Disoluciones para la activación de la superficie del electrodo de trabajo

- **Disolución de EDC/NHSS 40 mM**: se prepara disolviendo 26.8 mg de *1*-etil-*3*-(*3*-dimetilaminopropil)carbodiimida y 29.8 mg de *N*-hidroxisulfosuccinimida y se disuelven en 3.45 mL de disolución reguladora MES 25 mM de pH 6.5.
- **Disolución de EDC/NHSS 100 mM**: se prepara disolviendo las cantidades necesarias de ambas sustancias en el volumen adecuado de disolución reguladora MES 25 mM de pH 5.0 para obtener una concentración 100 mM.
- **Disolución de EDC/NHSS 200 mM**: se prepara disolviendo las cantidades necesarias de ambas sustancias en el volumen adecuado de disolución reguladora MES 25 mM de pH 5.0 para obtener una concentración 200 mM.
- **Disolución de EDC 400 mM/NHSS 100 mM**: se prepara disolviendo las cantidades necesarias de ambas sustancias en el volumen adecuado de disolución reguladora PBS' 100 mM de pH 7.0.

- **Polímero Mix&Go™**: disolución polimérica comercial (Anteo Technologies).

4.3.6. Disoluciones para el bloqueo de la superficie electródica

- **Blocker™ Casein in PBS**: disolución comercial que contiene caseína al 1% (p/v) en disolución reguladora PB 100 mM, NaCl 150 mM de pH 7.4 y KATHON™ como agente antimicrobiano (Thermo Fisher).
- **Disolución de biotina 0.5 mg/mL**: se prepara disolviendo 1 mg de *D*-biotina (Gerbu) en 2 mL de disolución reguladora PBS de pH 7.4.
- **Disolución de biotina 1.5 mg/mL**: se prepara disolviendo 1.5 mg de *D*-biotina (Gerbu) en 1 mL de disolución reguladora PBS de pH 7.4.
- **Disolución de BSA al 2% (p/v) en PBS de pH 7.4**: se prepara disolviendo la cantidad necesaria de albúmina de suero bovino (Gerbu) en el volumen adecuado de disolución reguladora PBS de pH 7.4.
- **Disolución de BSA al 2% (p/v) en Sample Diluent**: se prepara disolviendo la cantidad necesaria de albúmina de suero bovino (Gerbu) en el volumen adecuado de Sample Diluent.
- **Disolución de BSA al 5% (p/v) en PB 100 mM de pH 7.4**: se prepara disolviendo la cantidad necesaria de albúmina de suero bovino (Gerbu) en el volumen adecuado de disolución reguladora PB 100 mM de pH 7.4.

4.3.7. Disoluciones para la medida electroquímica

- **Disolución de ferri- y ferrocianuro potásico 2 mM en PB 50 mM de pH 6.0**: se prepara disolviendo 0.0066 g de $K_3Fe(CN)_6$ (Sigma) y

0.0084 g de $K_4Fe(CN)_6 \cdot 3H_2O$ (Sigma) en 10 mL de PB 50 mM de pH 6.0.

- **Disolución de ferri- y ferrocianuro potásico 2 mM en PB 100 mM de pH 7.4**: se prepara disolviendo 0.0066 g de $K_3Fe(CN)_6$ (Sigma) y 0.0084 g de $K_4Fe(CN)_6 \cdot 3H_2O$ (Sigma) en 10 mL de PB 100 mM de pH 7.4.

- **Disolución de ferri- y ferrocianuro potásico 2 mM en PBS de pH 7.4**: se prepara disolviendo 0.0066 g de $K_3Fe(CN)_6$ (Sigma) y 0.0084 g de $K_4Fe(CN)_6 \cdot 3H_2O$ (Sigma) en 10 mL de PBS de pH 7.4.

- **Disolución de ferri- y ferrocianuro potásico 5 mM en KCl 100 mM de pH 7.0**: se prepara disolviendo 0.0164 g de $K_3Fe(CN)_6$ (Sigma), 0.0211 g de $K_4Fe(CN)_6 \cdot 3H_2O$ (Sigma) y 0.0746 g de KCl (Panreac) en 10 mL de agua.

- **Disolución de ferri- y ferrocianuro potásico 5 mM en PB 100 mM de pH 7.4**: se prepara disolviendo 0.0164 g de $K_3Fe(CN)_6$ (Sigma) y 0.0211 g de $K_4Fe(CN)_6 \cdot 3H_2O$ (Sigma) en 10 mL de PB 100 mM de pH 7.4.

- **Disolución de hidroquinona 1 mM**: se prepara disolviendo 11 mg de hidroquinona (Sigma) en 1 mL de PB 50 mM de pH 6.0, realizándose posteriormente una dilución 1/100 en el mismo medio.

- **Disolución de hidroquinona 1 mM**: se prepara disolviendo 11 mg de hidroquinona (Sigma) en 1 mL de PB 100 mM de pH 7.4, realizándose posteriormente una dilución 1/100 en el mismo medio.

- **Disolución de peróxido de hidrógeno 50 mM**: se disuelven 50 µL de H_2O_2 (30% v/v, Sigma) en 1 mL de PB 50 mM de pH 6.0, realizándose posteriormente una dilución 1/10 en el mismo medio.

4.3.8. Otros reactivos y disoluciones

- ***2*-bromoetilamina**: Sigma, 99%
- ***4,4'*-bipiridina**: Sigma, 98%.
- ***11*-azido-*3, 6, 9*-trioxaundecan-*1*-amina**: Sigma, 90%.
- **Acetonitrilo**: Sigma, 99.8%.
- **Ácido *p*-aminobenzoico (*p*-ABA)**: Acros, 99%.
- **Diclorometano**: Sigma ≥ 99.8%.
- **Dietiléter**: Sigma-Aldrich, ≥ 99.7%.
- **Disolución de etinilhidrazida 26.4 mM**: se prepara disolviendo 8.8 mg de etinilhidrazida (Chem Space) en 500 µL de disolución reguladora PBS 100 mM de pH 7.0.
- **Disolución de HCl 1 M**: se prepara tomando 4.14 mL de HCl (Labkem, 37% v/v) en un matraz aforado de 50 mL y enrasando con agua.
- **Disolución de HRP 100 µg/mL**: se prepara disolviendo 1 mg de HRP en 1 mL de disolución reguladora PBS de pH 7.4, realizándose posteriormente una dilución 1/10 en el mismo medio.
- **Disolución de NaCl (40% p/p)**: se prepara disolviendo 40 g de NaCl (Labkem) en 100 mL de agua.

- **Disolución de $NaIO_4$ 20 mM**: se prepara disolviendo 0.0043 g de $NaIO_4$ en 1 mL de disolución reguladora AcOH/AcO^- 100 mM de pH 5.5.
- **Disolución de NH_4Cl (60% p/p)**: se prepara pesando 60 g de NH_4Cl (Sigma) en 100 mL de agua.
- **Etanol absoluto**: VWR Chemicals, ≥ 99.9%.
- **Etanol**: Sigma, 96% v/v.
- **Etilenglicol anhidro**: Merck, 99.8%.
- **$FeCl_3 \cdot 6H_2O$**: Sigma-Aldrich, 97%.
- **$FeCl_2 \cdot 4H_2O$**: Sigma-Aldrich, ≥ 99%.
- **Hidroxibenzotiazol (HOBt)**: Sigma, 97%.
- **HNO_3**: Scharlau, 65% v/v.
- **HRP**: peroxidasa de rábano, que se suministra de forma liofilizada (50-150 U/mg, Sigma).
- **Metanol anhídrido**: Sigma-Aldrich, ≥ 99.8%.
- **$NaBH_4$**: Sigma, ≥ 96%.
- **$NaIO_4$**: Sigma, ≥ 96%.
- **Na_2SO_4 anhidro**: Merck, ACS reagent, ≥ 99%.
- **$NH_3 \cdot H_2O$**: Panreac, 25% v/v.
- **Nitrito de isoamilo**: Sigma, 96%.
- ***N*-metil-*2*-pirrolidona (NMP)**: Aldrich, ≥ 99%.
- ***N*,*N*'-dimetilformamida (DMF) anhídrida**: Sigma-Aldrich, 99.8%.

- **poli-HRP-Strept (85-R200)**: polímero de estreptavidina y peroxidasa de rábano, que se suministra en forma líquida con 600 ppm de *5*-bromo-*5*-nitro-*1,3*-dioxano como conservante (Fitzgerald).
- **Strept-HRP**: monómero de estreptavidina y peroxidasa de rábano, que se suministra de forma liofilizada (500 U, Roche).
- **Tween® 20**: monolaurato de polioxietilen(20)sorbitano, tensoactivo tipo polisorbato (Sigma, ≤ 3% agua).
- **Wash Buffer**: se prepara disolviendo 28 mL de Wash Buffer Concentrate (componente 895003 del DuoSet® Ancillary Reagent Kit 1 de R&D Systems) en 673 mL de agua.

4.4. MUESTRAS

La validación de los inmunosensores desarrollados se llevó a cabo empleando suero humano liofilizado (Sigma, S2257) obtenido de un muestra de sangre total coagulada, así como muestras de suero de individuos sanos, tanto de hombre como de mujer (BBI Solutions, SG610-2 y SG609-2, respectivamente), muestras de suero de pacientes con hipercolesterolemia (Abyntek, SG376-2), muestras de suero de pacientes con diabetes tipo 2 (Abyntek, SG187-2), muestras de suero de individuos sanos, con diferentes tipos de cáncer (colorrectal, mama y pulmón) y epidermólisis bullosa (proporcionadas por el Hospital Universitario La Paz y el Hospital Clínico San Carlos de Madrid, España) y muestras de saliva de individuos sanos fumadores y no fumadores.

Las muestras de suero proporcionadas por los citados hospitales se obtuvieron con el correspondiente consentimiento informado aprobado por los pacientes y el Comité de Ética de las Instituciones que, en el caso de las muestras de epidermólisis

bullosa, poseen Código HULP: PI-1602, adherido a las Directrices de Helsinki y a revisiones adicionales, Fortaleza 2013 (http://www.wma.net).

Finalmente, para la validación del inmunosensor desarrollado para la determinación de interferón gamma, se empleó un material biológico humano certificado de referencia (NIBSC, 87/586), de concentración conocida.

4.5. PROCEDIMIENTOS EXPERIMENTALES

4.5.1. Preparación de un inmunosensor basado en el empleo de un polímero conductor como modificador de la superficie electródica

4.5.1.1. Inmunosensor para la determinación de endoglina

La electropolimerización del monómero del ácido *1H*-pirrol-*1*-propiónico (PPA) sobre la superficie del electrodo serigrafiado de carbono se lleva a cabo sumergiendo el electrodo en una disolución 5 mM del monómero PPA que contiene KCl 500 mM, aplicando 20 ciclos sucesivos mediante voltamperometría cíclica entre 0.0 y 0.85 V a 100 mV/s. Seguidamente, se sumerge el electrodo modificado resultante (pPPA/SPCE) en una disolución de hidroquinona 1 mM en disolución reguladora fosfato 100 mM de pH 7.4, registrándose un voltamperograma cíclico de control entre –0.2 y 1.0 V a 50 mV/s [Serafín, 2017]. Posteriormente, se lava el electrodo con agua y se activan los grupos carboxílicos de la superficie electródica depositando 5 µL de una disolución de EDC/NHSS 100 mM de cada uno de ellos en disolución reguladora MES 25 mM de pH 5.0 y se deja reaccionar durante 30 minutos. A continuación, se lava y se incuban 5 µL de una disolución de 12.5 µg/mL de anticuerpo de captura (anti-CD105) en disolución reguladora MES 25 mM de pH 5.0, durante 60 minutos. Transcurrido el tiempo de incubación, se lava y se bloquean las posiciones reactivas de la superficie

electródica con 10 µL de disolución comercial Blocker™ Casein durante 30 minutos. Después, se lava y se añaden 5 µL de antígeno (CD105) en disolución reguladora PBS de pH 7.4. Tras 30 minutos, se lava como anteriormente y se depositan 5 µL de una disolución de 2 µg/mL de anticuerpo de detección (Biotin-anti-CD105) en disolución reguladora PBS de pH 7.4 + 1% BSA (p/v), que se incuba durante 60 minutos. Posteriormente, se lava y se depositan 5 µL de una dilución 1/500 de poli-HRP-Strept en disolución reguladora poli-Strept-HRP Stabilizer 85R-112, que se incuba durante 15 minutos. Finalmente, se lava y se añaden 10 µL de disolución reguladora PBS de pH 7.4.

Para la obtención de los amperogramas, se depositan 45 µL de una disolución de hidroquinona 1 mM y se registra la corriente obtenida cuando se aplica un potencial de –200 mV. Cuando la corriente de fondo se estabiliza, después de unos 100 segundos, se adicionan 5 µL de una disolución de peróxido de hidrógeno 50 mM, midiéndose la corriente al cabo de 200 segundos de reacción enzimática.

En la Figura 4.21 se muestran de forma esquematizada las distintas etapas implicadas en la construcción y el funcionamiento del inmunosensor desarrollado para la determinación de endoglina.

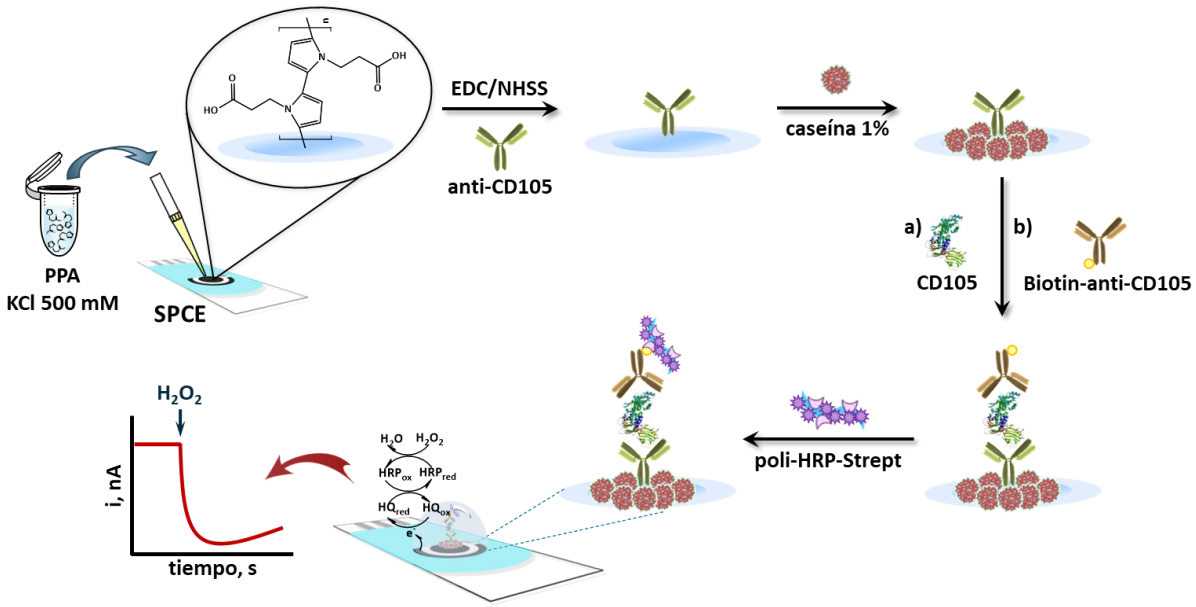

Figura 4.21. Esquema de las etapas implicadas en la preparación y el funcionamiento del inmunosensor poli-HRP-Strept-Biotin-anti-CD105-CD105-anti-CD105-pPPA/SPCE

4.5.2. Preparación de inmunosensores basados en la modificación de la superficie electródica con nanomateriales de carbono

4.5.2.1. Inmunosensor para la determinación de 8-isoprostano

Los nanocuernos de carbono, obtenidos en ausencia de catalizadores metálicos, mediante ablación de grafito con láser de CO_2, bajo corriente de argón a 760 Torr y a temperatura ambiente [Utsumi, 2005] se someten a un tratamiento oxidativo mediante calentamiento a 100°C en una disolución acuosa de peróxido de hidrógeno al 30% (v/v) [Zhang, 2007b]. Este tratamiento se realizó en el Instituto de Nanociencia, Nanotecnología y Materiales Moleculares (INAMOL) de la Universidad de Castilla-La Mancha (Toledo).

Para la preparación del inmunosensor se emplea una suspensión acuosa de 0.5 mg/mL de nanocuernos de carbono oxidados (HOOC-CNHs), depositándose 10 µL de la misma sobre el electrodo de trabajo y dejando secar.

Los grupos carboxílicos presentes en la superficie del electrodo de trabajo se activan incubándolos en 5 µL de una disolución de EDC/NHSS 100 mM de cada uno de ellos en disolución reguladora MES 25 mM de pH 5.0 durante 30 minutos. Seguidamente se lava con agua y se inmoviliza el anticuerpo de captura (anti-ISO) depositando 5 µL de una dilución 1/600 en disolución reguladora MES 25 mM de pH 5.0, dejándose incubar durante 60 minutos. Finalmente, se lava con agua y se bloquean las posiciones libres de la superficie electródica, depositando 5 µL de una disolución de BSA al 2% (p/v) en disolución reguladora Sample Diluent durante 30 minutos, para evitar posibles adsorciones inespecíficas. Al igual que anteriormente, transcurrido el tiempo de incubación, se lavan los electrodos con agua.

Una vez preparado el inmunosensor anti-ISO-HOOC-CNHs/SPCE, se lleva a cabo el inmunoensayo, de tipo competitivo directo, depositando, sobre la superficie del

electrodo de trabajo modificado, 5 µL de una disolución que contiene antígeno (ISO) de concentración variable y una dilución 1/500 del antígeno marcado con la enzima peroxidasa (HRP-ISO) en regulador Sample Diluent, incubándose durante 45 minutos. Por último, se lava y se añaden 10 µL de disolución reguladora Sample Diluent.

Para la obtención de los amperogramas, se depositan 45 µL de una disolución de hidroquinona 1 mM y se registra la corriente obtenida aplicando un potencial de –200 mV. Cuando la corriente de fondo se estabiliza, después de unos 100 segundos, se adicionan 5 µL de una disolución de peróxido de hidrógeno 50 mM, midiéndose la corriente al cabo de 200 segundos de reacción enzimática.

En la Figura 4.22 se muestra un esquema de la construcción y el funcionamiento del inmunosensor desarrollado para la determinación del compuesto tipo prostaglandina 8-isoprostano.

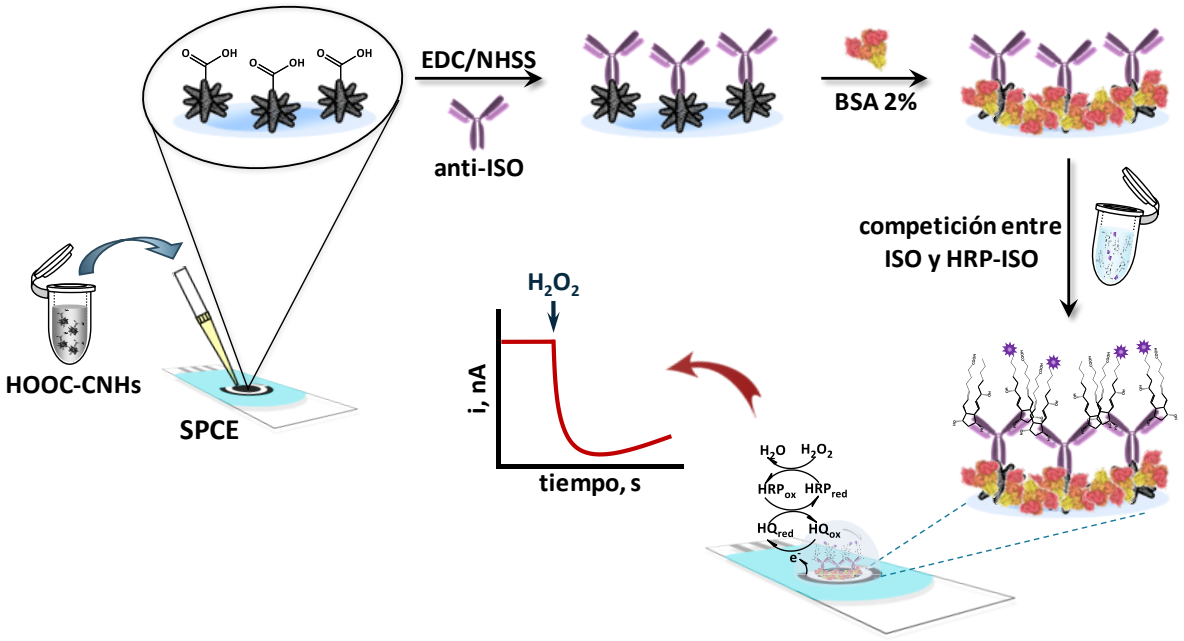

Figura 4.22. Esquema de las etapas implicadas en la preparación y el funcionamiento del inmunosensor HRP-ISO-anti-ISO-HOOC-CNHs/SPCE

4.5.2.2. Inmunosensor para la determinación de adiponectina

4.5.2.2.1. Preparación del material híbrido CMC-rGO

En primer lugar, se lleva a cabo una silanización del óxido de grafeno (GO), dispersando 100 mg de GO en 500 mL de etanol, con ayuda de un baño de ultrasonidos, durante 60 minutos. A continuación, se adicionan 50 mL de una disolución etanólica de (*3*-aminopropil) trietoxisilano (APTES) al 10% (v/v) y se agita la mezcla durante 12 horas a una temperatura entre 60 y 65°C. Transcurrido el tiempo de agitación, se elimina el disolvente con ayuda de un rotavapor, se lava el producto con etanol y se deja secar.

Por otro lado, se realiza la oxidación de la carboximetilcelulosa (CMC). Para ello, se disuelven 500 mg del polímero en 100 mL de agua y se añaden 540 mg de $NaIO_4$, dejándose agitar la mezcla durante 12 horas en oscuridad. Después, se añade 1 mL de etilenglicol y se mantiene la agitación durante 60 minutos más.

Posteriormente, se dializa el polímero oxidado en ausencia de luz y se mezcla con el óxido de grafeno silanizado, produciéndose el anclaje del polímero al material de carbono, agitándose la mezcla durante 60 minutos. Seguidamente, se añaden 2.5 g de $NaBH_4$ y se mantiene en agitación durante 12 horas. Una vez finalizado el tiempo de reacción, se elimina el disolvente, se lava con disolución reguladora PB 100 mM de pH 6.0 y se deja secar el producto obtenido [Araque, 2014].

En la Figura 4.23 se representa de forma esquemática el procedimiento seguido la preparación del material híbrido CMC-rGO.

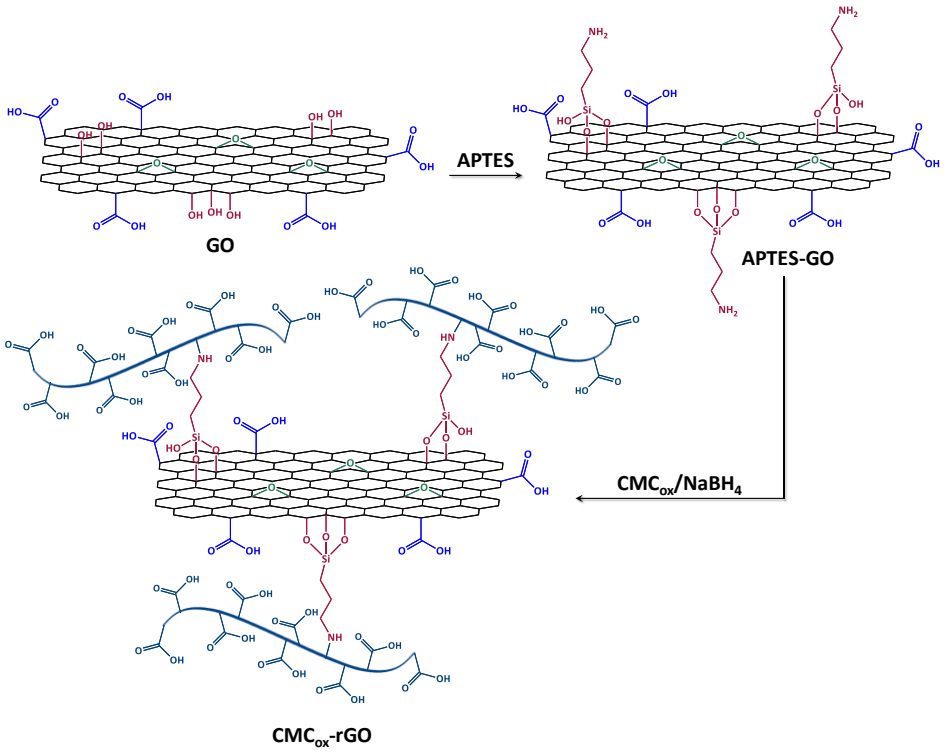

Figura 4.23. Representación esquemática del procedimiento de preparación del material híbrido CMC-rGO [Araque, 2014]

4.5.2.2.2. Preparación del inmunosensor

Inicialmente, se prepara una suspensión acuosa del material híbrido (CMC-rGO) previamente obtenido. Para ello, se dispersa 1 mg de CMC-rGO en 1 mL de agua y se mantiene en un baño de ultrasonidos durante 60 minutos. Posteriormente, se realiza una dilución 1/100 en el mismo medio y se mantiene en un baño de ultrasonidos durante 30 minutos. A continuación, se depositan 20 µL de la disolución diluida sobre el electrodo de trabajo, manteniéndose bajo una lámpara hasta que la gota se seca completamente. Después, se incuban sobre la superficie del electrodo 10 µL Mix&Go™ durante 30 minutos, lavando, a continuación, con agua y se inmoviliza el anticuerpo de captura depositando 5 µL de una dilución 1/300 en disolución reguladora MES 25 mM de pH 5.0, dejándose incubar durante 60 minutos. Seguidamente, se lava con agua y se bloquea la superficie electródica depositando 5 µL de una disolución de BSA al 5% (p/v) en disolución reguladora PB 100 mM de pH 7.4 durante 30 minutos. Posteriormente, se añaden 5 µL de la disolución de adiponectina (APN), se incuba durante 40 minutos, se lava con agua y se depositan

5 µL de una disolución de 2 µg/mL del anticuerpo de detección biotinilado (Biotin-anti-APN) en disolución reguladora PB 100 mM de pH 7.4 + 0.5% BSA (p/v), incubando durante 20 minutos. Transcurrido este tiempo de incubación, se lava con agua y se depositan 5 µL de una dilución 1/1000 de HRP-Strept en disolución reguladora PB 100 mM de pH 7.4 + 0.5% BSA (p/v) durante 20 minutos. Finalmente, se lava y se añaden 10 µL de disolución reguladora PB 100 mM de pH 7.4.

Para la obtención de los amperogramas, se depositan 45 µL de una disolución de hidroquinona 1 mM y se registra la corriente aplicando un potencial de –200 mV. Cuando la corriente de fondo se estabiliza, después de unos 100 segundos, se adicionan 5 µL de una disolución de peróxido de hidrógeno 50 mM, midiéndose la corriente al cabo de 200 segundos de reacción enzimática.

En la Figura 4.24 se muestran las etapas implicadas en la construcción y el funcionamiento del inmunosensor desarrollado para la determinación de adiponectina.

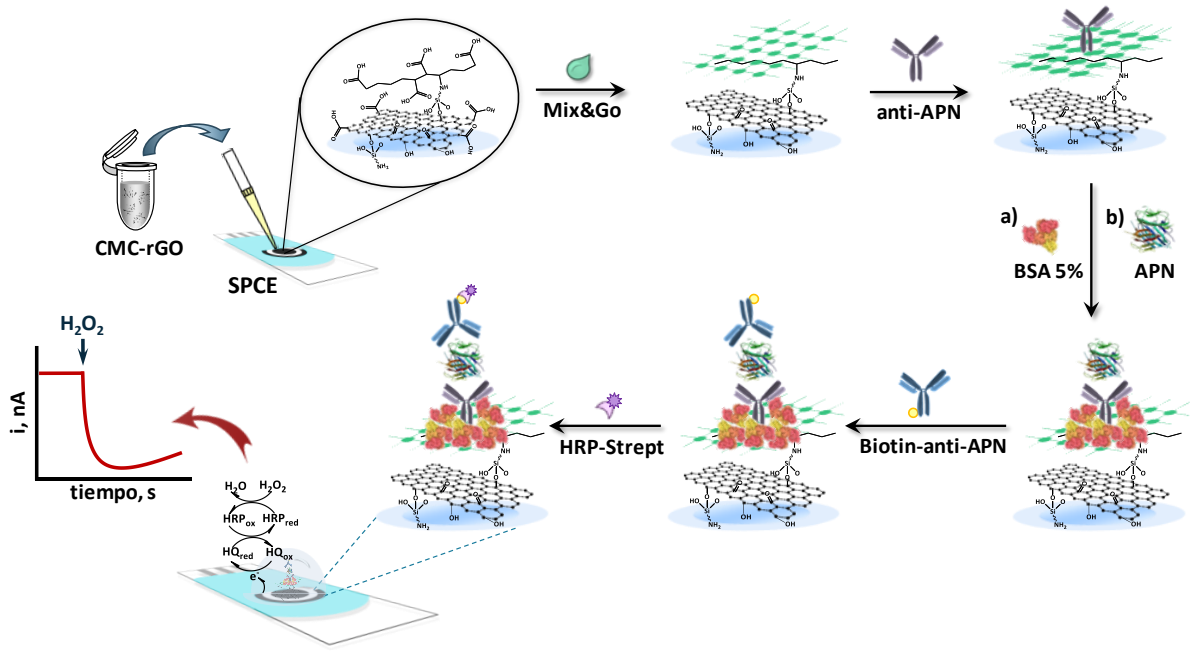

Figura 4.24. Esquema de las etapas implicadas en la preparación y el funcionamiento del inmunosensor HRP-Strept-Biotin-anti-APN-APN-anti-APN-CMC-rGO/SPCE

4.5.2.3. Inmunosensor para la determinación de factor de crecimiento transformante beta 1

4.5.2.3.1. Preparación de los nanotubos de carbono de pared múltiple funcionalizados con el grupo azida

En primer lugar, se preparan los nanotubos de carbono de pared múltiple carboxilados (HOOC-MWCNTs) por tratamiento con ácido nítrico a reflujo. Para ello, se pesan 25 mg de nanotubos y se introducen en un matraz de fondo redondo de 250 mL que contiene 85 mL de agua, que se sumerge en un baño de ultrasonidos durante 60 minutos para obtener una suspensión homogénea. A continuación, se añaden 16 mL de HNO_3 concentrado (65% v/v) y la mezcla se mantiene a reflujo durante 24 horas. Transcurrido ese tiempo, el producto resultante se deja enfriar a temperatura ambiente y se centrifuga a 4000 rpm durante 10 minutos. Posteriormente, se realizan sucesivos lavados con agua destilada hasta que la suspensión alcanza pH 7.0. Por último, el producto resultante se seca en la estufa a 60°C [Hu, 2011].

A continuación, se pesan 25 mg de nanotubos de carbono de pared múltiple carboxilados y se dispersan en 3.45 mL de disolución reguladora MES 25 mM de pH 6.5, que contiene 26.8 mg de *1*-etil-*3*-(*3*-dimetilaminopropil)carbodiimida (EDC) y 29.8 mg de *N*-hidroxisulfosuccinimida (NHSS), incubándose la suspensión durante 120 minutos, con agitación magnética en ausencia de luz. Después, se añaden 4.55 µL de *11*-azido-*3,6,9*-trioxaundecan-*1*-amina y se incuba como anteriormente durante 48 horas. Transcurrido el tiempo de incubación, se centrifuga a 4000 rpm durante 10 minutos y se realizan dos lavados, el primero con disolución reguladora PBS 10 mM de pH 7.0 y el segundo con agua destilada. Finalmente, el producto se deja secar en la estufa a 37°C [Qi, 2012].

En la Figura 4.25 se representa de forma esquemática el procedimiento seguido para la preparación de los nanotubos de carbono de pared múltiple funcionalizados con el grupo azida.

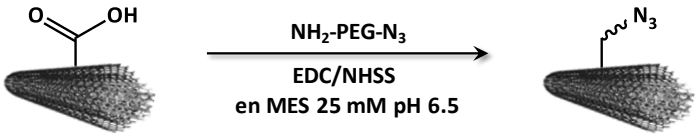

Figura 4.25. Representación esquemática del procedimiento seguido para la preparación de los nanotubos de carbono de pared múltiple funcionalizados con el grupo azida [Qi, 2012]

4.5.2.3.2. Preparación de la inmunoglobulina G etinilada empleando succinimidil-3-propiolato

Para preparar la inmunoglobulina G etinilada se sigue, con algunas modificaciones, el procedimiento descrito por Qi *et al.* [Qi, 2012], que implica la síntesis previa de succinimidil-*3*-propiolato. Para ello, se añaden, gota a gota, 10 mL de una disolución que contiene 1.14 g de *N,N'*-diciclohexilcarbodiimida (DCC) sobre otra disolución que contiene 0.39 g de ácido propargílico y 0.64 g de *N*-hidroxisuccinimida (NHS) en 30 mL de acetato de etilo. La disolución resultante se incuba a 4°C con agitación durante 8 horas. Transcurrido el tiempo de incubación, se filtra la disolución, empleando un embudo Büchner. Posteriormente, se elimina el disolvente con ayuda de un rotavapor y se disuelve el residuo obtenido en 15 mL de acetato de etilo. A continuación, el residuo se lava dos veces empleando un embudo de decantación, primero con 15 mL de una disolución saturada de cloruro sódico (40 g de NaCl por cada 100 g de agua) y después con 15 mL de una disolución saturada de cloruro amónico (60 g de NH_4Cl por cada 100 g de agua). Seguidamente, se lava con agua y se añade sulfato sódico anhidro como desecante en cantidad suficiente, como desecante hasta que el Na_2SO_4 no se apelmace. Seguidamente, se filtra la disolución, con ayuda de un filtro de pliegues, y se elimina el disolvente en un rotavapor. Después, se purifican los cristales del sólido obtenidos, mediante recristalización a -20°C, disolviéndolos previamente en la mínima cantidad de acetato de etilo. Una vez recristalizado el sólido, se evapora el disolvente a 37°C, con ayuda de un rotavapor, se raspa el sólido obtenido y se almacena en un vial a 8°C hasta su utilización.

Figura 4.26. Esquema de la síntesis del succinimidil-3-propiolato [Qi, 2012]

Una vez sintetizado el succinimidil-*3*-propiolato (Figura 4.26), se prepara una disolución de 2 mg/mL de inmunoglobulina G (anti-mouse-IgG) y se mezcla con 250 µL de una disolución de 1 mg/mL de succinimidil-*3*-propiolato en disolución reguladora carbonato 250 mM de pH 9.0 y 625 µL de disolución reguladora carbonato 250 mM de pH 9.0, para obtener un volumen total de 1 mL. La disolución resultante se incuba a 4°C con agitación durante 24 horas y transcurrido ese tiempo, se filtra la disolución, empleando un filtro de centrifuga Amicon® Ultra de 10 K a 1400 rpm y 8°C durante 10 minutos y se realizan cinco lavados cada uno con 500 µL de disolución reguladora PBS 10 mM de pH 7.0, centrifugando cada vez a 14000 rpm y 8°C, durante 10 minutos. Finalmente, se voltea el filtro y se centrifuga a 1000 rpm y 8°C durante 10 minutos, llevando el residuo obtenido a un volumen final de 125 µL con disolución reguladora PBS 10 mM de pH 7.0, obteniéndose, de este modo, una disolución de 1 mg/mL de la inmunoglobulina G etinilada (IgG etinilada).

En la Figura 4.27 se representa de forma esquemática la preparación de la inmunoglobulina G etinilada.

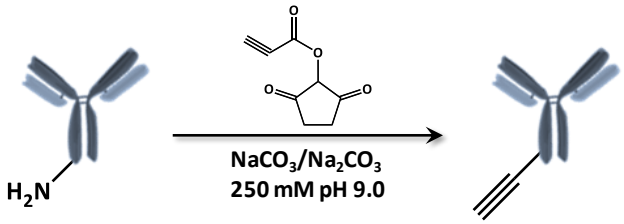

Figura 4.27. Representación esquemática de la preparación de la inmunoglobulina G etinilada empleando el procedimiento descrito por Qi *et al.* [Qi, 2012]

4.5.2.3.3. Preparación de la inmunoglobulina G etinilada empleando peryodato sódico

Con fines comparativos, se empleó también el procedimiento descrito por Le *et al.* [Le, 2013] (Figura 4.28), para la obtención de la inmunoglobulina G etinilada.

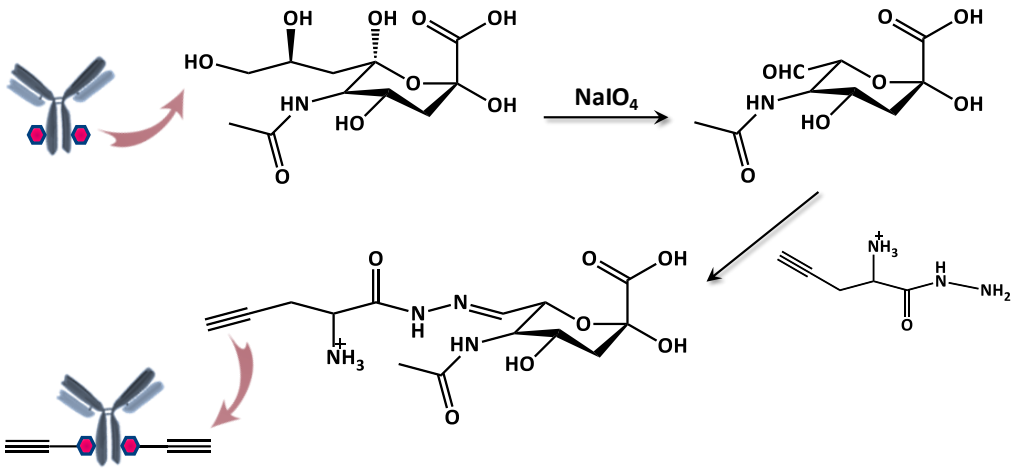

Figura 4.28. Representación esquemática de la reacción de formación de la inmunoglobulina G etinilada empleando el procedimiento descrito por Le *et al.* [Le, 2013]

En este caso, se añaden 50 µL de una disolución de peryodato sódico 20 mM en disolución reguladora AcOH/AcO^- 100 mM de pH 5.5 a 800 µL de una disolución de 2 mg/mL de inmunoglobulina G y la mezcla se incuba en un baño de hielo y ausencia de luz durante 30 minutos. A continuación, se filtra la disolución a 1400 rpm y 4°C empleando un filtro de centrifuga Amicon® Ultra de 10 K, durante 15 minutos. Posteriormente, se realizan tres lavados con disolución reguladora PBS 100 mM de pH 7.2, centrifugando a 14000 rpm y 4°C durante 15 minutos. Después, se voltea el filtro y se centrifuga a 1000 rpm y 4°C durante 2 minutos. Transcurrido este tiempo, se añade al residuo una disolución de 8.8 mg de etinilhidrazida en 500 µL de reguladora PBS 100 mM de pH 7.0 y se incuba durante 2 horas a 25°C. Después, se filtra la mezcla a 14000 rpm y 4°C durante 15 minutos con ayuda de otro Amicon® Ultra de 10 K, se realizan cinco lavados empleando disolución reguladora PBS 100 mM de pH 7.2 y un último lavado con disolución reguladora PBS 100 mM de pH 7.0. Por último, se voltea el filtro y se centrifuga a 1000 rpm y 4°C durante 10 minutos, llevando el residuo

obtenido a un volumen final de 800 µL con disolución reguladora PBS 10 mM de pH 7.0.

4.5.2.3.4. Preparación de los nanotubos de carbono de pared múltiple funcionalizados con inmunoglobulina G etinilada

Los nanotubos funcionalizados con el anticuerpo han de prepararse justo antes de ser utilizados. De este modo, en un tubo eppendorf de 1.5 mL se añaden 67.5 µL de una dilución 1/100 de la inmunoglobulina etinilada en disolución reguladora PBS 10 mM de pH 7.0, 45 µL de una disolución de ácido ascórbico 5 mM y 45 µL de una disolución de sulfato de cobre 5 mM, ambas en el mismo medio. Finalmente se adicionan 157.5 µL de una suspensión de 0.5 mg/mL de nanotubos de carbono funcionalizados con el grupo azida se incuban toda la noche a 4°C con agitación magnética (Figura 4.29).

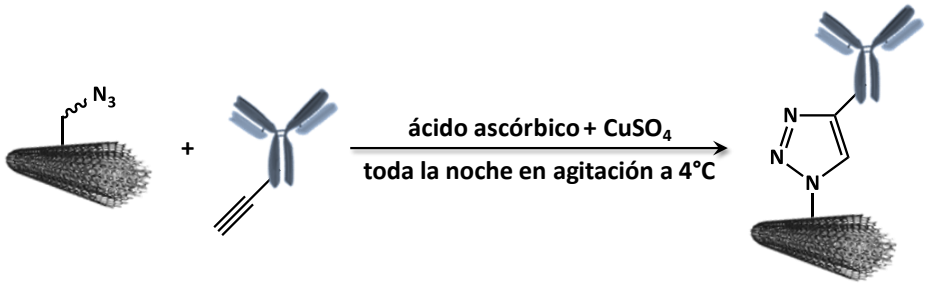

Figura 4.29. Representación esquemática de la cicloadición 1,3-dipolar de Huisgen catalizada por cobre (I) entre azidas y alquinos terminales

4.5.2.3.5. Preparación del inmunosensor

Inicialmente, se depositan 5 µL de la suspensión de nanotubos de carbono de pared doble funcionalizados con la inmunoglobulina G etinilada (IgG-MWCNTs) (*Apartado 4.5.2.3.4. de este capítulo*) y se dejan secar al aire. A continuación, se bloquea la superficie electródica con 5 µL de disolución comercial Blocker™ Casein, dejando incubar durante 30 minutos. Posteriormente, se lava con agua y se adicionan 5 µL de una disolución de 10 µg/mL de anticuerpo de captura (anti-TGF) en disolución reguladora PBS de pH 7.4 y se dejan durante 60 minutos. A continuación, se lava la

superficie electródica con agua y se añaden 5 µL de una disolución que contiene antígeno (TGF-β1) de concentración variable y 1 µg/mL de anticuerpo de detección biotinilado (Biotin-anti-TGF) en disolución reguladora Reagent Diluent 1, incubándose durante 60 minutos. Transcurrido este tiempo, se lava y se depositan 5 µL de una dilución 1/500 de poli-HRP-Strept en disolución reguladora poli-Strept-HRP Stabilizer 85R-112, que reacciona durante 15 minutos. Finalmente, se lava y se añaden 10 µL de disolución reguladora PBS de pH 7.4 hasta la realización de la medida.

Para la obtención de los amperogramas, se depositan 45 µL de una disolución de hidroquinona 1 mM y se registra la corriente obtenida cuando se aplica un potencial de –200 mV. Cuando la corriente de fondo se estabiliza, después de unos 100 segundos, se adicionan 5 µL de una disolución de peróxido de hidrógeno 50 mM, midiéndose la corriente al cabo de 200 segundos de reacción enzimática.

En la Figura 4.30 se muestran de forma esquematizada las etapas implicadas en la construcción y el funcionamiento del inmunosensor desarrollado para la determinación de factor de crecimiento beta 1.

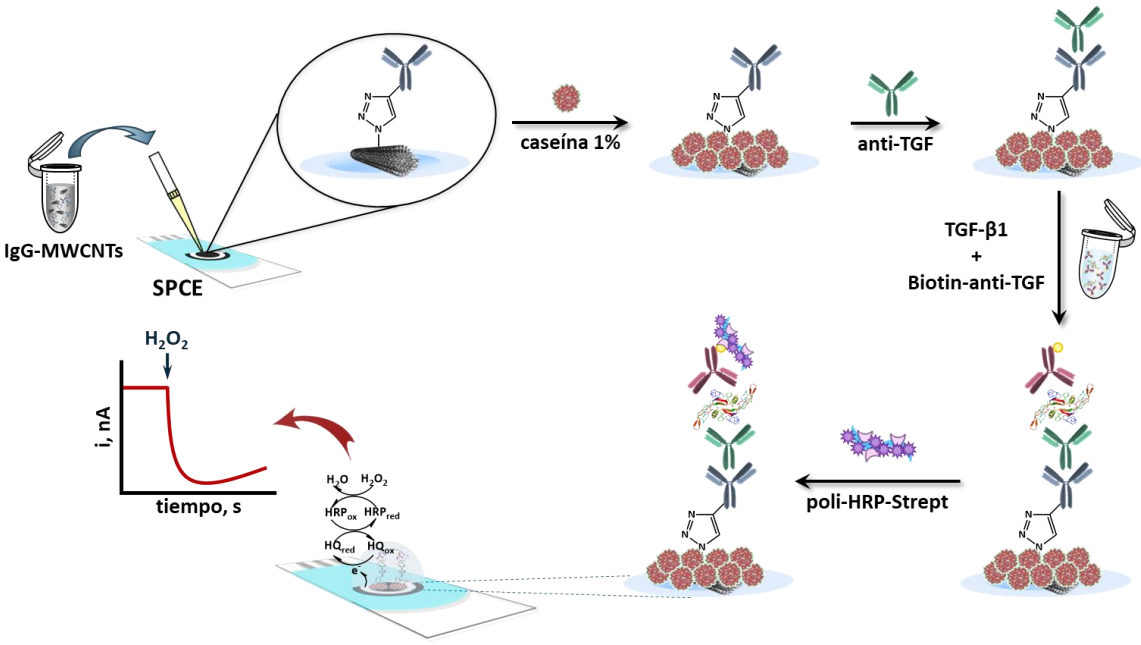

Figura 4.30. Esquema de las etapas implicadas en la preparación y el funcionamiento del inmunosensor poli-HRP-Strept-Biotin-anti-TGF-TGF-β1-anti-TGF-IgG-MWCNTs/SPCE

4.5.3. Preparación de inmunosensores basados en la modificación de la superficie electródica mediante *grafting* electroquímico

4.5.3.1. Inmunosensor para la determinación de interferón gamma

La modificación de la superficie del electrodo serigrafiado mediante *grafting* con ácido *p*-aminobenzoico se realiza llevando a cabo, en primer lugar, una reacción de diazotación del ácido con $NaNO_2$ en medio HCl y, posteriormente, un tratamiento electroquímico. Para ello, se disuelven 2 mg de ácido *p*-aminobenzoico en 2 mL de HCl 1 M, enfriando en un baño de hielo. Seguidamente se prepara la sal de diazonio adicionando gota a gota 38 µL de $NaNO_2$ 2 mM por cada 200 µL de la disolución de ácido *p*-aminobenzoico, con agitación constante en un baño de hielo. A continuación, se depositan 40 µL de esta disolución sobre la superficie de un electrodo serigrafiado de carbono y se realizan 10 ciclos en voltamperometría cíclica entre 0.0 y –1.0 V, a 200 mV/s. Finalmente se lava el electrodo abundantemente con agua y metanol y se deja secar al aire [Moreno-Guzmán, 2012].

Posteriormente, se lleva a cabo la activación de los grupos carboxílicos de la superficie del electrodo de trabajo. Para ello, se depositan 10 µL de una disolución de EDC/NHSS 100 mM de cada uno de ellos en disolución reguladora MES 25 mM de pH 5.0 y se deja incubar durante 30 minutos. Transcurrido este tiempo, se lava el electrodo con disolución reguladora MES 25 mM de pH 5.0 y se inmoviliza el anticuerpo de captura (anti-IFN), depositándose 5 µL de una disolución de 15 µg/mL de la misma en disolución reguladora MES de pH 5.0 e incubando durante 60 minutos. Transcurrido ese tiempo, se bloquean las posiciones libres del electrodo de trabajo, depositando 10 µL de una disolución de BSA al 2% (p/v) en disolución reguladora PBS de pH 7.4, durante 30 minutos. Tras la etapa de bloqueo, se lava nuevamente el electrodo con disolución reguladora PBS de pH 7.4 y se añaden 5 µL de la disolución

de antígeno (IFN-γ), incubando 60 minutos. A continuación, se lava y se añaden 5 µL de una disolución de 1.25 µg/mL de anticuerpo de detección biotinilado (Biotin-anti-IFN) en disolución reguladora PBS de pH 7.4, dejando incubar 45 minutos. Por último, se lava y se añaden 5 µL de una dilución 1/500 de HRP-Strept en la misma disolución reguladora, incubándose durante 20 minutos.

Para la obtención de los amperogramas, se depositan 45 µL de una disolución de hidroquinona 1 mM y se registra la corriente obtenida aplicando un potencial de –200 mV. Cuando la corriente de fondo se estabiliza, después de unos 50 segundos, se adicionan 5 µL de una disolución de peróxido de hidrógeno 50 mM, midiéndose la corriente al cabo de 200 segundos de reacción enzimática.

En la Figura 4.31 se muestran las etapas implicadas en la construcción y el funcionamiento del inmunosensor desarrollado para la determinación de interferón gamma.

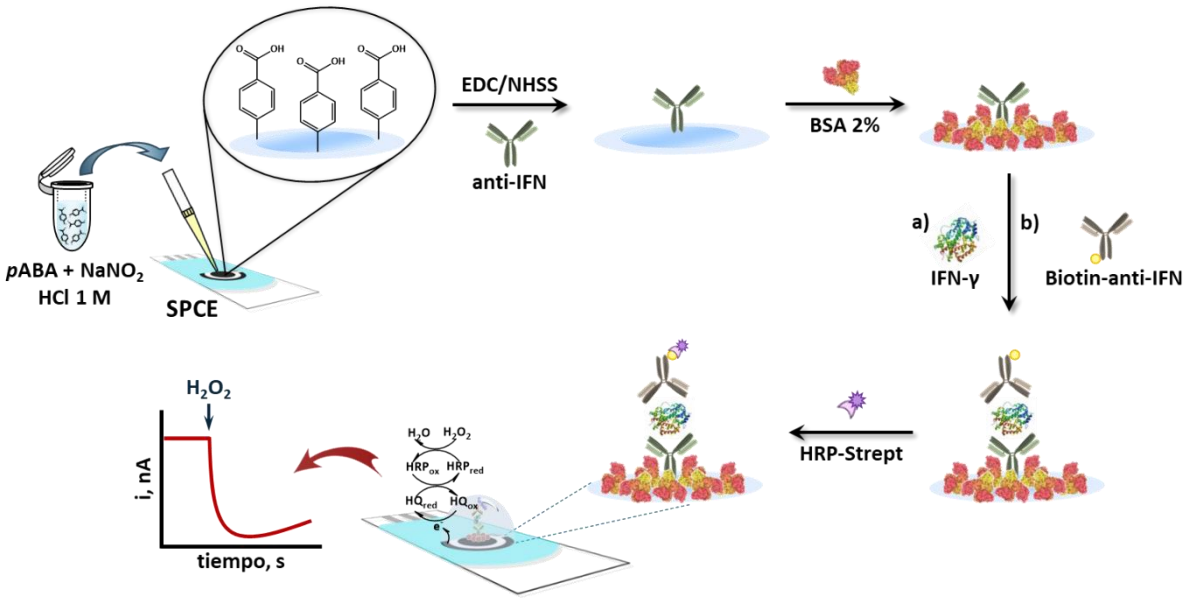

Figura 4.31. Esquema de las etapas implicadas en la preparación y el funcionamiento del inmunosensor HRP-Strept-Biotin-anti-IFN-IFN-γ-anti-IFN/SPCE

4.5.3.2. Inmunosensor dual para la determinación simultánea de factor de necrosis tumoral alfa e interleucina 1 beta

Para la modificación superficial de los electrodos se emplearon nanotubos de carbono de pared doble modificados con ácido *p*-aminobenzoico (HOOC-Phe-DWCNTs), preparados en el Instituto de Nanociencia, Nanotecnología y Materiales Moleculares (INAMOL) de la Universidad de Castilla-La Mancha (Toledo). Para ello, se dispersa 1 mg de HOOC-Phe-DWCNTs en 2 mL de agua, se añaden 27.4 µL de Tween® 20 y se introducen en un baño de ultrasonidos durante 60 minutos. A continuación, se depositan 0.5 µL de la suspensión sobre cada una de las superficies electródicas de trabajo y se dejan secar al aire. Esta operación se realiza por triplicado hasta depositar un total de 1.5 µL de la dispersión de nanotubos sobre cada uno de los electrodos de trabajo.

Posteriormente, se activa la superficie electródica incubando 2.5 µL del polímero Mix&Go™ durante 60 minutos. Transcurrido este tiempo, se lava con agua y se inmoviliza sobre cada electrodo de trabajo el correspondiente anticuerpo de captura (anti-TNF o anti-IL) depositando 2.5 µL de una disolución de 4 µg/mL de cada uno de ellos en disolución reguladora MES 25 mM de pH 5.0 e incubando durante 60 minutos, lavando después con agua. El bloqueo de las posiciones libres de las superficies electródicas se lleva a cabo depositando 2.5 µL de una disolución de BSA al 2% (p/v) en PBS de pH 7.4 durante 30 minutos, lavando después con agua. Seguidamente se añaden 2.5 µL de la disolución de antígeno (TNF-α o IL-1β) en disolución reguladora PBS de pH 7.4 y se incuba durante 60 minutos. A continuación, se lava con agua y se depositan 2.5 µL de una disolución de 0.5 µg/mL de los respectivos anticuerpos de detección biotinilados (Biotin-anti-TNF o Biotin-anti-IL) en disolución reguladora PBS de pH 7.4, incubándose durante 45 minutos. Posteriormente, se lava con agua y se depositan 2.5 µL de una dilución 1/500 de poli-HRP-Strept en disolución reguladora poli-Strept-HRP Stabilizer 85R-112 y se

incuba durante 15 minutos. Finalmente, se lava y se añaden 10 µL de disolución reguladora PBS de pH 7.4.

Para la obtención de los amperogramas, se depositan 45 µL de una disolución de hidroquinona 1 mM y se registra la corriente obtenida aplicando un potencial de –200 mV. Cuando la corriente de fondo se estabiliza, después de unos 100 segundos, se adicionan 5 µL de una disolución de peróxido de hidrógeno 50 mM, midiéndose la corriente al cabo de 200 segundos de reacción enzimática.

En la Figura 4.32 se muestra un esquema de las etapas implicadas en la construcción y el funcionamiento del inmunosensor desarrollado para la determinación simultánea de factor de necrosis tumoral alfa e interleucina 1 beta.

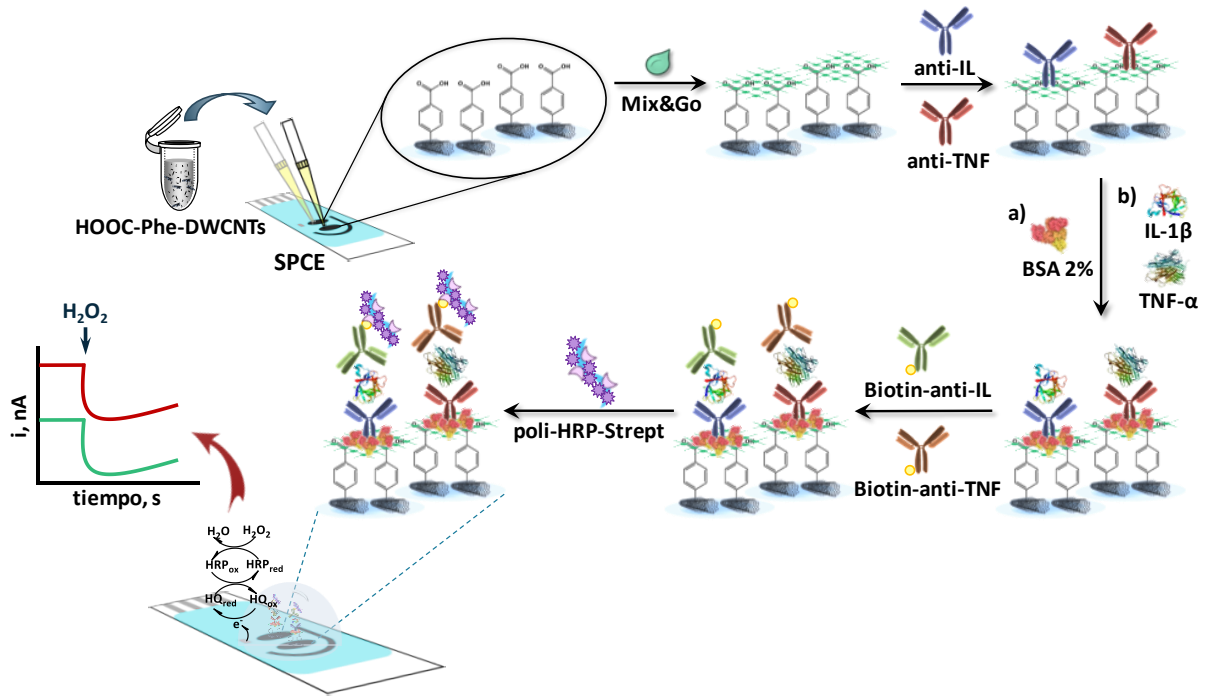

Figura 4.32. Esquema de las etapas implicadas en la preparación del inmunosensor dual para la determinación simultánea de las citoquinas pro-inflamatorias TNF-α e IL-1β

4.5.4. Preparación de inmunosensores basados en el empleo de nanomateriales híbridos funcionalizados con biomoléculas como estrategia de amplificación de la señal

4.5.4.1. Inmunosensor para la determinación de factor de crecimiento transformante beta 1 empleando nanotubos de carbono funcionalizados con aminoviológeno como etiqueta portadora de amplificación de la señal

4.5.4.1.1. Funcionalización de los nanotubos de carbono de pared simple con aminoviológeno

La funcionalización de los nanotubos de carbono de pared simple con aminoviológeno (V-Phe-SWCNTs) se ha realizado en el Instituto de Nanociencia, Nanotecnología y Materiales Moleculares (INAMOL) de la Universidad de Castilla-La Mancha (Toledo) empleando un método en varias etapas. En la primera de ellas, se sintetiza el compuesto bromuro de *1*-(*3*-aminoetil)-*4,4'*-bipiridinio, mezclando 500 mg de *4,4'*-bipiridina y 71.4 mg de *2*-bromoetilamina en 10 mL de acetonitrilo y manteniendo la mezcla a reflujo durante 90 minutos. Una vez enfriada la mezcla, se filtra el precipitado y se redisuelve en *N,N'*-dimetilformamida (DMF) caliente, para eliminar la sal di-alquilada por filtración. Finalmente, para obtener el producto mono-alquilado, como un sólido blanco, se añade dietiléter.

La segunda etapa corresponde a la oxidación de los nanotubos de carbono de pared simple. Para ello, se pesan 20 mg de dichos nanotubos y se dispersan en 40 mL de *N*-metil-*2*-pirrolidona, empleando un baño de ultrasonidos durante 10 minutos. Después, se añaden 457 mg de ácido *p*-aminobenzoico (*p*-ABA) y 0.54 mL de nitrito de isoamilo y se agita la mezcla bajo atmósfera de nitrógeno a 70°C durante 24 horas. Una vez transcurrido este tiempo, la mezcla se filtra a través de una membrana PTFE

de 0.1 µm de tamaño de poro y se lava con *N,N'*-dimetilformamida, metanol y diclorometano, hasta que el filtrado sea translúcido, obteniéndose el nanomaterial de carbono oxidado como un sólido de color negro.

Por último, se realiza la síntesis del híbrido aminoviológeno-nanotubos de carbono de pared simple (V-Phe-SWCNTs), dispersando 8 mg de los nanotubos oxidados en 20 mL de *N,N'*-dimetilformamida. Seguidamente se añaden 21.9 mg de *N,N'*-diciclohexilcarbodiimida (DCC), 14.4 mg de hidroxibenzotiazol (HOBt) y 16 mg de *1*-(*3*-aminoetil)-*4,4'*-bipiridinio, bajo corriente de argón. La suspensión se mantiene en un baño de ultrasonidos durante 10 minutos y, posteriormente, se calienta a 60°C durante 3 días. A continuación, el sólido se separa empleando una membrana PTFE de 0.1 µm de tamaño de poro y se lava con *N,N'*-dimetilformamida, metanol y diclorometano. Después, el sólido se redisuelve en *N,N'*-dimetilformamida, se añaden 16 mg de *2*-bromoetilamina y la mezcla se calienta a 120°C durante 24 horas. Transcurrido este tiempo, se filtra la suspensión a través de una membrana PTFE de 0.1 µm de tamaño de poro. Finalmente, el sólido se lava con *N,N'*-dimetilformamida, metanol y diclorometano, obteniéndose el híbrido (V-Phe-SWCNT).

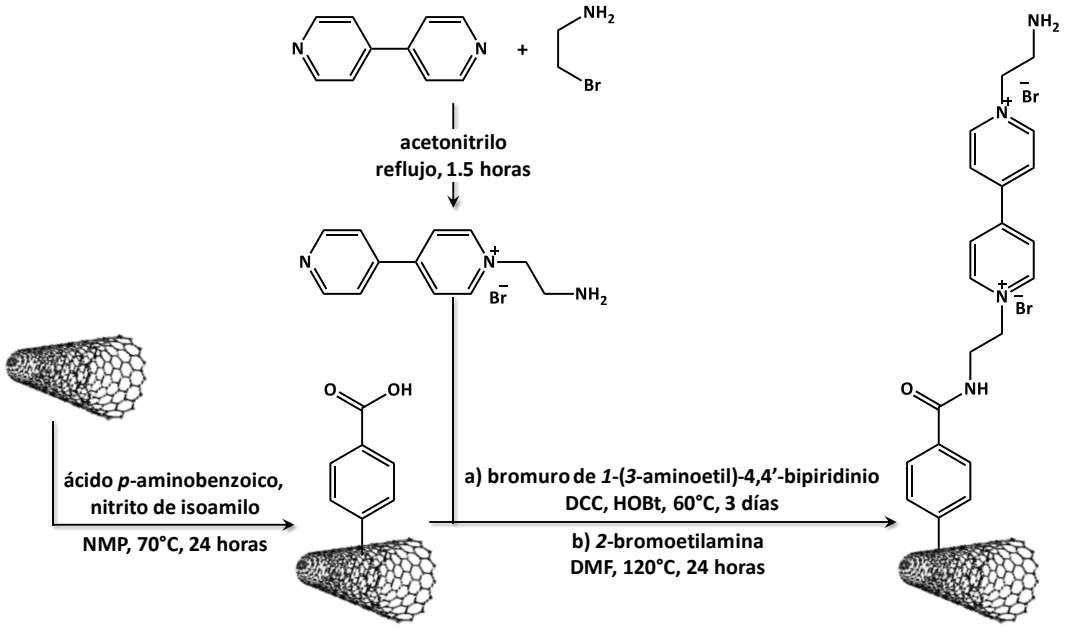

Figura 4.33. Representación esquemática de la síntesis de los nanotubos de carbono de pared simple funcionalizados con aminoviológeno

En la Figura 4.33 se representan de forma esquemática todos los pasos seguidos para llevar a cabo la síntesis de los nanotubos de carbono de pared simple funcionalizados con aminoviológeno.

4.5.4.1.2. Preparación del conjugado de nanomaterial funcionalizado con biomoléculas

Para obtener 100 µL del conjugado aminoviológeno-nanotubos de carbono de pared simple-anticuerpo-peroxidasa (V-Phe-SWCNT(-HRP)-anti-TGF), se mezclan 50 µL de una disolución de EDC/NHSS 200 mM de cada uno de ellos en disolución reguladora MES 25 mM de pH 5.0, con 50 µL de una disolución de 4 mg/mL de ácido tereftálico en disolución reguladora PB de pH 8.0, 100 µL de una disolución de 40 µg/mL de la enzima peroxidasa (HRP) en disolución reguladora PBS de pH 7.4, 100 µL de una disolución de 4 µg/mL de anticuerpo (anti-TGF) en disolución reguladora PBS de pH 7.4 y 100 µL de 0.5 mg/mL de V-Phe-SWCNTs en agua. La mezcla se incuba con agitación y en ausencia de luz durante 3 horas y transcurrido este tiempo, la mezcla se centrifuga a 14000 rpm y 8°C durante 10 minutos. Después, se retira el sobrenadante y se realizan dos lavados con 500 µL de disolución reguladora PBS de pH 7.4. Por último, el sólido se resuspende en 100 µL de disolución reguladora PBS de pH 7.4 (Figura 4.34).

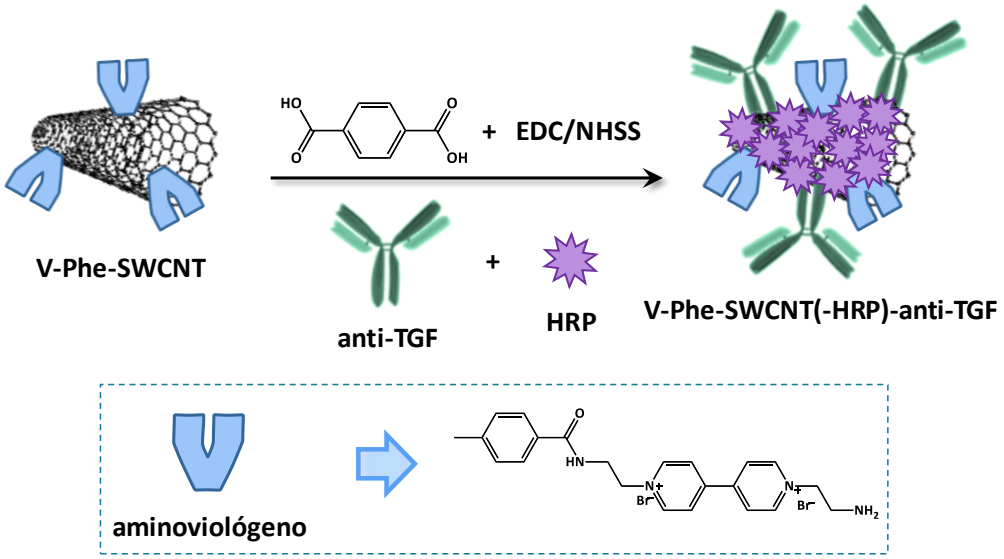

Figura 4.34. Representación esquemática de la preparación del híbrido V-Phe-SWCNT(-HRP)-anti-TGF

4.5.4.1.3. Preparación del inmunosensor

La modificación de la superficie del electrodo serigrafiado mediante *grafting* con ácido *p*-aminobenzoico se lleva a cabo siguiendo el procedimiento descrito en el *Apartado 4.5.3.1.* de este capítulo. Después, se activan los grupos carboxílicos de la superficie del electrodo de trabajo, depositando 5 µL de una disolución de EDC/NHSS 100 mM de cada uno de ellos en disolución reguladora MES 25 mM de pH 5.0 y se deja incubar durante 30 minutos. Seguidamente, se lava el electrodo con agua y se inmoviliza la estreptavidina, depositándose 5 µL de una disolución de 200 µg/mL de la misma en disolución reguladora MES 25 mM de pH 5.0 e incubándose durante 60 minutos. Tras este tiempo, se lava y se depositan 5 µL de una disolución de 7.5 µg/mL de anticuerpo de captura (Biotin-anti-TGF) en disolución reguladora PBS de pH 7.4, dejando reaccionar durante 60 minutos. La siguiente etapa, consistente en el bloqueo de los grupos activados que han quedado libres de anticuerpo, se realiza depositando 5 µL de una disolución de 0.5 mg/mL de biotina en disolución reguladora PBS de pH 7.4 e incubando 30 minutos. Tras la etapa de bloqueo, se lava y se añaden 5 µL de la disolución de antígeno (TGF-β1), incubando 60 minutos. Finalmente, se lava con agua y se añaden 5 µL del conjugado V-Phe-SWCNT(-HRP)-anti-TGF y, tras 60 minutos, se lava y se depositan 10 µL de disolución reguladora PBS de pH 7.4.

Para la obtención de los amperogramas, se depositan 45 µL de una disolución reguladora PB 50mM de pH 6.0 y se registra la corriente obtenida aplicando un potencial de –300 mV. Cuando la corriente de fondo se estabiliza, después de unos 100 segundos, se adicionan 5 µL de una disolución de peróxido de hidrógeno 50 mM, midiéndose la corriente al cabo de 200 segundos de reacción enzimática.

En la Figura 4.35 se muestran las etapas implicadas en la construcción y el funcionamiento del inmunosensor desarrollado para la determinación de factor de crecimiento beta 1 empleando el conjugado V-Phe-SWCNT(-HRP)-anti-TGF para la amplificación de la señal.

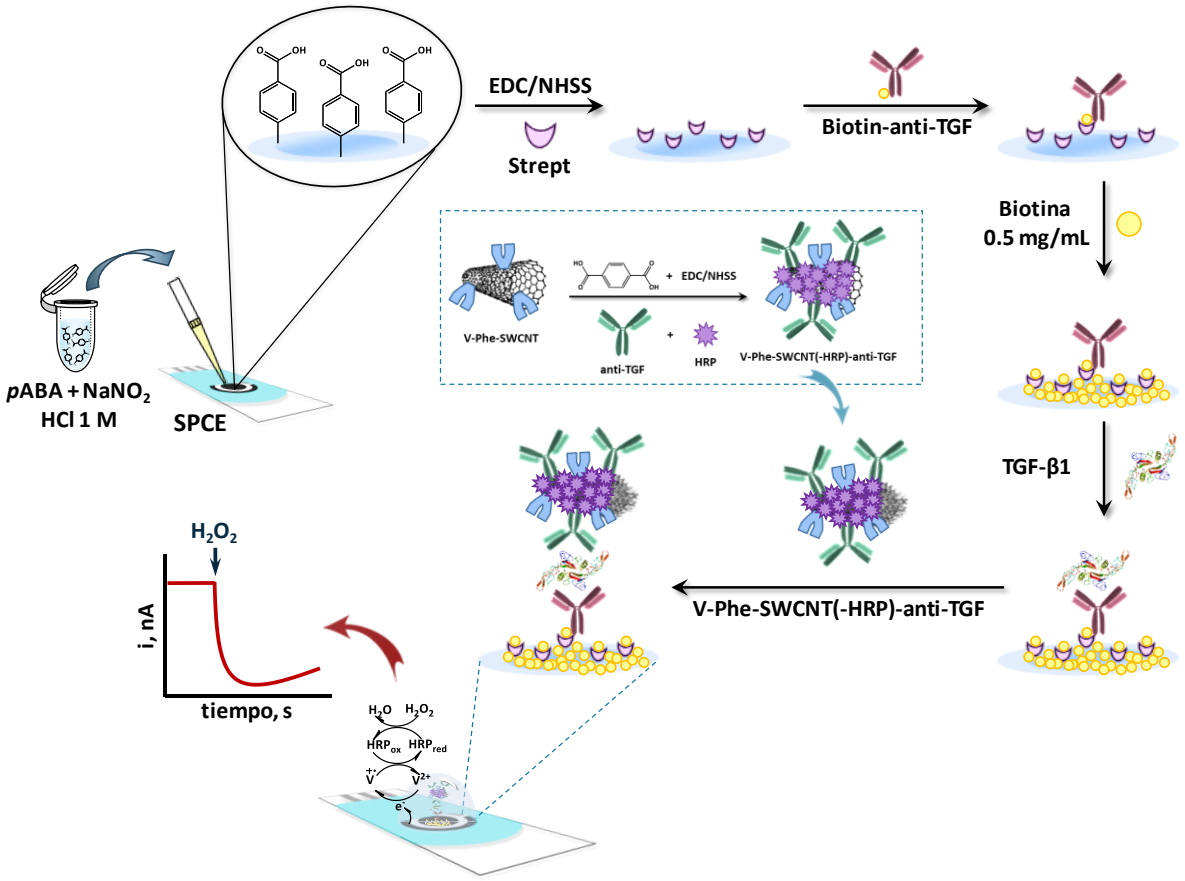

Figura 4.35. Esquema de las etapas implicadas en la preparación y el funcionamiento del inmunosensor V-Phe-SWCNT(-HRP)-anti-TGF-TGF-β1-Biotin-anti-TGF-Strept/SPCE

4.5.4.2. Inmunosensor para la determinación de fetuina A humana

4.5.4.2.1. Modificación de los nanotubos de carbono de pared múltiple con nanopartículas magnéticas

En primer lugar, se lleva a cabo la oxidación de los nanotubos de carbono de pared múltiple (HOOC-MWCNTs) siguiendo el procedimiento descrito por Hu *et al.* (*Apartado 4.5.2.3.1.* de este capítulo). Después, se prepara una suspensión homogénea de estos nanotubos, añadiendo 19.4 mg de los mismos a 10 mL de agua, y se añaden 13.1 mg de $FeCl_3 \cdot 6H_2O$ y 5.9 mg de $FeCl_2 \cdot 4H_2O$, ajustándose el pH entre 10 y 11 con $NH_3 \cdot H_2O$ al 25%, introduciendo la mezcla en un baño de ultrasonidos bajo atmósfera de nitrógeno durante 30 minutos. Transcurrido este tiempo, la mezcla se retira del baño y se mantiene a 80°C con agitación magnética bajo atmósfera de

nitrógeno durante 60 minutos (Figura 4.36). Cuando el sistema alcanza temperatura ambiente, se lava con agua el nanomaterial obtenido (HOOC-mMWCNTs) hasta alcanzar pH neutro y se seca en la estufa a 37°C [Zhang, 2014].

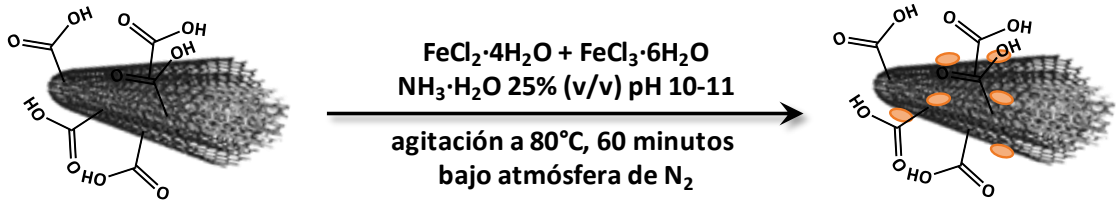

Figura 4.36. Magnetización de los nanotubos de carbono de pared múltiple carboxilados

4.5.4.2.2. Preparación del conjugado de material magnético funcionalizado con biomoléculas

Se dispersan 1.5 mg de nanotubos de carbono de pared múltiple magnéticos (HOOC-mMWCNTs) en 2 mL de disolución reguladora PBS' 100 mM de pH 7.0 en un baño de ultrasonidos durante 30 minutos. A continuación, se añade 1 mL de una disolución 400 mM de EDC y 100 mM de NHSS en disolución reguladora PBS' 100 mM de pH 7.0 y se incuba en oscuridad con agitación magnética durante 6 horas. Seguidamente, se centrifuga la suspensión a 1400 rpm y temperatura ambiente durante 5 minutos, se retira el sobrenadante y se realizan tres lavados con 1 mL de disolución reguladora PBS' 10 mM de pH 7.0. Tras el último lavado, se añade 1 mL de una disolución que contiene 5 µg/mL de anticuerpo (anti-HFA) y 1 mg/mL de peroxidasa de rábano (HRP) en disolución reguladora PBS' 100 mM de pH 7.0 y se incuba durante 24 horas con agitación magnética. Después, se centrifuga la mezcla a 1400 rpm y temperatura ambiente durante 5 minutos, se retira el sobrenadante y se realizan tres lavados con 1 mL de disolución reguladora PBS' 10 mM de pH 7.0. Finalmente, el residuo se resuspende en 1 mL de disolución reguladora PBST' 100 mM de pH 7.0 (Figura 4.37).

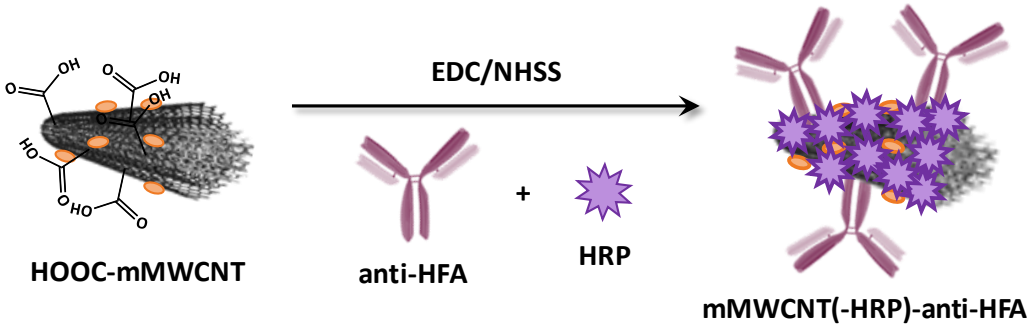

Figura 4.37. Representación esquemática de la preparación del híbrido mMWCNTs(-HRP)-anti-HFA

4.5.4.2.3. Preparación del inmunosensor

En primer lugar, se modificaron los electrodos serigrafiados de carbono mediante *grafting* con ácido *p*-aminobenzoico (*p*-ABA) siguiendo el procedimiento descrito por Liu *et al.* [Liu, 2000]. Este procedimiento se basa en la oxidación electroquímica del grupo amino del anillo aromático sobre la superficie del electrodo de carbono, lo que da lugar a la formación del catión radical y su unión a la superficie electródica por formación de un enlace carbono-nitrógeno. Para ello, se sumerge el electrodo serigrafiado de carbono en una mezcla de *p*-ABA y $LiClO_4$ en etanol absoluto y se realizan 3 barridos sucesivos mediante voltamperometría cíclica entre 0.0 y 0.6 V a 30 mV/s. Seguidamente, los electrodos modificados se lavan con agua destilada y se dejan secar al aire. La segunda etapa de preparación del inmunosensor implica la activación de los grupos carboxilo superficiales. Para ello, se deposita sobre su superficie un volumen 10 µL de una disolución de EDC/NHSS 100 mM de cada uno de ellos en disolución reguladora MES 25 mM de pH 5.0, y se deja incubar durante 30 minutos. Por último, la superficie electródica se modifica con estreptavidina, depositando 5 µL de una disolución de la proteína de 600 µg/mL en disolución reguladora MES 25 mM de pH 5.0 e incubando durante 60 minutos.

Seguidamente, se depositan 5 µL de una disolución de 7 µg/mL de anticuerpo de captura (Biotin-anti-HFA) en disolución reguladora PBS de pH 7.4 y se incuba durante 60 minutos. A continuación, se lavan los electrodos y se bloquean las posiciones reactivas de la superficie del electrodo de trabajo que han quedado libres, incubando 5 µL de una disolución de 1.5 mg/mL de biotina en disolución reguladora

PBS de pH 7.4 durante 30 minutos. Tras la etapa de bloqueo, se lava y se añaden 5 µL de una disolución de antígeno (HFA), que se incuba durante 60 minutos. Seguidamente se lava la superficie del electrodo y se depositan 5 µL del conjugado de nanomaterial magnético (mMWCNTs(-HRP)-anti-HFA) durante 60 minutos. Finalmente, se lava y se añaden 10 µL de disolución reguladora PBS de pH 7.4.

Para la obtención de los amperogramas, se depositan 45 µL de una disolución de hidroquinona 1 mM y se registra la corriente obtenida aplicando un potencial de –200 mV. Cuando la corriente de fondo se estabiliza, después de unos 100 segundos, se adicionan 5 µL de una disolución de peróxido de hidrógeno 50 mM, midiéndose la corriente al cabo de 200 segundos de reacción enzimática. En la Figura 4.38 se muestran las etapas implicadas en la construcción y el funcionamiento del inmunosensor desarrollado para la determinación de fetuina A humana.

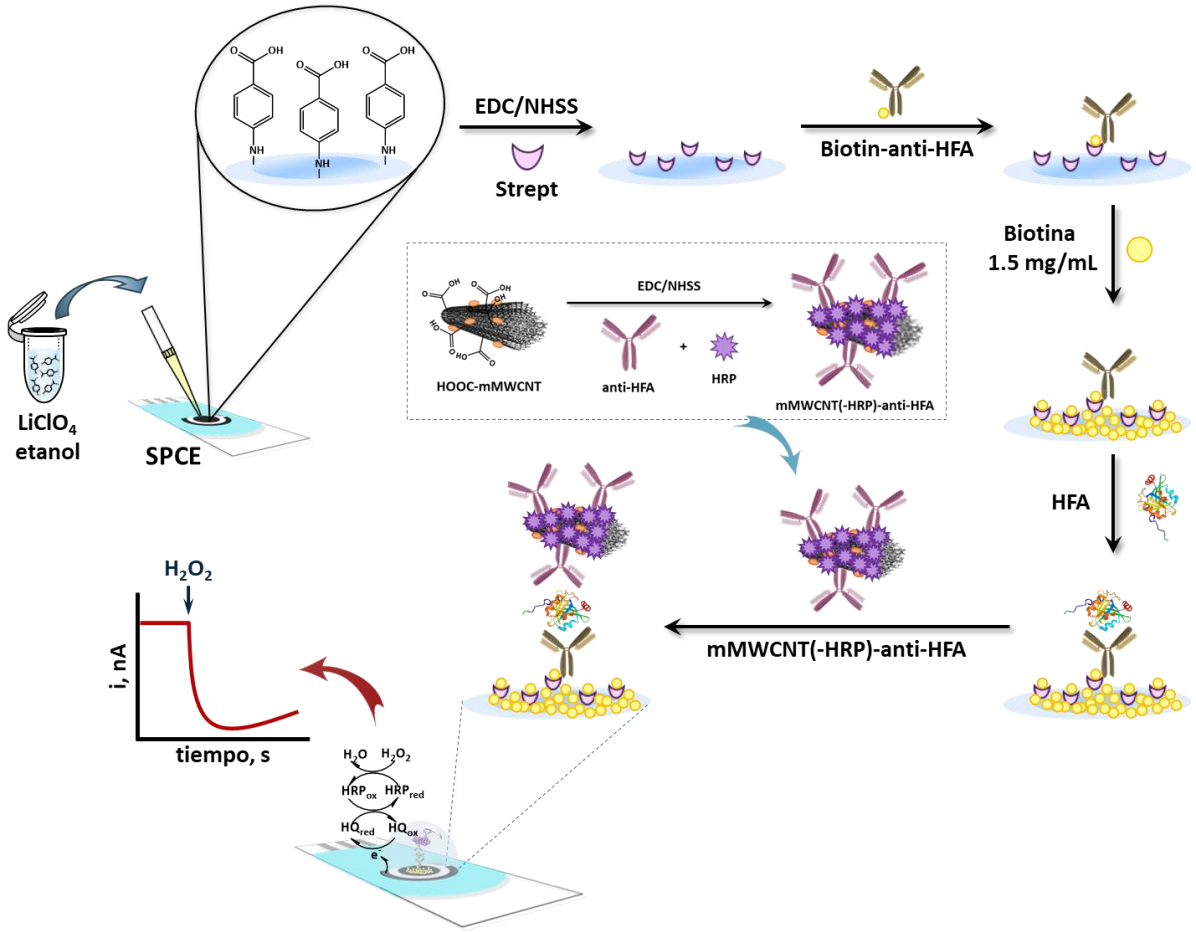

Figura 4.38. Esquema de las etapas implicadas en la preparación y el funcionamiento del inmunosensor mMWCNT(-HRP)-anti-HFA-HFA-Biotin-anti-HFA-Strept/SPCE

4.6. ANÁLISIS DE MUESTRAS

4.6.1. Determinación de endoglina en suero

El inmunosensor desarrollado se aplicó al análisis de muestras de suero humano pertenecientes a cinco individuos sanos, así como a tres pacientes con cáncer colorrectal, tres con cáncer de mama, tres con cáncer de pulmón y dos con epidermólisis bullosa.

Para evitar el efecto matriz se realiza una dilución 1/50 de las muestras con disolución reguladora PBS de pH 7.4, realizándose la determinación de CD105 por interpolación de la señal proporcionada por las muestras en el calibrado de disoluciones patrón. Tras la determinación, los resultados obtenidos empleando el inmunosensor, se comparan con los proporcionados por un inmunoensayo tipo ELISA empleando el kit DuoSet® ELISA Development System (DY1097) de R&D Systems.

4.6.2. Determinación de 8-isoprostano en suero

En primer lugar, se analizó un suero humano comercial, que se presenta de forma liofilizada y se conserva a 4°C. Una vez reconstituido en 5 mL de agua, se suplementa con concentraciones creciente de 8-isoprostano (30, 35 y 40 pg/mL) y, a continuación, se diluye a la mitad empleando una dilución 1/500 del antígeno marcado con la enzima peroxidasa (HRP-ISO) en regulador Sample Diluent, no siendo necesario ningún tratamiento adicional de la muestra.

Por otro lado, para poder determinar la concentración total de 8-isoprostano en las muestras de suero de individuos sanos es necesario llevar a cabo una hidrólisis de las lipoproteínas y fosfolípidos a los que pudiera estar unido. Comúnmente, para hidrolizar el enlace éster, se emplea un tratamiento básico. En este caso, se añaden 100 µL de NaOH 10 N sobre 400 µL de muestra y se incuba a 45°C durante 120 minutos. Posteriormente, se añaden 100 µL de HCl 10 N, apareciendo un precipitado blanco

lechoso, que se separa del sobrenadante centrifugando a 12000 rpm durante 5 minutos. Antes de llevar a cabo la etapa de inmunorreconocimiento, se comprueba que el pH del sobrenadante se encuentre entre 6 y 8.

En ambos casos, la determinación de 8-isoprostano se lleva a cabo por interpolación de la señal proporcionada por la muestra en el calibrado de disoluciones patrón.

Además, los resultados obtenidos para las muestras de suero humano de individuos sanos, empleando el inmunosensor desarrollado, se validan realizando un inmunoensayo tipo ELISA empleando los mismos reactivos, incluidos en el kit ELISA OxiSelect™ (STA-337) de Cell Biolabs, Inc.

4.6.3. Determinación de adiponectina en suero

El inmunosensor desarrollado se aplica al análisis de dos muestras de suero, una de ellas perteneciente a un paciente con hipercolesterolemia y la otra a un paciente con diabetes tipo 2.

Como tratamiento previo de la muestra es necesario realizar una dilución 1/50 de la misma en disolución reguladora PB 100 mM de pH 7.4. Sin embargo, esta dilución no es suficiente para evitar completamente el efecto matriz. Por lo tanto, es necesario realizar un calibrado de adiciones estándar, añadiendo concentraciones crecientes (entre 1 y 3 μg/mL) del estándar de adiponectina sobre las muestras de suero diluidas, con el fin de poder determinar la concentración de adiponectina en las muestras.

Como en los casos anteriores, los resultados obtenidos empleando el inmunosensor desarrollado se validan utilizando el kit ELISA ab108786 de Abcam.

4.6.4. Determinación de factor de crecimiento transformante beta 1 en suero

Por un lado, se analiza un suero humano liofilizado comercial enriquecido con distintas concentraciones de TGF-β1 (25, 75 y 125 pg/mL). Seguidamente, se realiza una dilución 1/100 en disolución reguladora Reagent Diluent 1, que permite evitar el efecto matriz.

Por otro lado, también se determina la concentración de TGF-β1 en dos muestras de suero humano pertenecientes a una mujer sana y a un paciente con hipercolesterolemia. En este caso, también es necesario llevar a cabo una dilución 1/100 en disolución reguladora Reagent Diluent 1 para evitar el efecto matriz.

La determinación de esta citoquina en las muestras se lleva a cabo por interpolación de la señal proporcionada por las mismas en el calibrado de disoluciones patrón.

Además, los resultados obtenidos para las muestras de suero humano no enriquecido se validan mediante un inmunoensayo tipo ELISA empleando el kit DuoSet® ELISA Development System (DY240–05) de R&D Systems.

4.6.5. Determinación de interferón gamma en un material biológico humano certificado y saliva

La utilidad del inmunosensor se demuestra, en primer lugar, mediante el análisis del contenido de IFN-γ en un material biológico certificado de referencia, de concentración conocida, que se presenta en forma liofilizada y se conserva a –20°C. Este material, además de una concentración conocida de interferón gamma, contiene 6 mg de albúmina de suero humano y disolución reguladora PBS y se reconstituye en 1 mL de agua. Una vez reconstituido este material, es necesario realizar una dilución 1/1000 empleando disolución reguladora PBS de pH 7.4, no siendo necesario ningún tratamiento adicional de la muestra.

Por otra parte, también se lleva a cabo la determinación de interferón gamma en muestras de saliva pertenecientes a cuatro individuos sanos. La toma de muestra de saliva se realiza empleando el dispositivo comercial Salivette®, que posteriormente se centrifuga a 3000 rpm durante 10 minutos.

Una vez evaluada la ausencia de efecto matriz, la determinación de IFN-γ en las muestras se lleva a cabo por interpolación de la señal proporcionada por las muestras en el calibrado de disoluciones patrón.

Para validar los resultados obtenidos en ambos casos empleando el inmunosensor desarrollado se realiza también un inmunoensayo tipo ELISA de las muestras empleando los mismos reactivos, incluidos en el kit DuoSet® ELISA Development System (DY285B–05) de R&D Systems.

4.6.6. Determinación simultánea de factor de necrosis tumoral alfa e interleucina 1 beta en suero y saliva

En este caso, se analiza un suero humano liofilizado comercial, enriquecido con distintas concentraciones de TNF-α e IL-β y dos muestras de saliva humana pertenecientes a dos individuos sanos, un hombre fumador y una mujer no fumadora. La toma de muestra de saliva se lleva a cabo siguiendo el procedimiento descrito en el *Apartado 4.6.5.* de este capítulo.

Como en el caso anterior, una vez evaluada la ausencia de efecto matriz, la determinación de ambas citoquinas en las muestras se lleva a cabo por interpolación de las señales proporcionadas por las muestras en los calibrados de disoluciones patrón.

Finalmente, los resultados obtenidos se validan mediante un inmunoensayo tipo ELISA empleando los kits DuoSet® ELISA Development System DY210–05 y DY201–05 para la determinación de TNF-α e IL-β, respectivamente, empleados en la preparación del inmunosensor para la determinación de estas citoquinas.

4.6.7. Determinación de factor de crecimiento transformante beta 1 en saliva

La utilidad del inmunosensor desarrollado se demuestra mediante el análisis de cuatro muestras de saliva pertenecientes a dos individuos sanos fumadores y dos no fumadores. La toma de muestra de saliva se lleva a cabo como en casos anteriores.

Como anteriormente, una vez evaluada la ausencia de efecto matriz, la determinación de TGF-β1 en las muestras se lleva a cabo por interpolación de la señal proporcionada por las muestras en el calibrado de disoluciones patrón, comparándose los resultados obtenidos proporcionados por el inmunosensor con los proporcionados por un inmunoensayo tipo ELISA empleando los mismos biorreactivos, incluidos en el kit DuoSet® ELISA Development System (DY240–05) de R&D Systems.

4.6.8. Determinación de fetuina A humana en saliva

El inmunosensor desarrollado se aplica a la determinación de fetuina A humana en dos muestras de saliva pertenecientes a dos individuos sanos, un varón fumador y una mujer no fumadora. La toma de muestra de saliva se realiza de igual modo que anteriormente. En este caso, es necesario llevar a cabo una dilución 1/100 previa de la muestra con disolución reguladora PBS de pH 7.4 para evitar el efecto matriz. De este modo, la determinación de HFA en las muestras se lleva a cabo por interpolación de la señal proporcionada por las muestras en el calibrado de disoluciones patrón.

Los resultados obtenidos se validan mediante un inmunoensayo tipo ELISA empleando el kit DuoSet® ELISA Development System (DY1184) de R&D Systems.

5

Resultados y Discusión

5.1. INMUNOSENSOR BASADO EN EL EMPLEO DE UN POLÍMERO CONDUCTOR COMO MODIFICADOR DE LA SUPERFICIE ELECTRÓDICA

Como se ha señalado en la *Introducción* de esta Memoria, la utilidad de los polímeros conductores electrónicos para la preparación de biosensores de afinidad se centra en aquellos materiales que poseen grupos funcionales capaces de inmovilizar las biomoléculas mediante enlace covalente, uniendo esta propiedad a las demás ventajas de estos polímeros para su empleo en aplicaciones electroquímicas. Lamentablemente, existen muy pocos materiales que posean estas características. Uno de ellos, el ácido poli(pirrolpropiónico) (pPPA), es el empleado para construir la plataforma electródica y el inmunosensor que se describe a continuación.

5.1.1. Inmunosensor para la determinación de endoglina

Las propiedades de la CD105 y el interés que presenta su determinación ya han sido descritas en el *Apartado 3.3.2.2.2*. La relación que guardan las variaciones de concentración de esta proteína en suero humano y otros fluidos biológicos con el proceso de envejecimiento, en particular con la inflamación y enfermedades relacionadas, así como la escasez de métodos existentes para su determinación llevó a desarrollar en este trabajo el inmunosensor electroquímico que se describe a continuación, que satisface los niveles de sensibilidad y exactitud requeridos en la práctica clínica. Como se verá, la plataforma inmunosensora se desarrolló sobre electrodos desechables de carbono (SPCEs) modificados con pPPA electrodepositado y consiste en un esquema tipo sándwich empleando un anticuerpo secundario biotinilado marcado con un polímero de estreptavidina y peroxidasa, con el fin de obtener una señal amperométrica amplificada.

5.1.1.1. Configuración del inmunosensor

Las etapas implicadas en la preparación y el funcionamiento del inmunosensor electroquímico para la determinación de endoglina aparecen representadas esquemáticamente en la Figura 4.21 de la *Parte Experimental*. Tal como allí se describe, la inmovilización del anticuerpo anti-CD105 se realizó por unión covalente a los grupos carboxilo del polímero depositado en la superficie del electrodo. La determinación de endoglina se lleva a cabo amperométricamente a un potencial de reducción de –200 mV, empleando peróxido de hidrógeno como sustrato enzimático e hidroquinona como mediador redox (Figura 5.1).

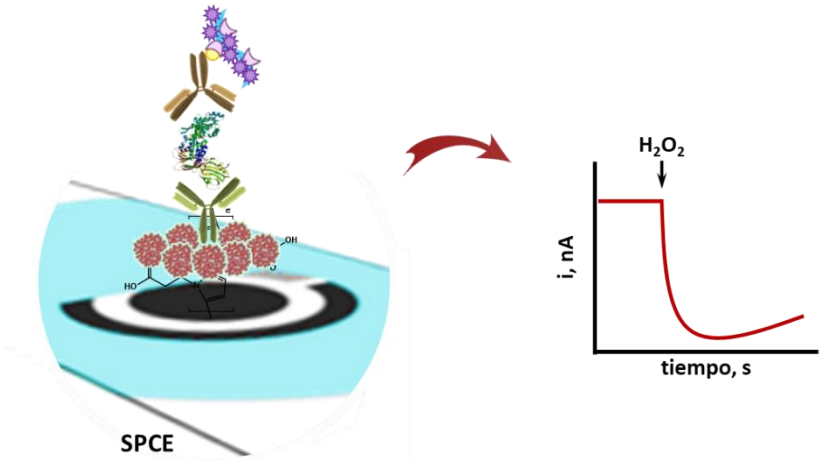

Figura 5.1. Esquema del funcionamiento del inmunosensor para la determinación de CD105

5.1.1.2. Optimización de las variables experimentales

Las variables implicadas en la preparación y el funcionamiento del inmunosensor se optimizaron con el objetivo de alcanzar la máxima sensibilidad y un amplio intervalo lineal para la determinación del biomarcador. Estas variables fueron: la concentración y el tiempo de incubación del anticuerpo de captura, las condiciones de la etapa de bloqueo, la concentración y el tiempo de incubación del anticuerpo de detección biotinilado y el tipo y dilución del conjugado enzimático. En cada caso, el criterio seguido para seleccionar el valor óptimo fue la obtención de la mayor relación (S/R) entre la corriente debida a la interacción específica (S), originada por la reacción de reconocimiento del antígeno por el anticuerpo, y la no específica (R). A

continuación, se describen los estudios de optimización realizados, resumiendo finalmente en la Tabla 5.1 los resultados obtenidos.

Influencia de la concentración y el tiempo de incubación del anticuerpo de captura

La concentración del anticuerpo inmovilizado sobre la superficie del electrodo juega un papel decisivo en la sensibilidad y el intervalo lineal del inmunoensayo. Para seleccionar la más adecuada se midieron las respuestas de varios inmunosensores preparados por deposición de 5 µL de disoluciones de anti-CD105 en concentración comprendida entre 5 y 17.5 µg/mL sobre la superficie del electrodo modificado con pPPA durante 60 minutos. Los resultados obtenidos aparecen representados en la Figura 5.2.

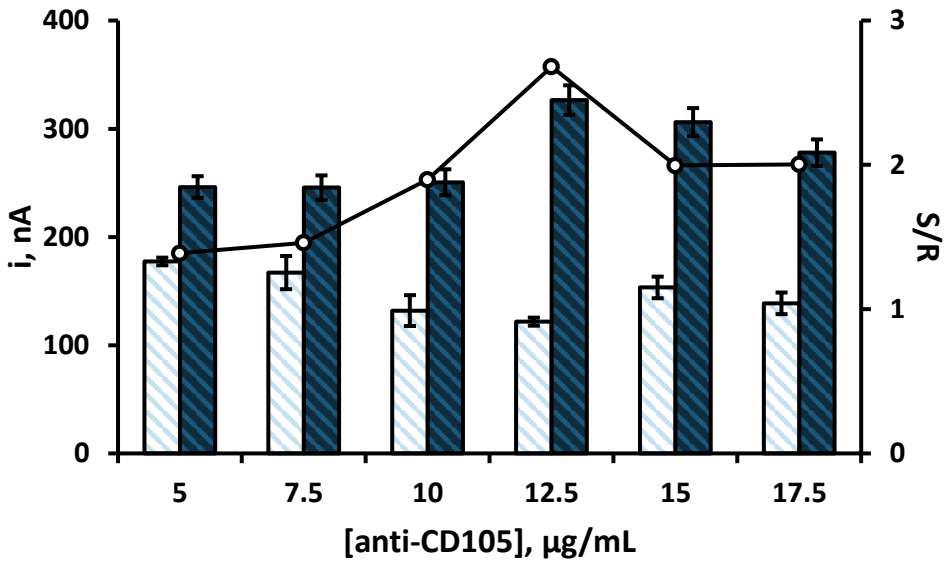

Figura 5.2. Efecto de la concentración de anti-CD105 sobre la respuesta del inmunosensor: ECD/NHSS, 100 mM, 10 µL, 30 min; anti-CD105, 5 µL, 60 min; Blocker™ Casein, 5 µL, 60 min; CD105, 0 (□) o 1 (■) ng/mL, 5 µL, 60 min; Biotin-anti-CD105, 2 µg/mL, 5 µL, 60 min; HRP-Strept, 1/1000, 5 µL, 20 min

Como puede observarse, la mayor relación entre las señales específica e inespecífica se obtiene para una concentración de anticuerpo de 12.5 µg/mL, por lo que este fue el valor seleccionado para estudios posteriores. Los valores más bajos de corriente en presencia de endoglina obtenidos para concentraciones de anticuerpo superiores al elegido pueden atribuirse al impedimento estérico originado en presencia de una cantidad excesiva de anticuerpo inmovilizado sobre la superficie

electródica, que dificulta la reacción de reconocimiento antígeno-anticuerpo [Eletxigerra, 2016].

En relación al tiempo de incubación (Figura 5.3), se observa que el valor óptimo es de 60 minutos, ya que se alcanza la mayor relación S/R.

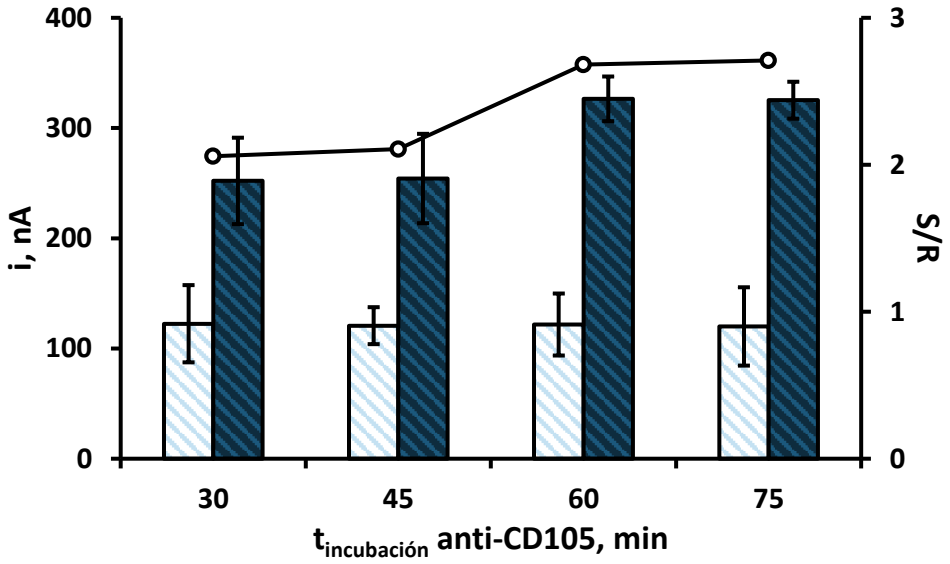

Figura 5.3. Efecto del tiempo de incubación del anti-CD105 sobre la respuesta del inmunosensor: ECD/NHSS, 100 mM, 10 µL, 30 min; anti-CD105, 12.5 µg/mL, 5 µL; Blocker™ Casein, 5 µL, 60 min; CD105, 0 (□) o 1 (■) ng/mL, 5 µL, 60 min; Biotin-anti-CD105, 2 µg/mL, 5 µL, 60 min; HRP-Strept, 1/1000, 5 µL, 20 min

Influencia de la etapa de bloqueo

Para evitar o, al menos, minimizar las adsorciones inespecíficas en la superficie del electrodo, que pueden llegar a incrementar notablemente la señal de fondo del inmunosensor, es necesario incorporar una etapa de bloqueo tras la inmovilización del anticuerpo de captura. En este caso se investigaron dos posibles agentes bloqueantes: caseína y BSA, por ser reactivos comúnmente empleados para esta aplicación, y se utilizaron dos concentraciones diferentes para cada uno de ellos. En la Figura 5.4 se han representado las respuestas obtenidas con distintos inmunosensores preparados en presencia de CD105 en disolución, así como las respuestas inespecíficas obtenidas en su ausencia. Como puede apreciarse, la mayor relación entre las señales específica e inespecífica se obtuvo al emplear un 1% de caseína (Blocker™ Casein) como agente bloqueante.

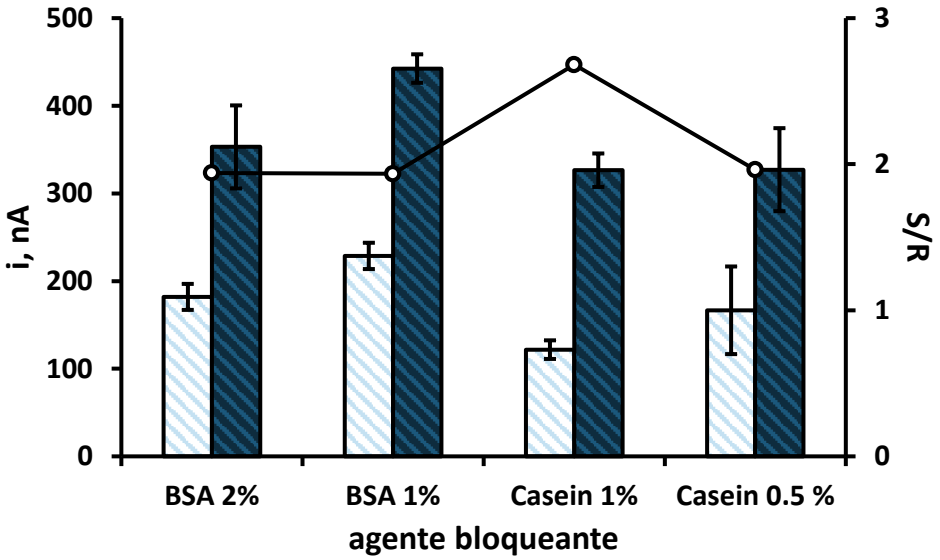

Figura 5.4. Efecto del agente bloqueante sobre la respuesta del inmunosensor: ECD/NHSS, 100 mM, 10 µL, 30 min; anti-CD105, 12.5 µg/mL, 5 µL, 60 min; agente bloqueante, 5 µL, 60 min; CD105, 0 (□) o 1 (■) ng/mL, 5 µL, 60 min; Biotin-anti-CD105, 2 µg/mL, 5 µL, 60 min; HRP-Strept, 1/1000, 5 µL, 20 min

En cuanto al tiempo de incubación del agente bloqueante (Figura 5.5), se observa que un tiempo de 30 minutos es suficiente para reducir al máximo la señal debida a las adsorciones inespecíficas, manteniendo la señal específica prácticamente constante. Tiempos de incubación superiores a 30 minutos hacen que la corriente debida a las señales específicas disminuya ligeramente. Por ello, dicho valor fue elegido para estudios posteriores.

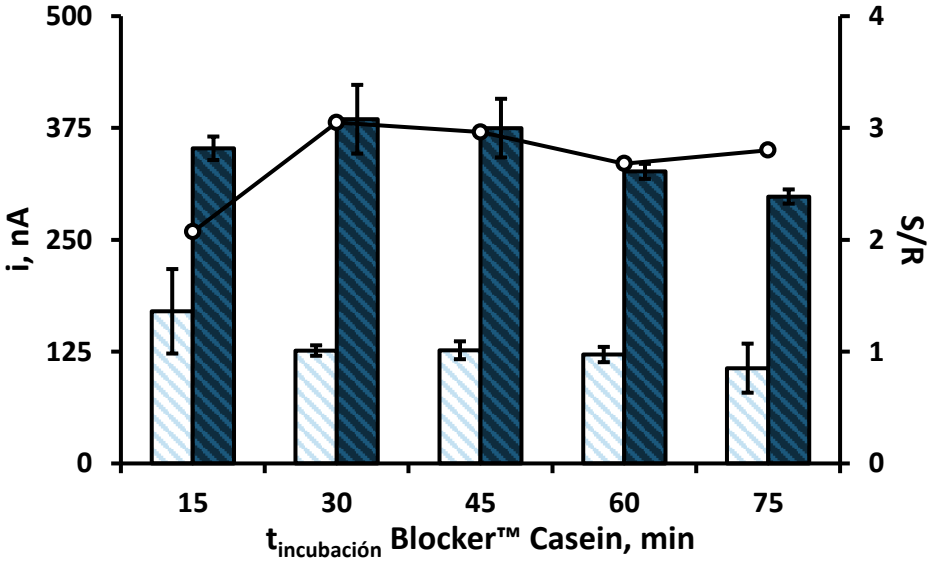

Figura 5.5. Efecto del tiempo de incubación del agente bloqueante sobre la respuesta del inmunosensor: ECD/NHSS, 100 mM, 10 µL, 30 min; anti-CD105, 12.5 µg/mL, 5 µL, 60 min; Blocker™ Casein, 5 µL; CD105, 0 (□) o 1 (■) ng/mL, 5 µL, 60 min; Biotin-anti-CD105, 2 µg/mL, 5 µL, 60 min; HRP-Strept, 1/1000, 5 µL, 20 min

Influencia de la concentración y el tiempo de incubación del anticuerpo de detección biotinilado

Este estudio se realizó preparando distintos inmunosensores con la concentración del anticuerpo de captura optimizada previamente y disoluciones de anticuerpo de detección conteniendo entre 1 y 4 µg/mL, en ausencia y en presencia de 1 ng/mL de CD105. La Figura 5.6 permite apreciar cómo la intensidad de corriente registrada aumenta a medida que lo hace la concentración de Biotin-anti-CD105, estabilizándose a partir de 2 µg/mL. Como puede observarse, para esta concentración se obtiene la mayor relación de señales específica a inespecífica, por lo que fue el valor seleccionado para la preparación del inmunosensor.

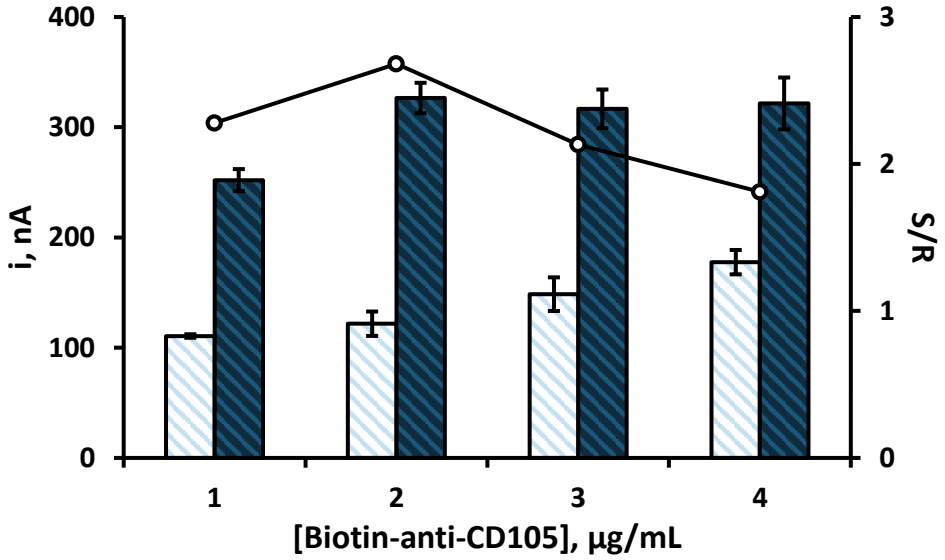

Figura 5.6. Efecto de la concentración de Biotin-anti-CD105 sobre la respuesta del inmunosensor: ECD/NHSS, 100 mM, 10 µL, 30 min; anti-CD105, 12.5 µg/mL, 5 µL, 60 min; Blocker™ Casein, 5 µL, 30 min; CD105, 0 (□) o 1 (■) ng/mL, 5 µL, 60 min; Biotin-anti-CD105, 5 µL, 60 min; HRP-Strept, 1/1000, 5 µL, 20 min

Con respecto al tiempo de incubación del anticuerpo de detección biotinilado, en la Figura 5.7 se han representado los resultados del estudio realizado, entre 30 y 75 minutos, que permiten concluir que un periodo de incubación de 45 minutos es adecuado para la preparación del inmunosensor, siendo asimismo algo superior la reproducibilidad de las medidas.

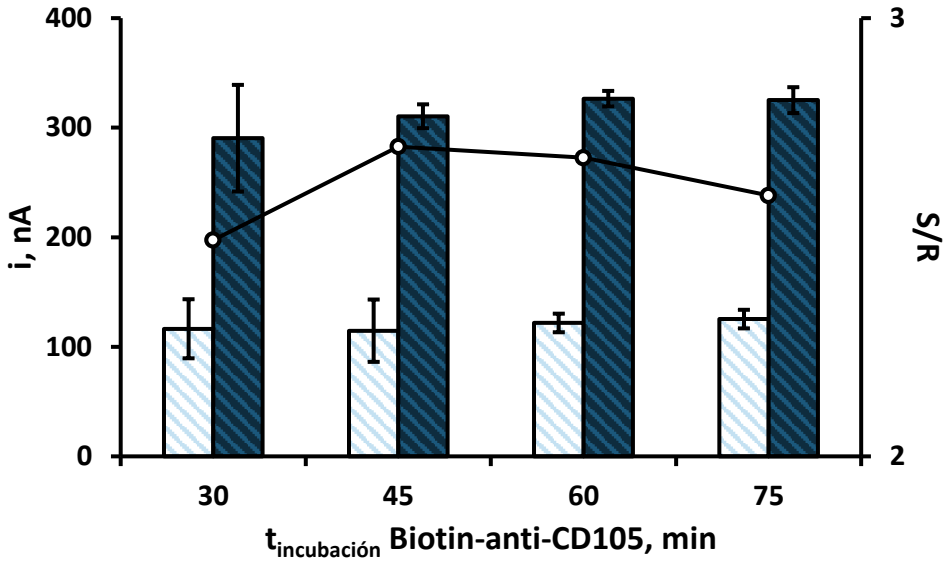

Figura 5.7. Efecto del tiempo de incubación de Biotin-anti-CD105 sobre la respuesta del inmunosensor: ECD/NHSS, 100 mM, 10 µL, 30 min; anti-CD105, 12.5 µg/mL, 5 µL, 60 min; Blocker™ Casein, 5 µL, 30 min; CD105, 0 (□) o 1 (■) ng/mL, 5 µL, 60 min; Biotin-anti-CD105, 2 µg/mL, 5 µL; HRP-Strept, 1/1000, 5 µL, 20 min

Influencia del tipo y la dilución del conjugado enzimático

Todas las optimizaciones anteriores se han realizado utilizando el conjugado HRP-Strept como etiqueta enzimática para la obtención de las respuestas electroquímicas del inmunosensor. Sin embargo, como se ha señalado, para la obtención de señales amperométricas de mayor magnitud, la configuración del inmunosensor desarrollado se completó utilizando un polímero de estreptavidina y peroxidasa (poli-HRP-Strept) en lugar del conjugado enzimático habitual (HRP-Strept). En la Figura 5.8, las respuestas obtenidas mediante el empleo del polímero empleando distintas diluciones, se comparan con la que se alcanza con el conjugado HRP-Strept en dilución 1/1000. Como puede observarse, en presencia del conjugado poli-HRP-Strept la señal específica aumenta notablemente, lo que puede atribuirse a la mayor carga enzimática, manteniéndose prácticamente constante la señal obtenida en ausencia de analito. En este caso, como óptima para la preparación del inmunosensor, se eligió la dilución 1/500.

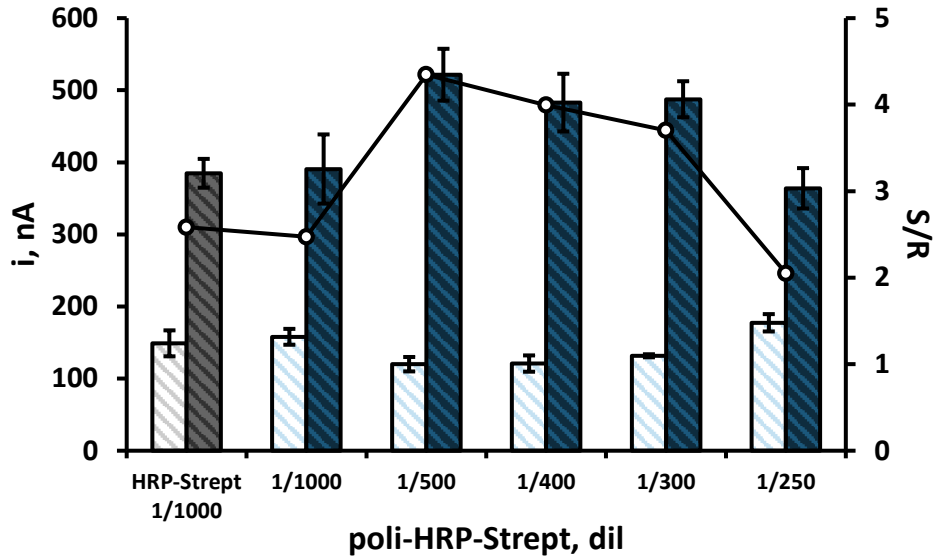

Figura 5.8. Efecto del tipo de conjugado enzimático sobre la respuesta del inmunosensor: ECD/NHSS, 100 mM, 10 µL, 30 min; anti-CD105, 12.5 µg/mL, 5 µL, 60 min; Blocker™ Casein, 5 µL, 30 min; CD105, 0 (□) o 1 (■) ng/mL, 5 µL, 60 min; Biotin-anti-CD105, 2 µg/mL, 5 µL, 60 min; conjugado enzimático, 5 µL, 20 min

Una vez estudiada la influencia de las variables que afectan a la preparación y el funcionamiento del inmunosensor, en la Tabla 5.1 se resumen los resultados obtenidos.

Tabla 5.1. Optimización de las variables experimentales implicadas en la construcción del inmunosensor poli-HRP-Strept-Biotin-anti-CD105-CD105-anti-CD105-pPPA/SPCE

VARIABLE EXPERIMENTAL	INTERVALO EVALUADO	VALOR SELECCIONADO
[anti-CD105], µg/mL	5 – 17.5	12.5
$t_{incubación}$ anti-CD105, min	30 – 75	60
agente bloqueante	Blocker™ Casein, BSA	Blocker™ Casein
Blocker™ Casein, %	0.5 – 1	1
$t_{incubación}$ Blocker™ Casein, min	15 – 75	30
[Biotin-anti-CD105], µg/mL	1 – 4	2
$t_{incubación}$ Biotin-anti-CD105, min	30 – 75	45
conjugado enzimático	HRP-Strept, poli-HRP-Strept	poli-HRP-Strept
HRP-Strept, dil	1/250 – 1/1000	1/500

5.1.1.3. Caracterización de la superficie electródica

Las etapas involucradas en la modificación de la superficie electródica se caracterizaron mediante espectroscopia de impedancia electroquímica sobre una disolución de $Fe(CN)_6^{3-/4-}$ 2 mM preparada en disolución reguladora PB 50 mM de pH 6.0.

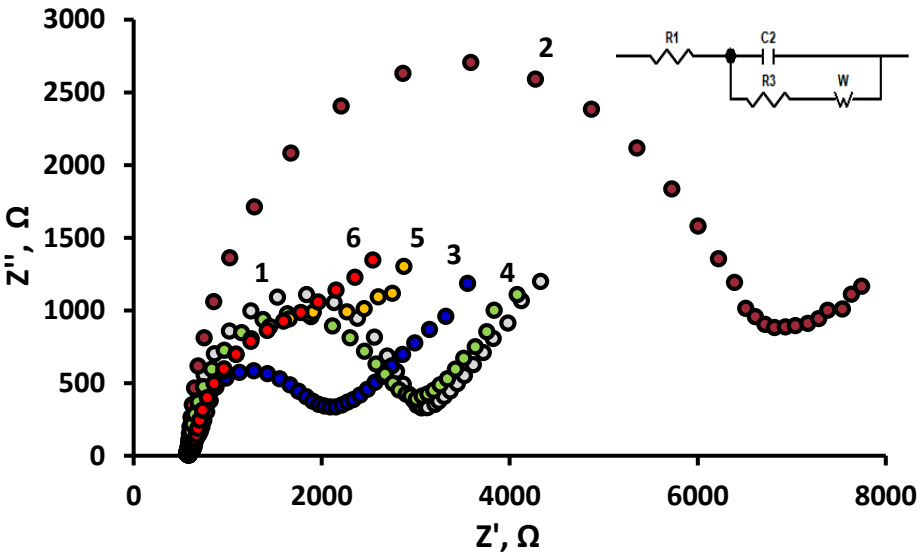

Figura 5.9. Diagramas de Nyquist registrados para: a) 1) SPCE, 2) pPPA/SPCE, 3) activación con EDC/NHSS, 4) anti-CD105-pPPA/SPCE, 5) bloqueo con Blocker™ Casein y 6) CD105-CD105-anti-CD105-pPPA/SPCE en una disolución $Fe(CN)_6^{3-/4-}$ 2 mM en PB 50 mM de pH 6.0

Los resultados obtenidos, representados en forma de espectros de Nyquist (Figura 5.9), muestran un aumento considerable de la resistencia a la transferencia de carga al modificar el electrodo serigrafiado, con R_{ct} = 2383 Ω (curva 1), obteniéndose un valor de R_{ct} = 5887 Ω para el electrodo pPPA/SPCE (curva 2). Este resultado es consecuencia de dos efectos: por un lado, la repulsión electrostática existente entre la sonda redox, aniónica, y los grupos carboxílicos presentes en el polímero, disociados al pH de trabajo y, por otro, a la baja conductividad relativa del polímero. Posteriormente, en la curva 3 se observa que la activación de los grupos carboxílicos con EDC/NHSS provoca una disminución drástica de R_{ct} (1331 Ω), que puede atribuirse a la neutralización de la carga negativa de los grupos carboxílicos confinados en la superficie del electrodo después de la reacción de activación. Como era de esperar, la resistencia R_{ct} aumenta notablemente después de la incorporación del anticuerpo de

captura (2180 Ω) debido al carácter aislante de la biomolécula inmovilizada sobre la superficie electródica. El bloqueo de las posiciones libres del electrodo con caseína origina un nuevo aumento en el valor de R_{ct} (2246 Ω) y, finalmente, tras la posterior incorporación del antígeno, este vuelve a incrementarse (2354 Ω), como corresponde a la interacción con el anticuerpo específico.

5.1.1.4. Calibrado y características analíticas

La Figura 5.10 muestra el calibrado construido con el inmunosensor desarrollado bajo las condiciones de trabajo optimizadas anteriormente empleando disoluciones estándar de CD105, así como algunas de las respuestas amperométricas utilizadas para su elaboración. Las barras de error se calcularon a partir de la desviación estándar de las medidas realizadas con tres inmunosensores diferentes. Como puede observarse, existe una relación lineal entre la intensidad de corriente registrada y el logaritmo de la concentración de CD105, entre 0.18 y 20 ng/mL, que se ajusta a la ecuación Δi, nA = (476 ± 12) log ([CD105], ng/mL) – (406 ± 1) (R^2 = 0.996), donde Δi es la diferencia entre la intensidad de corriente medida en ausencia y presencia del anticuerpo de captura [Serafín, 2017]. Este intervalo lineal, cubriendo más de dos órdenes de magnitud, es adecuado para la determinación de CD105 en muestras de suero, teniendo en cuenta las concentraciones esperadas, que se encuentran al nivel de ng/mL en este tipo de muestra [Takahashi, 2001]. El límite de detección, 140 pg/mL, se calculó como la concentración más baja que puede ser estadísticamente discriminada de la señal proporcionada por el blanco, de acuerdo con la expresión $\overline{x} + 3 \cdot s$, donde *s* es la desviación estándar calculada a partir de las respuestas amperométricas obtenidas para diez réplicas en ausencia de analito, en unidades de concentración, ng/mL.

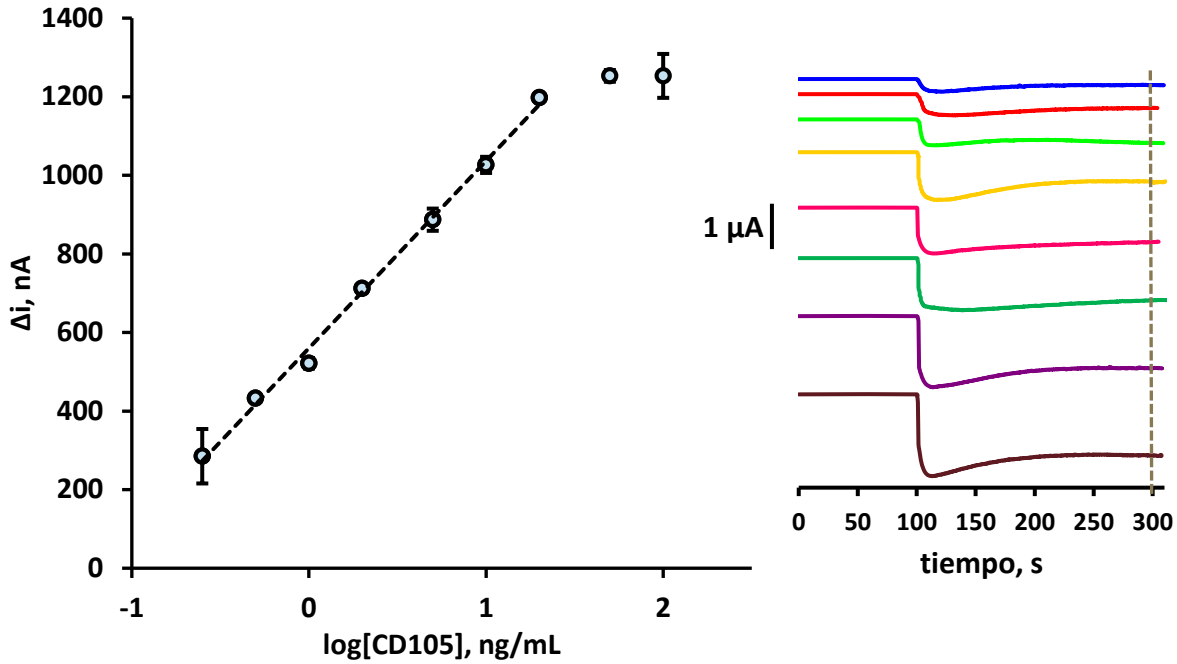

Figura 5.10. Calibrado para la determinación de CD105 empleando el inmunosensor poli-HRP-Strept-Biotin-anti-CD105-CD105-anti-CD105-pPPA/SPCE

Cuando se comparan las características analíticas del método propuesto con las de las dos únicas configuraciones descritas en la bibliografía, pueden extraerse algunas conclusiones. Por ejemplo, cabe destacar que la nueva configuración mejora el límite de detección del diseño propuesto por Zeng *et al.* [Zeng, 2012] con LOD = 900 pg/mL, que requiere además largos tiempos de preparación. Asimismo, dichas características son también ligeramente mejores que las obtenidas empleando un inmunosensor basado en partículas magnéticas carboxiladas como sustrato para la inmovilización del anticuerpo de captura [Torrente-Rodríguez, 2016] y que posee un intervalo lineal comprendido entre 0.8 y 10 ng/mL, con un límite de detección de 200 pg/mL.

5.1.1.5. Estudio de selectividad

En este apartado se ha evaluado el efecto sobre la respuesta del inmunosensor de la presencia de otros compuestos, especialmente otras proteínas, que pueden coexistir con la CD105 en suero humano. Para ello se han comparado las señales amperométricas proporcionadas por distintos inmunosensores preparados con 0 y 1 ng/mL de CD105, en ausencia y en presencia de los siguientes compuestos: albúmina

de suero bovino (BSA), inmunoglobulina G humana (hIgG), hemoglobina (HB), factor de crecimiento transformante beta 1 (TGF-β1), interleucina 6 (IL-6), interleucina 1 beta (IL-1β), E-cadherina (E-Cad), ácido úrico (UA), ácido ascórbico (AA), proteína recombinante ErbB2 humana (ErbB2), proteína recombinante p53 humana de longitud completa (p53), receptor de cadherina-17 (Cad17R) y receptor de factor de crecimiento de fibroblastos 4 (FGFR4).

Los resultados mostrados en la Figura 5.11 ponen de manisfiesto que niguno de estos compuestos da lugar a una interferencia significativa en la determinación de CD105 a los niveles de concentracion ensayados, demostrando así la alta selectividad de la configuración desarrollada.

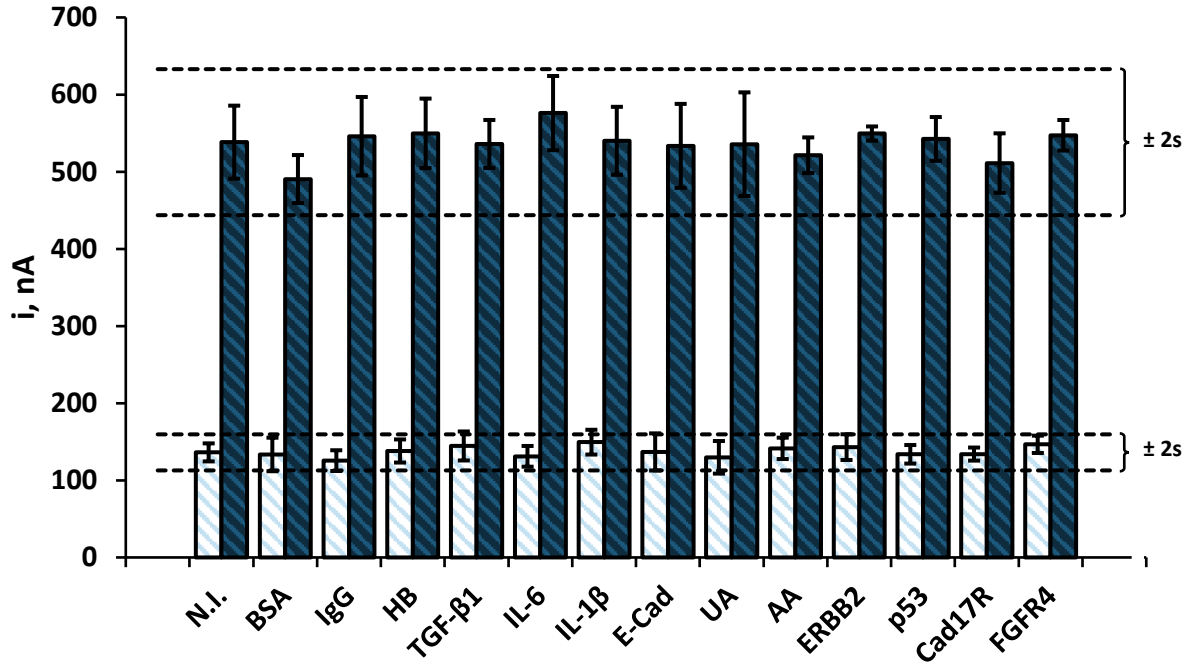

Figura 5.11. Selectividad del inmunosensor poli-HRP-Strept-Biotin-anti-CD105-CD105-anti-CD105-pPPA/SPCE evaluando la respuesta del mismo con 0 (□)o 1 (■) ng/mL de CD105 fente a 5 mg/mL de BSA, 1 mg/mL de hIgG, 5 mg/mL de HB, 50 ng/mL de TGF-β1, 300 pg/mL de IL-6, 50 pg/mL de IL-1β, 55 ng/mL de E-Cad, 100 µg/mL de UA, 7 µg/mL de AA, 15 ng/mL de ErbB2, 200 pg/mL de p53, 55 ng/mL de Cad17R y 1 ng/mL de FGFR4

5.1.1.6. Estudios de reproducibilidad y estabilidad

La repetibilidad de las medidas amperométricas y la reproducibilidad del procedimiento de preparación del inmunosensor se estudiaron investigando las

respuestas de distintos inmunosensores en ausencia y presencia de 1 ng/mL de CD105, preparados en el mismo día o en días diferentes. En estas condiciones se obtuvieron, en el primer caso, valores de RSD del 3.8 y 5.2%, respectivamente, y del 4.9 y 5.7% para inmunosensores preparados en distintos días. Estos resultados ponen de manifiesto la buena precisión de las medidas y del procedimiento completo de preparación del inmunosensor.

Por otro lado, se evaluó la estabilidad del inmunoconjugado anti-CD105-pPPA/SPCE preparando en el mismo día distintos electrodos modificados con el anticuerpo de captura que, tras el bloqueo de las posiciones libres de la superficie electródica con un 1% de caseína (Blocker™ Casein), se almacenaron en seco a –20°C. Después, de forma sucesiva, cada día de trabajo se prepararon tres inmunosensores a partir de los electrodos modificados con el inmunoconjugado previamente almacenados y se realizaron las medidas de la respuesta amperométrica para 1 ng/mL de CD105.

En la Figura 5.12 se ha representado el gráfico de control en el que los márgenes establecidos corresponden a ± 3 veces la desviación estándar de las medidas realizadas el primer día de trabajo. Como puede observarse, la media de las tres medidas realizadas cada día se encuentra dentro del intervalo establecido el primer día durante al menos 43 días, lo que demuestra la excelente estabilidad de almacenamiento de los inmunoconjugados anti-CD105-pPPA/SPCE en las condiciones indicadas.

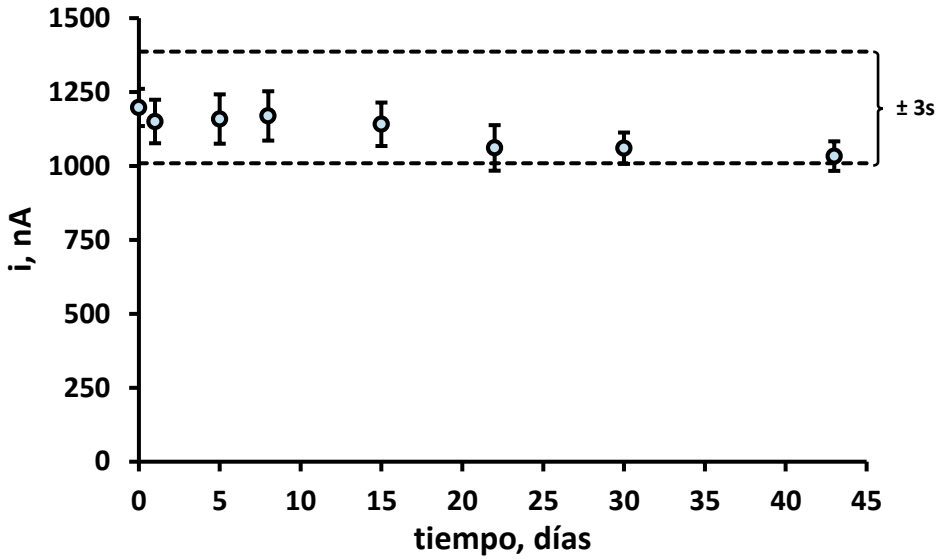

Figura 5.12. Gráfico de control para la evaluación de la estabilidad de almacenamiento del conjugado anti-CD105-pPPA/SPCE

5.1.1.7. Aplicación a la determinación de endoglina en suero

Se sabe que la endoglina juega un papel relevante en diversas enfermedades. A su relación con los procesos de envejecimiento hay que añadir que las variaciones de su concentración también permiten monitorizar procesos cancerosos y una enfermedad rara, la epidermólisis bullosa. En este trabajo, con el fin de demostrar la utilidad del inmunosensor desarrollado, se analizaron diferentes muestras de suero humano procedentes de individuos sanos y de pacientes con cáncer colorrectal, con cáncer de mama, con cáncer de pulmón y con epidermólisis bullosa.

Primeramente, se evaluó la posible existencia de efecto matriz comparando la pendiente de la curva de calibrado correspondiente a disoluciones estándar de CD105 con las pendientes de calibrado obtenidas al suplementar distintas diluciones de suero humano (0, 1/2, 1/3, 1/5, 1/10, 1/50 y 1/100) en disolución reguladora PBS de pH 7.4. De este modo, la ausencia de diferencias significativas entre los valores de la pendiente de la curva de calibrado obtenida para los estándares de CD105 en disolución reguladora (476 ± 12) nA y para las muestras 50 veces diluidas de suero de individuos sanos (475 ± 8) nA, con cáncer de mama (477 ± 7) nA y epidermólisis bullosa

(470 ± 30) nA, demostró que esta dilución es suficiente para evitar el efecto matriz. Por lo tanto, la determinación de CD105 puede llevarse a cabo por interpolación de la señal proporcionada por las muestras, tras una dilución 1/50 de las mismas, en el calibrado de disoluciones estándar, sin que sea necesario aplicar ningún otro tratamiento adicional a la muestra.

Los resultados obtenidos, por triplicado, empleando el inmunosensor se compararon con los proporcionados por el kit DuoSet® ELISA Development System (DY1097) de R&D Systems basado en el empleo de los mismos inmunoreactivos. En la gráfica de la Figura 5.13, se aprecian claramente las diferencias entre la concentración de CD105 de los sueros procedentes de individuos sanos y la de los pacientes con cáncer o epidermólisis bullosa.

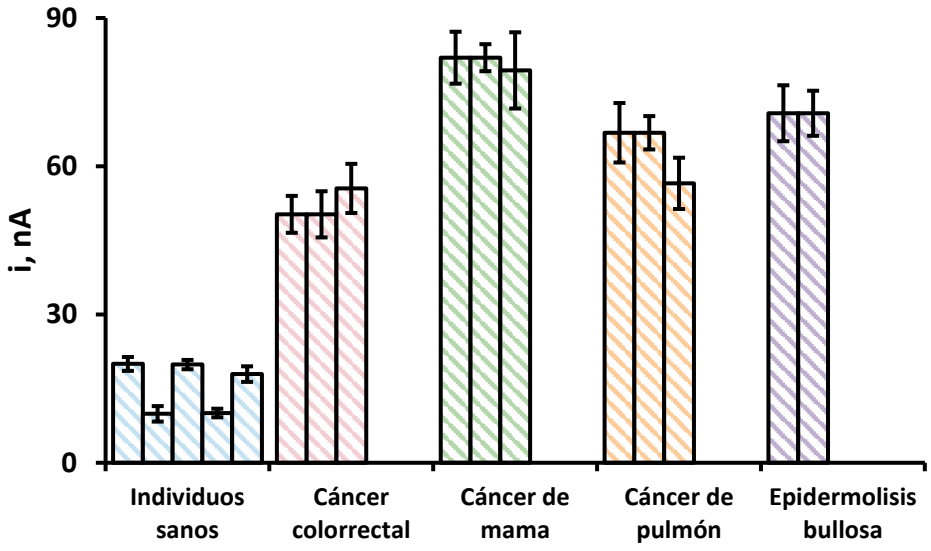

Figura 5.13. Concentraciones de CD105 encontradas en las muestras de suero analizadas empleando el inmunosensor poli-HRP-Strept-Biotin-anti-CD105-CD105-anti-CD105-pPPA/SPCE. Las barras de error se han estimado como ±3s, donde s es la desviación estándar relativa de las medidas por triplicado

Como se puede observar en la Tabla 5.2, no existen diferencias significativas entre los resultados obtenidos por ambos métodos. Esta afirmación se verificó mediante la representación de las concentraciones medias obtenidas con el inmunosensor para cada una de las muestras frente a las proporcionadas por el inmunoensayo ELISA, lo que dio como resultado una recta (R^2 = 0.998) de pendiente 1.01 ± 0.02 y ordenada en el origen –0.8 ± 1.0. La excelente correlación encontrada

con los intervalos de confianza para los valores de pendiente y ordenada en el origen (a un nivel de significación del 0.05), incluyendo el 1 y el 0, respectivamente, indicaron que la metodología desarrollada no presenta errores sistemáticos.

Tabla 5.2. Determinación de CD105 en muestras de suero empleando el inmunosensor poli-HRP-Strept-Biotin-anti-CD105-CD105-anti-CD105-pPPA/SPCE

MUESTRA	INMUNOSENSOR ng/mL (*n* = 3)*	ELISA ng/mL (*n* = 3)*
individuo sano 1	19 ± 2	20 ± 2
individuo sano 2	12 ± 2	10 ± 2
individuo sano 3	20 ± 1	20 ± 1
individuo sano 4	11 ± 1	10 ± 1
individuo sano 5	18 ± 2	18 ± 2
cáncer colorectal 1	50 ± 4	50 ± 4
cáncer colorectal 2	64 ± 3	67 ± 5
cáncer colorectal 3	57 ± 5	56 ± 5
cáncer de mama 1	81 ± 1	82 ± 5
cáncer de mama 2	86 ± 5	89 ± 3
cáncer de mama 3	84 ± 4	79 ± 8
cáncer de pulmón 1	67 ± 5	67 ± 6
cáncer de pulmón 2	59 ± 4	59 ± 3
cáncer de pulmón 3	58 ± 3	57 ± 5
epidermolisis bullosa 1	71 ± 5	71 ± 6
epidermolisis bullosa 2	75 ± 9	76 ± 5

* valor medio ± t·s/Vn

5.1.1.8. Conclusiones

En este trabajo se ha descrito la preparación y el funcionamiento de un inmunosensor integrado para la determinación de CD105, basado en la inmovilización covalente del anticuerpo de captura sobre la superficie de un electrodo serigrafiado de carbono modificado con pPPA empleando la química del EDC/NHSS.

El inmunosensor amperométrico posee atractivas características analíticas en términos de sensibilidad, selectividad y estabilidad. Si bien el límite de detección alcanzado es similar al del método ELISA, sin embargo, es importante mencionar que, con el inmunosensor, la determinación se puede realizar en un tiempo mucho menor (135 minutos frente a 280 minutos), una vez inmovilizado el anticuerpo de captura y realizado el bloqueo en ambos casos.

La simplicidad, rapidez, bajo coste, portabilidad y capacidad de multiplexado de la metodología desarrollada para la cuantificación de CD105 a bajas concentraciones en muestras complejas sin aplicar alguno salvo la dilución, la hacen más compatible con los requisitos clínicos que los métodos disponibles actualmente para la determinación de este biomarcador. Por ello, se considera que el inmunosensor desarrollado podría emplearse como dispositivo de control en el punto de atención para llevar a cabo la determinación de este analito en entornos de recursos limitados (clínicas ambulatorias, junto a las camas de los pacientes o en el propio hogar), fuera de los laboratorios de análisis clínicos centralizados.

5.2. INMUNOSENSORES BASADOS EN LA MODIFICACIÓN DE LA SUPERFICIE ELECTRÓDICA CON NANOMATERIALES DE CARBONO

Dentro de este apartado se presentan los resultados obtenidos en la determinación de 8-isoprostano (ISO) basada en la modificación electródica con nanocuernos de carbono, en la de adiponectina (APN) sobre un electrodo modificado con el nanomaterial híbrido de óxido de grafeno reducido y carboximetilcelulosa y, finalmente, en la de factor de crecimiento transformante beta 1 (TGF-β1) basada en la inmovilización del anticuerpo de captura, mediante una reacción tipo *"click"*, sobre superficies electródicas modificadas con nanotubos de carbono de pared múltiple.

5.2.1. Inmunosensor para la determinación de 8-isoprostano

Como ya se ha comentado en la *Introducción*, los isoprostanos son marcadores estables del estrés oxidativo, formados *in situ* a partir de los fosfolípidos de la membrana celular, siendo el 8-isoprostano el biomarcador más apropiado para evaluar el daño oxidativo *in vivo* producido en el organismo.

El inmunosensor puesto a punto en este trabajo es el primero descrito en la bibliografía para esta aplicación. La configuración propuesta implica la modificación de la superficie electródica con nanocuernos de carbono (CNHs) oxidados, que contienen una alta concentración de restos carboxílicos aprovechados para la posterior unión covalente del anticuerpo de captura. Tras la modificación del electrodo, se establece un inmunoensayo de tipo competitivo entre el analito y el mismo marcado con la enzima peroxidasa. El inmunosensor resultante permite la obtención de un calibrado con un intervalo de linealidad adecuado para llevar a cabo la determinación de este analito en muestras de suero, siendo límite de detección de 12 pg/mL.

5.2.1.1. Configuración del inmunosensor

Las etapas implicadas en la preparación y funcionamiento del inmunosensor electroquímico desarrollado para la determinación de 8-isoprostano aparecen representadas de forma esquemática en la Figura 4.22 de la *Parte Experimental*. Primeramente, se inmoviliza el anticuerpo anti-ISO sobre el electrodo serigrafiado de carbono previamente modificado con CNHs carboxilados, se bloquea con BSA y se establece un inmunoensayo tipo competitivo directo entre el antígeno (ISO) y el antígeno marcado con la enzima (HRP-ISO) (Figura 5.14). La detección electroquímica se lleva a cabo empleando hidroquinona como mediador redox y peróxido de hidrógeno como sustrato enzimático, registrándose la señal amperométrica aplicando un potencial de reducción de –200 mV.

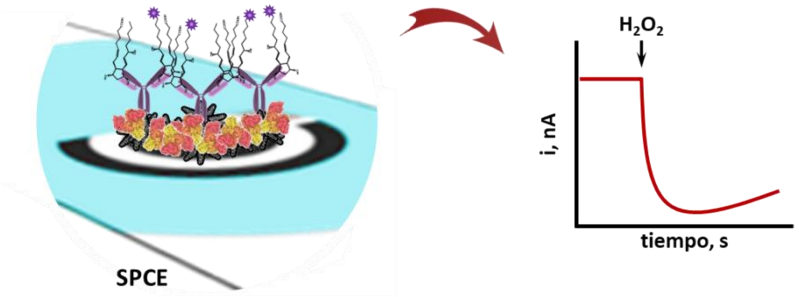

Figura 5.14. Esquema del funcionamiento del inmunosensor para la determinación de ISO

5.2.1.2. Optimización de las variables experimentales

Como en otros estudios, el criterio elegido para la optimización de las variables experimentales fue la mayor relación obtenida entre las respuestas amperométricas de los inmunosensores preparados en ausencia y en presencia de 0.75 y 1.5 ng/mL de ISO.

Influencia de la dilución del anticuerpo de captura inmovilizado

La carga del anticuerpo de captura (anti-ISO) inmovilizada sobre la superficie del electrodo de trabajo modificado con CNHs carboxilados se optimizó midiendo la respuesta amperométrica de diferentes inmunosensores preparados con disoluciones de anti-ISO a dilución entre 1/200 y 1/1200 con empleando disoluciones del antígeno

de diferentes concentraciones (0, 0.75 o 1.5 ng/mL) que compiten con disoluciones del antígeno marcado de dilución 1/100. En la Figura 5.15 se muestran los resultados obtenidos. Las barras de error corresponden a la desviación estándar obtenida para cada medida por triplicado.

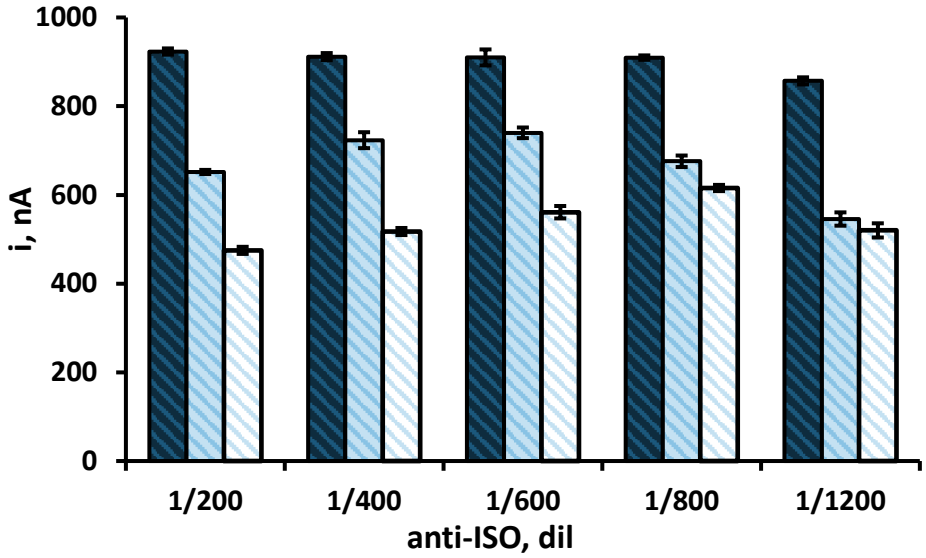

Figura 5.15. Efecto de la dilución de anti-ISO sobre la respuesta del inmunosensor: HOOC-CNHs, 0.5 mg/mL, 10 µL; ECD/NHSS, 100 mM, 5 µL, 30 min; anti-ISO, 5 µL, 60 min; BSA, 2%, 5 µL, 30 min; ISO, 0 (■), 0.75 (▨) y 1.5 (□) ng/mL + HRP-ISO, 1/100, 5 µL; 60 min

Como se puede observar, las corrientes medidas con los inmunosensores en ausencia de analito no varían con la carga de anti-ISO hasta llegar a una dilución 1/800, mostrando una ligera disminución para diluciones superiores, lo que indica la saturación de la superficie del electrodo con el anticuerpo. Además, a pesar de que se emplea una concentración relativamente alta de HRP-ISO (dilución 1/100), existe una buena competición entre el antígeno y el antígeno marcado por los sitios de unión del anticuerpo de captura, lo que da lugar a una disminución significativa de la corriente para una concentración de antígeno de 0.75 y 1.5 ng/mL. Sin embargo, se observan mayores cambios en la corriente registrada para diferentes concentraciones de antígeno, a diluciones de anticuerpo de captura inferiores a 1/800, lo que puede atribuirse a la mayor concentración de anticuerpo inmovilizado en la superficie del electrodo a la que es capaz de unirse el antígeno. Dado que diluciones 1/200, 1/400 y 1/600 del anticuerpo proporcionan resultados similares y con el fin de evitar un gasto

excesivo de anticuerpo en el ensayo, se seleccionaron las dos diluciones mayores de anticuerpo (1/400 y 1/600) para estudios posteriores.

Con respecto al tiempo de incubación del anticuerpo de captura sobre la superficie del electrodo de trabajo, se comprobó que un tiempo de 60 minutos es adecuado para obtener una buena sensibilidad.

Influencia de la dilución de antígeno marcado con la enzima

La concentración de antígeno marcado, HRP-ISO, utilizada para la competición con el antígeno analito se optimizó (Figura 5.16) estudiando la respuesta de diferentes inmunosensores preparados con diluciones 1/600 o 1/400 de anti-ISO y concentraciones de 0, 0.75 y 1.5 ng/mL de ISO, así como diluciones de HRP-ISO entre 1/100 y 1/1000. Como era de esperar, para ambas diluciones de anticuerpo (Figura 5.16a y 5.16b), las corrientes obtenidas para una concentración fija de antígeno disminuyen a medida que lo hace la concentración de HRP-ISO. En cuanto a la competición entre el antígeno y el mismo marcado con HRP, puede observarse que la mayor relación de señales se obtiene para diluciones 1/500 y 1/200 de HRP-ISO y diluciones 1/600 y 1/400 de anti-ISO, respectivamente.

Como se ha visto, existe una estrecha relación entre las concentraciones de anti-ISO y HRP-ISO como corresponde al tipo de configuración competitiva desarrollada en este caso. Por ello, la optimización final de ambas variables, orientada a elegir las condiciones adecuadas que permitan determinar concentraciones más bajas de ISO se realizó obteniendo calibrados para concentraciones de antígeno entre 0 y 200 pg/mL y distintas diluciones de anti-ISO y HRP-ISO (no representados). Las ecuaciones de la porción lineal de dichos calibrados proporcionaron valores de las pendientes de 0.85 ± 0.02 nA mL/pg y 0.46 ± 0.05 nA mL/pg para diluciones 1/500 de HRP-ISO y 1/600 de anti-ISO y para 1/200 de HRP-ISO y 1/400 de anti-ISO, respectivamente. Según estos resultados, las condiciones elegidas como óptimas para la preparación del inmunosensor fueron una dilución 1/500 de HRP-ISO y 1/600 de anti-ISO.

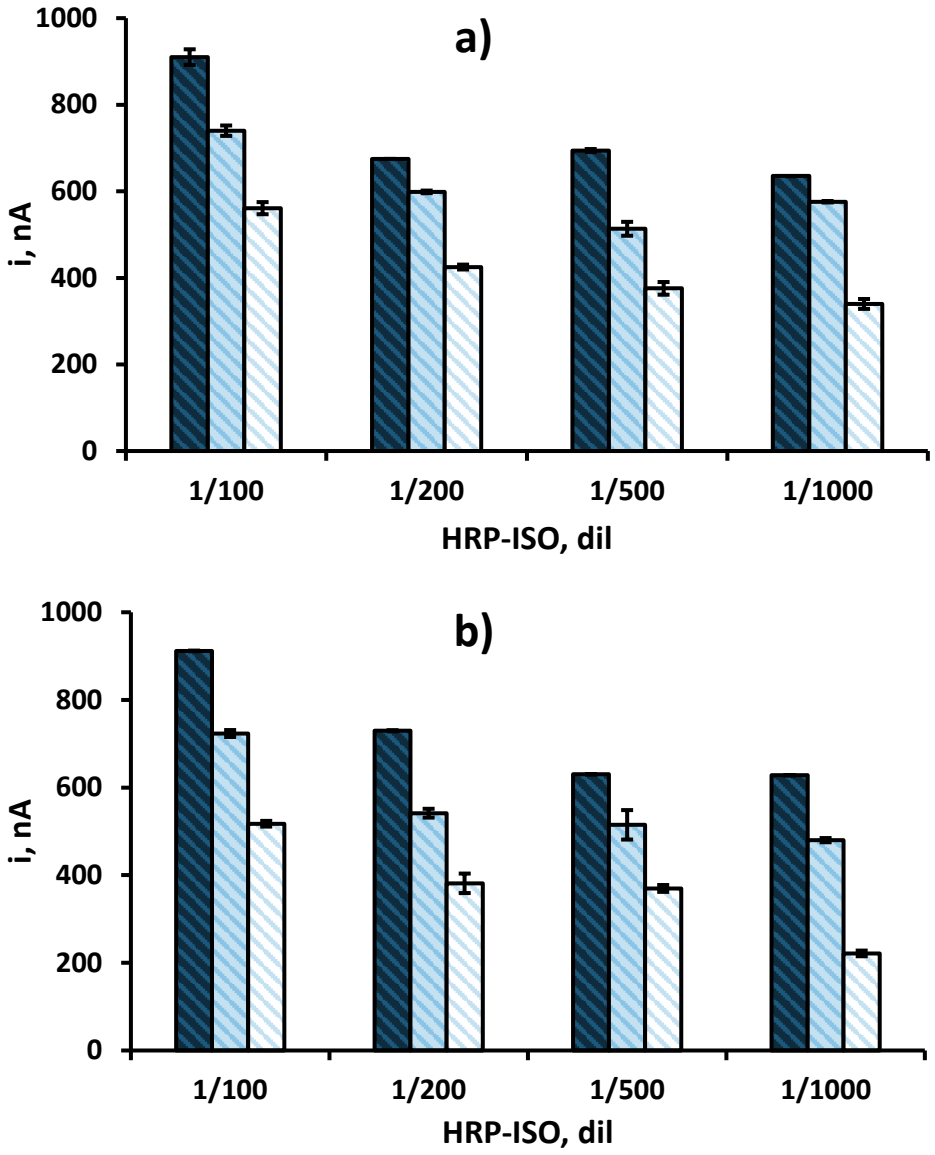

Figura 5.16. Efecto de la dilución de HRP-ISO sobre la respuesta del inmunosensor: HOOC-CNHs, 0.5 mg/mL, 10 µL; ECD/NHSS, 100 mM, 5 µL, 30 min; anti-ISO; a) 1/600 o b) 1/400, 5 µL, 60 min; BSA, 2%, 5 µL, 30 min; ISO, 0 (■), 0.75 (▨) y 1.5 (▨) ng/mL + HRP-ISO, 5 µL, 60 min

Influencia de la etapa de bloqueo

Con el objetivo de minimizar las adsorciones no específicas de inmunorreactivos sobre las posiciones libres de la superficie electródica, se aplicó una etapa de bloqueo empleando BSA, caseína y leche en polvo, agentes bloqueantes comunes en estas aplicaciones, estudiando su influencia en la respuesta del inmunosensor preparado en ausencia y en presencia de ISO. En cada caso se depositaron 5 µL de cada solución de bloqueo sobre el electrodo previamente modificado con el anticuerpo de captura (dilución 1/600) y, a continuación, una

dilución 1/500 de HRP-ISO con 0 o 500 pg/mL de antígeno. Los resultados obtenidos se muestran en la Figura 5.17. Como puede observarse, la mayor diferencia entre la señal específica e inespecífica se obtuvo utilizando BSA al 2% (p/v). Además, se demostró que un tiempo de incubación de 30 minutos era suficiente para garantizar un bloqueo efectivo.

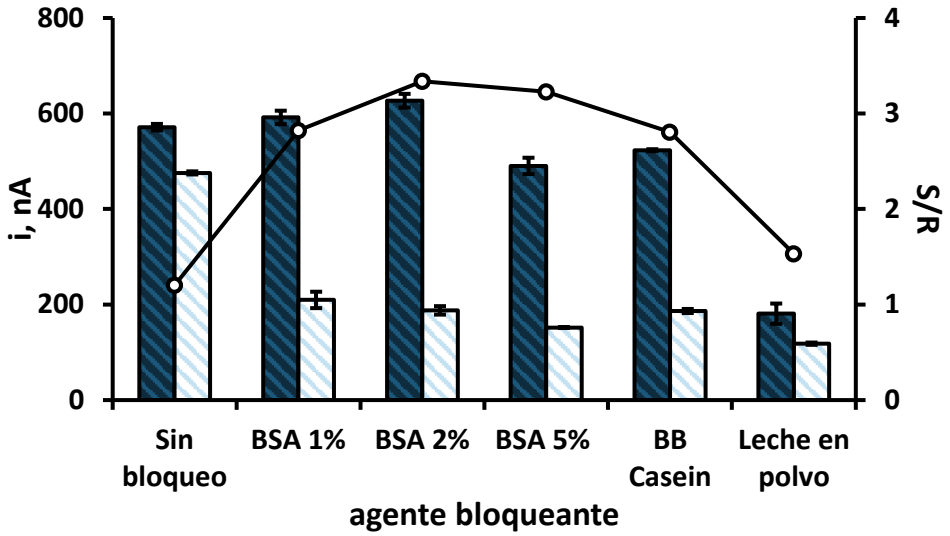

Figura 5.17. Efecto del agente bloqueante sobre la respuesta del inmunosensor: HOOC-CNHs, 0.5 mg/mL, 10 µL; ECD/NHSS, 100 mM, 5 µL, 30 min; anti-ISO; 1/600, 5 µL, 60 min; agente bloqueante, 5 µL, 30 min; ISO, 0 (■) y 0.5 (□) ng/mL + HRP-ISO, 1/500, 5 µL, 60 min

Influencia del tiempo de competición entre el antígeno y el antígeno marcado con la enzima

El tiempo de competición es el intervalo de tiempo durante el cual el antígeno y el antígeno marcado con la enzima compiten por los sitios de unión del anticuerpo. La adecuada elección de esta variable es determinante ya que condiciona, en gran medida, la respuesta del inmunosensor. Por ello, se optimizó en el intervalo de 15 a 60 minutos, obteniéndose los resultados que se muestran en la Figura 5.18.

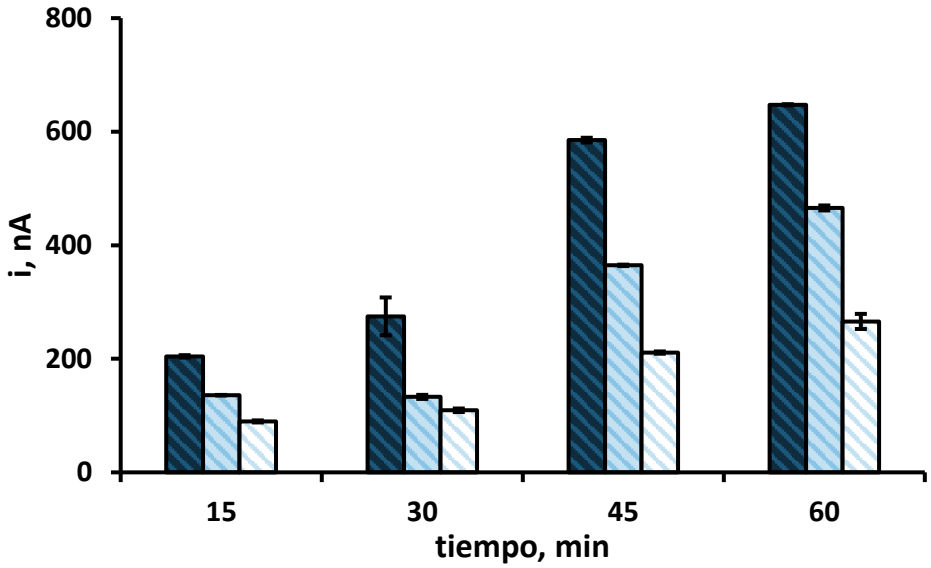

Figura 5.18. Efecto del tiempo de competición entre ISO y HRP-ISO sobre la respuesta del inmunosensor: HOOC-CNHs, 0.5 mg/mL, 10 µL; ECD/NHSS, 100 mM, 5 µL, 30 min; anti-ISO; 1/600, 5 µL, 60 min; BSA, 2%, 5 µL, 30 min; ISO, 0 (■), 0.75 (▨) y 1.5 (□) ng/mL + HRP-ISO, 1/500, 5 µL

Como puede observarse, las corrientes registradas para una misma concentración de ISO aumentan con el tiempo de incubación de la mezcla sobre el electrodo anti-ISO-HOOC-CNHs/SPCE. Sin embargo, la relación entre las señales obtenidas en ausencia y en presencia de la misma concentración de ISO es mayor para un tiempo de competición de 45 minutos. Por este motivo, se eligió este valor como óptimo, lo que permitió asimismo acortar el tiempo de ensayo.

Finalmente, a modo de resumen, en la Tabla 5.3 se recogen las variables estudiadas, así como los intervalos evaluados y los valores seleccionados en cada caso para estudios posteriores. La optimización de las variables relacionadas con la modificación del electrodo con el nanomaterial de carbono se realizó en investigaciones anteriores llevadas a cabo en nuestro grupo de investigación [Ojeda, 2014].

Tabla 5.3. Optimización de las variables experimentales implicadas en la construcción del inmunosensor HRP-ISO-anti-ISO-HOOC-CNHs/SPCE

VARIABLE EXPERIMENTAL	INTERVALO EVALUADO	VALOR SELECCIONADO
anti-ISO, dil	1/200 – 1/1200	1/600
HRP-ISO, dil	1/100 – 1/1000	1/500
$t_{competición}$ ISO + HRP-ISO, min	10 – 60	45
agente bloqueante	BSA, Blocker™ Casein, leche en polvo	BSA
BSA, %	1, 2, 5	2

5.2.1.3. Caracterización de la superficie electródica

La monitorización de las diferentes etapas involucradas en la preparación del inmunosensor se realizó mediante espectroscopia de impedancia electroquímica (EIS). La Figura 5.19a muestra los diagramas de Nyquist registrados para el electrodo serigrafiado de carbono desnudo (SPCE), el modificado con los nanocuernos de carbono carboxilados (HOOC-CNHs/SPCE), el modificado con el anticuerpo de captura (anti-ISO-CNHs/SPCE) y para el inmunosensor completo (HRP-ISO-anti-ISO-CNHs/SPCE) utilizando como sonda redox una disolución de $Fe(CN)_6^{3-/4-}$ 5mM en KCl 100 mM de pH 7.0.

Como era de esperar, la resistencia a la transferencia de carga en el electrodo desnudo es notablemente mayor (R_{ct} = 284 Ω) que la obtenida para el electrodo modificado con los nanocuernos de carbono (R_{ct} = 15 Ω). Esto es debido a la elevada conductividad eléctrica de este material. Al modificar la superficie electródica con el anticuerpo de captura, la resistencia aumenta ligeramente (R_{ct} = 45 Ω), como consecuencia del efecto aislante de las biomoléculas inmovilizadas. Finalmente, la inmovilización del antígeno marcado con la enzima condujo a un aumento adicional de la resistencia (R_{ct} = 338 Ω), debido al carácter aislante del bioconjugado.

En la Figura 5.19b se muestran los voltamperogramas cíclicos para las mismas superficies y en el mismo medio. Como puede observarse, los resultados son

consistentes con los obtenidos por EIS. Así, se observó un aumento notable en los valores de la corriente de pico de oxidación y reducción del par redox $Fe(CN)_6^{3-/4-}$ cuando la superficie del electrodo se modificó con los nanocuernos de carbono, mientras que la inmovilización del anticuerpo de captura sobre la superficie electródica y la formación de inmunocomplejos con el antígeno marcado con la enzima produjeron ligeras disminuciones de las corrientes de pico debido al bloqueo parcial de la superficie electródica. Estos resultados permiten confirmar la modificación del electrodo y la inmovilización de las biomoléculas.

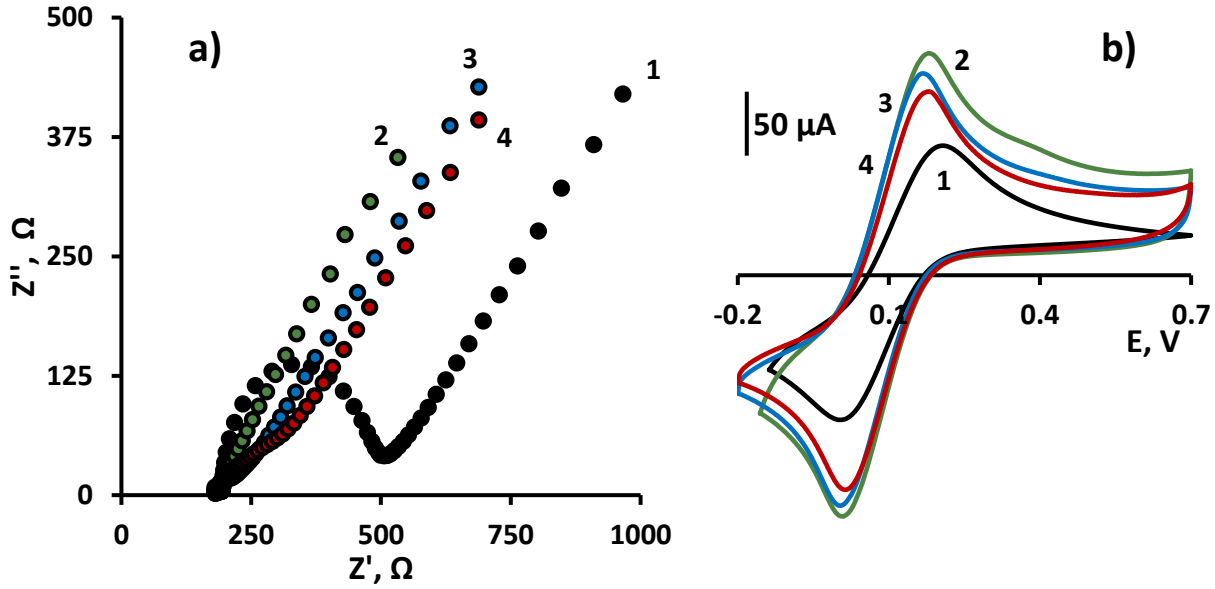

Figura 5.19. a) Diagramas de Nyquist y b) voltamperogramas clíclicos registrados para: 1) SPCE, 2) HOOC-CNHs/SPCE, 3) anti-ISO-HOOC-CNHs/SPCE y 4) HRP-ISO-anti-ISO-HOOC-CNHs/SPCE en una disolución $Fe(CN)_6^{3-/4-}$ 5 mM en KCl 100 mM de pH 7.0

5.2.1.4. Calibrado y características analíticas

En la Figura 5.20 se representa el calibrado obtenido empleando las condiciones experimentales previamente optimizadas. Como puede observarse, existe una relación lineal entre la intensidad de corriente y la concentración de 8-isoprostano entre 0 y 700 pg/mL (R^2 = 0.998), con una pendiente de (–850 ± 8) nA·mL/pg y una ordenada en el origen de (623 ± 3) nA.

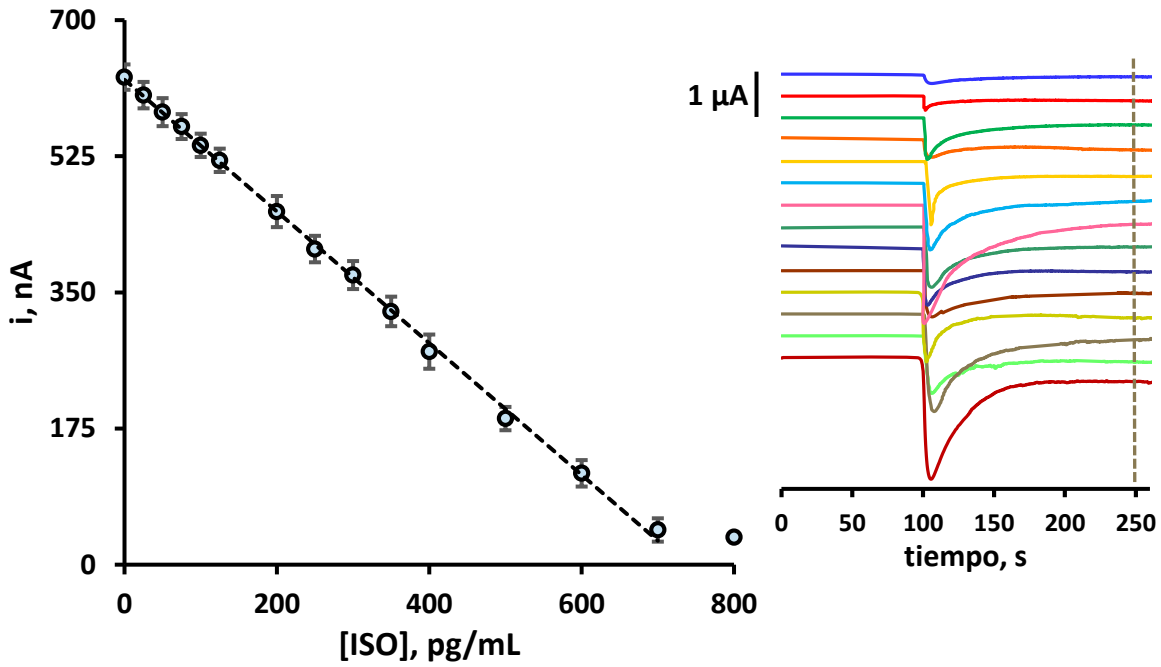

Figura 5.20. Calibrado para la determinación de ISO empleando el inmunosensor HRP-ISO-anti-ISO-HOOC-CNHs/SPCE

El límite de detección, de 12 pg/mL, se calculó como la concentración más baja que puede ser estadísticamente discriminada de la señal proporcionada por el blanco, a partir de la expresión $\bar{x}+3\cdot s$, donde *s* es la desviación estándar calculada a partir de las respuestas amperométricas obtenidas para diez réplicas en ausencia de 8-isoprostano, en unidades de concentración, pg/mL. Asimismo, el límite de cuantificación obtenido fue de 19 pg/mL, de acuerdo con la expresión $\bar{x}+10\cdot s$.

Dado que los niveles de concentración normales de este analito encontrados en individuos sanos están comprendidos entre unas pocas decenas y unos pocos cientos de pg/mL [Cabral de Faria, 2014; Vassalle, 2003], las características analíticas del inmunosensor desarrollado son adecuadas para la determinación de este analito en muestras de interés clínico.

5.2.1.5. Estudio de selectividad

La selectividad del inmunosensor depende fundamentalmente de la especificidad del anticuerpo de captura empleado y, para su evaluación, es preciso conocer el nivel de respuesta del mismo frente a otras especies, es decir, su reactividad

cruzada, en comparación con la respuesta frente a un blanco. Las especies investigadas en este caso para evaluar la selectividad del inmunosensor competitivo HRP-ISO-anti-ISO-CNHs/SPCE fueron diversas proteínas como adiponectina (APN), albúmina de suero bovino (BSA), colesterol (Chol), ceruloplasmina (Cp), factor de crecimiento transformante beta 1 (TGF-β1), factor de necrosis tumoral alfa (TNF-α), hemoglobina (HB), interleucina 6 (IL-6) e interleucina 8 (IL-8), que pueden estar presentes en muestras de suero humano junto al analito de interés.

Para ello, se compararon las respuestas amperométricas obtenidas para inmunosensores preparados en ausencia de ISO (máxima señal) o en presencia de 50 pg/mL del mismo y, a su vez, en ausencia y en presencia de cada uno de los compuestos ensayados al nivel de concentración que cabe esperar en dichas muestras. Los resultados mostrados en la Figura 5.21 ponen de manifiesto que ninguna de estas proteínas supone, a los niveles ensayados, una interferencia significativa en la determinación de este isoprostano.

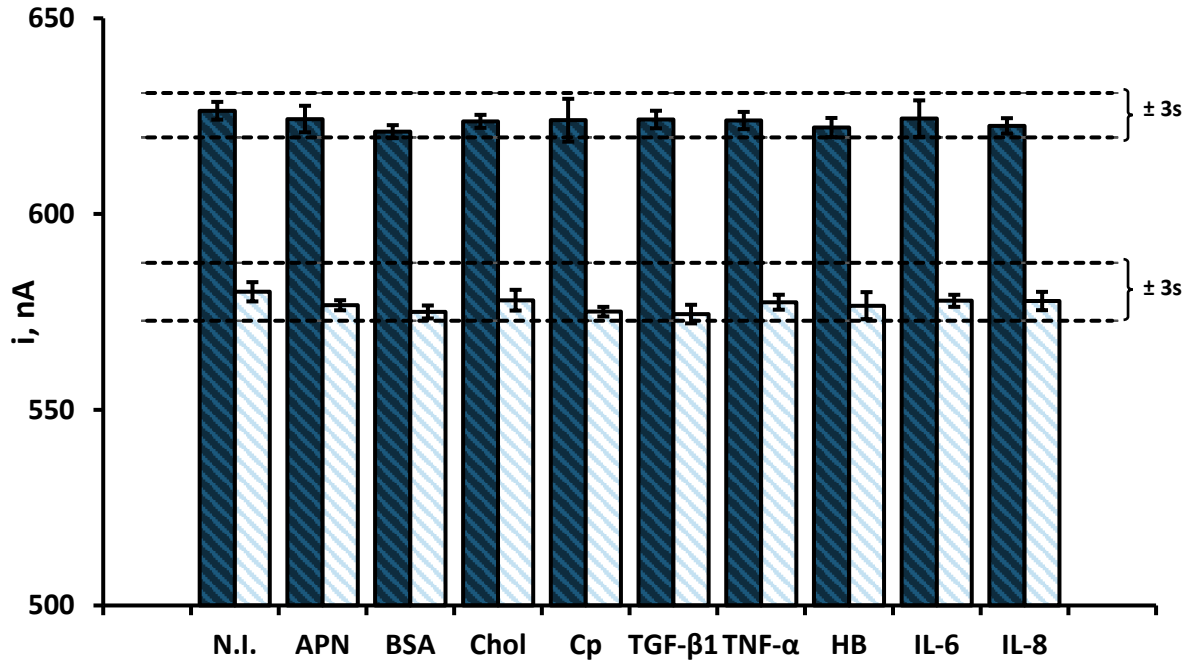

Figura 5.21. Selectividad del inmunosensor HRP-ISO-anti-ISO-HOOC-CNHs/SPCE evaluando la respuesta del mismo con 0 (■) o 50 (□) pg/mL de ISO frente a 20 µg/mL de APN, 5 mg/mL de BSA, 20 µg/mL de Chol, 500 µg/mL de Cp, 500 pg/mL de TGF-β1, 100 pg/mL de TNF-α, 50 µg/mL de HB, 50 pg/mL de IL-6 y 30 pg/mL de IL-8

5.2.1.6. Estudios de reproducibilidad y estabilidad

La repetibilidad y reproducibilidad de las medidas amperométricas se evaluó midiendo la respuesta de seis inmunosensores diferentes preparados en ausencia y en presencia de 50 pg/mL de ISO el mismo día o en días diferentes. Los resultados obtenidos proporcionaron valores de desviación estándar relativa, RSD, para los inmunosensores preparados el mismo día, del 0.36 y 0.35%, respectivamente, mientras que los valores de RSD para inmunosensores preparados en diferentes días fueron del 0.53 y 0.40%, respectivamente. Estos valores, inferiores al 2%, demuestran que el proceso de fabricación del inmunosensor es fiable y que las respuestas obtenidas con diferentes inmunosensores preparados de la misma manera son altamente reproducibles.

Por otro lado, también se evaluó la estabilidad del electrodo modificado con el anticuerpo de captura. Para ello se prepararon diferentes electrodos modificados con anti-ISO que, tras el bloqueo de la superficie electródica con BSA al 2%, se almacenaron en seco a –20°C. Posteriormente, en diferentes días, se construyó el inmunosensor completo mediante incubación de éste en la disolución del antígeno marcado con la enzima durante 45 minutos y se midió la respuesta amperométrica en ausencia de ISO.

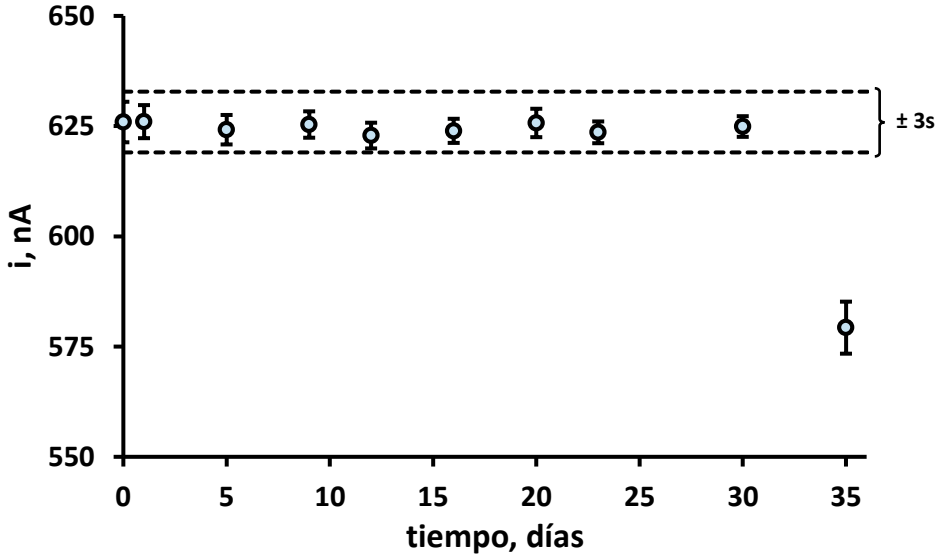

Figura 5.22. Gráfico de control para la evaluación de la estabilidad de almacenamiento del conjugado anti-ISO-HOOC-CNHs/SPCE

En la Figura 5.22 se muestra el gráfico control construido tomando como referencia el valor medio de 3 medidas obtenidas el primer día, en ausencia de ISO y empleando una dilución 1/500 de HRP-ISO.

Los resultados obtenidos permiten apreciar que la respuesta de los inmunosensores se mantiene dentro de los límites de control establecidos como ± 3 veces la desviación estándar de las medidas realizadas el primer día de trabajo, durante 30 días.

Esta característica tiene una gran importancia desde el punto de vista de la utilidad práctica del inmunosensor, ya que demuestra que es posible preparar varios conjugados, almacenarlos en las condiciones indicadas y, posteriormente, en el momento que se precise, construir el inmunosensor para su uso inmediato.

5.2.1.7. Aplicación a la determinación de 8-isoprostano en suero

Siguiendo el procedimiento descrito en el *Apartado 4.6.2.* de la *Parte Experimental*, el inmunosensor desarrollado se aplicó a la determinación de ISO en dos tipos de muestras de suero: suero humano liofilizado enriquecido con distintas concentraciones de analito y suero humano perteneciente a dos individuos sanos.

Para el análisis de la muestra de suero liofilizado, se evaluó en primer lugar la posible existencia de efecto matriz construyendo un calibrado con muestra enriquecida con distintas concentraciones de analito (entre 30 y 40 pg/mL). Después, se llevó a cabo la comparación estadística de las pendientes de la recta de regresión obtenida, (i_p, nA = (–896 ± 3) [ISO, ng/mL] + (624 ± 1) nA) con la correspondiente al calibrado empleando disoluciones estándar de isoprostano (i_p, nA = (–850 ± 8) [ISO, ng/mL] + (623 ± 3) nA). La aplicación del test de la *t* de Student proporcionó un valor calculado de la *t* experimental, (t_{exp} = 1.247) inferior al valor tabulado, (t_{tab} = 4.303) para un nivel de significación del 0.05. Estos resultados

permiten concluir que no existen diferencias significativas entre las pendientes de los dos calibrados, que aparecen superpuestas en la Figura 5.23, pudiéndose determinar la concentración de ISO en suero por interpolación directa de la señal proporcionada por la muestra en el calibrado de disoluciones estándar.

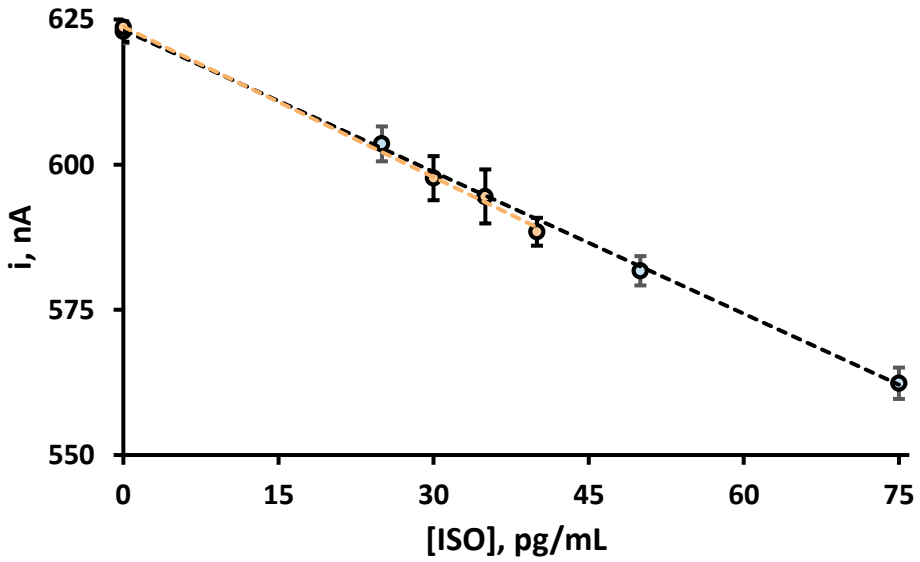

Figura 5.23. Superposición de las señales obtenidas para el suero liofilizado enriquecido (●) en el calibrado de disoluciones estándar (●)

En la Tabla 5.4 se resumen los resultados obtenidos en las determinaciones por triplicado, para los distintos niveles de enriquecimiento de la muestra.

Tabla 5.4. Determinación de ISO en muestras de suero humano liofilizado empleando el inmunosensor HRP-ISO-anti-ISO-HOOC-CNHs/SPCE

[ISO] AÑADIDO, pg/mL	[ISO] RECUPERADO, pg/mL*	RECUPERACIÓN, %*
30	30 ± 4	100 ± 1
35	33 ± 7	95± 6
40	42 ± 3	101 ± 4

* valor medio ± t·s/√n

Como se observa, los porcentajes de recuperación se encuentran entre el 95 y el 101%, lo que pone de manifiesto la gran fiabilidad de la metodología propuesta para la determinación de este analito en este tipo de muestra, siguiendo un protocolo de trabajo de gran simplicidad.

Por otro lado, se analizó el contenido total de 8-isoprostano en dos muestras de suero pertenecientes a individuos sanos, siendo necesario llevar a cabo, en primer lugar, una hidrólisis de las lipoproteínas y fosfolípidos a los que pudiera estar unido este isoprostano, siguiendo para ello el procedimiento descrito en el *Apartado 4.6.2.* de la *Parte Experimental*. Al igual que anteriormente, una vez comprobada la ausencia de efecto matriz, la determinación de ISO se llevó a cabo por interpolación de la intensidad de corriente proporcionada por las muestras en el calibrado de disoluciones estándar. Posteriormente, los resultados obtenidos se validaron comparándolos con los proporcionados por el kit ELISA de Cell Biolabs, siguiendo el procedimiento de ensayo especificado por la casa comercial. Los resultados obtenidos por ambos métodos se resumen en la Tabla 5.5.

Tabla 5.5. Determinación de ISO en muestras de suero de individuos sanos empleando el inmunosensor HRP-ISO-anti-ISO-HOOC-CNHs/SPCE

MUESTRA	INMUNOSENSOR, pg/mL (n = 6)*	ELISA, pg/mL (n = 6)*
hombre sano (SG610-2, BBI)	403 ± 7	408 ± 5
mujer sana (SG609-2, BBI)	394 ± 4	398 ± 3

* valor medio ± t·s/√n

Finalmente, se empleó el test *t* de Student para comparar estadísticamente los resultados proporcionados por ambos métodos, obteniéndose valores de t_{exp} de 1.714 y 1.107, para las muestras de hombre y mujer, respectivamente, ambos inferiores al valor teórico para las condiciones del experimento (t_{tab} = 2.228). Estos resultados confirman que no existen diferencias significativas entre ambas metodologías a un nivel de significancia de 0.05, quedando demostrada asimismo la utilidad del inmunosensor desarrollado para la determinación del contenido total de ISO en muestras de suero humano en concentraciones clínicamente relevantes.

5.2.1.8. Conclusiones

En este trabajo se ha desarrollado el primer inmunosensor electroquímico para la determinación de 8-isoprostano basado en la modificación de un electrodo

serigrafiado de carbono con nanocuernos de carbono de pared simple carboxilados (HOOC-CNHs) sobre los que se inmoviliza covalente el anticuerpo de captura (anti-ISO). Una vez establecido un esquema de inmunoensayo de tipo competitivo directo, se ha podido determinar la concentración de este analito, obteniéndose una gran sensibilidad debida tanto a la alta conductividad del nanomaterial empleado como al elevado número de restos carboxílicos presente en la superficie del electrodo modificado, que permite la inmovilización eficiente de una gran cantidad de anticuerpo de captura. En general se ha visto que las características analíticas del inmunosensor electroquímico mejoran las proporcionadas por los métodos convencionales de inmunoensayo tipo ELISA. Por último, la utilidad del inmunosensor se ha demostrado mediante la determinación de ISO en muestras de suero liofilizado enriquecido y de suero humano perteneciente a dos individuos sanos, siendo los resultados obtenidos en todos los casos estadísticamente comparables con los proporcionados por el correspondiente kit ELISA comercial.

5.2.2. Inmunosensor para la determinación de adiponectina

Para la preparación de este inmunosensor se hizo uso del nanomaterial híbrido formado con óxido de grafeno reducido y carboximetilcelulosa (CMC-rGO) utilizándolo como modificador de la superficie de los electrodos serigrafiados. Como ya se ha explicado en la *Introducción*, la adiponectina (APN) es una citoquina expresada específicamente en los adipocitos del tejido adiposo y su actividad está relacionada con los procesos inflamatorios, la obesidad y la vejez.

5.2.2.1. Configuración del inmunosensor

En la Figura 4.24 de la *Parte Experimental* se representaron las etapas de preparación y funcionamiento del inmunosensor para la determinación de APN. En ella se aprecia cómo, una vez modificado el electrodo serigrafiado de carbono con el material híbrido CMC-rGO, se añade el polímero Mix&Go™ sobre los grupos carboxílicos superficiales para inmovilizar posteriormente de forma orientada el anticuerpo de captura. A continuación, se establece un esquema de inmunoensayo tipo sándwich empleando el antígeno y el anticuerpo de detección biotinilado. La reacción de afinidad antígeno-anticuerpo se monitorizó empleando estreptavidina marcada con la enzima peroxidasa, obteniéndose la señal analítica como en casos anteriores, empleando hidroquinona como medidador redox y peróxido de hidrógeno como sustrato enzimático, aplicando un potencial de –200 mV.

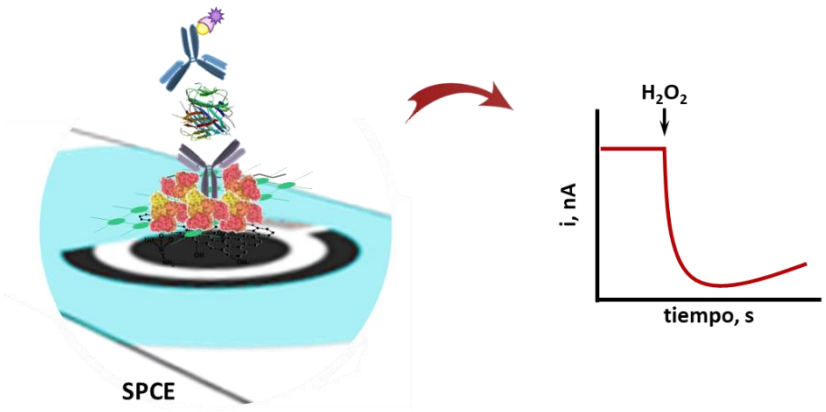

Figura 5.24. Esquema del funcionamiento del inmunosensor para la determinación de APN

5.2.2.2. Optimización de las variables experimentales

Con el objetivo de obtener las mejores características analíticas para la determinación de adiponectina, se optimizaron las distintas variables experimentales que influyen en la configuración y la respuesta del inmunosensor desarrollado. Como ya se ha comentado en apartados anteriores, se consideró como valor óptimo para cada una de las variables aquél que proporcionaba una mayor relación entre las corrientes específica e inespecífica (S/R) del inmunosensor, preparado respectivamente con y sin el antígeno APN.

Elección del método de inmovilización del anticuerpo de captura

Como se ha comentado anteriormente, la estrategia utilizada para inmovilizar el anticuerpo anti-APN sobre los grupos carboxílicos de la superficie del electrodo modificado consistió en añadir el polímero Mix&Go™ formado por una serie de complejos metálicos seleccionados por su elevada eficiencia para enlazar anticuerpos a través de su región Fc. Los resultados obtenidos empleando este método se compararon con el utilizado habitualmente, que implica el empleo del sistema EDC/NHSS para la activación de los grupos carboxílicos seguido de la formación de uniones tipo amida, con los restos amina de las proteínas.

En la Figura 5.25 se comparan las respuestas amperométricas del inmunosensor desarrollado para la determinación de APN haciendo uso de las dos alternativas para inmovilizar el anticuerpo anti-APN.

Como se puede comprobar, el uso del material polimérico Mix&Go™ proporcionó una mayor relación entre las señales obtenidas en ausencia y presencia del antígeno, a pesar de que las intensidades de corriente de ambas señales son menores que cuando se emplea el sistema de la carbodiimida, demostrando así que el empleo de este material es más adecuado para el desarrollo de esta configuración.

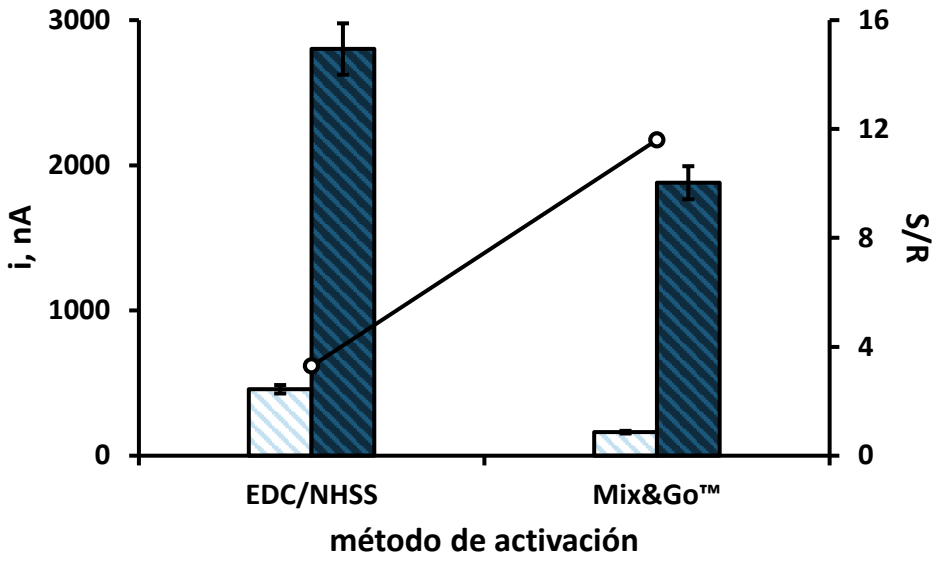

Figura 5.25. Efecto de la estrategia de inmovilización de anti-APN sobre la respuesta del inmunosensor: CMC-rGO, 20µL; EDC/NHSS, 100 mM, 10 µL, 30 min o Mix&Go™, 10 µL, 60 min; anti-APN, 1/300, 5 µL, 60 min; BSA, 5%, 5 µL, 30 min; APN, 0 (□) y 2 (■) µg/mL, 5 µL, 40 min; Biotin-anti-APN, 2 µg/mL, 5 µL, 20 min; HRP-Strept, 1/1000, 5µL, 15 min

Elección de la superficie electródica

Para evaluar la idoneidad del nanomaterial híbrido CMC-rGO usado como modificador electródico en la construcción del inmunosensor para la determinación de APN, se compararon los resultados proporcionados por los electrodos serigrafiados modificados con el híbrido de óxido de grafeno reducido y carboximetilcelulosa (CMC-rGO) con los de dos nanomateriales simples nanotubos de carbono de pared múltiple carboxilados (HOOC-MWCNTs) y óxido de grafeno reducido (rGO). Para ello se construyeron distintos inmunosensores inmovilizando los anticuerpos de captura sobre estas superficies utilizando el material polimérico Mix&Go™ en todos los casos.

Como puede observarse en la Figura 5.26, la señal obtenida en presencia de adiponectina es considerablemente mayor cuando se modifica el electrodo con el híbrido CMC-rGO, lo que probablemente se debe al elevado número de grupos carboxílicos superficiales presentes en la carboximetilcelulosa que posibilita la inmovilización de una mayor cantidad de anticuerpo.

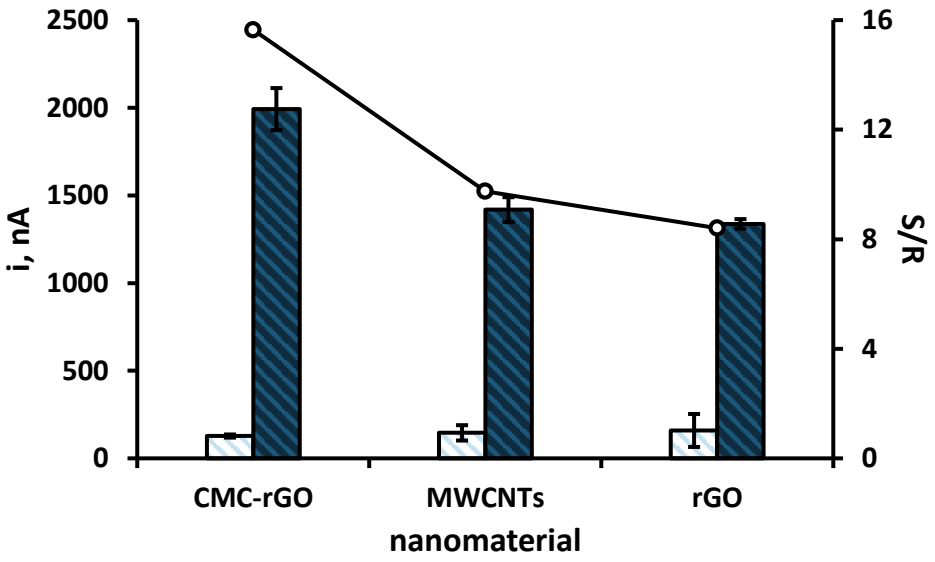

Figura 5.26. Efecto de la modificación de la superficie electródica sobre la respuesta del inmunosensor: CMC-rGO, HOOC-MWCNTs o rGO, 20µL; Mix&Go™, 10 µL, 60 min; anti-APN, 1/300, 5 µL, 60 min; BSA, 5%, 5 µL, 30 min; APN, 0 (□) y 2 (■) µg/mL, 5 µL, 40 min; Biotin-anti-APN, 2 µg/mL, 5 µL, 20 min; HRP-Strept, 1/1000, 5µL, 15 min

Influencia del tiempo de incubación del material polimérico Mix&Go™

Este estudio se realizó depositando 10 µL de Mix&Go™ sobre la superficie del electrodo de trabajo modificada previamente con 20 µL de CMC-rGO y dejando reaccionar durante 30 ó 60 min. Pasado este tiempo, se añadieron 5 µL de una dilución 1/300 de anti-APN en disolución reguladora MES 25 mM de pH 5.0 y se mantuvo a temperatura ambiente durante una hora en condiciones de humedad. Una vez inmovilizado el anticuerpo de captura, se adicionaron 5 µL de disolución de BSA al 5 % (p/v) en medio reguladora PB 100 mM de pH 7.4 y 5 µL de una disolución de 0 o 2 µg/mL de APN en la misma disolución reguladora, dejando incubar durante 40 minutos. Seguidamente se depositaron 5 µL de una disolución de 2 µg/mL de Biotin-anti-APN preparada en PB 100 mM de pH 7.4 + 0.5% BSA (p/v) durante 20 minutos. Por último, se añadieron 5 µL de una dilución 1/1000 de HRP-Strept en disolución PB 100 mM de pH 7.4 en presencia de un 0.5% de BSA (p/v) durante 15 minutos. Los resultados obtenidos se han representado en la Figura 5.27.

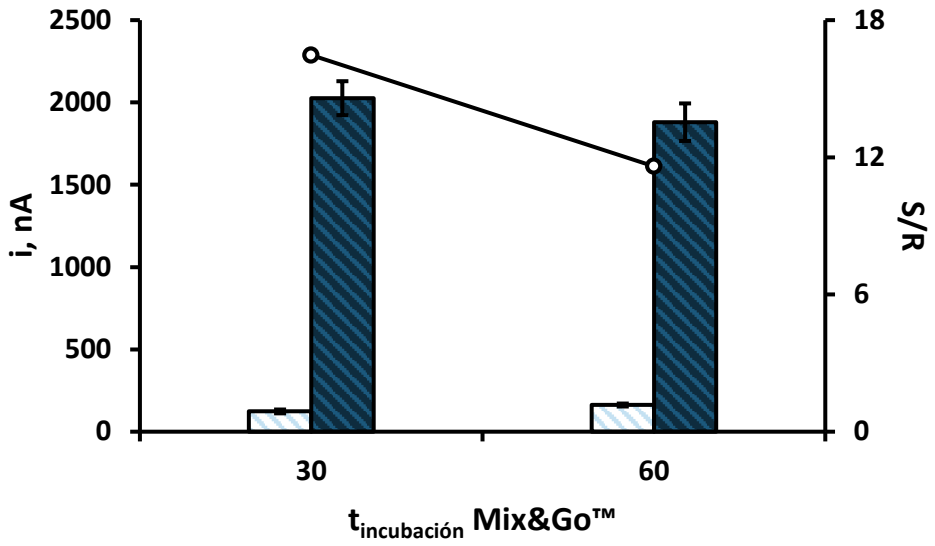

Figura 5.27. Efecto del tiempo de incubación del material polimérico Mix&Go™ sobre la respuesta del inmunosensor: CMC-rGO, 20µL; Mix&Go™, 10 µL; anti-APN, 1/300, 5 µL, 60 min; BSA, 5%, 5 µL, 30 min; APN, 0 (□) y 2 (■) µg/mL, 5 µL, 40 min; Biotin-anti-APN, 2 µg/mL, 5 µL, 20 min; HRP-Strept, 1/1000, 5µL, 15 min

Puede verse que no existe una diferencia notable entre ambos resultados, pero la señal en presencia de APN es ligeramente superior y la del blanco es algo inferior, dando lugar a una mayor relación S/R, por lo que se eligió el menor de estos tiempos, lo que además contribuye a una menor duración del procedimiento de preparación del inmunosensor.

Influencia de la concentración del anticuerpo de captura y el pH de incubación

Con el fin de elegir la concentración óptima de anticuerpo de captura para la preparación del inmunosensor, se estudiaron las respuestas específicas e inespecíficas obtenidas empleando diluciones de anti-APN comprendidas entre 1/37.5 y 1/450 y manteniendo constante el resto de variables experimentales. Como puede observarse en la Figura 5.28, se obtiene un máximo para la respuesta específica empleando una dilución 1/300 de anti-APN inmovilizado sobre la superficie del electrodo modificado. Concentraciones mayores dan lugar a una disminución de la corriente registrada, probablemente debido a la mayor dificultad para producirse la reacción de afinidad antígeno-anticuerpo. Estos resultados, así como la mayor relación S/R, llevaron a elegir esta dilución para estudios posteriores.

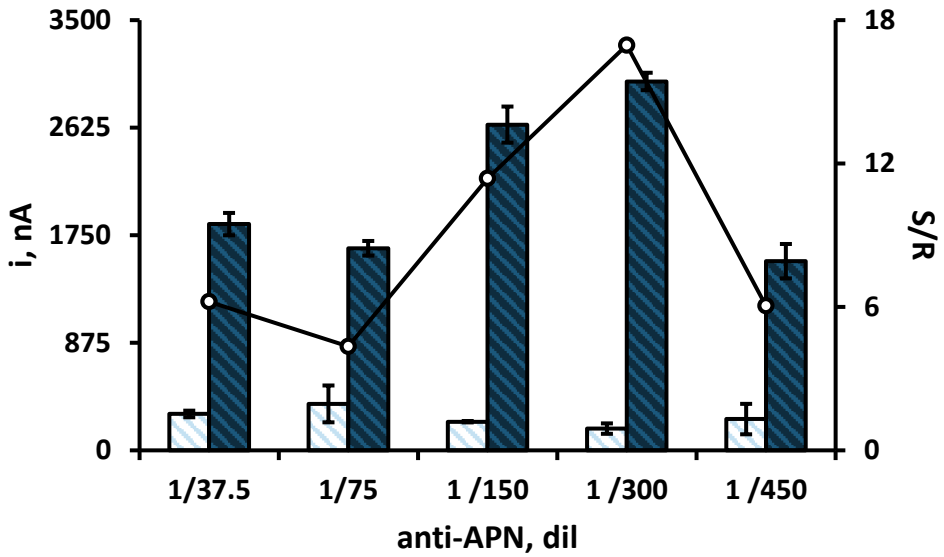

Figura 5.28. Efecto de la concentración de anti-APN sobre la respuesta del inmunosensor: CMC-rGO, 20µL; Mix&Go™, 10 µL, 30 min; anti-APN, 5 µL, 60 min; BSA, 5%, 5 µL, 30 min; APN, 0 (□) y 2 (■) µg/mL, 5 µL, 40 min; Biotin-anti-APN, 2 µg/mL, 5 µL, 20 min; HRP-Strept, 1/1000, 5µL, 15 min

En cuanto al pH de la disolución de anti-APN, al que se realiza la incubación, los resultados que se muestran en la Figura 5.29 demuestran que el valor más adecuado es pH 5, que fue el seleccionado para llevar esta etapa, utilizando disolución reguladora MES 25 mM para su ajuste.

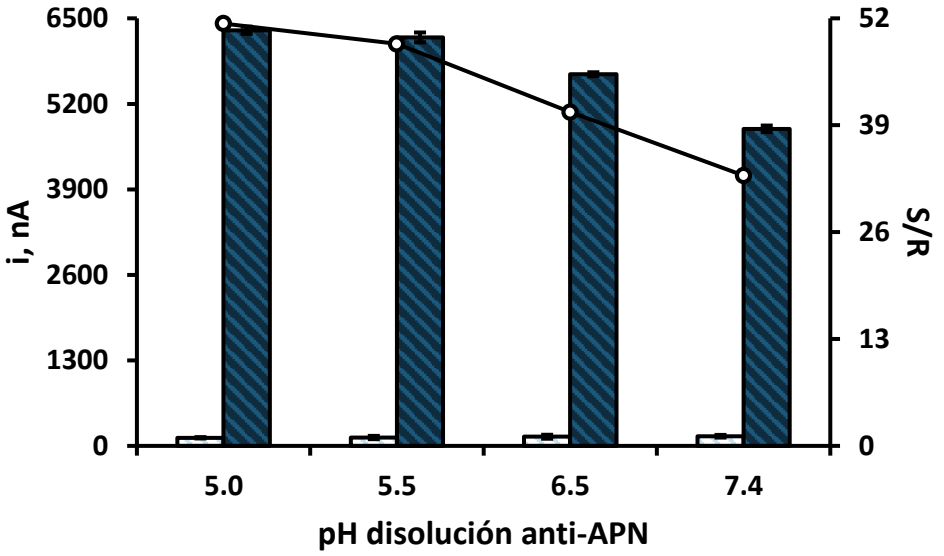

Figura 5.29. Efecto del pH de la disolución de anti-APN sobre la respuesta del inmunosensor: CMC-rGO, 20µL; Mix&Go™, 10 µL, 30 min; anti-APN, 1/300, 5 µL, 60 min; BSA, 5%, 5 µL, 30 min; APN, 0 (□) y 10 (■) µg/mL, 5 µL, 40 min; Biotin-anti-APN, 2 µg/mL, 5 µL, 20 min; HRP-Strept, 1/1000, 5µL, 15 min

Influencia de la etapa de bloqueo

Como en otros casos, con el objetivo de disminuir al máximo las señales debidas a adsorciones inespecíficas de los inmunorreactivos sobre la superficie del electrodo, se estudiaron las condiciones experimentales para el bloqueo de las posiciones reactivas libres de dicha superficie. Para ello, en primer lugar, se ensayaron diferentes agentes bloqueantes de uso común: BSA, caseína y leche en polvo. Se prepararon disoluciones de cada una de estas sustancias en disolución reguladora PB 100 mM de pH 7.4, a las concentraciones usuales, y se registraron las señales amperométricas de los inmunosensores preparados añadiendo, en cada caso, tras la inmovilización del anticuerpo de captura, 5 µL de la disolución del correspondiente agente bloqueante.

Los resultados que aparecen en la Figura 5.30 muestran un mejor comportamiento para los inmunosensores preparados en presencia de BSA. La respuesta específica de este inmunosensor es más alta, encontrándose una señal inespecífica menor, de modo que la relación entre ambas resulta óptima.

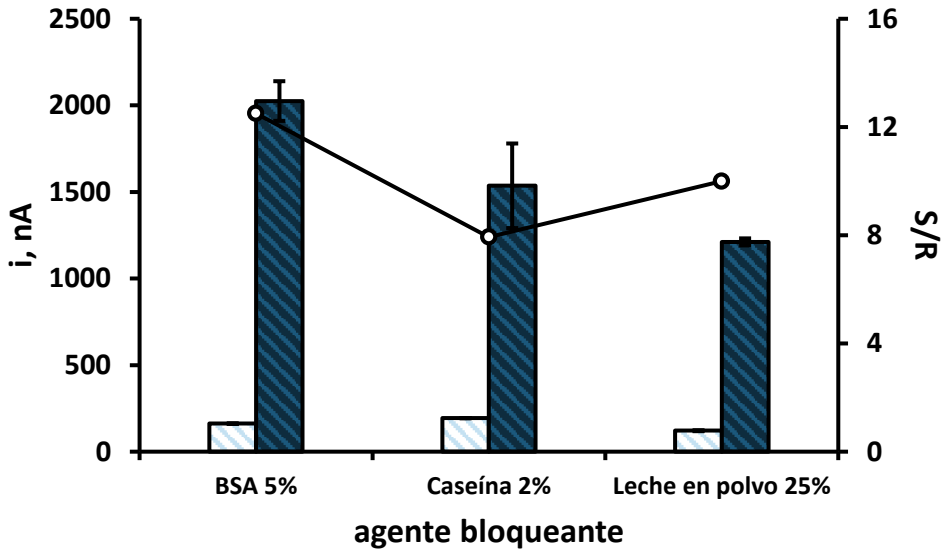

Figura 5.30. Efecto del agente bloqueante sobre la respuesta del inmunosensor: CMC-rGO, 20µL; Mix&Go™, 10 µL, 30 min; anti-APN, 1/300, 5 µL, 60 min; agente bloqueante, 5 µL, 30 min; APN, 0 (□) y 2 (■) µg/mL, 5 µL, 40 min; Biotin-anti-APN, 2 µg/mL, 5 µL, 20 min; HRP-Strept, 1/1000, 5µL, 15 min

Una vez elegido el algente bloqueante, se estudió la posible ventaja de añadir BSA al 0.5% (p/v) a las disoluciones de anticuerpo de detección biotinilado (Biotin-anti-APN) y de conjugado enzimático (HRP-Strept). La adición de agente

bloqueante a las disoluciones de reactivos auxiliares es una práctica común que contribuye a rebajar las señales debidas a adsorciones inespecíficas mejorando el efecto obtenido añadiendo dicho agente a la superficie del electrodo tras la inmovilización del anticuerpo de captura. Para hacer este estudio se realizaron medidas con varios inmunosensores preparados del modo habitual, a partir de disoluciones de Biotin-anti-APN y HRP-Strept en presencia o ausencia de un 0.5% (p/v) de BSA, manteniendo constante el resto de las variables.

Los resultados obtenidos (Figura 5.31) permiten apreciar que la adición de BSA a las disoluciones de los biorreactivos proporciona una respuesta inespecífica menor, lo que puede ser debido probablemente a que la adición de agente bloqueante sobre la superficie del inmunosensor anti-APN-CMC-rGO/SPCE no es suficiente para evitar todas las posibles adsorciones no específicas que se pueden originar sobre el electrodo y que son responsables de la mayor corriente residual de las medidas amperométricas. Teniendo en cuenta, además, que la presencia de BSA al nivel de concentración utilizado no disminuye la respuesta específica del inmunosensor, se optó por añadir este BSA a estas disoluciones.

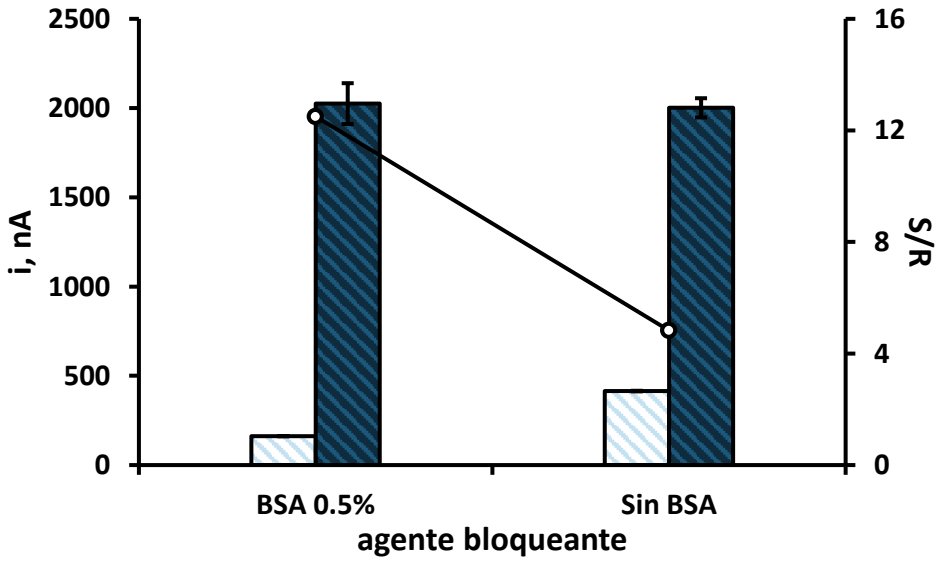

Figura 5.31. Efecto del agente bloqueante sobre la respuesta del inmunosensor: CMC-rGO, 20µL; Mix&Go™, 10 µL, 30 min; anti-APN, 1/300, 5 µL, 60 min; BSA, 5%, 5 µL, 30 min; APN, 0 (□) y 2 (■) µg/mL, 5 µL, 40 min; Biotin-anti-APN, 2 µg/mL, 5 µL, 20 min; HRP-Strept, 1/1000, 5µL, 15 min

Influencia de la concentración del anticuerpo de detección biotinilado

La concentración óptima de Biotin-anti-APN para la preparación del inmunosensor se eligió por comparación de las señales amperométricas registradas en ausencia y presencia de antígeno, empleando concentraciones de Biotin-anti-APN entre 1 y 4 µg/mL, con los resultados que aparecen en la Figura 5.32. En ella se aprecia un aumento de la respuesta específica del inmunosensor al aumentar la concentración de Biotin-anti-APN debido a la mayor cantidad de conjugado enzimático unido al electrodo. Por otra parte, como era de esperar, este aumento conlleva asociado un incremento de la señal inespecífica. Por tanto, teniendo en cuenta la mejor relación entre ambas señales, se eligió una concentración de 2 µg/mL de Biotin-anti-APN para estudios posteriores.

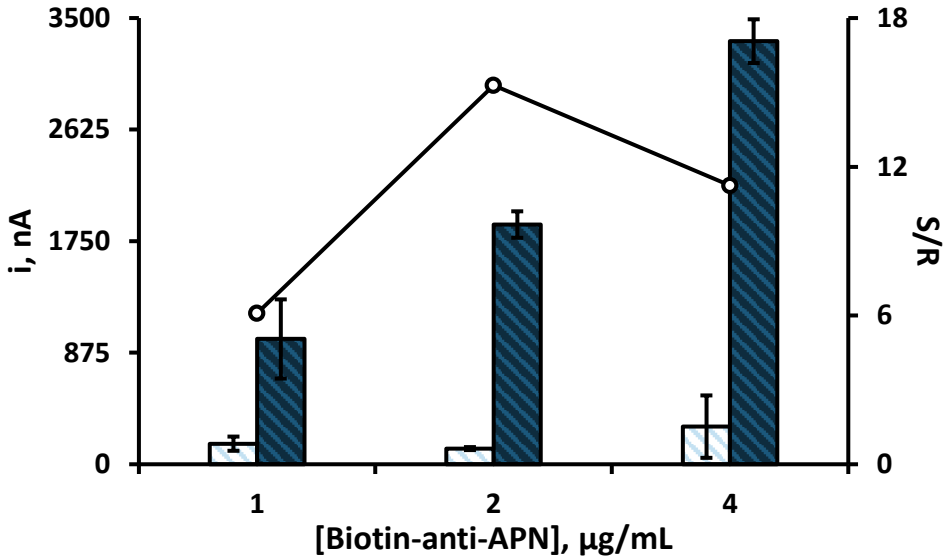

Figura 5.32. Efecto de la concentración de Biotin-anti-APN sobre la respuesta del inmunosensor: CMC-rGO, 20µL; Mix&Go™, 10 µL, 30 min; anti-APN, 1/300, 5 µL, 60 min; BSA, 5%, 5 µL, 30 min; APN, 0 (□) y 2 (■) µg/mL, 5 µL, 40 min; Biotin-anti-APN, 5 µL, 20 min; HRP-Strept, 1/1000, 5µL, 15 min

Influencia de la dilución del conjugado enzimático

La última etapa de la preparación de esta configuración consiste en la incorporación del conjugado enzimático HRP-Strept, responsable de la reducción del sustrato enzimático (H_2O_2) en presencia de hidroquinona como mediador redox. Este estudio se realizó preparando diferentes inmunosensores con diluciones de

HRP-Strept, entre 1/500 y 1/2000, en disolución reguladora PB 100 mM de pH 7.4 + 0.5% BSA (p/v), que se incubó durante 15 minutos.

En la Figura 5.33 se han representado los resultados obtenidos, observándose una mayor relación entre las señales específica e inespecífica cuando se emplea una dilución 1/1000.

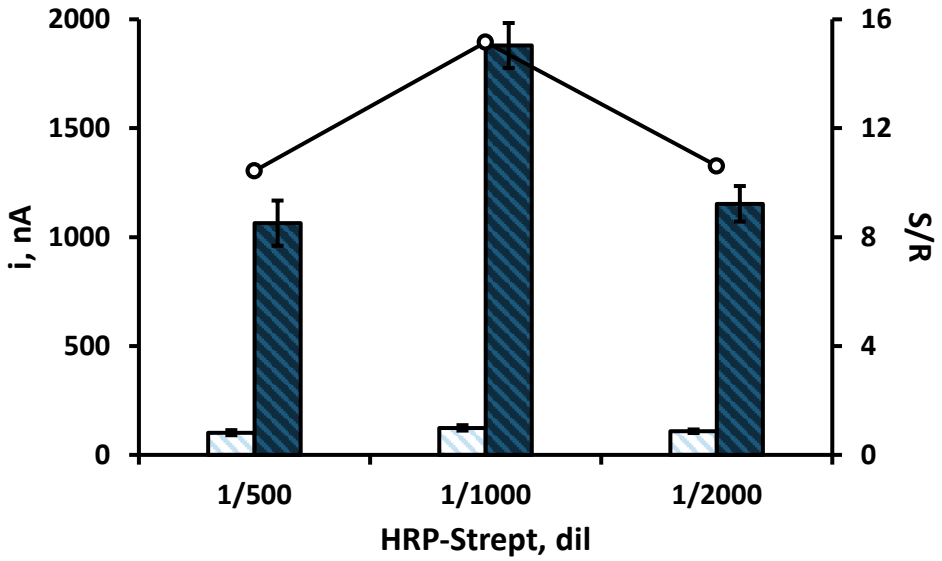

Figura 5.33. Efecto de la dilución de HRP-Strept sobre la respuesta del inmunosensor: CMC-rGO, 20µL; Mix&Go™, 10 µL, 60 min; anti-APN, 1/300, 5 µL, 60 min; BSA, 5%, 5 µL, 30 min; APN, 0 (□) y 2 (■) µg/mL, 5 µL, 40 min; Biotin-anti-APN, 2 µg/mL, 5 µL, 20 min; HRP-Strept, 5µL, 15 min

Influencia del tiempo de incubación del antígeno

Por último, se optimizó el tiempo de incubación del analito, APN, sobre el inmunosensor. Para ello, una vez depositado el antígeno sobre el inmunoconjugado anti-APN-CMC-rGO/SPCE, éste se incubó durante 20, 40 o 60 minutos antes de proseguir con las etapas posteriores. Como puede verse en la Figura 5.34, un mayor periodo de incubación origina un rápido aumento de la respuesta específica, así como también una mejora en la relación de estas respuestas respecto a las debidas a adsorciones no específicas. Estos resultados llevaron a elegir el tiempo de una hora, máximo periodo estudiado, como el más apropiado para la preparación del inmunosensor.

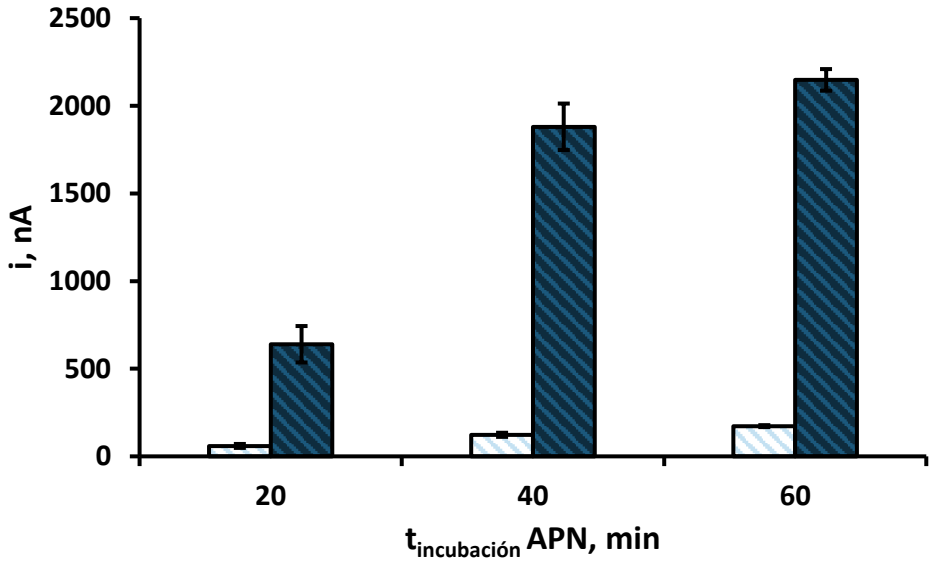

Figura 5.34. Efecto del tiempo de incubación de APN sobre la respuesta del inmunosensor: CMC-rGO, 20µL; Mix&Go™, 10 µL, 60 min; anti-APN, 1/300, 5 µL, 60 min; BSA, 5%, 5 µL, 30 min; APN, 0 (□) y 2 (■) µg/mL, 5 µL; Biotin-anti-APN, 2 µg/mL, 5 µL, 20 min; HRP-Strept, 1/1000, 5µL, 15 min

En la Tabla 5.6 se recogen, a modo de resumen, las variables estudiadas, así como los intervalos evaluados y los valores seleccionados en cada caso.

Tabla 5.6. Optimización de las variables experimentales implicadas en la construcción del inmunosensor HRP-Strept-Biotin-anti-APN-APN-anti-APN-CMC-rGO/SPCE

VARIABLE EXPERIMENTAL	INTERVALO EVALUADO	VALOR SELECCIONADO
método inmovilización anti-APN	EDC/NHSS, Mix&Go™	Mix&Go™
$t_{incubación}$ Mix&Go™, min	30 – 60	30
anti-APN, dil	1/37.5 – 1/450	1/300
agente bloqueante	BSA 5%, caseína 2%, leche en polvo 50%	BSA 5%
[Biotin-anti-APN], µg/mL	1 – 4	2
$t_{incubación}$ Biotin-anti-APN, min	20 – 60	40
HRP-Strept, dil	1/500 – 1/2000	1/1000

5.2.2.3. Caracterización de la superficie electródica

La espectroscopia de impedancia electroquímica se empleó para monitorizar las etapas implicadas en la construcción del inmunosensor, mostrándose en la

Figura 5.35 los diagramas de Nyquist registrados. Como era de esperar, la modificación de la superficie electródica con el material híbrido (CMC-rGO/SPCE) produjo un aumento en la resistencia a la transferencia electrónica (R_{ct}, de 682 a 1013 Ω), como consecuencia de la repulsión electrostática entre la sonda redox y los grupos carboxílicos cargados negativamente presentes en el material. La posterior incorporación del material polimérico Mix&Go™ condujo a un aumento adicional de la resistencia (R_{ct}, = 1334 Ω) debido a la menor conductividad de la superficie electródica modificada. La inmovilización del anticuerpo de captura provocó un aumento notable en el valor de R_{ct} hasta 2247, confirmando la eficacia del procedimiento de inmovilización. Las etapas posteriores de la preparación del inmunosensor dieron lugar a mayores valores de R_{ct} como consecuencia de la incorporación de biorreactivos aislantes que dificultan la transferencia de carga en la superficie del electrodo.

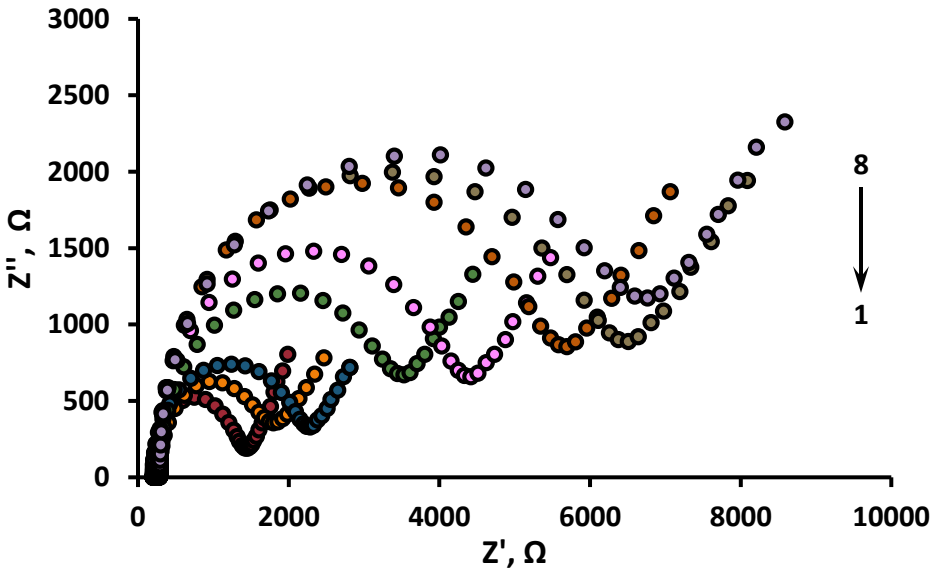

Figura 5.35. Diagramas de Nyquist registrados para: a) 1) SPCE, 2) CMC-rGO/SPCE, 3) Mix&Go™-CMC-rGO/SPCE, 4) anti-APN-CMC-rGO/SPCE , 5) BSA-anti-APN-CMC-rGO/SPCE, 6) APN-anti-APN-CMC-rGO/SPCE, 7) Biotin-anti-APN-APN-anti-APN-CMC-rGO/SPCE y 8) HRP-Strept-Biotin-anti-APN-APN-anti-APN-CMC-rGO/SPCE en una disolución $Fe(CN)_6^{3-/4-}$ 5 mM en PB 100 mM de pH 7.4

5.2.2.4. Calibrado y características analíticas

Trabajando en las condiciones experimentales previamente optimizadas, se estableció un calibrado para la determinación de APN empleando el inmunosensor

HRP-Strept-Biotin-anti-APN-APN-anti-APN-CMC-rGO/SPCE. En la Figura 5.36 se ha representado dicho calibrado, observándose la forma sigmoidal típica de estas configuraciones, mostrándose a la derecha algunos de los amperogramas obtenidos. El tramo lineal se extiende desde 0.5 hasta 10 µg/mL de analito y que responde a la ecuación i, nA = (2356 ± 81) log ([APN], µg/mL) + (1264 ± 46) con R^2 = 0.995. Teniendo en cuenta los niveles de APN que cabe esperar en suero humano, este intervalo de concentración es adecuado para llevar a cabo su determinación en este tipo de muestras.

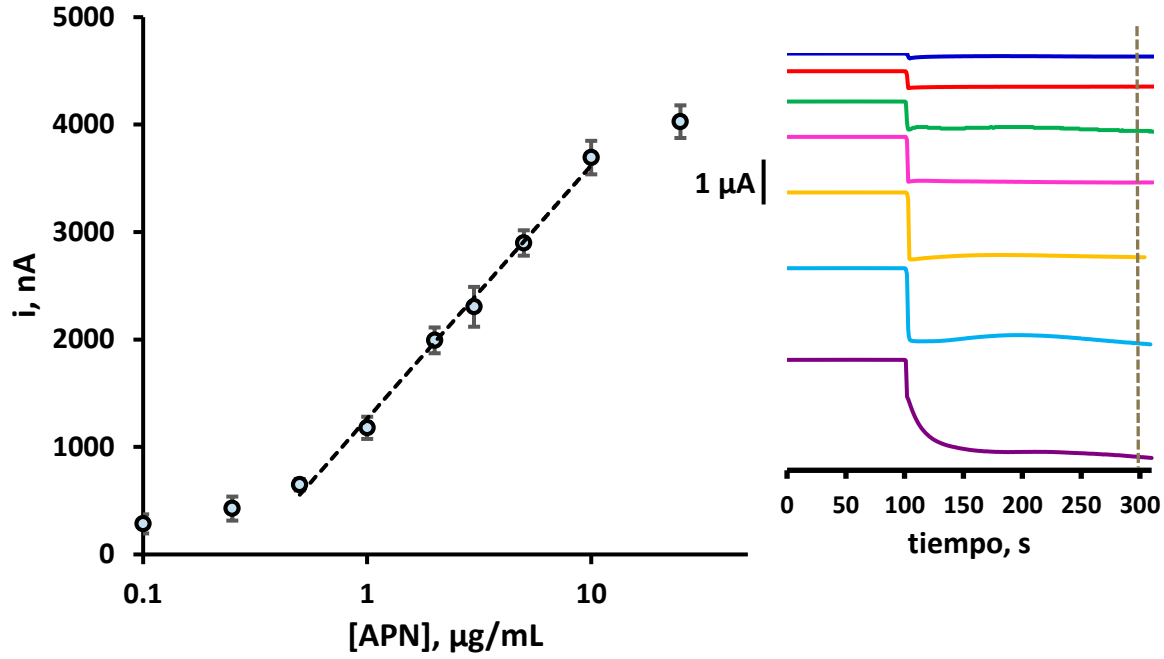

Figura 5.36. Calibrado para la determinación de APN empleando el inmunosensor HRP-Strept-Biotin-anti-APN-APN-anti-APN-CMC-rGO/SPCE

5.2.2.5. Estudio de selectividad

La selectividad del inmunosensor desarrollado se evaluó frente a otras proteínas presentes de forma natural en el organismo y que, por tanto, pueden actuar como potenciales interferentes. Para ello, se midieron las respuestas de distintos inmunosensores en ausencia o en presencia de 3 µg/mL de adiponectina y, a su vez, en ausencia y presencia del compuesto interferente (albúmina de suero bovino (BSA), ceruloplasmima (Cp), proteína C reactiva (CRP), grelina (GHRL) y factor de necrosis tumoral alfa (TNF-α)). Como se observa en la Figura 5.37, los resultados obtenidos

ponen de manifiesto que ninguna de las proteínas a los niveles de concentración ensayados supone una interferencia significativa en la determinación de APN, demostrándose así la alta especificidad de los inmunorreactivos utilizados. Además, al potencial de detección utilizado, tampoco se ha observado que otras sustancias electroactivas, como ácido ascórbico o ácido úrico, interfieran en la detección de adiponectina empleando el inmunosensor desarrollado.

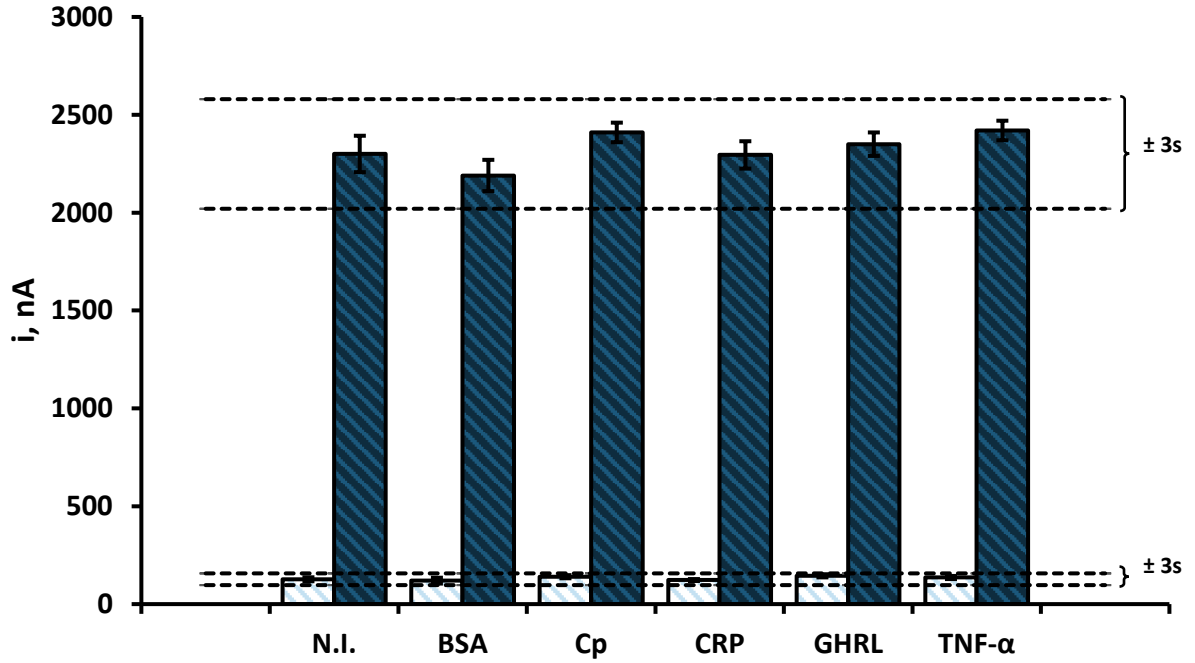

Figura 5.37. Selectividad del inmunosensor HRP-Strept-Biotin-anti-APN-APN-anti-APN-CMC-rGO/SPCE evaluando la respuesta del mismo con 0 (□)o 3 (■) µg/mL de APN frente a 5 mg/mL de BSA, 500 µg/mL de Cp, 1 µg/mL de CRP, 0.5 ng/mL de GHRL y 100 pg/mL de TNF-α

5.2.2.6. Estudios de reproducibilidad y estabilidad

La repetitividad y la reproducibilidad de las medidas amperométricas se evaluó preparando distintos inmunosensores en ausencia y presencia de 2 µg/mL de APN, en el mismo día o en días diferentes. En estas condiciones se obtuvieron valores de RSD del 6.3 y 7.3%, para inmunosensores preparados el mismo día, y del 5.2 y 5.9% para inmunosensores preparados en días diferentes, lo que pone de manifiesto que la precisión alcanzada es aceptable respecto al procedimiento completo de preparación del inmunosensor. Por otro lado, se estudió la estabilidad del inmunoconjugado anti-APN-CMC-rGO/SPCE. Para ello, se prepararon el mismo día distintos electrodos

modificados con el anticuerpo de captura y, tras el bloqueo de la superficie del electrodo de trabajo con BSA al 5%, se almacenaron en seco a –20°C. Cada día de trabajo se prepararon tres inmunosensores y se realizaron las medidas de la respuesta amperométrica en presencia de 7.5 µg/mL de APN. En la Figura 5.38 se ha representado un gráfico de control en el que se señalan los límites de ±3s correspondientes a la medida de la respuesta del inmunosensor el primer día de trabajo.

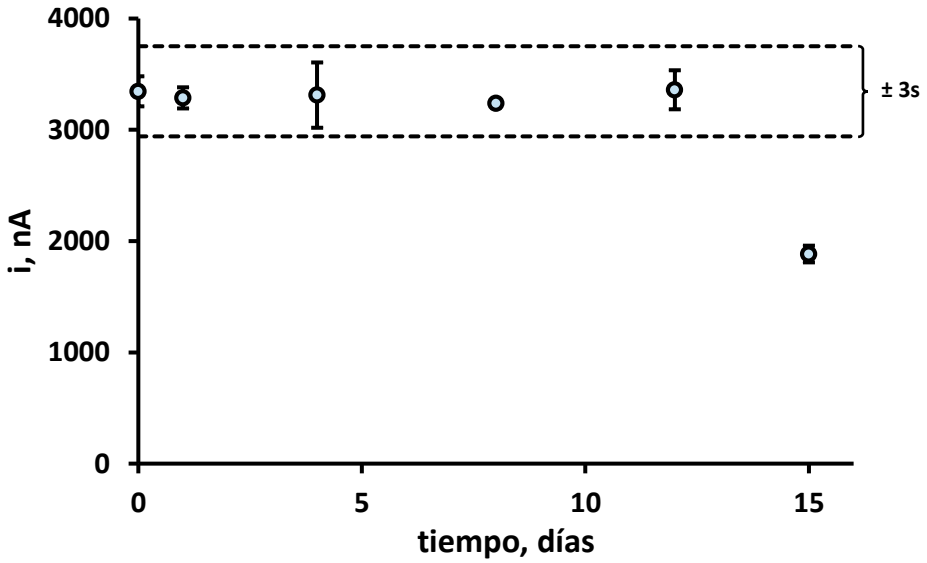

Figura 5.38. Gráfico de control para la evaluación de la estabilidad de almacenamiento del conjugado anti-APN-CMC-rGO/SPCE

Como puede observarse, la media de las tres medidas realizadas cada día se encuentra dentro del intervalo establecido el primer día durante, al menos, 12 días, poniéndose de manifiesto la buena estabilidad de los inmunoconjugados anti-APN-CMC-rGO/SPCE cuando se almacenan en seco a –20°C.

5.2.2.7. Aplicación a la determinación de adiponectina en suero

Para demostrar la aplicabilidad del inmunosensor desarrollado al análisis de muestras reales de interés clínico, se realizó la determinación de esta citoquina en dos muestras de suero humano, una de ellas perteneciente a un paciente con hipercolesterolemia y la otra a un paciente con diabetes tipo 2. Como se ha comentado

anteriormente, la concentración de APN en suero de individuos sanos oscila entre las unidades y las decenas de µg/mL. Sin embargo, en individuos con hipercolesterolemia se han observado mayores concentraciones de APN, siendo menores que en el caso de individuos con diabetes tipo 2.

Como se describe en el *Apartado 4.6.3*. de la *Parte Experimental*, es necesario realizar una dilución 1/50 de la muestra de suero en disolución reguladora PB 100 mM de pH 7.4. Sin embargo, con esta dilución no se evita por completo el efecto matriz, por lo que es necesario realizar un calibrado de adiciones estándar, añadiendo concentraciones crecientes (entre 1 y 3 µg/mL) del patrón de APN sobre las muestras de suero diluidas, con el fin de poder determinar la concentración de esta citoquina en dichas muestras. Es importante destacar que diluciones menores de la muestra en disolución reguladora dieron como resultado grandes disminuciones en el valor de la pendiente del calibrado y, como consecuencia, de la sensibilidad del ensayo.

En la Tabla 5.7 se comparan los resultados obtenidos empleando el inmunosensor con los obtenidos empleando el kit ELISA ab108786 de Abcam, siguiendo el procedimiento de ensayo especificado por la casa comercial.

Tabla 5.7. Determinación de APN en muestras de suero empleando el inmunosensor

MUESTRA	INMUNOSENSOR µg/mL (*n* = 3)*	ELISA µg/mL (*n* = 3)*
hipercolesterolemia	15 ± 2	17 ± 3
diabetes tipo 2	10 ± 2	9 ± 2

* valor medio ± t·s/√n

Los resultados obtenidos confirman que no existen diferencias significativas entre ambas metodologías, quedando demostrada la utilidad del inmunosensor desarrollado para la determinación de APN en muestras de suero humano de individuos con hipercolesterolemia y diabetes tipo 2.

5.2.2.8. Conclusiones

En este trabajo se describe por primera vez la preparación y el funcionamiento de un inmunosensor electroquímico desechable utilizando el híbrido CMC-rGO como plataforma electródica. El excelente comportamiento de este material híbrido, junto con la capacidad del material polimérico Mix&Go™ para inmovilizar de forma estable y orientada el anticuerpo de captura permitió el desarrollo de un inmunosensor para la determinación de APN. Las características analíticas del método desarrollado son apropiadas para la determinación de este analito en muestras de suero humano, obteniéndose resultados concordantes con los proporcionados por un kit ELISA comercial. Es importante destacar ventajas como el menor tiempo de ensayo empleando el inmunosensor (inferior a 2 horas) frente a las más de 5 horas que requiere el inmunoensayo ELISA convencional, y el menor consumo de reactivos y de muestras. Todas estas características hacen de este dispositivo una alternativa muy atractiva para la determinación de esta citoquina.

5.2.3. Inmunosensor para la determinación de factor de crecimiento transformante beta 1

Para la preparación de esta configuración se utilizaron nanotubos de carbono de pared múltiple (MWCNTs) como modificadores de la superficie electródica. El nanomaterial fue funcionalizado con grupos azida para emplearlo como sustrato para la inmovilización del anticuerpo de captura a través de una reacción de cicloadición azida-alquino catalizada por cobre (I) (CuAAC) con inmunoglobulina G etinilada. Como se ha explicado en la *Introducción*, la denominada *"click chemistry"*, de la que esta reacción es la principal representante, se ha convertido en una herramienta eficiente para la inmovilización de biomoléculas. Las ventajas de esta estrategia combinadas con la elevada conductividad de los nanotubos de carbono ha permido desarrollar un inmunosensor estable y de elevada sensibilidad para la determinación de esta citoquina.

5.2.3.1. Configuración del inmunosensor

En la Figura 4.30 de la *Parte Experimental* se representó un esquema de la preparación y funcionamiento del inmunosensor desarrollado. Como se puede apreciar, los nanotubos de carbono funcionalizados con el grupo azida reaccionan con la IgG etinilada mediante la reacción de cicloadición cataizada por ion cuproso. Posteriormente, el anticuerpo de captura anti-TGF se inmoviliza sobre el conjugado IgG-MWCNTs y tras una etapa previa de bloqueo con caseína, tiene lugar la reacción de afinidad con el antígeno TGF-β1 añadiéndose finalmente el anticuerpo de detección biotinilado (Biotin-anti-TGF). Por último, la reacción de afinidad se monitoriza electroquímicamente con el sistema HRP/H_2O_2/HQ (Figura 5.39).

En los apartados que vienen a continuación se caracterizan los nanotubos de carbono modificados con el grupo azida, se optimizan las variables experimentales y se caracterizan las diversas etapas de preparación de inmunosensor. Finalmente, se establecen las características analíticas, se realizan los estudios de selectividad del

inmunoensayo y los de estabilidad y se aplica el inmunosensor desarrollado a la determinación de esta citoquina en muestras de suero.

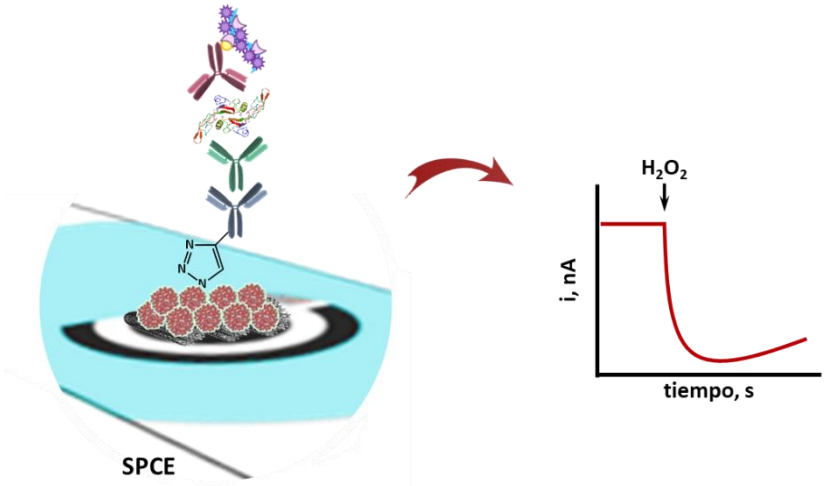

Figura 5.39. Esquema del funcionamiento del inmunosensor para la determinación de TGF-β1

5.2.3.2. Caracterización del nanomaterial azida-MWCNTs

El nanomaterial de carbono funcionalizado con grupos azida se caracterizó empleando la técnica de espectrometría FTIR con los resultados que se han representado en la Figura 5.40. En dicha figura se comparan los espectros obtenidos para la azida comercial utilizada para la funcionalización (*11*-azido-*3,6,9*-trioxaundecan-*1*-amina) y los nanotubos funcionalizados. Como se puede observar, en ambos casos aparece una banda característica a 2106 cm^{-1}, correspondiente al modo de estiramiento simétrico del grupo $–N_3$, que demuestra la funcionalización de los nanotubos de carbono de pared múltiple con el grupo azida. Sin embargo, esta banda no aparece en el espectro registrado para el conjugado IgG-MWCNTs, lo que sugiere la unión exitosa del anticuerpo a través del grupo alquino.

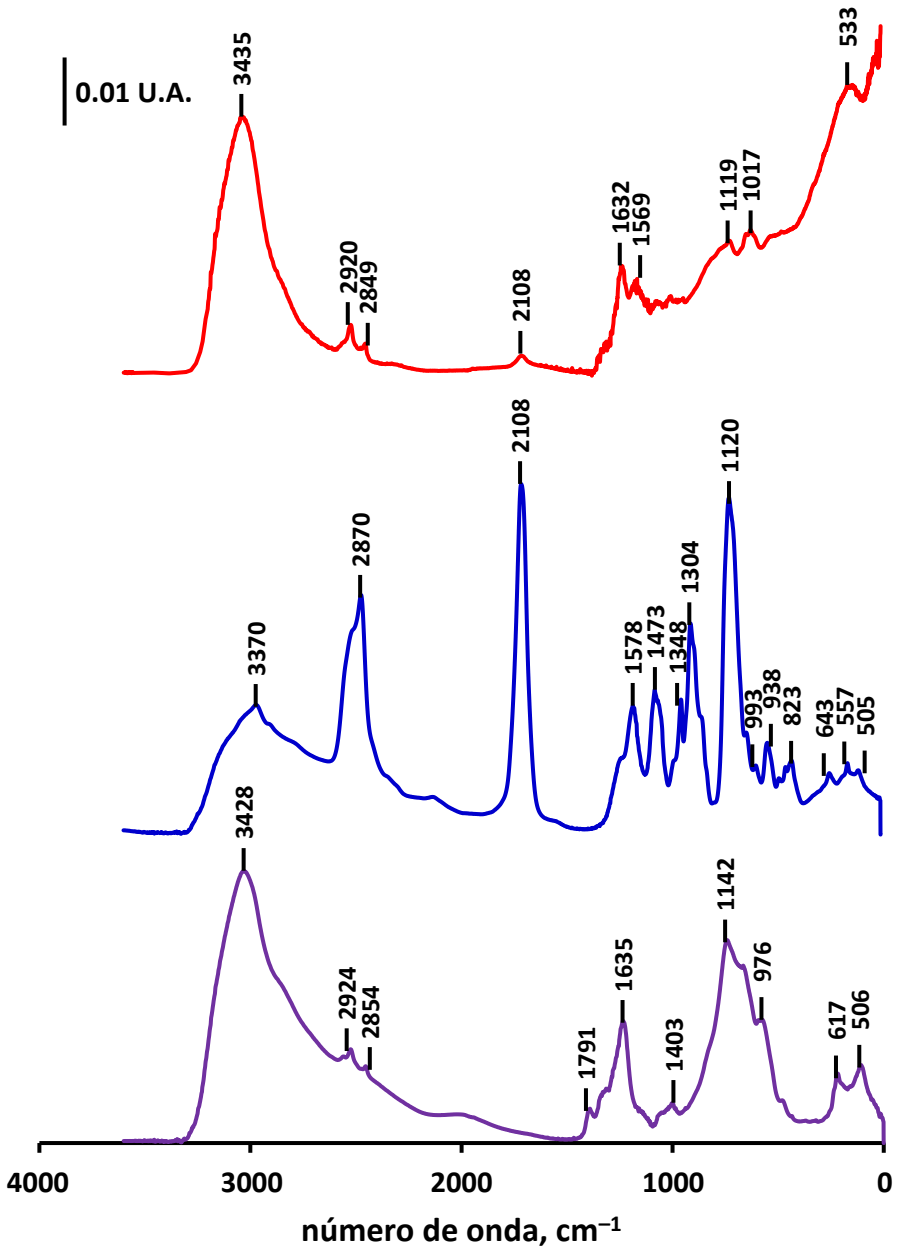

Figura 5.40. Espectros FTIR de: azida-MWCNTs (–), *11*-azido-*3,6,9*-trioxaundecan-*1*-amina (–) e IgG-MWCNTs (–)

5.2.3.3. Optimización de las variables experimentales

Al igual que en otros inmunosensores desarrollados en este trabajo, las variables que afectan a la obtención del conjugado IgG-MWCNTs, así como las implicadas en la preparación y el funcionamiento del inmunosensor para TGF-β1 se optimizaron siguiendo el criterio de la mejor relación señal específica a señal inespecífica (S/R).

Elección del método de funcionalización de la inmunoglobulina G

Para obtener el derivado alquinilado de la IgG se ensayaron dos procedimientos diferentes utilizando los reactivos succinimidil-*3*-propiolato [Qi, 2012] o peryodato sódico [Le, 2013]. Estos procedimientos, obtenidos de la bibliografía y aplicados con ligeras modificaciones, se describieron en los *Apartados 4.5.2.3.2* y *4.5.2.3.3* de la *Parte Experimental*. Para elegir el método de derivatización más adecuado, se compararon las respuestas amperométricas obtenidas empleando diferentes inmunosensores en ausencia o en presencia de 200 pg/mL de TGF-β1 utilizando la IgG etinilada siguiendo el procedimiento descrito en el *Apartado 4.5.2.3.5* de la *Parte Experimental*.

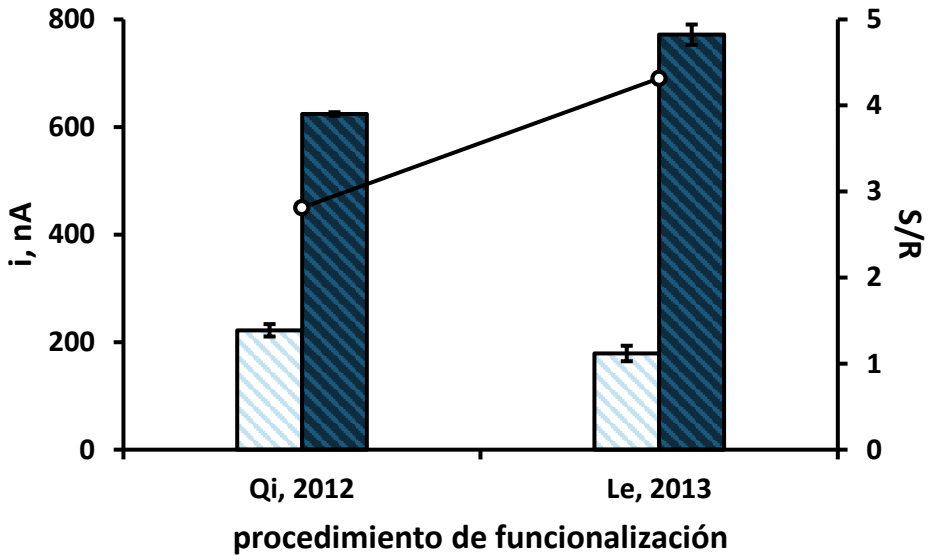

Figura 5.41. Efecto del método de funcionalización de la IgG etinilada sobre la respuesta del inmunosensor: IgG-MWCNTs, 10 µg/mL, 5 µL; Blocker™ Casein; 5 µL, 30 min; anti-TGF, 10 µg/mL, 5 µL, 60 min; TGF-β1, 0 (□) o 200 (■) pg/mL y Biotin-anti-TGF, 1 µg/mL, 5 µL, 60 min; HRP-Strept, 1/2000, 5 µL, 20 min

Como puede observarse en la Figura 5.41, la relación entre las señales específica e inespecífica es un 25% mayor cuando se emplea el procedimiento descrito por Le *et al.* [Le, 2013] para la preparación de la IgG etinilada. Este resultado se debe probablemente a que el peryodato sódico oxida selectivamente los grupos *1,2*-diol de los carbohidratos presentes en la región Fc de la IgG, lo que permite su modificación de forma orientada. Esta circunstancia no se da cuando se utiliza el otro procedimiento, por lo que se eligió el del peryodato sódico para el trabajo posterior.

Influencia de la concentración de la inmunoglobulina G etinilada

Se estudió la influencia de la concentración de la IgG etinilada necesaria para reaccionar con los MWCNTs funcionalizados con el grupo azida para la obtención del inmunoconjugado IgG-MWCNTs. Para ello, se midió la respuesta amperométrica de los inmunosensores preparados empleando disoluciones de la inmunoglobulina de 5, 10 y 20 µg/mL para la obtención del inmunoconjugado, en ausencia y en presencia de 100 pg/mL de TGF-β1, en cada caso. Como se muestra en la Figura 5.42, la mayor relación entre las señales específica e inespecífica se obtuvo empleando una concentración de 10 µg/mL de IgG etinilada.

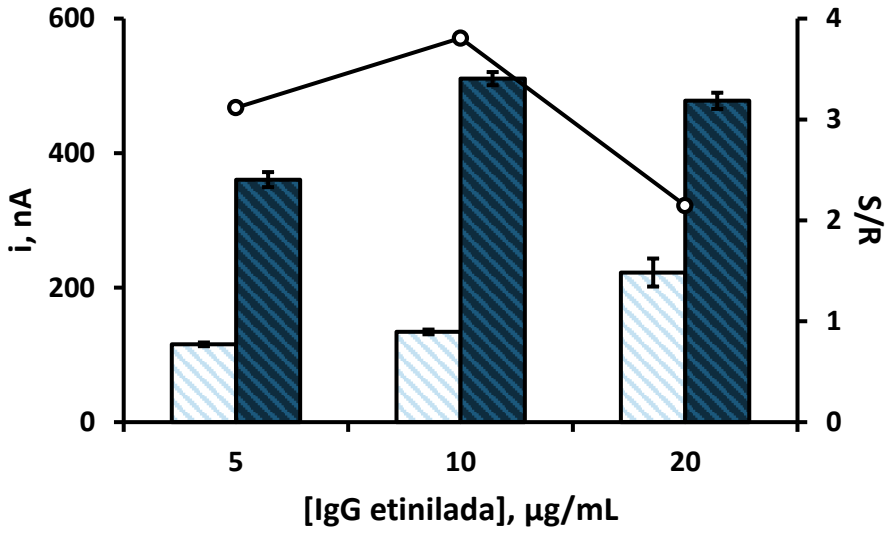

Figura 5.42. Efecto de la concentración de IgG etinilada sobre la respuesta del inmunosensor: IgG-MWCNTs, 5 µL; Blocker™ Casein; 5 µL, 30 min; anti-TGF, 10 µg/mL, 5 µL, 60 min; TGF-β1, 0 (□) o 100 (■) pg/mL y Biotin-anti-TGF, 1 µg/mL, 5 µL, 60 min; HRP-Strept, 1/2000, 5 µL, 20 min

Influencia de la relación entre la inmunoglobulina G etinilada y los nanotubos de carbono de pared múltiple funcionalizados con el grupo azida

Entre las ventajas del empleo de los MWCNTs destacan su elevada conductividad y sus propiedades electrocatalíticas. Sin embargo, una desventaja es que su empleo como modificadores de la superficie electródica proporciona una elevada corriente de fondo. En este caso, además, dicha corriente de fondo depende de la concentración de IgG funcionalizada conjugada a los nanotubos. Así, una

concentración escasa de dicha IgG en el inmunoconjugado podría dejar una gran cantidad de posiciones reactivas libres, difíciles de bloquear, que darían lugar a una corriente de fondo de magnitud relativamente elevada. Por lo contrario, una concentración excesiva de IgG etinilada enlazada a los MWCNTs funcionalizados con los grupos azida podría originar impedimento estérico que ocasionaría una inmovilización ineficaz del anticuerpo de captura anti-TGF.

En la Figura 5.43 se muestran las señales amperométricas obtenidas empleando varios inmunosensores preparados utilizando distintas proporciones de la suspensión de nanotubos de carbono de pared múltiple funcionalizados con el grupo azida y la inmunoglobulina G etinilada, en ausencia y en presencia de TGF-β1. A la vista de los resultados obtenidos se eligió como óptima una relación 1:1 entre ambos.

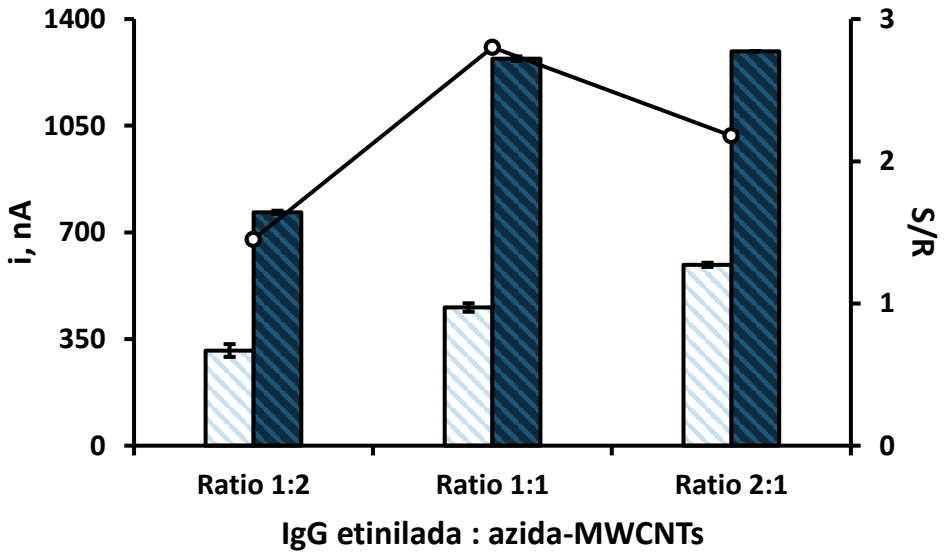

Figura 5.43. Efecto del ratio entre la concentración de IgG etinilada y los azida-MWCNTs sobre la respuesta del inmunosensor: IgG-MWCNTs, 5 µL; Blocker™ Casein; 5 µL, 30 min; anti-TGF, 10 µg/mL, 5 µL, 60 min; TGF-β1, 0 (□) o 100 (■) pg/mL y Biotin-anti-TGF, 1 µg/mL, 5 µL, 60 min; HRP-Strept, 1/2000, 5 µL, 20 min

Influencia de la etapa de bloqueo

Con el objetivo de disminuir al máximo las uniones inespecíficas de los distintos inmunorreactivos sobre la superficie del electrodo IgG-MWCNTs/SPCE, después de la inmovilización de los nanotubos de carbono de pared múltiple funcionalizados con la IgG etinilada y de forma previa a la incorporación del anticuerpo de captura (anti-TGF) se incluyó una etapa de bloqueo incubando el electrodo modificado con el conjugado

en diferentes disoluciones de agentes bloqueantes, en las concentraciones empleadas habitualmente en la preparación de inmunosensores.

En la Figura 5.44 se muestran los resultados obtenidos en ausencia y en presencia de TGF-β1, incubándose las diferentes disoluciones bloqueantes durante 30 minutos. Como puede apreciarse, la disolución comercial de caseína (Blocker™ Casein) es el agente bloqueante más efectivo, puesto que la relación entre las señales específica e inespecífica es mucho mayor que en los otros dos casos.

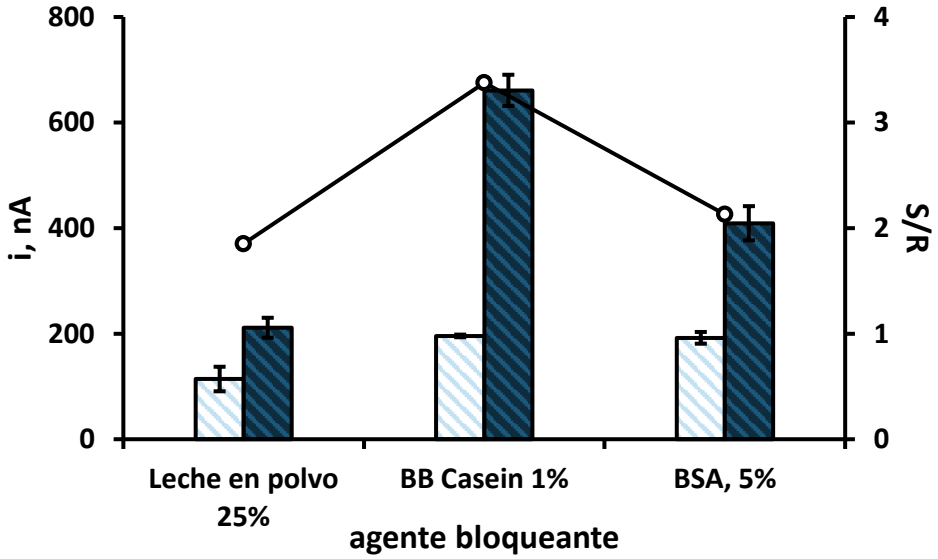

Figura 5.44. Efecto del agente bloqueante sobre la respuesta del inmunosensor: IgG-MWCNTs, 10 µg/mL, 5 µL; agente bloqueante; 5 µL, 30 min; anti-TGF, 10 µg/mL, 5 µL, 60 min; TGF-β1, 0 (▨) o 100 (■) pg/mL y Biotin-anti-TGF, 1 µg/mL, 5 µL, 60 min; HRP-Strept, 1/2000, 5 µL, 20 min

Influencia de la concentración del anticuerpo de captura

La concentración del anticuerpo de captura juega un papel decisivo en la sensibilidad de los inmunosensayos y en la amplitud del intervalo lineal. Para optimizar esta variable, se midió la respuesta amperométrica de distintos inmunosensores preparados por inmovilización de 5 µL de disoluciones de anti-TGF en el intervalo de concentraciones comprendido entre 5 y 20 µg/mL, durante 60 minutos sobre los electrodos IgG-MWCNTs/SPCE, en ausencia y en presencia de 100 pg/mL de TGF-β1.

De este modo, como se observa en la Figura 5.45, la concentración óptima de anticuerpo de captura es de 10 µg/mL, ya que la relación entre las señales específica

e inespecífica es mayor. La disminución de esta relación para mayores concentraciones de anticuerpo se debe probablemente a la existencia de impedimento estérico que dificulta la formación de los inmunocomplejos.

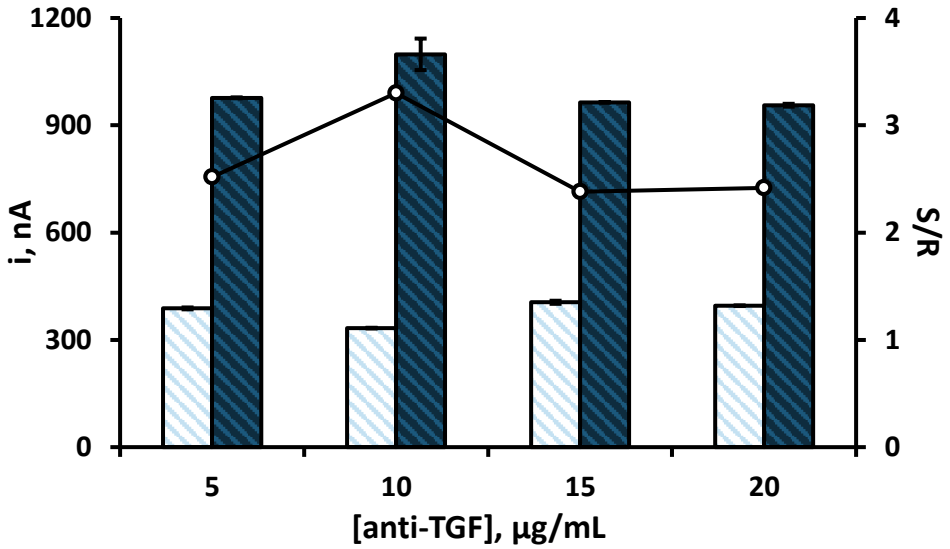

Figura 5.45. Efecto de la concentración de anti-TGF sobre la respuesta del inmunosensor: IgG-MWCNTs, 10 µg/mL, 5 µL Blocker™ Casein; 5 µL, 30 min; anti-TGF, 5 µL, 60 min; TGF-β1, 0 (□) o 100 (■) pg/mL y Biotin-anti-TGF, 1 µg/mL, 5 µL, 60 min; poli-HRP-Strept, 1/500, 5 µL, 20 min

Influencia de las etapas de incubación del antígeno y del anticuerpo de detección biotinilado

Para seleccionar los tiempos de incubación del antígeno TGF-β1 sobre el inmunosensor anti-TGF-IgG-MWCNTs/SPCE y del anticuerpo biotinilado sobre el bioelectrodo resultante, TGF-anti-TGF-IgG-MWCNTs/SPCE, se evaluó la respuesta obtenida en ausencia y en presencia de 200 pg/mL de TGF-β1. Al mismo tiempo, se evaluó también la posibilidad de acortar los tiempos de ensayo llevando a cabo una única etapa de incubación en una mezcla de ambos biorreactivos, en lugar de realizar dos etapas de incubación en cada una de estas disoluciones por separado.

Como puede observarse en la Figura 5.46, la corriente obtenida en presencia de TGF-β1 es mucho mayor cuando se lleva a cabo la incubación en la disolución del antígeno y del anticuerpo biotinilado en dos etapas por separado, si bien también se observa un aumento considerable de la señal inespecífica. Debido a la imposibilidad de disminuir dicha señal incluso añadiendo agente bloqueante (BSA al 1% (p/v)) a las

disoluciones de los inmunorreactivos de forma adicional a la etapa de bloqueo optimizada previamente con caseína, se optó por llevar a cabo la incubación de los dos biorreactivos en una etapa conjunta ya que es superior la relación de señales obtenida en presencia y en ausencia de analito, además de ser menor el tiempo de análisis.

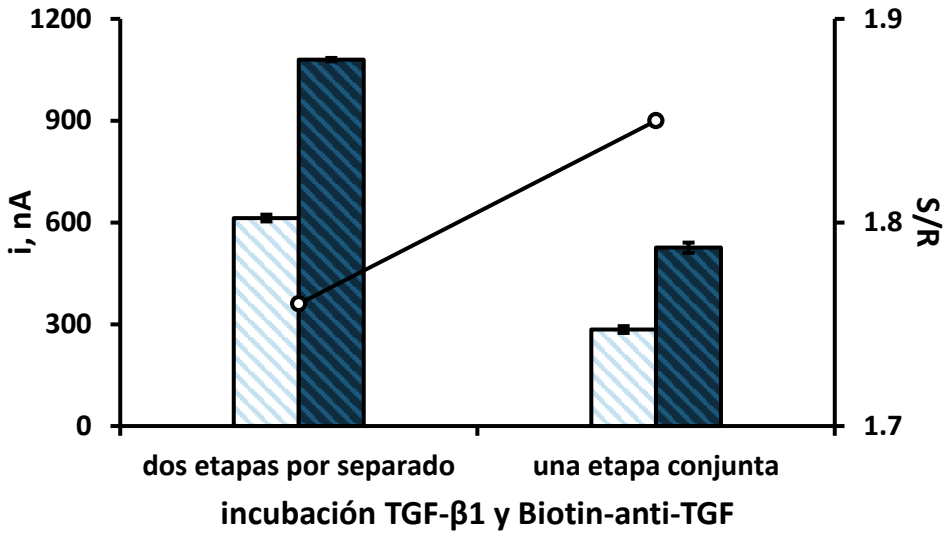

Figura 5.46. Efecto de la incubación de TGF-β1 y Biotin-anti-TGF sobre la respuesta del inmunosensor: IgG-MWCNTs, 10 µg/mL, 5 µL Blocker™ Casein; 5 µL, 30 min; anti-TGF, 10 µg/mL, 5 µL, 60 min; TGF-β1, 0 (□) o 200 (■) pg/mL; Biotin-anti-TGF, 1 µg/mL, 5 µL, 60 min; poli-HRP-Strept, 1/500, 5 µL, 20 min

Influencia de la concentración del anticuerpo de detección biotinilado

Por lo que respecta a la influencia de la concentración de Biotin-anti-TGF sobre la respuesta del inmunosensor, en la Figura 5.47 se muestran los resultados obtenidos para concentraciones comprendidas entre 0.5 y 10 µg/mL. Como puede observarse, la señal inespecífica aumenta gradualmente al aumentar la concentración de Biotin-anti-TGF, mientras que la señal específica, obtenida en presencia de TGF-β1, crece hasta una concentración de 1 µg/mL del anticuerpo de detección biotinilado, estabilizándose para valores superiores. En vista de los resultados obtenidos, se eligió la citada concentración de 1 µg/mL, puesto que proporciona la mayor diferencia entre las señales específica e inespecífica.

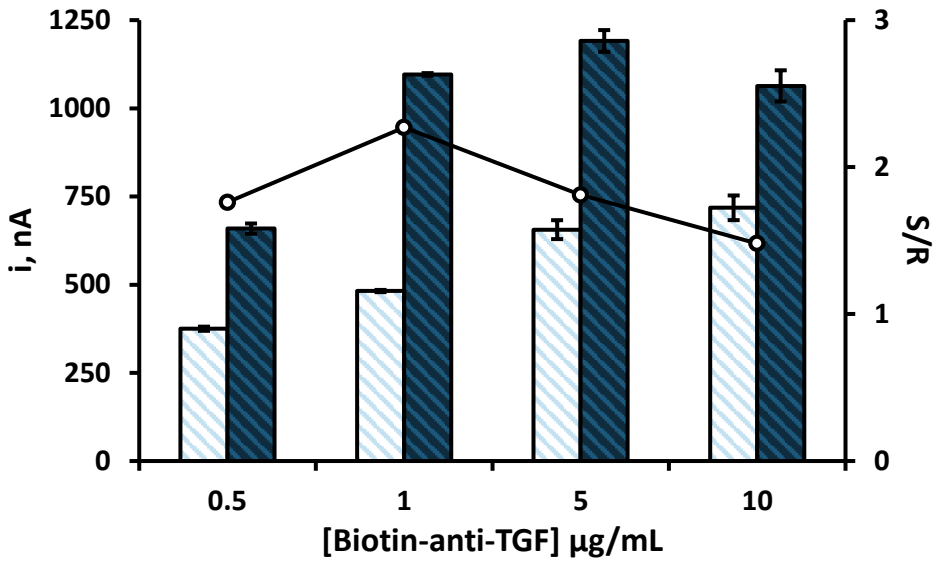

Figura 5.47. Efecto de la concentración de Biotin-anti-TGF sobre la respuesta del inmunosensor: IgG-MWCNTs, 10 µg/mL, 5 µL; Blocker™ Casein, 5 µL, 30 min; anti-TGF, 10 µg/mL, 5 µL, 60 min; TGF-β1, 0 (□) o 200 (■) pg/mL y Biotin-anti-TGF, 5 µL, 60 min; poli-HRP-Strept, 1/500, 5 µL, 20 min

Influencia del tipo y la dilución del conjugado enzimático

Con el objetivo de obtener una mayor sensibilidad, se utilizó una estrategia de amplificación de la señal electroquímica obtenida con el inmunosensor empleando un polímero de estreptavidina y peroxidasa (poli-HRP-Strept) cuyo efecto sobre la respuesta amperométrica se comparó con la obtenida empleando el conjugado de estreptavidina y peroxidasa convencional (HRP-Strept).

Como cabía esperar, los resultados mostrados en la Figura 5.48 ponen de manifiesto un aumento considerable de la intensidad de corriente registrada en presencia del antígeno cuando se emplea el polímero (poli-HRP-Strept), lo que se debe probablemente a la mayor cantidad de enzima presente sobre el electrodo que cuando se emplea el conjugado convencional. Además, aunque usando poli-HRP-Strept se observa también una mayor corriente en ausencia de TGF-β1 debida a las adsorciones inespecíficas, la relación de señales es considerablemente mayor, por lo que se eligió el polímero para la preparación del inmunosensor.

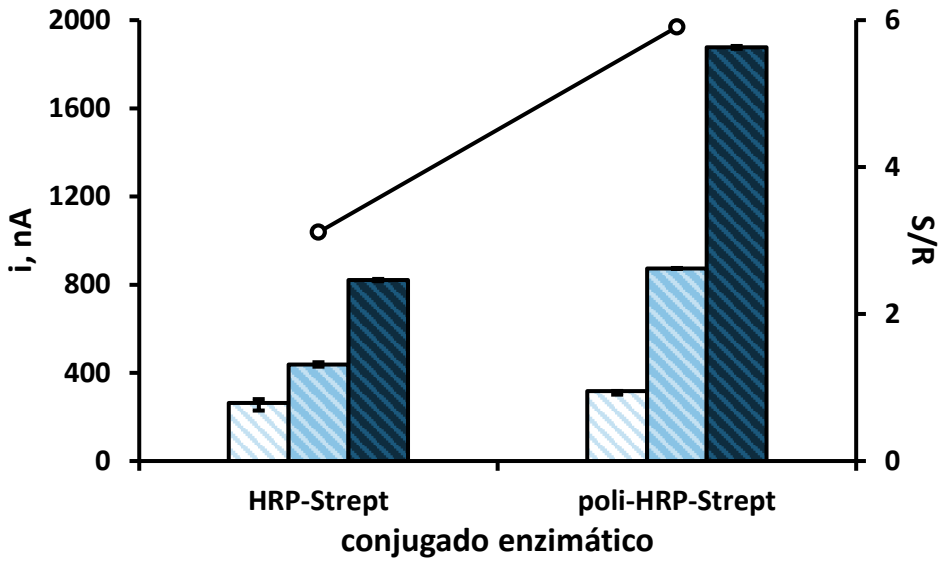

Figura 5.48. Efecto del tipo de conjugado enzimático sobre la respuesta del inmunosensor: IgG-MWCNTs, 10 µg/mL, 5 µL Blocker™ Casein; 5 µL, 30 min; anti-TGF, 10 µg/mL, 5 µL, 60 min; TGF-β1, 0 (□), 100 (▨) o 200 (■) pg/mL y Biotin-anti-TGF, 5 µL, 60 min; conjugado enzimático, 5 µL, 20 min

Finalmente, una vez elegida esta opción, se optimizó la dilución del conjugado poli-HRP-Strept con los resultados que aparecen en la Figura 5.49 se muestran los resultados obtenidos para diluciones del polímero comprendidas entre 1/250 y 1/2000.

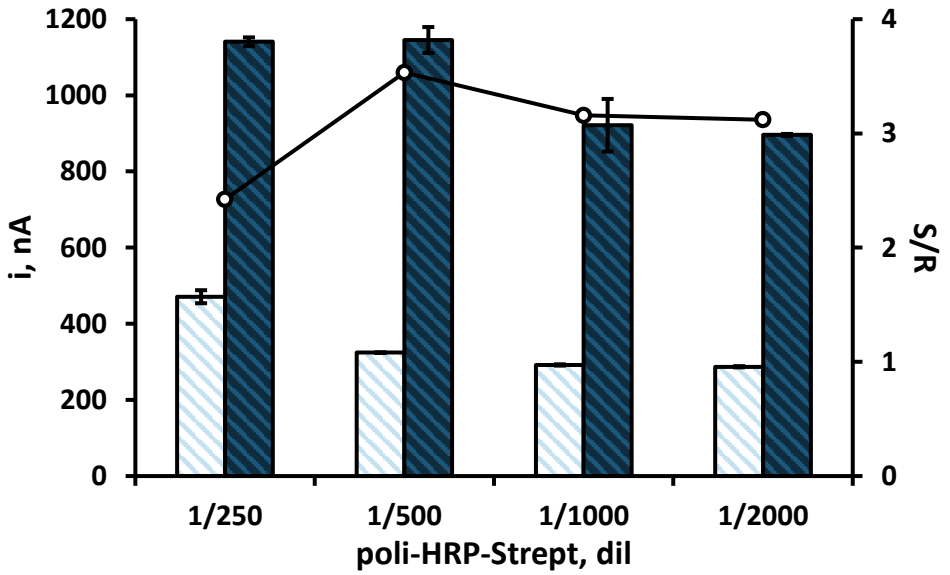

Figura 5.49. Efecto de la dilución de poli-HRP-Strept sobre la respuesta del inmunosensor: IgG-MWCNTs, 10 µg/mL, 5 µL Blocker™ Casein; 5 µL, 30 min; anti-TGF, 10 µg/mL, 5 µL, 60 min; TGF-β1, 0 (□) o 100 (■) pg/mL y Biotin-anti-TGF, 5 µL, 60 min; poli-HRP-Strept, 5 µL, 20 min

Como puede observarse, la dilución 1/500 es la que proporciona una mayor relación entre las señales específica e inespecífica, por lo que se eligió para estudios posteriores.

Por último, los resultados obtenidos en estos estudios se resumen en la Tabla 5.8, donde se recogen las distintas variables, los intervalos evaluados y los valores seleccionados para estudios posteriores.

Tabla 5.8. Optimización de las variables experimentales implicadas en la construcción del inmunosensor poli-HRP-Strept-Biotin-anti-TGF-TGF-β1-anti-TGF-IgG-MWCNTs/SPCE

VARIABLE EXPERIMENTAL	INTERVALO EVALUADO	VALOR SELECCIONADO
método de funcionalización de la IgG	Qi, 2012; Le, 2013	Le, 2013
[IgG etinilada], µg/mL	5 – 20	10
Relación IgG/MWCNTs	1:2 – 2:1	1:1
agente bloqueante	BSA, Blocker™ Casein, leche en polvo	Blocker™ Casein
[anti-TGF], µg/mL	5 – 20	10
[Biotin-anti-TGF], µg/mL	0.5 – 10	1
incubación TGF-β1 y Biotin-anti-TGF	1 o 2 etapas	1 etapa
conjugado enzimático	HRP-Strept, poli-HRP-Strept	poli-HRP-Strept
poli-HRP-Strept, dil	1/250 – 1/2000	1/500

5.2.3.4. Caracterización de la superficie electródica

Las etapas involucradas en la modificación de la superficie electródica se monitorizaron mediante espectroscopia de impedancia electroquímica (EIS). La Figura 5.50. muestra los diagramas de Nyquist registrados para el electrodo serigrafiado de carbono desnudo (SPCE) así como para los diferentes electrodos modificados tras la deposición de los nanotubos de carbono funcionalizados con el grupo azida (azida-MWCNTs/SPCE), una vez conjugada la IgG alquinil-funcionalizada (IgG-MWCNTs/SPCE), y tras la incorporación del anticuerpo de captura

(anti-TGF-IgG-MWCNTs/SPCE) utilizando una disolución de $Fe(CN)_6^{4-/3-}$ 5 mM preparada en disolución reguladora PBS de pH 7.4 como sonda redox. En la Figura 5.50 se han representado también los circuitos equivalentes empleados para ajustar a dichas representaciones.

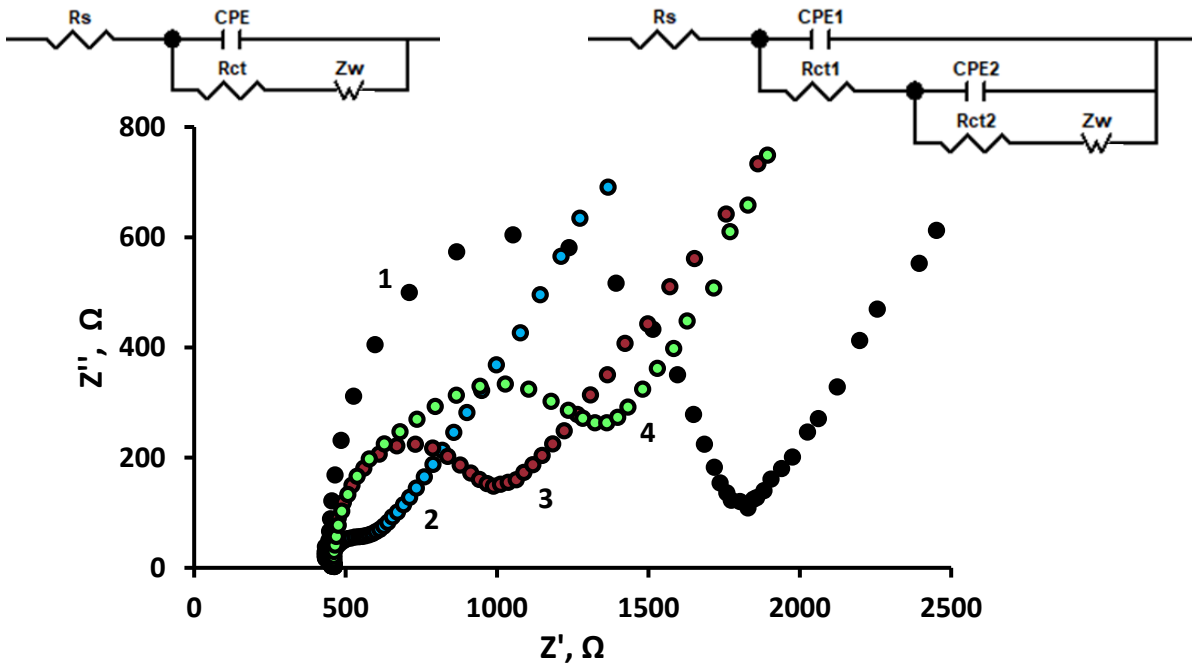

Figura 5.50. Diagramas de Nyquist registrados para: a) 1) SPCE, 2) azida-MWCNTs/SPCE, 3) IgG-MWCNTs/SPCE y 4) anti-TFG-IgG-MWCNTs/SPCE en una disolución $Fe(CN)_6^{3-/4-}$ 5 mM en PBS de pH 7.4

Los diagramas 1, 2 y 3 se ajustan bien a un circuito de Randles, mientras que el diagrama 4 se ajusta mejor al circuito equivalente representado a la derecha, que pone de manifiesto la coexistencia de algunas zonas de la superficie electródica recubiertas con el anticuerpo de captura con otras directamente expuestas a la sonda redox. Efectivamente, la presencia de circuitos RC dispuestos en paralelo sugieren la presencia sobre la superficie electródica de una película con un espesor no uniforme o bien con defectos o poros [Bardini, 2015].

En cuanto a la resistencia a la transferencia de carga (R_{ct}) en el electrodo desnudo, su valor es notablemente mayor (1247 Ω) que cuando se incorporan los nanotubos de carbono de pared doble funcionalizados con el grupo azida (240 Ω), debido a la elevada conductividad de los MWCNTs. Asimismo, la resistencia aumentó hasta los 658 Ω al incorporar el conjugado IgG-MWCNTs, como consecuencia del

efecto aislante de la biomolécula. La inmovilización posterior del anticuerpo de captura condujo a un aumento adicional de la resistencia a la transferencia electrónica (865 Ω), debido al bloqueo aún mayor de la superficie modificada. Estos resultados confirman la inmovilización eficaz del conjugado anti-TGF-IgG-MWCNTs sobre la superficie electródica.

5.2.3.5. Calibrado y características analíticas

Utilizando las condiciones experimentales optimizadas anteriormente y empleando la amperometría como técnica de medida, se obtuvo el calibrado para la determinación de TGF-β1 que se muestra en la Figura 5.51 junto a algunos de los amperogramas obtenidos para distintas concentraciones de TGF-β1. Como cabe esperar, en la configuración tipo sándwich desarrollada, un incremento en la concentración de TGF-β1 se traduce en una mayor concentración de Biotin-anti-TGF inmovilizada sobre el electrodo y, por tanto, también del conjugado poli-HRP-Strept, lo que da lugar a un incremento en la intensidad de corriente obtenida. En este caso, se obtuvo una relación lineal entre la intensidad de corriente y la concentración de TGF-β1 entre 5 y 200 pg/mL, siendo la ecuación de la recta de calibrado $\Delta i, nA = (5.6 \pm 0.1)$ ([TGF-β1], pg/mL) + (32.5 ± 0.9) ($R^2 = 0.995$), donde Δi es la corriente obtenida tras la sustracción de la corriente de fondo medida para el inmunosensor en ausencia de antígeno. Es de destacar que este intervalo es adecuado para la determinación de esta citoquina en suero humano ya que los niveles de concentración encontrados en individuos sanos están comprendidos entre 0.1 y 25 ng/mL [Grainger, 2000]. El límite de detección obtenido, 1.3 pg/mL, se calculó como la concentración más baja que puede ser estadísticamente discriminada de la señal proporcionada por el blanco, de acuerdo con la expresión $\bar{x} + 3 \cdot s$, donde s es la desviación estándar calculada a partir de las respuestas amperométricas obtenidas para diez réplicas en ausencia de TGF-β1, en unidades de concentración, pg/mL. Asimismo, el límite de cuantificación alcanzado fue de 4.3 pg/mL, obtenido a partir de la expresión $\bar{x} + 10 \cdot s$.

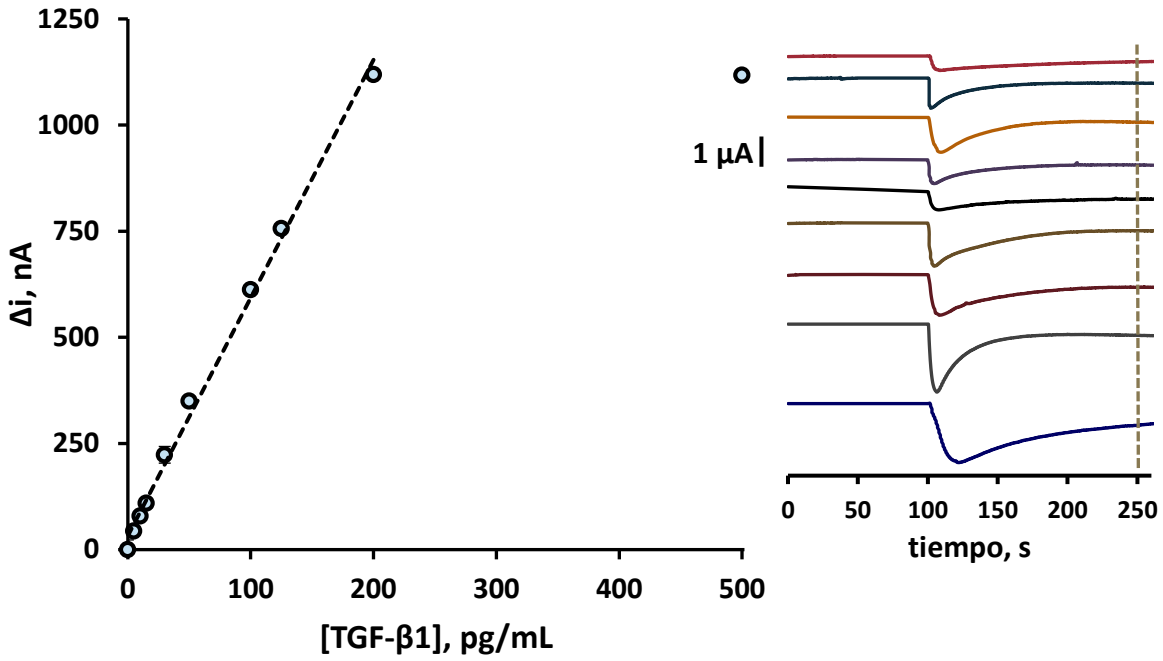

Figura 5.51. Calibrado para la determinación de TGF-β1 empleando el inmunosensor poli-HRP-Strept-Biotin-anti-TGF-TGF-β1-anti-TGF-IgG-MWCNTs/SPCE

Cuando se comparan las características analíticas obtenidas con el inmunosensor desarrollado con las proporcionadas por los kits ELISA comerciales mostrados en la Tabla 3.6 de la *Introducción*, pueden observarse algunas diferencias. En el caso de los kits ELISA, aparecen intervalos lineales que abarcan desde las pocas decenas a varios miles de pg/mL con límites de detección de pocas unidades de pg/mL. Sin embargo, hay que mencionar que la mayoría de los calibrados son logarítmicos, lo que redunda en una menor precisión. Además, los tiempos de ensayo son mucho más largos, consumiendo algo más de 3 horas, frente a los 80 minutos del inmunosensor, contando en ambos casos a partir del momento en que se inmoviliza el anticuerpo de captura. Por otra parte, el límite de detección alcanzado con el método desarrollado en este trabajo es más de 200 veces inferior al obtenido con el aptasensor desarrollado por Matharu *et al.* [Matharu, 2014] y más de 100 veces inferior al obtenido por el inmunosensor impedimétrico Yao *et al.* [Yao, 2016].

5.2.3.6. Estudio de selectividad

Para evaluar la selectividad del inmunosensor desarrollado, se compararon las respuestas amperométricas obtenidas en ausencia y en presencia de 125 pg/mL de TGF-β1 y, a su vez, en ausencia y en presencia de cada uno de los compuestos ensayados como interferentes, a los niveles de concentración que se pueden encontrar en muestras de suero de individuos sanos. Los compuestos ensayados fueron: adiponectina (APN), albúmina de suero bovino (BSA), bilirrubina (BIL), colesterol (Chol), ceruloplasmina (Cp), factor de necrosis tumoral alfa (TNF-α), grelina (GHRL), hemoglobina (HB), interleucina 6 (IL-6), interleucina 8 (IL-8) y proteína C reactiva (CRP). Los resultados obtenidos, que se muestran en la Figura 5.52, demostraron que ninguna de estas proteínas, a los niveles de concentración ensayados, supone una interferencia significativa en la determinación de TGF-β1 empleando el inmunosensor, demostrando así la alta selectividad de la configuración desarrollada.

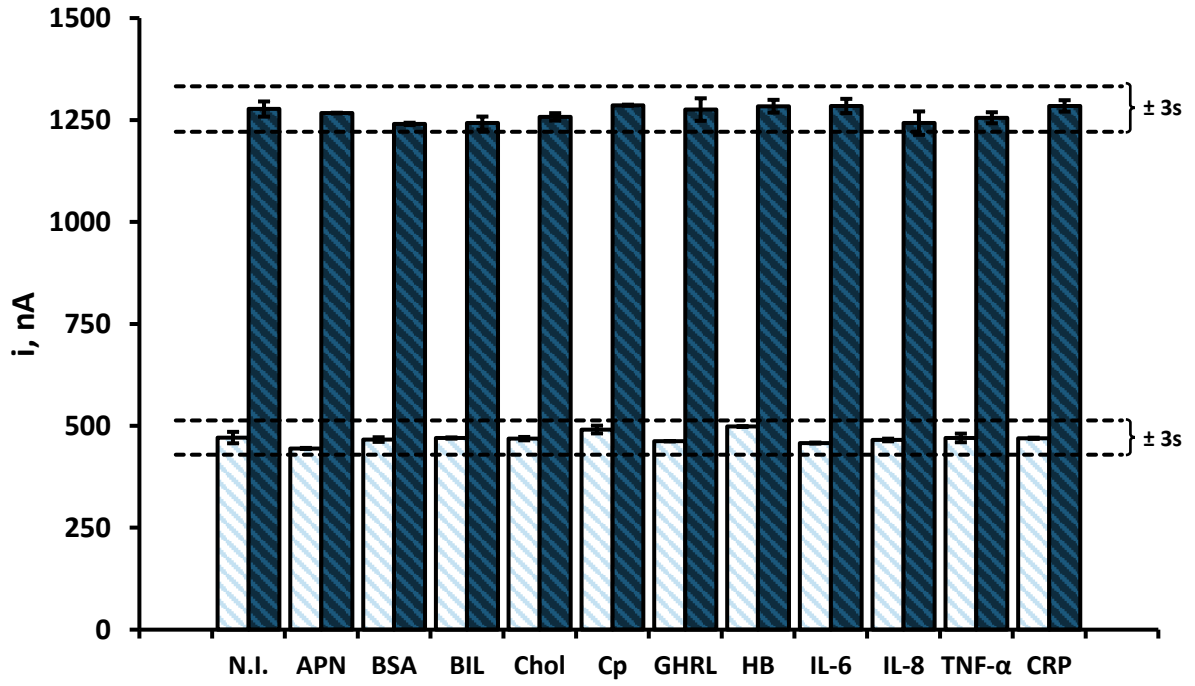

Figura 5.52. Selectividad del inmunosensor poli-HRP-Strept-Biotin-anti-TGF-TGF-β1-anti-TGF-IgG-MWCNTs/SPCE evaluando la respuesta del mismo con 0 (□) o 125 (■) pg/mL de TGF-β1 frente a 20 µg/mL de APN, 5 µg/mL de BSA, 190 ng/mL de BIL, 20 µg/mL de Chol, 500 µg/mL de Cp, 100 pg/mL de TNF-α, 500 pg/mL de GHRL, 50 µg/mL de HB, 50 µg/mL de IL-6, 30 pg/mL de IL-8 y 1 µg/mL de CRP

5.2.3.7. Estudios de reproducibilidad y estabilidad

Los estudios de repetibilidad de las medidas se realizaron midiendo la respuesta amperométrica de cinco inmunosensores diferentes fabricados el mismo día, en ausencia y en presencia de 125 pg/mL de TGF-β1. Los valores de RSD obtenidos fueron del 1.5 y 2.7 %, respectivamente. Asimismo, la reproducibilidad de las medidas se evaluó también empleando cinco inmunosensores preparados en distintos días, obteniendo valores de RSD del 1.9 y 2.5 %, en ausencia y en presencia de la misma concentración de TGF-β1, respectivamente. Estos resultados demuestran la buena precisión de las medidas y ponen de manifiesto que el procedimiento de fabricación del inmunosensor es fiable y reproducible.

También se estudió la estabilidad del inmunoconjugado anti-TGF-IgG-MWCNTs/SPCE. Para ello, se prepararon en el mismo día distintos electrodos modificados con el anticuerpo de captura que, tras la etapa de bloqueo con caseína (Blocker™ Casein), se almacenaron en condiciones de humedad a 8°C, depositando sobre ellos un volumen de 20 µL de disolución Reagent Diluent 1 recomendada por la casa comercial. Después, de forma sucesiva, cada día de trabajo se prepararon tres inmunosensores a partir de los electrodos previamente modificados con el inmunoconjugado y se realizaron las medidas de la respuesta amperométrica en presencia de 125 pg/mL de TGF-β1.

En la Figura 5.53 se ha representado el gráfico de control en el que los márgenes establecidos corresponden a ± 3 veces la desviación estándar de las medidas realizadas el primer día de trabajo. Como puede observarse, la media de las tres medidas realizadas cada día se encuentra dentro del intervalo establecido el primer día durante, al menos, 40 días (no se estudiaron tiempos superiores), poniéndose de manifiesto la excelente estabilidad de almacenamiento de los inmunoconjugados anti-TGF-IgG-MWCNTs/SPCE cuando se almacenan en condiciones de humedad a 8°C.

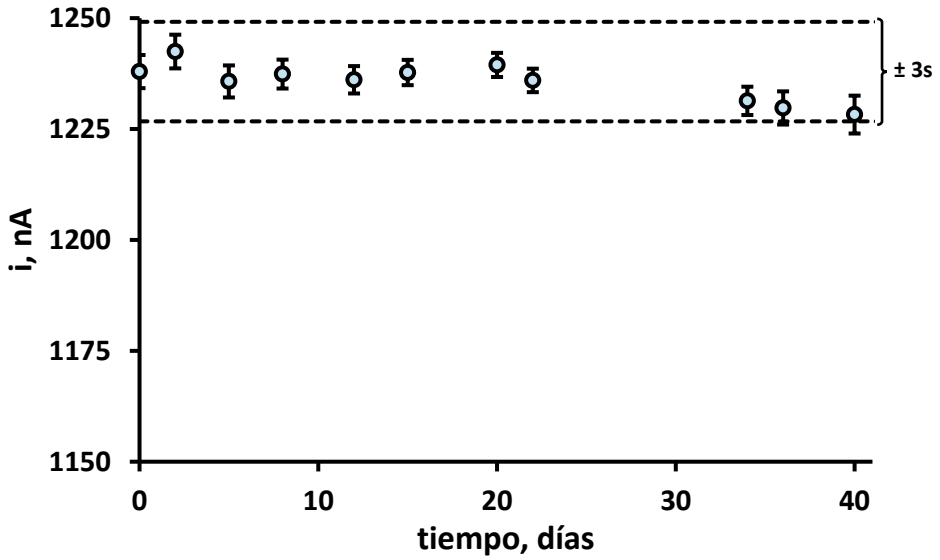

Figura 5.53. Gráfico de control para la evaluación de la estabilidad de almacenamiento del conjugado anti-TGF-IgG-MWCNTs/SPCE

5.2.3.8. Aplicación a la determinación de factor de crecimiento transformante beta 1 en suero

La utilidad analitica del inmunosensor desarrollado se ha demostrado mediante aplicación a la determinación de TGF-β1 en muestras de suero siguiendo el protocolo descrito en el *Apartado 4.6.4.* del *Desarrollo Experimental*.

En primer lugar, se analizó la muestra de suero humano liofilizado evaluando la posible existencia de efecto matriz. En la Figura 5.54 se recogen las respuestas amperométricas obtenidas empleando distintas diluciones del suero en disolución reguladora PBS de pH 7.4, en ausencia y en presencia de una concentración final de 125 pg/mL de TGF-β1. Como se puede observar, para una dilución 1/10 de suero liofilizado en PBS de pH 7.4 se observa un ligero efecto matriz debido a los componentes de la matriz del suero. Sin embargo, a partir de una dilución 1/50 el efecto matriz desaparece. Teniendo en cuenta la elevada sensibilidad de la configuración desarrollada y con el objetivo de asegurar por completo la eliminación de cualquier efecto matriz, se seleccionó una dilución 1/100 como la más adecuada para la determinación de TGF-β1 en suero humano.

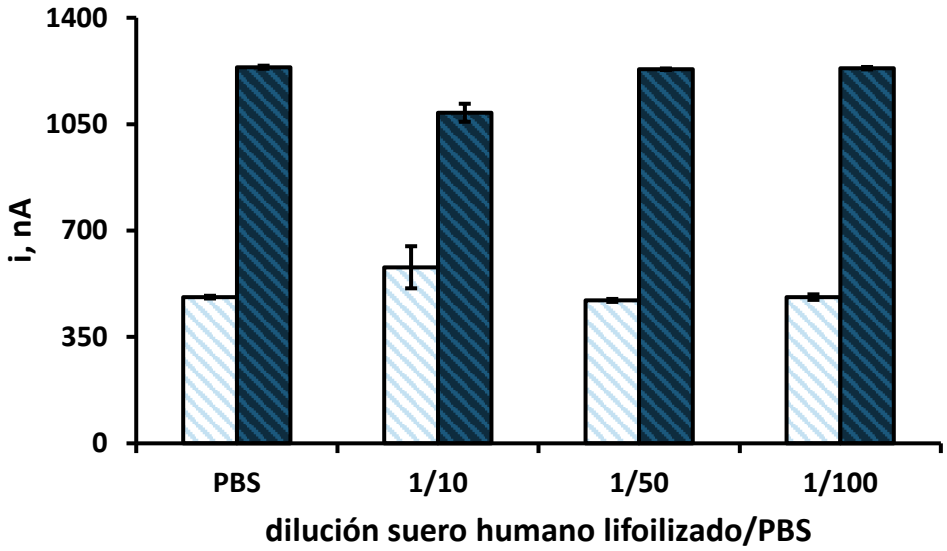

Figura 5.54. Evaluación de la influencia de la dilución del suero humano liofilizado en la respuesta amperométrica del inmunosensor poli-HRP-Strept-Biotin-anti-TGF-TGF-β1-anti-TGF-IgG-MWCNTs/SPCE

A continuación se construyó una curva de calibrado de la muestra enriqueciendo el suero liofilizado (dilución 1/100) con distintas concentraciones de analito (25, 75 y 125 pg/mL) y se comparó la pendiente de la ecuación de calibrado (5.57 ± 0.01) nA mL/pg con la obtenida empleando disoluciones estándar, (5.6 ± 0.1) nA mL/pg, no existiendo diferencias significativas entre estos dos valores.

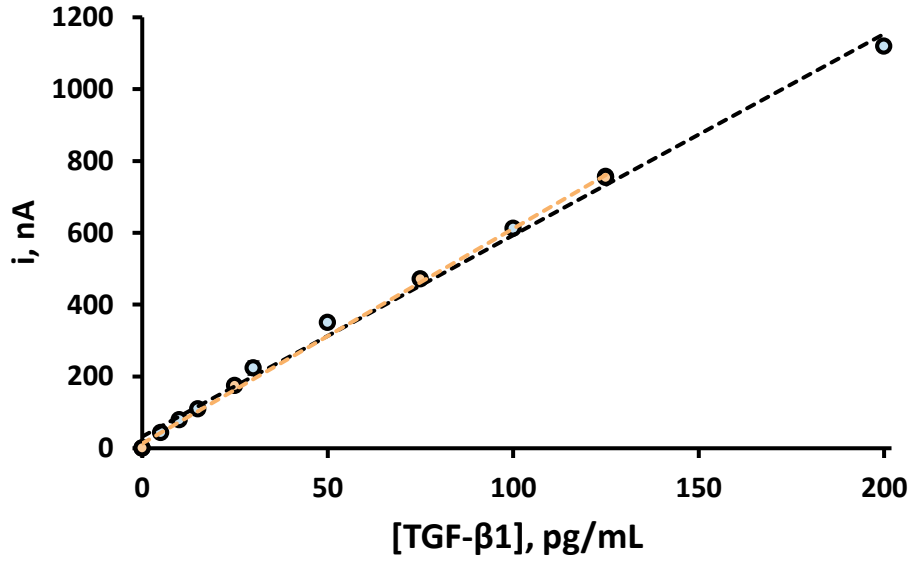

Figura 5.54. Superposición de las señales obtenidas para el suero liofilizado enriquecido (●) en el calibrado de disoluciones estándar (○)

En la Figura 5.55 se han superpuesto ambos calibrados observándose una gran similitud entre ambas rectas. Estos resultados demuestran que a la dilución aplicada

es posible determinar la concentración de TGF-β1 en suero por interpolación directa de la señal proporcionada por la muestra en el calibrado de disoluciones estándar.

En la Tabla 5.9 se resumen los resultados obtenidos en la determinación, por triplicado, para las muestras enriquecidad con distintas concentraciones de TGF-β1.

Tabla 5.9. Determinación de TGF-β1 en muestras de suero humano liofilizado empleando el inmunosensor poli-HRP-Strept-Biotin-anti-TGF-TGF-β1-anti-TGF-IgG-MWCNTs/SPCE

[TGF-β1] AÑADIDO, pg/mL	[TGF-β1] RECUPERADO, pg/mL*	RECUPERACIÓN, %*
25	25 ± 2	100 ± 9
75	76 ± 3	101 ± 4
125	123 ± 1	98 ± 1

* valor medio ± t·s/√n

Como puede observarse, los porcentajes de recuperación se encuentran entre el 98 y el 101%, lo que pone de manifiesto la elevada fiabilidad de la metodología propuesta para la determinación de este analito en este tipo de muestra, siguiendo un protocolo de trabajo tan simple. Además, al igual que en otras configuraciones presentadas en esta Memoria, se compararon los resultados obtenidos empleando el inmunosensor con los obtenidos empleando el kit DuoSet® ELISA Development System (DY240–05) de R&D Systems, siguiendo el procedimiento de ensayo especificado por la casa comercial (Tabla 5.10).

Tabla 5.10. Determinación de TGF-β1 en muestras de suero empleando el inmunosensor

MUESTRA	INMUNOSENSOR ng/mL (*n* = 3)*	ELISA ng/mL (*n* = 3)*
individuo sano (SG609-2, BBI)	1.38 ± 0.05	1.40 ± 0.02
hipercolesterolemia (SG376-2, BBI)	2.11 ± 0.06	2.10 ± 0.04

* valor medio ± t·s/√n

Los resultados obtenidos confirman que no existen diferencias significativas entre ambas metodologías, quedando demostrada la utilidad del inmunosensor desarrollado para la determinación de TGF-β1 en muestras de suero humano en

concentraciones clínicamente relevantes en individuos sanos y en pacientes de hipercolesterolemia.

5.2.3.9. Conclusiones

En este trabajo se ha desarrollado un nuevo inmunosensor amperométrico para la determinación de TGF-β1 basado en una plataforma electródica compuesta de nanotubos de carbono de pared múltiple funcionalizados con grupos azida e inmunoglobulina G etinilada mediante una reacción CuAAC. Esta estrategia permite la inmovilización orientada de los anticuerpos de captura, preservando su actividad biológica. A continuación, se estableció una configuración tipo sándwich empleando poli-HRP-Strept como estrategia de amplificación de la señal obteniendo así una configuración con un excelente rendimiento analítico en términos de sensibilidad, rango lineal clínicamente relevante, reproducibilidad, estabilidad de almacenamiento y selectividad. Las características analíticas obtenidas mejoran, en términos generales, el rendimiento analítico de los kits ELISA comerciales y del inmunosensor impedimétrico encontrado en la bibliografía. Finalmente, la aplicabilidad del inmunosensor desarrollado se ha demostrado mediante el análisis de suero humano, requiriendo un tratamiento de muestra mínimo.

5.3. INMUNOSENSORES BASADOS EN LA MODIFICACIÓN DE LA SUPERFICIE ELECTRÓDICA MEDIANTE *GRAFTING* ELECTROQUÍMICO

En este grupo se describen las configuraciones de inmunosensores preparados mediante *grafting* o injertado de radicales de sales de diazonio formadas a partir de arilaminas. Este procedimiento, empleado para la inmovilizacion covalente de anticuerpos, se ha empleado tanto para modificar la superficie de los electrodos utilizados como plataformas de detección como para el desarrollo de etiquetas portadoras para amplificación de la respuesta electroquímica. Así, en primer lugar, se va a describir la configuración más sencilla, empleada para la determinación de IFN-γ. Seguidamente se detallarán los estudios realizados para la determinación simultánea de TNF-α e IL-1β sobre un electrodo modificado con nanotubos de carbono de pared doble funcionalizados con la sal de diazonio del ácido *p*-aminobenzoico (*p*-ABA) y, por último, se presentan los inmunosensores desarrollados para TGF-β1 y para HFA, que tienen en común el empleo de nanomateriales como portadores de biomoléculas para detección amplificada.

5.3.1. Inmunosensor para la determinación de interferón gamma

Como se ha comentado anteriormente, el interferón gamma (IFN-γ) es una citoquina pro-inflamatoria, crítica en la respuesta inmune innata y adaptativa. Los niveles normales de IFN-γ en saliva son del orden de unidades de pg/mL [Ghallab, 2010], por lo que, para su determinación en este tipo de muestra es necesario desarrollar métodos altamente sensibles y precisos. En este trabajo se ha desarrollado un inmunosensor electroquímico empleando un esquema de inmunoensayo tipo sándwich que implica el uso de plataformas electródicas

modificadas con ácido *p*-ABA mediante la técnica del *grafting* o injertado electroquímico para la inmovilización covalente del anticuerpo de captura anti-IFN, así como un anticuerpo de detección biotinilado y el conjugado HRP-Strept.

5.3.1.1. Configuración del inmunosensor

Las etapas implicadas en la preparación y funcionamiento del inmunosensor electroquímico desarrollado para la determinación de interferón gamma se representaron esquemáticamente en la Figura 4.31 de la *Parte Experimental*. Como puede observarse, una vez funcionalizada la superficie electródica con los radicales aril diazonio del *p*-ABA mediante *grafting* electroquímico [Moreno-Guzmán, 2012], el anticuerpo anti-IFN se inmoviliza covalentemente, se bloquean las posiciones libres de la superficie electródica con BSA y se incorporan el antígeno (IFN-γ) y el anticuerpo de detección biotinilado (Biotin-anti-IFN). Finalmente, la reacción de afinidad se monitoriza electroquímicamente empleando un conjugado de estreptavidina y peroxidasa (HRP-Strept) con peróxido de hidrógeno e hidroquinona como mediador redox, detectándose la quinona generada mediante amperometría a un potencial de –200 mV vs Ag.

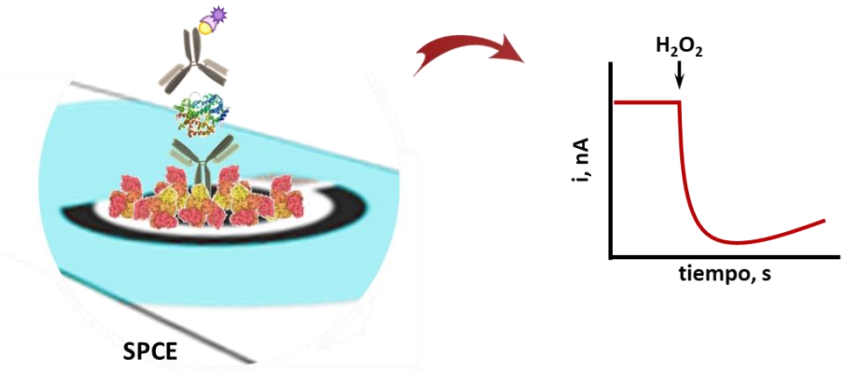

Figura 5.56. Esquema del funcionamiento del inmunosensor para la determinación de IFN-γ

5.3.1.2. Optimización de las variables experimentales

Como en casos anteriores, las variables experimentales implicadas en la preparación y el funcionamiento del inmunosensor se han optimizado con el objetivo

de alcanzar la máxima sensibilidad y un amplio intervalo lineal para la determinación de IFN-γ. Del mismo modo, el criterio seguido para seleccionar el valor óptimo fue la obtención de la mayor relación entre la corriente proporcionada por la reacción de reconocimiento del antígeno por el anticuerpo, y la no específica obtenida en ausencia de IFN-γ (S/R).

Influencia de la concentración y el tiempo de incubación del anticuerpo de captura

La concentración del anticuerpo de captura inmovilizado sobre la superficie del electrodo de trabajo es una variable crucial a la hora de obtener una buena sensibilidad del inmunoensayo. Para su optimización se inmovilizaron 5 µL de las disoluciones de anti-IFN, en el intervalo de concentraciones comprendido entre 5 y 20 µg/mL preparadas en disolución reguladora MES 25 mM de pH 5.0, dejándose incubar durante una hora sobre la superficie del electrodo. Como se observa en la Figura 5.57, las respuestas específicas aumentan con la concentración de anticuerpo de captura hasta 15 µg/mL, donde se alcanza probablemente el nivel de saturación. Por ello, dicho valor fue escogido como óptimo para estudios posteriores.

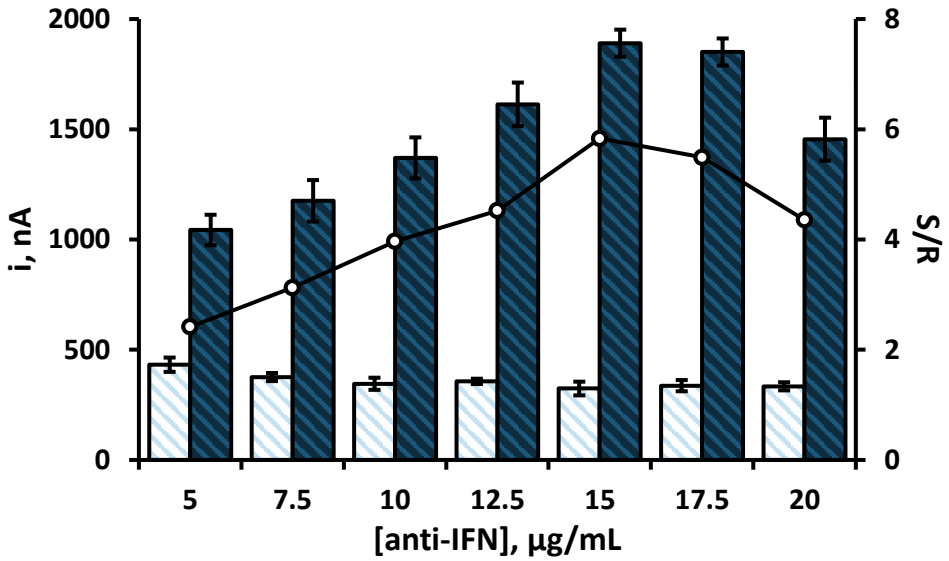

Figura 5.57. Efecto de la concentración de anti-IFN sobre la respuesta del inmunosensor: ECD/NHSS, 100 mM, 10 µL, 30 min; anti-IFN, 5 µL, 60 min; BSA, 1%, 5 µL, 30 min; IFN-γ, 0 (□) y 1 (■) ng/mL, 5 µL, 60 min; Biotin-anti-IFN, 0.5 µg/mL, 5 µL, 60 min; HRP-Strept, 1/500, 5µL, 20 min

En cuanto al tiempo de incubación del anticuerpo, los resultados representados en la Figura 5.58, demuestran que un tiempo de 60 minutos es adecuado para alcanzar la mayor relación de señales.

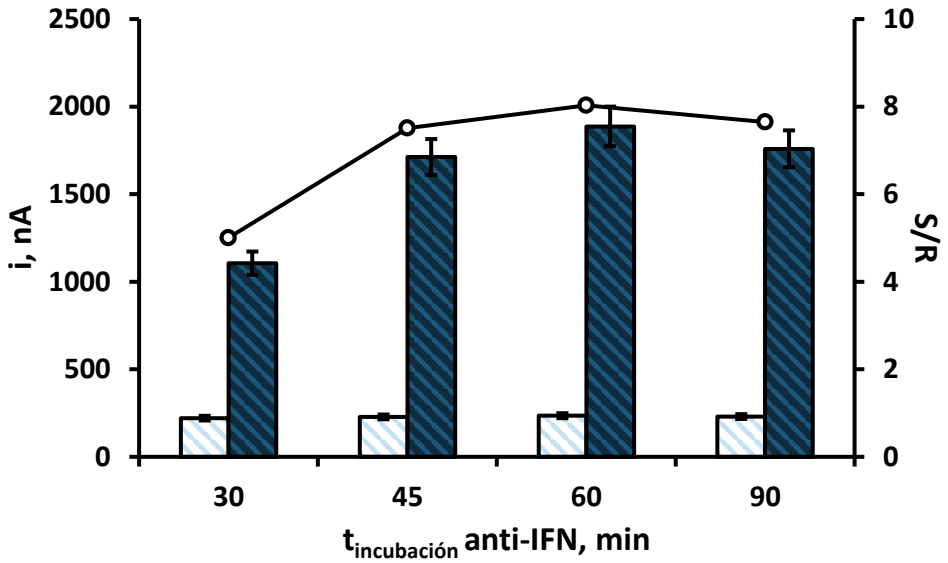

Figura 5.58. Efecto del tiempo de incubación de anti-IFN sobre la respuesta del inmunosensor: ECD/NHSS, 100 mM, 10 µL, 30 min; anti-IFN, 5 µL; BSA, 1%, 5 µL, 30 min; IFN-γ, 0 (□) y 1 (■) ng/mL, 5 µL, 60 min; Biotin-anti-IFN, 0.5 µg/mL, 5 µL, 60 min; HRP-Strept, 1/500, 5µL, 20 min

Influencia de la etapa de bloqueo

Para minimizar en la medida de lo posible la señal debida a las adsorciones inespecíficas sobre la superficie del electrodo, se probaron distintas concentraciones de BSA, así como el uso de caseína (disolución comercial Blocker™ Casein) como agentes bloqueantes, empleando un tiempo de incubación de 30 minutos tras la inmovilización del anticuerpo de captura.

Los resultados mostrados en la Figura 5.59 revelan que el bloqueo más eficiente de la superficie electródica tiene lugar empleando BSA al 2% (p/v). En esas condiciones, la corriente inespecífica obtenida en ausencia de IFN-γ es inferior al 16% de la obtenida cuando se incuba en una disolución 1 ng/mL de antígeno sobre el inmunosensor.

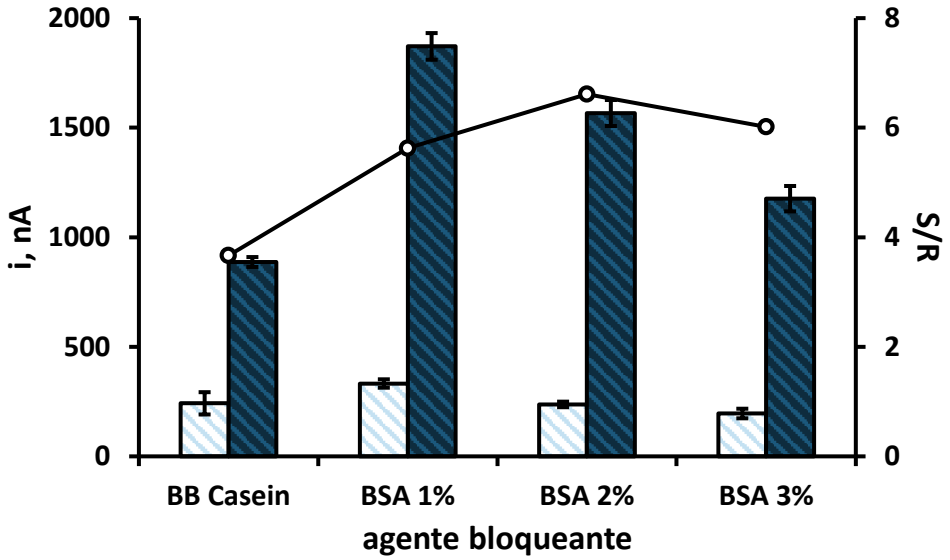

Figura 5.59. Efecto del agente bloqueante sobre la respuesta del inmunosensor: ECD/NHSS, 100 mM, 10 µL, 30 min; anti-IFN, 15 µg/mL, 5 µL, 60 min; agente bloqueante, 5 µL, 30 min; IFN-γ, 0 (□) y 1 (■) ng/mL, 5 µL, 60 min; Biotin-anti-IFN, 0.5 µg/mL, 5 µL, 60 min; HRP-Strept, 1/500, 5µL, 20 min

Influencia de la concentración y el tiempo de incubación del anticuerpo de detección biotinilado

La influencia de la concentración de Biotin-anti-IFN sobre la respuesta del inmunosensor se estudió en el intervalo de 0.25 a 2 µg/mL preparando diferentes inmunosensores con 15 µg/mL de anti-IFN en ausencia y en presencia de 1 ng/mL de antígeno.

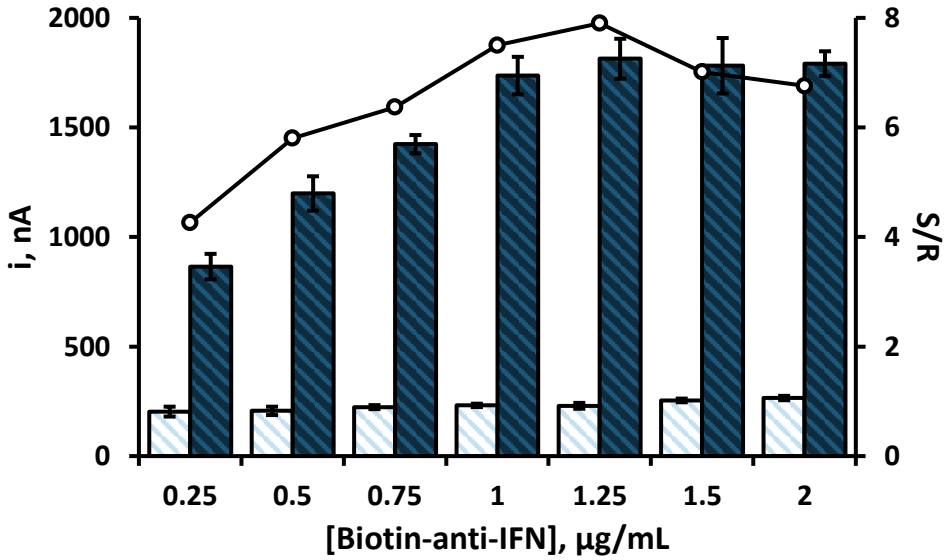

Figura 5.60. Efecto de la concentración de Biotin-anti-IFN sobre la respuesta del inmunosensor: ECD/NHSS, 100 mM, 10 µL, 30 min; anti-IFN, 15 µg/mL, 5 µL, 60 min; BSA, 2%, 5 µL, 30 min; IFN-γ, 0 (□) y 1 (■) ng/mL, 5 µL, 60 min; Biotin-anti-IFN, 5 µL, 60 min; HRP-Strept, 1/500, 5µL, 20 min

Como puede observarse en la Figura 5.60, la intensidad de corriente aumenta al aumentar la concentración de anticuerpo de detección biotinilado entre 0.25 y 1.25 µg/mL. Para concentraciones superiores, la intensidad de corriente se mantiene prácticamente constante. De este modo, la mayor relación de señales se obtiene para una concentración de anticuerpo de 1.25 µg/mL, siendo esta la concentración elegida.

En cuanto al tiempo de incubación de este anticuerpo sobre el inmunosensor, los resultados obtenidos (Figura 5.61), permiten deducir que 45 minutos son suficientes para obtener la mayor relación de señales.

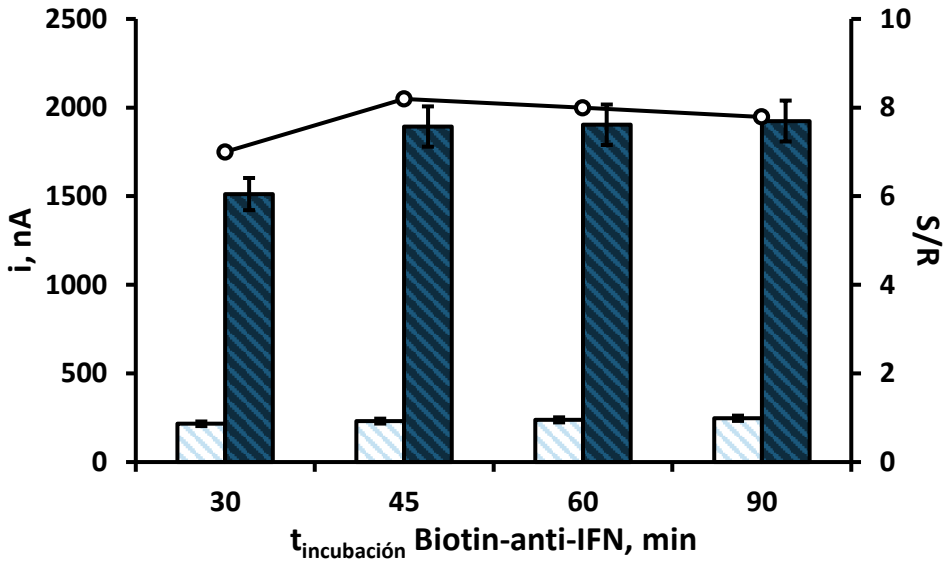

Figura 5.61. Efecto del tiempo de incubación de Biotin-anti-IFN sobre la respuesta del inmunosensor: ECD/NHSS, 100 mM, 10 µL, 30 min; anti-IFN, 15 µg/mL, 5 µL, 60 min; BSA, 2%, 5 µL, 30 min; IFN-γ, 0 (□) y 1 (■) ng/mL, 5 µL, 60 min; Biotin-anti-IFN, 1.25 µg/mL, 5 µL; HRP-Strept, 1/500, 5µL, 20 min

Influencia de la dilución del conjugado enzimático

Con el objetivo de alcanzar la mayor sensibilidad en la determinación de IFN-γ, se estudió la influencia de la dilución del conjugado enzimático (HRP-Strept) sobre la respuesta del inmunosensor. En la Figura 5.62 se puede observar que la intensidad de corriente debida a la señal específica disminuye a medida que lo hace la dilución del conjugado enzimático, obteniéndose la máxima relación S/R para una dilución 1/500.

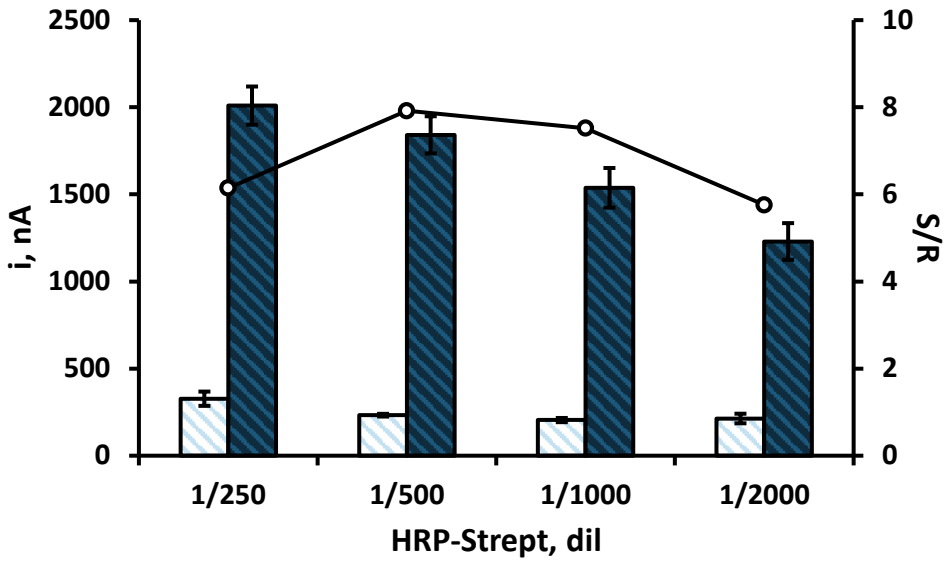

Figura 5.62. Efecto de la dilución de HRP-Strept sobre la respuesta del inmunosensor: ECD/NHSS, 100 mM, 10 µL, 30 min; anti-IFN, 15 µg/mL, 5 µL, 60 min; BSA, 2%, 5 µL, 30 min; IFN-γ, 0 (□) y 1 (■) ng/mL, 5 µL, 60 min; Biotin-anti-IFN, 1.25 µg/mL, 5 µL, 60 min; HRP-Strept, 5µL, 20 min

En la Tabla 5.11 se resumen las variables estudiadas, así como los intervalos evaluados y los valores seleccionados en cada caso para estudios posteriores.

Tabla 5.11. Optimización de las variables experimentales implicadas en la construcción del inmunosensor HRP-Strept-Biotin-anti-IFN-IFN-γ-anti-IFN/SPCE

VARIABLE EXPERIMENTAL	INTERVALO EVALUADO	VALOR SELECCIONADO
[anti-IFN], µg/mL	5 – 20	15
$t_{incubación}$ anti-IFN, min	30 – 90	60
agente bloqueante	Blocker™ Casein, BSA	BSA
BSA, %	1 – 3	2
[Biotin-anti-IFN], µg/mL	0.25 – 2	1.25
$t_{incubación}$ Biotin-anti-IFN, min	30 – 90	45
HRP-Strept, dil	1/250 – 1/2000	1/500

5.3.1.3. Caracterización de la superficie electródica

Una vez optimizadas las variables experimentales implicadas en la construcción y el funcionamiento del inmunosensor desarrollado, las distintas etapas de preparación del mismo se han monitorizado mediante espectroscopia de impedancia electroquímica utilizando una disolución de $Fe(CN)_6^{3-/4-}$ 2 mM preparada en PBS

de pH 7.4 (Figura 5.63). Como puede observarse, la modificación del SPCE desnudo con *p*-ABA da lugar a un gran aumento en la resistencia a la transferencia de carga (R_{ct}, de 646 Ω a 4187 Ω) debido a la repulsión electrostática entre la sonda redox aniónica presente en la disolución y los grupos carboxílicos de la superficie electródica disociados al pH de medida. Seguidamente, la activación con EDC/NHSS conduce a una drástica disminución del valor de R_{ct} (497 Ω) debida probablemente a la neutralización parcial de las cargas negativas. Finalmente, como era de esperar, tras la inmovilización de anti-IFN la resistencia a la transferencia de carga vuelve a aumentar (R_{ct} = 1143 Ω) debido al carácter aislante del anticuerpo inmovilizado sobre la superficie electródica.

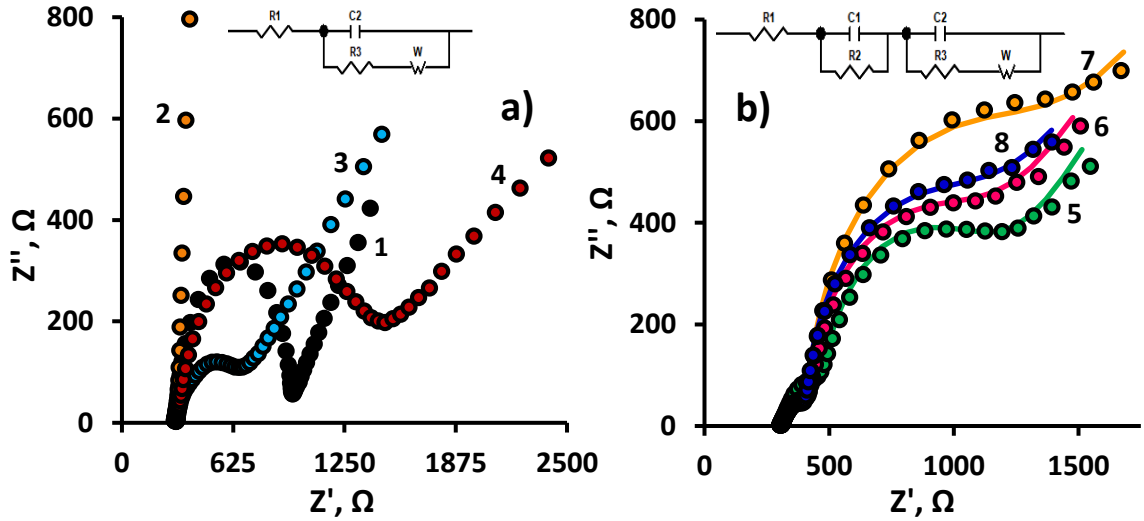

Figura 5.63. Diagramas de Nyquist registrados para: a) 1) SPCE, 2) *p*-ABA-SPCE, 3) EDC/NHSS-*p*-ABA-SPCE, 4) anti-IFN/SPCE y b) 5) BSA-anti-IFN/SPCE, 6) IFN-γ-anti-IFN/SPCE, 7) Biotin-anti-IFN-IFN-γ-anti-IFN/SPCE y 8) HRP-Strept-Biotin-anti-IFN-IFN-γ-anti-IFN/SPCE en una disolución $Fe(CN)_6^{3-/4-}$ 2 mM en PBS de pH 7.4

Es importante destacar la aparición de dos semicírculos en el diagrama de Nyquist a partir de la etapa de bloqueo, lo que puede atribuirse a la formación de una superficie electródica heterogénea consistente en zonas con dos capas diferentes. Debido a este cambio, para un mejor ajuste a los espectros de impedancia obtenidos, se han propuesto dos circuitos equivalentes, siendo el más adecuado a la segunda situación experimental (Figura 5.63b), constituido por dos circuitos RC, como se comprueba al superponer la correspondiente simulación sobre los gráficos de Nyquist obtenidos experimentalmente [Baraket, 2014], el representado en dicha figura, en el que la resistencia, R_2, correspondiente al segundo semicírculo del gráfico de Nyquist

describe la transferencia electrónica a través de las biomoléculas inmovilizadas, incluyendo BSA, IFN-γ, Biotin-anti-IFN y HRP-Strept. El aumento de la resistencia a la transferencia de carga que se observa tras la incubación del antígeno y después de la inmovilización del anticuerpo de detección biotinilado se explica como debido tanto al carácter aislante de las biomoléculas como a la repulsión electrostática entre la biotina, que se encuentra disociada al pH de trabajo, y la sonda redox aniónica en disolución. Finalmente, la disminución de la resistencia a la transferencia de carga que se aprecia al incubar el electrodo en la disolución de HRP-Strept se ha atribuido a la neutralización parcial de las cargas negativas de la biotina al pH de trabajo.

5.3.1.4. Calibrado y características analíticas

En la Figura 5.64 se representa el calibrado obtenido para la determinación de IFN-γ empleando las condiciones experimentales previamente optimizadas. Como puede observarse, existe una relación lineal entre la intensidad de corriente y el logaritmo de la concentración del analito entre 2.5 y 2000 pg/mL (R^2 = 0.996), con una pendiente de (591 ± 12) nA·mL/pg y una ordenada en el origen de (121 ± 26) nA.

El límite de detección, 1.65 pg/mL, se calculó como la concentración más baja que puede ser estadísticamente discriminada de la señal proporcionada por el blanco, de acuerdo con la expresión $\overline{x} + 3 \cdot s$, donde *s* es la desviación estándar calculada a partir de las respuestas amperométricas obtenidas para diez réplicas en ausencia de interferón gamma, en unidades de concentración, pg/mL. Asimismo, el límite de cuantificación alcanzado fue de 1.95 pg/mL, de acuerdo con la expresión $\overline{x} + 10 \cdot s$.

Teniendo en cuenta que los niveles de concentración normales de esta citoquina encontrados en saliva de individuos sanos son del orden de algunas unidades de pg/mL [Ghallab, 2010], puede decirse que las características analíticas del inmunosensor desarrollado son adecuadas para la determinación de este analito en este tipo de muestra.

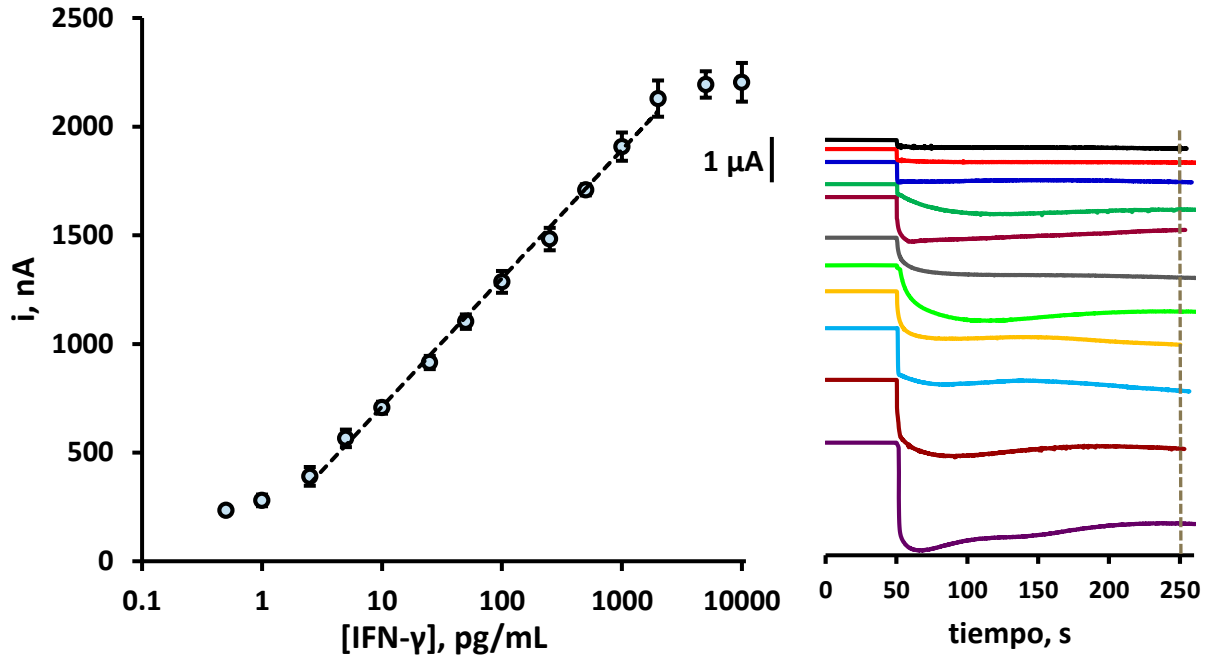

Figura 5.64. Calibrado para la determinación de IFN-γ empleando el inmunosensor HRP-Strept-Biotin-anti-IFN-IFN-γ-anti-IFN/SPCE

5.3.1.5. Estudio de selectividad

El interferón gamma se determina habitualmente en fluidos biológicos en los que coexiste naturalmente con muchas otras sustancias presentes a diferentes concentraciones y que podrían interferir en la determinación de este analito con el inmunosensor. Para estudiar la selectividad del método desarrollado se midieron las respuestas amperométricas del inmunosensor frente a diversas sustancias como ácido ascórbico (AA), albúmina de suero bovino (BSA), glucosa (Glu), hemoglobina (HB), inmunoglobulina G humana (hIgG), interleucina 1 beta (IL-1β), interleucina 6 (IL-6) e interleucina 8 (IL-8), ligando de receptor activador para el factor nuclear kappaB (RANKL), factor de crecimiento transformante beta 1 (TGF-β1), factor de necrosis tumoral alfa (TNF-α) y ácido úrico (UA), que están presentes en muestras de suero humano. Para ello, se compararon las respuestas amperométricas obtenidas para inmunosensores preparados en ausencia de IFN-γ o en presencia de este en una concentración de 1 ng/mL y, a su vez, en ausencia y en presencia de cada uno de los compuestos ensayados al nivel de concentración que cabe esperar en suero humano.

Los resultados mostrados en la Figura 5.65 ponen de manifiesto que ninguna de estas especies supone, a los niveles ensayados, una interferencia significativa en la determinación de esta citoquina, demostrando así la alta selectividad de la configuración desarrollada.

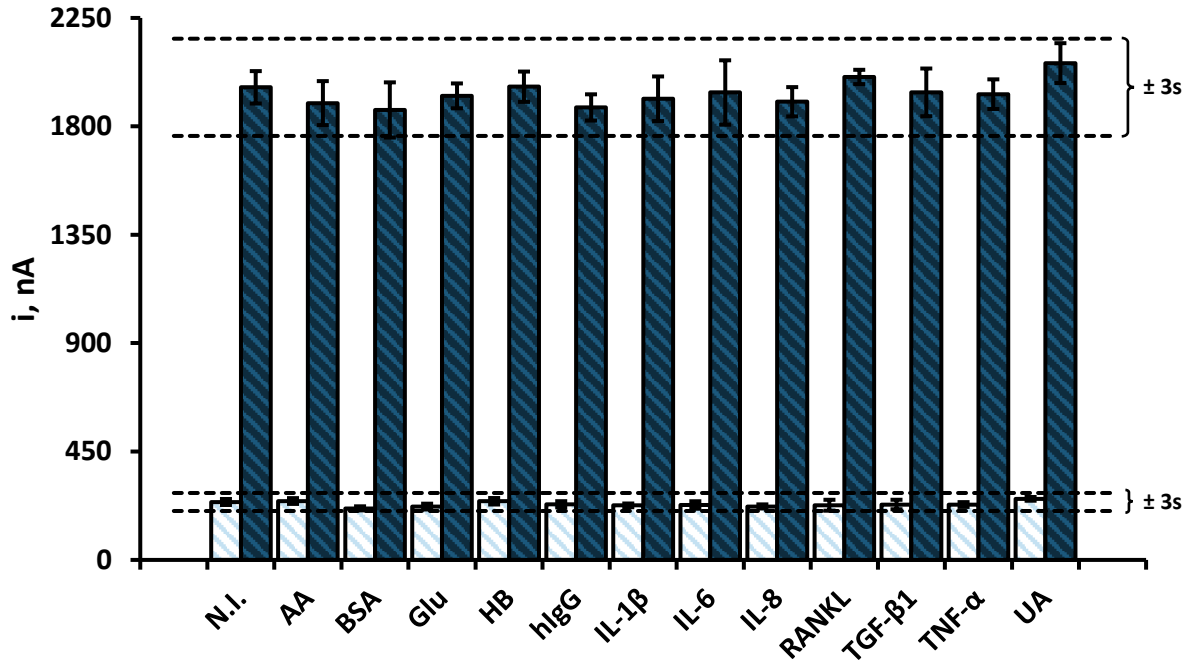

Figura 5.65. Selectividad del inmunosensor HRP-Strept-Biotin-anti-IFN-IFN-γ-anti-IFN/SPCE evaluando la respuesta del mismo con 0 (□) ó 1 (■) ng/mL de IFN-γ frente a 7 µg/mL de AA, 5 mg/mL de BSA, 1 mg/mL de Glu, 5 mg/mL de HB, 1 mg/mL de hIgG, 50 pg/mL de IL-1β, 300 pg/mL de IL-6, 300 pg/mL de IL-8, 100 pg/mL de RANKL, 50 pg/mL de TGF-β1, 200 pg/mL de TNF-α y 10 µg/mL de UA

5.3.1.6. Estudios de reproducibilidad y estabilidad

Los estudios de repetitividad y reproducibilidad se realizaron por medida de las respuestas amperométricas de distintos inmunosensores preparados en ausencia o en presencia de 1 ng/mL de IFN-γ el mismo día o en días diferentes. En estas condiciones se obtuvieron valores de RSD del 1.4 y 1.8%, para inmunosensores preparados el mismo día, y de 2.1 y 2.6% para inmunosensores preparados en días diferentes, lo que pone de manifiesto que el procedimiento de fabricación del inmunosensor es fiable y presenta una buena reproducibilidad. También se evaluó la estabilidad del anticuerpo de captura sobre la superficie del electrodo, anti-IFN/SPCE. Para ello, se prepararon en el mismo día distintos inmunoconjugados y, tras el bloqueo de la superficie del

electrodo de trabajo con BSA al 2%, se almacenaron en seco a –20°C. Cada día de trabajo se prepararon tres inmunosensores a partir de los electrodos modificados almacenados y se realizaron las medidas de la respuesta amperométrica para 1 ng/mL de IFN-γ. En la Figura 5.66 se ha representado el gráfico de control en el que los márgenes establecidos corresponden a ± 3 veces la desviación estándar de las medidas realizadas el primer día de trabajo. Como puede observarse, la media de las tres medidas realizadas cada día se encuentra dentro del intervalo establecido el primer día durante 40 días, poniéndose de manifiesto la excelente estabilidad de almacenamiento de los conjugados anti-IFN/SPCE cuando se almacenan en seco a –20°C. Esta característica es de gran importancia puesto que demuestra que es posible preparar varios inmunoconjugados, almacenarlos en las condiciones indicadas y, posteriormente, utilizarlos a demanda para llevar a cabo la determinación de IFN-γ en el momento que se precise.

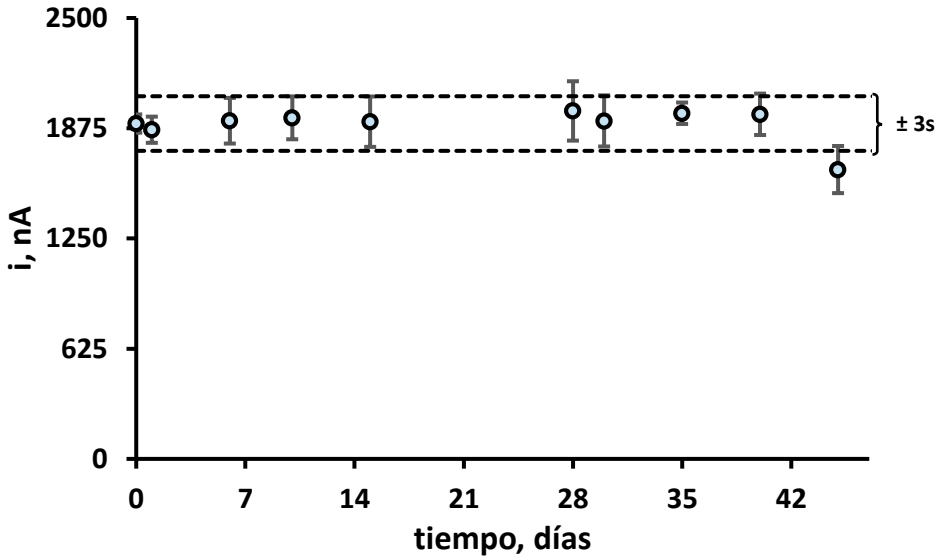

Figura 5.66. Gráfico de control para la evaluación de la estabilidad de almacenamiento del conjugado anti-IFN/SPCE

5.3.1.7. Aplicación a la determinación de interferón gamma en un material biológico humano certificado y saliva

El método desarrollado para la determinación de IFN-γ con el inmunosensor HRP-Strept-Biotin-anti-IFN-IFN-γ-anti-IFN/SPCE se ha validado mediante su aplicación a la determinación de esta citoquina en un material biológico humano certificado de referencia que contiene una concentración de interferón gamma de 12.5 ng/mL, aproximadamente. Además, también se ha evaluado su utilidad para la determinación de bajas concentraciones de este analito en muestras reales analizando muestras de saliva de cuatro individuos voluntarios sanos, siguiendo el procedimiento descrito en el *Apartado 4.6.5.* de la *Parte Experimental*.

En primer lugar, se estudió la posible existencia de efecto matriz en el material biológico de referencia comparando la pendiente del calibrado construido con disoluciones estándar de IFN-γ en disolución reguladora PBS de pH 7.4 con la del obtenido a partir de una dilución 1/1000 del material biológico en disolución reguladora PBS de pH 7.4 enriquecida con distintas concentraciones de IFN-γ. En estas condiciones, las ecuaciones de los calibrados fueron, respectivamente, i, nA = (593 ± 1) log ([IFN-γ], pg/mL) + (115 ± 2) e i, nA = (591 ± 12) log ([IFN-γ], pg/mL) + (121 ± 26) con valores de las pendientes muy parecidos entre sí. La comparación estadística de dichas pendientes se realizó empleando el test *t* de Student, para lo cual se calculó el valor de t_{exp}, que se comparó con el valor tabulado, t_{tab}, a un nivel de significación del 0.05, haciendo uso de la expresión:

$$t_{\exp} = \frac{|b_1 - b_2|}{\sqrt{s_1^2 + s_2^2}}$$

siendo b_1 y b_2 las pendientes de las rectas de calibrado y s_1 y s_2 las desviaciones estándar respectivas, obtenidas por el método de mínimos cuadrados de cada una ellas. Aplicando este criterio se obtuvo un valor de t_{exp} de 0.186, que es inferior al valor

teórico para las condiciones del experimento (t_{tab} = 2.262) y un nivel de significación del 0.05, lo que demuestra que no existen diferencias significativas entre las pendientes de las curvas de calibrado. En la figura Figura 5.67 se muestran las dos rectas superpuestas, poniendo de manifiesto la gran similitud entre ellas. De acuerdo con estos resultados, es posible determinar la concentración de IFN-γ en este material por interpolación directa de la corriente proporcionada por la muestra en el calibrado de disoluciones estándar tras una dilución 1/1000 del mismo en disolución reguladora PBS de pH 7.4. De esta forma se obtuvo una concentración media de IFN-γ de 12.5 ± 0.2 ng/mL, siendo el valor de RSD del 1.6% (n = 9), que corresponde a una recuperación media del (100 ± 2)%. Este resultado está de acuerdo con la concentración media, 12.3 ± 0.5 ng/mL, obtenida empleando el kit ELISA comercial.

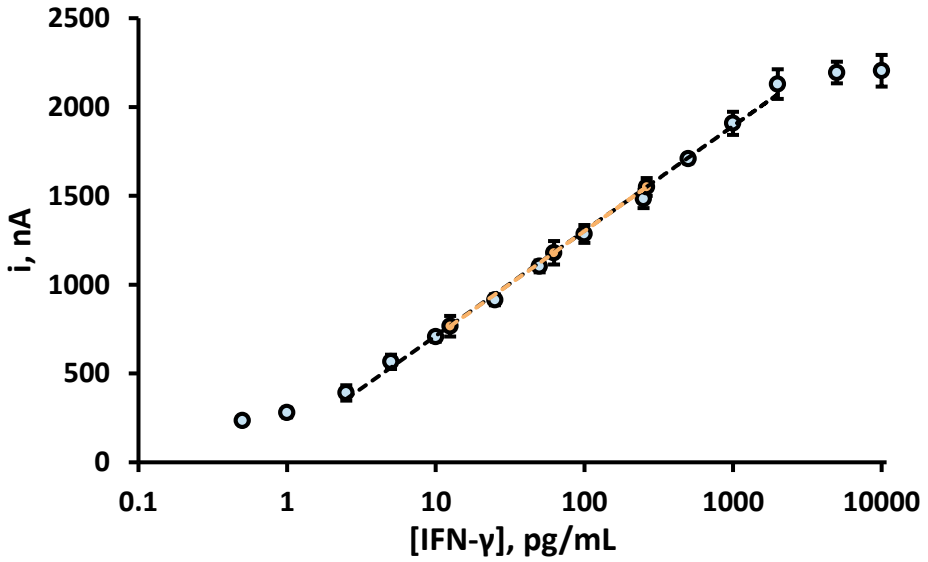

Figura 5.67. Superposición de las señales obtenidas para el material biológico de referencia enriquecido (○) en el calibrado de disoluciones estándar (○)

En cuanto a las muestras de saliva, también se demostró la ausencia de efecto matriz comparando la pendiente de la curva de calibrado construida con disoluciones estándar de IFN-γ en disolución reguladora PBS de pH 7.4 con la de la construida a partir de cada una de las muestras de saliva suplementadas con distintas concentraciones de IFN-γ, como anteriormente. En este caso, los valores de t_{exp} para cada una de las muestras de saliva fueron 0.993, 1.398, 1.277 y 1.352, respectivamente. Todos estos valores son inferiores al valor teórico establecido para las condiciones del

experimento (t_{tab} = 2.262) a un nivel de significación del 0.05. Por tanto, es posible llevar a cabo la determinación de este analito en muestras de saliva por interpolación de la señal amperométrica proporcionada por la muestra en el calibrado de disoluciones estándar, sin que sea necesario ningún pretratamiento de la muestra. Además, los resultados obtenidos fueron validados mediante el empleo del kit DuoSet® ELISA Development System (DY285B–05) de R&D Systems, observándose que los métodos eran estadísticamente comparables entre sí (Tabla 5.12), lo que pone de manifiesto la utilidad del inmunosensor desarrollado para la determinación de IFN-γ a bajas concentraciones en muestras de saliva, sin necesidad de pretratamiento salvo la dilución según el procedimiento que se describe en el *Apartado 4.6.5.* de la *Parte Experimental*.

Tabla 5.12. Determinación de IFN-γ en muestras de saliva de individuos sanos empleando el inmunosensor HRP-Strept-Biotin-anti-IFN-IFN-γ-anti-IFN/SPCE

MUESTRA	INMUNOSENSOR, pg/mL (*n* = 6)*	ELISA, pg/mL (*n* = 3)*
voluntario 1	8.4 ± 0.3	8.2 ± 0.4
voluntario 2	7.3 ± 0.2	7.1 ± 0.3
voluntario 3	7.6 ± 0.2	7.5 ± 0.3
voluntario 4	7.2 ± 0.3	7.2 ± 0.5

* valor medio ± t·s/√n

5.3.1.8. Conclusiones

En este trabajo se ha preparado un inmunosensor electroquímico para la determinación de IFN-γ basado en la modificación superficial de un electrodo serigrafiado de carbono desechable con ácido *p*-aminobenzoico seguido de la unión covalente del anticuerpo de captura y el establecimiento de un inmunoensayo tipo sándwich. Esta configuración ha hecho posible la determinación de la citoquina empleando un calibrado semilogarítmico con un intervalo lineal comprendido entre 2.5 y 2000 pg/mL y un límite de detección de 1.65 pg/mL. Estas características, junto a la elevada precisión y selectividad, lo hacen adecuado para la determinación de

IFN-γ en muestras biológicas, habiéndose aplicado a la cuantificación de esta proteína en un material biológico de referencia certificado y muestras de saliva de cuatro individuos voluntarios a niveles clínicamente relevantes, siendo únicamente necesario realizar una dilución 1/1000 en disolución reguladora PBS de pH 7.4 en el caso del material biológico de referencia y una dilución 1/100 de las muestras de saliva.

5.3.2. Inmunosensor dual para la determinación simultánea de factor de necrosis tumoral alfa e interleucina 1 beta

Como se ha indicado, estas citoquinas, TNF-α e IL-1β, son típicamente pro-inflamatorias [Zhang, 2007], y su determinación es importante para el seguimiento de este tipo de enfermedades y otros procesos relacionados. Sin embargo, su determinación supone un reto, debido a la baja concentración de ambas especies, sobre todo en el caso de la saliva, donde su concentración es de pocos pg/mL [Mazloum-Ardakani, 2014]. Esto hace que se requieran métodos analíticos precisos, fiables y suficientemente sensibles.

Como se ha comentado anteriormente, son numerosos los métodos disponibles para la determinación de TNF-α, mientras que en el caso de la IL-1β son escasos. Asimismo, no existe ninguna metodología descrita previamente en la bibliografía para la determinación simultánea de ambas citoquinas. Por este motivo, en este trabajo se describe la puesta a punto de una plataforma inmunosensora integrada para determinación simultánea de TNF-α e IL-1β, que satisface los requisitos de sensibilidad, selectividad y reproducibilidad para su aplicación en el análisis de muestras clínicas. Se han aprovechado las ventajas que ofrece el empleo de electrodos serigrafiados de carbono duales para el diseño de configuraciones múltiplex, así como la elevada conductividad de los nanotubos de carbono de pared doble (DWCNTs) para diseñar un inmunosensor basado en la inmovilización de los anticuerpos de captura específicos para cada antígeno sobre estos nanotubos funcionalizados con grupos *4*-carboxifenilo empleando el reactivo polimérico Mix&Go™. La configuración desarrollada se aplicó con buenos resultados a la determinación simultánea de ambas citoquinas en suero y saliva, demostrando así su utilidad para el análisis de muestras de interés clínico.

5.3.2.1. Configuración del inmunosensor

La Figura 4.32 de la *Parte Experimental* aparecen esquematizadas las etapas implicadas en la preparación y funcionamiento del inmunosensor electroquímico desarrollado para la determinación simultánea de TNF-α e IL-1β. Según se describe, sobre las superficies de los electrodos de trabajo, una vez modificadas con nanotubos de carbono de pared doble funcionalizados con grupos *4*-carboxifenilo (HOOC-Phe-DWCNTs), se añade el polímero Mix&Go™ para inmovilizar, a continuación, de forma orientada cada uno de los anticuerpos de captura. Después se establece el esquema de inmunoensayo tipo sándwich, incorporando los antígenos y los anticuerpos de detección biotinilados. La reacción de afinidad se monitoriza electroquímicamente como anteriormente (Figura 5.68).

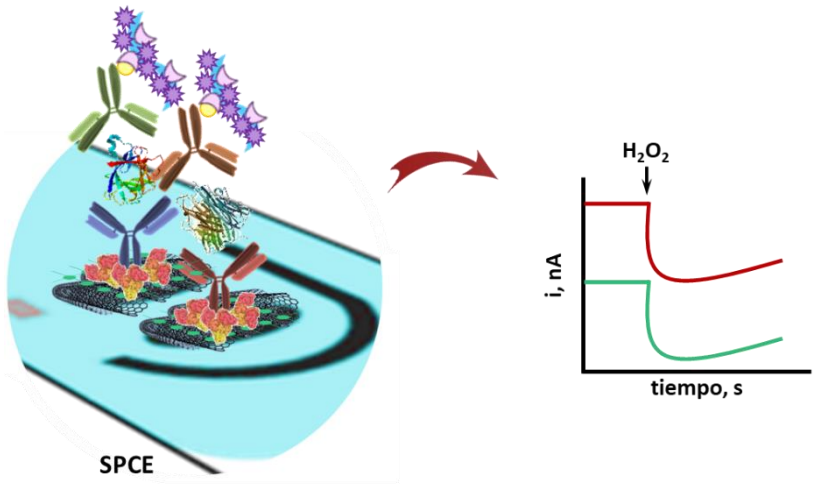

Figura 5.68. Esquema del funcionamiento del inmunosensor para la determinación simultánea de TNF-α e IL-1β

5.3.2.2. Optimización de las variables experimentales

Con el fin de obtener la configuración de un inmunosensor electroquímico dual que permitiera llevar a cabo la determinación simultánea de las dos citoquinas del modo más sensible, se llevó a cabo la optimización de las variables experimentales implicadas en la preparación y el funcionamiento de cada una de las plataformas por separado, empleando electrodos serigrafiados de carbono sencillos. Las variables estudiadas fueron: a) la concentración y el tiempo de incubación del anticuerpo de captura, b) el tipo de agente bloqueante y su concentración, c) la concentración y el

tiempo de incubación del anticuerpo de detección biotinilado y d) el tipo de marcaje enzimático y la dilución del mismo.

Elección del método de inmovilización de los anticuerpos de captura

Con el fin de elegir el mejor método para inmovilizar los anticuerpos de captura anti-TNF y anti-IL sobre la superficie electródica modificada con HOOC-Phe-DWCNTs, se realizó un estudio comparativo aplicando dos procedimientos diferentes. El primero de ellos emplea la estrategia de inmovilización habitualmente utilizada, que hace uso del sistema de la carbodiimida/hidroxisuccinimida para la activación de los grupos carboxílicos y posterior formación de uniones tipo amida con las funciones amina presentes en los anticuerpos, mientras que el segundo hace uso del reactivo Mix&Go™ que, como se ha visto anteriormente, es un material polimérico de complejos metálicos seleccionados por su elevada eficacia para enlazar anticuerpos a través de su región Fc [Ooi, 2014], orientando y proporcionando una alta estabilidad a la configuración resultante [Muir, 2007].

En la Figura 5.69 se comparan las respuestas amperométricas obtenidas aplicando estos procedimientos a la preparación de los inmunosensores HRP-Strept-Biotin-anti-TNF-α-anti-TNF-Phe-DWCNTs/SPCE y HRP-Strept-Biotin-anti-IL-1β-anti-IL-Phe-DWCNTs/SPCE.

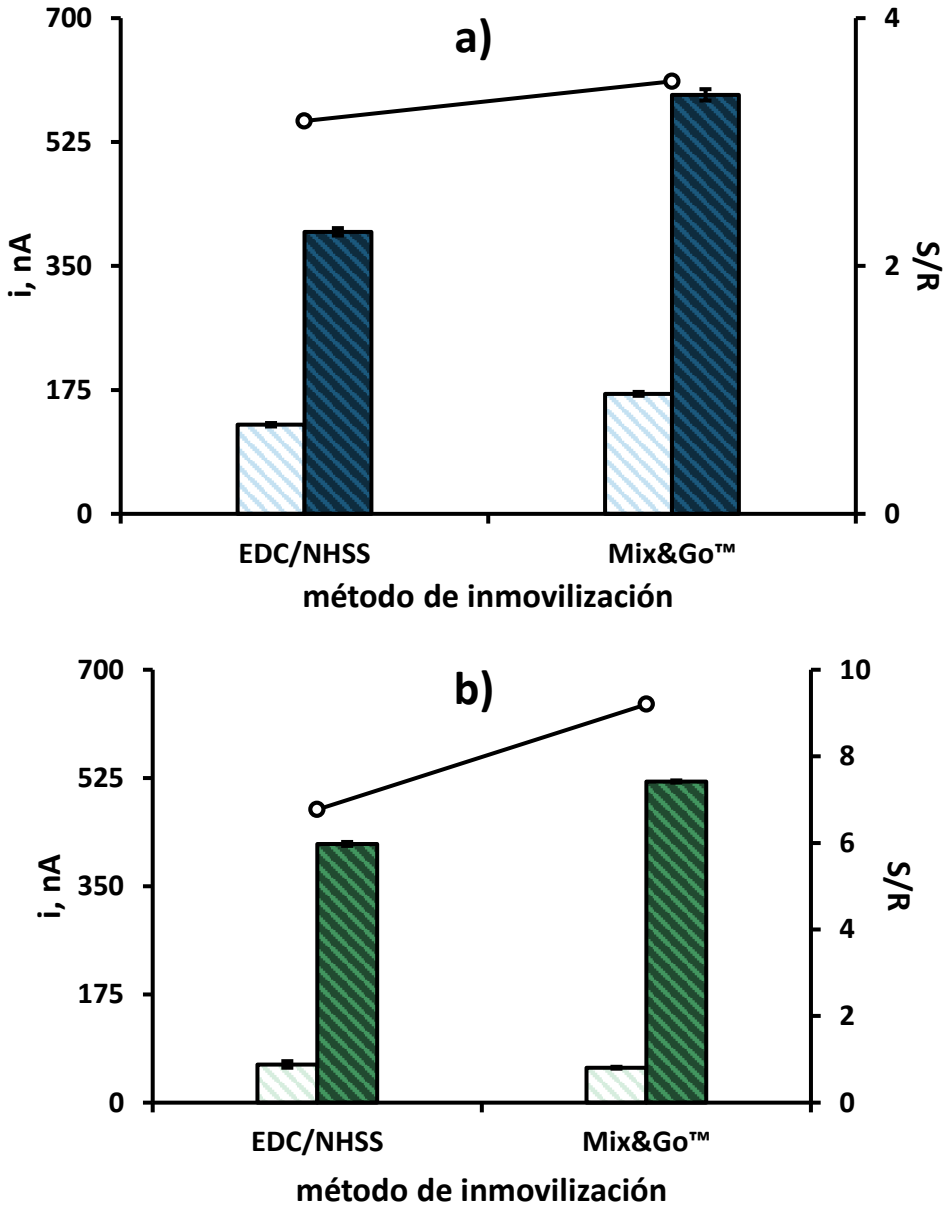

Figura 5.69. Efecto de la estrategia de inmovilización de anti-TNF y anti-IL sobre la respuesta de los inmunosensores: HOOC-Phe-DWCNTs, 3 µL; EDC/NHSS, 100 mM, 5 µL, 30 min o Mix&Go™, 5 µL, 60 min; anti-TNF. 4 µg/mL o anti-IL, 6 µg/mL 5 µL, 60 min; BSA, 1%, 5 µL, 30 min; TNF-α, 0 (□) y 50 (■) pg/mL o IL-1β, 0 (□) y 250 (■) pg/mL, 5 µL, 60 min; Biotin-anti-TNF o Biotin-anti-IL, 0.5 µg/mL, 5 µL, 60 min; HRP-Strept, 1/2000, 5µL, 20 min

Como se puede observar, al emplear el material polimérico Mix&Go™ se obtuvo una mayor relación entre las intensidades de corriente registradas en presencia y ausencia de los antígenos lo que se debe probablemente a que los anticuerpos de captura respectivos se encuentran orientados adecuadamente sobre la superficie electródica.

Influencia de la concentración y el tiempo de incubación de los anticuerpos de captura

La influencia de la concentración de cada anticuerpo de captura (anti-TNF o anti-IL) inmovilizado sobre los electrodos HOOC-Phe-DWCNTs/SPCEs, haciendo uso del reactivo polimérico Mix&Go™ se evaluó comparando las respuestas amperométricas obtenidas empleando distintos inmunosensores para concentraciones de 0 o 50 pg/mL de TNF-α o IL-1β. La preparación de los inmunosensores implica la deposición de 5 μg/mL de disoluciones de distinta concentración de los respectivos anticuerpos de captura y la aplicación del procedimiento descrito en el *Apartado 4.5.3.2.* de la *Parte Experimental*, empleando una concentración de 0.5 μg/mL de los correspondientes anticuerpos de detección biotinilados y una dilución 1/2000 del conjugado de estreptavidina y peroxidasa para la monitorización de la reacción de afinidad.

Así, la Figura 5.70a muestra que la relación entre las señales específica e inespecífica aumenta al aumentar la concentración de anti-TNF inmovilizado sobre la superficie electródica hasta alcanzar una concentración de 4 μg/mL, disminuyendo ligeramente para concentraciones superiores. Con respecto a la intensidad de corriente registrada en el caso de la IL-1β (Figura 5.70b), los valores medidos alcanzaron una mayor relación entre las señales específica e inespecífica para concentraciones de anticuerpo de captura inmovilizado entre 4 y 6 μg/mL, eligiéndose 6 μg/mL como valor óptimo.

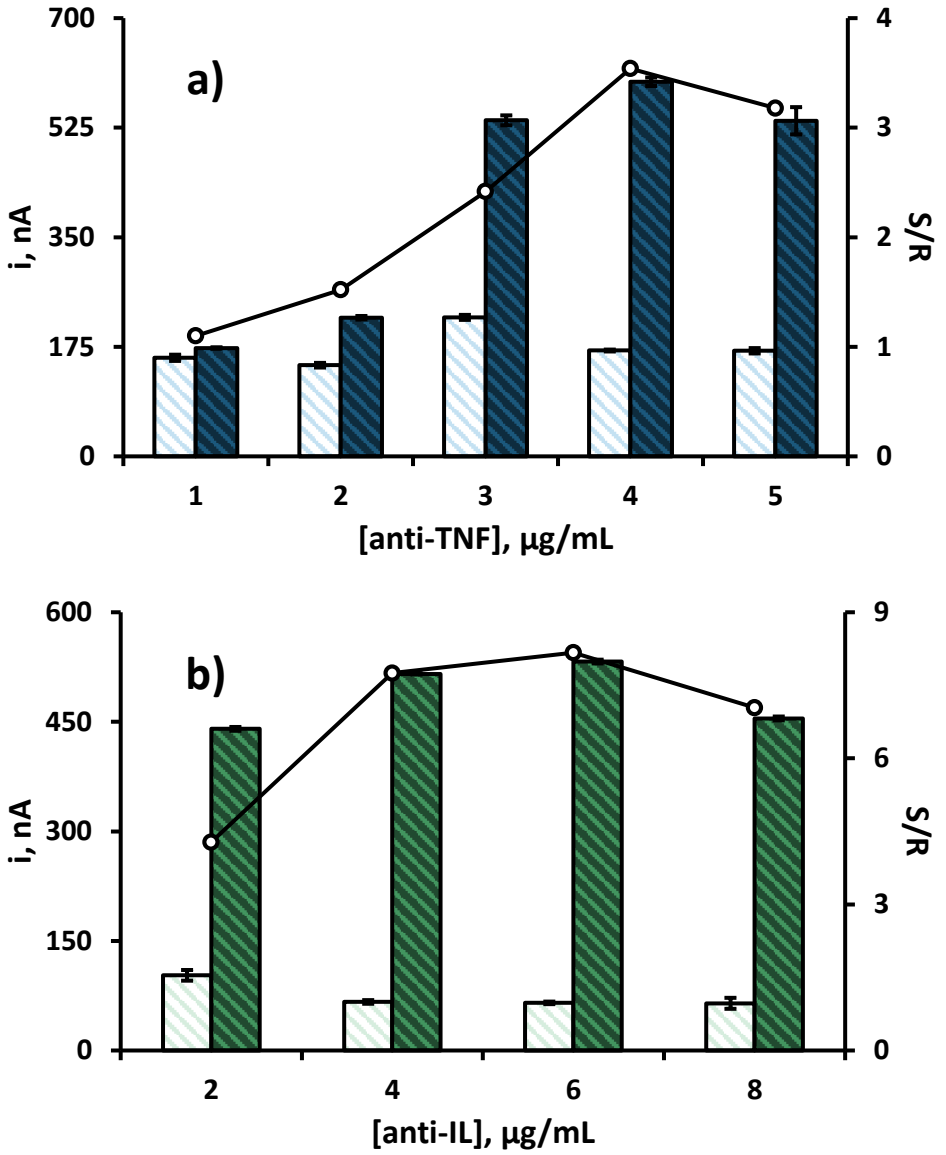

Figura 5.70. Efecto de la concentración de a) anti-TNF y b) anti-IL sobre la respuesta de los inmunosensores: HOOC-Phe-DWCNTs, 3 µL; Mix&Go™, 5 µL, 60 min; anti-TNF o anti-IL, 5 µL, 60 min; BSA, 2%, 5 µL, 30 min; TNF-α, 0 (□) y 50 (■) pg/mL o IL-1β, 0 (□) y 250 (■) pg/mL, 5 µL, 60 min; Biotin-anti-TNF o Biotin-anti-IL, 0.5 µg/mL, 5 µL, 60 min; HRP-Strept, 1/2000, 5µL, 20 min

Por otro lado, también se optimizó el tiempo de incubación de las disoluciones de los anticuerpos de captura sobre la superficie electródica. Los resultados mostrados en la Figura 5.71 indican que un tiempo de incubación de 60 minutos es adecuado para la preparación de ambas configuraciones.

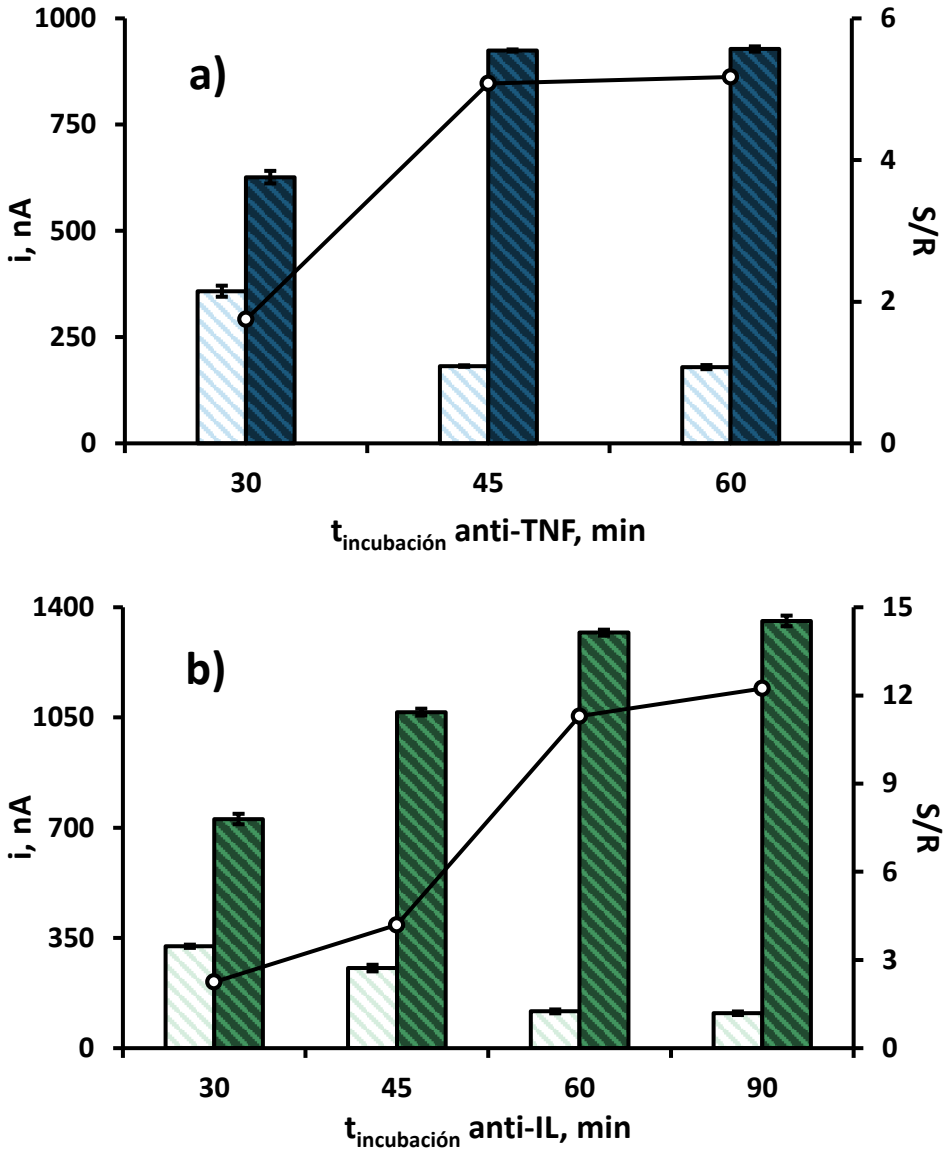

Figura 5.71. Efecto del tiempo de incubación de a) anti-TNF y b) anti-IL sobre la respuesta de los inmunosensores: HOOC-Phe-DWCNTs, 3 µL; Mix&Go™, 5 µL, 60 min; anti-TNF, 4 µg/mL o anti-IL, 6 µg/mL, 5 µL; BSA, 2%, 5 µL, 30 min; TNF-α, 0 (□) y 50 (■) pg/mL o IL-1β, 0 (□) y 250 (■) pg/mL, 5 µL, 60 min; Biotin-anti-TNF o Biotin-anti-IL, 0.5 µg/mL, 5 µL, 60 min; poli-HRP-Strept, a) 1/1000 o b) 1/500, 5µL, 15 min

Influencia de la etapa de bloqueo

Con el objetivo de minimizar posibles fenómenos de adsorción inespecífica sobre la superficie del electrodo, se evaluaron distintas estrategias de bloqueo, analizando el efecto de varios reactivos adecuados para este propósito: BSA en distintas concentraciones, disolución de caseína comercial (Blocker™ Casein) o leche en polvo. Para ello se depositan 5 µL de cada disolución de bloqueo sobre los electrodos previamente modificados con los anticuerpos de captura y se deja incubar

durante un tiempo preestablecido de 30 minutos y, a continuación, cada inmunosensor se prepara en ausencia o presencia de 250 pg/mL de cada antígeno.

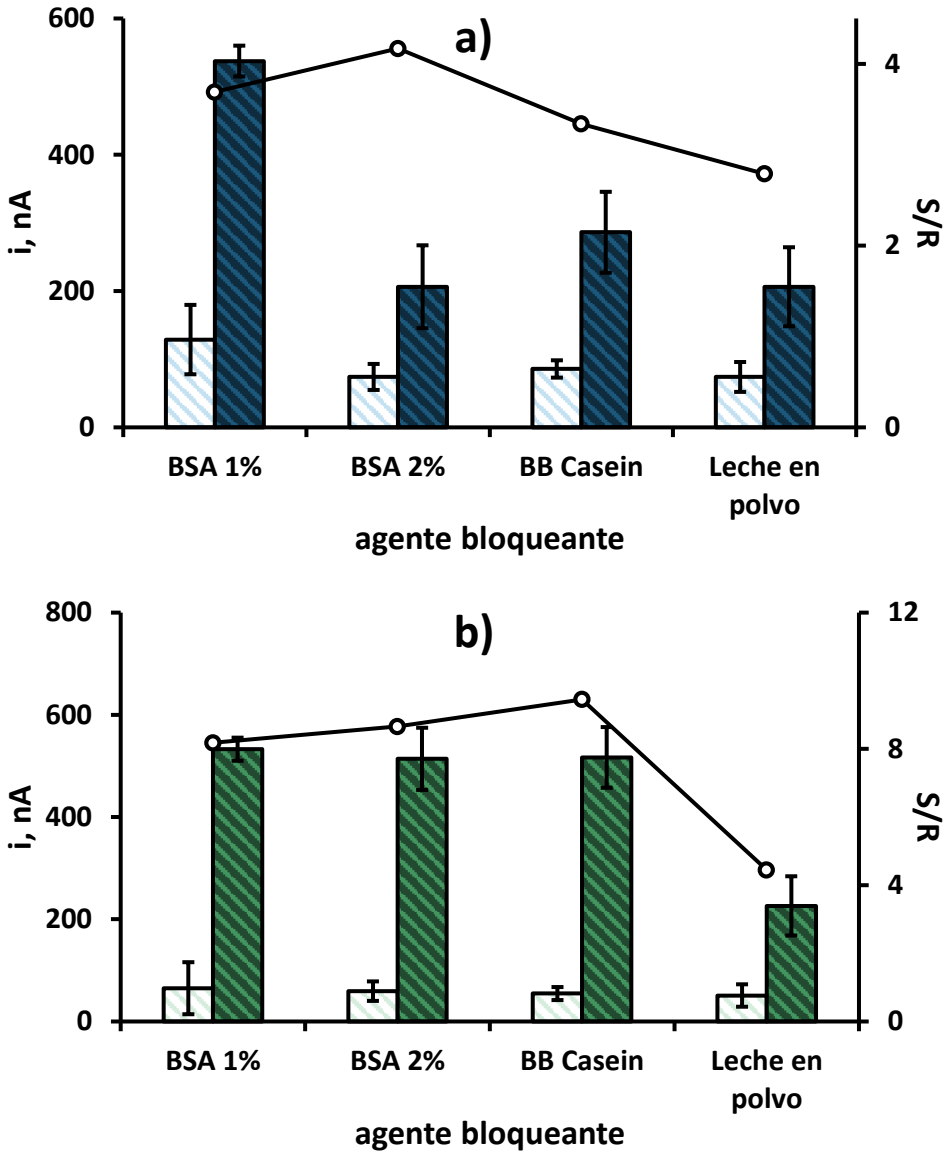

Figura 5.72. Efecto del agente bloqueante sobre la respuesta de los inmunosensores: HOOC-Phe-DWCNTs, 3 µL; Mix&Go™, 5 µL, 60 min; (a) anti-TNF, 4 µg/mL o (b) anti-IL, 6 µg/mL, 5 µL, 60 min; agente bloqueante, 5 µL, 30 min; TNF-α, 0 (□) y 50 (■) pg/mL o IL-1β, 0 (□) y 250 (■) pg/mL, 5 µL, 60 min; (a) Biotin-anti-TNF o (b) Biotin-anti-IL, 0.5 µg/mL, 5 µL, 60 min; HRP-Strept, 1/2000, 5µL, 20 min

Los resultados que se muestran en la Figura 5.72a para el inmunosensor de la TNF-α revelan una mayor relación entre las señales específica e inespecífica para un 2% de BSA, siendo similar esta relación cuando se bloquea con BSA al 2% o con caseína en el inmunosensor de la IL-1β (Figura 5.72b). Por ello, se eligió un 2% de BSA como

agente bloqueante, seleccionando asimismo un tiempo de incubación de 30 minutos, que es suficiente para minimizar eficazmente las adsorciones inespecíficas.

Influencia de la concentración y el tiempo de incubación de los anticuerpos de detección biotinilados

Para optimizar la concentración de los anticuerpos de detección biotinilados, Biotin-anti-TNF y Biotin-anti-IL, se prepararon diferentes inmunosensores, en ausencia o presencia de 50 pg/mL de TNF-α y en ausencia o presencia de 250 pg/mL de IL-1β, incubando, durante 60 minutos disoluciones de Biotin-anti-TNF de concentraciones comprendidas entre 0.25 y 0.75 µg/mL y de Biotin-anti-IL de concentraciones comprendidas entre 0.25 y 1 µg/mL, respectivamente.

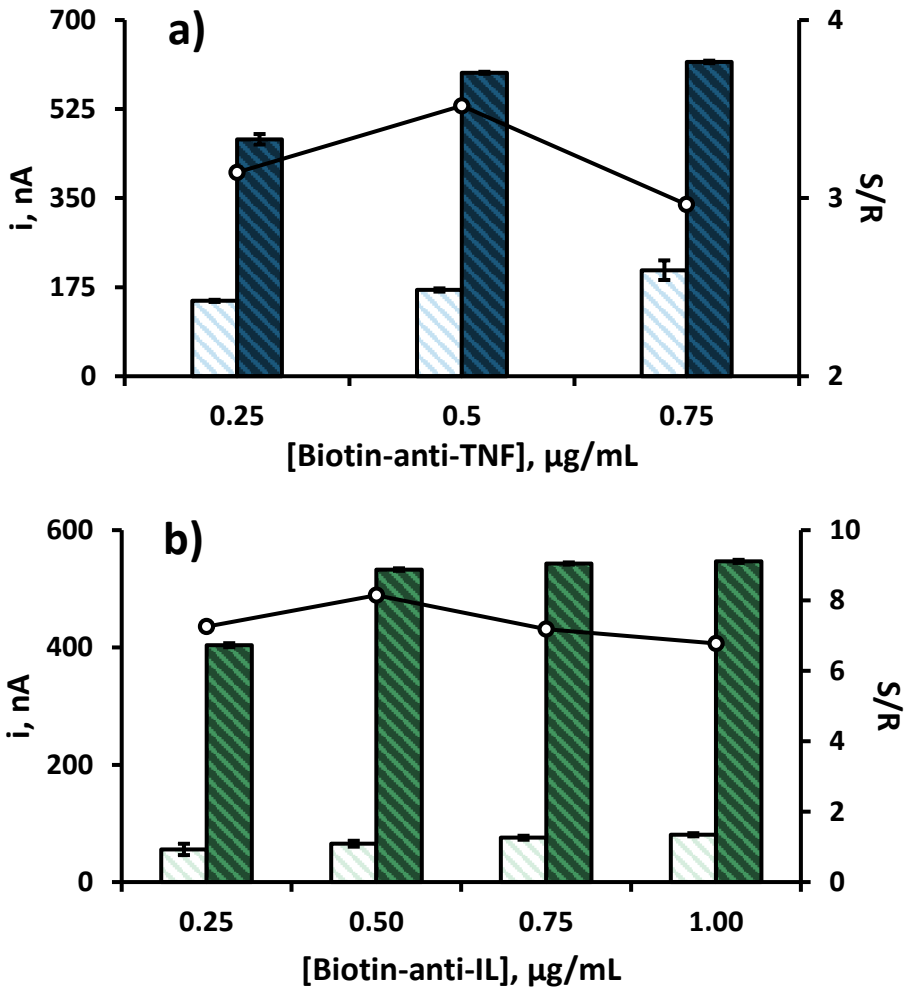

Figura 5.73. Efecto de la concentración de a) Biotin-anti-TNF y b) Biotin-anti-IL sobre la respuesta de los inmunosensores: HOOC-Phe-DWCNTs, 3 µL; Mix&Go™, 5 µL, 60 min; anti-TNF, 4 µg/mL o anti-IL, 6 µg/mL, 5 µL, 60 min; BSA, 2%, 5 µL, 30 min; TNF-α, 0 (□) y 50 (■) pg/mL o IL-1β, 0 (□) y 250 (■) pg/mL, 5 µL, 60 min; Biotin-anti-TNF o Biotin-anti-IL, 5 µL, 60 min; HRP-Strept, 1/2000, 5µL, 20 min

Como se puede ver en la Figura 5.73, los valores de intensidad de corriente en presencia de antígeno aumentan ligeramente para ambas citoquinas con la concentración del anticuerpo biotinilado correspondiente, incrementándose también la señal inespecífica. Así, se obtiene una mayor relación entre las corrientes específica e inespecífica para una concentración de 0.5 µg/mL de cada uno de los anticuerpos biotinilados, valor que se seleccionó para ambos Inmunosensores.

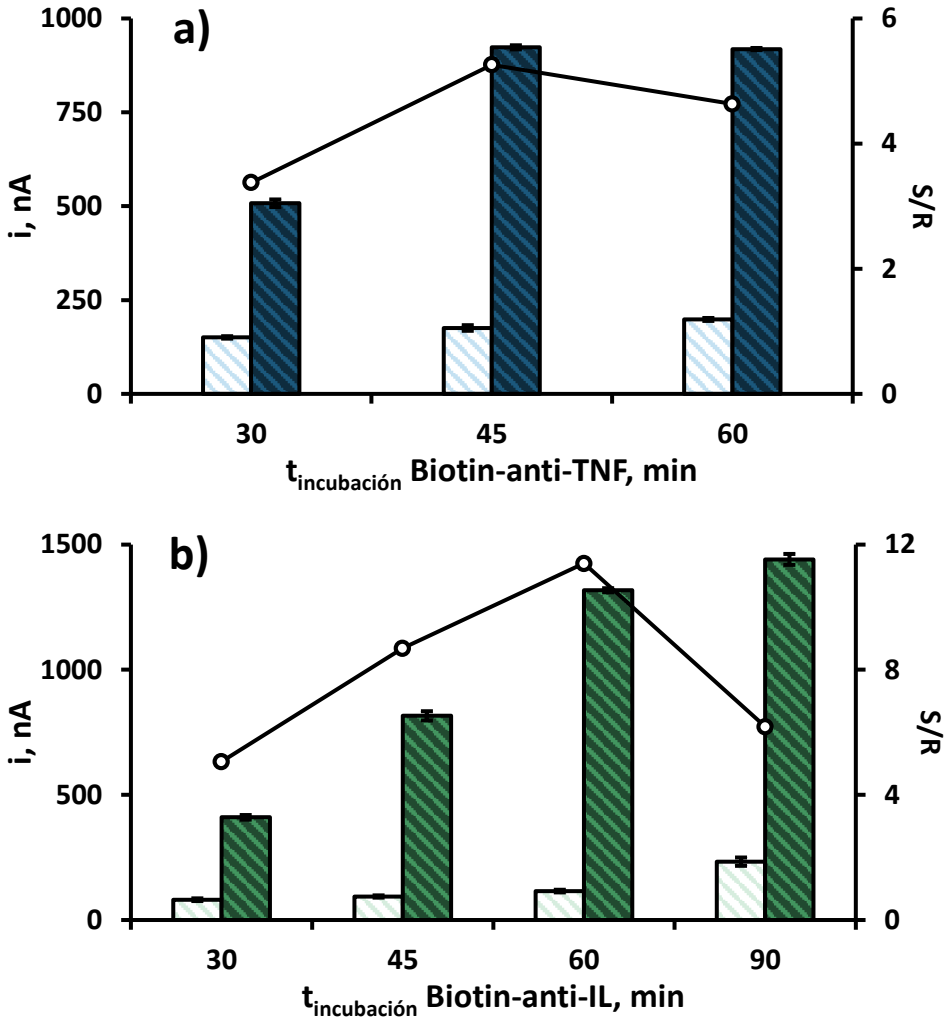

Figura 5.74. Efecto del tiempo de incubación de a) anti-TNF y b) anti-IL sobre la respuesta de los inmunosensores: HOOC-Phe-DWCNTs, 3 µL; Mix&Go™, 5 µL, 60 min; anti-TNF, 4 µg/mL o anti-IL, 6 µg/mL, 5 µL, 60 min; BSA, 2%, 5 µL, 30 min; TNF-α, 0 (□) y 50 (■) pg/mL o IL-1β, 0 (▨) y 250 (▩) pg/mL, 5 µL, 60 min; Biotin-anti-TNF o Biotin-anti-IL, 0.5 µg/mL, 5 µL; poli-HRP-Strept, a) 1/1000 o b) 1/500, 5µL, 15 min

Por otro lado, también se evaluó el tiempo de incubación en las disoluciones de los anticuerpos biotinilados Biotin-anti-TNF y Biotin-anti-IL requerido para la formación de los inmunocomplejos. Para ello, se midió la respuesta de distintos inmunosensores aplicando tiempos comprendidos entre 30 y 60 minutos y entre 30 y

90 minutos, respectivamente. Como se observa en la Figura 5.74, en ambos casos, la mayor relación S/R se obtuvo para un tiempo de incubación de 60 minutos.

Influencia del tipo y la dilución del conjugado enzimático

Con el fin de obtener una mayor sensibilidad, se estudió el efecto de distintos conjugados enzimáticos sobre la respuesta de los inmunosensores para TNF-α e IL-1β.

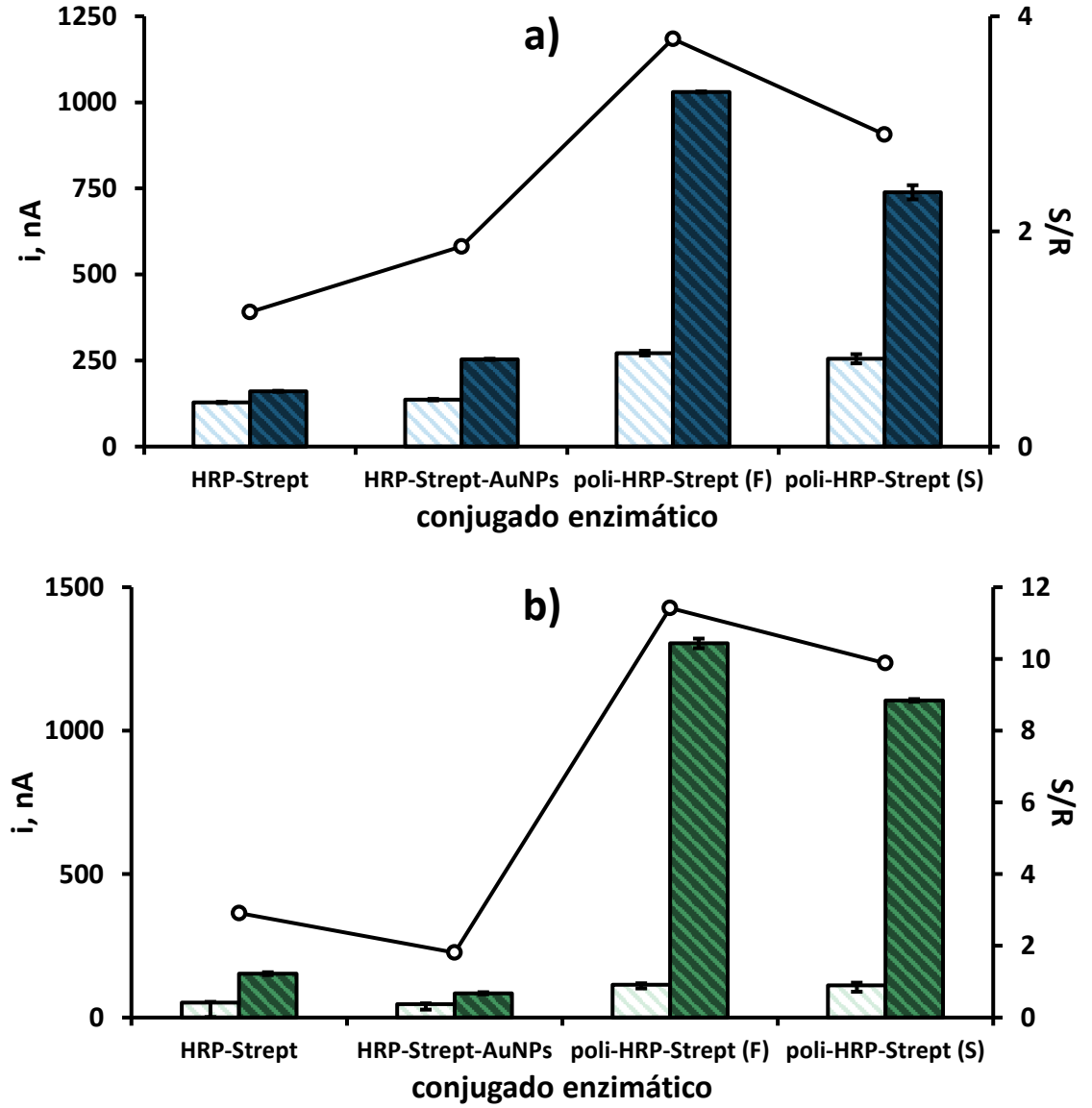

Figura 5.75. Efecto del tipo de conjugado enzimático sobre la respuesta de los inmunosensores: HOOC-Phe-DWCNTs, 3 µL; Mix&Go™, 5 µL, 60 min; anti-TNF, 4 µg/mL o anti-IL, 6 µg/mL, 5 µL, 60 min; BSA, 2%, 5 µL, 30 min; TNF-α, 0 (□) y 10 (■) pg/mL o IL-1β, 0 (□) y 25 (▩) pg/mL, 5 µL, 60 min; Biotin-anti-TNF o Biotin-anti-IL, 0.5 µg/mL, 5 µL, 60 min; HRP-Strept, 1/2000, HRP-Strept-AuNPs, 1/2, poly-HRP-Strept (F), 1/500, poli-HRP-Strept (S), 1/500, 5µL, 15 min

En la Figura 5.75 se muestran los resultados obtenidos empleando el monómero HRP-Strept convencional, el mismo monómero conjugado con nanopartículas de oro (HRP-Strept-AuNPs) y dos polímeros comerciales poli-HRP-Strept.

Como puede observarse, los inmunosensores construidos con los conjugados poliméricos, poli-HRP-Strept, proporcionaron una corriente específica mucho mayor como corresponde a la presencia de una mayor cantidad de peroxidasa sobre el electrodo. Asimismo, se observa una mayor relación de señales empleando el producto comercial de la compañía Fitzgerald, que probablemente contiene un mayor número de moléculas de peroxidasa.

Con respecto al efecto de la dilución del conjugado enzimático poly-HRP-Strept de Fitzgerald, ambos inmunosensores exhiben un comportamiento similar en presencia de analito, observándose una disminución de la corriente específica a medida que la concentración del conjugado enzimático disminuye (Figura 5.76).

Sin embargo, la relación entre las señales específica e inespecífica aumenta ligeramente hasta una dilución 1/1000 en el inmunosensor de la TNF-α, mientras que permanece aproximadamente constante para el inmunosensor de IL-1β en el intervalo de diluciones estudiado. A partir de estos resultados, con el fin de homogeneizar la preparación del inmunosensor dual, se seleccionó una dilución 1/500 para ambos.

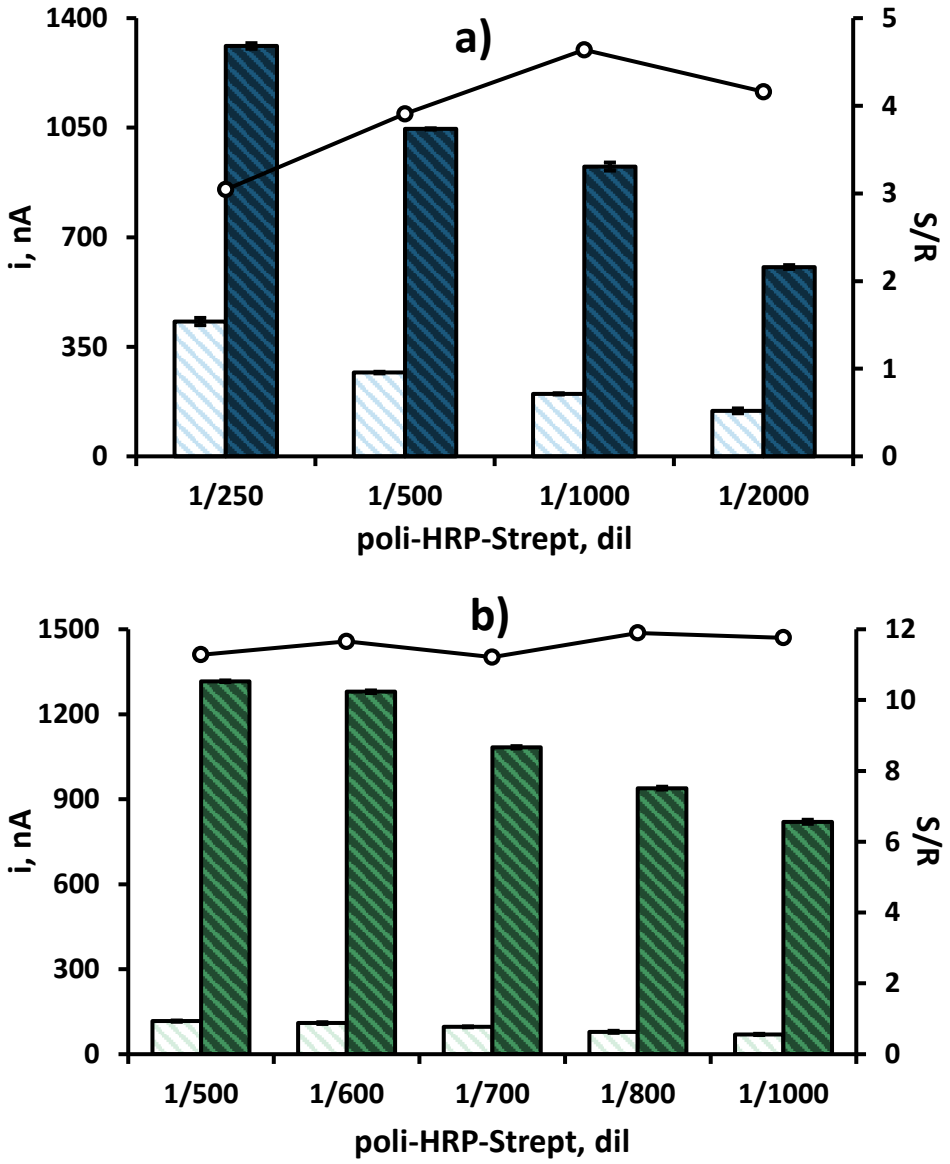

Figura 5.76. Efecto de la dilución de poli-HRP-Strept sobre la respuesta de los inmunosensores: HOOC-Phe-DWCNTs, 3 µL; Mix&Go™, 5 µL, 60 min; anti-TNF, 4 µg/mL o anti-IL, 6 µg/mL, 5 µL, 60 min; BSA, 2%, 5 µL, 30 min; TNF-α, 0 (□) y 10 (■) pg/mL o IL-1β, 0 (□) y 25 (■) pg/mL, 5 µL, 60 min; Biotin-anti-TNF o Biotin-anti-IL, 0.5 µg/mL, 5 µL, 60 min; poli-HRP-Strept, 1/500, 5µL, 15 min

En la Tabla 5.13 se resumen las variables estudiadas, así como los intervalos evaluados y los valores seleccionados para estudios posteriores para cada una de las configuraciones derrolladas con el criterio de la mejor relación S/R.

Tabla 5.13. Optimización de las variables experimentales implicadas en la construcción del inmunosensor dual

VARIABLE EXPERIMENTAL	INTERVALO EVALUADO	VALOR SELECCIONADO
método inmovilización anti-TNF y anti-IL	EDC/NHSS Mix&Go™ Micro	Mix&Go™ Micro
$[Ab_{captura}]$, µg/mL	1 – 5 (TNF-α) 2 – 8 (IL-1β)	4 (TNF-α) 6 (IL-1β)
$t_{incubación}$ $Ab_{captura}$, min	30 – 60 (TNF-α) 30 – 90 (IL-1β)	60
agente bloqueante	BSA, Blocker™ Casein, leche en polvo	BSA
BSA	1 – 2	2
[Biotin-$Ab_{detección}$], µg/mL	0.25– 0.75 (TNF-α) 0.25 – 1 (IL-1β)	0.5
$t_{incubación}$ Biotin-$Ab_{detección}$, min	30 – 90	60
conjugado enzimático	HRP-Strept, HRP-Strept-AuNPs, poli-HRP-Strept (Fitzgerald), poli-HRP-Strept (Sigma)	poli-HRP-Strept (Fitzgerald)
poli-HRP-Strept, dil	1/250 – 1/1000	1/500

5.3.2.3. Calibrados y características analíticas

Una vez optimizadas las condiciones experimentales para los inmunosensores de TNF-α e IL-1β individuales sobre los electrodos HOOC-Phe-DWCNTs/SPCE, se procedió a la construcción del inmunosensor para la determinación simultánea de ambas citoquinas sobre un electrodo serigrafiado de carbono dual. Empleando este electrodo, se obtuvieron los calibrados que se muestran en la Figura 5.77. Las barras de error se calcularon a partir de las medidas proporcionadas por tres electrodos duales diferentes para cada uno de los analitos a las concentraciones estudiadas. La variación de la intensidad de corriente con el logaritmo de la concentración de TNF-α se ajusta linealmente a la ecuación i, nA = (746 ± 16) log ([TNF-α], pg/mL) + (245 ± 22) (R^2 = 0.999), entre 1 y 200 pg/mL (Figura 5.77a), mientras que para IL-1β, entre 0.5 y 100 pg/mL, la ecuación i, nA = (624 ± 15) log ([IL-1β], pg/mL) + (393 ± 18) (R^2 = 0.996) (Figura 5.77b). Estos intervalos de concentración, que abarcan dos

órdenes de magnitud, son adecuados para la determinación de las citoquinas en muestras clínicas, a nivel de las unidades de pg/mL [M. Mazloum-Ardakani, 2014].

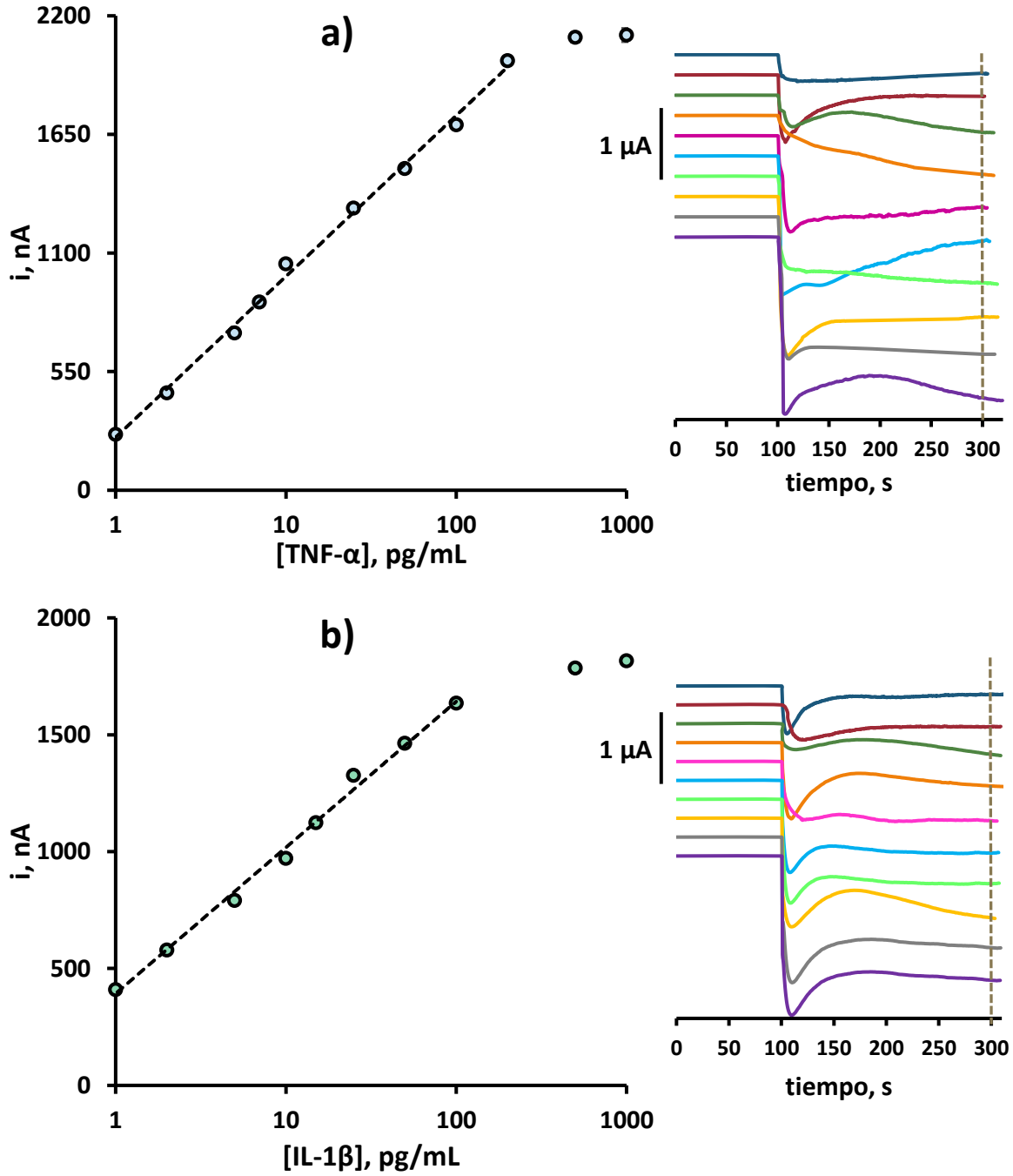

Figura 5.77. Calibrados para la determinación simultánea de TNF-α e IL-1β empleando el inmunosensor dual poli-HRP-Strept-Biotin-anti-TNF-TNF-α-anti-TNF-Phe-DWCNTs/SPCE y poli-HRP-Strept-Biotin-anti-IL-IL-1β-anti-IL-Phe-DWCNTs/SPCE

Por otro lado, los límites de detección alcanzados fueron de 0.85 pg/mL para el inmunosensor de TNF-α y de 0.38 pg/mL para el inmunosensor de IL-1β, calculados siguiendo el criterio $\overline{x}+3\cdot s$, donde *s* es la desviación estándar calculada a partir de las

respuestas amperométricas obtenidas para diez réplicas del blanco, es decir, en ausencia de analito (TNF-α o IL-1β), en unidades de concentración, pg/mL.

5.3.2.4. Estudio de selectividad

Debido a la proximidad entre los dos electrodos de trabajo, es importante investigar la posible reactividad cruzada de una citoquina en el inmunosensor de la otra. Con este propósito se compararon las respuestas amperométricas registradas empleando, por un lado, el inmunosensor poli-HRP-Strept-Biotin-anti-TNF-TNF-α-anti-TNF-Phe-DWCNTs/SPCE en presencia de 25 pg/mL de IL-1β con las obtenidas empleando 0 o 10 pg/mL de TNF-α (Figura 5.78a) y, por otro, el inmunosensor poli-HRP-Strept-Biotin-anti-IL-IL-1β-anti-IL-Phe-DWCNTs/SPCE en presencia de 10 pg/mL de TNF-α con las obtenidas empleando 0 o 25 pg/mL de IL-1β (Figura 5.78b).

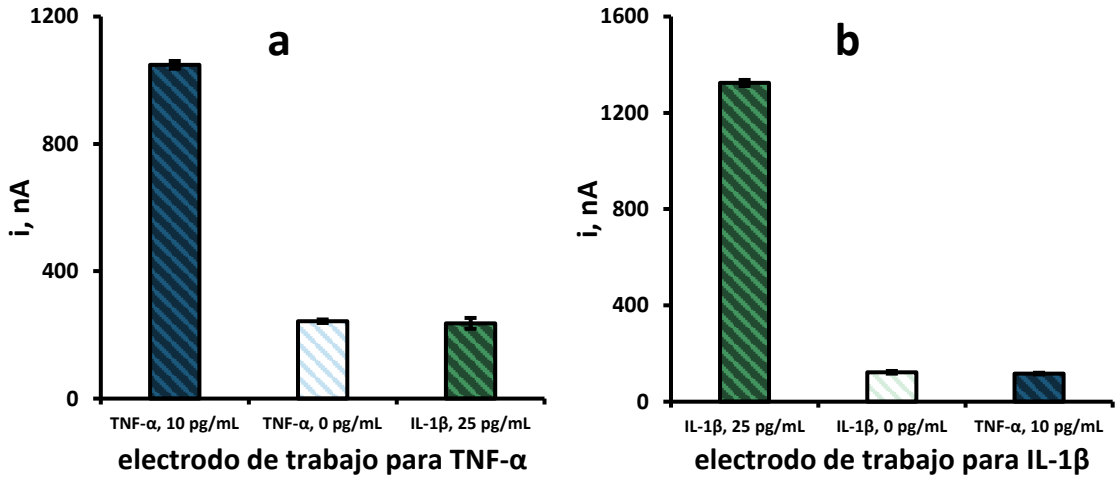

Figura 5.78. Respuesta del inmunosensor poli-HRP-Strept-Biotin-anti-TNF-TNF-α-anti-TNF-Phe-DWCNTs/SPCE con 0 (□), 10 (■) pg/mL de TNF-α y 25 (■) pg/mL de IL-1β y del inmunosensor poli-HRP-Strept-Biotin-anti-IL-IL-1β-anti-IL-Phe-DWCNTs/SPCE con 0 (□), 25 (■) pg/mL de IL-1β y 10 (■) pg/mL de TNF-α

Los resultados obtenidos muestran claramente que no existen diferencias significativas entre las respuestas amperométricas de ambos inmunosensores en ausencia del antígeno objetivo y en presencia del antígeno interferente, lo que demuestra la especificidad de los anticuerpos utilizados.

Además, al igual que en otros casos, las citoquinas TNF-α e IL-1β se encuentran en las muestras de interés clínico tales como suero y saliva junto con otros compuestos

que pueden actuar como interferentes en su determinación. En este apartado, se estudió el efecto de las siguientes especies: adiponectina (APN), albúmina de suero bovino (BSA), colesterol (Chol), proteína C reactiva (CRP), hemoglobina (HB), interleucina 6 (IL-6), interleucina 8 (IL-8), factor de crecimiento transformante beta 1 (TGF-β1), bilirrubina (BIL), ceruloplasmina (Cp), grelina (GHRL) y leptina (Lep), no observándose interferencia por parte de ninguna de estas especies en ninguna de las dos determinaciones (Figura 5.79).

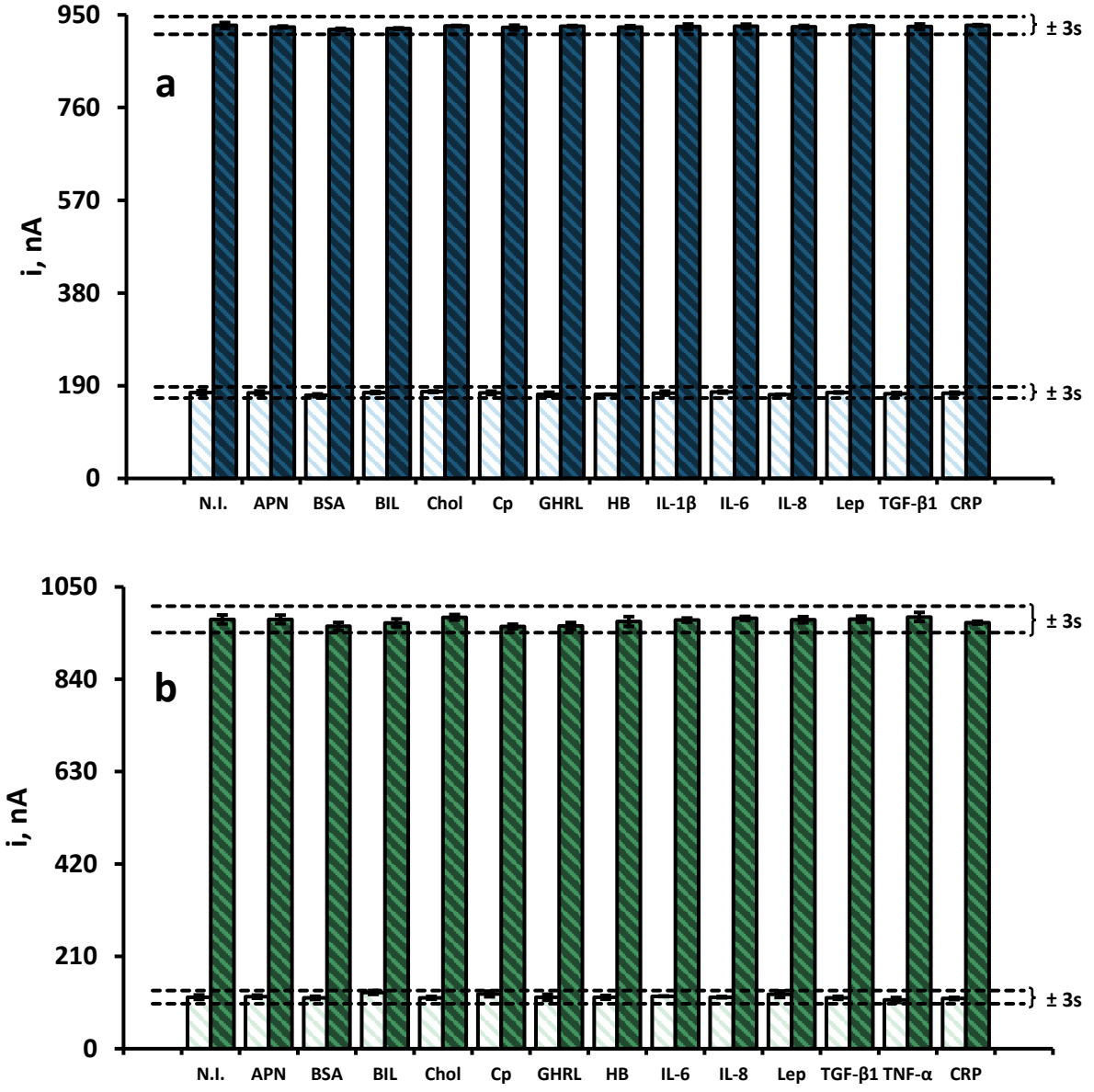

Figura 5.79. Selectividad del inmunosensor dual evaluando la respuesta del mismo con 0 (□) y 10 (■) pg/mL de TNF-α o 0 (□) y 25 (▩) pg/mL de IL-1β frente a 20 µg/mL de APN, 5 mg/mL de BSA, 190 ng/mL de BIL, 20 µg/mL de Chol, 500 µg/mL de Cp, 500 pg/mL de GHRL, 50 µg/mL de HB, 50 pg/mL de IL-1 β, 50 pg/mL de Il-6, 30 pg/mL de IL-8, 500 pg/mL de TGF-β1, 5 ng/mL de Lep y 1 µg/mL de CRP

5.3.2.5. Estudios de reproducibilidad y estabilidad

La reproducibilidad de las medidas amperométricas se evaluó con diferentes inmunosensores duales preparados en el mismo día y en días diferentes, en ausencia o en presencia de 100 pg/mL de TNF-α o de 50 pg/mL de IL-1β, obteniéndose valores de desviación estándar relativa (RSD) del 0.3 y 0.7% para la TNF-α (*n*=5) y del 0.6 y 2.7% para la IL-1β (*n*=4), respectivamente, para los ensayos realizados en el mismo día, así como del 0.5 y 0.7% para la TNF-α (*n*=5) y 0.8 y 3.7% para la IL-1β (*n*=4), respectivamente, para las medidas registradas en días diferentes. Estos resultados demuestran una buena repetibilidad y reproducibilidad de las medidas y una buena precisión en la fabricación y el funcionamiento de la plataforma inmunosensora electroquímica dual desarrollada.

Por otro lado, se evaluó la estabilidad de los inmunoconjugados anti-TNF-Phe-DWCNTs/SPCE y anti-IL-Phe-DWCNTs/SPCE que, tras su bloqueo con BSA al 2%, se almacenaron en seco a –20°C. De este modo, el mismo día se prepararon varios inmunoconjugados que se utilizaron posteriormente para construir, en días diferentes, los inmunosensores duales completos, registrando su respuesta amperométrica en presencia de 100 pg/mL de TNF-α y 50 pg/mL de IL-1β.

Como puede observarse en el gráfico de control representado en la Figura 5.80, cuyos márgenes corresponden a ± 3 veces la desviación estándar de las medidas realizadas el primer día de trabajo, la media de las tres medidas realizadas cada día se encuentra dentro del intervalo señalado durante al menos 40 días en ambos casos, lo que demuestra una relativamente prolongada estabilidad de almacenamiento.

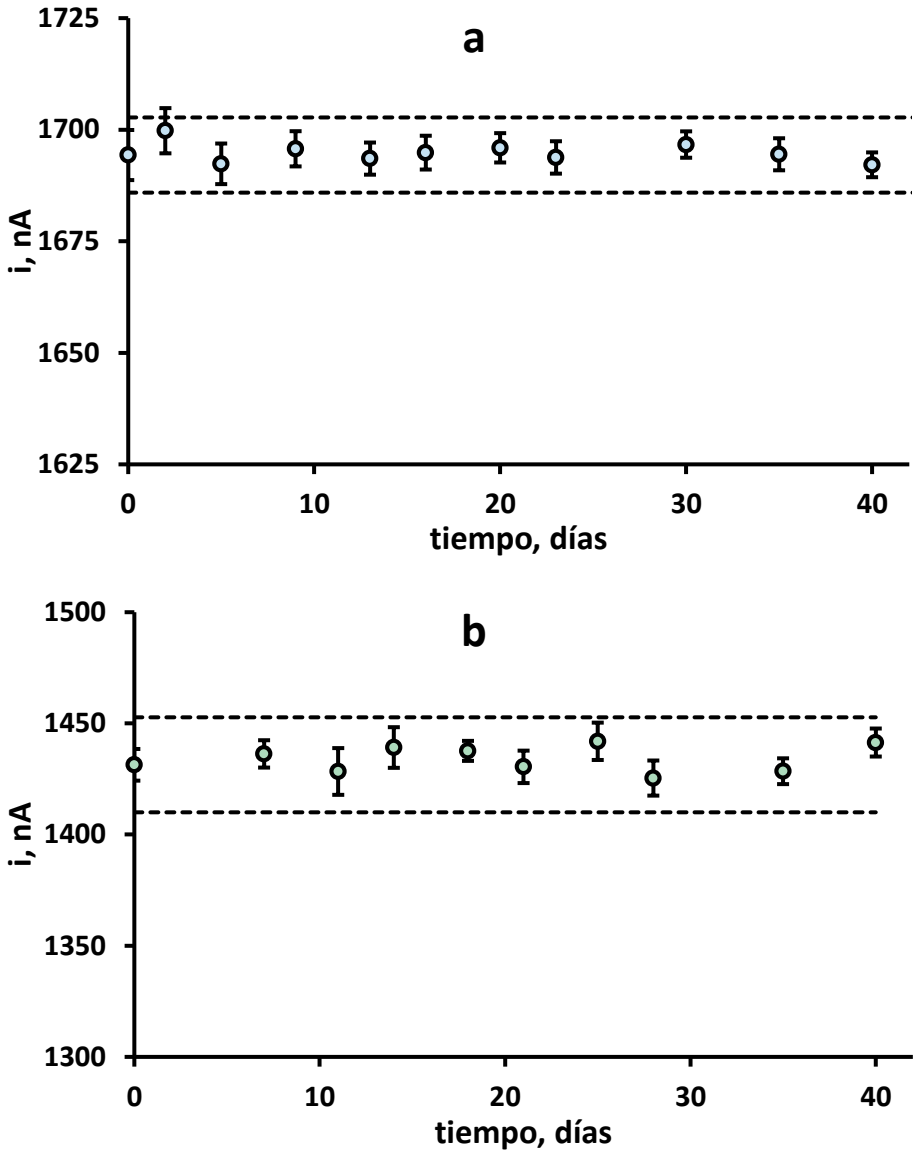

Figura 5.80. Gráfico de control para la evaluación de la estabilidad de almacenamiento de los conjugados anti-TNF-Phe-SWCNTs/SPCE y anti-IL-Phe-SWCNTs/SPCE

5.3.2.6. Aplicación a la determinación simultánea de factor de necrosis tumoral alfa e interleucina 1 beta en suero y saliva

La utilidad analítica del inmunosensor dual se demostró mediante su aplicación a la determinación simultánea de TNF-α e IL-1β en suero humano liofilizado enriquecido con distintas concentraciones de cada uno de los analitos, a niveles clínicamente relevantes [Arica, 2005; Dogan, 2006], y en saliva procedente de cuatro individuos sanos, siguiendo el procedimiento descrito en el *Apartado 4.6.6.* de la *Parte*

Experimental. Al igual que en otros casos, en primer lugar, se evaluó la posible existencia de efecto matriz en la muestra de suero liofilizado. Para ello se construyó un calibrado enriqueciendo el suero liofilizado con 5, 10 y 15 pg/mL de TNF-α, y 2.5, 5 y 7.5 pg/mL de IL-1β. Posteriormente se compararon las pendientes de las ecuaciones de calibrado obtenidas previamente con disoluciones estándar, 746 ± 16 y 624 ± 15 nA por década de concentración para TNF-α e IL-1β, respectivamente, con las pendientes de los calibrados obtenidos para las muestras enriquecidas con diferentes concentraciones de cada una de las citoquinas, ip, nA = (766 ± 12) log ([TNF-α], pg/mL) + (238 ± 13) nA e ip, nA = (614 ± 72) log ([IL-1β], pg/mL) + (389 ± 49) nA.

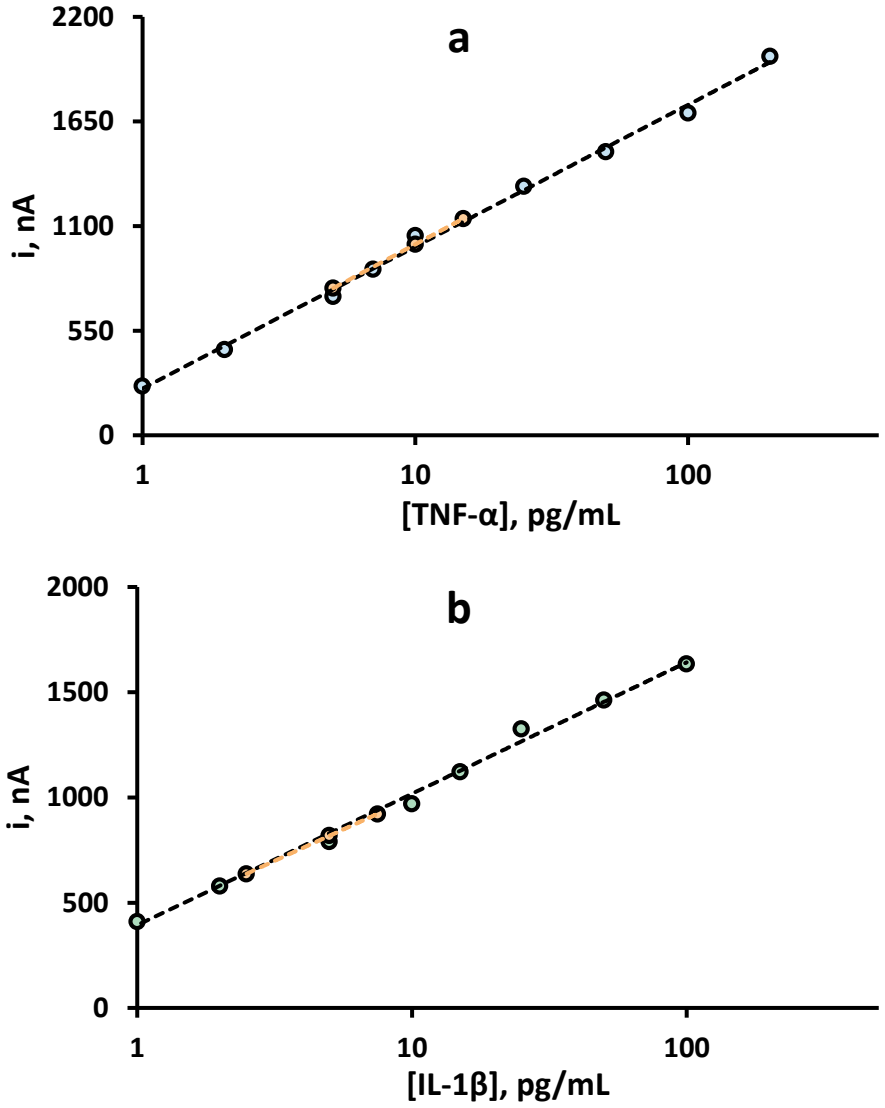

Figura 5.81. Superposición de las señales obtenidas para el suero liofilizado enriquecido (●) en el calibrado de disoluciones estándar de TNF-α (○) e IL-1β (○)

Como anteriormente, esta comparación se llevó a cabo empleando el test *t* de Student, donde el valor calculado de la *t* de Student experimental, (t_{exp} = 1.231 para la TNF-α y t_{exp} = 1.655 para la IL-1β) es inferior al valor de *t* de Student tabulada, (t_{tab} = 2.306) a un nivel de significación del 0.05. Estos resultados permiten deducir que no existen diferencias significativas entre las pendientes de las curvas de calibrado en ambos medios (Figura 5.81), pudiéndose determinar la concentración de ambas citoquinas en suero por interpolación directa de las señales proporcionadas por la muestra en los calibrados de disoluciones estándar.

En la Tabla 5.14 se resumen los resultados obtenidos en la determinación por triplicado de las muestras de suero analizadas.

Tabla 5.14. Determinación de TNF-α e IL-1β en muestras de suero humano liofilizado empleando el inmunosensor dual

[TNF-α] AÑADIDO, pg/mL	[TNF-α] RECUPERADO, pg/mL*	RECUPERACIÓN, %*
5	5.1 ± 0.2	99 ± 8
10	10.2 ± 0.6	98 ± 6
15	15.7 ± 0.9	98 ± 8
[IL-1β] AÑADIDO, pg/mL	**[IL-1β] RECUPERADO, pg/mL***	**RECUPERACIÓN, %***
2.5	2.5 ± 0.2	102 ± 7
5	4.9 ± 0.4	102 ± 5
7.5	7.3 ± 0.5	104 ± 6

* valor medio ± t·s/√n

Como se observa, los porcentajes de recuperación se encuentran entre el 98 y el 104%, lo que pone de manifiesto la gran fiabilidad de la metodología propuesta para la determinación de estos analitos en este tipo de muestra, siguiendo un protocolo de trabajo que se caracteriza por su simplicidad.

En el caso de las muestras de saliva de individuos sanos, una vez comprobada la ausencia de efecto matriz, la determinación de TNF-α e IL-1β se llevó a cabo por interpolación de la intensidad de corriente proporcionada por las muestras en los

calibrados de disoluciones estándar. Posteriormente, los resultados obtenidos se validaron comparándolos con los proporcionados por los kits ELISA correspondientes, siguiendo el procedimiento de ensayo especificado por la casa comercial. Los resultados obtenidos por ambos métodos se resumen en la Tabla 5.15. Además, al igual que anteriormente, se empleó el test *t* de Student para comparar estadísticamente los resultados, obteniéndose valores de t_{exp} de 0.10 y 0.67 para la TNF-α y de 0.27 y 0.17 de IL-1β, para las muestras, respectivamente, ambos inferiores al valor teórico para las condiciones del experimento (t_{tab} = 2.201). Estos resultados confirman que no existen diferencias significativas entre ambas metodologías a un nivel de significación del 0.05, quedando demostrada la utilidad del inmunosensor dual desarrollado para la determinación del contenido TNF-α e IL-1β en muestras de saliva humana en concentraciones clínicamente relevantes.

Tabla 5.15. Determinación de TNF-α e IL-1β en muestras de saliva empleando el inmunosensor dual

MUESTRA	INMUNOSENSOR TNF-α, pg/mL*	ELISA TNF-α, pg/mL*
hombre fumador	13.3 ± 0.5	13.5 ± 0.9
mujer no fumadora	11.2 ± 0.3	11.3 ± 0.7
MUESTRA	**INMUNOSENSOR IL-1β, pg/mL***	**ELISA IL-1β , pg/mL***
hombre fumador	13.3 ± 0.5	13.5 ± 0.9
mujer no fumadora	11.2 ± 0.3	11.3 ± 0.7

* valor medio ± t·s/√n

Al igual que anteriormente, se empleó el test *t* de Student para comparar estadísticamente los resultados, obteniéndose valores de t_{exp} de 0.10 y 0.67 para la TNF-α y de 0.27 y 0.17 de IL-1β, para el hombre fumador y la mujer no fumadora, respectivamente, ambos inferiores al valor teórico para las condiciones del experimento (t_{tab} = 2.201). Estos resultados confirman que no existen diferencias significativas entre ambas metodologías a un nivel de significancia de 0.05, quedando demostrada la utilidad del inmunosensor dual desarrollado para la determinación del

contenido TNF-α e IL-1β en muestras de suero humano en concentraciones clínicamente relevantes.

5.3.2.7. Conclusiones

En este trabajo se ha descrito por primera vez la preparación, funcionamiento y aplicación de una plataforma electroquímica dual para la determinación simultánea de las citoquinas TNF-α e IL-1β. El inmunosensor desarrollado se basa en el empleo de electrodos serigrafiados de carbono modificados con nanotubos de carbono de pared doble funcionalizados con grupos *p*-carboxifenilo. Además de las ventajas de este nanomaterial, el uso del reactivo polimérico Mix&Go™ permite llevar a cabo la inmovilización orientada de los dos anticuerpos de captura a través de la región glicosilada, lo que facilita la preparación del inmunosensor. Por otro lado, el empleo de una configuración tipo sándwich con amplificación de la señal por medio del conjugado poli-HRP-Strept permitió el desarrollo de un método sensible para la determinación simultánea de TNF-α e IL-1β con características analíticas mejoradas respecto de los métodos encontrados en la bibliografía y de los inmunoensayos tipo ELISA comerciales para la determinación individual de estos compuestos. Finalmente, la utilidad del inmunosensor dual desarrollado se demostró mediante su aplicación a la determinación simultánea de ambas citoquinas, en concentraciones clínicamente relevantes, en fluidos biológicos como suero y saliva.

Un factor importante a destacar es que tiempo de ensayo con el inmunosensor es mucho menor que cuando se utilizan los kits ELISA. En efecto, para la determinación simultánea de las dos citoquinas, el inmuosensor dual requiere aproximadamente dos horas y media una vez que se han inmovilizados los respectivos anticuerpos de captura. Sin embargo, los inmunoensayos convencionales con los kits ELISA requieren tiempos de ensayo de cuatro horas y cuarenta minutos para cada una de las determinaciones. Por otro lado, el volumen de muestra empleado es mucho menor, con solo 2.5 µL cada vez, frente a los 100 µL que se requieren en el inmunoensayo ELISA.

5.4. INMUNOSENSORES BASADOS EN EL EMPLEO DE NANOMATERIALES HÍBRIDOS FUNCIONALIZADOS CON BIOMOLÉCULAS COMO ESTRATEGIA DE AMPLIFICACIÓN DE LA SEÑAL

En este apartado se describen dos configuraciones de inmunosensores desarrollados en la Tesis Doctoral con la característica común de estar basados en el empleo de materiales híbridos de nanotubos de carbono como portadores de los respectivos anticuerpos de detección para su uso como sistemas de amplificación de la respuesta electroquímica. En primer lugar, se presentan los resultados obtenidos con el inmunosensor preparado para el factor de crecimiento transformante beta 1 (TGF-β1) utilizando MWCNTs funcionalizados con anti-TGF, aminoviológeno y peroxidasa y, a continuación, se comentarán los correspondientes al inmunosensor para fetuina A humana (HFA), empleando en este caso un híbrido de nanotubos y nanopartículas magnéticas con anti-HFA y peroxidasa.

5.4.1. Inmunosensor para la determinación de factor de crecimiento transformante beta 1 empleando nanotubos de carbono funcionalizados con aminoviológeno como etiqueta portadora de amplificación de la señal

Como se ha comentado anteriormente, el factor de crecimiento transformante beta 1 (TGF-β1) es una citoquina perteneciente a la familia estructural de las TGF-βs multifuncionales que regulan una gran variedad de procesos biológicos. En particular, la TGF-β1 participa en la respuesta inmune e inflamatoria [Tsapenko, 2013] y se considera un buen biomarcador de la fibrosis hepática, el carcinoma de vejiga o algunas enfermedades renales. La concentración de TGF-β1 en saliva de individuos

sanos se encuentra alrededor de las pocas decenas de pg/mL [Yousefzadeh, 2006; Brand, 2014]. Por su parte, los viológenos son derivados de la *4,4'*-bipiridina que poseen un comportamiento electroquímico reversible correspondientes a sus tres posibles estados de oxidación: $V^{2+} \leftrightarrow V^{+\bullet} \leftrightarrow V^{0}$. Se ha visto que este comportamiento redox promueve la transferencia electrónica entre la superficie electródica y las proteínas, con la consiguiente disminución del sobrepotencial óhmico [Lee, 2016]. En este trabajo, como se ha indicado, el aminoviológeno (V) inmovilizado sobre nanotubos de carbono de pared simple (SWCNTs) se ha utilizado como marcador redox para la detección de TGF-β1.

La metodología empleada para la preparación del inmunosensor implica los siguientes pasos: a) preparación de los conjugados V-Phe-SWCNT(-HRP)-anti-TGF mediante la unión covalente de la enzima y el anticuerpo al material híbrido V-Phe-SWCNT; b) construcción de la plataforma sensora mediante la inmovilización del anticuerpo biotinilado (Biotin-anti-TGF) sobre electrodos serigrafiados funcionalizados mediante grafting con *p*-ABA y modificados con estreptavidina y c) implementación del inmunoensayo tipo sándwich para TGF-β1 mediante el uso de conjugados V-Phe-SWCNT(-HRP)-anti-TGF como etiquetas portadoras para amplificación de la señal.

5.4.1.1. Configuración del inmunosensor

En la Figura 4.35. de la *Parte Experimental* se han representado las etapas de preparación del inmunosensor para la determinación de TGF-β1. Como puede obsevarse, en primer lugar, se modifica la superficie de un electrodo serigrafiado de carbono mediante grafting con *p*-ABA. Tras la activación de los grupos carboxílicos se modifica la superficie con estreptavidina y se inmoviliza el anticuerpo de captura biotinilado (anti-TGF). Posteriormente, se bloquean con biotina las posiciones libres de la superficie electródica y se incorpora el antígeno (TGF-β1). Por último, se incorpora el bioconjugado V-Phe-SWCNT(-HRP)-anti-TGF, donde el aminoviológeno

actúa como mediador redox, llevándose a cabo la detección amperométrica del antígeno por adición de peróxido de hidrógeno a un potencial de reducción de –300 mV (Figura 5.82).

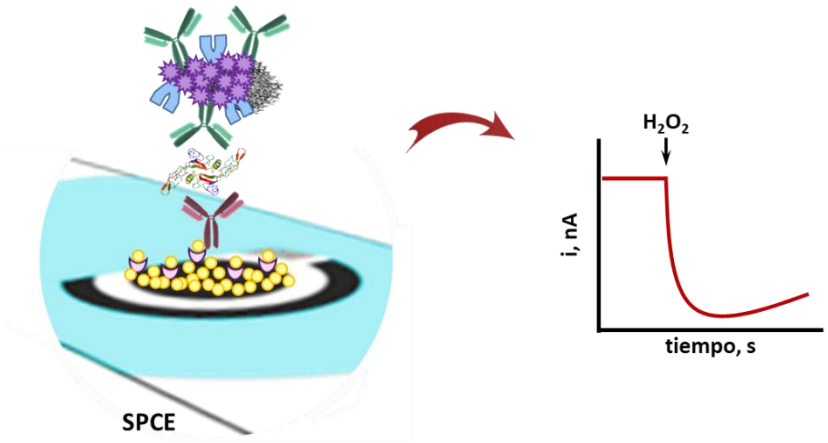

Figura 5.82. Esquema del funcionamiento del inmunosensor para la determinación deTGF-β1 empleando híbridos de aminoviológeno y SWCNTs como etiqueta portadora para la amplificación de la señal

5.4.1.2. Caracterización del nanomaterial

El material híbrido de nanotubos de carbono de pared simple funcionalizado con aminoviológeno, V-Phe-SWCNTs, se caracterizó empleando análisis termogravimétrico (TGA), espectrometría FTIR, espectroscopias Raman y UV-visible y el test de Kaiser. Mediante análisis termogravimétrico se cuantificó el grado de funcionalización del híbrido de nanotubos de carbono y se estimó la cantidad de grupos funcionales anclados a los mismos. Para ello, las muestras se calentaron desde 40 a 1000°C a una velocidad de 10°C/min en atmósfera de nitrógeno. Como puede observarse en el termograma de la Figura 5.83, a 600°C hay una pérdida de peso del 10.3% para los nanotubos de carbono de pared simple desnudos (SWCNTs), del 24.4% para los nanotubos de carbono de pared simple carboxilados (HOOC-Phe-SWCNTs) y del 33.3% para el material híbrido de nanotubos de carbono de pared simple funcionalizados con aminoviológeno, V-Phe-SWCNTs. De este modo, se estimó que el número de grupos carboxílicos funcionales presentes en el nanotubo es de 1 por cada 50 átomos de carbono y, con el mismo cálculo, que el número de grupos aminoviológenos funcionales es de 1 por cada 114 átomos de carbono.

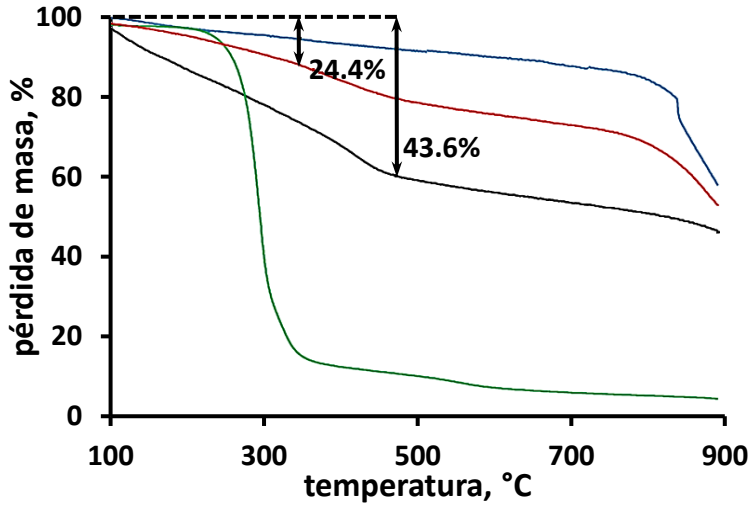

Figura 5.83. Perfil termogravimétrico de: SWCNTs (–), HOOC-SWCNTs (–) V-Phe-SWCNTs (–) y V (–)

El espectro Raman de los nanotubos de carbono de pared simple representado en la Figura 5.84 muestra dos bandas características: la banda D, de baja intensidad, a 1292 cm^{-1} y la banda G a 1595 cm^{-1}, siendo la relación entre ellas, I_D/I_G igual a 0.09. Después de la funcionalización, la intensidad de la banda D, asociada a la transformación de los carbonos con geometría sp^2 a sp^3, aumenta considerablemente, lo que indica la incorporación de un resto orgánico sobre la superficie de los nanotubos de carbono, haciéndose considerablemente mayor la relación entre ambas bandas, I_D/I_G de 0.54, que se corresponde a la incorporación del grupo aminoviológeno.

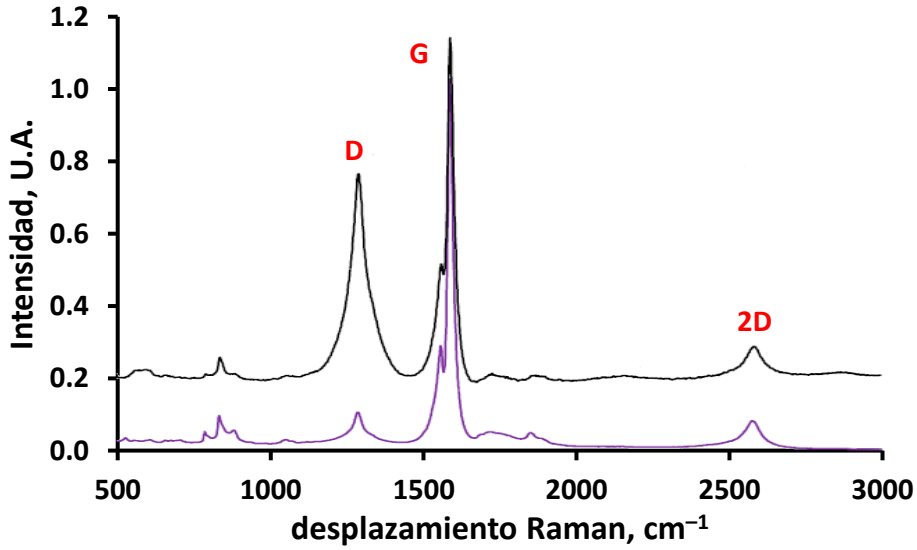

Figura 5.84. Espectro Raman a $\lambda_{excitación}$ = 785 nm de: SWCNTs (–) y V-Phe-SWCNTs (–)

La Figura 5.85a muestra la zona RBM de los nanotubos de carbono antes y después de la reacción de Tour. La reducción de la intensidad de las bandas también confirma la incorporación de distintos grupos funcionales a los SWCNTs. Además, la banda G^+ es sensible a la transferencia de carga, como se muestra en la Figura 5.85b. La banda G se desplaza hacia arriba 2 cm^{-1} en el espectro del híbrido de nanotubos de carbono de pared simple funcionalizados con aminoviológeno en comparación con el espectro de los nanotubos de carbono de pared simple desnudos [Davies, 2014; Voggu, 2008]. Este resultado confirma que el aminoviológeno, aceptor de electrones, está unido al esqueleto del nanotubo de carbono.

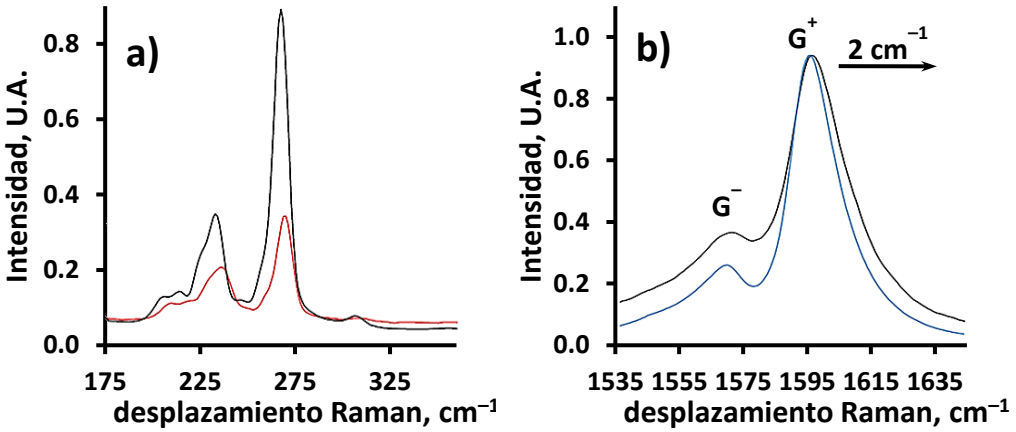

Figura 5.85. Espectros Raman comparativos de: a) la zona RBM a $\lambda_{excitación}$ = 785 nm antes (–) y después (–) de la funcionalización y b) la región próxima a la banda G a $\lambda_{excitación}$ = 785 nm de los SWCNTs (–) y los V-Phe-SWCNTs (–)

La espectrometría infrarroja por Transformada de Fourier (FTIR) proporciona información importante sobre la unión covalente del aminoviológeno sobre la superficie de los nanotubos de carbono de pared simple (Figura 5.86). En comparación con el espectro de los nanotubos de carbono de pared simple desnudo, el espectro del híbrido de nanotubos de carbono funcionalizados con aminoviológeno muestra las bandas características de las vibraciones del esqueleto en el plano del dominio grafítico a 1554 cm^{-1}, el modo de estiramiento alifático C–H a 2919 cm^{-1} y el C–H aromático cerca de 3005 cm^{-1}. Además, aparecen picos de gran intensidad atribuidos a las unidades de aminoviológeno a 3450 cm^{-1} (vibración N–H) y 1095 cm^{-1} (enlace C–N). Además, se observa un nuevo pico a 1642 cm^{-1} que se puede asignar a

un modo de estiramiento amida-carbonilo, que indica la unión química del aminoviológeno a la pared del nanotubo de carbono.

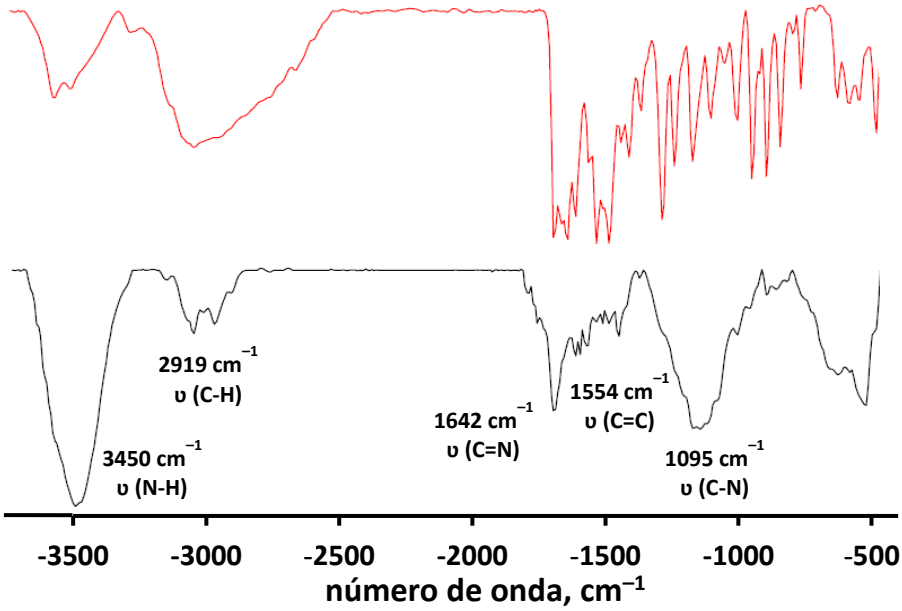

Figura 5.86. Espectros FTIR de: V (–) y V-Phe-SWCNTs (–)

Los resultados obtenidos mediante espectroscopia UV-visible están de acuerdo con los anteriores. Así en la Figura 5.87a, en la que se ha representado el espectro UV-visible del híbrido V-SWCNTs, aparece un pico a 382 nm, que no aparece en el espectro de los SWNCTs, demostrando así la incorporación del mediador. Por otro lado, la presencia de la amina primaria en el híbrido se confirmó mediante el test de Kaiser para aminas primarias, donde la ninhidrina reacciona con el grupo *N*-terminal del híbrido V-Phe-SWNCTs dando lugar a un color azul intenso (Figura 5.87b) [Tuci, 2012].

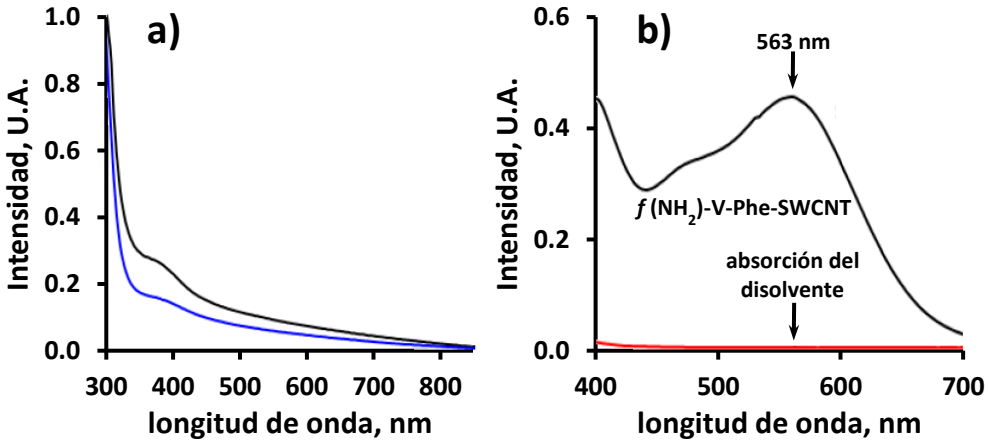

Figura 5.87. a) Espectro UV-visible en NMP de: bromuro de *1*-(*3*-aminoetil)-*4,4'*-bipiridinio (–) y V-Phe-SWCNTs (–); b) registro del test de Kaiser para los V-Phe-SWCNTs

A continuación, se preparó el bioconjugado V-Phe-SWCNT(-HRP)-anti-TGF por inmovilización covalente de la enzima peroxidasa (HRP) y el anticuerpo de detección (anti-TGF) sobre los nanotubos de carbono funcionalizados con aminoviológeno (V-Phe-SWCNT), tal y como se describe en el *Apartado 4.5.4.1.2.* de la *Parte Experimental*. Con el fin de lograr la inmovilización estable de un número elevado de biomoléculas sobre la superficie del nanomaterial híbrido, se llevó a cabo la unión covalente de los anticuerpos de detección anti-TGF a los grupos carboxílicos presentes en el material previa activación con el sistema EDC/NHSS. Por otro lado, se hizo uso del ácido tereftálico para enlazar los anticuerpos anti-TGF a los grupos aminoviológeno presentes en el híbrido V-Phe-SWCNT [Rahim-Ruslinda, 2013].

Una vez sintetizado el material híbrido bioconjugado, su caracterización se llevó a cabo por espectroscopia UV-visible e infrarroja por Transformada de Fourier. El espectro de absorción del material híbrido bioconjugado muestra una banda característica a 266 nm que se corresponde con la presencia de la biomolécula inmovilizada sobre la superficie del material (Figura 5.88a). Por su parte, el espectro FT-IR del material híbrido V-Phe-SWCNT(-HRP)-anti-TGF (Figura 5.88b) muestra una banda más amplia para la vibración característica de flexión O-H a 3429 cm^{-1}, así como nuevas bandas a 803, 656 y 478 cm^{-1}, en la región característica de las proteínas, que confirman la unión del anticuerpo. Asimismo, las bandas características del material híbrido se mantuvieron.

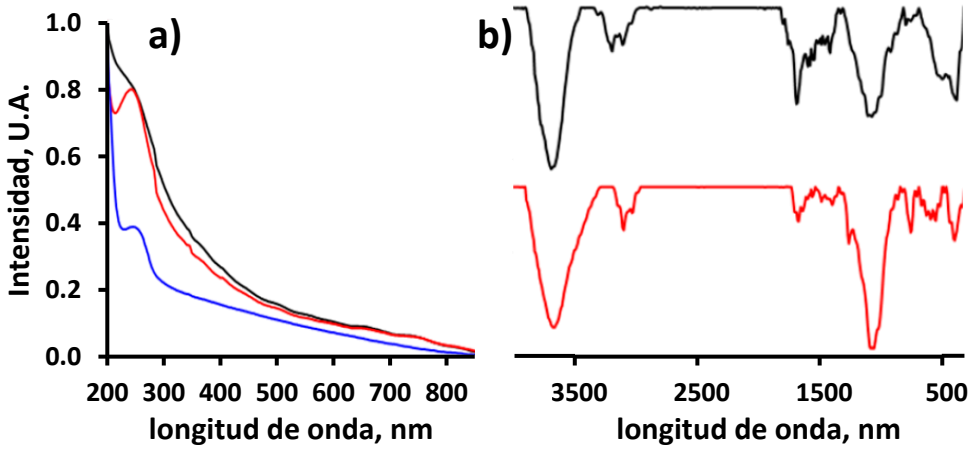

Figura 5.88. a) Espectro de absorción en H_2O_2 de: V-Phe-SWCNT (–), V-Phe-SWCNT-HRP (–) y V-Phe-SWCNT-(HRP)-anti-TGF (–); b) espectro FTIR de: V-Phe-SWCNT (–) y V-Phe-SWCNT(-HRP)-anti-TGF (–)

Por otro lado, en la Figura 5.89a se muestran los voltamperogramas cíclicos registrados en disoluciones preparadas en ausencia y presencia de H_2O_2 en un intervalo de potencial entre 0.0 y –0.8 V vs Ag, para el material híbrido V-Phe-SWCNT/SPCE (curvas 1 y 3) y el material híbrido modificado con la enzima V-Phe-SWCNT-HRP/SPCE (curvas 2 y 4). Como puede observarse, este último bioconjugado proporciona una respuesta más sensible a la reducción de H_2O_2 debido a la presencia de la enzima.

Por otro lado, la comparación de los voltamperogramas cíclicos de electrodos modificados con el conjugado SWCNT-HRP (Figura 5.89b) y con el conjugado de nanotubos-viológeno con peroxidasa (V-Phe-SWCNTs-HRP) (Figura 5.89c), registrados ambos en presencia y en ausencia de peróxido de hidrógeno, permitió apreciar que la señal respecto del blanco es superior para en conjugado de nanotubos funcionalizados con el aminoviologeno lo que puede atribuirse al papel de los grupos viológeno electroactivos del material híbrido V-Phe-SWCNT, a los que se ha atribuido una actividad pseudo-peroxidasa [Dong, 1997]. Este comportamiento está de acuerdo con lo descrito por Jia *et al.* [Jia, 2008] para la reducción electroquímica de H_2O_2 sobre un electrodo de carbono vítreo modificado con nanopartículas de oro y tetrabromuro de *N,N'*-bis(*3*-aminopropil-*4,4'*-bipiridinio) en ausencia y en presencia de la enzima peroxidasa.

Aunque la corriente catódica de los voltamperogramas cíclicos aumenta a medida que el potencial se hace más negativo, se seleccionó un potencial de detección de –0.3 V para llevar a cabo las medidas amperométricas para determinación de TGF-β1, con el objetivo de evitar posibles interferencias de sustancias electroactivas que puedan estar presentes en las muestras clínicas analizadas.

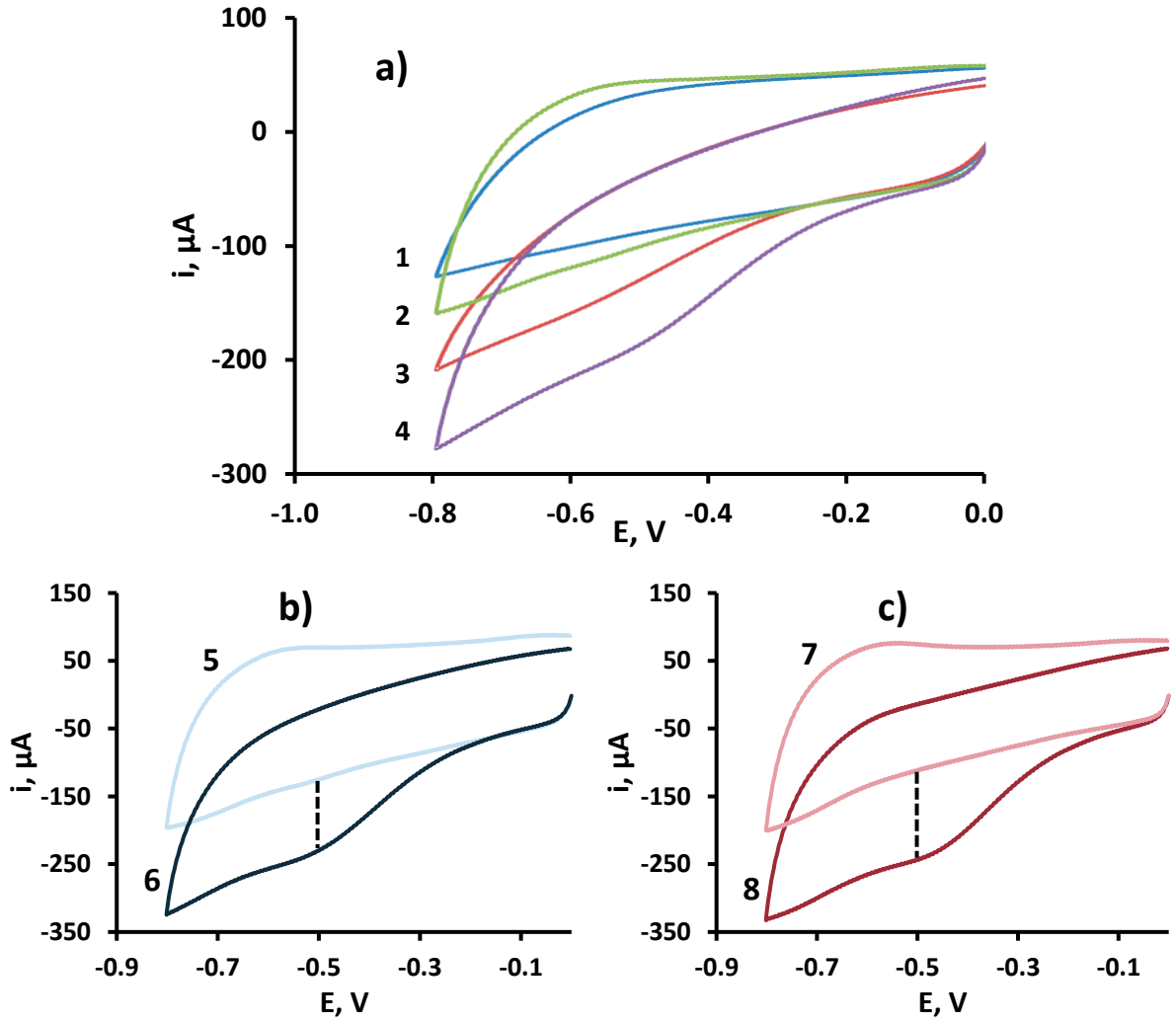

Figura 5.89. Voltamperogramas cíclicos registrados en disolución reguladora PB 100 mM de pH 6.0 de: a) V-Phe-SWCNT/SPCE (curvas 1 y 3) y V-Phe-SWCNT-HRP/SPCE (curvas 2 y 4). Los voltamperogramas cíclicos 1 y 2 contienen H_2O_2 0.044 mM. b) SWCNT-HRP/SPCE en ausencia (curva 5) y en presencia (curva 6) de H_2O_2 0.044 mM y c) V-Phe-SWCNT-HRP/SPCE en ausencia (curva 7) y en presencia (curva 8) de H_2O_2 0.044 mM

5.4.1.3. Optimización de las variables experimentales

Se optimizaron las variables que afectan a la preparación del material híbrido funcionalizado y las implicadas en la preparación del inmunosensor con los resultados que se describen a continuación.

Influencia de la concentración de estreptavidina

La influencia de la carga de estreptavidina inmovilizada en la superficie del electrodo sobre la respuesta amperométrica del inmunosensor para la determinación de TGF-β1 se estudió inmovilizando diferentes concentraciones de esta proteína, entre

100 y 300 µg/mL, sobre la superficie de los electrodos serigrafiados de carbono modificados por *grafting* con ácido *p*-ABA, tras su activación. Posteriormente, se construyeron los diferentes inmunosensores, en ausencia y presencia de 125 pg/mL de TGF-β1, empleando una disolución de Biotin-anti-TGF de 7.5 µg/mL y una disolución de bloqueo que contenía 0.5 mg/mL de biotina. Los conjugados V-Phe-SWCNT(-HRP)-anti-TGF se prepararon con 10 µg/mL de la enzima peroxidasa y 2 µg/mL del anticuerpo de detección. Finalmente, la corriente amperométrica se registró, empleando hidroquinona como mediador redox, en presencia de peróxido de hidrógeno como sustrato enzimático, a un potencial de reducción de –0.3 V. Como se muestra en la Figura 5.90, la mejor relación entre la señal específica e inespecífica se obtuvo para una concentración de estreptavidina de 200 µg/mL, por lo que este fue el valor seleccionado para estudios posteriores.

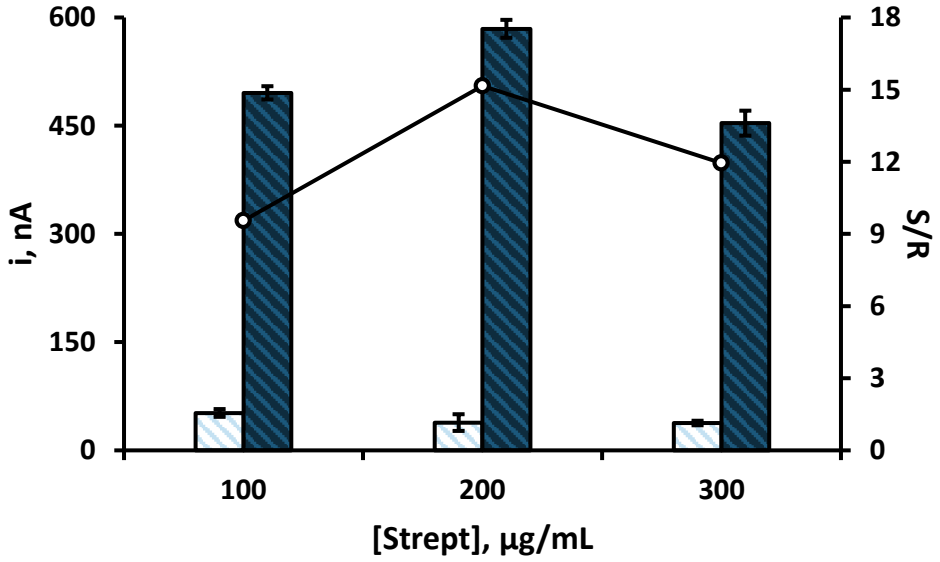

Figura 5.90. Efecto de la concentración de Strept sobre la respuesta del inmunosensor: Strept, 5 µL, 60 min; Biotin-anti-TGF, 7.5 µg/mL, 5 µL, 60 min; Biotin, 0.5 mg/mL, 5 µL, 30 min; TGF-β1, 0 (□) o 125 (■) pg/mL, 5 µL, 60 min; V-Phe-SWCNT(-HRP)-anti-TGF, 5 µL, 60 min

Influencia de la concentración de anticuerpo de captura biotinilado

Usando las condiciones experimentales descritas anteriormente, se optimizó también la concentración del anticuerpo de captura biotinilado Biotin-anti-TGF estudiando el intervalo comprendido entre 2.5 y 10 µg/mL. En la Figura 5.91 se muestran los registros de las señales amperométricas obtenidas con los

inmunosensores completos para las distintas concentraciones de anticuerpo de captura biotiniado, en ausencia y presencia de 125 pg/mL de TGF-β1. Como se observa, la señal debida a las adsorciones inespecíficas disminuye al aumentar la cantidad de anticuerpo inmovilizado sobre la superficie del electrodo. Asimismo, la señal específica aumenta a medida que lo hace la concentración de Biotin-anti-TGF hasta 7.5 µg/mL, estabilizándose para valores superiores.

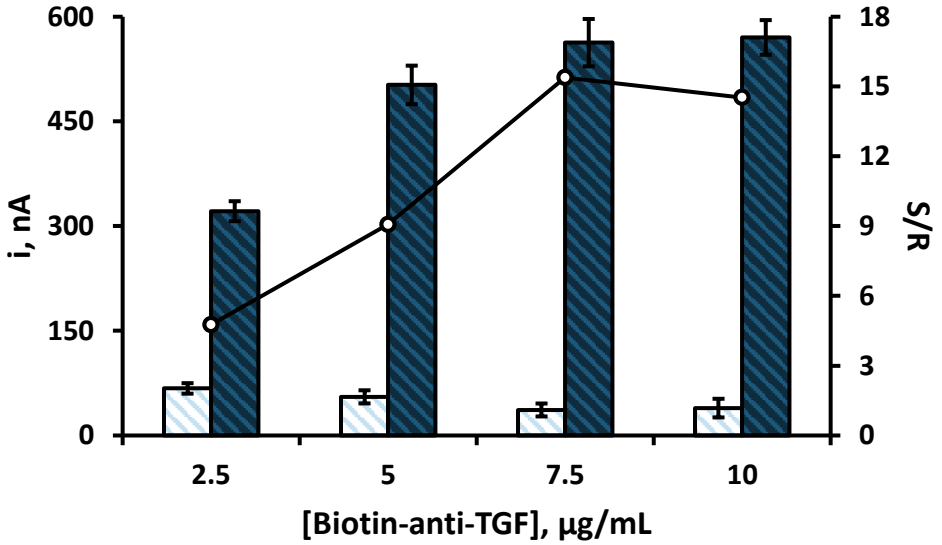

Figura 5.91. Efecto de la concentración de Biotin-anti-TGF sobre la respuesta del inmunosensor: Strept, 200 µg/mL, 5 µL, 60 min; Biotin-anti-TGF, 5 µL, 60 min; Biotin, 0.5 mg/mL, 5 µL, 30 min; TGF-β1, 0 (□) o 125 (■) pg/mL, 5 µL, 60 min; V-Phe-SWCNT(-HRP)-anti-TGF, 5 µL, 60 min

Influencia de la proporción de nanotubos de carbono funcionalizados con aminoviológeno en el conjugado V-Phe-SWCNT(-HRP)-anti-TGF

Como se ha comentado anteriormente, los nanotubos de carbono poseen numerosas ventajas debidas a su elevada conductividad y sus propiedades electrocatalíticas, lo que los hace muy atractivos para el desarrollo de inmunosensores electroquímicos. Sin embargo, su presencia puede originar una elevada corriente de fondo, por lo que la concentración del nanomaterial a emplear debe ser controlada cuidadosamente. En este caso fue necesario elegir la proporción adecuada de V-Phe-SWCNTs que se añade a la disolución que contiene el anticuerpo anti-TGF y la enzima peroxidasa. Se sabe que el uso de una concentración demasiado baja de

biomoléculas en relación a la cantidad del conjugado V-Phe-SWCNTs dejaría una gran cantidad de posiciones reactivas libres dando lugar a una corriente de fondo importante. Por el contrario, una elevada concentración de biomoléculas podría originar impedimento estérico, lo que dificultaría la reacción de reconocimiento antigénico por parte del anticuerpo de detección presente en el nanomaterial híbrido.

Como se describe en el *Apartado 4.5.4.1.2.* de la *Parte Experimental* y se muestra en la Figura 4.34, para obtener 100 µL del conjugado V-Phe-SWCNT(-HRP)-anti-TGF, se mezclan 50 µL de una disolución de EDC/NHSS con 50 µL de ácido tereftálico 4 mg/mL, 100 µL de una disolución de 40 µg/mL de HRP, 100 µL de una disolución de 4 µg/mL del anticuerpo (anti-TGF) y 50, 100 ó 200 µL de 0.5 mg/mL de V-Phe-SWCNTs en agua. Tras 3 horas incubación se centrifuga y el sólido se resuspende en 100 µL de disolución reguladora PBS de pH 7.4. De esta forma, se obtienen conjugados en los que la relación entre volumen de suspensión V-Phe-SWCNTs y el volumen final del conjugado es 1/2, 1/1 y 2/1.

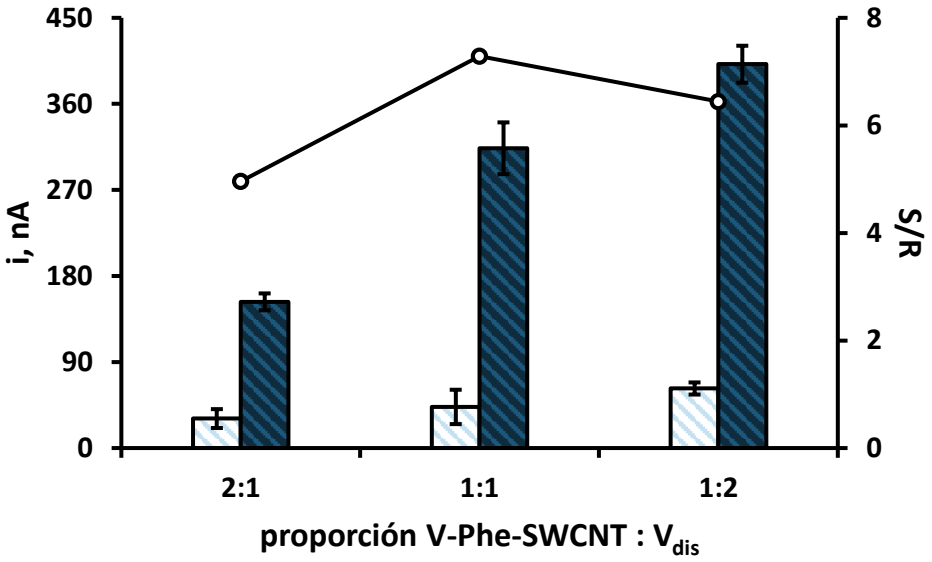

Figura 5.92. Efecto de la proporción de V-Phe-SWCNT frente al volumen de disolución sobre la respuesta del inmunosensor: Strept, 200 µg/mL, 5 µL, 60 min; Biotin-anti-TGF, 5 µg/mL, 5 µL, 60 min; Biotin, 0.5 mg/mL, 5 µL, 30 min; TGF-β1, 0 (□) o 125 (■) pg/mL, 5 µL, 60 min; V-Phe-SWCNT(-HRP)-anti-TGF, 5 µL, 60 min

En la Figura 5.92 se muestran los resultados obtenidos trabajando en estas condiciones. La señal específica aumenta a medida que lo hace el volumen de conjugado, lo que demuestra el mayor número de biomoléculas inmovilizadas. Sin

embargo, como era de esperar, también aumenta la señal inespecífica obtenida para inmunosensores preparados con dichos conjugados en ausencia de antígeno. Como puede apreciarse, la mayor relación de señales se obtiene cuando se emplea un volumen intermedio, 100 µL, de suspensión V-Phe-SWCNTs para preparar el conjugado (proporción 1:1).

Influencia de la concentración de enzima peroxidasa

Con el objetivo de implementar un protocolo más simple y rápido, la inmovilización de la enzima peroxidasa y el anticuerpo de detección sobre el material híbrido previamente sintetizado se realizó en una sola etapa, incubándolo en una disolución que contiene ambas biomoléculas. En estas condiciones se estudió la influencia de la concentración de peroxidasa en el material híbrido empleando disoluciones que contienen 2.5, 5, 10 y 20 µg/mL de HRP y una concentración constante de anticuerpo de detección anti-TGF de 2 µg/mL.

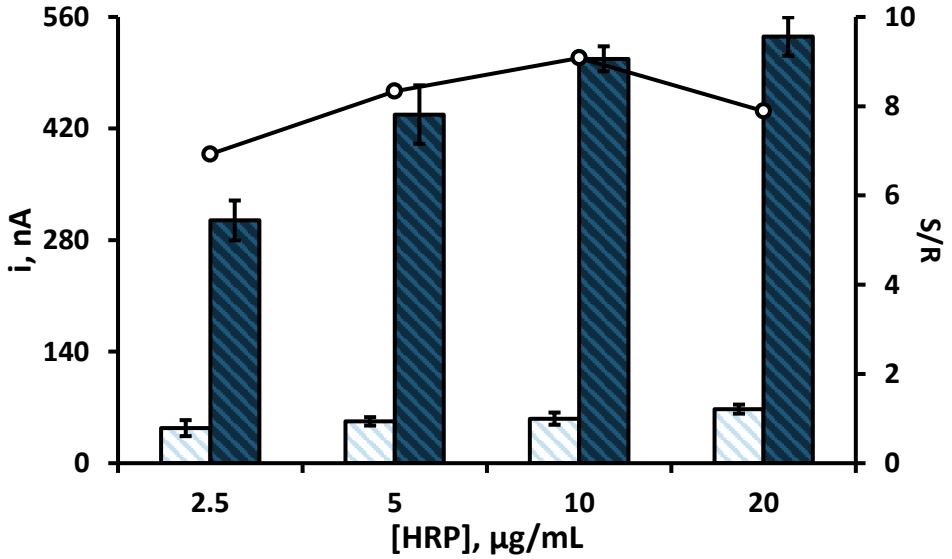

Figura 5.93. Efecto de la concentración de HRP sobre la respuesta del inmunosensor: Strept, 200 µg/mL, 5 µL, 60 min; Biotin-anti-TGF, 7.5 µg/mL, 5 µL, 60 min; Biotin, 0.5 mg/mL, 5 µL, 30 min; TGF-β1, 0 (□) o 125 (■) pg/mL, 5 µL, 60 min; V-Phe-SWCNT(-HRP)-anti-TGF, 5 µL, 60 min

Los resultados mostrados en la Figura 5.93 ponen de manifiesto que la intensidad de corriente medida para las respuestas específicas y no específicas aumentan con la concentración de enzima en todo el intervalo investigado,

obteniéndose la mayor relación entre las señales específica a inespecífica para 10 µg/mL.

Influencia de la concentración de anticuerpo de detección

En esta configuración, el anticuerpo de detección anti-TGF se inmoviliza covalentemente en el nanomaterial híbrido V-Phe-SWCNTs(-HRP). Para optimizar su carga, se estudió el efecto del aumento de la concentración de dicha biomolécula sobre la respuesta del inmunosensor en el intervalo de 1 a 3 µg/mL con los resultados que se muestran en la Figura 5.94. En ella se observa que la mejor relación de señales aparece para una concentración de 2 µg/mL.

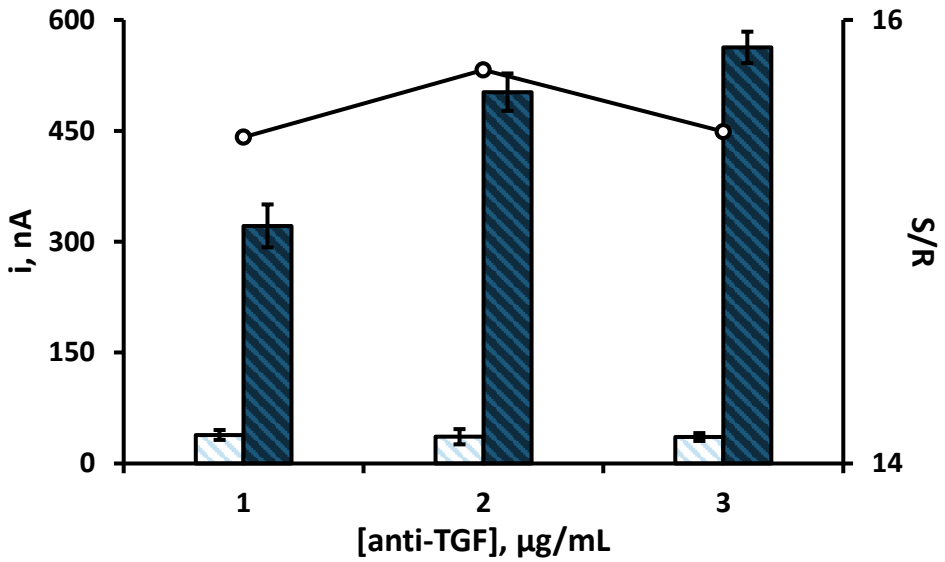

Figura 5.94. Efecto de la concentración de anti-TGF sobre la respuesta del inmunosensor: Strept, 200 µg/mL, 5 µL, 60 min; Biotin-anti-TGF, 7.5 µg/mL, 5 µL, 60 min; Biotin, 0.5 mg/mL, 5 µL, 30 min; TGF-β1, 0 (□) o 125 (■) pg/mL, 5 µL, 60 min; V-Phe-SWCNT(-HRP)-anti-TGF, 5 µL, 60 min

A modo de resumen, en la Tabla 5.16 se recogen las variables estudiadas, así como los intervalos evaluados y los valores seleccionados para cada una de ellas.

Tabla 5.16. Optimización de las variables experimentales implicadas en la construcción del inmunosensor V-Phe-SWCNT(-HRP)-anti-TGF-TGF-β1-Biotin-anti-TGF-Strept/SPCE

VARIABLE EXPERIMENTAL	INTERVALO EVALUADO	VALOR SELECCIONADO
[Strept], µg/mL	100 – 300	200
[Biotin-anti-TGF], µg/mL	2.5 – 10	7.5
V-Phe-SWCNTs, proporción	1:2 – 2:1	1:1
[HRP], µg/mL	2.5 – 20	10
[anti-TGF], µg/mL	1 – 3	2

5.4.1.4. Calibrado y características analíticas

En la Figura 5.95 se representa el calibrado obtenido con el inmunosensor desarrollado bajo las condiciones de trabajo previamente optimizadas. Las barras de error se calcularon, en cada caso, a partir de tres medidas realizadas con tres inmunosensores diferentes.

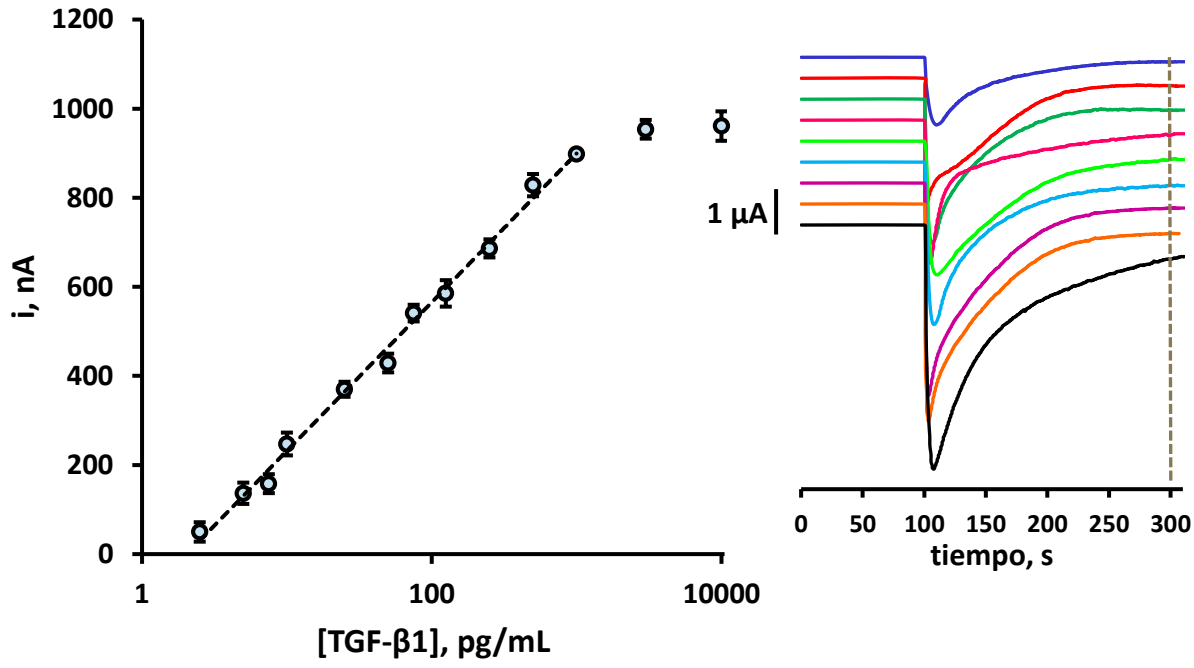

Figura 5.95. Calibrado para la determinación de TGF-β1 empleando el inmunosensor V-Phe-SWCNT(-HRP)-anti-TGF-TGF-β1-Biotin-anti-TGF-Strept/SPCE

Como puede observarse, existe una relación lineal entre la intensidad de corriente y el logaritmo de la concentración de TGF-β1 entre 2.5 y 1000 pg/mL que se

ajusta a la ecuación i, nA = (332 ± 9) log ([TGF-β1], pg/mL) – (99 ± 18) (R^2 = 0.996). Este intervalo, que cubre casi tres órdenes de magnitud, es adecuado para la determinación de esta citoquina en muestras de saliva, teniendo en cuenta que la concentración esperada se encuentra en torno a las pocas decenas de pg/mL [Yousefzadeh, 2006; Brand, 2014]. El límite de detección, de 0.95 pg/mL, se calculó de acuerdo con el criterio $\overline{x} + 3 \cdot s$, donde *s* es la desviación estándar, expresada en unidades de concentración.

Estas características analíticas mejoran notablemente las obtenidas con otros inmunosensores descritos en trabajos anteriores. Así, por ejemplo, la concentración más baja del calibrado, 2.5 pg/mL, es seis veces menor que la obtenida empleando inmunosensores basados en el empleo de partículas magnéticas carboxílicas [Sánchez-Tirado, 2017]. Además, el inmunosensor descrito en este trabajo proporciona un intervalo de linealidad más amplio, casi un orden de magnitud mayor, con una pendiente 60 veces mayor y un límite de detección ligeramente menor que el inmunosensor descrito con anterioridad, basado en el empleo de una reacción tipo *"click"* como estrategia de inmovilización del anticuerpo de captura [Sánchez-Tirado, 2016]. Además, el inmunosensor desarrollado exhibe un límite de detección notablemente más bajo que otros reportados en la bibliografía, como los proporcionados por un aptasensor, 1 ng/mL, [Matharu, 2014] y un inmunosensor impedimétrico, 0.570 ng/mL [Yao, 2016].

Por otro lado, las características analíticas del inmunosensor propuesto mejoran también las de los kits ELISA comerciales. Por ejemplo, el DuoSet® ELISA Development System (DY240–05) de R&D Systems proporciona una respuesta de absorbancia directamente proporcional al log[TGF-β1] entre 31 y 1000 pg/mL y requiere un tiempo de ensayo de 5 horas y 20 minutos, notablemente más largo que el necesario para preparar el inmunosensor electroquímico preparado en este trabajo (2 horas y 30 minutos), contando el tiempo de ensayo, en ambos casos, a partir de la inmovilización del anticuerpo de captura.

5.4.1.5. Estudio de selectividad

La selectividad de la configuración desarrollada se evaluó comparando las respuestas amperométricas obtenidas en ausencia y en presencia de 50 pg/mL de TGF-β1 y, a su vez, en ausencia y en presencia de cada uno de los compuestos ensayados como interferentes: ácido ascórbico (AA), adiponectina (APN), albúmina de suero bovino (BSA), cortisol (CL), inmunoglobulina G humana (hIgG), interleucina 1 beta (IL-1β), interleucina 6 (IL-6), interleucina 8 (IL-8), factor de necrosis tumoral alfa (TNF-α) y ácido úrico (UA) (Figura 5.96).

Los resultados obtenidos demostraron que ninguna de estas proteínas a los niveles de concentración ensayados supone una interferencia significativa en la determinación de TGF-β1 empleando el inmunosensor, demostrando así la alta selectividad de la configuración desarrollada.

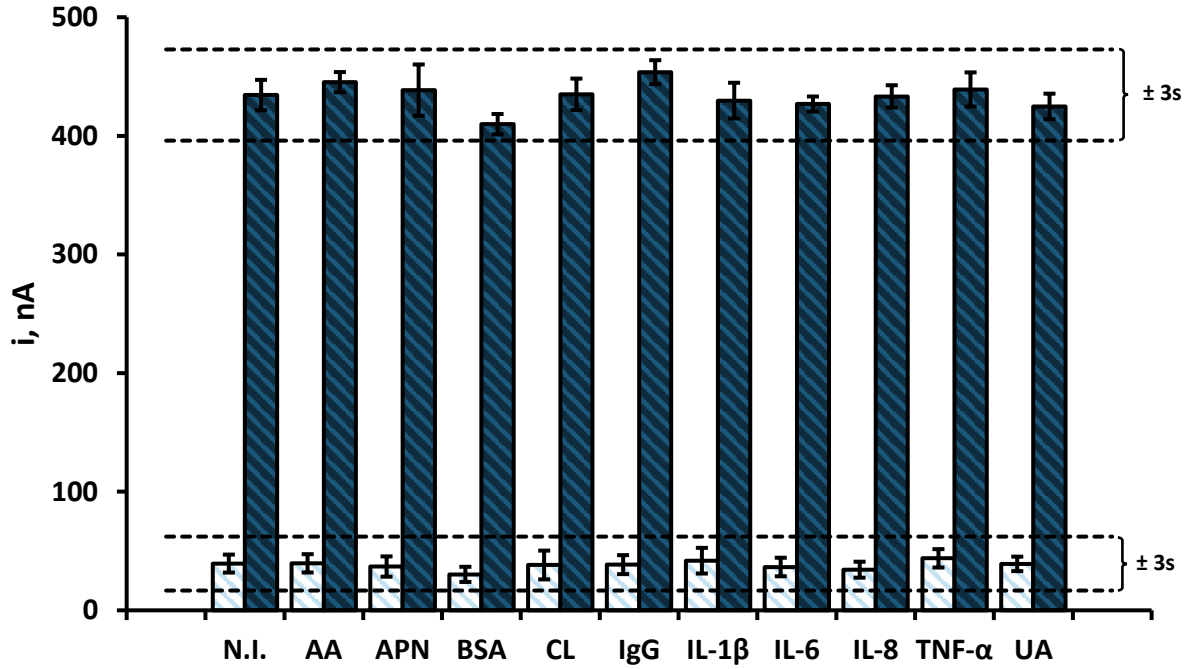

Figura 5.96. Selectividad del inmunosensor V-Phe-SWCNT(-HRP)-anti-TGF-TGF-β1-Biotin-anti-TGF-Strept/SPCE evaluando la respuesta del mismo con 0 (□ ó 50 (■) pg/mL de TGF-β1 frente a 370 µg/mL de AA, 5 pg/mL de APN, 50 ng/mL de BSA, 12 ng/mL de CL, 50 ng/mL de hIgG, 50 pg/mL de IL-1β, 50 pg/mL de IL-6, 250 pg/mL de IL-8, 10 pg/mL de TNF-α y 50 µg/mL de UA

5.4.1.6. Estudios de reproducibilidad y estabilidad

La repetibilidad de las medidas se evaluó midiendo la respuesta amperométrica de cinco inmunosensores diferentes fabricados el mismo día, en ausencia y en presencia de 125 pg/mL de TGF-β1. Los valores de RSD obtenidos fueron del 3.4 y 3.1 %, respectivamente. Del mismo modo, la reproducibilidad de las medidas se evaluó también empleando cinco inmunosensores preparados en distintos días, obteniendo valores de RSD del 6.5 y 7.2 %, en ausencia y en presencia de la misma concentración de TGF-β1, respectivamente. Estos resultados demuestran la buena precisión de las medidas y ponen de manifiesto que el procedimiento de fabricación del inmunosensor es fiable y reproducible.

También se estudió la estabilidad de los inmunoconjugados Biotin-anti-TGF-Strept/SPCE y V-Phe-SWCNT(-HRP)-anti-TGF.

En el primer caso, se prepararon en el mismo día distintos electrodos modificados con el anticuerpo de captura que, tras el bloqueo de la superficie del electrodo de trabajo con biotina, se almacenaron en condiciones de humedad a 8°C, depositando sobre ellos un volumen de 20 µL de disolución reguladora PBS. Después, de forma sucesiva, cada día de trabajo se prepararon tres inmunosensores a partir de estos electrodos previamente modificados con el inmunoconjugado y se realizaron las medidas de la respuesta amperométrica en presencia de 125 pg/mL de TGF-β1.

En la Figura 5.97 se ha representado un gráfico de control en el que los márgenes establecidos corresponden a ± 3 veces la desviación estándar de las medidas realizadas el primer día de trabajo. Como puede observarse, la media de las tres medidas realizadas cada día se encuentra dentro del intervalo establecido el primer día durante, al menos, 30 días (no se estudiaron tiempos superiores), poniéndose de manifiesto la excelente estabilidad de almacenamiento de los inmunoconjugados Biotin-anti-TGF-Strept/SPCE cuando se almacenan en condiciones de humedad a 8°C.

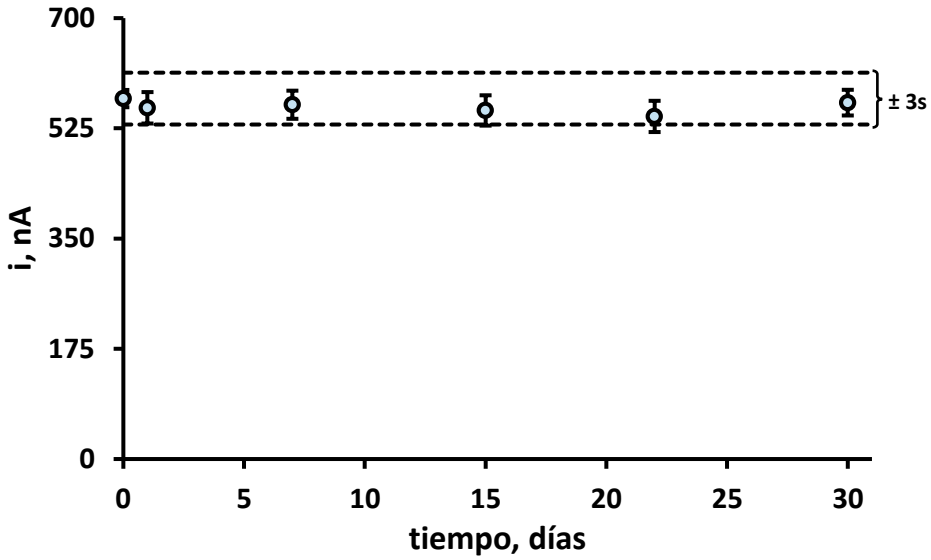

Figura 5.97. Gráfico de control para la evaluación de la estabilidad de almacenamiento del conjugado Biotin-anti-TGF-Strept/SPCE

En el caso del inmunoconjugado V-Phe-SWCNT(-HRP)-anti-TGF, se preparó, en el mismo día, un volumen mayor de la suspensión de material híbrido funcionalizado con las biomoléculas y se almacenaron distintas alícuotas en disolución reguladora PBS de pH 7.4 a 8°C. Posteriormente, de forma sucesiva, cada día de trabajo se prepararon tres inmunosensores utilizando el material híbrido funcionalizado con las biomoléculas previamente preparado y se realizaron las medidas de la respuesta amperométrica en presencia de 125 pg/mL de TGF-β1.

En la Figura 5.98 se ha representado un gráfico de control en el que, como en estudios anteriores, los márgenes establecidos corresponden a ± 3 veces la desviación estándar de las medidas realizadas el primer día de trabajo. Puede observarse que la media de las tres medidas realizadas cada día se encuentra dentro del intervalo establecido el primer día durante, al menos, 14 días (no se estudiaron tiempos superiores), poniéndose de manifiesto una adecuada estabilidad de almacenamiento de los inmunoconjugados V-Phe-SWCNT(-HRP)-anti-TGF cuando se almacenan en las condiciones indicadas.

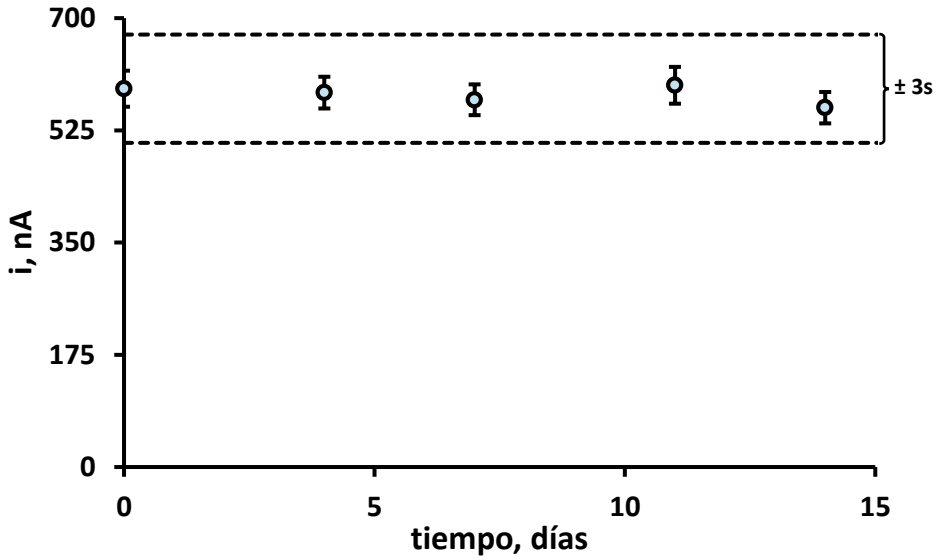

Figura 5.98. Gráfico de control para la evaluación de la estabilidad de almacenamiento del conjugado V-Phe-SWCNT(-HRP)-anti-TGF

5.4.1.7. Aplicación a la determinación de factor de crecimiento transformante beta 1 en saliva

La utilidad del inmunosensor se demostró mediante su aplicación a la determinación de TGF-β1 en muestras de saliva de cuatro individuos sanos, dos fumadores y dos no fumadores, siguiendo el procedimiento descrito en el *Apartado 4.6.7.* de la *Parte Experimental*.

En primer lugar, la posible existencia de efecto matriz se examinó por comparación de las pendientes de las rectas de calibrado construidas mediante el enriquecimiento de las muestras de saliva con concentraciones sucesivas del estándar de TGF-β1 con la obtenida empleando disoluciones estándar del analito. La aplicación del test *t* de Student proporcionó unos valores de t_{exp} de 0.969, 0.615, 0.254 y 0.221, inferiores al t_{tab} (2.179) a un nivel de significación de 0.05.

Teniendo esto en cuenta, la determinación de TGF-β1 se llevó a cabo por interpolación de la intensidad de corriente proporcionada por las muestras en el calibrado de disoluciones estándar. Posteriormente, los resultados obtenidos se validaron comparándolos con los proporcionados por el kit ELISA DuoSet® ELISA

Development System (DY240–05) de R&D Systems, siguiendo el procedimiento de ensayo especificado por la casa comercial. Los resultados obtenidos por ambos métodos se resumen en la Tabla 5.17.

Tabla 5.17. Determinación de TGF-β1 en muestras de saliva empleando el inmunosensor V-Phe-SWCNT(-HRP)-anti-TGF-TGF-β1-Biotin-anti-TGF-Strept/SPCE

MUESTRA	INMUNOSENSOR ng/mL (*n* = 5)*	ELISA ng/mL (*n* = 4)*
fumador 1	27.6 ± 0.2	27.3 ± 0.2
fumador 2	26.4 ± 0.5	26.3 ± 0.1
no fumador 1	21.2 ± 0.6	21.2 ± 0.1
no fumador 2	22.8 ± 0.3	22.7 ± 0.5

* valor medio ± t·s/√n

5.4.1.8. Conclusiones

En este trabajo se ha sintetizado un nanomaterial híbrido (V-Phe-SWCNT) para, una vez incorporada la enzima peroxidasa y el anticuerpo de detección anti-TGF, obtener el conjugado V-Phe-SWCNT(-HRP)-anti-TGF, para ser empleado como etiqueta portadora para la amplificación de la señal. La implementación de un inmunoensayo tipo sándwich unida al empleo de dicho material permitió obtener unas mejores características analíticas, en términos de intervalo dinámico lineal, sensibilidad, estabilidad y límite de detección, que las de otros inmunosensores descritos previamente y las de los inmunoensayos tipo ELISA comerciales.

Además, el inmunosensor desarrollado demostró su utilidad analítica por aplicación a la determinación de TGF-β1 en cuatro muestras de saliva de individuos voluntarios sanos, sin necesidad de tratamiento previo excepto la dilución.

5.4.2. Inmunosensor para la determinación de fetuina A humana

La fetuina A humana (HFA), también llamada glicoproteína α2-Heremans-Schmid, se considera un biomarcador de obesidad, resistencia a la insulina y diabetes tipo 2. Asimismo, se han observado concentraciones séricas altas de esa cistatina en individuos con hígado graso o inflamado [Yilmaz, 2010], aumentando el riesgo de que padezcan diabetes tipo 2 [Dabrowska, 2015]. Por otro lado, la síntesis de la HFA está negativamente regulada durante la lesión y la inflamación [Choi, 2016], actuando esta proteína como un potente inhibidor de la precipitación del fosfato de calcio y el proceso de calcificación. Existe además una estrecha relación entre la HFA y la enfermedad periodontal que hace que la determinación de esta cistatina en saliva sea especialmente relevante.

En este trabajo, la preparación del inmunosensor para la determinación de HFA implica los siguientes pasos: a) preparación de conjugados basados en nanotubos de carbono magnéticos mMWCNTs(-HRP)-anti-HFA mediante la unión covalente de la enzima y el anticuerpo a material híbrido MWCNTs/Fe_3O_4, b) construcción de la plataforma sensora mediante la inmovilización del anticuerpo biotinilado (Biotin-anti-TGF) sobre electrodos serigrafiados funcionalizados mediante grafting con *p*-ABA y modificados con estreptavidina y c) implementación del inmunoensayo tipo sándwich para HFA mediante el uso de conjugados mMWCNTs(-HRP)-anti-HFA como etiquetas portadoras para amplificación de la señal.

5.4.2.1. Configuración del inmunosensor

El esquema del funcionamiento del inmunosensor desarrollado para la determinación de HFA se representó en la Figura 4.38 de la *Parte Experimental*. Como ya se ha comentado, el inmunosensor emplea electrodos serigrafiados de carbono modificados mediante grafting con *p*-ABA, si bien en este caso, la reacción de funcionalización de la superficie electródica se realizó en etanol absoluto y en

presencia de $LiClO_4$, de acuerdo con un proceso electroquímico de oxidación que genera grupos carboxifenilamino [Liu, 2000] con ligeras modificaciones. Tras la activación de los grupos carboxílicos con EDC y NHSS, se inmoviliza la estreptavidina y se incorpora el anticuerpo de captura biotinilado (Biotin-anti-HFA), se bloquean las posiciones libres del electrodo y se incorpora el antígeno y el conjugado de nanomaterial magnético obteniendo así el inmunosensor mMWCNTs(-HRP)-anti-HFA-HFA-anti-HFA-Biotin-Strept-Phe-SPCE. La señal analítica se obtiene empleando hidroquinona como mediador redox y peróxido de hidrógeno como sustrato enzimático, registrándose la señal amperométrica a un potencial de reducción de –200 mV (Figura 5.99).

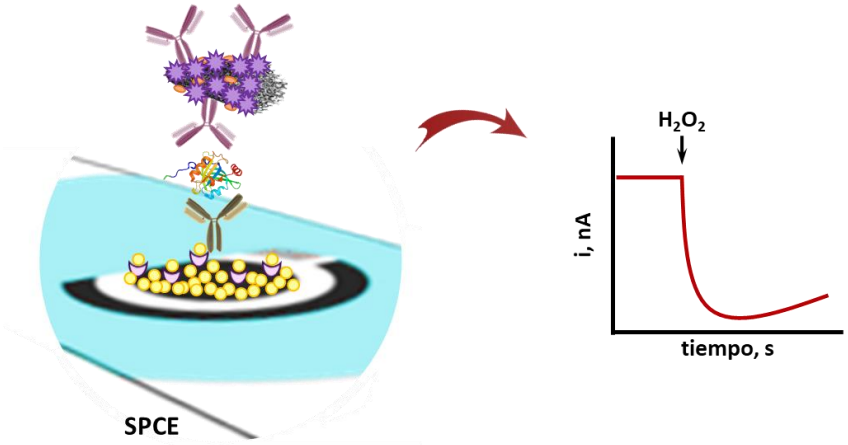

Figura 5.99. Esquema del funcionamiento del inmunosensor para la determinación de HFA

5.4.2.2. Caracterización del nanomaterial

Los nanotubos de carbono de pared múltiple magnéticos (mMWCNTs) se caracterizaron mediante diferentes técnicas: microscopia electrónica de barrido (SEM), microscopia electrónica de transmisión (TEM), difracción de rayos X (XRD) y espectrometría de dispersion de energía de rayos X (EDS). En la Figura 5.100 se muestran las micrografías obtenidas para los nanotubos de carbono sin modificar y modificados mediante un tratamiento en medio acuoso con cloruros férrico y ferroso, donde se puede apreciar la presencia de partículas de Fe_3O_4 unidas a la superficie de los nanotubos de carbono en este último caso.

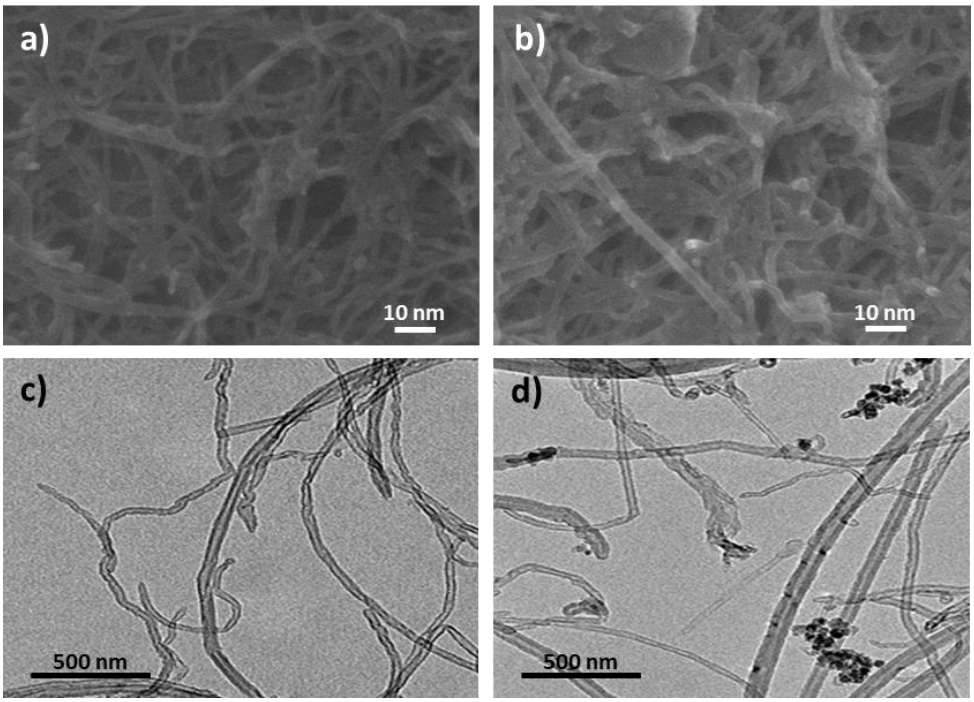

Figura 5.100. Microscopia electrónica de barrido (SEM) de: a) MWCNTs y b) mMWCNTs y microscopia electrónica de transmisión (TEM) de: c) MWCNTs y d) mMWCNTs

Los espectros de difracción de rayos X de los MWCNTs y mMWCNTs se muestran en la Figura 5.101.

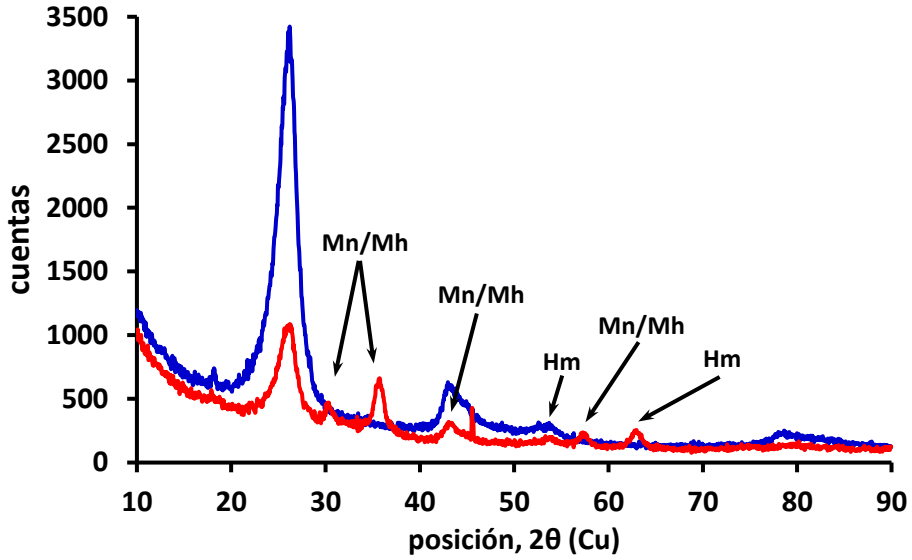

Figura 5.101. Espectro de difracción de rayos X (XRD) de: HOOC-MWCNTs (–) y HOOC-mMWCNTs (–)

Como se puede observar, los picos correspondientes a la estructura de los MWCNTs (–), que también aparecen en el espectro de los mMWCNTs (–), junto con otros picos que pueden ser atribuidos a diferentes tipos comunes de óxidos de hierro

[Gong, 2009; Kim, 2010]. Así, los picos que aparecen a un valor de 2θ de 30.2, 35.7, 43.3 y 57.2° pueden asignarse a magnetita (Mn, Fe_3O_4) o a magnemita (Mh, γ-Fe_2O_3). Asimismo, los picos que aparecen a un valor de 2θ de 53.9 y 62.8° pueden atribuirse a la presencia de óxidos de hierro no magnéticos (Hm, α-Fe_2O_3).

En la Figura 5.102. se muestra el análisis mediante espectrometría de energía dispersiva de rayos X (EDS), donde queda demostrada la presencia de hierro, oxígeno y carbono en los mMWCNTs.

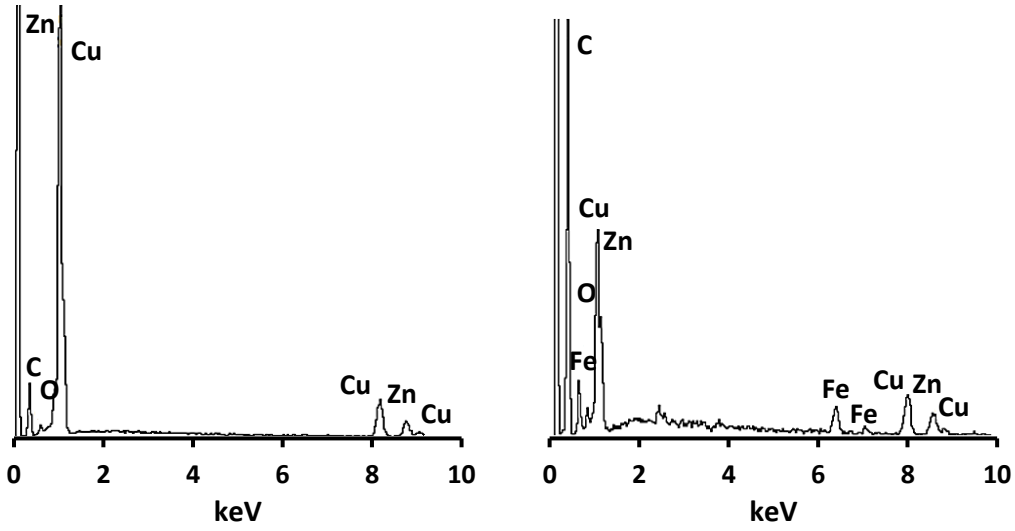

Figura 5.102. Análisis de composición por fluorescencia de rayos X por energía dispersiva (EDS)

Finalmente, en la Figura 5.103 se muestra la curva de histéresis de magnetización a temperatura ambiente para los mMWCNTs, que se obtuvo empleando un magnetómetro de muestra vibrante. Esta curva se comparó con la obtenida para los MWCNTs y las partículas de Fe_3O_4 puras, obtenidas en las mismas condiciones de reacción.

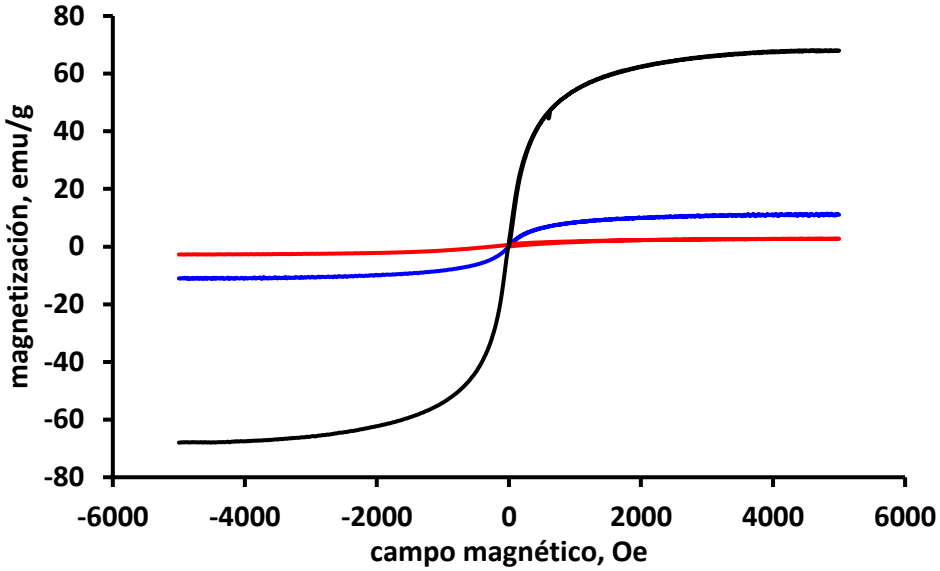

Figura 5.103. Curva de magnetización de: a) Fe_3O_4 (–), b) HOOC-MWCNTs (–) y c) HOOC-mMWCNTs (–)

Los resultados obtenidos demostraron el comportamiento superparamagnético de los HOOC-mMWCNTs, con una magnetización de saturación de 9.89 emu/g, que, como se esperaba, es significativamente menor que la obtenida para las partículas de Fe_3O_4 (62.12 emu/g) debido a la presencia de nanotubos de carbono en el material [Gan, 2010; Liu,2014].

Finalmente, como se muestra en la Figura 5.104, al aplicar un campo magnético externo con ayuda de un imán de neodimio, los nanotubos de carbono carboxilados se mantienen homogéneamente dispersos, mientras que los modificados con partículas de Fe_3O_4 tienden a agregarse en torno al imán, debido a la atracción magnética.

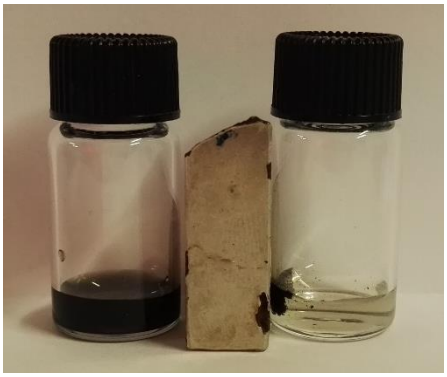

Figura 5.104. Fotografía que muestra a la izquierda del imán de neodimio una suspensión de 1 mg/mL de HOOC-MWCNTs y a la derecha otra de 1 mg/mL de HOOC-mMWCNTs

5.4.2.3. Optimización de las variables experimentales

La puesta a punto del inmunosensor mMWCNT(-HRP)-anti-HFA-HFA-Biotin-anti-HFA-Strept/SPCE requiere una cuidadosa selección de las variables experimentales implicadas en su preparación y funcionamiento. A continuación, se describen los resultados obtenidos en los estudios correspondientes.

Influencia de la concentración de estreptavidina

La estreptavidina inmovilizada sobre la superficie del electrodo es la reponsable de la unión de afinidad con el anticuerpo de captura biotinilado. Esta variable fue optimizada preparando diferentes inmunosensores por incubación de 5 µL de estreptavidina en un intervalo de concentraciones entre 200 y 800 µg/mL en disolución reguladora MES 25 mM de pH 5.0 durante 60 minutos sobre el electrodo HOOC-Phe-SPCE previamente activado con el sistema EDC /NHSS (Figura 5.105).

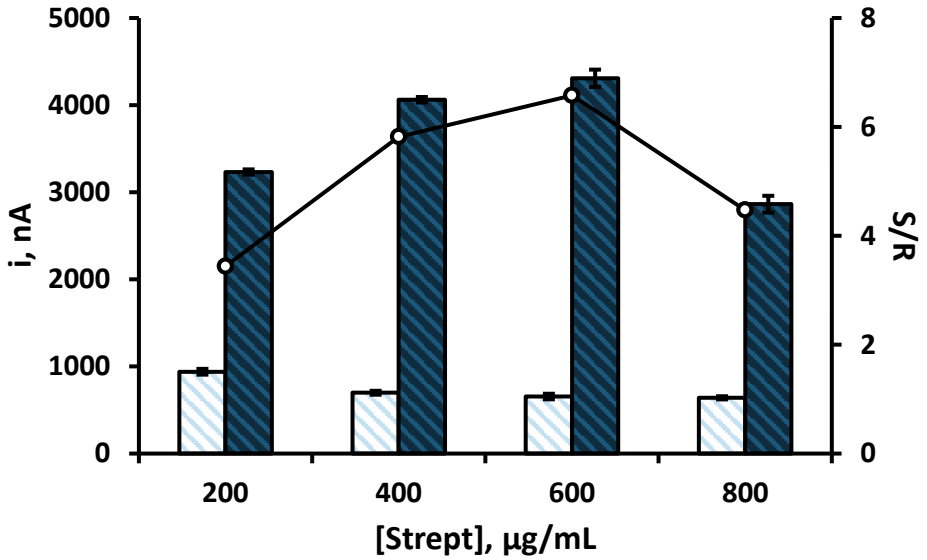

Figura 5.105. Efecto de la concentración de Strept sobre la respuesta del inmunosensor: Strept, 5 µL, 60 min; Biotin-anti-HFA, 7 µg/mL, 5 µL, 60 min; Biotin, 0.5 mg/mL, 5 µL, 30 min; HFA, 0 (□) o 250 (■) pg/mL, 5 µL, 60 min; mMWCNT(-HRP)-anti-HFA, 5 µL, 60 min

Como puede observarse, en presencia de 250 pg/mL de HFA, al aumentar la concentración de estreptavidina lo hace la señal de corriente hasta 600 µg/mL de estreptavidina, disminuyendo para concentraciones superiores, probablemente debido a fenómenos de impedimento estérico que dificultan la inmovilización

posterior del anticuerpo de captura biotinilado o la posterior inmovilización del antígeno y/o del conjugado que contiene el anticuerpo de detección. Asimismo, en ausencia de HFA, la señal debida a las adsorciones inespecíficas disminuye ligeramente al aumentar la concentración de estreptavidina, lo que puede atribuirse a un mayor bloqueo de la superficie electródica. De este modo, la máxima relación entre las señales específica e inespecífica se obtiene para una concentración de estreptavidina de 600 µg/mL.

Influencia de la concentración de anticuerpo de captura biotinilado

Esta variable fue optimizada inmovilizando 5 µL de disoluciones de distinta concentración de Biotin-anti-HFA en el intervalo de 5 a 12 µg/mL, durante una hora sobre los electrodos. Como es habitual, se llevaron a cabo medidas comparativas en ausencia y en presencia de 250 pg/mL de HFA (Figura 5.106).

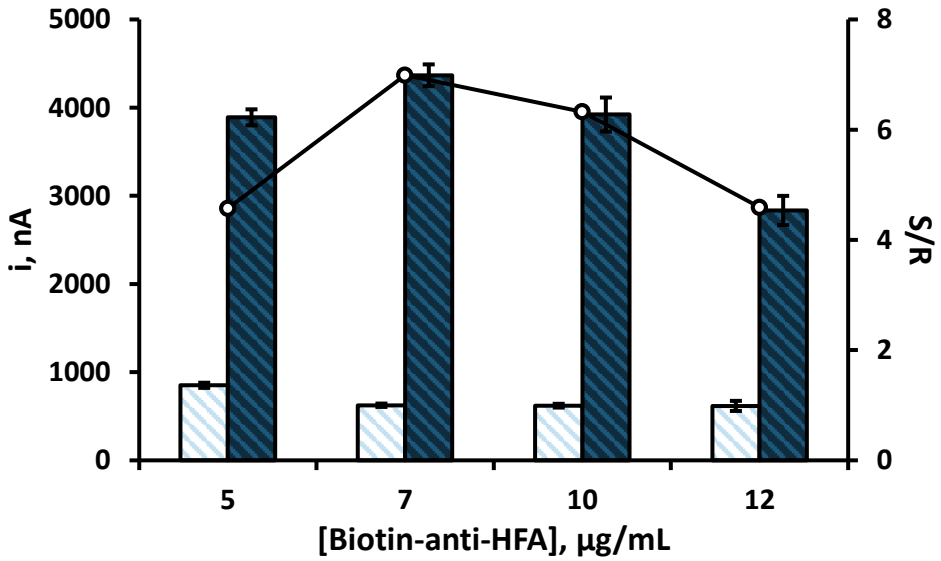

Figura 5.106. Efecto de la concentración de Biotin-anti-HFA sobre la respuesta del inmunosensor: Strept, 600 µg/mL, 5 µL, 60 min; Biotin-anti-HFA, 60 min; Biotin, 0.5 mg/mL, 5 µL, 30 min; HFA, 0 (□) o 250 (■) pg/mL, 5 µL, 60 min; mMWCNT(-HRP)-anti-HFA, 5 µL, 60 min

La concentración de Biotin-anti-HFA que proporciona una mayor relación de señales específica e inespecífica es de 7 µg/mL. Concentraciones superiores de anticuerpo de captura dieron lugar a una disminución de la respuesta en presencia de HFA, probablemente debido a la presencia de una concentración excesiva de anticuerpo.

Influencia de la etapa de bloqueo

Con el objetivo de minimizar al máximo la señal correspondiente a las adsorciones inespecíficas se realizaron diversos estudios para optimizar el bloqueo de la superficie del electrodo. Así, aunque anteriormente se había utilizado una concentración de 0.5 mg/mL de biotina como agente bloqueante, para dicha optimización se realizaron ensayos empleando distintas concentraciones de biotina, así como añadiendo un 1% de BSA a la disolución de biotina inicial. Los resultados mostrados en la Figura 5.107, revelan un bloqueo eficiente empleando 1.5 mg/mL de biotina durante 30 minutos.

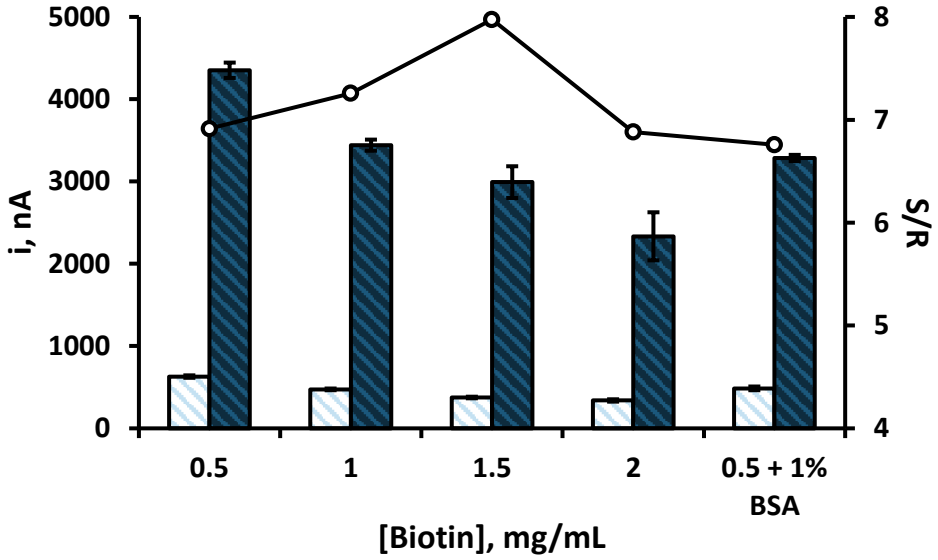

Figura 5.107. Efecto del agente bloqueante sobre la respuesta del inmunosensor: Strept, 600 µg/mL, 5 µL, 60 min; Biotin-anti-HFA, 7 µg/mL, 60 min; agente bloqueante, 5 µL, 30 min; HFA, 0 (□) o 250 (■) pg/mL, 5 µL, 60 min; mMWCNT(-HRP)-anti-HFA, 5 µL, 60 min

Puede observarse también que la adición de BSA a la disolución inicial de biotina da lugar a peores resultados, produciendo una disminución de la señal específica respecto a la obtenida añadiendo la misma concentración (0.5 mg/mL) de biotina únicamente al electrodo, mientras que en ausencia de antígeno las señales son muy similares.

Influencia de la concentración de enzima peroxidasa

Para optimizar la concentración de enzima peroxidasa empleada en la preparación del inmunoconjugado mMWCNT(-HRP)-anti-HFA, se estudió su efecto sobre la respuesta del inmunosensor en el intervalo de 1 a 2.5 mg/mL. Los resultados obtenidos en ausencia y en presencia de HFA, recogidos en la Figura 5.108, permiten seleccionar una concentración de 1 mg/mL para estudios posteriores.

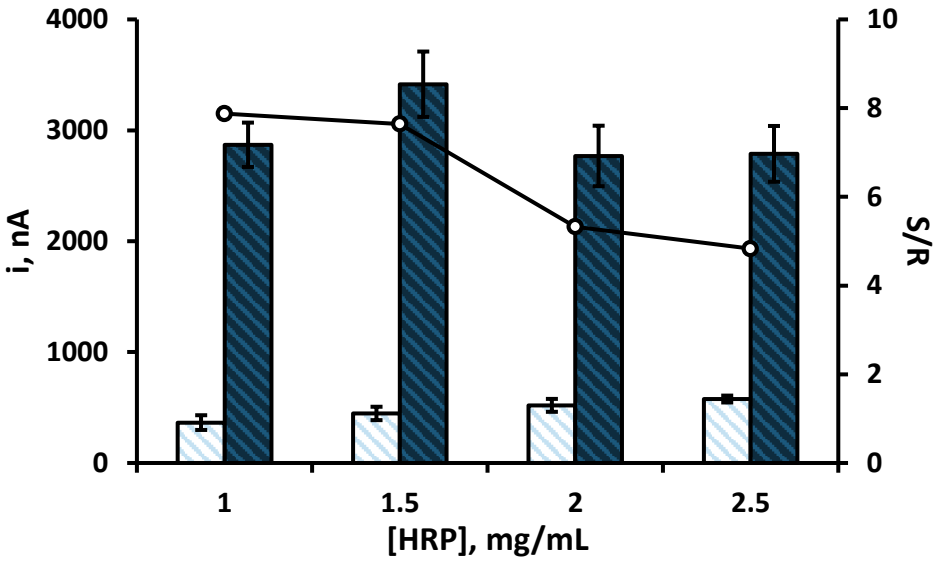

Figura 5.108. Efecto de la concentración de HRP sobre la respuesta del inmunosensor: Strept, 600 µg/mL, 5 µL, 60 min; Biotin-anti-HFA, 7 µg/mL, 60 min; biotin, 5 µL, 30 min; HFA, 0 (□) o 250 (■) pg/mL, 5 µL, 60 min; mMWCNT(-HRP)-anti-HFA, 5 µL, 60 min

Influencia de la concentración de anticuerpo de detección

Para elegir la concentración de anti-HFA empleada en la preparación del conjugado mMWCNTs(-HRP)-anti-HFA se prepararon inmunosensores empleando distintos inmunoconjugados obtenidos a partir de diferentes concentraciones de anti-HFA, comprendidas entre 2.5 y 10 µg/mL, y una concentración de HRP de 1 mg/mL en todos los casos (Figura 5.109).

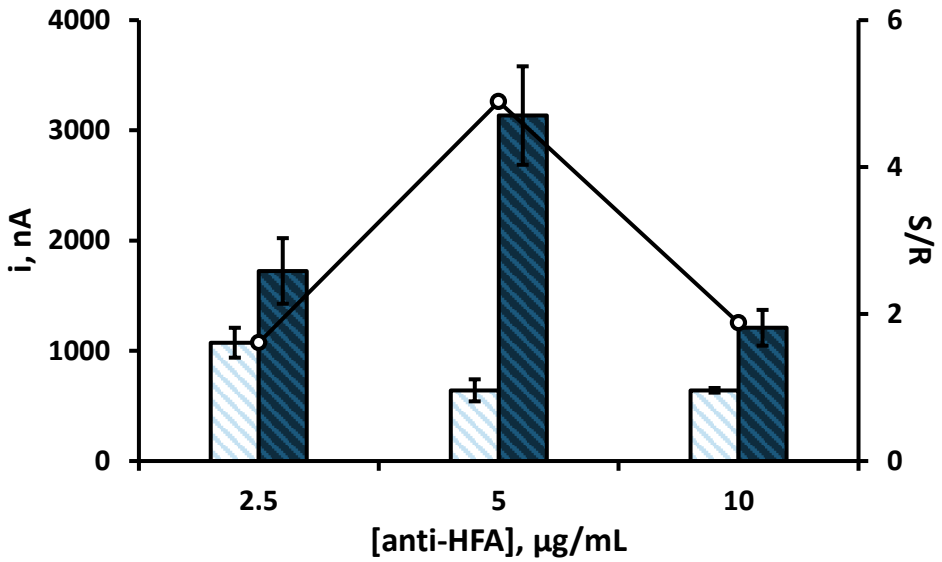

Figura 5.109. Efecto de la concentración de anti-HFA sobre la respuesta del inmunosensor: Strept, 600 µg/mL, 5 µL, 60 min; Biotin-anti-HFA, 7 µg/mL, 60 min; biotin, 5 µL, 30 min; HFA, 0 (□) o 250 (■) pg/mL, 5 µL, 60 min; mMWCNT(-HRP)-anti-HFA, 5 µL, 60 min

A la vista de los resultados obtenidos, se eligió una concentración de anti-HFA de 5 µg/mL, ya que proporciona una mejor relación de señales obtenidas en presencia y ausencia de HFA.

En la Tabla 5.18 se recogen, a modo de resumen, las variables estudiadas, así como los intervalos evaluados y los valores seleccionados en cada caso para estudios posteriores.

Tabla 5.18. Optimización de las variables experimentales implicadas en la construcción del inmunosensor mMWCNT(-HRP)-anti-HFA-HFA-Biotin-anti-HFA-Strept/SPCE

VARIABLE EXPERIMENTAL	INTERVALO EVALUADO	VALOR SELECCIONADO
[Strept], µg/mL	200 – 800	600
[Biotin-anti-TGF], µg/mL	5 – 12	7
agente bloqueante	biotina (0.5 – 2 mg/mL) 0.5 mg/mL biotina + 1% BSA	1.5 mg/mL biotina
conjugado enzimático	HRP-IgG, mMWCNT(-HRP)-anti-HFA	mMWCNT(-HRP)-anti-HFA
[anti-TGF], µg/mL	2.5 – 10	5
[HRP], µg/mL	1 – 2.5	1

5.4.2.4. Caracterización de la superficie electródica

Todas las etapas involucradas en la preparación del inmunosensor se han monitorizado empleando espectroscopia de impedancia electroquímica (EIS) y voltamperometría cíclica (CV) utilizando una disolución de $Fe(CN)_6^{3-/4-}$ 2 mM como par redox en disolución reguladora PBS de pH 7.4. La Figura 5.110a muestra cómo tras la modificación del electrodo serigrafiado de carbono con *p*-ABA la resistencia a la transferencia de carga aumenta de 376 a 1885 Ω. Esto es debido, como ya se ha señalado anteriormente, a la repulsión electrostática entre los grupos carboxílicos presentes en la superficie electródica, que están disociados al pH de trabajo, y la sonda redox también con carga negativa. Después de la activación de los grupos carboxílicos y de la inmovilización de la estreptavidina, el valor de R_{ct} disminuyó drásticamente hasta 957 Ω, probablemente debido a la neutralización parcial de la carga negativa en la superficie electródica. Como se esperaba, se observaron aumentos sucesivos en la resistencia después de la incubación en la disolución del anticuerpo biotinilado (R_{ct} = 1513 Ω) y tras la etapa de bloqueo con biotina (R_{ct} = 1711 Ω) (curvas 4 y 5) lo que se atribuye, por un lado, al efecto de estas proteínas bloqueando la transferencia electrónica y, por otro, a la repulsión electrostática entre la biotina (que está disociada al pH de trabajo) y la sonda redox aniónica en la solución, también carga negativamente. Sorprendentemente, la adición del antígeno HFA provocó una disminución en la resistencia a la transferencia de carga (R_{ct} = 1497 Ω), lo que se explica si se tiene en cuenta que la adición del antígeno compensa parcialmente la carga negativa de la biotina en la superficie del electrodo, siendo el gráfico de Nyquist similar al obtenido antes de la etapa de bloqueo. Finalmente, el diámetro del semicírculo decrece (R_{ct} = 1184 Ω) al incorporar el material inmunoconjugado mMWCNT(-HRP)-anti-HFA, debido a la presencia de nanotubos de carbono, que facilitan la transferencia electrónica en la interfase electrodo-disolución.

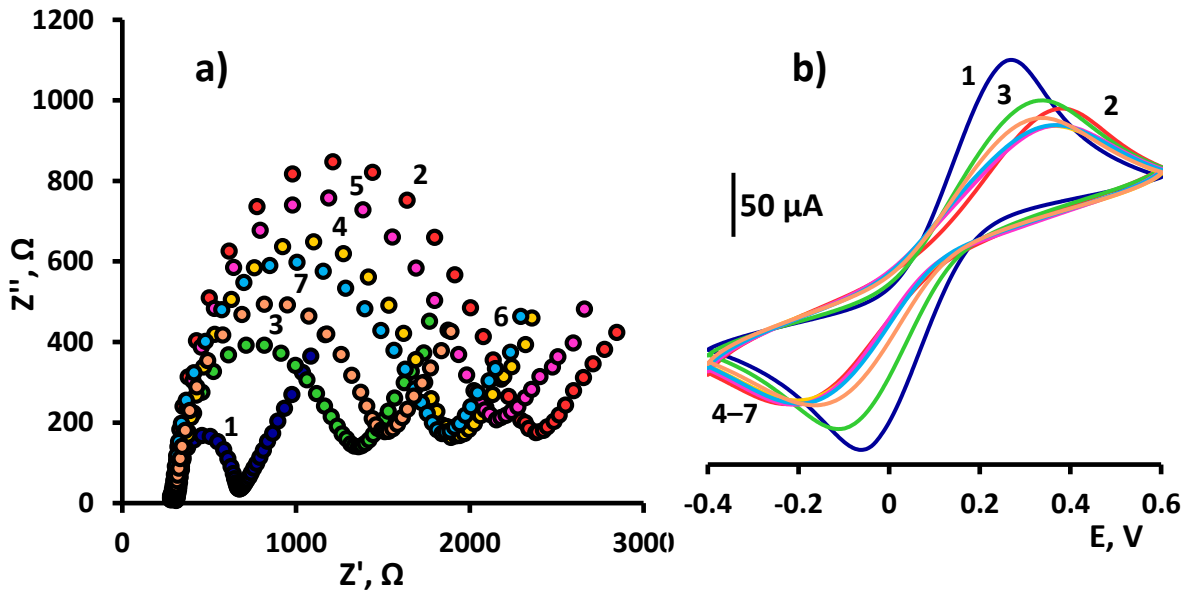

Figura 5.110. a) Diagramas de Nyquist y b) voltamperogramas clíclicos registrados para: 1) SPCE, 2) *p*-ABA/SPCE, 3) Strept/SPCE, 4) Biotin-anti-HFA-Strept/SPCE, 5) bloqueo con biotina, 6) HFA-Biotin-anti-HFA-Strept/SPCE y 7) mMWCNT(-HRP)-anti-HFA-HFA-Biotin-anti-HFA-Strept/SPCE en una disolución $Fe(CN)_6^{3-/4-}$ 2 mM en PBS de pH 7.4

Conclusiones similares se extrajeron a partir de los resultados obtenidos mediante voltamperometría cíclica (Figura 5.110b), especialmente en las primeras etapas de la preparación del inmunosensor. El voltamperograma correspondiente al electrodo serigrafiado desnudo (curva 1) muestra los picos de oxidación y reducción característicos del par redox a valores de potencial de +0.27 y –0.06 V, respectivamente, siendo las corrientes anódica y catódica poseen aproximadamente la misma magnitud (130 µA). La posterior modificación del electrodo con ácido *p*-aminobenzoico (curva 2) provocó una disminución en la corriente de pico y una mayor separación de los picos anódico y catódico debido a la repulsión electrostática entre la sonda redox y los grupos carboxílicos disociados en la superficie del electrodo. Cuando se inmoviliza la estreptavidina (curva 3), se restablece parcialmente la reversibilidad del voltamperograma, probablemente debido a una menor repulsión electrostática. La incorporación sucesiva del resto de inmunorreactivos provocó ligeras variaciones en los voltamperogramas cíclicos hacia un comportamiento menos reversible, como consecuencia de la presencia de capas aislantes de espesor creciente sobre la superficie del electrodo, aumentando ligeramente la reversibilidad en presencia del conjugado de nanotubos de carbono.

5.4.2.5. Calibrado y características analíticas

Empleando las condiciones experimentales optimizadas anteriormente y la amperometría como técnica de medida, se obtuvo el calibrado para la determinación de HFA registrando las señales a un potencial de –200 mV.

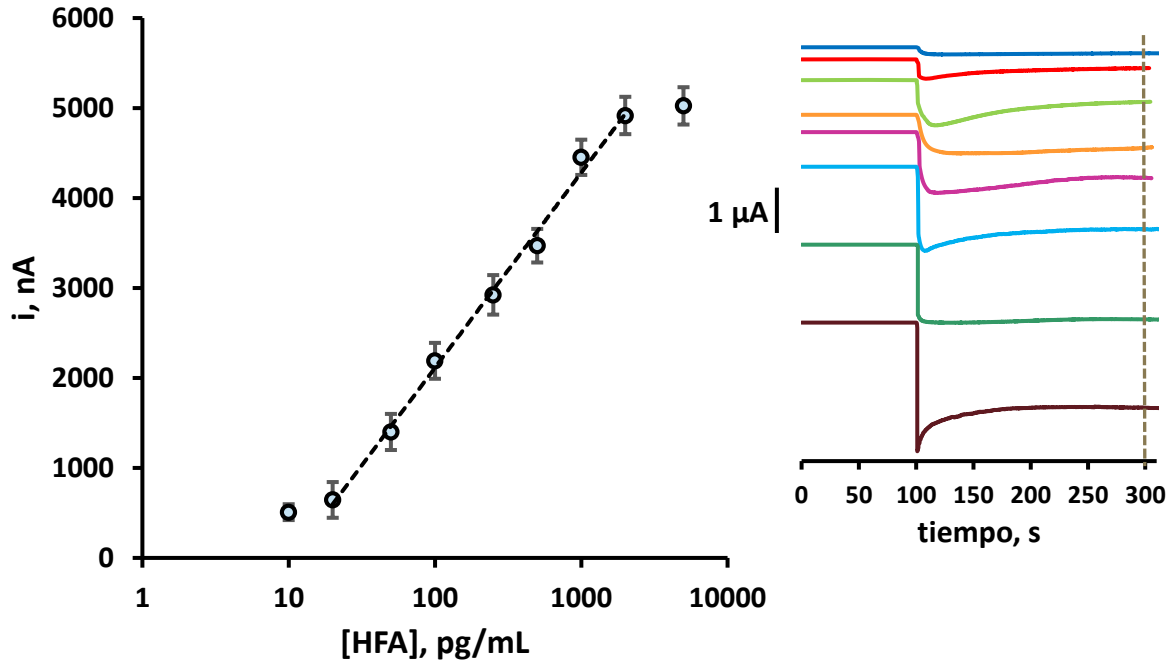

Figura 5.111. Calibrado para la determinación de HFA empleando el inmunosensor mMWCNT(-HRP)-anti-HFA-HFA-Biotin-anti-HFA-Strept/SPCE

La Figura 5.111 muestra la curva de calibrado correspondiente a los amperogramas mostrados a la derecha. La representación de la corriente en estado estacionario frente al logaritmo de la concentración de HFA se ajusta a la ecuación i, nA = (2168 ± 67) log ([HFA], pg/mL) – (2222 ± 163) (R^2 = 0.995), mostrando un intervalo lineal comprendido entre 20 y 2000 pg/mL de HFA. Este margen es adecuado para la determinación de HFA en muestras biológicas, ya que los niveles de HFA en suero son del orden de los mg/mL [Wu, 2014] y en saliva del orden de los µg/mL [Karabakan, 2016]. Además, la sensibilidad obtenida permite aplicar un elevado grado de dilución, minimizando de este modo el efecto matriz usual en muestras biológicas complejas.

El límite de detección, 16 pg/mL, se calculó, como en casos anteriores, de acuerdo con el criterio $\overline{x}+3{\cdot}s$, donde s es la desviación estándar, expresada en

unidades de concentración. Por su parte, el límite de cuantificación alcanzado fue de 53 pg/mL, de acuerdo con la expresión $\overline{x}+10\cdot s$.

5.4.2.6. Comparación entre diferentes estrategias de detección

Como se ha visto, la configuración desarrollada empleando el conjugado mMWCNTs(-HRP)-anti-HFA como etiqueta portadora de los anticuerpos de captura y la peroxidasa, proporciona una elevada sensibilidad. De acuerdo con Zhang *et al.* [Zhang, 2014], esto es debido a que dicho conjugado ofrece una elevada área superficial y es capaz de promover la transferencia electrónica entre la disolución y el electrodo. Pero, además, la presencia de las nanopartículas magnéticas probablemente contribuyen a aumentar la conductividad de los nanotubos de carbono y la capacidad para la inmovilización de biomoléculas. Para estudiar el efecto de estas nanopartículas, se compararon las medidas realizadas con el inmunosensor preparado con nanotubos de carbono magnéticos o no (mMWCNTs o MWCNTs), con los resultados representados en la Figura 5.112. Como puede observarse, el calibrado obtenido empleando mMWCNT(-HRP)-anti-HFA (▨) presenta una mayor pendiente (2168 ± 67 nA por década de concentración) que la que se obtiene utilizado el conjugado MWCNT(-HRP)-anti-HFA (▩) (1210 ± 50 nA por década de concentración). La mayor sensibilidad conseguida en presencia de mMWCNTs revela la contribución favorable de las partículas magnéticas para mejorar la conductividad. Por otro lado, en la misma figura se han representado también (▧) los resultados obtenidos en ausencia de enzima peroxidasa con el fin de comprobar la actividad pseudo-peroxidasa de las nanopartículas magnéticas. Puede verse que la sensibilidad es mucho menor cuando se utilizan los nanotubos magnéticos conjugados con el anticuerpo, mMWCNT-anti-HFA en ausencia de enzima, ya que la catálisis enzimática de la peroxidasa sobre la reacción del peróxido de hidrógeno es mucho más importante que la débil actividad pseudo-peroxidasa de dichas partículas.

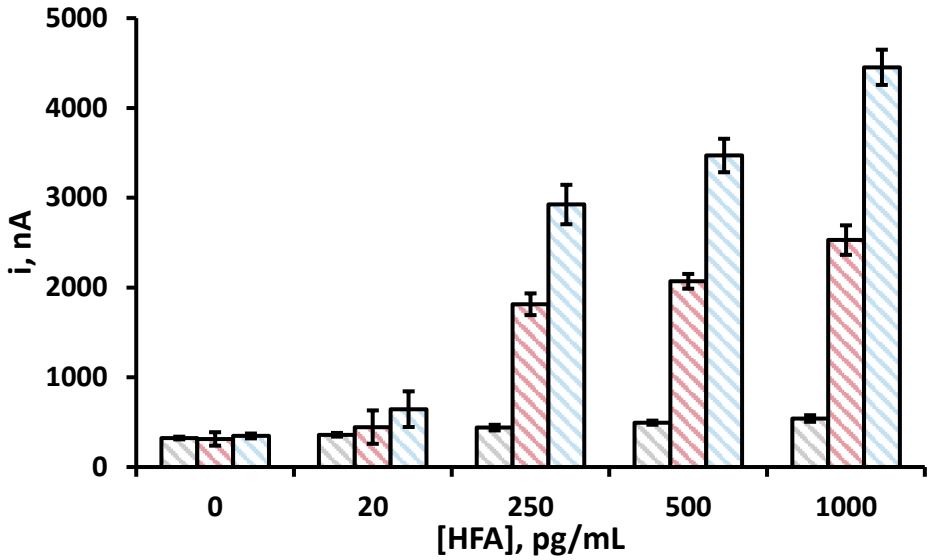

Figura 5.112. Calibrados obtenidos empleando: Strept, 600 µg/mL, 5 µL, 60 min; Biotin-anti-HFA, 7 µg/mL, 5 µL, 60 min; Biotin, 1.5 mg/mL, 5 µL, 30 min; HFA, 5 µL, 60 min y a) mMWCNT-anti-HFA (▨), donde i, nA = (100 ± 20) log ([HFA], pg/mL) + (220 ± 40); b) MWCNT(-HRP)-anti-HFA (▨), donde i, nA = (1210 ± 50) log ([HFA], pg/mL) – (1100 ± 100) y mMWCNT(-HRP)-anti-HFA (▨), donde i, nA = (2168 ± 67) log ([HFA], pg/mL) – (2222 ± 163), 5 µL,60 min

Finalmente, para destacar el efecto amplificador de los conjugados mMWCNT(-HRP)-anti-HFA, las respuestas del inmunosensor preparado con este conjugado se compararon con las obtenidas empleando un anticuerpo secundario marcado con la misma enzima. Como puede verse en la Figura 5.113, la corriente medida en presencia de HFA fue tres veces mayor utilizando el conjugado de nanotubos magnéticos.

Estos resultados muestran que los conjugados son útiles como portadores de biomoléculas para la amplificación de la señal. Además, es importante resaltar que, aunque se origina un fuerte aumento de la corriente debida a las interacciones específicas útiles para la detección de HFA, las respuestas inespecíficas representan únicamente el 13% de aquellas, lo que ofrece una elevada relación S/R.

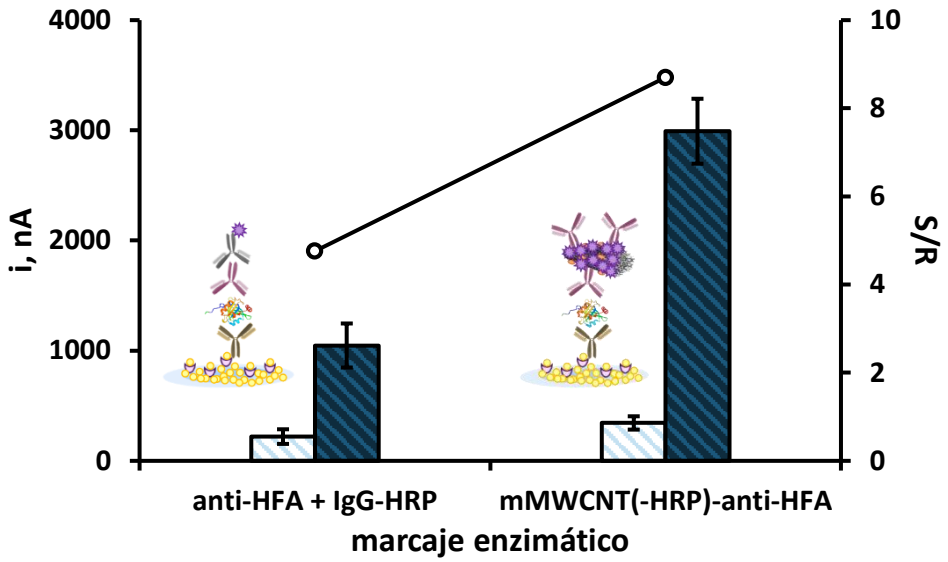

Figura 5.113. Efecto del tipo de marcaje enzimático sobre la respuesta del inmunosensor: Strept, 600 µg/mL, 5 µL, 60 min; Biotin-anti-HFA, 7 µg/mL, 60 min; biotin, 5 µL, 30 min; HFA, 0 (□) o 250 (■) pg/mL, 5 µL, 60 min; mMWCNT(-HRP)-anti-HFA o anti-HFA y HRP-IgG, 5 µL, 60 min

5.4.2.7. Estudio de selectividad

Para estudiar la selectividad del inmunosensor desarrollado para la determinación de HFA, se compararon las respuestas amperométricas obtenidas en ausencia y en presencia de 250 pg/mL de HFA y, a su vez, en ausencia y en presencia de cada uno de los compuestos ensayados como interferentes, en este caso: albúmina de suero bovino (BSA), creatinina (CR), ácido ascórbico (AA), interleucina 1 beta (IL-1β), interleucina 6 (IL-6), interleucina 8 (IL-8), cortisol (CL), estradiol (E2), inmunoglobulina G humana (hIgG), factor de necrosis tumoral alfa (TNF-α), factor de crecimiento transformante beta 1 (TGF-β1) y ácido úrico (UA).

Los resultados mostrados en la Figura 5.114 ponen de manisfiesto que niguna de estas proteínas supone una interferencia significativa en la determinación de HFA a los niveles de concentracion indicados, demostrando así la alta selectividad de la configuración desarrollada.

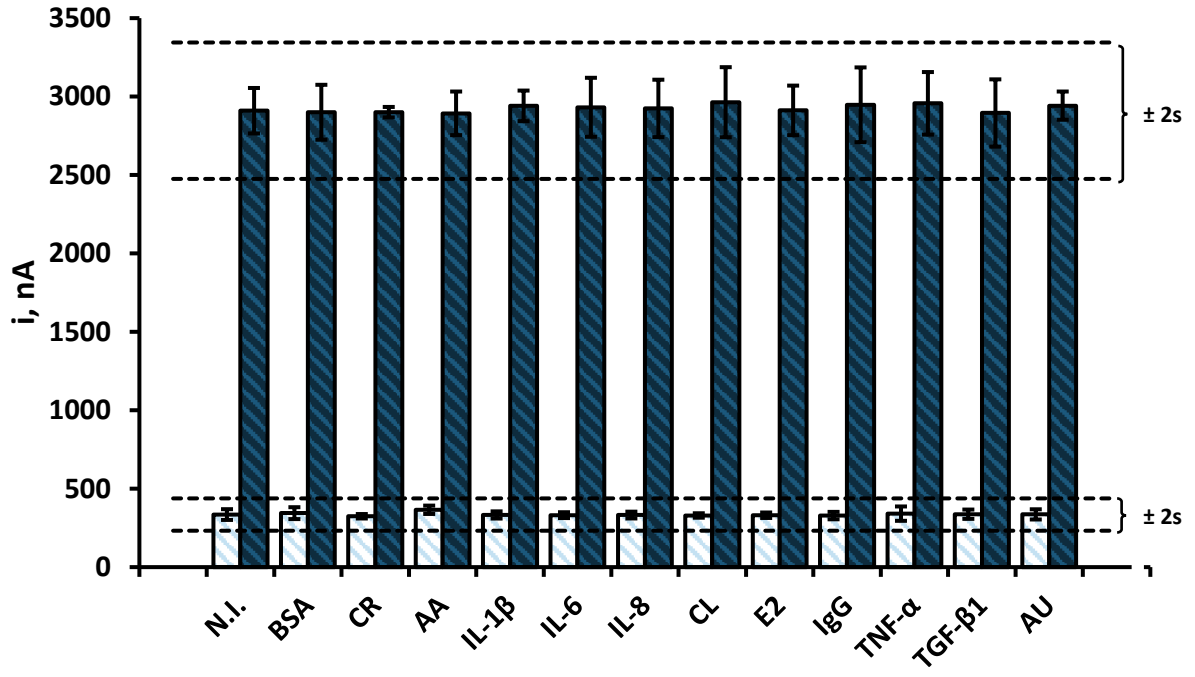

Figura 5.114. Selectividad del inmunosensor mMWCNT(-HRP)-anti-HFA-HFA-Biotin-anti-HFA-Strept/SPCE evaluando la respuesta del mismo con 0 (□)o 250 (■) pg/mL de HFA fente a 5 mg/mL de BSA, 10 pg/mL de AA, 50 pg/mL de IL-1β, 50 pg/mL de IL-6, 250 pg/mL de IL-8, 12 ng/mL de CL, 200 pg/mL de E2, 50 ng/mL de hIgG, 200 pg/mL de TNF-α, 500 pg/mL de TGF-β1 y 50 µg/mL de AU

5.4.2.8. Estudios de reproducibilidad y estabilidad

Los estudios de repetibilidad de las medidas se realizaron midiendo la respuesta amperométrica de ocho inmunosensores diferentes, preparados el mismo día, en ausencia y presencia de 250 pg/mL de HFA, siendo los valores de RSD obtenidos del 6.7 y 7.4%, respectivamente. Por otro lado, la reproducibilidad se evaluó midiendo la respuesta de inmunosensores preparados en diferentes días, obteniéndose valores de RSD del 7.2 y 7.5%, en ausencia y presencia de 250 pg/mL de HFA. Asimismo, estos resultados demuestran la buena precisión de las medidas y ponen de manifiesto que el procedimiento de fabricación del inmunosensor es fiable y reproducible.

Por otro lado, para evaluar la estabilidad del inmunoconjugado Biotin-anti-HFA-Strept-Phe-SPCE, se prepararon distintos electrodos modificados, se almacenaron en seco a –20°C y, después, cada día de trabajo se construyó a partir de ellos el inmunosensor completo en presencia de 250 pg/mL de HFA.

En la Figura 5.115 se ha representado un gráfico de control tomando como valor central el valor medio para tres medidas amperométricas realizadas el primer día del estudio, donde los márgenes establecidos corresponden a ± 3 veces la desviación estándar de las medidas realizadas el primer día de trabajo.

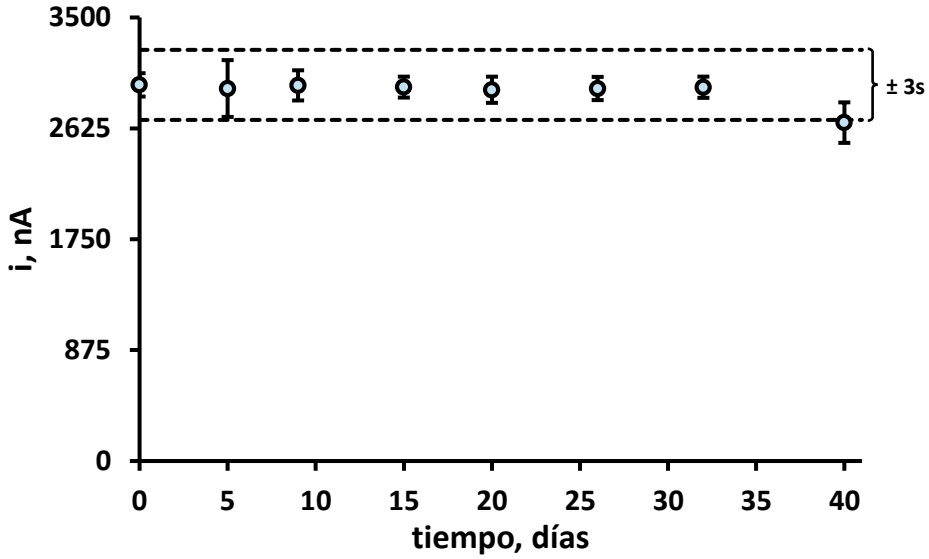

Figura 5.115. Gráfico de control para la evaluación de la estabilidad de almacenamiento del conjugado Biotin-anti-HFA-Strept/SPCE

Como puede observarse, las respuestas amperométricas permanecieron dentro de los límites de control durante 32 días, sin pérdida significativa de la respuesta inicial durante el periodo de estudio. Como ya se ha señalado en apartados anteriores, esta característica tiene una gran importancia desde el punto de vista de la utilidad práctica del inmunosensor, puesto que disponer de electrodos modificados preparados con antelación permite una reducción del tiempo de análisis.

También se realizaron estudios de estabilidad del conjugado de nanotubos mMWCNT(-HRP)-anti-HFA. Para ello, se preparó el conjugado y se dispersó en 1 mL de disolución reguladora PBST 100 mM de pH 7.0, almacenándose a 8°C.

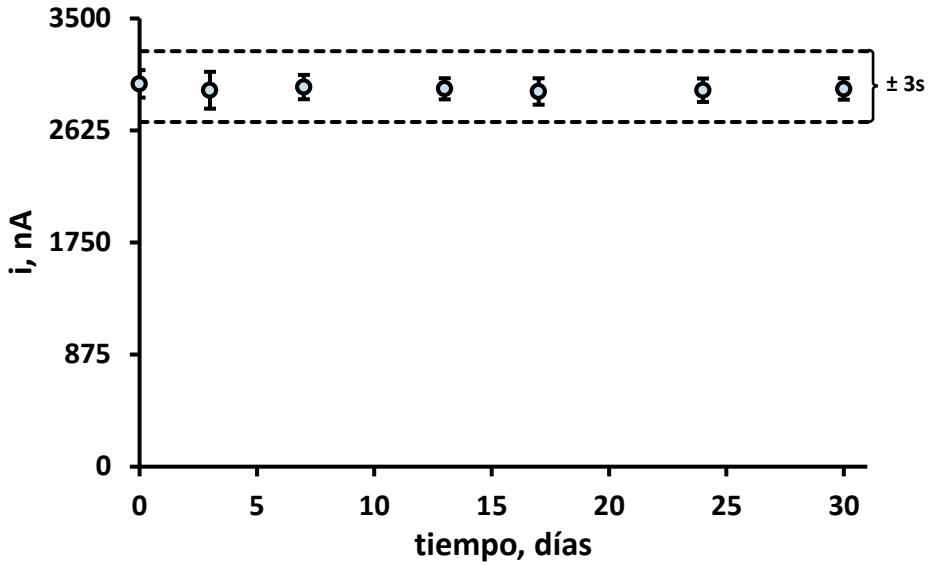

Figura 5.116. Gráfico de control para la evaluación de la estabilidad de almacenamiento del conjugado mMWCNT(-HRP)-anti-HFA

Como se puede ver en la Figura 5.116, el inmunosensor preparado con este inmunoconjugado proporcionó respuestas dentro de los límites de control establecidos el primer día durante 30 días, poniendo de manifiesto la posibilidad de disponer del material inmunoconjugado almacenado para su uso cuando se precise, lo que nuevamente conduce a una disminución del tiempo de análisis.

5.4.2.9. Aplicación a la determinación de fetuina A humana en saliva

La utilidad del inmunosensor desarrollado para el análisis de muestras clínicas se ha comprobado mediante el análisis de dos muestras de saliva proporcionadas por dos individuos sanos, un fumador y un no fumador. Este tipo de muestra se ha elegido porque, como se ha comentado anteriormente, la HFA posee un papel clave en la detección de procesos inflamatorios dentales [Doğan, 2016]. Además, la saliva es un fluido biológico muy atractivo para el diagnóstico de distintas enfermedades, puesto que su recolección es sencilla, barata, no invasiva, segura e indolora, entre otras ventajas [Campuzano, 2017]. Por otro lado, con el objetivo de minimizar el posible efecto matriz y ajustar la concentración de HFA en las muestras dentro del rango de linealidad obtenido con el inmunosensor, se estudiaron distintos factores de dilución

en disolución reguladora PBS de pH 7.4, observándose que una dilución 1/100 de la muestra es suficiente para evitar este efecto. Así, en la Figura 5.117 se muestran superpuestos los calibrados correspondientes a las señales proporcionadas por el material biológico diluido 100 veces y enriquecido con concentraciones crecientes de fetuina, con el calibrado obtenido para disoluciones estándar de fetuina A humana. Como puede apreciarse ambos calibrados son muy similares.

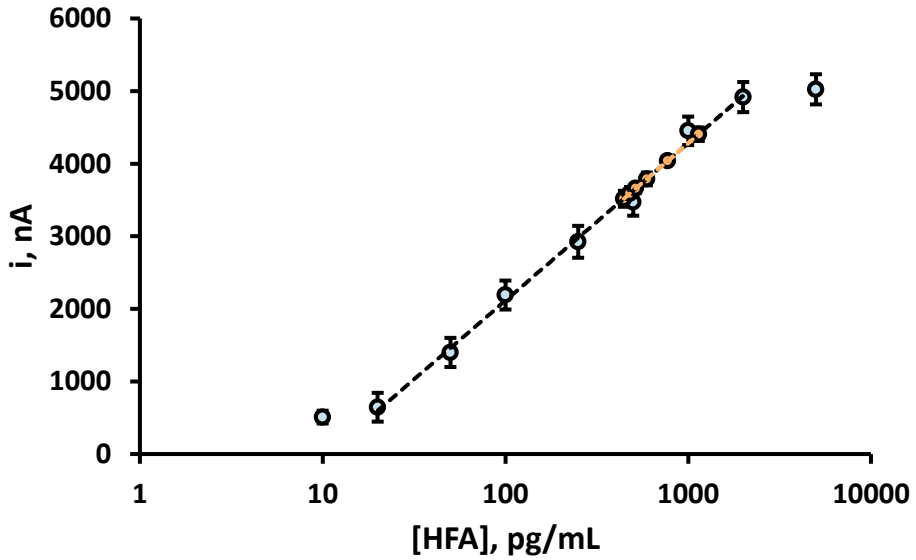

Figura 5.117. Superposición de las señales obtenidas para el material biológico de referencia enriquecido (●) en el calibrado de disoluciones estándar (○)

Asimismo, se ha realizado la comparación estadística de las pendientes para los calibrados de fetuina en saliva de individuo fumador y no fumador (2.16 ± 0.03 y 2.17 ± 0.03 µA por década de concentración, respectivamente) con la obtenida para el calibrado de disoluciones estándar (2.17 ± 0.07 µA por década de concentración) mediante el test de la *t* de Student, obteniéndose valores de t_{exp} mucho más bajos que los tabulados (t_{tab} = 2.262) a un nivel de significación de 0.05. Estos resultados permiten la determinación de HFA en saliva directamente mediante la interpolación de la señal proporcionada por la muestra diluida en el calibrado de disoluciones estándar.

En la Tabla 5.19 se comparan las concentraciones de HFA encontradas en las muestras de saliva empleando el inmunosensor desarrollado con las obtenidas

empleando el kit ELISA, siguiendo el procedimiento de ensayo especificado por la casa comercial.

Tabla 5.19. Determinación de HFA en muestras de saliva empleando el inmunosensor mMWCNT(-HRP)-anti-HFA-HFA-Biotin-anti-HFA-Strept/SPCE

MUESTRA	INMUNOSENSOR ng/mL (*n* = 5)*	ELISA ng/mL (*n* = 4)*
fumador	44.6 ± 0.5	44.8 ± 0.8
no fumador	43.0 ± 0.2	42.9 ± 0.6

* valor medio ± t·s/√n

Como puede observarse, existe un excelente acuerdo entre los resultados obtenidos por ambos métodos, los cuales también están en concordancia con los valores encontrados en la bibliografía para la saliva de individuos sanos, 41 ng/mL [Doğan, 2016].

5.4.2.10. Conclusiones

En este trabajo se ha descrito el primer inmunosensor amperométrico para la determinación de fetuina A humana. La estrategia diseñada incluye la modificación de la superficie del electrodo serigrafiado de carbono mediante *grafting* oxidativo con ácido *p*-aminobenzoico para la posterior unión covalente de estreptavidina, y el establecimiento de un formato de inmunoensayo tipo sándwich con Biotin-anti-HFA como anticuerpo de captura, empleando un inmunoconjugado mMWCNT(-HRP)-anti-HFA como etiqueta portadora para la amplificación de la señal.

La estrategia seguida proporciona importantes ventajas analíticas, en términos sensibilidad y amplio intervalo lineal, con respecto a los inmunoensayos tipo ELISA comerciales y al único inmunosensor electroquímico cronoimpedimétrico para la determinación de HFA descrito hasta ahora en la bibliografía. También es importante destacar que el inmunosensor desarrollado puede usarse para la determinación de este analito en muestras de saliva a bajos niveles de concentración, no siendo ningún

tratamiento de la muestra salvo la dilución. Otras ventajas relevantes del inmunosensor desarrollado son la gran reproducibilidad de las medidas y la excelente estabilidad de almacenamiento.

Por último, este diseño puede extenderse fácilmente a la determinación de otros biomarcadores, dada la facilidad de modificación de la superficie del electrodo de carbono y de preparación de los nanotubos magnéticos modificados con las biomoléculas específicas.

6

Conclusions

Partial conclusions to the research work done in this Doctoral Thesis have been exposed throughout the previous sections in which the milestones reached were highlighted and the characteristics of the developed configurations have been compared with other methodologies previously described in the literature.

In a broad context, through the experiments carried out, the electroanalytical advantages of electrochemical grafting or the use of the conducting polymer poly(pyrrolepropionic) acid and different carbon nanomaterials, as well as the application of novel immobilization techniques for developing analytical devices and methods for determining "*inflammageing"* biomarkers that are competitive with existing procedures have been explored. Likewise, poly-HRP-Strept and carbon nanotubes-modified hybrids have also been used successfully as carrier nanotags for signal amplification.

It is important to highlight that in this Doctoral Thesis the preparation and functioning of the first electrochemical immunosensors for the determination of 8-isoprostane and human fetuin A and for the simultaneous determination of tumor necrosis factor alpha and interleukin 1 beta have been described. Besides, the first disposable electrochemical immunosensor making use of a rGO/CMC hybrid nanostructured electrode have also been described.

It has been demonstrated that the analytical methods developed with these novel immunosensors exhibit better analytical characteristics in terms of sensitivity, clinically relevant linear range, reproducibility, storage stability and selectivity than other immunoassay-based procedures described previously.

In addition, most of the methodologies proposed in this work require shorter analysis times and lower reagents consumption than others based on different techniques and, in all cases, the results obtained demonstrated a good precision, the values of the relative standard deviations for repeatability and reproducibility ranging between 0.35 and 7.50, thus demonstrating the reliability for fabrication protocols of the devices.

Finally, but importantly, all the immunosensors have demonstrated their practical utility by application to the determination of the selected biomarkers at physiological levels in certified biological reference material, serum and/or saliva, providing good results.

7

Bibliografía

A

[ABCAM ab46025]: Human IFN-γ ELISA Kit *(https://www.abcam.com/human-ifn-gamma-elisa-kit-ab46025.html)*

[ABCAM ab46087]: Human TNF-α ELISA Kit *(https://www.abcam.com/human-tnf-alpha-elisa-kit-ab46087.html)*

[ABCAM ab99968]: Human Adiponectin ELISA Kit *(https://www.abcam.com/human-adiponectin-elisa-kit-ab99968.html)*

[ABCAM ab100507]: Human CD105 ELISA Kit *(https://www.abcam.com/human-cd105-elisa-kit-endoglin-ab100507.html)*

[ABCAM ab100647]: Human TGF-β1 ELISA Kit *(https://www.abcam.com/human-tgf-beta-1-elisa-kit-ab100647.html)*

[ABCAM ab108855]: Human Fetuin A ELISA Kit *(https://www.abcam.com/human-fetuin-a-elisa-kit-ahsg-ab108855.html)*

[ABCAM ab175819]: 8-isoprostane ELISA Kit *(https://www.abcam.com/8-isoprostane-elisa-kit-ab175819.html)*

[ABCAM ab214025]: Human IL-1β ELISA Kit *(https://www.abcam.com/human-il-1-beta-elisa-kit-ab214025.html)*

[Abernethy, 2012]: N. Abernethy, E. Chung, B.T. Fontanelle, Y. Gao, D. Jennins, M.M. Koudijs, D. Lim, L. Yang, T. Ling, P. Vukovic, A. Wong, N.J. Maeji, Metal polymers: a glue to immobilize proteins onto synthetic surfaces, *44th Oak Ridge Conference: emerging technologies for 21st Century diagnostics, San José, California* (2012).

[Abnova KA0017]: Human ADIPOQ ELISA Kit *http://www.abnova.com/products/products_detail.asp?catalog_id=KA0017)*

[Ahmed, 2018]: W. Ahmed, A. Elhissi, V. Dhanak, K. Subramani, Carbon nanotubes: applications in cancer therapy and drug delivery research in K. Subramani, W. Ahmed,

Emerging nanotechnologies in dentistry. A volume in micro and nano technologies, 2nd Edition, *Elsevier* (2018) 371–389.

[Ahuja, 2007]: T. Ahuja, I.A. Mir, D. Kumar, Rajesh, Biomolecular immobilization on conducting polymers for biosensing applications, *Biomaterials* 28 (2007) 791–805.

[Ajima, 2005]: K.Ajima, M. Yudasaka, T. Murakami, A. Maigné, K. Shiba, S. Iijima, Carbon nanohorns as anticancer drug carriers, *Mol. Pharm.* 2 (2005) 475–480.

[Alwarappan, 2009]: S. Alwarappan, A. Erdem, C. Liu, C.Z. Li, Probing the electrochemical properties of graphene nanosheets for biosensing applications, *J. Phys. Chem. C* 113 (2009) 8853–8857.

[Antibodies Online ABIN2944828]: 8-isoprostane ELISA Kit *(https://www.antibodies-online.com/kit/2944828/8-Isoprostane+ELISA+Kit/)*

[Araque, 2014]: E. Araque, R. Villalonga, M. Gamella, A. Sánchez, P. Martínez-Ruiz, V. García-Baonza, J.M. Pingarrón, Water-soluble reduced Graphene oxide-carboxymethylcellulose hybrid nanomaterial for electrochemical biosensor design, *ChemPlusChem* 79 (2014) 1334–1341.

[Arica, 2005]: O. Arica, M. Aral, S. Sasmaz, P. Ciragil, Serum levels of TNF-α, IFN-γ, IL-6, IL-12, IL-17 and IL-18 in patients with active psoriasis and correlation with disease severity, *Mediat. Inflamm.* 5 (2005) 273–279.

[Arita, 1999]: Y. Arita, S. Kihara, N. Ouchi, M. Takahashi, K. Maeda, J. Miyagawa, K. Hotta, I. Shimomura, T. Nakamura, K. Miyaoka, H. Kuriyama, M. Nishida, S. Yamashita, K. Okubo, K. Matsubara, M. Muraguchi, Y. Ohmoto, T. Funahashi, Y. Matsuzawa, Paradoxical decrease of an adipose-specific protein, adiponectin in obesity, *Biochem. Biophys. Res. Commun.* 257 (1999) 79–83.

[Aviva Systems Biology OKAG00159]: Human Endoglin ELISA Kit *(https://www.avivasysbio.com/endoglin-elisa-kit-human-96-wells-okag00159.html)*

[Aydin, 2018]: E.B. Aydin, M. Aydin, M.K. Sezgintürk, Highly sensitive electrochemical immunosensor based on polythiophene polymer with densely populated carboxyl groups as

immobilization matriz for detection of interleukin 1β in human serum and saliva, *Sens. Actuators B Chem.* 270 (2018) 18–27.

[Azam, 2014]: S. Azam, R.T. Rahman, Z. Lou, Y. Tang, S.M. Raqib, J.S. Jothi, Review: advancements and application of immunosensors in the analysis of food contaminants, *Nus. Bioscience* 6 (2014) 186–195.

B

[Bakiner, 2014]: O. Bakiner, E. Bozkirli, D.T. Ertugrul, N. Sezgin, M.E. Ertorer, Plasma fetuin-A levels are reduced in patients with hypothyroidism, *Eur. J. Endocrinol.* 170 (2014) 411–418.

[Banerjee, 1992]: M. Banerjee, K.H. Kang, J.D. Morrow, L.J. Roberts II, J.H. Newman, Effects of a novel prostaglandin, 8-epi-$PGF_{2\alpha}$, in rabbit lung in situ, *Am. J. Physiol.* 263 (1992) H660–H663.

[Baraket, 2014]: A. Baraket, M. Lee, N. Zine, M.G. Trivella, M. Zabala, J. Bausells, M. Sigaud, N. Jaffrezic-Renault, A. Errachid, A fully integrated electrochemical BioMEMS fabrication process for cytokine detection: application for heart failure, *Procedia Eng.* 87 (2014) 377–379.

[Bardini, 2015]: L. Bardini EIS 101, an introduction to electrochemical impedance spectroscopy, *Technical Report* (2015) 21–23.

[Barrouin, 2015]: M. Barrouin, Mas in myocardial infarction and congestive heart failure in T. Unger, U.M. Steckelings, R.A.S. dos Santos, The protective arm of the renin angiotensin system (RAS). Functional aspects and therapeutic implications, 1st Edition, *Elsevier* (2015) 191–195.

[B-Bridge K1001-1]: Human total full length mature Adiponectin ELISA Kit *(https://www.biocat.com/products/K1001-1-BR)*

[Bélanger, 2011]: D. Bélanger, J. Pinson, Electrografting: a powerful method for surface modification, *Chem. Soc. Rev.* 40 (2011) 3995–4048.

[Bertók, 2013]: T. Bertók, P. Gemeiner, M. Mikula, P. Gemeiner, J. Tkac, Ultrasensitive impedimetric lectin based biosensor for glycoproteins containing sialic acid, *Microchim. Acta* 180 (2013) 151–159.

[Betteridge, 2000]: D.J. Betteridge, What is oxidative stress? *Metabolism* 49 (2000) 3–8.

[Biogems BGK01584]: Human IL-1β ELISA Kit *(https://www.bio-gems.com/elisa-kits-pre/bgk-human-il-1-pre-coated-elisa-kit.html)*

[Biolegend 430104]: ELISA MAX™ Deluxe Set Human IFN-γ *(https://www.biolegend.com/en-gb/products/human-ifn-gamma-elisa-max-deluxe-2227)*

[Biolegend 437004]: ELISA MAX™ Deluxe Set Human IL-1β *(https://www.biolegend.com/fr-fr/products/human-il-1beta-elisa-max-deluxe-7064)*

[Biolegend 437707]: LEGEND MAX™ Free Active TGF-β1 ELISA Kit *(https://www.biolegend.com/en-us/products/legend-max-free-active-tgf-beta1-elisa-kit-with-pre-coated-plates-7080)*

[Biomatik EKA51839]: Human IFN-γ ELISA Kit *(https://www.biomatik.com/elisa-kits/ifn-gamma-human-elisa-kit-cat-eka51839/)*

[Biomatik EKA51975]: Human Endoglin ELISA Kit *(https://www.biomatik.com/elisa-kits/endoglin-human-elisa-kit-cat-eka51975/)*

[Biomatik EKA52040]: Human Fetuin A ELISA Kit *(https://www.biomatik.com/elisa-kits/fetuin-a-human-elisa-kit-cat-eka52040/)*

[BioVendor RD191023100]: Human high sensitivity (Sandwich) Adiponectin ELISA Kit *(https://www.biovendor.com/adiponectin-human-elisa-high-sensitivity-sandwich)*

[BioVendor RD191037100]: Human Fetuin A (AHSG) ELISA Kit *(https://www.biovendor.com/fetuin-a-ahsg-human-elisa)*

[Biovision K4779-100]: Human TNF-α ELISA Kit *(https://www.biovision.com/documentation/datasheets/K4779.pdf)*

[Boster EK0392]: Human IL-1β ELISA Kit PicoKine™ *(https://www.bosterbio.com/human-il-1-beta-picokine-trade-elisa-kit-ek0392-boster.html)*

[Boster EK0525]: Human TNF-α ELISA Kit PicoKine™ *(https://www.bosterbio.com/human-tnf-alpha-picokine-trade-elisa-kit-ek0525-boster.html)*

[Boster FEK0644]: Human CD105 Picokine™ Fast ELISA Kit *(https://www.bosterbio.com/human-cd105-picokine-trade-fast-elisa-kit-fek0644-boster.html)*

[Brand, 2014]: H.S. Brand, A.J.M. Ligtenberg, E.C.I. Veerman, Saliva and wound healing in A.J.M. Ligtenberg, E.C.I. Veerman, Saliva: secretion and functions, 1st Edition, *Karger* (2014) 52–60.

[Brozena, 2010]: A.H. Brozena, J. Moskowitz, B. Shao, S. Deng, H. Liao, K.J. Gaskeil, Y.H. Wang, Outer wall selectively oxidized, water-soluble double-walled carbon nanotubes, *J. Am. Chem. Soc.* 132 (2010) 3932–3938.

C

[Cabral de Faria, 2014]: A.P. Cabral de Faria, V. Fontana, R. Modolo, N.R. Bararo, A.R. Sabbatini, I.F. Pansani, S.E. Ferreira-Melo, H. Moreno, 8-isoprostane levels are associated with endothelial dysfunction in resistant hypertension, *Clin. Chim. Acta* 433 (2014) 179–183.

[Campuzano, 2017]: S. Campuzano, P. Yáñez-Sedeño, J.M. Pingarrón, Electrochemical bioaffinity sensors for salivary biomarkers detection, *TrAC Trends Alan. Chem.* 86 (2017) 14–24.

[Cavanagh, 2012]: M.M. Cavanagh, C.M. Weyand, J. Goronzy, Chronic inflammation and aging: DNA damages tips the balance, *Curr. Opin. Immunol.* 24 (2012) 488–493.

[Cayman Chemical 516351]: 8-isoprostane ELISA Kit *(https://www.caymanchem.com/product/516351/8-isoprostane-elisa-kit)*

[Cayman Chemical 589201]: Human TNF-α ELISA Kit *(https://www.caymanchem.com/product/589201/tnf-%CE%B1-(human)-elisa-kit)*

[Cell Biolabs Inc STA-337]: 8-iso-prostaglandin F2a Assay *(https://www.cellbiolabs.com/8-iso-prostaglandin-f2a-assay)*

[Chen, 2010]: D. Chen, L. Tang, J. Li, Graphene-based materials in electrochemistry, *Chem. Soc. Rev.* 39 (2010) 3157–3180.

[Chen, 2014]: Y. Chen, T.S. Pui, P. Kongsuphol, K.C. Tang, S.K. Arya, Aptamer-based array electrodes for quantitative interferon-γ detection, *Biosens. Bioelectron.* 53 (2014) 257–262.

[Chiang, 2010]: C.Y. Chiang, M.L. Hsieh, K.W. Huang, L.K. Chau, C.M. Chang, S.R. Lyu, Fiber-optic particle plasmon resonance sensor for detection of interleukin-1β in synovial fluids, *Biosens. Bioelectron.* 26 (2010) 1036–1042.

[Choi, 2016]: K.M. Choi, The impact of organokines on insulin resistance, inflammation and atherosclerosis, *Endocrinol. Metab.* 31 (2016) 1–6.

[Chu, 2017]: Z. Chu, H. Dai, Y. Liu, Y. Lin, Development of a semiconductor-based electrochemical sensor for interferon-γ detection, *Int. J. Electrochem. Sci.* 12 (2017) 9141–9149.

[Chung, 2009]: K.F. Chung, Cytokines in P.J. Barnes, J.M. Drazen, S.I. Rennard, N.C. Thomson, Asthma and COPD: basic mechanisms and clinical management, 2nd Edition, *Elsevier* (2009) 327–341.

[Cohen, 1975]: S. Cohen, Antibody structure, *J. Clin, Pathol. Supple. (Assoc. Clin. Pathol.)* 6 (1975) 1–7.

[Coplan, 2009]: J.D. Copla, J.G. Kral, E.L.P. Smith, L.A. Rosenblum, Mother-infant interaction in the variable foraging demand model in L.R. Squire, Encyclopedia of Neuroscience, 1st Edition, *Elsevier* (2009) 981–987.

[Costa, 2008]: M.J. Costa, D.A. Monteiro, A.L. Oliveira-Neto, F.T. Rantin, A.L. Kalinin, Oxidative stress biomarkers and heart function in bullfrog tadpoles exposed to Roundup Original, *Ecotoxicology* 17 (2008) 153–163.

[Creative Diagnostics DEIA5014]: 8-isoprostane Express EIA Kit *(https://www.creative-diagnostics.com/8-Isoprostane-Express-EIA-Kit-107321-471.htm)*

[Cusabio CSB-E10030]: Human Soluble Endoglin ELISA Kit *(https://www.cusabio.com/ELISA-Kit/Human-Soluble-EndoglinsENGsCD105-ELISA-Kit-76486.html)*

D

[Dabrowska, 2015]: A.M. Dabrowska, J.S. Taracha, B. Wojtysiak-Duma, D. Dumac, Fetuin-A (AHSG) and its usefulness in clinical practice. Review of the literature, *Biomed. Pap. Med. Fac. Univ. Palacky Olomouc Czech Repub.* 159 (2015) 352–359.

[Dallas, 2008]: S.L. Dallas, T. Alliston, L.F. Bonewald, Transforming growth factor-β in J.P. Bilezikian, L.G. Raisz, T.J. Martin, Principles of bone biology, 3rd Edition, *Elsevier* (2008) 1145–1166.

[Davies, 2014]: P. Davies, I. Kratochvilová, C. Ewels, T. Aqeel, N, Martin, V. Fal'ko, T. Enoki, A. Rodriguez-Fortea, K. Kaneko, A. Turak, C. Buono, V. Kovalenko, P. Ajayan, M. Heggie, V. Khare, A. Hirsch, T. Gspann, A. Windle, P. Costa, M. Shaffer, J. Casado, M.Chan-Park, R. Busquets, Doping and theory: general discussion, *Faraday Discuss.* 173 (2014) 233–256.

[Dawidczyk, 2013]: T.J. Dawidczyk, H. Kong, H.E. Katz, Organic semiconductors (OSCs) for electronic chemical sensors in O. Ostroverkhova, Handbook of organic materials for optical and (opto)electronicdevices. Properties and applications, 1st Edition, *Woodhead Publishing* (2013) 577–596.

[de Gonzalo-Calvo, 2000]: D. de Gonzalo-Calvo, K. Neitzert, M. Fernández, I. Vega-Naredo, B. Caballero, M. García-Macía, F.M. Suárez, M.J. Rodríguez-Colunga, J.J. Solano, A. Coto-Montes, Differential inflammatory responses in aging and disease: TNF-alpha and IL-6 as possible biomarkers, *Free Radic. Biol. Med.* 49 (2000) 733–737.

[De Paula, 2016]: F.J.A. De Paula, D.M. Black, C.J. Rosen, Osteoporosis and bone biology in S. Melmed, K.S. Polonsky, R.R. Larsen, H.M. Kronenberg, Williams textbook of endocrinology, 13th Edition, *Elsevier* (2016) 1323–1364.

[Delamar, 1992]: M. Delamar, R. Hitmi, J. Pinson, M. Savéant, Covalent modification of carbon surfaces by grafting of functionalized aryl radicals produced from electrochemical reduction of diazonium salts, *J. Am. Chem. Soc.* 114 (1992) 5883–5884.

[Detroit R&D 8iso1]: 8-isoprostane ELISA Kit *(https://www.detroitrandd.com/store/hypertension-stroke/8-isoprostane-elisa)*

[Dinarello, 2009]: C.A. Dinarello, Immunological and inflammatory functions of the interleukin-1 family, *Ann. Rev. Immunol.* 27 (2009) 519–550.

[Dinarello, 2013]: C.A. Dinarello, Overview of the interleukin-1 family of ligands and receptors, *Semin. Immunol.* 25 (2023) 389–393.

[Ding, 2017]: S. Ding, C. Mosher, X.Y. Lee, S.R. Das, A.A. Cargil, X. Tang, B. Chen, E.S. McLamore, C. Gomes, J.M. Hostetter, J.C. Claussen, Rapid and label-free detection of interferon gamma via an electrochemical aptasensor comprising a ternary surface monolayer on a gold interdigitated electrode array, *ACS Sens.* 2 (2017) 210–217.

[Doehner, 2011]: W. Doehner, S. von Haehling, S.D. Anker, Alterations in nutrituin and body mass in heart failure in D.L. Mann, Hearth failure: a companion to Braunwald's heart disease, 2nd Edition, *Elsevier* (2011) 330–345.

[Dogan, 2006]: Y. Dogan, S. Akarsu, B. Ustundag, E. Yilmaz, M.K. Gurgoze, Serum IL-1β, IL-2 and IL-6 in insulin-dependent diabetic children, *Mediat. Inflamm.* 1 (2006) 1–6.

[Doğan, 2016]: G.E. Doğan, T. Demír, E. Laloğlu, E. Sağlam, H. Aksoy, A. Yildirim, F. Akçay, Patients with dental calculus have increased saliva and gingival crevicular fluid fetuin-A levels but no association with fetuin-A polymorphisms, *Braz. Oral. Res.* 30 (2016) e129.

[Dong, 1997]: S. Dong, J. Li, Self-assembled monolayers of thiols on gold electrodes for bioelectrochemistry and biosensors, *Bioelectrochem. Bioenerg.* 42 (1997) 7–13.

[Dong, 2006]: T. Ahuja, I.A. Mir, D. Kumar, Rajesh, Sensitive amperometric immunosensing using polypyrrolepropionic acid films for biomolecule immobilization, *Anal. Chem.* 78 (2006) 7424–7431.

[Drake, 2006]: R.R. Drake, E.E. Schwegler, G. Malik, J. Diaz, T. Block, A. Mehta, O.J. Semmes, Lectin capture strategies combined with mass spectrometry for the discovery of serum glycoprotein biomarkers, *Mol. Cell. Proteom.* 5 (2006) 1957–1967.

[Duff, 2003]: S.E. Duff, C. Li, J.M. Garland, S. Kumar, CD105 is important for angiogenesis: evidence and potential applications, *FASEB J.* 17 (2003) 984–992.

[Dziegielewska, 1990]: K.M. Dziegielewska, W.M. Brown, S.J. Casey, D.L. Christie, R.C. Foreman, R.M. Hill, N.R. Saunders, The complete cDNA and amino acid sequence of bovine fetuin, *J. Biol. Chem.* 265 (1990) 4354–4357.

E

[Eagle Bioscience 8IS39-K01 0]: 8-isoprostane ELISA Assay Kit *(https://eaglebio.com/product/8-isoprostane-elisa-assay-kit/)*

[Eagle Biosciences FET39-K01]: Human Fetuin A ELISA Assay Kit *(https://eaglebio.com/product/fetuin-a-elisa-assay-kit/)*

[Ealick, 1991]: S.E. Ealick, W.J. Cook, S. Vijay-Kumar, M. Carson, T.L. Nagabhushan, P.P. Trotta, C.E. Bugg, Three-dimensional structure of recombinant human interferon-gamma, *Science* 252 (1991) 698–702.

[eBioscience 88-7346]: Human TNF-α ELISA Kit *(https://www.thermofisher.com/elisa/product/TNF-alpha-Human-Uncoated-ELISA-Kit-with-Plates/88-7346-22)*

[EIAab E0701h]: Human 8-isoprostane ELISA Kit *(http://eiaab.com/UploadFiles//2010922594664204.pdf)*

[El Ayadi, 2018]: A. El Ayadi, D.N. Herndon, C.C. Finnerty, Biomarkers in burn patient care in D.N. Herndon, Total burn care, 5th Edition, *Elsevier* (2018) 232–235.

[Elabscience E-EL-H0108]: Human IFN-γ ELISA Kit *(https://www.elabscience.com/p-human_ifn_%CE%B3(interferon_gamma)_elisa_kit-17971.html)*

[Eletxigerra, 2014]: U. Eletxigerra, J. Martínez-Perdiguero, S. Merino, R. Villalonga, J.M. Pingarrón, S. Campuzano, Amperometric magnetoimmunoassay for the direct detection of tumor necrosis factor alpha biomarker in human serum, *Anal. Chim. Acta.* 838 (2014) 37–44.

[Eletxigerra, 2016]: U. Eletxigerra, J. Martínez-Perdiguero, S. Merino, R. Barderas, V. Ruiz-Valdepeñas Montiel, J.M. Pingarrón, S. Campuzano, Estrogen receptor α

determination in serum, cell lysates and breast cancer cells using an amperometric magnetoimmunosensing platform, *Sens. Biosensing Res.* 7 (2016) 71–76.

[Eley, 2009]: B.S. Eley, D.W. Beatty, The basic immunology of tuberculosis in H.S. Schaaf, A.I. Zumla, J.M. Grange, M.C. Raviglione, W.W. Yew, J.R. Starke, M. Pai, P.R. Donald, Tuberculosis: a comprehensive clinical reference, 1st Edition, *Saunders* (2009) 75–86.

[Enzo ADI-900-091]: Direct 8-iso-$PGF_{2\alpha}$ ELISA Kit *(http://www.enzolifesciences.com/ADI-900-091/direct-8-iso-pgf2alpha-elisa-kit/)*

[Enzo ADI-900-099]: Human TNF-α ELISA Kit *(http://www.enzolifesciences.com/ADI-900-099/tnf-alpha-human-elisa-kit/)*

[Enzo ADI-900-130]: Human IL-1β ELISA Kit *(http://www.enzolifesciences.com/ADI-900-130A/il-1beta-human-elisa-kit/)*

[Enzo ADI-900-155]: Human TGF-β1 ELISA Kit *(http://www.enzolifesciences.com/ADI-900-155/tgf-beta1-elisa-kit/)*

[Enzo ALX-850-337-KI01]: Human Adiponectin ELISA Kit *(http://www.enzolifesciences.com/ALX-850-377/adiponectin-human-elisa-kit/)*

[Epitope Diagnostics KT-800]: Human Fetuin A ELISA Kit *(http://www.epitopediagnostics.com/kt800)*

F

[Fialkow, 2007]: L. Fialkow, Y. Wang, G.P. Downey, Reactive oxygen and nitrogen species as signaling molecules regulating neutrophil function, *Free Radic. Biol. Med.* 15 (2007) 153–164.

[Fragoulis, 2008]: G.E. Fragoulis, H.M. Moutsopoulos, Chronic inflammation (inflammaging) and its potential contribution to age-associated diseases, *J. Gerontol. A Biol. Sci. Med. Sci.* 69 (2014) S4–S9.

[Franceschi, 2014]: C. Franceschi, J. Campisi, Inflammation and aging, *Arch. Hellen. Med.* 25 (2014) 24–32.

[Frijhoff, 2015]: J. Frijhoff, P.G. Winyard, N. Zarkovic, S.S. Davies, R. Stocker, D. Cheng, A.R. Knight, E.L. Taylor, J. Oettrich, T. Ruskovska, A.C. Gasparovic, A. Cuadrado, D. Weber, H.E. Poulse, T. Grune, H.H.H.W. Schmidt, P. Ghezzi, Clinical relevance of biomarkers of oxidative stress, *Antioxid. Redox Signal.* 23 (2015) 1144–1170.

G

[Gagné, 2014]: F. Gagné, Oxidative stress in F. Gagné, Biochemical ecotoxicology: principles and methods, 1st Edition, *Elsevier* (2014) 103–115.

[Gan, 2010]: N. Gan, N.X. Luo, T.H. Li, L. Zheng, M.J. Ni, A non-enzyme amperometric immunosensor or rapid determination of human immunodeficiency virus p24 based on magnetism controlled carbon nanotubes modified printed electrode, *Chin. J. Anal. Chem.* 38 (2010) 1556–1562.

[Gao, 2015]: H. Gao, H. Duan, 2D and 3D graphene materials: preparation and bioelectrochemical applications, *Biosens. Bioelectron.* 65 (2015) 404–419.

[Garzón, 2009]: L. Garzón, Á. Cavero, Eye, light, life and evolution, *Arch. Med.* 1 (2009) 1–6.

[Gebert, 2017]: J. Gebert, M. Schnölzer, U. Warnken, J. Kopitz, Combining click chemistry-based proteomics with dox-inducible gene expression, *Methods Enzymol.* 585 (2017) 295–327.

[Ghallab, 2010]: N.A. Ghallab, N. El-Wakeel, O.G. Shaker, Levels of salivary IFN-gamma, TNF-alfa and TNF receptor-2 as prognostic markers in (erosive) oral lichen planus, *Mediators Inflamm.* 847632 (2010) 1–7.

[Grainger, 1995]: D.J. Grainger, D.E. Mosedale, J.C. Metcalfe, P.L. Weissberg, P.R. Kemp, Active and acid-activatable TGF-β in human sera, platelets and plasma, *Clin. Chim. Acta* 235 (1995) 11–31.

[Grainger, 2000]: D.J. Grainger, D.E. Mosedale, J.C. Metcalfe, TGF-beta in blood: a complex problem, *Cytokine Growth Factor Rev.* 11 (2000) 133–145.

[Green, 2011]: A.A. Green, M.C. Hersam, Properties and application of double-walled carbon nanotubes sorted by outer-wall electronic type, *ACS Nano* 5 (2011) 1459–1467.

[Gong, 2009]: J.L. Gong, B. Wang, G.M. Zeng, C.P. Yang, C.G. Niu, Q.Y. Niu, Y. Zhou, W.J. Liang, Removal of cationic dyes from aqueous solution using magnetic multi-wall carbon nanotube nanocomposite as adsorbent, *J. Hazard. Mater.* 164 (2009) 1517–1522.

[Goustin, 2011]: A.S. Goustin, A.B. Abou-Samra, The "thrifty" gene encoding Ahsg/Fetuin-A meets the insulin receptor: insights into the mechanism of insulin resistance, *Cell. Signal.* 23 (2011) 980–990.

[Guerrero, 2018]: S. Guerrero, L. Agüí, P. Yáñez-Sedeño, J.M. Pingarrón, Screen-printed gold electrodes functionalized with grafted p-aminobenzoic acid for the construction of electrochemical immunosensors. Determination of TGF-β1 cytokine in human plasma, *Electroanal.* 30 (2018) 1327–1335.

[Gulcelik, 2013]: N.E. Gulcelik, M. Halil, S. Ariogui, A. Usman, Adipocytokines and aging: adiponectin and leptin, *Minerva Endocrinol.* 38 (2013) 203–210.

H

[Haldón, 2015]: E. Haldón, M.C. Nicasio, P.J. Pérez, Copper-catalysed azide-alkyne cycloadditions (CuAAC): an update, *Org. Biomol. Chem.* 13 (2015) 9528–9550.

[Halliwell, 1994]: B. Halliwell, C.E. Cross, Oxygen-derived species: their relation to human disease and environmental stress, *Environ. Health Perspect.* 102 (1994) 5–12.

[Hayama, 2010]: S. Hayama, T. Higuchi, H. Miyakoshi, Y. Nakano, Analytical evaluation of a high-molecular.weight (HMW) adiponectin chemiluminescent enzyme immunoassay, *Clin. Chim. Acta* 411 (2010) 2073–2078.

[He, 2017]: Z.Y. He, X.W. Wei, Y.Q. Wei, Recent advances of nanostructures in antimicrobial therapy in A.M. Grumezescu, Antimicrobial nanoarchitectonics. From synthesis to applications, 1st Edition, *Elsevier* (2017) 167–194.

[Hein, 2008]: C.D. Hein, X.M. Liu, D. Wang, Click chemistry, a powerful tool for pharmaceutical sciences, *Pharm. Res.* 25 (2008) 2216–2230.

[Hernández, 2011]: K. Hernández, R. Fernández-Lafuente, Control of protein immobilization: coupling immobilization and site-direct mutagenesis to improve biocatalyst or biosensor performance, *Enzyme Microb. Technol.* 48 (2011) 107–122.

[Hinck, 1996]: A.P. Hinck, S.J. Archer, S.W. Qian, A.B. Roberts, M.B. Sporn, J.A. Weatherbee, M.L. Tsang, R. Lucas, B.L. Zhang, J.Wenker, D.A. Torchia, Transforming growth factor beta 1: three-dimensional structure in solution and comparison with the X-ray structure of transforming growth factor beta 2, *Electrochemistry* 35 (1996) 8517–8534.

[Hirako, 2016]: S. Hirako, Adiponectin in Y. Takei, H. Ando, K. Tsutsui, Handbook of hormones. Comparative endocrinology for basic and clinical research, 1st Edition, *Elsevier* (2016) 308–309.

[Ho, 2013]: E. Ho, K.K. Galougahi, C.C. Liu, R. Bhindi, Biological markers of oxidative stress: applications to cardiovascular research and practice, *Redox Biol.* 1 (2013) 483–491.

[Holban, 2016]: A.M. Holban, A.M. Grumezescu, E. Andronescu, Inorganic nanoarchitectonics designed for drug delivery and anti-infective surfaces in A.M. Grumezescu, Surface chemistry of nanobiomaterials. Applications of nanobiomaterials volume 3, 1st Edition, *Elsevier* (2016) 301–327.

[Hold, 2008]: G.L. Hold, E.M. El-Omar, Genetic aspects of inflammation and cancer, *Biochem. J.* 410 (2008) 225–235.

[Honkanen, 1997]: E. Honkanen, A.M. Teppo, T. Törnroth, P.H. Groop, C. Grönhagen-Riska, Urinary transforming growth factor-β1 in membranous glomerulonephritis, *Nephrol. Dial. Transplant.* 12 (1997) 2562–2568.

[Hou, 2013]: Y. Hou, T. Li, H. Huang, H. Quan, X. Miao, M. Yang, Electrochemical immunosensor for the detection of tumor necrosis factor α based on hydrogel preparaed from ferrocene modified amino acid, *Sens. Actuators B Chem.* 182 (2013) 605–609.

[Hu, 2011]: Y. Hu, Z. Zhao, Q. Wan, Facile preparation of carbon nanotube-conducting polymer network for sensitive electrochemical immunoassay of Hepatitis B surface antigen in serum, *Bioelectrochem.* 81 (2011) 59–64.

[Huang, 2015]: H. Huang, R. Yan, M. Liu, J. Zhou, J. Tan, X. Zhang, X.H. Hu, Y. Huang, W. He, J. Wu, G. Luo, Role of dentritic epidermal T lymphocytes in immune rejection of skin allograft in mice and its mechanism, *Zhonghua Shao Shang Za Zhi* 31 (2015) 125–129.

[Huddam, 2013]: B. Huddam, A. Azak, G. Koçak, N. Bayraktar, S. Sezer, The relationship between serum fetuin-a, cystatin.-c levels, and microalbuminaria in patients with metabolic syndrome, *J. Clin. Lab. Anal.* 27 (2013) 317–322.

[Hummers, 1958]: W.S. Hummers, R.E. Offerman, Preparation of graphitic oxide, *J. Am. Chem. Soc.* 80 (1958) 1339.

[Hycult Biotech HK307-01]: Human TNF-α ELISA Kit *(https://www.hycultec.de/hk307-01)*

[Ijzermans, 1989]: J.N.M. Ijzermans, R.L. Marquet, Interferon-gamma: a review, *Immunobiol.* 179 (1989) 456–473.

[Invitrogen BMS224-2]: Human IL-1β ELISA Kit *(https://www.thermofisher.com/elisa/product/IL-1-beta-Human-ELISA-Kit/BMS224-2)*

[Invitrogen BMS249-4]: Human TGF-β1 ELISA Kit *(https://www.thermofisher.com/elisa/product/TGF-beta-1-Human-ELISA-Kit/BMS249-4)*

[Invitrogen BMS2065TEN]: Human TGF-β1 (LAP) ELISA Kit *https://www.thermofisher.com/elisa/product/TGF-beta-1-LAP-Human-ELISA-Kit/BMS2065TEN)*

[Invitrogen KHP0041]: Human Adiponectin ELISA Kit *(https://www.thermofisher.com/elisa/product/Adiponectin-Human-ELISA-Kit/KHP0041)*

J

[Jackson, 2013]: P. Jackson, N.R. Jacobsen, A. Baun, R. Birkedal, D. Kühnel, K.A. Jensen, U. Vogel, H. Wallin, Bioaccumulation and ecotoxicity of carbon nanotubes, *Chem. Cent. J.* 7 (2013) 154.

[Jahnen-Dechent, 2011]: W. Jahnen-Dechent, A. Heiss, C. Schäfer, M.Ketteler, Fetuin-A regulation of calcified matrix metabolism, *Circ. Res.* 108 (2011) 1494–1509.

[Jia, 2008]: J. Jia, Hydrogen peroxide biosensor based on horseradish peroxidase-Au nanoparticles al t viologen grafted glassy carbon electrode, *Microchim. Acta* 163 (2008) 237–241.

[Ju, 2017]: H. Ju, G. Lai, F. Yan, Introduction in H. Ju, G. Lai, F. Yan, Immunosensing for detection of protein biomarkers, 1st Edition, *Elsevier* (2017) 1–30.

[Jura, 2016]: M. Jura, L.P. Kozak, Obesity and related consequences to ageing, *Age* 38 (2016) 1–18.

K

[Kak, 2018]: G. Kak, M. Raza, B.K. Tiwari, Interferon-gamma (IFN-γ): exploring its implications in infectious diseases, *Biomol. Concepts* 9 (2018) 64–79.

[Kalabay, 2002]: L. Kalabay, L. Jakab, Z. Prohaszka, G. Fust, Z. Benko, L. Telegdy, Z. Lorincz, P. Zavodoszky, P. Arnaud, B. Fekete, Human fetuin/alpha2HS-glycoprotein level as a novel indicator of liver cell function and short-term mortality in patients with liver cirrhosis and liver cancer, *Eur. J. Gastroenterol. Hepatol.* 14 (2002) 389–394.

[Karabakan, 2016]: M. Karabakan, A. Bozkurt, M. Gunay, B.K. Aktas, E. Hirik, M. Aydin, B. Nuhoglu, Association between serum fetuin-A level and erectile function, *Andrologia* 48 (2016) 787–792.

[Karak, 2012]: N. Karak, Vegetable oil-based polymer nanocomposites in N. Karak, Vegetable oil-based polymers. Properties, processing and applications, 1st Edition, *Woodhead Publishing* (2012) 271–309.

[Karandikar, 2017]: S. Karandikar, A. Mirani, V. Waybhase, V.B. Petravale, S. Patankar, Nanovaccines for oral delivery-formulation strategies and challenges in E. Andronescu, A.M. Grumezescu, Nanostructures for oral medicine. A volume in micro and nano technologies, 1st Edition, *Elsevier* (2017) 263–293.

[Karousis, 2016]: N. Karousis, I. Suarez-Martinez, C.P. Ewel, N. Tagmatachis, Structure, properties, functionalization, and applications of carbon nanohorns, *Chem. Rev.* (2016) 4850–4883.

[Kim, 2010]: I.T. Kim, G.A. Nunnery, K. Jacob, J. Schwartz, X. Liu, R. Tannenbaum, Synthesis, characterization, and alignment of magnetic carbon nanotubes tethered with maghemite nanoparticles, *J. Phys. Chem.* 114 (2010) 6944–6951.

[Kirkwood, 2009]: T.B.L. Kirkwood, Genetic of age-dependent human disease in J.F. Halter, J.G. Ouslander, M.E. Tinetti, S.Studenski, K.P. High, S. Asthana Hazzard's geriatric medicine and gerontology, 6th Edition, *McGraw-Hill Medical* (2009) 15–21.

[Klein, 2016]: S. Klein, J.A. Romjin, Obesity in S. Melmed, K.S. Polonsky, R.R. Larsen, H.M. Kronenberg, Williams textbook of endocrinology, 13th Edition, *Elsevier* (2016) 1633–1659.

[Koch, 2000]: A.E: Koch, The role of angiogenesis in rheumatoid arthritis: recent developments, *Ann. Rheum. Dis.* 59 (2000) i65–i71.

[Kongsuphol, 2014]: P. Kongsuphol, H. Hwee Ng, J.P. Pursey, S.K. Arya, C.C. Wong, E. Stulz, M.K. Park, EIS-based biosensor for ultra-sensitive detection of TNF-α from non-diluted human serum, *Biosens. Bioelectron.* 61 (2014) 274–279.

[Kramer, 2016]: I.M. Kramer, TGFβ and signaling through receptor serine/threonine protein kinases in I.M. Kramer, Signal transduction, 3rd Edition, *Elsevier* (2016) 887–933.

[Krause, 2015]: C.E. Krause, B.A. Otieno, G.W. Bishop, G. Phadke, L. Choquette, R.V. Lalla, D.E. Peterson, J.F. Rusling, Ultrasensitive microfluidic array for serum pro-inflammatory

cytokines and C-reactive protein to assess oral mucositis risk in cancer patients, *Anal. Bioanal. Chem.* 407 (2015) 7239–7243.

[Kropf, 1997]: J. Kropf, J.O. Schurek, A. Wollner, A. Gressner, Immunological measurement of transforming growth factor-beta I (TGF-β1) in blood; assay development and comparison, *Clin. Chem.* 43 (1997) 1965–1974.

L

[Lacy, 2017]: P. Lacy, Eosinophil cytokines in allergy in M. Foti, M. Locati, Cytokine effectors functions in tissues, 1st Edition, *Elsevier* (2017) 173–218.

[Le, 2013]: H.T. Le, J.G. Jang, J.Y. Park, C.W. Lim, T.W. Kim, Antibody functionalization with a dual reactive hydrazine/click crosslinker, *Anal. Biochem.* 435 (2013) 68–73.

[Lebreton, 1979]: J. Lebreton, F. Joisel, J. Raoult, B. Lannuzel, J. Rogez, G. Humbert, Serum concentration of human alpha 2 HS glycoprotein during the inflammatory process: evidence that alpha 2 HS glycoprotein is a negative acute-phase reactant, *J. Clin, Invest.* 64 (1979) 1118–1129.

[Lee, 2016]: D. Lee, Y.H. Kim, S. Park, Enzyme electrode platform using methyl viologen electrochemically immobilized on carbon materials, *J. Electrochem. Soc.* 163 (2016) G93–G98.

[Li, 2012]: T. Li, Z. Si, L. Hu, H. QI, M. Yang, Prussian Blue-functionalized ceria nanoparticles as label for ultrasensitive detection of tumor necrosis factor-α, *Sens. Actuators B Chem.* 171–172 (2012) 1060–1065.

[Liang, 2014]: J. Liang, Z. Wang, G. Liu, J. Zhan, L. Jiang, Z. Jiang, Association of dialysate calcium concentration with fetuin A level and carotid intima-media thickness in peritoneal dialysis patient, *Ren. Fail.* 36 (2014) 65–68.

[Liébana, 2016]: S. Liébana, G.A. Drago, Bioconjugation and stabilisation of biomolecules in biosensors, *Essays Biochem.* 60 (2016) 59–68.

[Lim, 2007]: P. Lim, J.P. Collet, S. Moutereau, N. Guigui, L. Mitchell-Heggs, S. Loric, M. Bernard, S. Benhamed, G. Montalescot, J.L. Rande, P. Gueret, Fetuin-A is an independent predictor of death after ST-elevation myocardial infarction, *CLin, Chem.* 53 (2007) 1835–1840.

[Liu, 2000]: J. Liu, L. Cheng, B. Liu, S. Dong, Covalent modification of a glassy carbon surface by 4-aminobenzoic acid and its application in fabrication of a polyoxometalates-consisting monolayer and multilayer films, *Langmuir* 16 (2000) 74718–7476.

[Liu, 2009]: W. Liu, J.D. Morrow, H. Yin, Quantification of F_2-isoprostanes as reliable index of oxidative stress *in vivo* using gas chromatography-mass spectrometry (GC-MS) method, *Free Radic. Biol. Med.* 15 (2009) 1101–1107.

[Liu, 2010]: X. Liu, H. Li, F. Wang, S. Zhu, Y. Wang, G. Xu, Functionalized single-walled carbon nanohorns for electrochemical bioensing, *Biosens. Bioelectron.* 25 (2010) 2194–2199.

[Liu, 2010b]: Y. Liu, N. Tuleouva, E. Ramanculov, A. Revzin, Aptamer-based electrochemical biosensor for interferon gamma detection, *Anal. Chem.* 82 (2010) 8131–8136.

[Liu, 2014]: C.C. Liu, S. Sadhasivan, S. Savitha, F.H. Lin, Fabrication of multiwalled carbon nanotubes.magnetite nanocomposite as an effective ultra-sensing platform for the early screening of nasopharyngeal carcinoma by luminescence immunoassay, *Talanta* 122 (2014) 195–200.

[Liu, 2015]: C. Liu, G. Xiang, D. Jiang, L. Liu, F. Liu, F. Luo, X. Pu, An electrochemical aptasensor detection of IFN-γ using graphene and a dual signal amplification strategy based on the exonuclease-mediated surface-initiated enzymatic polymerization, *Analyst* 140 (2015) 7784–7791.

[Lopez-Castejon, 2011]: G. Lopez-Castejon, D. Brough, Understanding the mechanism of IL-1β secretion, *Cytokine Growth Factor Rev.* 22 (2011) 189–195.

[LSBio LS-F567]: Human IFN-γ ELISA Kit *(https://www.lsbio.com/elisakits/human-ifn-gamma-interferon-gamma-elisa-kit-sandwich-elisa-ls-f567/567)*

[LSBio LS-F2548]: Human TGF-β1 ELISA Kit *(https://www.lsbio.com/elisakits/human-tgfb1-tgf-beta-1-elisa-kit-sandwich-elisa-ls-f2548/2548)*

[LSBio LS-F2668]: Human AHSG/Fetuin A ELISA Kit *(https://www.lsbio.com/elisakits/human-ahsg-fetuin-a-elisa-kit-sandwich-elisa-ls-f2668/2668)*

[Ludwig, 1980]: F.C. Ludwig, M.E. Smoke, The measurement of biological age, *Exp. Aging Res.* 6 (1980) 497–522.

M

[Maeda, 1998]: H. Maeda, T. Akaike, Nitric oxide and oxygen radicals in infection, inflammation and cancer, *Biochemistry* 63 (1998) 854–865.

[Mak, 2006]: T.W. Mak, M.E. Saunders, Cytokines and cytokines receptors in T.W. Mak, M.E. Saunders, The immune response. Basic and clinical principles, 1st Edition, *Elsevier* (2006) 463–516.

[Maring, 2012]: J.A. Maring, M. Trojanowska, P. ten Dijke, Role of endoglin in fibrosis and scleroderma, *Int. Rev. Cel. Mol. Bio.* 297 (2012) 295–308.

[Markey, 2017]: K.A. Markey, G.R. Hill, Cytokines in hematopoietic stem cell transplantation in M. Foti, M. Locati, Cytokine effector functions in tissues, 1st Edition, *Academic Press* (2017) 219–236.

[Martins, 2015]: V.L. Martins, M.P. Caley, K. Moore, Z. Szentpetery, S.T. Marsh, D.F. Murrell, M.H. Kim, M. Avari, J.A. McGrath, R. Cerio, A. Kivisaari, V.M. Kähäri, K. Hodivala-Dilke, C.H. Brennan, M. Chen, J.F. Marshall, E.A. O'Toole, Suppression of TGFβ and angiogenesis by type VII collagen in cutaneous SCC, *J. Natl. Cancer Inst.* 108 (2015) 1–11.

[Matharu, 2014]: Z. Matharu, D. Patel, Y. Gao, A. Haque, Q. Zhou, A. Revzin, Detecting TGF-β release from liver cells using an aptasensor integrated with microfluidics, *Anal. Chem.* 86 (2014) 8865–8872.

[Mazloum-Ardakani, 2014]: M. Mazloum-Ardakani, L. Hosseinzadeh, Z. Taleat, Two kinds of electrochemical immunoassays for the tumor necrosis factor α in human serum using screen-printed graphite electrodes modified with poly(anthranilic acid), *Microchim. Acta* 181 (2014) 917–924.

[Mazloum-Ardakani, 2015]: M. Mazloum-Ardakani, L. Hosseinzadeh, A. Khoshroo, Label-free electrochemical immunosensor for detection of tumor necrosis factor α based on fullerene-functionalized carbon nanotubes/ionic liquid, *J. Electroanal. Chem.* 757 (2015) 58–64.

[Mazloum-Ardakani, 2015b]: M. Mazloum-Ardakani, L. Hosseinzadeh, K. Khoshroo, Ultrasensitive electrochemical immunosensor for detection of tumor necrosis factor-α based on functionalized MWCNT-gold nanoparticle/ionic liquid nanocomposite, *Electroanal.* 27 (2015) 2518–2526.

[McEnaney, 1999]: B. McEnaney, Structure and bonding in carbon materials in T.D. Burchell, Carbon materials for advanced technologies, 1st Edition, *Elsevier* (1999) 1–33.

[McInnes, 2017]: I.B. McInnes, Cytokines in G.S. Firestein, R.C. Budd, S.E. Gabriel, I.B. McInnes, J.R. O'Dell Kelley and Firestein's Textbook of rheumatology, 10th Edition, *Elsevier* (2017) 396–407.

[Mercodia 10-1193-01]: Human Adiponectin ELISA Kit *(http://diagenics-co-uk.s3.amazonaws.com/documents/mercodia-10119301.pdf)*

[Merrill, 1993]: J.E. Merrill, O. Martínez-Maza, Cytokines in AIDS-associated nervous and immune system dysfunction, *Meth. Neuroscience* 17 (1993) 243–266.

[Mesiano, 2019]: S. Mesiano, Endocrinology of human pregnancy and fetal-placental neuroendocrine development in J.F. Strauss III, R.L. Barbieri, Yen and Jaffe's reproductive endocrinology, 8th Edition, *Elsevier* (2019) 256–284.

[Messini, 2013]: I.E. Messini, C.I. Messini, K. Dafopoulos, Obesity in PCOS and infertility in T. Mahmood, S. Arulkumaran, Obesity, 1st Edition, *Elsevier* (2013) 99–116.

[Milne, 2011]: G.L. Milne, H. Yin, K.D. Hardy, S.S. Davies, L.J. Roberts II, Isoprostane generation and function, *Chem. Rev.* 111 (2011) 5973–5996.

[Min, 2008]: K. Min, M. Cho, S.Y. Han, Y.B. Shim, J. Ku, C. Ban, A simple and direct electrochemical detection of interferon-γ using its RNA and DNA aptamers, *Biosens. Bioelectron.* 23 (2008) 1819–1824.

[Miyawaki, 2008]: J. Miyawaki, M. Yudasaka, T. Azami, Y. Kubo, S. Iijima, Toxicity of single-walled carbon nanohorns, *ACS Nano* 2 (2008) 213–226.

[Mizuno, 2015]: K. Mizuno, H. Kataoka, Analysis of urinary 8-isoprostane as an oxidative stress biomarker by stable isotope dilution using automated online in-tube solid-phase microextraction coupled with liquid chromatography-tandem mass spectrometry, *J. Pharm. Biomed. Anal.* 112 (2015) 36–42.

[Montuschi, 1999]: P. Montuschi, M. Corradi, G. Ciabattoni, J. Nightingale, S.A. Kharitonov, P.J. Barnes, Increased 8-isoprostane, a marker of oxidative stress, in exhaled condensate of asthma patients, *Am. J. Respir. Crit. Care Med.* 160 (1999) 216–220.

[Moreno-Guzmán, 2012]: M. Moreno-Guzmán, I. Ojeda, R. Villalonga, A. González-Cortés, P. Yáñez-Sedeño, J.M. Pingarrón, Ultrasensitive detection of adrenocorticotropin hormone (ACTH) using disposable phenylboronic-modified electrochemical immunosensors, *Biosens. Bioelectron.* 35 (2012) 82–86.

[Morrow, 1990]: J.D. Morrow, K.E. Hill, R.F. Burk, T.M. Nammour, K.F. Badr, L.J. Roberts II, A series of prostaglandin F2-like compounds ate produced in vivo in humans by a non-cyclooxygenase, free radical-catalyzed mechanism, *Proc. Natl. Acad. Sci.* 87 (1990) 9383–9387.

[Moschou, 2016]: D. Moschou, L. Greathead, P. Pantelidis, P. Kelleher, H. Morgan, T. Prodromakis, Amperometric IFN-γ immunosensors with commercially fabricated PCB sensing electrodes, *Biosens. Bioelectron.* 86 (2016) 805–810.

[Muir, 2007]: B.W. Muir, M.C. Barden, S.P. Collet, A.D. Gorse, R. Monteiro, L. Yang, N.A.M. McDougall, S. Gould, N.J. Maeji, High-throughput optimization of surfaces for antibody immobilization using metal complexes, *Anal. Biochem.* 363 (2007) 97–107.

[Musi, 2014]: N. Musi, R. Guardado-Mendoza, Adipose tissue as an endocrine organ in A. Ulloa-Aguirre, P.M. Conn, Cellular endocrinology in health and disease, 1st Edition, *Elsevier* (2014) 229–237.

[MyBioSource MBS703511]: Human Endoglin ELISA Kit *(https://www.mybiosource.com/eng-human-elisa-kits/endoglin/703511)*

N

[Nagaraj, 2010]: V.J. Nagaraj, S. Aithal, S. Eaton, M. Bothara, P. Wiktor, S. Prasad, NanoMonitor: a miniature electronic biosensor for glycan biomarker detection, *Nanomed.* 5 (2010) 369–378.

[Nassiri, 2011]: F. Nassiri, M.D. Cusimano, B.W. Scheithauer, F. Rotondo, A. Fazio, G.M. Yousef, L.V. Syro, K. Kovacs, R.V: Lloyd, Endoglin (CD105): a review of its role in angiogenesis and tumor diagnosis, progression and therapy, *Anticancer Res.* 31 (2011) 2283–2290.

[Novoselov, 2008]: K.S. Novoselov, P. Blake, M.I. Katsnelson, Graphene: electronic properties in K.H.J. Buschow, R.W. Cahn, M.C. Flemings, B. Ilschner, E.J. Kramer, S. Mahajan, P. Veyssière, Encyclopedia of materials: science and technology, 2nd Edition, *Elsevier* (2008) 1–6.

[Novus Biologicals NBP1-83741]: Human TNF-α ELISA Kit (Colorimetric) *(https://www.novusbio.com/products/tnf-alpha-elisa-kit_nbp1-83741)*

[Novus Biologicals NBP1-91174]: Human IFN-γ ELISA Kit (Colorimetric) *(https://www.novusbio.com/products/ifn-gamma-elisa-kit_nbp1-91174)*

O

[Oettgen, 2012]: H. Oettgen, D.H. Broide, Introduction to mechanism of allergic disease in S.T. Holgate, M.K. Church, D.H. Broide, F.D. Martínez, Allergy, 4th Edition, *Elsevier* (2012) 1–32.

[Ojeda, 2014]: I. Ojeda, B. Garcinuño, M. Moreno-Guzmán, A. González-Cortés, M. Yudasaka, S. Iijima, F. Langa, P. Yáñez-Sedeño, J.M. Pingarrón, Carbon nanohorns as a scaffold for the construction of disposable electrochemical immunosensing platforms. Application to the determination of fibrinogen in human plasma and urine, *Anal. Chem.* 86 (2014) 7749–7756.

[Ojeda, 2015]: I. Ojeda, M. Barrejón, L.M. Arellano, A. González-Cortés, P. Yáñez-Sedeño, F. Langa, J.M. Pingarrón, Grafted-double walled carbon nanotubes as electrochemical platforms for immobilization of antibodies using a metallic-complex chelating polymer:

application to the determination of adiponectin cytokine in serum, *Biosens. Bioelectron.* 74 (2015) 24–29.

[Oliveira, 2018]: W.F: Oliveira, G.M.M. Silva, P.E. Cabral, M.D.L. Oliveira, C.A.S. Andrade, M.V. Silva, L.C.B.B. Coelho, G. Machado, M.T.S. Correira, Titanium dioxide nanotubes functionalized with cratylia mollis seed lectin, cramoll, enhanced osteoblast-like cells adhesion and proliferation, *Mater. Sci.Eng. C Mater. Biol. Appl.* 1 (2018) 664–672.

[Ooi, 2014]: H.W. Ooi, S.J. Cooper, C.Y. Huang, D. Jennins, E. Chung, N.J. Maeji, A.K. Whittaker, Coordination complexes as molecular glue for immobilization of antibodies on cyclic olefin copolymer surfaces, *Anal. Biochem.* 456 (2014) 6–13.

[Opal, 2000]: S.M. Opal, V.A. DePalo, Anti-inflammatory cytokines, *Chest.* 117 (2000) 1162–1172.

[Origene EA100480]: Human AHSG/Fetuin A ELISA Kit *(http://www.origene.com.cn/assets/Documents/ELISA%20Kits/EA100480.pdf)*

P

[Pal, 2012]: D. Pal, S. Dasgupta, R. Kundu, S. Maitra, G. Das, S. Mukhopadhyay, S. Ray, S.S. Majumdar, S. Bhattacharya, Fetuin-A acts as an endogenous ligand of TLR4 to promote lipid-induced insulin resistance, *Nat. Med.* 18 (2012) 1279–1285.

[Park, 2011]: S.J. Park, M.K. Seo, Comprehension of nanocomposites, *Interface Sci. Technol.* 18 (2011) 777–819.

[Pei, 2012]: S. Pei, H.M. Cheng, The reduction of graphene oxide, *Carbon* 50 (2012) 3210–3228.

[Peral de Castro, 2015]: C. Peral de Castro, S.A. Jones, J. Harris, Autophagy controls the production and secretion of IL-1β: underlying mechanisms in M.A. Hayat Autophagy: cancer, other pathologies, inflammation, immunity, infection, and aging. Volume 6: regulation of autophagy and selective autophagy, 1st Edition, *Elsevier* (2015) 201–209.

[Peralta-Zaragoza, 2001]: O. Peralta-Zaragoza, A. Lagunas-Martínez, V. Madrid-Marina, Transforming growth factor beta-1: structure, function and regulation mechanisms in cancer, *Salud Pública Mex.* 43 (2001) 340–351.

[Perkin Elmer AL209C]: Human Adiponectin AlphaLISA Detection Kit *(https://www.perkinelmer.com/es/product/alphalisa-adiponectin-kit-500-assay-pts-al209c)*

[Phoenix Pharmaceuticals EK-ADI-01]: Human Adiponectin globular form ELISA Kit *(https://phoenixpeptide.com/products/view/Assay-Kits/EK-ADI-01)*

[Piro, 2017]: B. Piro, S. Reisberg, Recent advances in electrochemical immunosensors, *Sensors* 17 (2017) 794.

[Porwal, 2017]: M. Porwal, V. Rastogi, A. Kumar, An overview on carbon nanotubes, *Bioequiv. Availab.* 3 (2017) 114–116.

[Pospieszny, 2015]: T. Pospieszny, Steroidal conjugates: synthesis, spectroscopic, and biological studies, *Stud. Nat. Prod. Chem.* 46 (2015) 169–200.

[Praticò, 2002]: D. Praticò, Oxidative imbalance and lipid peroxidation in Alzheimer's disease, *Drug Dev. Res.* 56 (2002) 446–451.

[Prosnitz, 2018]: A. Prosnitz, J.R. Gruen, V. Bhandari, The basic immunology of tuberculosis in R. Pyeritz, B. Korf, W. Grody, Emery and Rimoin's principles and practice of medical genetics and genomics, 7th Edition, *Academic Press* (2018) 1–22.

[Pui, 2013]: T.S. Pui, P. Konsuphol, S.K. Arya, T. Bansal, Detection of tumor necrosis factor (TNF-α) in cell culture medium with label free electrochemical impedance spectroscopy, *Sens. Actuators B Chem.* 181 (2013) 494–500.

[Pumera, 2007]: M. Pumera, Carbon nanotubes contain residual metal catalyst nanoparticles even after washing with nitric acid at elevated temperature because these metal nanoparticles are sheathed by several graphene sheets, *Langmuir* 23 (2007) 6453–6458.

[Punbusayakul, 2013]: N. Punbusayakul, S. Talapatra, M. Ajayan, W. Surareungchai, Label-free as-grown double wall carbon nanotubes bundles for *Salmonella typhimurium* immunoassay, *Chem. Cent. J.* 7 (2013) 1–8.

Q

[Qi, 2012]: H. Qi, C. Ling, R. Huang, X. Qiu,, L. Shangguan, Q. Gao, C. Zhang, Functionalization of single-walled carbon nanotubes with protein by click chemistry as sensing platform for sensitized electrochemical immunoassay, *Electrochim. Acta* 63 (2012) 76–82.

[Quintanilla, 2013]: M. Quintanilla, J.R. Ramirez, E. Pérez-Gómez, D. Romero, B. Velasco, M. Letarte, J.M. López-Novoa, C. Bernabéu, Expression of the TGF-β coreceptor endoglin in epidermal keratinocytes and its dual role in multistage mouse skin carcinogenesis, *Oncogene* 22 (2003) 5976–5985.

[Qureshi, 2010]: A. Qureshi, J.H. Niazi, S. Kallempudi, Y. Gurbuz, Label-free capacitive biosensor for sensitive detection of multiple biomarkers using gold interdigitated capacitor arrays, *Biosens. Bioelectron.* 25 (2010) 2318–2313.

R

[Rahim Ruslinda, 2013]: A. Rahim Ruslinda, K. Tanabe, S. Ibori, X. Wang, H. Kawarada, Effects of diamond-FET-based RNA aptamer sensing for detection of real sample of HIV-1 Tat protein, *Biosens. Bioelectron.* 40 (2013) 277–282.

[Ramírez, 2012]: M.M. Ramírez, C. Sánchez, Tumor necrosis factor-α, insulin resistance, the lipoprotein metabolism and obesity in humans, *Nutr. Hops.* 27 (2012) 1751–1757.

[Ravussin, 2016]: E. Ravussin, S.R. Smith, Role of the adipocyte in metabolism and endocrine function in J.L. Jameson, L.J. De Groot, D.M. de Kretser, L.C. Giudice, A.B. Grossman, S. Melmed, J.T. Potts Jr, G.C. Weir, Endocrinology: adult and pediatric, 7th Edition, *Elsevier* (2016) 627–647.

[Ray, 2015]: S.C. Ray, Application and uses of graphene in S.C. Ray, Applications of graphene and graphene-oxide based nanomaterials. A volume in micro and nano technologies, 1st Edition, *William Andrew* (2015) 1–38.

[RayBiotech ELH-Endoglin-1]: Human Endoglin ELISA Kit *(https://www.raybiotech.com/human-endoglin-elisa-kit-for-serum-plasma-cell-culture-supernatants-and-urine/)*

[RayBiotech ELH-IFNg-1]: Human IFN-γ ELISA Kit *(https://www.raybiotech.com/human-ifn-gamma-elisa-kit-for-serum-plasma-cell-culture-supernatant-and-urine/)*

[RayBiotech ELH-IL1b]: Human IL-1β ELISA Kit *(https://www.raybiotech.com/human-il-1-beta-elisa-kit-for-serum-plasma-cell-culture-supernatant-and-urine/)*

[RayBiotech ELH-TGF-b1-1]: Human TGF-β1 ELISA Kit *(https://www.raybiotech.com/human-tgf-beta-1-elisa-kit-for-serum-plasma-cell-culture-supernatants-and-urine/)*

[RayBiotech ELH-TNFa]: Human TNF-α ELISA Kit *(https://www.raybiotech.com/human-tnf-alpha-elisa-kit/)*

[Rea, 2018]: I.M. Rea, D.S. Gibson, V. McGilligan, S.E. McNerlan, H.D. Alexander, O.A. Ross, Age and age-related diseases: role of inflammation triggers and cytokines, *Front. Immunol.* 9 (2018) 586.

[Reed, 1999]: C. Reed, Z.Q. Fu, J. Wu, Y.N. Xue, R.W. Harrison, M.J. Chen, I.T. Weber, Crystal structure of TNF-alpha mutant R31D with greater affinity for receptor R1 compared with R2, *Protein Eng.* 10 (1999) 1101–1107.

[Reff, 1982]: M.E. Reff, E.L. Schneider, Biological markers of aging, *NIH Publication* 82-2221 (1982).

[Reynolds, 2005]: J.L. Reynolds, J.N. Skepper, R. McNair, T. Kasama, K. Gupta, P.L. Weissberg, W. Jahnen-Dechent, C.M. Shanahan, Multifunctional roles for serum protein fetuin-a inhibition of human vascular smooth muscle cell calcification, *J. Am. Soc. Nephrol.* 16 (2005) 2920–2930.

[Rho, 2009]: J. Rho, M.H.A. Roehrl, J.Y. Wang, Glycoproteomic analysis of human lung adenocarcinomas using glycoarrays and tandem mass spectrometry: differential expression and glycosylation patterns of vimentin and fetuin A isoforms, *Protein J.* 28 (2009) 148–160.

[Robinson, 2016]: K.N. Robinson, M. Teran-Garcia, From infancy to aging: biological and behavioral modifiers of Fetuin-A, *Biochimie.* 124 (2016) 141–149.

[Rossi, 2012]: E. Rossi, C. Langa, A. Gilsanz, F.J. Blanco, J. Ayllón, E. Villar, L.M. Botella, C. Cabañas, M. Shaw, C. Bernabeu, Characterization of chicken endoglin, a member of the zona pellucida family of proteins, and its tissue expression, *Gene* 491 (2012) 31–39.

[Rossi, 2013]: E. Rossi, F. Sanz-Rodriguez, N. Eleno, A. Düwell, F.J. Blanco, C. Langa, L.M. Botella, C. Cabañas, J.M. López-Novoa, C. Bernabeu, Endothelial endoglin is involved in inflammation: role in leukocyte adhesion and transmigration, *Blood* 121 (2013) 403–415.

[Ruecha, 2019]: N. Ruescha, K. Shin, O. Chailapakul, N. Rodthongkum, Label-free paper-based electrochemical impedance immunosensor for human interferon gamma detection, *Sens. Actuators B Chem.* 279 (2019) 298–304.

[Ryan, 2004]: K.A. Ryan, M.F. Smith, M.K. Sanders, P.B. Ernst, Reactive oxygen and nitrogen species differentially regulate Toll-like receptor 4-mediated activation of NF-kappa B and interleukin-8 expression, *Infect. Immun.* 72 (2004) 2123–2130.

[Ryffel, 1993]: B. Ryffel, Pathology induced by inflammatory cytokines: introduction, *Int. Rev. Exp. Pathol.* 34 (1993) 3–6.

[R&D Systems DB100B]: Human TGF-β1 Quantikine ELISA Kit *(https://www.rndsystems.com/products/human-tgf-beta-1-quantikine-elisa-kit_db100b)*

[R&D Systems DIF50]: Human IFN-γ Quantikine ELISA Kit *(https://www.rndsystems.com/products/human-ifn-gamma-quantikine-elisa-kit_dif50)*

[R&D Systems DFTA00]: Human Fetuin A Quantikine ELISA Kit *(https://www.rndsystems.com/products/human-fetuin-a-quantikine-elisa-kit_dfta00)*

[R&D Systems DLB50]: Human IL-1β Quantikine ELISA Kit *(https://www.rndsystems.com/products/human-il-1-beta-il-1f2-quantikine-elisa-kit_dlb50)*

[R&D Systems DNDG00]: Human Endoglin/CD105 Quantikine ELISA Kit *(https://www.rndsystems.com/products/human-endoglin-cd105-quantikine-elisa-kit_dndg00)*

S

[Saito, 2017]: T. Saito, M. Bokhove, R. Croci, S. Zamora-Caballero, L. Han, M. Letarte, D. de Sanctis, L. Jovine, Structural basis of the human endoglin-BMP9 interaction: insights into BMP signaling and HHT1, *Cell. Rep.* 19 (2017) 1917–1928.

[Sakwe, 2010]: A.M. Sakwe, R. Koumangoye, S.J. Goodwin, J. Ochieng, Fetuin-A (α_2HS-glycoprotein) is a major serum adhesive protein that mediates growth signaling in breast tumor cells, *J. Biol. Chem.* 285 (2010) 41827–41835.

[Sánchez-Tirado, 2016]: E. Sánchez-Tirado, A. González-Cortés, P. Yáñez-Sedeño, J.M. Pingarrón, Carbon nanotubes functionalized by click chemistry as scaffolds for the preparation of electrochemical immunosensors. Application to the determination of TGF-beta 1 cytokine, *Analyst* 141 (2016) 5730–5737.

[Sánchez-Tirado, 2017]: E. Sánchez-Tirado, G. Martínez-García, A. González-Cortés, P. Yáñez-Sedeño, J.M. Pingarrón, Electrochemical immunosensor for sensitive determination of transforming growth factor (TGF)-β1 in urine, *Biosens. Bioelectron.* 88 (2017) 9–14.

[Serafín, 2017]: V. Serafín, R.M. Torrente-Rodríguez, M. Batlle, P. García de Frutos, S. Campuzano, P. Yáñez-Sedeño, J.M. Pingarrón, Electrochemical immunosensor for receptor tyrosine kinase AXL using poly(pyrrolepropionic acid)-modified disposable electrodes, *Sens. Actuators B Chem.* 240 (2017) 1251–1256.

[Shapiro, 1998]: L. Shapiro, P.E. Scherer, The crystal structure of a complement-1q family protein suggest an evolutionary link to tumor necrosis factor, *Curr. Biol.* 8 (1998) 335–338.

[Sharma, 2016]: M. Sharma, J.A. McClung, N.G. Abraham, Adiponectin: a mediator of obesity, insulin resistance, diabetes, and the metabolic syndrome in W.S. Aronow, J.A. McClung, Translational research in coronary artery disease. Pathophysiology to treatment, 1st Edition, *Elsevier* (2013) 33–42.

[Shen, 2014]: Y.J. Shen, A.R. Lam, S.W.S. Ho, C.X. Koo, N. Le Bert, S. Gasser, Cancer pathogenesis and DNA sensing in K.J. Ishii, C.K. Tang, Biological DNA sensor. The impact of nucleic acids on diseases and vaccinology, 1st Edition, *Elsevier* (2014) 205–229.

[Shi, 2009]: L. hi, X. Liu, W. Niu, H. Li, S. Han, J. Chen, G. Xu, Hydrogen peroxide biosensor based on direct electrochemistry of soybean peroxidase immobilized on single.walled carbon nanohorn modified electrode, *Biosens. Bioelectron.* 24 (2009) 1159–1163.

[Silva, 2016]: P.M.S. Silva, A.L.R. Lima, B.V.M. Silva, L.C.B.B. Coelho, R.F. Dutra, M.T.S. Correia, Cratylia mollis lectin nanoelectrode for differential diagnostic of prostate cancer and bening prostatic hyperplasia based on label-free detection, *Biosens. Bioelectron.* 85 (2016) 171–177.

[Singh, 2012]: M. Singh, P.K. Sharma, V.K. Garg, S.C. Mondal, A.K. Singh, N. Kumar, Role of fetuin-A in atherosclerosis associated with diabetic patients, *J. Pharm. Pharmacol.* 64 (2012) 1703–1708.

[Smirnov, 2016]: I.V. Smirnov, I.V. Gryazeva, M.P. Samoylovich, L.A. Terekhina, A.A. Pinevich, O.A. Shashkova, I.Y. Krutetskaia, D.I. Sokolov, S.A. Selkov, N.N. Nikolsky, V.B. Klimovich, Different pairs of monoclonal antibodies detect variable amounts of soluble endoglin in human blood plasma, *Immunochem. Immunopathol.* 2 (2016) 473–482.

[Sobrova, 2012]: P. Sobrova, M. Ryvolova, D. Huska, J. Hubalek, I. Provaznik, V. Adam, R. Kizek, Voltammetry of adiponection and its interactions with collagen on a carbon paste electrode at femtogram level, *Int. J. Electrochem. Sci.* 7 (2012) 1–12.

[Sprott, 1985]: R.L. Sprott, E.L. Schneider, Biomarkers of aging in S. Hart, Proceedings of the International Conference on Nutrition and Aging, 1st Edition, *A. R. Liss* (1985) 43–52.

[Stansfield, 2014]: W.E. Stansfield, M. Ranek, A. Pendse, J.C. Schisler, S. Wang, T. Pulinilkunnil, M.S. Willis, The pathophysiology of cardiac hypertrophy and heart failure in M.S. Willis, J.W. Homeister, J.R. Stone, Cellular and molecular pathobiology of cardiovascular disease, 1st Edition, *Elsevier* (2014) 51–78.

[Stefan, 2013]: N. Stefan, H.U. Häring, Circulating fetuin-A and free fatty acids interact to predict insulin resistance in humans, *Nat. Med.* 19 (2013) 394–395.

[Stemcell Technologies #02004]: Human IL-1β ELISA Kit *(https://www.stemcell.com/human-il-1-beta-elisa-kit.html)*

[Sultani, 2012]: M. Sultani, A.M. Stringer, J.M. Bowen, R.J. Gibson, Anti-inflammatory cytokines: important immunoregulatory factors contributing to chemotherapy-induced gastrointestinal mucositis, *Chemother. Res. Prac.* 490804 (2012) 1–11.

[Sun, 2013]: Z.Sun, L. Deng, H. Gan, R. Shen, M. Yang, Y. Zhang, Sensitive immunosensor for tumor necrosis factor α based on dual signal amplification of ferrocene modified

self-assembled peptide nanowire and glucose oxidase functionalized gold nanorod, *Biosens. Bioelectron.* 39 (2013) 215–219.

[Szekanecz, 1995]: Z. Szekanecz, G.K. Haines, L.A. Harlow, M.R. Shah, T.W. Fong, R. Fu, S.J. Lin, G. Rayan, A.E. Koch, Increased synovial expression of transforming growth factor (TGF)-beta receptor endoglin and TGF-beta 1 in rheumatoid arthritis: possible interactions in the pathogenesis of the disease, *CLin. Inmunol. Immunopathol.* 76 (1995) 187–194.

T

[Takahashi, 2001]: N. Takahashi, R. Kawanishi-Tabata, A. Haba, M. Tabata, Y. Haruta, H. Tsai, B.K. Seon, Association of serum endoglin with metastasis in patients with colorectal, breast, and other solid tumors, and suppressive effect of chemotherapy on the serum endoglin, *Clin. Cancer Res.* 7 (2001) 524–532.

[Tanaka, 2004]: H. Tanaka, H. Kanoh, M. El-Merraoui, W.A. Steele, M. Yudasaka, S. Iijima, K. Kaneo, Quantum effects on hydrogen adsorption in internal nanospaces of single-wall carbon nanohorns, *J. Phys. Chem. B* 108 (2004) 17457–17465.

[Tedeschi, 2003]: L. Tedeschi, C. Domenici, A. Ahluwalia, F. Baldini, A. Mencaglia, Antibody immobilisation on fibre optic TIRF sensors, *BIosens. Bioelectron.* 19 (2003) 85–93.

[Teles, 2008]: F.R.R Teles, L.P. Fonseca, Applications of polymers for biomolecule immobilization in electrochemical biosensors, *Mater. Sci. Eng. C* 28 (2008) 1530–1543.

[ThermoFisher EHAHSG]: Human AHSG/Fetuin A ELISA Kit *(https://www.thermofisher.com/elisa/product/ASHG-Fetuin-A-Human-ELISA-Kit/EHAHSG)*

[ThermoFisher EHENG]: Human Endoglin (CD105) ELISA Kit *(https://www.thermofisher.com/elisa/product/Endoglin-CD105-Human-ELISA-Kit/EHENG)*

[ThermoFisher EHIFNG]: Human IFN-γ ELISA Kit *(https://www.thermofisher.com/elisa/product/IFN-gamma-Human-ELISA-Kit/EHIFNG)*

[Torrente-Rodríguez, 2016]: R.M. Torrente-Rodríguez, S. Campuzano, V. Ruiz-Valdepeñas-Montiel, M. Pedrero, M.J. Fernández-Acereño, R. Barderas,

J.M. Pingarrón, Rapid endoglin determination in serum samples using an amperometric magneto-actuated disposable immunosensing platform, *J. Pharm. Biomed. Anal.* 129 (2016) 288–293.

[Tsapenko, 2013]: M.V. Tsapenko, R.E. Nwoko, T.M. Borland, N.V. Voskoboev, A. Pflueger, A.D. Rule, J.C. Lieske, Measurement of urinary TGF-β1 in patients with diabetes mellitus and normal controls, *Clin. Biochem.* 46 (2013) 1430–1435.

[Tuci, 2012]: G. Tuci, C.M.Vinattieri, L. Luconi, M. Ceppatelli, S. Cicchi, A. Brandi, J. Filippi, M. Melucci, G. Giambastiani, "Click" on tubes: a versatile approach towards multimodal functionalization of SWCNTs, *Chem. Eur. J.* 18 (2012) 8454–8463.

U

[USBiological 028519]: Human TGF-β1 ELISA BioAssay™ Kit *(https://www.probiotek.com/productos/reactivos/otros/kit-de-elisa-bioassay-factor-de-crecimiento-transformante-beta-1-tgfb1/)*

[Utsumi, 2005]: S. Utsumi, J. Miyawaki, H. Tanaka, Y. Hattori, T. Itoi, N. Ichikuni, H. Kanoh, M. Yudasaka, S. Iijima, K. Kaneko, Opening mechanism of internal nanoporosity of single-wall carbon nanohorn, *J. Phys. Chem. B* 109 (2005) 14319–14324.

[Uygun, 2018]: Z.O. Uygun, Ç. Şahin, M. Yilmaz, Y. Akçaya, A. Akdemir, F. Sağın, Fullerene-PAMAM(G5) composite modified impedimetric biosensor to detect Fetuin-A in real blood samples, *Anal. Biochem.* 542 (2018) 11–15.

V

[Vaidya, 2010]: V.S. Vaidya, J.V. Bonventre, M.A: Ferguson, Biomarkers of acute kidney injury in C.A. McQueen, Comprehensive toxicology, 2nd Edition, *Elsevier* (2010) 197–211.

[Vashit, 2011]: S.K. Vashit, C.K. Dixit, B.D. MacCraith, R. O'Kennedy, Effect of antibody immobilization strategies on the analytical performance of a surface plasmon resonance-based immunoassay, *Analyst* 136 (2011) 4431–4436.

[Vashit, 2014]: S.K. Vashit, E.M. Schneider, J.H.T. Luong, Surface plasmon resonance-based immunoassay for human fetuin A, *Analyst* 139 (2014) 2237–2242.

[Vashit, 2015]: S.K. Vashit, E.M. Schneider, J.H.T. Luong, Rapid sandwich ELISA-based in vitro diagnostic procedure for the highly-sensitive detection of human fetuin A, *Biosens. Bioelectron.* 67 (2015) 73–78.

[Vassalle, 2003]: C. Vassalle, N. Botto, M.G. Andreassi, S. Berli, A. Biagini, Evidence for enhanced 8-isoprostane plasma levels, as index of oxidative stress in vivo, in patients with coronary artery disease, *Coron. Artery Dis.* 14 (2003) 213–218.

[Vaughan, 2017]: O.R. Vaughan, F.J. Rosario, T.L. Powell, T. Jansson, Regulation of placental amino acid transport and fetal growth, *Prog. Mol. Biol. Transl. Sci.* 145 (2017) 217–251.

[Villarreal, 2017]: C.C. Villarreal, T. Pham, P. Ramnani, A. Mulchandani, Carbon allotropes as sensors for environmental monitoring, *Curr. Opin. Electrochem.* 3 (2017) 106–113.

[Voggu, 2008]: R. Voggu, C.S. Rout, A.D. Franklin, T.S. Fisher, C.N.R. Rao, Extraordinary sensitivity of the electronic structure and properties of single-walled carbon nanotubes to molecular charge-transfer, *J. Phys, Chem. C* 34 (2008) 13053–13056.

[Vukovic, 2014]: P. Vukovic, R. De las Heras, L. Yang, T. Ling, D. Jennins, T. Baumgartner, E. Chung, B.T. Ohse, Y. Gao, S. Cooper, A. Wong, C. Munian, C.Y. Huang, N.J. Maeji, Simple and versatile protein immobilization onto surfaces by multi-point non-covalent metal chelation, *Anteo Diagnostics* (2014).

W

[Walter, 2010]: M.R. Walter, Structure of IFNγ and its receptors in R.A. Bradshaw, E.A. Dennis, Handbook of cell signaling, 2nd Edition, *Academic Press* (2010) 261–263.

[Wang, 1995]: Z. Wang, G. Ciabattoni, C. Créminon, J. Lawson, G.A. Fitzgerald, C. Patrono, J. Maclouf, Immunological characterization of urinary 8-epi-prostaglandin F2 alpha excretion in man, *J. Pharmacol. Exp. Ther.* 275 (1995) 94–100.

[Wang, 2006]: J. Wang, G. Liu, M.H. Engelhard, Y. Lin, Sensitive immunoassay of a biomarker tumor necrosis factor-α based on poly(guanine)-functionalized silica nanoparticle label, *Anal. Chem.* 78 (2006) 6974–6979.

[Wang, 2012]: H. Wang, A.E. Sama, Anti-inflammatory role of fetuin-A in injury and infection, *Curr. Mol. Med.* 12 (2012) 625–633.

[Wang, 2016]: Y. Wang, G.H. Mazurek, E.C. Alocilja, Measurement of interferon gamma concentration using an electrochemical immunosensor, *J. Electrochem. Soc.* 163 (2016) B140–B145.

[Wang, 2017]: X. Wang, X. Han, A. Ma, L. Chen, H. Liang, A. Litifu, F. Xue, Fabrication of electrochemical immunosensor for interferon-γ determination and its application of tuberculosis diagnosis, *Int. J. Electrochem. Sci.* 12 (2017) 7262–7271.

[Weng, 2013]: S. Weng, M. Chen, C. Zhao, A. Liu, L. Lin, Q. Liu, J. Lin. X. Lin, Label-free electrochemical immunosensor based on $K_3[Fe(CN)_6]$ as signal for facile and sensitive determination of tumor necrosis factor-alpha, *Sens. Actuators B Chem.* 184 (2013) 1–7.

[Woods, 2012]: J.A. Woods, K.R. Wilund, S.A. Martin, B.M. Kistler, Exercise, inflammation and aging, *Aging Dis.* 3 (2012) 130–140.

[Wu, 2008]: P. Wu, D.G. Castner, D.W. Grainger, Diagnostic devices as biomaterials: a review of nucleic acid and protein microarray surface performance issues, *J. Biomater. Sci. Polym. Ed.* 19 (2008) 725–753.

[Wu, 2012]: Z.C. Wu, J.T. Yu, Y. Li, L. Tan, Clusterin in Alzheimer's disease, *Adv. Clin. Chem.* 56 (2012) 155–173.

[Wu, 2012b]: K. WU, H. Qiu, J. Hu, N. Sun, Z. Zhu, M. Li, Z. Shi, Electrochemistry of double-wall carbon nanotubes encapsulating C_{60} and their spectral characterization, *Carbon* 50 (2012) 4401–4408.

[Wu, 2013]: C.Y. Wu, J. Martel, W.Y. Cheng, C.C. He, D.M. Ojcius, J.D. Young, Membrane vesicles nucleate mineralo-organic nanoparticles and induce carbonate apatite precipitation in human body fluids, *J. Biol. Chem.* 288 (2013) 30571–30584.

[Wu, 2014]: Y.X. Wu, C.Y. Li, Y.L. Deng, Patients with nephrolithiasis had lower fetuin-A protein level in urine and renal tissue, *Urolithiasis* 42 (2014) 29–37.

X

[Xia, 2015]: J. Xia, D. Song, Z. Wang, F. Zhang, M. Yang, R. Gui, L. Xia, S. Bi, Y. Xia, Y. Li, L. Xia, Single electrode biosensor for simultaneous determination of interferon gamma and lysozyme, *Biosens. Bioelectron.* 68 (2015) 55–61.

[Xia, 2017]: X. Xia, W. Chen, J. McDermott, J.D.J Han, Molecular and phenotypic biomarkers of aging, *F1000Research* 860 (2017) 1–10.

Y

[Yan, 2013]: G.P. Yan, Y.H. Wang, X.X. He, K.M. Wang, J.Q. Liu, Y.D. Du, A highly sensitive label-free electrochemical aptasensor for interferon-gamma detection based on graphene controlled assembly and nuclease cleavage-assisted target recycling amplification, *Biosens. Bioelectron.* 44 (2013) 57–63.

[Yáñez-Sedeño, 2016]: P. Yáñez-Sedeño, A. González-Cortés, L. Agüí, J.M. Pingarrón, Uncommon carbon nanostructures for the preparation of electrochemical immunosensors, *Electroanalysis* 28 (2016) 1679–1691.

[Yáñez-Sedeño, 2017]: P. Yáñez-Sedeño, S. Campuzano, J.M. Pingarrón, Carbon nanostructures for tagging in electrochemical biosensing: a review, *J. Carbon Res.* 3 (2017) 1–30.

[Yao, 2016]: Y. Yao, J. Bao, Y. Lu, D. Zhang, S. Luo, X. Cheng, Q. Zhang, S. Li, Q. Liu, Biomarkers of liver fibrosis detecting with electrochemical immunosensor on clinical serum, *Sens. Actuators B Chem.* 222 (2016) 127–132.

[Yi, 2009]: J.K. Yi, J.W. Chang, W. Han, J.W. Lee, E. Ko, D.H. Kim, J. Bae, J. Yu, C. Lee, M. Yu, D. Noh, Autoantibody to tumor antigen, alpha 2-HS glycoprotein: a novel biomarker of breast cancer screening and diagnosis, *Cancer Epidemiol. Biomark. Prev.* 18 (2009) 1357–1364.

[Yilmaz, 2010]: Y.Yilmaz, O.Yonal, R. Kurt, F. Ari, A.Y. Oral, C.A. Celikel, S. Korkmaz, E. Ulukaya, O. Ozdogan, N. Imeryuz, E. Avsar, C. Kalayci, Serum fetuin A/α2HS-glycoprotein levels in patients with non-alcoholic fatty liver disease: relation with liver fibrosis, *Ann. Clin. Biochem.* 47 (2010) 549–553.

[Yin, 2011]: Z. Yin, Y. Liu, L.P. Jiang, J.J. Zhu, Electrochemical immunosensor of tumor necrosis factor α based on alkaline phosphatase functionalized nanospheres, *Biosens. Bioelectron.* 26 (2011) 1890–1894.

[Yousefzadeh, 2006]: G. Yousefzadeh, B. Larijani, A. Mohammadirad, R. Heshmat, G. Dehghan, R. Rahimi, M. Abdollahi, Determination of oxidative stress status and concentration of TGF-β1 in the blood and saliva of osteoporotic subjects, *Ann. NY Acad. Sci.* 1091 (2006) 142–150.

[Yu, 1999]: B. Yu, M. Blaber, A.M. Groneborn, G.M. Clore, D.L. Caspar, Disordered water within a hydrophobic protein cavity visualized by x-ray crystallography, *Proc. Natl. Acad. Sci. USA* 96 (1999) 103–108.

[Yuanyuan, 2006]: X. Yuanyuan, X. Shanhong, B. Chao, C. Shaofeng, A micro amperometric immunosensor for detection of human immunoglobulin, *Science in China Series F* 49 (2006) 397–408.

Z

[Zeng, 2012]: S. Zeng, S. Wang, L. Wang, L. Yang, Z. Chen, Z. Liang, A novel CD105 determination system based on an ultrasensitive bioelectrochemical strategy with Pt nanoparticles, *Sensors* 12 (2012) 13471–13479.

[Zhang, 2007]: J.M. Zhang, J. Ann, Cytokines, inflammation and pain, *Int. Anesthesiol. Clin.* 45 (2007) 27–37.

[Zhang, 2007b]: M. Zhang, M. Yudasaka, K. Ajima, J. Miyawaki, Si Iijima, Light-assisted oxidation of single-wall carbon nanohorns for abundant creation of oxygenated groups that enable chemical modifications with proteins to enhance biocompatibility, *ACS Nano* 1 (2007) 265–272.

[Zhang, 2010]: J. Zhang, J. Lei, C. Xu, L. Ding, H. Ju, Carbon nanohorns sensitized electrochemical immunosensor for rapid detection of microcystin-LR, *Anal. Chem.* 82 (2010) 1117–1122.

[Zhang, 2010b]: J. Zhang, H. Yang, G. Shen, P. Cheng, J. Zhang, S. Guo, Reduction of graphene oxide via L-ascorbic acid, *Chem. Commun.* 46 (2010) 1112–1114.

[Zhang, 2012]: M. Zhang, S.M. June, T.E. Long, Principles of step-growth polymerization (polycondensation and polyaddition) in K. Matyjaszewski, M. Möller, Polymer science: a comprehensive reference, 1st Edition, *Elsevier* (2012) 7–47.

[Zhang, 2014]: Q. Zhang, X. Chen, F. Tu, C. Yao, Ultrasensitive enzyme-free electrochemical immunoassay for free thyroxine based on three dimensionally ordered macroporous chitosan-Au nanoparticles hybrid film, *Biosens. Bioelectron.* 59 (2014) 377-383.

[Zhang, 2015]: Y. Zhang, Y. Yan, B. Zhang, W. Zhu, Y. He, Fabrication of an interferon-gamma-based ITO detector for latent tuberculosis diagnosis with high stability and lower cost, *J. Solid State Electrochem.* 19 (2015) 3111–3119.

[Zhang, 2016]: Y. Zhang, B. Zhang, X. Ye, L. Huang, Z. Jiang, S. Tan, X. Cai, Electrochemical immunosensor for interferon-γ based on disposable ITO detector and HRP-antibody-conjugated nano gold as signal tag, *Mater. Sci. Eng. C* 59 (2016) 577–584.

[Zhu, 2014]: S. Zhu, J. Zhang, X. Zhao, H. Wang, G. Xu, J. You, Electrochemical behavior and voltammetric determination of L-tryptophan and L-tyrosine using a glassy carbon electrode modified with single-walled carbon nanohorns, *Microchim. Acta* 181 (2014) 445–451.

[Zhu, 2016]: M. Zhu, Y. Tang, Q. Wen, J. Li, P. Yang, Dynamic evaluation of cell-secreted interferon gamma in response to drug stimulation via a sensitive electro-chemiluminiscence immunosensor based on a glassy carbon electrode modified with graphene oxide, polyaniline nanofibers, magnetic beads and gold nanoparticles, *Microchim. Acta* 183 (2016) 1739–1748.

8

Publicaciones

Electrochimica Acta 292 (2018) 887–894

Amperometric determination of endoglin in human serum using disposable immunosensors constructed with poly(pyrrolepropionic) acid-modified electrodes

Electrochimica Acta 292 (2018) 887–894

Contents lists available at ScienceDirect

Electrochimica Acta

journal homepage: www.elsevier.com/locate/electacta

Amperometric determination of endoglin in human serum using disposable immunosensors constructed with poly(pyrrolepropionic) acid-modified electrodes

E. Martínez-Periñán [a], E. Sánchez-Tirado [a], A. González-Cortés [a], R. Barderas [b], J.M. Sánchez-Puelles [c], L. Martínez-Santamaría [d], S. Campuzano [a], P. Yáñez-Sedeño [a, *], J.M. Pingarrón [a]

[a] Department of Analytical Chemistry, Faculty of Chemistry, University Complutense of Madrid, 28040, Madrid, Spain
[b] UFIEC, CROSADIS, National Institute of Health Carlos III, Majadahonda, 28222, Madrid, Spain
[c] Departamento de Medicina Celular y Molecular, Centro de Investigaciones Biológicas, Consejo Superior de Investigaciones Científicas, 28040, Madrid, Spain
[d] Department of Bioengineering, UC3M, CIEMAT, IIS-Fundación Jiménez Díaz, CIBER de Enfermedades Raras (CIBERER), Madrid, Spain

ARTICLE INFO

Article history:
Received 21 July 2018
Received in revised form
19 September 2018
Accepted 2 October 2018
Available online 3 October 2018

Keywords:
Endoglin
CD105
Human serum
Electrochemical immunosensor
Serum

ABSTRACT

An amperometric immunosensor for the determination of the biomarker endoglin (CD105) to comply with the requirements of sensitivity and accuracy demanded in clinical practice is reported in this work. The immunosensing platform is implemented onto disposable electrodes modified with poly(-pyrrolepropionic) acid (pPPA). The methodology involves a sandwich configuration and labeling of the biotinylated detector antibody with poly-HRP-streptavidin for signal amplification. Amperometric detection of hydrogen peroxide reduction in the presence of HQ was employed as analytical readout. The different steps involved in the immunosensor preparation were monitored by electrochemical impedance spectroscopy. The resulting immunosensor provided a linear range between 0.18 and 20 ng mL^{-1}, adequate for the determination of CD105 in serum, with a detection limit (LOD) of 140 pg mL^{-1}. These analytical characteristics improve those reported previously for other electrochemical immunosensors. A good reproducibility of the measurements, an excellent storage stability of the anti-CD105-pPPA/SPCE bioplatforms and an excellent selectivity of the resulting immunosensors were found. The usefulness of the immunosensors was tested by analyzing human serum samples collected from healthy individuals and patients of colorectal, breast and lung cancer and epidermolysis bullosa. The results were successfully validated against those provided by an ELISA kit.

© 2018 Elsevier Ltd. All rights reserved.

1. Introduction

Human endoglin (CD105) is a 180 kDa homodimeric hypoxia-inducible cell transmembrane type III glycoprotein, densely expressed on the surface of angiogenic proliferating endothelial cells that acts as an auxiliary receptor for the transforming growth factor (TGF) family of cytokines. This protein plays a significant role in angiogenesis, a crucial process involved in several physiological and pathological conditions such as cancer [1,2]. The stronger CD105 expression found in a wide range of endothelial tumors, including colon, breast, brain, lung, prostate and cervical cancer, compared to normal tissues, suggests the possible involvement of CD105 in tumor angiogenesis [3–5]. In fact, increasing levels of CD105 in biological fluids from affected patients may be used as an indicator for disease progression and risk of metastasis [6,7]. CD105 circulating levels have been found to be altered in response to chemotherapy and, therefore, their monitoring can be useful for both the evaluation of the response of patients to treatment, especially to antiangiogenic therapies, and in tracing disease recurrence.

Increased CD105 levels are also detected in inflamed tissues. The protein modulates TGF-β induced production [8] and, therefore, is not involved only in cancer but also in the development and progression of other important diseases related to angiogenesis such as

* Corresponding author.
E-mail address: yseo@quim.ucm.es (P. Yáñez-Sedeño).

https://doi.org/10.1016/j.electacta.2018.10.015
0013-4686/© 2018 Elsevier Ltd. All rights reserved.

preeclampsia [9], rheumatoid arthritis [10] and skin diseases such as epidermolysis bullosa [11].

Various immunoassay methods for the detection of CD105 have been reported so far [12] related with cancer treatment [2] or diagnostics of preeclampsia [13]. ELISA kits available from Thermo Scientific [14] or SigmaAldrich [15] are examples of commercial kits involving sandwich-type configurations with anti-CD105 capture antibodies, biotinylated anti-CD105, and peroxidase (HRP)-streptavidin conjugates. These kits provide dynamic ranges extending from units to thousands of pg mL^{-1} with minimum detectable doses (MDD), calculated statistically from the zero signal value, of units of pg mL^{-1}. An important disadvantage of these methods is the long analysis time required (five hours). More simple immunoassays involving capture and HRP-labeled detection antibody as immunoreagents are also available. For instance, the ELISA kit from Sino Biologicals [16] provides a calibration plot ranging from 62.5 to 4000 pg mL^{-1} CD105 with a MDD value of 36 pg mL^{-1} in an assay time of 3 h 40 min.

Regarding electrochemical immunosensors, to our knowledge only two configurations have been reported so far. A sandwich type immunosensor involved immobilization of anti-CD105 capture antibody on a mercaptoethylamine self-assembled monolayer (SAM) onto a gold nanoparticles (AuNPs)–modified gold electrode and the use of a detection antibody chemically linked to the electron mediator thionine and platinum nanoparticles (PtNPs) for signal amplification [17]. This approach provided a linear range from 1.3 to 200.0 ng mL^{-1} and a detection limit (LOD) of 0.9 ng mL^{-1}. However, it implies laborious and time consuming protocols for SAM modification of the electrode surface (26 h) and preparation of the labeled immunoconjugates (12.5 h). More recently, a sandwich-type immunosensor was implemented on the surface of magnetic microbeads (MBs) and used capture and HRP-detection antibodies as well as amperometric detection of hydrogen peroxide in the presence of hydroquinone (HQ). A linear relationship between 0.8 and 10.0 ng mL^{-1} and a LOD of 0.2 ng mL^{-1} were achieved [18]. It is worth to mention that although both immunosensors provide higher LODs than ELISA kits, the sensitivity is sufficient for the determination of the target protein in serum of patients diagnosed with cancer, where the mean values found using a radioimmunoassay were of 34.0 ± 26.8 and 63.8 ± 72.5 ng mL^{-1} in metastasis-negative (42) and positive (59) patients, respectively [19]. However, the great variability observed in these results highlights the need for developing methodologies that provide not only good sensitivity but also good reproducibility for the determination of this circulating biomarker.

Nowadays the use of electrodes modified with electropolymerized conducting polymers containing suitable functional groups offers an interesting strategy to develop electrochemical immunosensing platforms with enhanced performance. For example, poly(pyrrolepropionic) acid (pPPA), a conducting polymer with abundance of carboxyl groups, allows the immobilization of large bioreagents loadings and permeation of electroactive species to the electrode surface due to its porous structure [20]. Despite these interesting properties, only few examples of electrochemical immunosensors involving the use of pPPA as modifier of glassy carbon electrodes [21–24] and SPCEs [25] have been found in the literature.

In this work, a strategy able to comply with the requirements of sensitivity and accuracy demanded by the determination of CD105 is described. The immunosensing platform was implemented onto a disposable electrode modified with pPPA and involved a sandwich configuration as well as labeling of the biotinylated detector antibody with poly-HRP-streptavidin for signal amplification. Amperometric detection of hydrogen peroxide reduction in the presence of HQ was employed as analytical readout. The immunosensor provided a calibration plot with a linear range between 0.18 and 20 ng mL^{-1} CD105, a LOD value of 140 pg mL^{-1} CD105 and was successfully applied to the determination of the target analyte in serum samples from cancer or epidermolysis bullosa patients with minimal sample treatment.

2. Experimental

2.1. Apparatus and electrodes

Screen-printed carbon electrodes (SPCEs, 110 DRP) were used as electrochemical transducers DropSens-Metrohm (Oviedo, Spain). They are constituted of a 4 mm ∅-working electrode, a silver pseudo-reference electrode and a carbon counter electrode. A μ-Autolab type III potentiostat, operated by the GPES 4.7 software (EcoChemie), was employed for electropolymerization of PPA onto SPCEs. Electrochemical impedance spectroscopy (EIS) was carried out using an Autolab type III potentiostat controlled by the FRA2 software (EcoChemie). Amperometric measurements were performed with an INBEA Biosensor S.L. potentiostat using the Ib-Graph software. An Elmasonic Se60 (Elma) ultrasonic bath, a Vortex homogenizator (Velp Scientifica) and a Crison Basic 20+ pH-meter were also used. All electrochemical experiments were performed at room temperature.

2.2. Reagents and solutions

Mouse anti-human endoglin capture antibody (anti-CD105), from Human Endoglin/CD105 DuoSet Elisa Catalog Number: DY1097 from R&D Systems, was reconstituted with 1.0 mL 0.01 M phosphate buffer saline solution (PBS) of pH 7.4 containing 137 mM NaCl, 2.7 mM KCl, 8.1 mM Na_2HPO_4 and 1.5 mM KH_2PO_4. Anti-CD105 solutions were prepared by appropriate dilution with 25 mM 2-(*N*-morpholino)ethanesulfonic acid (MES, from Gerbu) buffer solution of pH 5.0. CD105 standard solutions and biotinylated goat anti-human endoglin (Biotin-anti-CD105), also from Human Endoglin/CD105 DuoSet Elisa, Catalog Number: DY1097 from R&D Systems, were prepared in 0.01 M PBS solution of pH 7.4 supplemented with 1% (w/v) BSA.

Pyrrole propionic acid (PPA) (Sigma-Aldrich, 97%) and KCl (Scharlau, 99.5%) were used. The electro-synthesis of pPPA polymer was made from 5 mM PPA +0.5 M KCl aqueous solutions. N-(3-dimethyl-aminopropyl)-N′-ethylcarbodiimide (EDC, Acros Organics) and N-hydroxysulfo-succinimide (Sulfo-NHS, Sigma-Aldrich) were used as activation agents for carboxyl groups confined at the electrode surface. 50 mg mL^{-1} solutions of EDC and Sulfo-NHS each in 25 mM MES buffer of pH 5 were used for this purpose. The blocking agent was a commercial 1% (w/v) casein solution prepared in 0.01 M PBS of pH 7 (Blocker™ Casein, Thermo Fisher). Solutions of streptavidin labeled with horseradish peroxidase (HRP-Strept, Roche), prepared in 0.1 M phosphate buffer (PB) of pH 7.4, and poly-HRP-Strept (85-R200), diluted in stabilizer solution (Fitzgerald), were also used. Hydrogen peroxide (Aldrich, 30% (w/w)) and hydroquinone (HQ, Sigma) were also employed. 0.05 M $K_3Fe(CN)_6$ and $K_4Fe(CN)_6$ (Sigma) solutions were prepared in 0.01 M PB of pH 7.4. Bovine serum albumin (BSA), immunoglobulin G (IgG), hemoglobin (HB), uric acid (UA) and ascorbic acid (AA), all from Sigma, transforming growth factor beta-1 (TGF-β1), interleukin 1 beta (IL-1β), E-cadherin (E-Cad), cadherin 17R (Cad17R), and fibroblast growth factor receptor 4 (FGFR4), all from R&D System Inc., interleukin 6 (IL-6, Abcam), recombinant human ErbB2 protein (ERBB2, Sino Biological Inc.), and recombinant full length human p53 protein (p53, EMD Millipore Corporation), were tested as potential interfering compounds. Solutions of these reagents were prepared in 0.01 M PBS of pH 7.4. All other chemicals

used were of analytical reagent grade. All solutions were prepared with deionized water obtained from a Milli-pore Milli-Q purification system (18.2 MΩ cm at 25 °C).

2.3. Procedures

2.3.1. Preparation of anti-CD105-pPPA/SPCE immunosensor

Electropolymerization of pPPA on the SPCE was carried out by immersing the electrode in the 5 mM PPA +0.5 M KCl solution and applying 20 successive voltammetric cycles between 0 and + 0.85 V vs Ag pseudo reference electrode at 100 mV s^{-1}. The resulting pPPA/SPCE was immersed into a 1 mM HQ solution in 0.1 M PB of pH 7.4, and a control cyclic voltammogram between −0.2 and + 1.0 V vs. the Ag pseudo-reference electrode at 50 mV s^{-1} was recorded. Thereafter, electrode surface confined carboxyl groups were activated by adding 10 μL of EDC/NHSS solution and allowing incubation for 30 min at 25 °C in a humidified chamber. The electrode was washed with 25 mM MES buffer of pH 5, and the anti-CD105 capture antibody was covalently attached to the activated pPPA/SPCE by dropping 5 μL of a 12.5 μg mL^{-1} antibody solution allowing incubation during 60 min at 25 °C. After washing with MES buffer, the unreacted activated groups on the anti-CD105-pPPA/SPCEs were blocked with 10 μL of 1% casein solution during 30 min. The anti-CD105-pPPA/SPCEs were washed with 0.1 M PB of pH 7.4, dried and used or stored at −20 °C in dry conditions.

2.3.2. Determination of CD105

5 μL of the antigen solution (or the sample) were added onto the anti-CD105-pPPA/SPCEs and incubated for 30 min. Thereafter, 5 μL of a 2 μg mL^{-1} Biotin-anti-CD105 solution were dropped onto the bioelectrode, incubated during 60 min, and washed with 0.1 M PB of pH 7.4. Subsequently, 5 μL of a 1:500 diluted poly-HRP-Strept solution were added and incubated for 15 min. After washing with 0.1 M PB of pH 7.4, a drop of this buffer was added on the resulting immunosensor and stored until use at room temperature. The determination of CD105 was accomplished by adding 45 μL of a 1 mM HQ solution (freshly prepared in 50 mM PB of pH 6.0) on the surface of the horizontally positioned poly-HRP-Strept-Biotin-anti-CD105-CD105-anti-CD105-pPPA/SPCE immunosensor and applying a potential of −200 mV vs the Ag pseudo-reference electrode. Once the background current was stabilized (100 s approximately), 5 μL of a 50 mM H_2O_2 solution freshly prepared in the same buffer were added and incubated for 200 s. Then, the cathodic current arising from the electrochemical reduction of benzoquinone was measured.

2.3.3. Analysis of serum samples

Serum samples were collected from patients affected by different types of cancer (colorectal, breast and lung cancer), as well as by epidermolysis bullosa. Epidermolysis bullosa patients were selected for age (18–40 years) and for being carriers of identical C7 mutation c.6527insC in exon 80 of the *COL7A1* gene. The samples as well as control sera from healthy individuals were provided by Hospital Universitario La Paz and Clínico San Carlos (Madrid, Spain) with informed consent approved by the patients and Ethics Committee of the Institutions (in case of epidermolysis bullosa samples, Code HULP: PI-1602, which adhered to Helsinki Guidelines and further reviews, Fortaleza 2013, http://www.wma.net/).

The samples were analyzed using poly-HRP-Strept-Biotin-anti-CD105-CD105-anti-CD105-pPPA/SPCE immunosensors after a fifty-fold sample dilution in 0.01 M PBS of pH 7.4. Validation of the method was performed by comparison of the obtained results with those provided by applying a conventional ELISA methodology using the same immunoreagents.

3. Results and discussion

Fig. 1 shows schematically the different steps implied in the preparation of the poly-HRP-Strept-Biotin-anti-CD105-CD105-anti-CD105-pPPA/SPCE immunosensors as well as the amperometric measurement principle. Upon electropolymerization of PPA on the SPCE by cyclic voltammetry, the anti-CD105 was covalently immobilized through carbodiimide/succinimide chemistry on the pPPA/SPCE (a) and the remaining free active sites were blocked with casein (b). A sandwich type immunoassay involving CD105 (c), Biotin-anti-CD105 (d) and poly-HRP-Strept (d) was then implemented. The affinity reaction was amperometrically monitored by adding H_2O_2 in the presence of HQ as the redox mediator.

3.1. Optimization of the experimental variables involved in the preparation of the immunosensor

The effect of different variables on the immunosensor response was evaluated. The tested variables were: anti-CD105 antibody loading on pPPA/SPCE and incubation time (a); Biotin-anti-CD105 loading on anti-CD105-pPPA/SPCE and incubation time (b); type and concentration of blocking agent (c); type of enzymatic tracer to label the Biotin-anti-CD105 conjugate (d) and poly-HRP-Strept concentration (e). The largest ratio between the currents measured in the presence (S) or in absence (N) of the target compound was taken as the selection criterion for each tested variable. Other variables involved in the immunosensor preparation such as the experimental conditions for pPPA electrodeposition onto SPCE were taken from previous work [25]. Furthermore, the conditions at which the amperometric currents from benzoquinone (BQ) generated by the HRP reaction using the H_2O_2/HQ system, were taken also from a previous work [26].

The results of the optimization studies are summarized in Table 1. Details are given in the Supporting Information and Figs. S1–S4.

Once the experimental variables were optimized, the different steps involved in the immunosensor preparation were monitored by electrochemical impedance spectroscopy (EIS) using 2 mM $Fe(CN)_6^{4-/3-}$ as the redox probe in 0.05 M PB of pH 6.0 (Fig. 2). As expected, the modification of the SPCE with pPPA gave rise to a large increase in the electron transfer resistance, R_{CT}, varying from 2383 Ω (bare SPCE) to 5887 Ω (pPPA/SPCE) as a consequence of two effects: a) the relatively low conductivity of the polymer and b) the electrostatic repulsion between the redox probe and the negatively charged carboxylate groups at the working pH. Activation with EDC/NHSS provoked a dramatic decrease of the R_{CT} value (1331 Ω) which can be explained by the neutralization of the negative charge of the surface confined −COOH groups after the activation reaction. A further increase in the R_{CT} value was observed after conjugation with anti-CD105 (2180 Ω) due to the partially insulating barrier on the electrode surface produced by the presence of the antibody. As expected, blocking with casein of the remaining unreacted sites led to an increase in the R_{CT} value (2246 Ω), and the subsequent incorporation of the antigen provoked a slightly higher R_{CT} value (2354 Ω).

3.2. Analytical figures of merit of the immunosensor

Fig. 3 displays the calibration plot for CD105 standard solutions constructed with the developed immunosensor under the optimized working conditions. Error bars were calculated from measurements carried out with three different immunosensors. Some typical recorded amperograms are also displayed in Fig. 3. The steady state current vs. logarithm of CD105 concentration followed the adjusted equation Δi, nA = (476 ± 12) log [CD105], ng mL^{-1} –

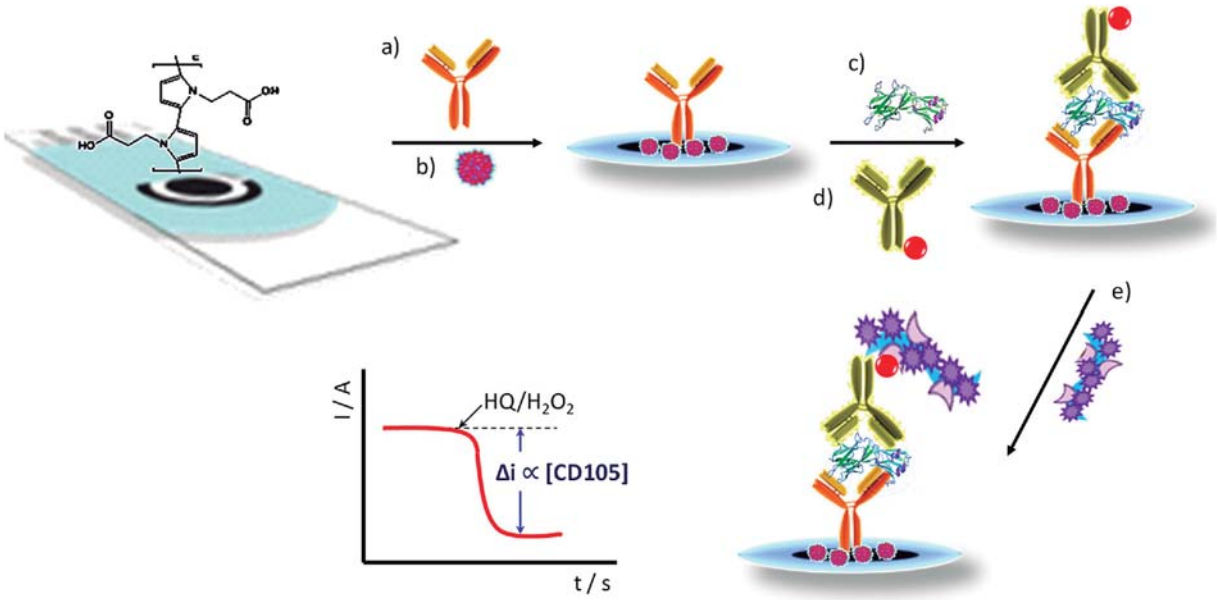

Fig. 1. Schematic display of the different steps involved in the preparation of the amperometric immunosensor for CD105 using pPPA-modified SPCEs: covalent immobilization of anti-CD105 (a), blocking step with casein (b), sandwich configuration using CD105 (c), Biotin-anti-CD105 (d), and poly-HRP-Strept conjugate (e).

Table 1
Optimization of the experimental variables affecting the performance of poly-HRP-Strept-anti-CD105-CD105-anti-CD105-pPPA/SPCE immunosensor for the amperometric determination of CD105.

Variable	Range (or compound) tested	Selected
Anti-CD105 loading, μg mL^{-1}	5–17.5	12.5
Incubation time for anti-CD105, min	30–75	60
Biotin-anti-CD105 loading, μg mL^{-1}	1–4	2
Incubation time for Biotin-anti-CD105, min	30–75	45
Type of blocking agent	casein, BSA	casein
Concentration of blocking agent, % (w/v)	1–2	1
Incubation time for casein, min	15–75	30
Enzymatic tracer to label the Biotin-anti-CD105	HRP-Strept, poly-HRP-Strept	poly-HRP-Strept
Poly-HRP-Strept dilution	1/1000–1/250	1/500

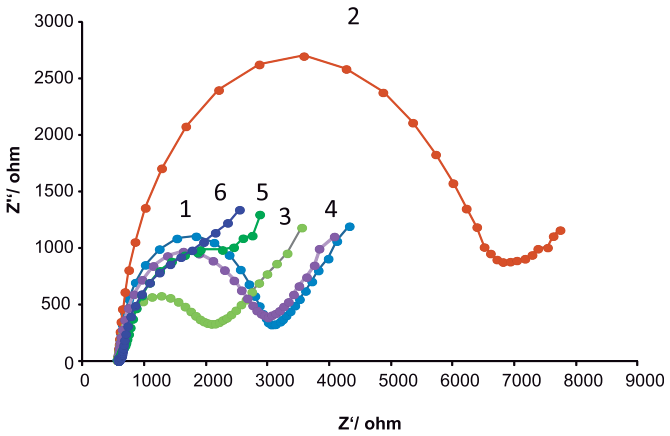

Fig. 2. Nyquist plots recorded in 2 mM $[Fe(CN)_6]^{3-/4-}$ in 0.05 M phosphate buffer solution of pH 6.0 at: SPCE (1); pPPA/SPCE (2); EDC/NHSS-activated pPPA/SPCE (3); anti-CD105-pPPA/SPCE (4); casein/anti-CD105-pPPA/SPCE (5); CD105-anti-CD105-pPPA/SPCE (6); 0.04–100,000 Hz frequency range with a 10 mV r.m.s. signal.

(406 ± 1) ($r^2 = 0.996$), where Δi is the difference between the currents measured in the presence and in the absence of capture antibody [25]. The range of linearity extended between 0.18 and 20 ng mL^{-1} covering more than two orders of magnitude and is adequate for the determination of CD105 in serum according to the expected concentrations, at the ng mL^{-1} level, in this type of sample [19], The LOD, 140 pg mL^{-1}, was calculated according to the $3 \times s_b$ criterion, where s_b was estimated as the standard deviation, expressed in concentration units, calculated from ten amperometric responses of the immunosensor in the absence of CD105. It is worth to mention that these analytical characteristics improve those reported by Zeng et al. with a LOD of 900 pg mL^{-1} [17], and are also slightly better than those obtained with an immunosensor using MBs [18] that exhibited a linear calibration plot from 0.8 to 10 ng mL^{-1} and a LOD of 200 pg mL^{-1} CD105.

The amperometric responses measured with five different immunosensors prepared on the same day for 0 and 1 ng mL^{-1} CD105 yielded relative standard deviation (RSD) values of 3.8% and 5.2% ($n = 5$), respectively. Moreover, the same measurements with five different immunosensors constructed on different days gave RSD values of 4.9% and 5.7% ($n = 5$), respectively, thus showing that the protocols used for the biosensor fabrication and the amperometric detection are suitable to allow a good reproducibility of the measurements.

The storage stability of anti-CD105-pPPA/SPCE bioelectrodes once the blocking step with casein was made, was also tested. Different anti-CD105-pPPA/SPCEs were prepared on the same day, stored under dry conditions at −20 °C, and employed to prepare

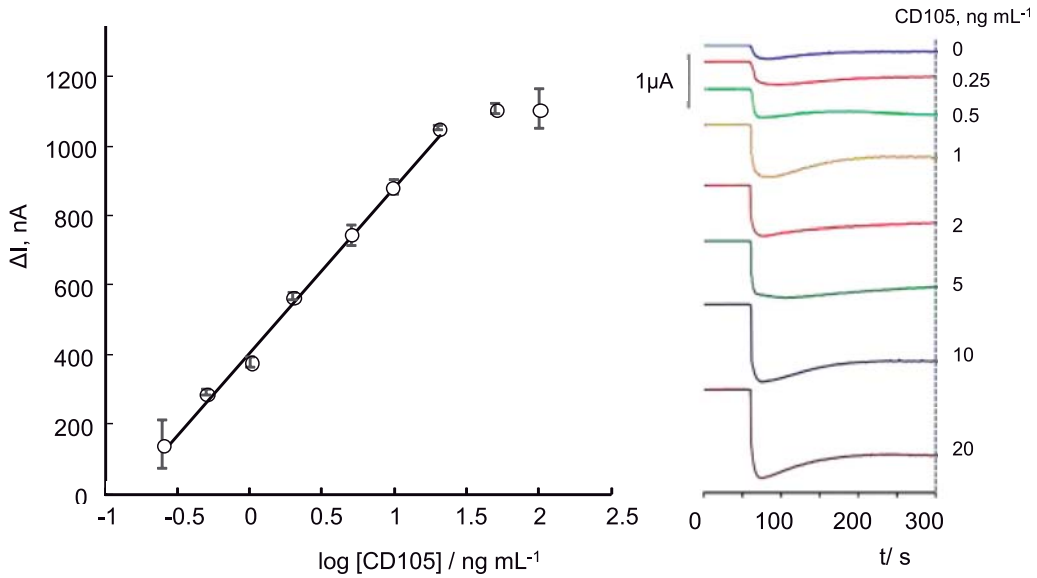

Fig. 3. Calibration plot (left) and real amperograms (right) recorded for the determination of CD105 standards at the poly-HRP-Strept-Biotin-anti-CD105-CD105-anti-CD105-pPPA/SPCE. Error bars estimated as triple of the standard deviation (n = 3).

immunosensors to measure 20 ng mL^{-1} CD105 each control day. The control chart shown in Fig. 4 indicates that the immunosensor responses remained within the control limits, set at ± 3s, were s was the standard deviation of the measurements carried out with 10 different immunosensors prepared the day 0 of this study, for at least 43 days (no longer storage times were tested). These results demonstrated the excellent stability of the anti-CD105-pPPA/SPCE bioplatforms.

3.3. Selectivity

The effect of the presence of other protein biomarkers and non-target compounds potentially co-existing with CD105 in human serum on the immunosensor response was evaluated. The amperometric responses provided by the developed immunosensors for 0 and 1 ng mL^{-1} CD105 standards were measured both in the absence and in the presence of the following compounds: BSA, IgG, hemoglobin (HB), transforming growth factor beta-1 (TGF-β1), interleukin 6 (IL-6), interleukin 1 beta (IL-1β), E-cadherin (E-Cad), uric acid (UA), ascorbic acid (AA), recombinant human ErbB2 protein (ERBB2), human p53 (p53), cadherin 17R (Cad17R) and fibroblast growth factor receptor 4 (FGFR4). The tested concentrations of these compounds were those reported as their normal levels in human serum. Fig. 5 shows clearly as no significant differences occurred between the currents measured in the absence or in the presence of these potential interferents, thus demonstrating the practical specificity of the immunosensor for the determination of CD105.

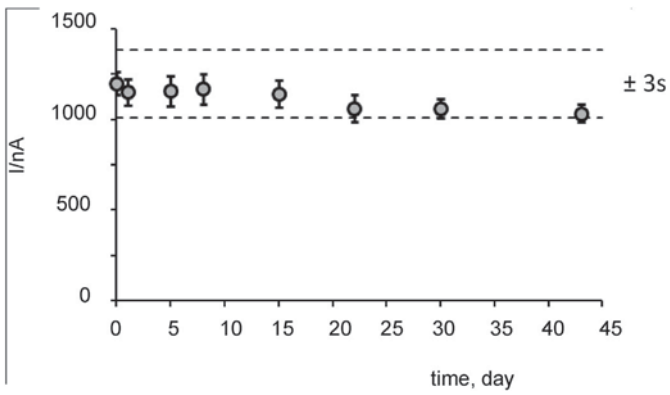

Fig. 4. Control chart constructed to check the storage stability of anti-CD105-pPPA/SPCE bioelectrodes upon storage at −20 °C under dry conditions. The central value was the average amperometric signals provided by 10 different immunosensors prepared the day 0 of the study for 20 ng mL^{-1} CD105. Upper and lower limits of control were set as three times the standard deviation (3s) of these measurements. Error bars estimated as triple of the standard deviation (n = 3).

3.4. Determination of CD105 in human serum samples

The real usefulness of the developed immunosensors was verified by analyzing human serum samples collected from healthy individuals (3) and patients of colorectal (3), breast (3) and lung (3) cancer, as well as from epidermolysis bullosa (2) patients. The potential existence of a matrix effect was evaluated by comparing the slope of the calibrations plot prepared with CD105 standards in buffered solutions with that constructed in serum after applying different dilution ratios (0, 1:2, 1:3, 1:5, 1:10, 1:50, and 1:100) with 0.01 M PBS of pH 7.4. The comparison of the slope of the calibrations plots obtained for CD105 standards prepared in buffered solutions (476 ± 12) and 50-times diluted healthy (475 ± 8), breast cancer (477 ± 7) and untreated epidermolysis bullosa (470 ± 30) patients, exemplified that this dilution was sufficient to avoid a significant matrix effect. Therefore, quantification of CD105 could be accomplished by interpolating the currents measured in the 1:50 diluted samples into the calibration plot prepared with CD105 standards, without any other sample treatment. The results obtained by triplicate with the immunosensor were compared with those provided by an ELISA kit that uses the same immunoreagents (Table 2). As it can be seen, no apparent differences exist between the results provided by the two methods. This was verified by means of a paired samples *t*-test (α = 0.05; p-value = 0.3). The plot of the mean concentrations obtained with the immunosensors vs. those provided by the ELISA kit resulted in a linear least-squares regression graph (r = 0.998) with a slope value of (1.01 ± 0.02)

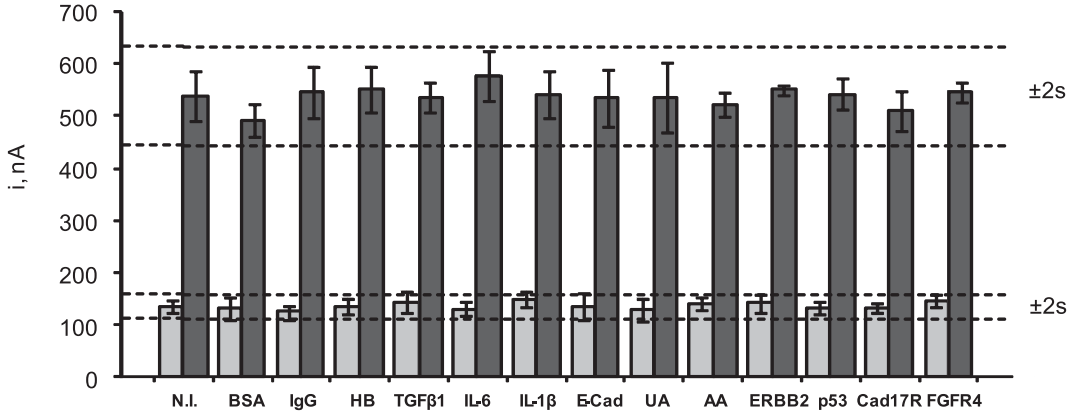

Fig. 5. Amperometric responses measured with the poly-HRP-Strept–Biotin-anti-CD105–CD105–anti-CD105–pPPA/SPCEs for 0 (grey bars) and 1 (black bars) ng mL^{-1} CD105 standards prepared in the presence of 5 mg mL^{-1} BSA, 1 mg mL^{-1} IgG, 5 mg mL^{-1} HB, 50 ng mL^{-1} TGF-β1, 300 pg mL^{-1} IL-6, 50 pg mL^{-1} IL-1β, 55 ng mL^{-1} E-Cad, 100 μg mL^{-1} UA, 7 μg mL^{-1} AA, 15 ng mL^{-1} ERBB2, 200 pg mL^{-1} p53, 55 ng mL^{-1} Cad17R, and 1 ng mL^{-1} FGFR4. Error bars estimated as triple of the standard deviation (n = 3).

Table 2
Determination of CD105 (in ng mL^{-1}) in human serum samples.

Patient		No.	Immunosensor, (n = 3)[a]	ELISA, (n = 3)[a]
Healthy		1	19 ± 2	20 ± 2
		2	12 ± 2	10 ± 2
		3	20 ± 1	20 ± 1
		4	11 ± 1	10 ± 1
		5	18 ± 2	18 ± 2
Cancer	Colorectal (CRC)	6	50 ± 4	50 ± 4
		7	64 ± 3	67 ± 5
		8	57 ± 5	56 ± 5
	Breast (BC)	9	81 ± 1	82 ± 5
		10	86 ± 5	89 ± 3
		11	84 ± 4	79 ± 8
	Lung (LC)	12	67 ± 5	67 ± 6
		13	59 ± 4	59 ± 3
		14	58 ± 3	57 ± 5
Epidermolysis bullosa (EB)		15	71 ± 5	71 ± 6
		16	75 ± 9	76 ± 5

[a] Mean value ± ts/√n.

and an intercept of (−0.8 ± 1.0). The highly satisfactory correlation found with confidence intervals for the slope and intercept values (at a significance level of α = 0.05) including the unit and the zero values, respectively, indicated that the developed methodology exhibited no systematic errors. It is important to mention that the LOD achieved with the immunosensor is similar to the lowest concentration standard recommended by the ELISA kit involving the same immunoreagents (140 vs 125 pg mL^{-1}), However, and

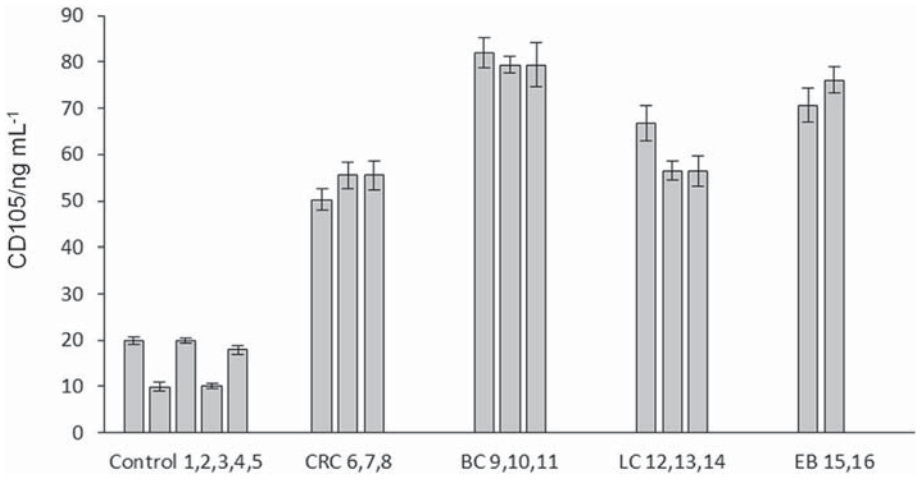

Fig. 6. CD105 concentration (in ng mL^{-1}) provided by the developed immunosensor in the serum samples analyzed. Error bars estimated as triple of the standard deviation (n = 3).

importantly, the immunosensor is able to perform the determination in half time than the ELISA kit (135 vs. 280 min) once the anti-CD105–pPPA/SPCEs and anti-CD105-plate were prepared and blocked, respectively. Moreover, the amperometric determination may be easily automated and implemented with portable and cost-effective instrumentation, making the developed immunosensor an attractive and user-friendly tool to monitor routinely CD105 serum levels even for decentralized analysis and more suitable than ELISA methods for bedside and emergency medicine. Additional advantages compared with the ELISA methodologies include the easy translation of the approach to determine other specific biomarkers limiting the hospital admission and stay (drastically alleviating the hospital expenses) [27,28] and the facile integration into multiplexed (similarly to the ELISA kits, it is possible to carry out 96 determinations at the same time by using the electrochemical ELISA plates marketed in recent years) platforms.

Importantly, the plot of data summarized in Table 2 (Fig. 6) visualizes clearly the differences in the CD105 concentration in the sera of healthy individuals and for cancer patients, thus supporting the relevant role of this protein as a cancer biomarker in human serum. In addition, it was also possible to discriminate between patients suffering epidermolysis bullosa, which exhibited also elevated CD105 levels in serum.

4. Conclusions

This work reports a novel disposable integrated inmunosensor for the determination of CD105 based on covalent immobilization of the capture antibody on pPPA-modified SPCEs using EDC/NHSS chemistry. The amperometric immunosensor exhibits a very attractive analytical performance in terms of sensitivity, selectivity and stability as well as successful applicability for the accurate determination of the endogenous content of the target protein in human serum samples from cancer and epidermolysis bullosa patients with no matrix effect upon a simple 50-times sample dilution. The simplicity, rapidity, affordability, portability, and multiplexing ability of the developed methodology to provide quantification of CD105 in small amounts of scarcely treated complex samples make it more compatible with the clinical requirements than the current available methods to bring the determination of this biomarker from the laboratory into point-of-care testing devices to perform on-site determinations even in resource-limited settings (outpatient clinics, near patients' beds or at home). Indeed, the feasibility to perform routine screening of this relevant target transmembrane glycoprotein (or other candidate circulating protein biomarkers) can allow continued investigation of its clinical relevance/role in physiological/pathological conditions improving patient management, therapy efficiency and high relevant diseases outcomes.

Acknowledgments

The financial support of the Spanish Ministerio de Economía y Competitividad CTQ2015-70023-R and CTQ2015-64402-C2-1-R, and SAF2014-53209-R Research Projects, the PI17CIII/00045 research project from AESI and the NANOAVANSENS Program from the Comunidad de Madrid (S2013/MT-3029). E.M-P. acknowledged Spanish Ministry (Economía, Industria y competitividad) for Juan de la Cierva-Formación fellow.

Appendix A. Supplementary data

Supplementary data to this article can be found online at https://doi.org/10.1016/j.electacta.2018.10.015.

References

[1] S.E. Duff, C. Li, J.M. Garland, S. Kumar, CD105 is important for angiogenesis: evidence and potential applications, FASEB. J. 17 (2003) 984–992.
[2] F. Nassiri, M.D. Cusimano, B.W. Scheithauer, F. Rotondo, A. Fazio, G.M. Yousef, L.V. Syro, K. Kovacs, R.V. Lloyd, Endoglin (CD105): a review of its role in angiogenesis and tumor diagnosis, progression and therapy, Anticancer Res. 31 (2011) 2283–2290.
[3] F.J. Burrows, E.J. Derbyshire, P.L. Tazzari, P. Amlot, A.F. Gazdar, S.W. King, M. Letarte, E.S. Vitetta, P.E. Thorpe, Up-regulation of endoglin on vascular endothelial cells in human solid tumors: implications for diagnosis and therapy, Clin. Cancer Res. 1 (1995) 1623–1634.
[4] B. Bodey, S.E. Siegel, H.E. Kaiser, Overexpression of endoglin (CD105): a marker of breast carcinoma-induced neo-vascularization, Anticancer Res. 18 (1998) 3621–3628.
[5] S. Kumar, A. Ghellal, C. Li, G. Byrne, N. Haboubi, J.M. Wang, N. Bundred, Breast carcinoma: vascular density determined using CD105 antibody correlates with tumor prognosis, Cancer Res. 59 (1999) 856–861.
[6] M. Quintanilla, J.R. Ramirez, E. Pérez-Gómez, D. Romero, B. Velasco, M. Letarte, J.M. López-Novoa, C. Bernabéu, Expression of the TGF-b coreceptor endoglin in epidermal keratinocytes and its dual role in multistage mouse skin carcinogenesis, Oncogene 22 (2003) 5976–5985.
[7] V.L. Martins, M.P. Caley, K. Moore, Z. Szentpetery, S.T. Marsh, D.F. Murrell, M.H. Kim, M. Avari, J.A. McGrath, R. Cerio, A. Kivisaari, V.M. Kähäri, K. Hodivala-Dilke, C.H. Brennan, M. Chen, J.F. Marshall, E.A. O'Toole, Suppression of TGFβ and angiogenesis by type VII collagen in cutaneous SCC, J. Natl. Cancer Inst. 108 (2015) djv293, https://doi.org/10.1093/jnci/djv293.
[8] E. Rossi, F. Sanz-Rodriguez, N. Eleno, A. Düwell, F.J. Blanco, C. Langa, L.M. Botella, C. Cabañas, J.M. López-Novoa, C. Bernaveu, Endothelial endoglin is involved in inflammation: role in leukocyte adhesion and transmigration, Blood 121 (2013) 403–415.
[9] P.K. Aggarwal, N. Chandel, V. Jain, V. Jha, The relationship between circulating endothelin-1, soluble fms-like tyrosine kinase-1 and soluble endoglin in preeclampsia, J. Hum. Hypertens. (2011) 1–6.
[10] A.E. Koch, The role of angiogenesis in rheumatoid arthritis: recent developments, Ann. Rheum. Dis. 59 (2000) i65–i71.
[11] C. Hümefeld, M. Mezger, J.S. Kern, A. Nysytöm, K. Brickner-Tuderman, I. Müller, R. Handgretinger, M. Röcken, One goal, different strategies – molecular and cellular approaches for the treatment of inherited skin fragility disorders, Exp. Dermatol. 22 (2013) 162–167.
[12] I.V. Smirnov, I.V. Gryazeva, M.P. Samoylovich, L.A. Terekhina, A.A. Pinevich, O.A. Shashkova, I.Y. Krutetskaia, D.I. Sokolov, S.A. Selkov, N.N. Nikolskiy, V.B. Klimovich, Different pairs of monoclonal antibodies detect variable amounts of soluble endoglin in human blood plasma, Immunochem. Immunopathol. 2 (2016) 473–482.
[13] A.L. Gregory, G. Xu, V. Sotov, M. Letarte, Review: the enigmatic role of endoglin in the placenta, Placenta 35 (2014) 593–599.
[14] www.thermofisher.com/order/catalog/product/EHENG.
[15] www.sigmaaldrich.com/catalog/product/sigma/rab0171?Lang=es&regin=ES.
[16] http://www.sinobiologicalcdn.com/reagent/KIT10149.pdf.
[17] S. Zeng, S. Wang, L. Wang, L. Yang, Z. Chen, Z. Liang, A novel CD105 determination system based on an ultrasensitive bioelectrochemical strategy with Pt nanoparticles, Sensors 12 (2012) 13471–13479.
[18] R.M. Torrente-Rodríguez, S. Campuzano, V. Ruiz-Valdepeñas-Montiel, M. Pedrero, M.J. Fernández-Aceñero, R. Barderas, J.M. Pingarrón, Rapid endoglin determination in serum samples using an amperometric magneto-actuated disposable immunosensing platform, J. Pharm. Biomed. Anal. 129 (2016) 288–293.
[19] N. Takahashi, R. Kawanishi-Tabata, A. Haba, M. Tabata, Y. Haruta, H. Tsai, B.K. Seon, Association of serum endoglin with metastasis in patients with colorectal, breast, and other solid tumors, and suppressive effect of chemotherapy on the serum endoglin, Clin. Cancer Res. 7 (2001) 524–532.
[20] H. Dong, X. Cao, C.M. Li, W. Hu, An in situ electrochemical surface plasmon resonance immunosensor with polypyrrole propylic acid film: comparison between SPR and electrochemical responses from polymer formation to protein immunosensing, Biosens. Bioelectron. 23 (2008) 1055–1062.
[21] H. Dong, C.M. Li, W. Chen, Q. Zhou, Z.-X. Zeng, J.H.T. Luong, Sensitive amperometric immunosensing using polypyrrolepropylic acid films for biomolecule immobilization, Anal. Chem. 78 (2006) 7424–7431.
[22] Y. Hu, Z. Zhao, Q. Wan, Facile preparation of carbon nanotube conducting polymer network for sensitive electrochemical immunoassay of Hepatitis B surface antigen in serum, Bioelectrochemistry 81 (2011) 59–64.
[23] V. Serafín, L. Agüí, P. Yáñez-Sedeño, J.M. Pingarrón, Electrochemical immunosensor for the determination of insulin-like growth factor-1 using electrodes modified with carbon nanotubes–poly(pyrrole propionic acid) hybrids, Biosens. Bioelectron. 52 (2014) 98–104.
[24] V. Serafín, L. Agüí, P. Yáñez-Sedeño, J.M. Pingarrón, Determination of prolactin hormone in serum and urine using an electrochemical immunosensor based on poly(pyrrolepropionic acid)/carbon nanotubes hybrid modified electrodes, Sens. Actuators B Chem. 195 (2014) 494–499.
[25] V. Serafín, R.M. Torrente-Rodríguez, M. Batlle, P. García de Frutos, S. Campuzano, P. Yáñez-Sedeño, J.M. Pingarrón, Electrochemical immunosensor for receptor tyrosine kinase AXL using poly(pyrrolepropionic acid)-modified disposable electrodes, Sens. Actuators B Chem. 240 (2017)

1251–1256.
[26] M. Eguílaz, M. Moreno-Guzmán, S. Campuzano, A. González-Cortés, P. Yáñez-Sedeño, J.M. Pingarrón, An electrochemical immunosensor for testosterone using functionalized magnetic beads and screen-printed carbon electrodes, Biosens. Bioelectron. 26 (2010) 517–522.
[27] M. Mascini, S. Tombelli, Biosensors for biomarkers in medical diagnostics, Biomarkers 13 (2008) 637–657.
[28] F. Ricci, G. Adornetto, G. Palleschi, A review of experimental aspects of electrochemical immunosensors, Electrochim. Acta 84 (2012) 74–83.

Supporting Information

AMPEROMETRIC DETERMINATION OF ENDOGLIN IN HUMAN SERUM USING DISPOSABLE IMMUNOSENSORS CONSTRUCTED WITH POLY(PYRROLEPROPIONIC) ACID-MODIFIED ELECTRODES

E. Martínez-Periñán[a], E. Sánchez-Tirado[a], A. González-Cortés[a], R. Barderas[b], J.M. Sánchez-Puelles[c], L. Martínez-Santamaría[d], S. Campuzano[a], P. Yáñez-Sedeño[a,*], J.M. Pingarrón[a].

[a] Department of Analytical Chemistry, Faculty of Chemistry, University Complutense of Madrid, 28040-Madrid, Spain.

[b] UFIEC, CROSADIS, National Institute of Health Carlos III, Majadahonda, 28222-Madrid, Madrid, Spain.

[c] Departamento de Medicina Celular y Molecular, Centro de Investigaciones Biológicas, Consejo Superior de Investigaciones Científicas, 28040-Madrid, Spain.

[d] Department of Bioengineering, UC3M; CIEMAT; IIS-Fundación Jiménez Díaz; CIBER de Enfermedades Raras (CIBERER), Madrid, Spain.

CONTENT

1. Effect of anti-CD105 loading and incubation time

The effect of the capture antibody loading on the response of the resulting immunosensor was studied by immobilizing 5 µL of anti-CD105 solutions in the 5 to 17.5 µg mL^{-1} concentration range and allowing 60 min for incubation. Fig. S1a shows that larger specific-to-unspecific current ratio was obtained for a 12.5 µg mL^{-1} concentration, thus this value was selected for the preparation of the immunosensor. The lower specific current observed at larger concentrations can be attributed to the steric hindrance of the antigen recognition when large amounts of the capture antibody are immobilized [1]. The time for incubation of anti-CD105 was tested in the 30 – 75 min range. The results shown in Fig. S1b led us to choose 60 min for further work.

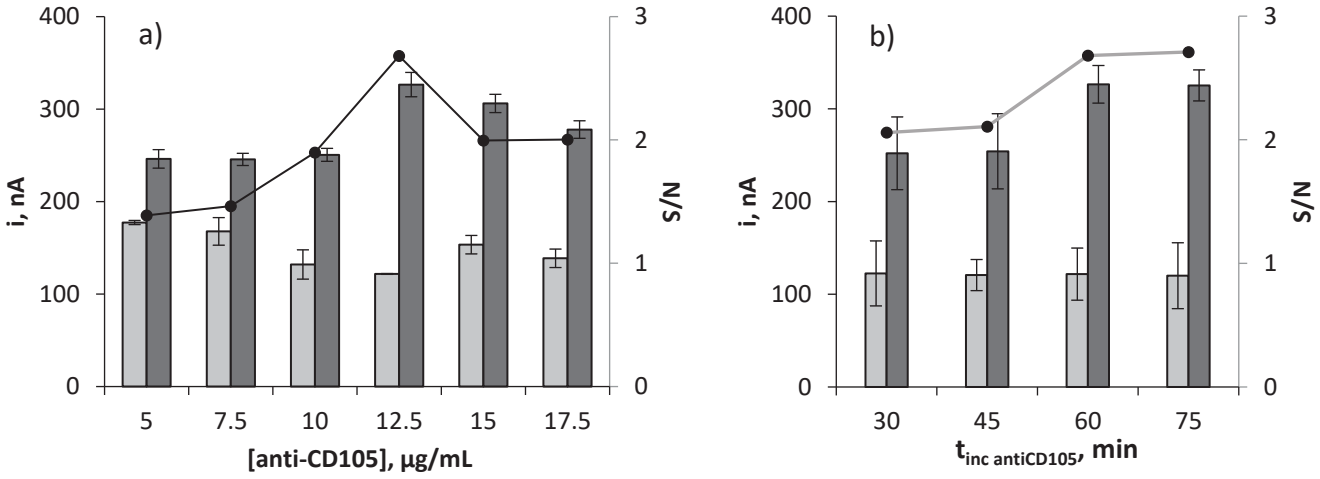

Fig. S1. Amperometric responses measured with the immunosensors in the absence (grey) or in the presence of 1.0 ng mL^{-1} CD105 (black) as a function of the anti-CD105 loading (5–17.5 µg mL^{-1}) a) and the anti-CD105 incubation time (30–75 min) b). Error bars estimated as triple of the standard deviation (n = 3).

2. Effect of Biotin-anti-CD105 loading and incubation time

Fig. S2a shows as the measured current increased with the Biotin-anti-CD105 concentration up to 2 µg mL^{-1} and levelled off for larger concentrations. Lower S/N ratios

were found for loadings above 2 μg mL^{-1} indicating a worse efficiency of the immunorecognition reaction. Therefore, a 2 μg mL^{-1} concentration of Biotin-anti-CD105 was selected for further work. Regarding the incubation time with the detector antibody in the 30–75 min range, Fig. S2b led us to select 60 min achieving also a better reproducibility for the preparation of Biotin-anti-CD105-CD105-anti-CD105-pPPA/SPCE.

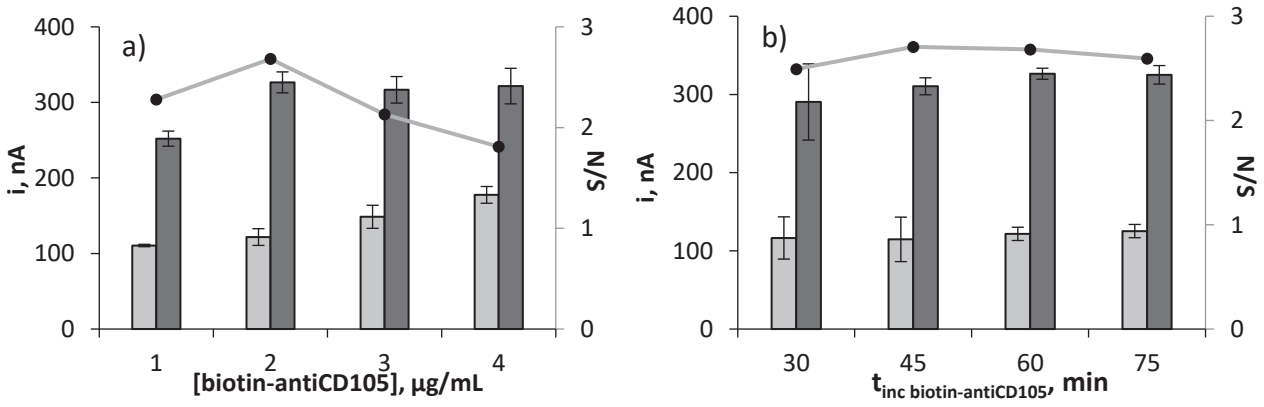

Fig. S2. Effect of the Biotin-anti-CD105 loading (a) and the incubation time (b) on the amperometric responses measured with HRP-Strept-Biotin-anti-CD105-CD105-anti-CD105-pPPA/SPCEs immunosensors in the absence (grey) or in the presence of 1.0 ng mL^{-1} CD105 (black). Error bars estimated as triple of the standard deviation (n = 3).

3. Optimization of the blocking step

Blocking of the free active sites on the electrode surface was carried out using BSA and casein solutions as well recognized reagents for minimizing unspecific adsorptions. Fig. S3a shows that lower unspecific responses and larger S/N ratios were achieved using 1% (w/v) casein. Regarding blocking time, 30 min were sufficient for an effective blocking (Fig. 3Sb).

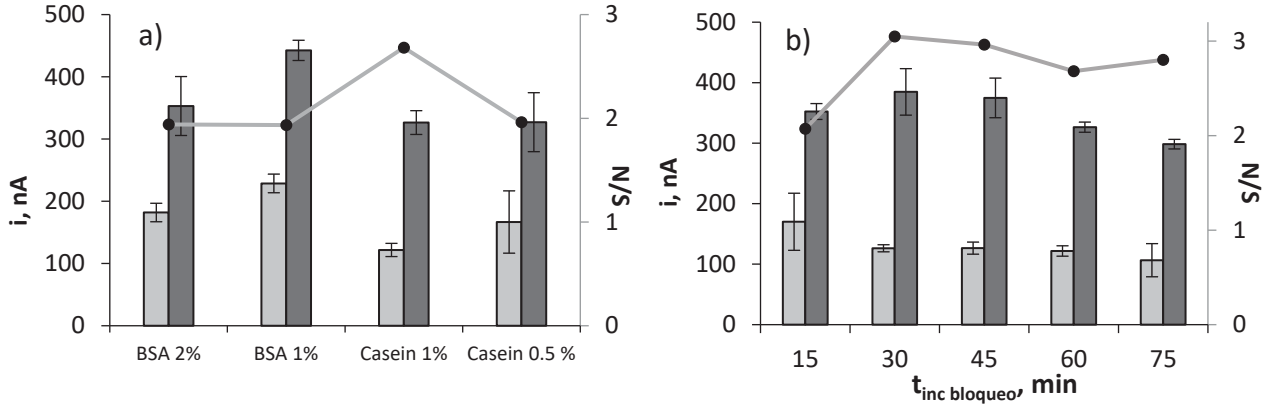

Fig. S3. Effect of the type (a) and incubation time of blocking agent (b) on the amperometric responses measured with HRP-Strept-Biotin-anti-CD105-CD105-anti-CD105-pPPA/SPCEs in the absence (grey) or in the presence of 1.0 ng mL^{-1} CD105 (black). Error bars estimated as triple of the standard deviation (n = 3).

4. Effect of the enzymatic tracer to label Biotin-anti-CD105 and of poly-HRP-Strept concentration

The effect of different enzymatic tracers on the response of the immunosensors was checked. Fig. S4 shows the results obtained by using HRP-Strept at the previously optimized concentration [2] and poly-HRP-Strept conjugate at different dilution ratios between 1/1,000 and 1/250. As expected, HRP-Strept polymers allowed achieving a remarkably larger specific current because of the larger loading of enzymes per antigen. Fig. S4 shows as a 1/500 dilution provided better S/N ratio.

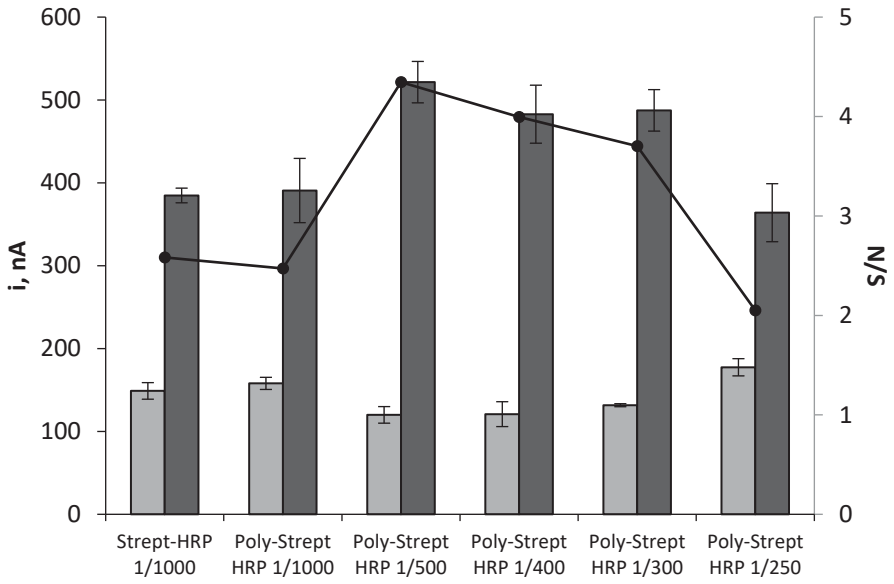

Fig. S4. Effect of the type and concentration of enzymatic tracer on the amperometric responses measured with the resulting Biotin-anti-CD105-CD105-anti-CD105-pPPA/SPCEs immunosensors in the absence (grey) or in the presence of 1.0 ng mL^{-1} CD105 (black). Error bars estimated as triple of the standard deviation (n = 3).

References

[1] U. Eletxigerra, J. Martínez-Perdiguero, S. Merino, R. Barderas, V. Ruiz-Valdepeñas Montiel, J.M. Pingarrón, S. Campuzano, Estrogen receptor α determination in serum, cell lysates and breast cancer cells using an amperometric magnetoimmunosensing platform. Sens. Biosensing Res. 7 (2016) 71–76.

[2] I. Ojeda, M. Moreno-Guzmán, A. González-Cortés, P. Yáñez-Sedeño, J. M. Pingarrón, Electrochemical magnetoimmunosensor for the ultrasensitive determination of interleukin-6 in saliva and urine using poly-HRP streptavidin conjugates as labels for signal amplification, Anal. Bioanal. Chem. 406 (2014) 6363–6371.

Journal of Electroanalytical Chemistry 793 (2017) 197–202

Electrochemical immunosensor for the determination of 8-isoprostane aging biomarker using carbon nanohorns-modified disposable electrodes

Journal of Electroanalytical Chemistry 793 (2017) 197–202

Contents lists available at ScienceDirect

Journal of Electroanalytical Chemistry

journal homepage: www.elsevier.com/locate/jelechem

Electrochemical immunosensor for the determination of 8-isoprostane aging biomarker using carbon nanohorns-modified disposable electrodes

E. Sánchez-Tirado [a], A. González-Cortés [a], M. Yudasaka [b], S. Iijima [c], F. Langa [d], P. Yáñez-Sedeño [a,*], J.M. Pingarrón [a]

[a] Department of Analytical Chemistry, Faculty of Chemistry, University Complutense of Madrid, Ciudad Universitaria s/n, 28040 Madrid, Spain
[b] Nanotube Research Center, National Institute of Advanced Industrial and Technology, Higashi, Tsukuba, Ibaraki 305-8565, Japan
[c] Department of Physics, Meijo University, Shiogamaguchi, Tenpaku-ku, Nagoya 468-8502, Japan
[d] Instituto de Nanociencia, Nanotecnología y Materiales Moleculares (INAMOL), Universidad de Castilla-La Mancha, 45071 Toledo, Spain

ARTICLE INFO

Article history:
Received 15 September 2016
Received in revised form 24 October 2016
Accepted 2 November 2016
Available online 4 November 2016

Keywords:
Aging biomarkers
Electrochemical immunosensors
8-isoprostane
Prostaglandin

ABSTRACT

The first electrochemical immunosensor for the determination of 8-isoprostane (8-iso prostaglandin F2α, ISO), one of the most reliable biomarkers of lipid peroxidation in the human body and of aging related to Alzheimer's disease or atherosclerosis is reported in this article. Disposable screen-printed carbon electrodes modified with carboxylated carbon nanohorns (CNHs) were employed as scaffolds for covalent immobilization of a specific anti-ISO antibody). A competitive immunoassay involving ISO and HRP-labeled antigen was designed and the determination of ISO was carried out by amperometry at −200 mV using the H_2O_2/hydroquinone (HQ) system. Under the optimized conditions, the immunosensor provides a linear response for ISO ($r^2 = 0.998$) extending up to 700 pg/mL, which is suitable for the determination of the target compound in human serum. The analytical performance of the immunosensor improves that claimed for ELISA kits in terms of linearity of the calibration plot, precision, with RSD values lower than 1%, and assay time (1 h 30 min), and exhibits a low limit of detection, 12 pg/mL, a long storage stability (30 days), and an excellent selectivity against other proteins that may be found in human serum. The analytical utility of the developed immunosensor was demonstrated by determining ISO in two types of human serum samples: lyophilized spiked serum, and real human serum from healthy male and female individuals with good results.

© 2016 Elsevier B.V. All rights reserved.

1. Introduction

Isoprostanes are prostaglandin–like compounds produced through the oxygen radical induced peroxidation of tissue phospholipids and lipoproteins [1]. Among them, 8-isoprostane (8-iso-prostaglandin F2α, ISO) (Fig. 1), a stable product of oxidative stress, is one of the most reliable biomarkers of lipid peroxidation in the human body [2], and of aging related to Alzheimer's disease or atherosclerosis [3]. Although detectable quantities of isoprostanes are usually present in tissues and biological fluids including plasma, saliva and urine, their levels increase as the oxidative damage increases [4]. Relatively high isoprostanes concentrations appear in smokers, and in patients suffering cardiovascular diseases, diabetes, obesity, hypercholesterolemia, metabolic syndrome [5], or cancer [6]. Although GC–MS and LC–MS/MS are the recommended techniques for the determination of 8-isoprostane in clinical samples [7,8], the methods, mainly applied to urine, are characterized by their high cost, extensive sample extraction and low throughput. As an alternative, ELISA immunoassays are also used. Table 1 summarizes the analytical characteristics claimed for various commercial ELISA kits for the determination of ISO. All configurations used involve competitive-type immunoassays and most of them use HRP-labeled immunoreagents and colorimetric detection upon H_2O_2 addition in the presence of 3,3′,5,5′-tetramethylbenzidine (TMB). Less common are those using acetylcholinesterase (AChE) or alkaline phosphatase-labeled ISO. The addition of Ellman's reagent containing the substrate of AChE or *p*-nitrophenyl phosphate, respectively, allows the colorimetric detection to be performed. Despite the claimed advantages of immunosensors versus ELISA concerning higher sensitivity and lower detection limits, better precision, and shorter assay times [9,10], no immunosensors for the determination of ISO have been described in the literature so far.

On the other hand, single-walled carbon nanohorns, SWCNHs (or simply CNHs), are a relatively new type of carbon allotrope consisting of a unique horn-shaped graphene with a diameter of 2–5 nm and a length of 40–50 nm [11]. CNHs assemble to form nanostructures shaped like dahlia flowers [12], with a diameter around 100 nm that enables an easy dispersion in liquids [13]. Another important feature is that

* Corresponding author.
E-mail address: yseo@quim.ucm.es (P. Yáñez-Sedeño).

http://dx.doi.org/10.1016/j.jelechem.2016.11.003
1572-6657/© 2016 Elsevier B.V. All rights reserved.

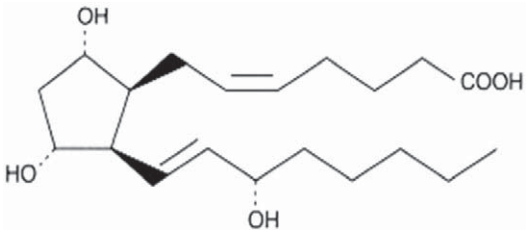

Fig. 1. Structure of 8-isoprostane (8-iso-prostaglandin F2α, ISO).

production of CNHs is performed in the absence of metal catalysts, so that they can be used directly without post treatment or purification [14]. Moreover, CNHs possess high conductivity, large surface area, and abundant oxidizable defects that provide a great number of oxygenated groups affordable for biomolecules immobilization [15]. Despite these interesting properties, scarce applications have been reported up to date related with the preparation of electrochemical immunosensors involving CNHs functionalized electrodes [16]. A competitive immunoassay design for the determination of microcystin-LR (MC-LR) involving covalent immobilization of the antigen to oxidized CNHs and the use of HRP-anti-MC-LR was reported by Zhang et al. [17]. More recently, a sandwich-type impedimetric immunosensor for α-fetoprotein (AFP) was prepared by linking HRP and GOx enzymes to CNHs and biocatalyzed precipitation in the presence of 4-chloro-1-naphthol and H_2O_2 which led to a significant enhancement of the signal from $Fe(CN)_6^{3-/4-}$ redox couple [18]. Our group also used carboxylated CNHs to construct electrochemical platform for the preparation of an immunosensor for fibrinogen (Fib) [19]. The approach involved the use of HOOC-CNHs deposited onto a SPCE to covalently immobilize Fib, and the establishment of an indirect competitive assay with horseradish peroxidase labeled Fib. A composite combining CNHs and alginic acid was also used to develop a sandwich-type enzyme-free immunosensor for carcinoembryonic antigen (CEA) [20]. The large concentration of immobilized antibodies provided a high sensitivity that was enhanced by using magnetic $NiCo_2O_4$ NPs decorated with hematin as labels for the secondary antibodies. A Chitosan/CNHs composite demonstrated to be also a suitable electrochemical platform to construct an electrochemical immunosensor for alpha-fetoprotein (AFP) [21].

In this work the first electrochemical immunosensor for the determination of ISO is reported. A simple and rapid strategy was developed involving the use of disposable screen-printed carbon electrodes modified with carboxylated CNHs as scaffolds for covalent immobilization of a specific antibody (anti-ISO). A competitive immunoassay involving the target antigen (ISO) and HRP-labeled antigen (HRP-ISO) was employed. ISO quantification was carried out by amperometry at −200 mV (vs. Ag pseudo-reference electrode) using the H_2O_2/hydroquinone (HQ) system. Therefore, the reduction current of the generated quinone at the SPCE surface was the analytical readout. All the steps involved in the preparation and performance of anti-ISO-CNHs/SPCE immunosensor were optimized and, under the optimized conditions, ISO could be determined with a high sensitivity. The analytical utility of the developed immunosensor was demonstrated by determining ISO in two types of human serum samples: lyophilized spiked serum, and real human serum from healthy male and female individuals with good results.

2. Experimental

2.1. Reagents and solutions

The rabbit anti-ISO capture antibody, the antigen (ISO), and the HRP-labeled antigen (HRP-ISO) used were the reagents included in the ELISA kit OxiSelect™ (STA-337) from Cell Biolabs. Working solutions from the antibody were prepared in a 25 mM 2-(*N*-morpholino) ethanesulfonic (MES, Gerbu) buffer solution of pH 5.0. Sample Diluent from Cell Biolabs was the solvent used to prepare ISO and HRP-ISO working solutions. CNHs were synthesized in the absence of metallic catalysts by graphite ablation with a CO_2 laser under argon atmosphere at 760 Torr and room temperature. The purity was higher than 90% and the 10% impurity was micrometer-sized graphitic balls [22]. CNHs oxidation was performed by treatment with a 30% H_2O_2 aqueous solution at ≈100 °C [23]. Activation of the carboxylic groups of CNHs for further immobilization of capture antibodies was made by using 1-ethyl-3-(3-dimethylaminopropyl)carbodiimide hydrochloride (EDC) and *N*-hydroxysulfosuccinimide (NHSS) (Acros Organics). Bovine serum albumin (BSA) from Gerbu was used as blocking agent. Compounds tested as potential interfering substances were: adiponectin (APN), ceruloplasmin (Cp), interleukin-6 (IL-6), interleukin-8 (IL-8) (Abcam), bilirubin (BR) (Aldrich), cholesterol (Chol), creatinin (CR), hemoglobin (HB) (Sigma), transforming growth factor β1 (TGF–β1), tumor necrosis factor α (TNF–α) (R&D Systems), and C reactive protein (CRP) (Fitzgerald). Hydrogen peroxide (Aldrich, 30% (w/w)) and hydroquinone (HQ) (Sigma) were used for the amperometric measurements.

Table 1
Analytical characteristics reported for various ELISA immunoassays for ISO determination.

Type of immunoassay	ELISA kit	Dynamic range, pg/mL	MDC, pg/mL	Precision, RSD % (inter/intra assays)	Assay time
Direct competitive between ISO and HRP-ISO Substrate: TMB	Eagle Bioscience (8IS39-K01)	10–5000	10	–	2 h 30 min
	Cayman Chemical (516351)	0.8–500	2.7	7.2%/15.5%	2 h
	Saphire Bioscience (133–16,456)	1.4–3000	18	≤10%/≤12.6%	3 h 30 min
	Neogen Corporation (430110)	50–10,000	30	≤10%/≤10%	2 h 40 min
	Cusabio (CSB-E12100h)	78–5000	19.5	<15%/<15%	2 h 30 min
	EIAab (E0701h)	1.56–100	1	–	4 h 30 min
	Abcam (ab175819)	5–5000	1	–	2 h 30 min
	Oxford Biomed. Res. (EA84)	50–100	–	–	2 h 30 min
	Abbexa Ltd. (abx055460)	16–1000	5	–	2 h 30 min
	US Biological (I9050)	100–1000	100	–	2 h 30 min
	Abnova (KA0443)	50–10,000	100	–	2 h 40 min
	Invitrogen (KHP0041)	500–16,000	100	3.8%/4.6%	2 h 20 min
	Northwest (NWK-IS002)	50–10,000	50	–	2 h 30 min
	Detroit R&D, Inc. (8Iso1)	500–16,000	100	–	2 h 30 min
	Cell Biolabs (STA-337)	50–200	50	–	2 h 30 min
Direct competitive between SO and AP-ISO Substrate: *p*NPP	IBL (CM500431)	23.4–3000	2.7	7.2%/15.5%	2 h
	CD Creative Diagnost. (DEIA6463)	40–100	40	12%/20%	3 h 30 min
	Enzo Life Sciences ADI-900-069	3–50,000	6.71	9.7–13.1%	<3 h
Direct competitive between ISO and AChE-ISO. Substrate: thiocholine	CD creatIve Diagnost. (DEIA5014)	40–100	10	12%/20%	3 h 30 min
	CD Creative Diagnost. (DEIA6464)	40–100	16.3	12%/20%	3 h 30 min

Abbreviations: MDC, minimum detectable concentration; ISO, 8 isoprostane; HRP-ISO, peroxidase-labeled isoprostane; TMB, 3,3′5,5′-tetramethylbenzidine; AChE-ISO, acetilcholinesterase-labeled isoprostane; *p*NPP, 4-nitrophenyl phosphate.

Deionized water from a Millipore Milli–Q (18.2 MΩ cm at 25 °C) purification system was also used.

Samples analyzed were lyophilized human serum (S2257, Sigma) spiked with 30, 35 and 40 pg/mL ISO, and real human serum samples from healthy male and female individuals (BBI Solutions, SG610–2 y SG609–2, respectively). Validation was accomplished by comparing the results with those obtained by using the OxiSelect™ ELISA kit (STA-337) from Cell Biolabs.

2.2. Apparatus and electrodes

Amperometric measurements were made with an INBEA potentiostat using the IbGraph software (INBEA S.L., Madrid, Spain). Screen-printed carbon electrodes (SPCEs, 110 DRP, ϕ4 mm) from DropSens (Oviedo, Spain) were used as working electrodes. These electrodes are provided with a silver pseudo-reference electrode and a carbon counter electrode. Electrochemical impedance spectrocopy was carried out with an Autolab type III potentiostat (Ecochemie) controlled by FRA2 software. Incubation steps were performed at 25 °C using an Optic Ivymen System constant temperature incubator shaker (Comecta S.A.) and pH measurements were made using a Crison Basic 20 + pH meter. A P-Selecta ultrasonic bath, an MPW-65R centrifuge (MPW Med. Instruments), and a Vortex homogenizator from Heidolph were also used. Absorbance measurements in the ELISA method were made using a Sunrise™ Tecan microplate reader provided with the Magellan software. All experiments were performed at room temperature.

2.3. Procedures

2.3.1. Preparation of the immunosensor

Oxidized CNHs (1 mg) were suspended in 2 mL of deionized water in an Eppendorf tube and ultrasonicated for 90 min. Once homogenized, a 5-μL aliquot was transferred to the electrode surface and dried under IR radiation. This operation was repeated by depositing another 5-μL aliquot. Activation of CNHs carboxyl groups was made by addition of 5 μL of a 0.1 M each EDC/NHSS mixture solution, prepared in 25 mM MES buffer solution of pH 5.0, onto CNHs/SPCE, and let to stand during 30 min. Thereafter, immobilization of the capture antibody was accomplished by adding 5 μL of a 1/600 diluted anti-ISO solution prepared in 25 mM MES buffer solution of pH 5.0, allowing incubation for 60 min at 25 °C. Then, the anti-ISO-CNHs/SPCE immunosensor was washed with deionized water and allowed drying in air. Next, a blocking step was applied by adding 5 μL of a 2% BSA solution and incubating for 30 min followed by washing with water. Finally, the resulting immunosensors were preserved by adding 50 μL of 50 mM phosphate buffer solution of pH 6.0 until use.

2.3.2. Immunoassay at anti-ISO-CNHs/SPCE

A competitive immunoassay scheme was employed for the determination of ISO. A mixture solution of the antigen (ISO) and the labeled antigen (HRP-ISO) was prepared in an Eppendorf tube with 5 μL of standard ISO solutions of variable concentration or the sample, and 5 μL of a 1/250 diluted HRP-ISO solution. Then, 5 μL from this mixture solution were dropped onto the as prepared anti-ISO-CNHs/SPCE and incubated for 45 min. Amperometric measurements were obtained after addition of 45 μL of a 1 mM HQ solution prepared in a 50 mM phosphate buffer solution of pH 6.0, and by applying a detection potential of −200 mV. Once the background current was stabilized (200 s approximately), a 5-μL aliquot of 50 mM hydrogen peroxide solution was added and, after a period of 200 s for allowing the enzymatic reaction to take place, the reduction current of the formed quinone was measured.

2.3.3. Analysis of human serum

As indicated above, two types of human serum samples were analyzed. Lyophilized solid serum was reconstituted in deionized water and, once spiked, it was 1:1 diluted with HRP-ISO solution. No further treatment was necessary. A simple treatment was applied to real serum samples. It consisted of the addition of 100 μL of 10 M NaOH to 400 μL of sample and incubation for 2 h at 45 °C. This treatment was applied to hydrolyze lipoprotein and phospholipid coupled ISO in order to measure both free and esterified ISO. Then, 100 μL of 10 M HCl were added to assist precipitation of lipoproteins and phospholipids. Centrifugation at 12,000 rpm for 5 min was carried out and the supernatant should be in the 6–8 pH range. In both cases, the determination of ISO was carried out by interpolation of the amperometric responses measured for the samples into the calibration plot constructed with ISO standards. Furthermore, validation of the results for real serum samples was accomplished by comparison with those provided by an ELISA method for human ISO from Cell Biolab. In this case, the protocol indicated in the supplier's directions was followed. In brief, this consisted of pipetting a mixture solution of ISO standards or samples and HRP-ISO into the anti-ISO coated-well plates and leaving an incubation time of 60 min. Then, colour development was achieved by addition of TMB substrate solution and after 20 min, an acid “stop solution” was added, and the absorbance was measured at 450 nm.

3. Results and discussion

The synthesis and characterization of CNHs were performed as described previously [19]. As indicated in the Experimental section, 30% aqueous H_2O_2 was used for CNHs oxidation and generation of carboxylic acid groups [23] for further antibodies immobilization. The fundamentals of the different steps involved in the immunoreaction occurring on the activated functionalized CNHs-modified SPCE as well as of the amperometric transduction strategy are schematically depicted in Fig. 2. Once carboxylated CNHs were adsorbed on the electrode surface, anti-ISO antibodies were covalently immobilized and the remaining active sites on the SPCE surface blocked with BSA. Thereafter, a competitive immunoassay strategy was designed by dropping onto the anti-ISO-CNHs/SPCE immunosensor a mixture solution of the target analyte and HRP-ISO. The amperometric response for ISO quantification was measured upon addition of H_2O_2 as HRP substrate in the presence of HQ as the redox mediator.

3.1. Optimization of experimental variables involved in the performance of the immunosensor

Variables involved in the preparation of the immunosensor and its electrochemical performance were optimized. The evaluated variables were: a) loading of anti-ISO antibody immobilized onto CNHs/SPCE; b) concentration of HRP-ISO conjugate; c) time for competition between ISO and HRP-ISO for the binding sites of the capture antibody; d) reagents and incubation time used for blocking the remaining unmodified sites on the electrode surface. Details on the optimization studies are provided in the Supporting Information and in Figs. S1–S4. Other variables such as the amount of CNHs adsorbed onto the electrode surface (5 μg) or the composition of the H_2O_2/HQ system and the detection potential were optimized in previous works [19,24].

3.2. Characterization of the immunosensor by electrochemical impedance spectroscopy and cyclic voltammetry

Electrochemical impedance spectroscopy (EIS) was employed to monitor the different steps involved in the preparation of the immunosensor. Fig. 3a shows the Nyquist plots recorded for bare SPCE, HOOC-CNHs/SPCE, anti-ISO-CNHs/SPCE, and HRP-ISO-anti-ISO-CNHs/SPCE, using 5 mM $Fe(CN)_6^{3-/4-}$ in 100 mM KCl of pH 7.0 as the redox probe. As it can be seen, the charge transfer resistance at the bare SPCE (curve 1) was notably higher (R_{CT} = 284 Ω) than that measured for the CNHs//SPCE (curve 2, R_{CT} = 15 Ω) due to the expected electron transfer promotion occurring at carbon nanohorns-modified electrodes. The resistance increased to 45 Ω when the anti-ISO

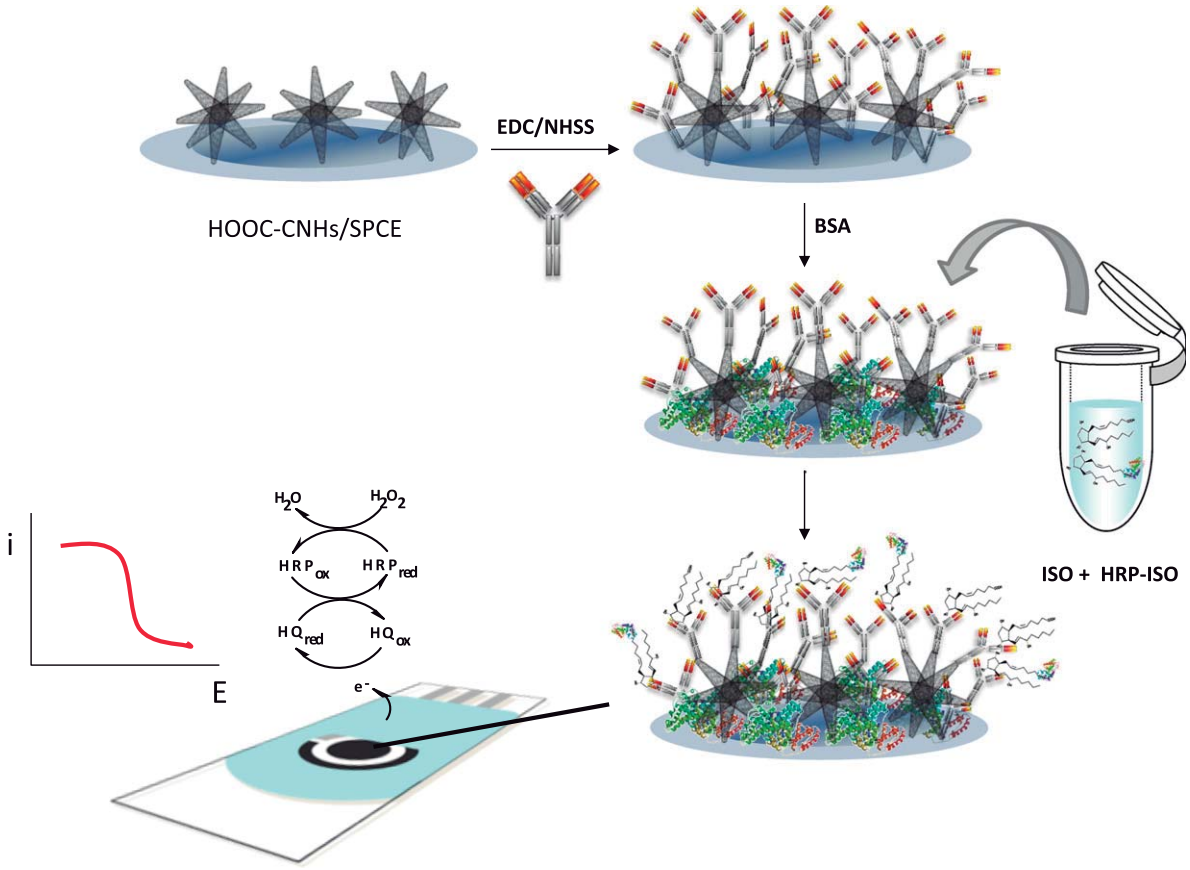

Fig. 2. Schematic display of the different steps involved in the preparation and functioning of the anti-ISO-CNHs/SPCE immunosensor.

antibodies were deposited onto the CNHs/SPCE surface (curve 3), as a consequence of the isolating effect provoked by the biomolecules. It is interesting to remark that despite this isolating effect, the R_{CT} value is notably low which points out the electron transfer promotion caused by the presence of CNHs as electrode modifying material. Subsequent immobilization of the HRP-labeled antigen led to a further resistance increase (curve 4) (R_{CT} = 338 Ω), due to the lower conductivity of the resulting biosurface. Fig. 3b shows cyclic voltammograms for the same redox probe solution recorded at SPCE, HOOC-CNHs/SPCE, anti-ISO-CNHs/SPCE, and HRP-ISO-anti-ISO-CNHs/SPCE. Results are consistent with those obtained by EIS. A noticeable increase in the oxidation and reduction peak current values for $Fe(CN)_6^{3-/4-}$ was observed when SPCEs were modified with HOOC-CNHs (voltammogram 2) which is attributed to the improved electron transfer upon modification with CNHs. Surface immobilization of anti-iSO and formation of the immunocomplexes with HRP-ISO (voltammograms 3 and 4, respectively) produced slight decreases in the peak current values most likely due to the high conductivity of the modified electrode surface despite immobilization of biomolecules. These results confirmed the suitability of the used procedures for the electrode modification and immobilization of anti-ISO antibodies onto CNHs/SPCEs.

3.3. Analytical figures of merit of the immunosensor

Fig. 4 shows the linear calibration plot (r^2 = 0.998) for ISO constructed by amperometry at −0.20 V with the anti-ISO-CNHs/SPCE immunosensor. The corresponding equation is: i_p, nA = (850 ± 8) [ISO, ng/mL] + (623 ± 3 nA), and the linear range extends up to

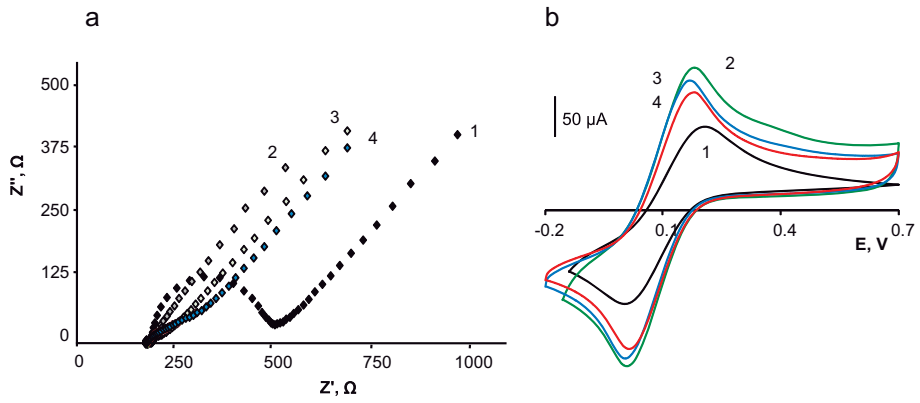

Fig. 3. Nyquist plots (a) and cyclic voltammograms (b) recorded for (1) bare SPCE, (2) CNHs//SPCE, (3) anti-ISO-CNHs/SPCE, and (4) HRP-ISO-anti-ISO-CNHs/SPCE with 5 mM $Fe(CN)_6^{3-/4-}$ in 100 mM KCl of pH 7.0.

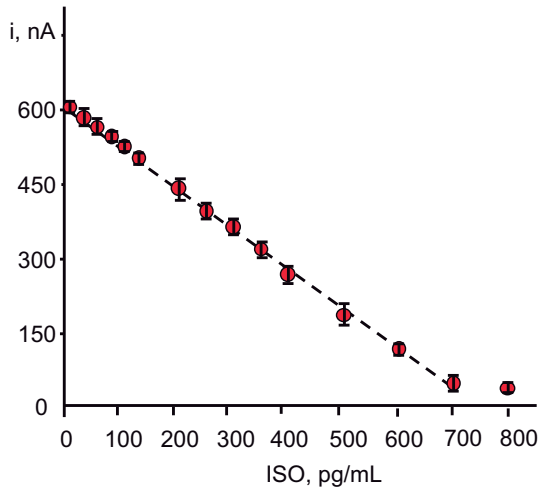

Fig. 4. Calibration plot for ISO constructed with the anti-ISO-CNHs/SPCE immunosensor. See text for the experimental conditions.

700 pg/mL ISO. Interestingly, this range is suitable for the determination of the target compound in human serum since the concentration levels found in healthy individuals are comprised between few tens and few hundreds of pg/mL [25,26]. The limit of detection, 12 pg/mL, was calculated as the lowest concentration that can be statistically discriminated from zero, according to the $\bar{x} + 3s$ criterion, where s was estimated as the standard deviation (n = 10) for the blank (measurements in the absence of ISO) in concentration units (pg/mL). The limit of quantification achieved, $\bar{x} + 10s$, was 19 pg/mL.

The reproducibility of the amperometric measurements was tested by repetitive measurements carried out for 0 and 50 pg/mL ISO carried out with six different immunosensors. Relative standard deviations values, RSD, of 0.36 and 0.35%, respectively were calculated for immunosensors prepared in the same day, while RSD values of 0.53 and 0.40%, respectively, were found for immunosensors prepared in different days. These results demonstrated an excellent accuracy of the amperometric measurements and indicated that the proposed method for the immunosensor preparation was reliable and reproducible. When these analytical figures of merit are compared with data provided for commercial ELISA kits using similar immunoreagents, some noticeable differences become apparent. ELISA kits usually provide non-linear dynamic ranges covering from several tens to thousands of pg/mL with minimum detectable concentrations (MDC) of tens (or even one hundred) pg/mL. These parameters are calculated mostly from nonlinear logarithmic plots and the precision levels are around 10% or higher. It is important to note that the criteria used to calculate the MDC values for these kits are rarely given in the commercial protocols. Moreover, the time lasted for the assay is remarkably longer with ELISA kits which mostly require 2 h 30 min versus 1 h 20 min needed when the immunosensor is used (counting, in both cases, since the immobilization of capture antibody). Therefore, it can be concluded that the analytical performance of the developed immunosensor, covering a wide linear range of clinically relevant ISO concentrations, improves, in general terms, the analytical performance claimed for ELISA kits.

The storage capability of the anti-ISO-CNHs/SPCE bioelectrode was also tested. Different immunosensors were prepared on the same day and stored at −20 °C under dry conditions. Then, the immunosensors were used in different days to measure solutions without ISO. A control chart was constructed (Fig. S5) by setting as control limits ±3s, where s was the standard deviation of the measurements (n = 10) carried out on the first day. The immunosensor responses remained inside the control limits for 30 days, decreasing for longer storage periods probably as a consequence of the loose of activity of the antibody. These results suggested the possibility of preparing a set of anti-ISO-CNHs/SPCEs immunosensors and keeping them under storage until their use for the analysis of samples was requested.

Regarding the selectivity of the immunosensor, it is important to remind that anti-ISO antibodies used were the same that those employed in the ELISA kit OxiSelect™ (STA-337) from Cell Biolabs. These antibodies exhibited a high specificity toward ISO (8-isoprostane, 8-iso-PGF2α), versus other types of similar compounds, with cross-reactivity factors of 4.6% (PGF1α) or 1.8% (PGF2α), and much lower CR% for other derivatives [http://www.cellbiolabs.com/8-iso-prostaglandin-f2a-assay]. Therefore, we tested the additional selectivity of the capture antibody by measuring the amperometric responses of the immunosensor for 0 and 50 pg/mL ISO in the presence of other proteins: adiponectin (APN), bovine serum albumin (BSA), bilirubin (BR), cholesterol (Chol), ceruloplasmin (Cp), transforming growth factor β1 (TGF), tumoral necrosis factor alpha (TNF), hemoglobin (Hb), interleukin-6 (IL-6), and interleukin-8 (IL-8) at concentration levels that can be found in serum of healthy individuals. Fig. 5 shows clearly as no significant differences were apparent between the currents measured in the absence or in the presence of these compounds, thus demonstrating the practical specificity of the immunosensor for the determination of ISO.

3.4. Determination of ISO in human serum

The developed immunosensor was applied to the determination of ISO in two types of human serum, lyophilized spiked serum, and real human serum from healthy male and female individuals by applying the procedures described in Section 2.3.3. Regarding lyophilized serum, the possible existence of matrix effects was initially evaluated by constructing a calibration plot for reconstituted serum and spiked with ISO over the 0 to 40 pg/mL concentration range. The equation for the corresponding linear calibration graph was: i_p, nA = (896 ± 3) [ISO, ng/mL)] + (624 ± 1, nA). No statistically significant difference was found with the slope value of the calibration plot constructed with ISO standard solutions as the Student's t_{exp} value, 1.247, was lower than the tabulated one, $t_{tab} = 4.303$ for a 0.05 significance level. Therefore, no significant matrix effect was found and the determination of ISO could be carried out by interpolation of the current values measured for the serum samples into the calibration plot constructed with ISO standard solutions. Table 2 summarizes the results obtained by triplicate for lyophilized serum spiked at three different concentration levels. Recoveries ranged between 95 and 101%, indicating the reliability of the approach to determine low ISO concentrations in this kind of sample following a very simple working protocol.

Furthermore, two real human sera from male and female healthy individuals were also analyzed. As it was described in the Experimental Section 2.3.3, a simple treatment was applied to these samples with the aim of hydrolizing lipoproteins and phospholipids to which ISO could be bound. This treatment was that recommended for the ELISA test for human ISO by Cell Biolab [http://www.cellbiolabs.com/8-iso-prostaglandin-f2a-assay].

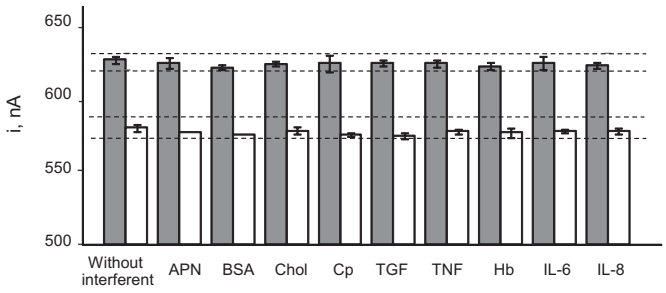

Fig. 5. Interferences study: 0 (grey) and 50 (white) pg/mL ISO in the presence of 20 μg/mL adiponectin (APN), 5 mg/mL BSA, 20 μg/mL cholesterol (Chol), 500 μg/mL ceruloplasmin (Cp), 500 pg/mL transforming growth factor β1 (TGF), 100 pg/mL tumor necrosis factor α (TNF), 50 μg/mL hemoglobin (Hb), 50 pg/mL interleukin 6 (IL-6), 30 pg/mL interleukin 8 (IL-8).

Table 2
Determination of ISO in human serum samples with anti-ISO-CNHs/SPCE immunosensors.

Lyophilized spiked serum		
ISO, pg/mL	ISO found, pg/mL (n = 3)	Recovery, %
30	30 ± 4	100 ± 1
35	33 ± 7	95 ± 6
40	42 ± 3	101 ± 4
Real human serum		
Type	Immunosensor, pg/mL (n = 6)	ELISA, pg/mL (n = 6)
Healthy male (SG610-2, BBI)	403 ± 7	408 ± 5
Healthy female (SG609-2, BBI)	394 ± 4	398 ± 3

Once verified the absence of matrix effects, the determination of ISO was carried out by interpolation of the amperometric responses for the samples into the calibration plot constructed with ISO standards. Validation of the obtained results was accomplished by comparing them with those provided by the OxiSelect™ (STA–337) ELISA kit from Cell Biolabs following the procedure specified in Section 2.3.3. The results obtained by both methods are summarized in Table 2. RSD values (n = 6) were in all cases lower than 2% exhibiting an excellent precision. The concentrations found were also statistically compared by means of the Student's *t*-test, obtaining t_{exp} values of 1.714 (male) and 1.107 (female) which were lower than tabulated *t* (2.228). These results confirm that no significant differences were apparent between both methodologies at a significance level of 0.05. All these results demonstrate clearly the usefulness of the developed immunosensor to determine ISO at clinically relevant concentrations in human serum.

4. Conclusions

The first immunosensor for the determination of the aging biomarker 8-isoprostane is reported in this paper. In order to improve the analytical performance of the immunosensor an electrochemical platform consisting of disposable SPCE modified with carboxylated CNHs has been used as scaffold for the covalent immobilization of specific anti-ISO antibodies. Using a competitive immunoassay, ISO can be determined in human serum with a high sensitivity derived not only from the high conductivity of CNHs but also because of the large number of oxygenated moieties present on the CNHs-modified electrode surface allowing subsequent high loading of capture antibodies. The analytical performance exhibited by the electrochemical immunosensor is excellent, improving, in general terms, that provided by ELISA kits. The usefulness of the immunosensor was demonstrated by determining ISO in lyophilized spiked serum, and real human serum from healthy male and female individuals with results in statistic agreement with those found by applying an ELISA kit.

Acknowledgements

Financial support from the Spanish Ministerio de Economía y Competitividad, Research Projects CTQ2015-70023-R and CTQ2015-71955-REDT, and the NANOAVANSENS Program from Comunidad de Madrid (S2013/MT-3029) is gratefully acknowledged.

Appendix A. Supplementary data

Supplementary data to this article can be found online at doi:10.1016/j.jelechem.2016.11.003.

References

[1] T. Petrosino, M. Serafini, Antioxidant modulation of F2-Isoprostanes in humans: a systematic review, Crit. Rev. Food Sci. Nutr. 54 (2014) 1202–1221.
[2] K. Mizuno, H. Kataoka, Analysis of urinary 8-isoprostane as an oxidative stress biomarker by stable isotope dilution using automated online in-tube solid-phase microextraction coupled with liquid chromatography–tandem mass spectrometry, J. Pharm. Biomed. Anal. 112 (2015) 36–42.
[3] G.L. Milne, Q. Dai, L.J. Roberts II, The isoprostanes-25 years later, Biochim. Biophys. Acta 1851 (2015) 433–445.
[4] T.A. McGowan, S.R. Dunn, B. Faulkner, K. Sharma, Stimulation of urinary TGF-β1 and isoprostanes in response to hyperglycemia in humans, Clin. J. Am. Soc. Nephrol. 1 (2006) 263–268.
[5] P. Montushi, P. Barnes, R.L. Jackson II, Insights into oxidative stress: the isoprostanes, Curr. Med. Chem. 14 (2007) 703–717.
[6] D.A. Barocas, S. Motley, M.S. Cookson, S.S. Chang, D.F. Penson, Q. Dai, G. Milne, L.J. Roberts II, J. Morrow, R.S. Concepcion, J.A. Smith Jr., J.H. Fowke, Oxidative stress measured by urine F2-isoprostane level is associated with prostate cancer, J. Urol. 185 (2011) 2102–2107.
[7] K.A. Smith, J. Shepherd, A. Wakil, E.S. Kilpatrick, A comparison of methods for the measurement of 8-isoPGF2α: a marker of oxidative stress, Ann. Clin. Biochem. 48 (2011) 147–154.
[8] J. Klawitter, M. Haschke, T. Shokati, J. Klawitter, U. Christians, Quantification of 15-F2α-isoprostane in human plasma and urine: results from enzyme-linked immunoassay and liquid chromatography/tandem mass spectrometry can not be compared, Rapid Commun. Mass Spectrom. 25 (2011) 463–468.
[9] I. Ojeda, M. Moreno-Guzmán, A. González-Cortés, P. Yáñez-Sedeño, J.M. Pingarrón, Electrochemical magnetoimmunosensor for the ultrasensitive determination of interleukin-6 in saliva and urine using poly-HRP streptavidin conjugates as labels for signal amplification, Anal. Bioanal. Chem. 406 (2014) 6363–6371.
[10] S. Guerrero, G. Martínez-García, V. Serafín, L. Agüí, P. Yáñez-Sedeño, J.M. Pingarrón, Electrochemical immunosensor for sensitive determination of the anorexigen peptide YY at grafted reduced graphene oxide electrode platforms, Analyst 140 (2015) 7527–7533.
[11] S. Zhu, J. Zhang, X. Zhao, H. Wang, G. Xu, J. You, Electrochemical behavior and voltammetric determination of L-tryptophan and L-tyrosine using a glassy carbon electrode modified with single-walled carbon nanohorns, Microchim. Acta 181 (2014) 445–451.
[12] L. Shi, X. Liu, W. Niu, H. Li, S. Han, J. Chen, G. Xu, Hydrogen peroxide biosensor based on direct electrochemistry of soybean peroxidase immobilized on single-walled carbon nanohorn modified electrode, Biosens. Bioelectron. 24 (2009) 1159–1163.
[13] J. Miyawaki, M. Yudasaka, T. Azami, Y. Kubo, S. Iijima, Toxicity of single-walled carbon nanohorns, ACS Nano 2 (2008) 213–226.
[14] H. Tanaka, H. Kanoh, M. El-Merraoui, W.A. Steele, M. Yudasaka, S. Iijima, K. Kaneko, Quantum effects on hydrogen adsorption in internal nanospaces of single-wall carbon nanohorns, J. Phys. Chem. B 108 (2004) 17457–17465.
[15] K. Ajima, M. Yudasaka, T. Murakami, A. Maigne, K. Shiba, S. Iijima, Carbon nanohorns as anticancer drug carriers, Mol. Pharm. 2 (2005) 475–480.
[16] P. Yáñez-Sedeño, A. González-Cortés, L. Agüí, J.M. Pingarrón, Uncommon carbon nanostructures for the preparation of electrochemical immunosensors, Electroanalysis 28 (2016) 1679–1691.
[17] J. Zhang, J. Lei, C. Xu, L. Ding, H. Ju, Carbon nanohorn sensitized electrochemical immunosensor for rapid detection of microcystin-LR, Anal. Chem. 82 (2010) 1117–1122.
[18] F. Yang, J. Han, Y. Zhuo, Z. Yang, R. Yuan, Highly sensitive impedimetric immunosensor based on single-walled carbon nanohorns as labels and bienzyme biocatalyzed precipitation as enhancer for cancer biomarker detection, Biosens. Bioelectron. 55 (2014) 360–365.
[19] I. Ojeda, B. Garcinuño, M. Moreno-Guzmán, A. González-Cortés, M. Yudasaka, S. Iijima, F. Langa, P. Yáñez-Sedeño, J.M. Pingarrón, Carbon nanohorns as a scaffold for the construction of disposable electrochemical immunosensing platforms. Application to the determination of fibrinogen in human plasma and urine, Anal. Chem. 86 (2014) 7749–7756.
[20] H. Dai, L. Gong, S. Zhang, G. Xu, Y. Li, Z. Hong, Y. Lin, All-in-one bioprobe devised with hierarchical-ordered magnetic $NiCo_2O_4$ superstructure for ultrasensitive dual-readout immunosensor for logic diagnosis of tumor marker, Biosens. Bioelectron. 77 (2016) 928–935.
[21] H. Dai, S. Zhang, L. Gong, Y. Li, G. Xu, Y. Lin, Z. Hong, The photoelectrochemical exploration of multifunctional TiO_2 meso-crystals and its enzyme-assisted biosensing application, Biosens. Bioelectron. 72 (2015) 18–24.
[22] S. Utsumi, M. Miyawaki, H. Tanaka, Y. Hattori, H. Itoi, N. Ichikuni, H. Kanoh, M. Yudasaka, S. Iijima, K. Kaneko, Opening mechanism of internal nanoporosity of single-wall carbon nanohorn, J. Phys. Chem. B 109 (2005) 14319–14324.
[23] M. Zhang, M. Yudasaka, K. Ajima, J. Miyawaki, S. Iijima, Light-assisted oxidation of single-wall carbon nanohorns for abundant creation of oxygenated groups that enable chemical modifications with proteins to enhance biocompatibility, ACS Nano 1 (2007) 265–272.
[24] M. Eguílaz, M. Moreno-Guzmán, S. Campuzano, A. González-Cortés, P. Yáñez-Sedeño, J.M. Pingarrón, An electrochemical immunosensor for testosterone using functionalized magnetic beads and screen-printed carbon electrodes, Biosens. Bioelectron. 26 (2010) 517–522.
[25] A.P. Cabral de Faria, V. Fontana, R. Modolo, N.R. Barbaro, A.R. Sabbatini, I.F. Pansani, S.E. Ferreira–Melo, H. Moreno, Plasma 8–isoprostane levels are associated with endothelial dysfunction in resistant hypertersion, Clin. Chim. Acta 433 (2014) 179–183.
[26] C. Vassalle, N. Botto, M.G. Andreassi, S. Berli, A. Biagini, Evidence for enhanced 8–isoprostane plasma levels, as indez of oxidative stress in vivo, in patients with coronary artery disease, Coron. Artery Dis. 14 (2003) 213–218.

Supporting Information.

- **Optimization of the experimental variables involved in the performance of the immunosensor**

- *Effect of the anti-ISO loading onto CNHs/SPCE*

- *Figure S1*

- *Effect of the HRP-ISO concentration*

- *Figure S2*

- *Optimization of the blocking step*

- *Figure S3*

- *Effect of the time for competition*

- *Figure S4*

- **Storage capability of the anti-ISO-CNHs/SPCE bioelectrode**

- *Figure S5*

- *Effect of the anti-ISO loading onto CNHs/SPCE*

The loading of anti-ISO immobilized on the CNHs/SPCE and the concentration of HRP-ISO used for the competitive immunoassay influenced each other and strongly affected the immunosensor response. Therefore, both variables were evaluated together in the same set of experiments. Figure S1a shows the results obtained with different immunosensors prepared by using anti-ISO solutions diluted in the 1:200 to 1:1200 range, and performing incubation with 0, 0.75 or 1.5 ng/mL ISO in competition with 1:100 diluted HRP-ISO solutions. The error bars correspond to the standard deviation

obtained from triplicate measurements in each case. As it can be observed, the currents measured with the immunosensors in the absence of ISO did not vary with the anti-ISO dilution up to a 1:800 factor, showing a slightly decrease for larger dilutions, indicating saturation of the electrode surface with the antibody for dilutions lower than 1:1200. Moreover, despite the relatively high concentration of HRP-ISO used, a good competition of the antigen for the binding sites of the antibody took place, this giving rise to a significant current decrease for 0.75 and 1.5 ng/mL ISO. However, larger current changes with different ISO concentrations were observed for anti-ISO dilutions lower than 1:800, which can be attributed to the larger amount of antibody on the electrode surface able to bind the antigen. Taking this into account, two antibody dilution factors: 1:600 and 1:400 were selected for further work. Regarding the time for incubation of anti-ISO on CNHs/SPCE, a period of 60 min was found to be adequate for both antibody loadings to obtain the best sensitivity.

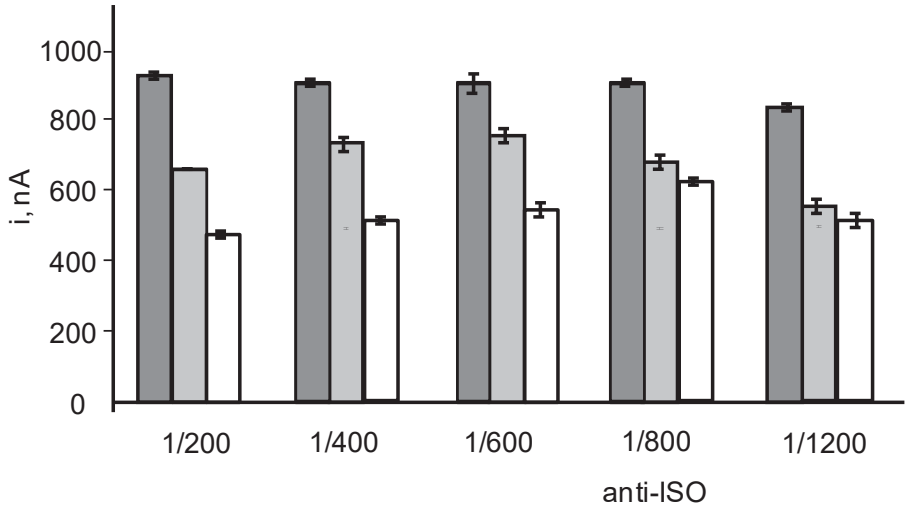

Figure S1. Effect of the anti-ISO loading on the immunosensor response for 0 (dark grey), 0.75 (light grey), 1.5 (white) ng/mL ISO, 5 μL, 60 min; CNHs, 10 μL; 100 mM EDC/NHSS, 5 μL, 30 min; anti–ISO, 5 μL, 60 min; 2% BSA, 5 μL, 30 min; HRP–ISO, 1/100 dilution, 5 μL, 60 min

- Effect of the HRP-ISO concentration

The concentration of HRP-ISO used for the competition with ISO antigen was also optimized (Figure S2). Different anti-ISO-CNHs/SPCE immunosensors were prepared with 1:600 or 1:400 diluted anti-ISO, and the responses for 0, 0.75 and 1.5 ng/mL ISO were measured for various HRP-ISO dilutions between 1:100 and 1:1000. As expected, current responses showed a decrease when the conjugate concentration decreased for both anti-ISO dilutions. Moreover, the competition with the antigen allowed noticeable changes in the current to be measured for 1:500 or 1:200 diluted HRP-ISO for 1:600 or 1:400 anti-ISO loading, respectively. Therefore, in order to select conditions adequate to measure low ISO concentrations, the characteristics of the calibration plots obtained between 0 and 200 pg/mL ISO using both experimental conditions were compared. The corresponding slope values of the linear calibration graphs were 0.85 ± 0.02 and 0.46 ± 0.05 nA mL/ng for 1:500 HRP-ISO and 1:600 anti-ISO, and 1:200 HRP-ISO and 1:400 anti-ISO, respectively. According to these results, 1:500 HRP-ISO and 1:600 anti-ISO were selected for the preparation of the immunosensor.

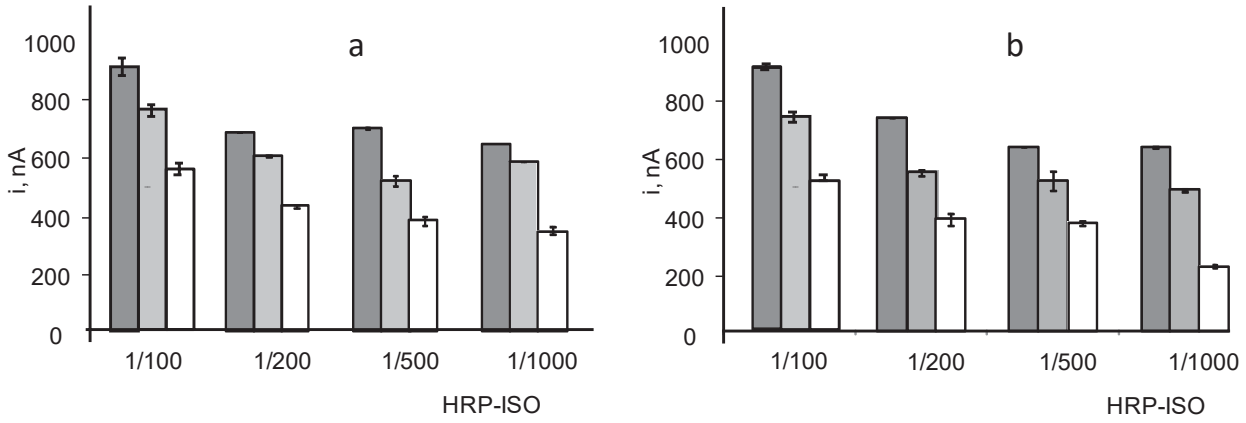

Figure S2. Effect of the HRP-ISO concentration on the immunosensor response for 0 (dark grey), 0.75 (light grey), 1.5 (white) ng/mL ISO, 5 µL, 60 min; CNHs, 10 µL; 100 mM EDC/NHSS, 5 µL, 30 min; anti–ISO, 1/600 dilution, (a), 1/400 dilution (b), 5 µL, 60 min; 2% BSA, 5 µL, 30 min; HRP–ISO, 5 µL, 60 min

- *Optimization of the blocking step*

In order to minimize non-specific adsorptions of immunoreagents on the remaining sites of the unmodified electrode surface, various studies concerning blocking of the electrode surface were made. The nature of the blocking agent, its concentration, and the incubation time employed to block the free sites on the anti-ISO-CNHs/SPCE surface (unspecific responses) were evaluated. BSA, casein and powder milk were tested as blocking agents using solutions with different concentrations: 1, 2 and 5% BSA, 1% casein, and 5% powder milk. The protocol consisted of adding 5 μL of each blocking solution on the anti-ISO-CNHs/SPCE prepared with 1:600 diluted anti-ISO, 1:500 HRP-ISO, and in the absence or in the presence of 0.5 ng/mL ISO. The obtained results are shown in Figure S3. As it can be observed, the best blocking conditions, with the highest specific-to-unspecific current ratio was achieved when using 2% BSA. Furthermore, a time for incubation of 30 min was shown to be enough to ensure an effective blocking.

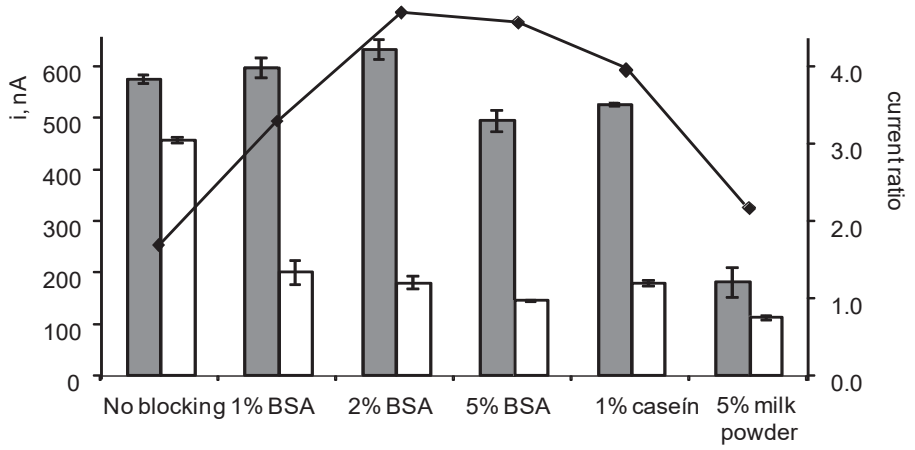

Figure S3. Optimization of the blocking step: CNHs, 10 μL; 100 mM EDC/NHSS, 5 μL, 30 min; anti–ISO 1/600 dilution, 5 μL, 60 min; blocking agent, 5 μL, 30 min; 0 (dark grey), 0.5 (white) ng/mL ISO, 5 μL, 60 min; HRP–ISO, 1/500 dilution, 5 μL, 60 min.

- *Effect of the time for competition*

The incubation time for competition was also optimized in the 15 to 60 min range with the results displayed in Figure S4. The measured current increased when the incubation of the ISO and HRP-ISO mixture solution onto the anti-ISO-CNHs/SPCE was longer. Taking into account that similar current values were obtained in the absence of ISO for 45 and 60 min but the signal change with respect to 0.75 ng/mL ISO was larger for the shorter time, 45 min was chosen as the time let for competition which also shortened the whole assay time.

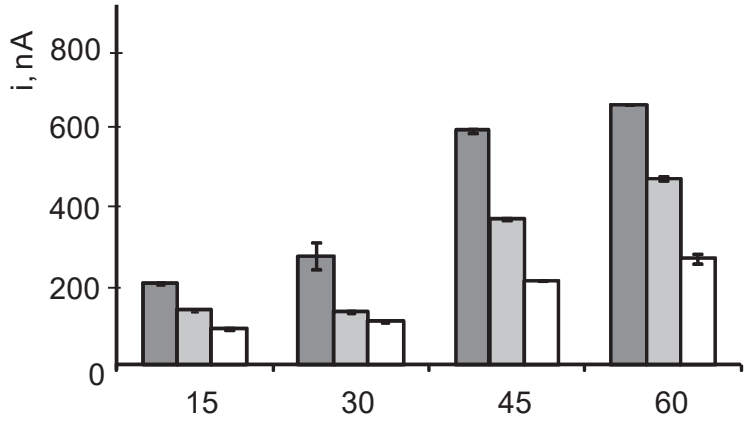

Figure S4. Effect of the incubation time for competition between ISO and HRP-ISO: CNHs, 10 μL; 100 mM EDC/NHSS, 5 μL, 30 min; anti–ISO 1/600 dilution, 5 μL, 60 min; 2% BSA, 5 μL, 30 min; 0 (dark grey), 0.75 (light grey) , 1.5 (white) ng/mL ISO, 5 μL, 60 min; HRP–ISO, 1/500 dilution, 5 μL

- Storage capability of the anti-ISO-CNHs/SPCE bioelectrode

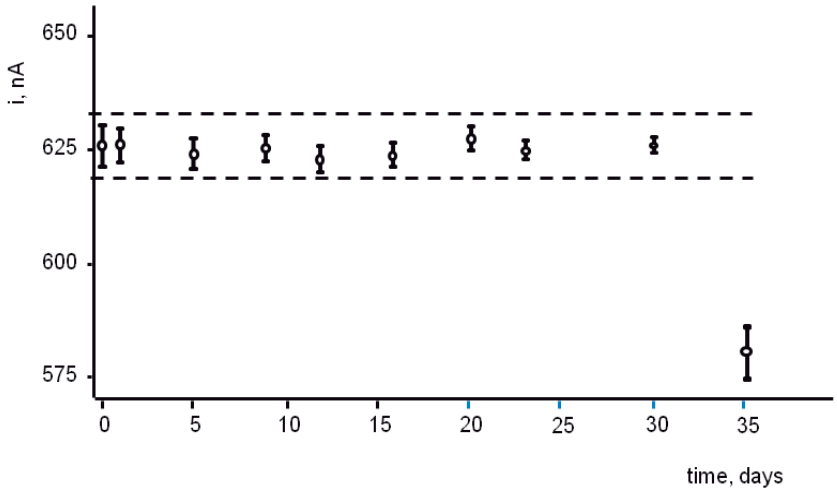

Figure S5. Control chart constructed to evaluate the storage stability of anti-ISO-CNHs/SPCE conjugates. Each point corresponds to the mean value of three successive measurements for 0 pg/mL ISO.

Sensors and Actuators B: Chemical 223 (2016) 89–94

An electrochemical immunosensor for adiponectin using reduced graphene oxide-carboxymethylcellulose hybrid as electrode scaffold

Sensors and Actuators B 223 (2016) 89–94

Contents lists available at ScienceDirect

Sensors and Actuators B: Chemical

journal homepage: www.elsevier.com/locate/snb

An electrochemical immunosensor for adiponectin using reduced graphene oxide–carboxymethylcellulose hybrid as electrode scaffold

C.B. Arenas, E. Sánchez-Tirado, I. Ojeda, C.A. Gómez-Suárez, A. González-Cortés, R. Villalonga, P. Yáñez-Sedeño*, J.M. Pingarrón

Department of Analytical Chemistry, Faculty of Chemistry, University Complutense of Madrid, 28040 Madrid, Spain

ARTICLE INFO

Article history:
Received 30 June 2015
Received in revised form 9 September 2015
Accepted 10 September 2015
Available online 12 September 2015

Keywords:
Graphene
Adiponectin
Electrochemical immunosensor
Carboxymethyl cellulose
Mix&Go™
Human serum

ABSTRACT

Reduced graphene oxide–carboxymethylcellulose hybrid (CMC–rGO) was used for the development of a novel electrochemical immunosensor for the determination of adiponectin (APN) cytokine. The hybrid material was synthesized by covalent binding of oxidized CMC to GO layers followed by chemical reduction with sodium borohydride. A sandwich-type immunoassay was employed involving the commercial metal-complexes based polymer Mix & Go™ for the stable and oriented immobilization of anti-APN capture antibody. Biotinylated-anti-APN and HRP-Strept were used for the assay configuration. The APN quantification was performed by amperometry at −200 mV using the hydrogen peroxide/hydroquinone enzyme substrate/mediator system. A sigmoidal calibration plot for APN in the 0.1–50 μg/mL range, with a linear portion in the 0.5–10.0 μg/mL APN concentration range was obtained. The calculated limit of detection ($3s_b/m$) was 61 ng/mL APN. The usefulness of the immunosensor was evaluated by analyzing human serum from hypercholesterolemia or diabetes patients.

© 2015 Elsevier B.V. All rights reserved.

1. Introduction

Graphene is nowadays widely accepted as an extremely suitable and versatile nanomaterial for electroanalytical applications [1]. However, characteristics such as high hydrophobicity of graphene nanosheets, low solubility, and aggregation occurrence are well known drawbacks for the practical use of this material. In particular, a major obstacle in the field of biosensors is the absence of functional moieties on graphene surface thus limiting the easy and efficient immobilization of biomolecules. This problem has been overcome by chemical derivatization although, in this case, structural damage of graphene nanosheets affecting their properties should be prevented. A convenient alternative to address this point consists of preparing graphene–polymer hybrids using macromolecules such as chitosan [2], hydroxypropyl cellulose [3], gelatin [4], or carboxymethylcellulose (CMC) [5]. In particular, CMC is a linear polymeric water-soluble cellulose derivative which has been employed to prepare graphene dispersions [6]. CMC–rGO hybrids combine the properties of both materials resulting in a highly conductive, hydrophilic, and biocompatible hybrid nanomaterial. A method for the synthesis of CMC–rGO hybrids by covalent binding of oxidized CMC to graphene oxide layers followed by chemical reduction with sodium borohydride was recently developed by our group. The resulting oxygen-rich conducting material was used for the fabrication of enzyme biosensors [5]. A different synthetic approach was that based on simple mixing of CMC and GO and CMC grafting by π–π stacking. The hybrid was used as coating material for glassy carbon electrodes and for the immobilization of hemoglobin investigating the direct electron transfer of the protein and its bioelectroactivity toward the reduction of NO and H_2O_2 [7]. Very recently, our group also used CMC–rGO hybrid for the preparation of an electrochemical DNA sensor for the detection of a target DNA sequence on the p53 tumor suppressor (TP53) gene [8].

In this paper, the CMC–rGO hybrid (synthesized as in Ref. [5]) was used for the first time to prepare an electrochemical immunosensor taking advantage of the excellent electrochemical behavior observed for the electrodes modified with this nanohybrid. Moreover, in order to ensure the stable and oriented binding of capture antibodies, a strategy involving the use of the Mix&Go™ reagent was implemented. This reagent is a commercial polymeric coating that contains several metallic complexes selected for their efficiency to bind proteins [9,10]. The polymer forms strong multivalent interactions with electron donating groups [11] such as the carboxylic moieties existing in CMC–rGO hybrids, where it can be retained. To immobilize antibodies, Mix&Go™ uses small molecule ligands to bind Fc domains as anchoring point. These ligands mimic binding domains from proteins A and G, and extend as two adjacent side-chains from a polymer backbone. In addition, the metal

* Corresponding author.
E-mail address: yseo@quim.ucm.es (P. Yáñez-Sedeño).

http://dx.doi.org/10.1016/j.snb.2015.09.055
0925-4005/© 2015 Elsevier B.V. All rights reserved.

complexes integrated into the polymer chains enhance binding of Fc domains providing a higher stability. The combination of CMC–rGO hybrids with the use of Mix&Go™ for antibody immobilization resulted in a convenient methodology to be used as a general route for the preparation of electrochemical immunosensors.

On the other hand, there is increasing evidence that the adipose processes are associated with alterations of several immunologic functions [12]. Adipose tissue has been revealed as an important endocrine organ producing various cytokines and hormones, among which adiponectin (APN) and leptin are the most abundant adipocyte products [13]. APN is a 244 amino acid protein involved in glucose and lipid metabolism [14] with a central role in the regulation of insulin resistance [15]. Average levels of several units [16] or tens [17,18] μg/mL APN in serum of healthy men and women have been found. In addition, increased APN concentrations have been observed with high-density lipoprotein-cholesterol levels. APN levels also correlate negatively with glucose and insulin concentrations, with low values in diabetic patients, as well as with liver fat content or visceral adiposity. All these relationships have led to consider APN as a possible biomarker for metabolic syndrome [15]. Therefore, monitoring of APN levels is proposed as a promising target for prevention and treatment of obesity, insulin resistance, hyperlipidemia and atherosclerosis. Currently, colorimetric immunoassays involving various commercially available ELISA kits are the usual methods for the determination of APN. These consist predominantly of sandwich-type immunoassays using HRP-labeled IgG or HRP-streptavidin to bind with anti-APN or biotinylated anti-APN secondary antibodies, respectively, and color development by using hydrogen peroxide and tetramethylbenzidine (TMB). These methods require long times of analysis which in some cases last more than 4 h.

In this work, a novel electrochemical immunosensor for APN, where anti-APN antibodies were immobilized using the Mix&Go™ polymer onto a CMC–rGO-modified screen-printed carbon electrode (SPCE), is reported. A sandwich-type immunoassay with biotinylated-anti-APN and HRP-Strept was implemented and the APN determination was performed by amperometry at −200 mV upon addition of hydrogen peroxide in the presence of hydroquinone. The usefulness of the immunosensor was evaluated by analyzing human serum from hypercholesterolemia or diabetes patients, and the results were successfully compared with those provided by a commercial ELISA kit.

2. Experimental

2.1. Reagents and solutions

Mouse polyclonal human anti-adiponectin (anti-APN) was purchased from Abnova. Human adiponectin peptide (APN) and rabbit polyclonal biotinylated anti-APN antibody (Biotin-anti-APN) were purchased from Abcam. Streptavidin labeled with HRP (HRP-Strept) was purchased from Roche. Hydroquinone (HQ) and hydrogen peroxide (30% w/v) were purchased from Sigma–Aldrich. Mix&Go™ polymer was from Anteo Diagnostics. Graphene oxide (NIT.GO.M.140.10) from Nanoinnova Technologies, low viscosity sodium carboxymethylcellulose (CMC, MW 29600 Da, 0.7 substitution degree, BDH), (3-aminopropyl)triethoxysilane (APTES, 99% Sigma), ethylene glycol (Merck), sodium periodate (Sigma), and sodium borohydride (Sigma), were also used. Sodium dihydrogen phosphate and di-sodium hydrogen phosphate were purchased from Scharlau. Bovine serum albumin (BSA) was purchased from GERBU Biotechnik, GmbH. Casein from bovine milk (Sigma) and semi-skimmed milk purchased in a local supermarket were also used. Buffer solutions used were 0.1 M phosphate buffer solution (PBS) of pH 7.4, 50 mM PBS of pH 6.0, and 25 mM 2-(N-morpholino)ethanesulfonic acid (MES) of pH 5.0. Cholesterol and insulin (Sigma) were tested as potentially interfering compounds. Deionized water was obtained from a Millipore Milli-Q purification system (18.2 MΩ cm).

2.2. Samples

Human serum samples from cholesterol and diabetic Type 2 patients were purchased from Abyntek (Refs. SG376-2 and SG187-2, respectively). For comparison purposes, the APN concentration in the samples was also determined by using a colorimetric ELISA kit from Abcam (Ref. ab 108786).

2.3. Apparatus and electrodes

All electrochemical measurements were made with a PGSTAT 12 potentiostat from Autolab. The electrochemical software was the general-purpose electrochemical system (GPES) (EcoChemie B.V.). Screen printed carbon electrodes (SPCEs, 110 DRP, ∅4 mm) were purchased from DropSens (Oviedo, Spain). These electrodes include a silver pseudoreference electrode and a carbon counter electrode. For homogenization of the solutions, an Optic Ivymen System constant temperature incubator shaker (Comecta S.A.) was used. All experiments were performed at room temperature.

2.4. Procedures

2.4.1. Preparation of the CMC–rGO/SPCEs

The CMC–rGO hybrid was prepared as described previously [5]. Briefly, a dispersion of 100 mg GO in 500 mL ethanol was prepared by ultrasonic stirring for 1 h. Then, 50 mL of an ethanolic 1% (v/v) APTES solution were added and GO was sylanized by continuous stirring for 12 h at 60–65 °C. Subsequently, the solvent was eliminated in a roto-evaporator and the resulting product was washed with ethanol, centrifuged, and let to dry in a desiccator. Separately, a solution of 500 mg CMC per 100 mL water was prepared. Then 540 mg $NaIO_4$ were added keeping under stirring for 12 h in the dark. Then, 1 mL ethyleneglycol was added and stirring was kept for 1 h. The resulting oxidized CMC was dialyzed in absence of light and mixed with the sylanized GO previously obtained, leaving under stirring during 1 h. Further, 2.5 g $NaBH_4$ were added and the mixture was stirred for 12 h. Subsequently, the solvent was eliminated and the resulting product was washed with a 0.1 M phosphate buffer solution of pH 6.0 and allowed drying. CMC–rGO/SPCEs were prepared by dropping 20 μL of a 10 μg/mL CMC–rGO aqueous solution onto the SPCE surface and allowing to dry.

2.4.2. Preparation of HRP-Strept-Biotin-anti-APN-APN-anti-APN-CMC-rGO/SPCE immunosensors

10 μL of Mix&Go™ polymer solution were dropped onto the CMC–rGO/SPCE surface and let stand for 30 min at room temperature. The modified electrode was then washed with deionized water and dried at room temperature. All further washing and drying steps were carried out similarly. Next, 5 μL of anti-APN 1/300 diluted with 25 mM MES of pH 5.0 were added and incubated during 60 min. After washing, 5 μL of a 5% BSA solution were added allowing incubation for 30 min. Then, 5 μL of a standard APN solution or the sample in 0.1 M PBS of pH 7.4 was dropped onto the electrode surface and left standing for 40 min. After washing, 5 μL of 2.0 μg/mL Biotin-anti-APN solution prepared in the presence of 0.5% BSA were added to the APN-anti-APN-CMC-rGO/SPCE and incubated for 20 min. Finally, 5 μL of a 1/1000 diluted HRP-Strept solution prepared in the presence of 0.5% BSA in PBS 0.1 M pH 7.4 were drop casted and incubated for 15 min.

2.4.3. Determination of APN

45 μL of a 1 mM HQ solution in PBS 50 mM pH 6.0 were dropped onto the surface of the HRP-Strept-Biotin-anti-APN-APN-anti-APN-CMC-rGO/SPCE immunosensor which was horizontally positioned, and a detection potential of −0.20 V was applied. The background current was allowed to stabilize (approx. 100 s) and 5 μL of a 50 mM H_2O_2 solution prepared in 50 mM PBS of pH 6.0 were added and incubation was allowed for 200 s. The steady-state current corresponding to the electrochemical reduction of benzoquinone was used as the analytical readout.

2.4.4. Samples analysis

The serum samples were homogenized by manual stirring. A 1:50 dilution with PBS buffer of pH 7.4 was carried out. The standard additions method adding APN in the 0–2 μg/mL concentration range was used for the analyte quantification.

3. Results and discussion

The different steps involved in the preparation and functioning of the developed immunosensor are illustrated in Fig. 1. Firstly, (step 1) graphene oxide was sylanized with APTES and the oxidized CMC was attached to the free amino groups on the graphene surface by reductive alkylation with $NaBH_4$ [5]. This protocol also caused reduction of the epoxy and carbonyl groups in the GO nanosheets. After dropping CMC–rGO onto SPCE (step 2), Mix&Go^{TM} was added and anti-APN antibodies were immobilized. After a blocking step with BSA, the immunoreaction with APN was performed (step 3) and the analyte was sandwiched with Biotin-anti-APN. HRP-Strept was then employed as the detection conjugate. As it was described in Section 2.4.3, once the HRP-Strept-Biotin-anti-APN-APN-anti-APN-CMC-rGO/SPCE immunosensor was prepared, the determination of APN (step 4) was carried out by amperometry at −0.2 V upon addition of H_2O_2 as HRP substrate and using hydroquinone as redox mediator.

In order to evaluate the suitability of the rGO–CMC hybrid as electrode scaffold for the preparation of the immunosensor, different nanostructuration approaches of the SPCEs were compared. Various APN immunosensors were constructed where the APN capture antibodies were immobilized using the polymer Mix&Go^{TM} and SPCEs were modified with carboxylated MWCNTs, reduced graphene oxide (rGO), and CMC–rGO.

Moreover, for comparison purposes, anti-APN antibodies were immobilized without using Mix&Go^{TM}. Immobilization was accomplished covalently by EDC/NHSS onto the –COOH rich CMC–rGO nanostructured electrode platform. Fig. 2 shows the amperometric currents measured for 0 and 2 μg/mL APN as well as the corresponding signal-to-background current ratios. As it can be observed, a larger ratio was obtained when the electrode platform was prepared with the hybrid nanomaterial. This can be attributed to the large amount of oxygenated groups on the CMC–rGO-modified electrode surface thus providing an efficient scaffold for large capture antibody immobilization loadings. This can be performed also by activation of carboxyl moieties by EDC/NHS chemistry allowing covalent binding through the amine groups. However, this usual methodology does not assure the proper orientation of the antibody. Conversely, the use of the Mix&Go^{TM} polymer for anti-APN immobilization allows an

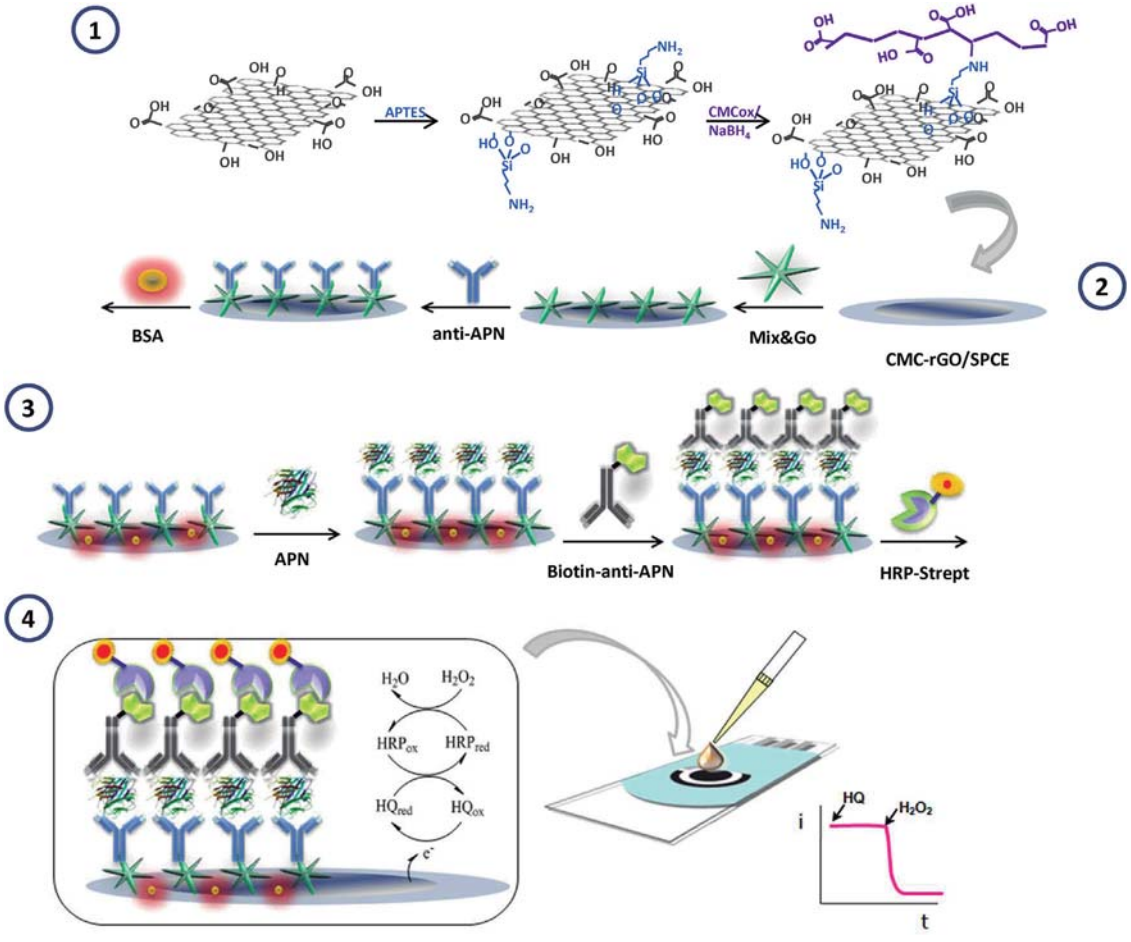

Fig. 1. Schematic display of the different steps involved in the construction of an electrochemical immunosensor for APN involving covalent immobilization of anti-APN onto Mix&Go^{TM}-CMC-rGO/SPCE.

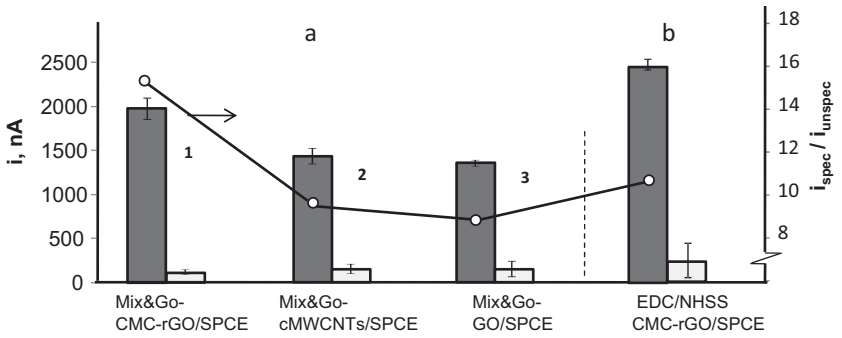

Fig. 2. Amperometric currents for 0 and 2 μg/mL APN measured with the HRP-Strept-Biotin-anti-APN-APN-anti-APN-CMC-rGO/SPCE immunosensor prepared by covalent immobilization of APN: (a) using Mix&Go™ onto CMC–rGO/SPCE (1), carboxylated MWCNTs/SPCE (2), and rGO/SPCE (3); (b) by activation with EDC/NHSS onto CMC–rGO/SPCE. See text and Table 1 for the experimental conditions.

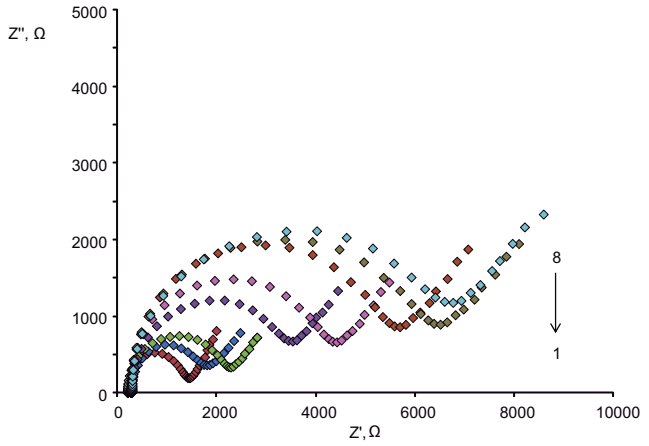

Fig. 3. Nyquist plots obtained by electrochemical impedance spectroscopy at (1) SPCE, (2) CMC–rGO/SPCE, (3) Mix&Go-CMC-rGO/SPCE, (4) anti-APN-CMC-rGO/SPCE, (5) anti-APN-(BSA)-Mix&Go-CMC-rGO/SPCE, (6) APN-anti-APN-(BSA)-Mix&Go-CMC-rGO/SPCE, (7) Biotin-anti-APN-APN-anti-APN-(BSA)-Mix&Go-CMC-rGO/SPCE, and (8) HRP-Strept-Biotin-anti-APN-APN-anti-APN-(BSA)-Mix&Go-CMC-rGO/SPCE in 5 mM $Fe(CN)_6^{3-/4-}$ 0.1 M PBS pH 7.4 solution.

enhanced specific-to-background current ratio to be obtained (Fig. 2) due to the remarkably low background current arising from unspecific adsorptions. Accordingly, this combined strategy of using the CMC–rGO hybrid nanomaterial as electrode scaffold (this nanomaterial was exploited for the first time in this work for the construction of an electrochemical immunosensor) and the Mix&Go™ polymer for capture antibody immobilization was employed for the preparation of the APN immunosensor.

Electrochemical impedance spectroscopy (EIS) was employed to monitor the steps involved in the electrode modification. Fig. 3 shows the Nyquist plots recorded at SPCE, CMC–rGO/SPCE, Mix&Go-CMC-rGO/SPCE, anti-APN-Mix&Go-CMC-rGO/SPCE, anti-APN-(BSA)-Mix&Go-CMC-rGO/SPCE, APN-anti-APN-(BSA)-Mix&Go-CMC-rGO/SPCE, Biotin-anti-APN-APN-anti-APN-(BSA)-Mix&Go-CMC-rGO/SPCE and HRP-Strept-Biotin-anti-APN-APN-anti-APN-(BSA)-Mix&Go-CMC-rGO/SPCE using 5 mM $Fe(CN)_6^{4-}$/$Fe(CN)_6^{3-}$ as the redox probe in 0.1 M PBS pH 7.4. As expected, SPCE modification with the hybrid material to obtain CMC–rGO/SPCE produced an increase in the charge transfer resistance, from 682 Ω up to 1013 Ω, as a consequence of the electrostatic repulsion between the redox probe and the negatively charged carboxylate groups. The subsequent incorporation of Mix&Go™ polymer led to a further resistance increase (R_{CT} = 1334 Ω) due to the lower conductivity of the modified electrode surface. The immobilization of the capture antibody provoked also a remarkable increase in the R_{CT} value up to 2247 Ω, which confirmed the efficiency of the immobilization procedure. The subsequent steps in the immunosensor preparation gave rise to larger R_{CT} values as a consequence of the incorporation of non-conducting compounds.

Table 1
Variables optimized and selected values regarding the performance of the HRP-Strept-Biotin-anti-APN-APN-anti-APN-CMC-rGO/SPCEs immunosensor.

Variable	Tested range	Selected value
Incubation time of Mix&Go (min)	30, 60	30
Anti-APN loading (dilution)	1/37.5–1/450	1/300
Blocking agent type	BSA, casein, milk	BSA
Biotin-anti-APN (μg/mL)	1–4	2
Incubation time for blocking (min)	15–60	30
HRP-Strept, dilution	1/500–1/2000	1/1000
Incubation time for APN	20, 40, 60	40

3.1. Optimization of the experimental variables

The different variables affecting the performance of the developed immunosensor were evaluated. These studies involved testing: (a) the incubation time with the Mix&Go™ polymer on the CMC–rGO/SPCE; (b) the loading of anti-APN and (c) the effect of pH value on the immobilization of anti-APN onto CMC–rGO/SPCE coated with Mix&Go™ polymer; (d) the blocking step; (e) the concentration of Biotin-anti-APN onto APN-anti-APN-CMC-rGO/SPCE; (f) the concentration of HRP-Strept onto Biotin-anti-APN-APN-anti-APN-CMC-rGO/SPCE; (g) the time for incubation of APN onto anti-APN-CMC-rGO/SPCE. Details on these optimization tests can be found in Supplementary material and in Figs. S1–S7. Table 1 summarizes the ranges checked for all the variables as well as the selected values for further work.

It should be mentioned here that other selected variables such as the pH and the detection potential values were the same than those optimized previously by our group using the same enzyme/redox mediator electrochemical detection system [19].

3.2. Analytical figures of merit of the immunosensor

Fig. 4 shows the calibration plot constructed by amperometry in stirred solutions using a detection potential of −0.20 V. A range of linearity (r^2 = 0.995) extending between 0.5 and 10 μg/mL was found according to the equation i nA = 1033 ln[APN] μg/mL + 1265. This range is suitable for the determination of the target analyte in human serum as the normal concentration levels are from several units to tens of μg/mL. The limit of detection was calculated according to the $3s_b/m$ criterion, where s_b was the standard deviation of the blank responses (in the absence of APN), s = ±21 nA (n = 10), and m was the slope of the linear range, 1033 nA per decade of concentration in μg/mL. The obtained value was 61 ng/mL. When

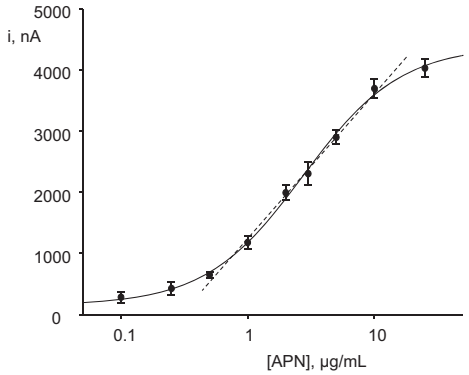

Fig. 4. Calibration plot for APN constructed with the HRP-Strept-Biotin-anti-APN-APN-anti-APN-CMC-rGO/SPCE immunosensor. See text and Table 1 for the experimental conditions.

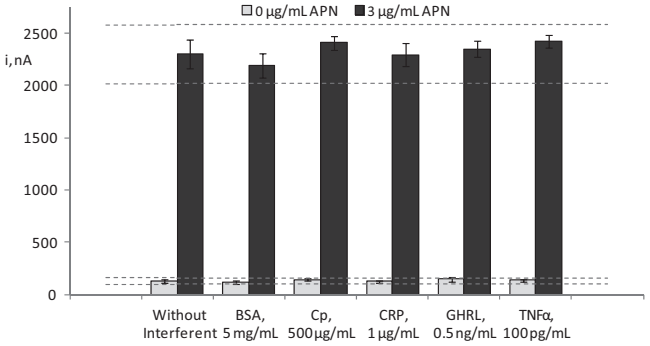

Fig. 5. Effect of the presence of BSA, ceruloplasmin (Cp), protein C-reactive (CRP), tumor necrosis factor alpha (TNFα), and ghrelin (GHRL) on the amperometric responses obtained for 0 (light gray) and 3 (dark gray) µg/mL APN at the HRP-Strept-Biotin-anti-APN-APN-anti-APN-(BSA)-Mix&Go-CMC-rGO/SPCE immunosensor.

these analytical characteristics are compared with data provided in the protocols of commercial ELISA kits using similar immunoreagents, some noticeable differences were apparent. Theses kits offer dynamic ranges that usually cover up to tenths of ng/mL with minimum detectable concentrations around tens of ng/mL. However, these parameters are calculated mostly from nonlinear logarithmic ranges and the precision levels are around 10% or higher. It is important to note that the criteria used to calculate the LOD values in the commercial protocols are rarely given. Moreover, the time lasted for the assay was remarkably longer with ELISA kits extending even over 5 h. Therefore, it could be concluded that the analytical characteristics of the developed immunosensor, covering a wide linear range of APN concentrations within the clinically relevant interval, improved, in general terms, those achieved with ELISA kits.

The reproducibility of the amperometric measurements was evaluated for 0 and 2 µg/mL APN solutions both on the same day and on different days with immunosensors prepared each time for each test. Relative standard deviation, RSD, values of 6.3 and 7.3% were obtained for 0 and 2 µg/mL for measurements carried out on the same day, respectively, whereas RSD values were 5.2 and 5.9%, respectively, for measurements on different days. These results showed that an acceptable precision was achieved regarding the whole procedure for immunosensor preparation.

The storage stability of the anti-APN-CMC-rGO/SPCE was also tested. In order to do that, different immunosensors were prepared on the same day, stored in dry at −20 °C, and employed to measure 7.5 µg/mL APN on different days according to the procedure described in Section 2. The control chart constructed (Fig. S7) by setting as control limits ±3*s*, were *s* was the standard deviation of the measurements ($n = 10$) carried out on the first day, indicated that the immunosensor responses remained inside the control limits for at least 12 days (no longer storage times were tested) demonstrating the good stability of the constructed anti-APN-CMC-rGO/SPCE.

The antibody used exhibited a great selectivity against other proteins different than APN. As it can be clearly seen in Fig. 5, the responses of the immunoelectrode in the absence and in the presence of 3 µg/mL APN, and in the presence of BSA, ceruloplasmin (Cp), C-reactive protein (CRP), ghrelin (GHRL) or tumor necrosis factor alpha (TNF-α) were not significantly different. Moreover, at the detection potential used, interference from electroactive substances such as ascorbic and uric acids was not observed either.

3.3. Determination of APN in human serum with the developed immunosensor

As it is described in Section 2.4.4, the serum samples were 1:50 diluted with the PBS buffer solution. A strong matrix effect was observed for these samples and, therefore, a dilution step was carried out in order to minimize such effect. Smaller dilution factors provoked a noticeable decrease in the slope value of the calibration plot and therefore in the sensitivity of the assay. Although the strong matrix effect was minimized upon the selected dilution factor, it could not be completely avoided. Accordingly, the determination of APN in the serum samples was accomplished by applying the standard additions method which involved the addition of 1–3 µg/mL APN and using a different immunosensor for each point of the standard additions plot.

The mean APN concentration values found ($n = 3$) were 15 ± 2 and 10 ± 2 µg/mL from sera of cholesterol and diabetic Type 2 patients, respectively. These results were compared with those obtained by using the Abcam ELISA kit for human adiponectin. The mean APN concentrations found ($n = 3$) were 17 ± 3 µg/mL (cholesterol) and 9 ± 2 µg/mL (diabetic) which were not statistically different from the values obtained with the immunosensor, thus demonstrating the usefulness of this approach for the determination of APN in this kind of clinical samples.

4. Conclusions

The first disposable electrochemical immunosensor making use of a rGO/CMC hybrid nanostructured electrode scaffold is described in this work. The excellent electrochemical behavior of this hybrid nanomaterial together with the ability of the metal-complexes based polymer Mix&Go^{TM} for the stable and oriented immobilization of specific capture antibody allowed the development of an immunosensor for the APN protein involved in glucose and lipid metabolism. The analytical performance of the developed immunosensor, with a detection limit of 61 ng/mL and great storage stability, was appropriate for the determination of the target analyte in human serum as it was demonstrated by comparing the results with those provided by a commercial ELISA kit. It is important to remark that a very significant advantage of the immunosensor versus the ELISA kit is related to the required time for the whole assay. While it takes less than 2 h from the antibody immobilization, the time when the ELISA kit is employed lasts almost 5 h.

Acknowledgments

Financial support of Spanish Ministerio de Economía y Competitividad, Research Project CTQ 2012-35041, and NANOAVANSENS Program from Comunidad de Madrid (S2013/MT-3029) is gratefully acknowledged.

Appendix A. Supplementary data

Supplementary data associated with this article can be found, in the online version, at http://dx.doi.org/10.1016/j.snb.2015.09.055.

References

[1] M. Pumera, A. Ambrosi, A. Bonanni, E.L.K. Chng, H.L. Poh, Trends Anal. Chem. 29 (2014) 954.
[2] H. Bao, Y. Pan, Y. Ping, N.G. Sahoo, T. Wu, L. Li, J. Li, L.H. Gan, Small 7 (2011) 1569.
[3] Q. Yang, X. Pan, K. Clarke, K. Li, Ind. Eng. Chem. Res. 51 (2012) 310.
[4] J. An, Y. Gou, C. Yang, F. Hu, C. Wang, Mater. Sci. Eng. C 33 (2013) 2827.
[5] E. Araque, R. Villalonga, M. Gamella, A. Sánchez, P. Martínez-Ruiz, V. García-Baonza, J.M. Pingarrón, ChemPlusChem 79 (2014) 1334.
[6] Q. Yang, X. Pan, F. Huang, K. Li, J. Phys. Chem. C 114 (2010) 3811.
[7] Y. Cheng, B. Feng, X. Yang, P. Yang, Y. Ding, Y. Chen, J. Fei, Sens. Actuators B 182 (2013) 288.
[8] B. Esteban-Fernández de Ávila, E. Araque, S. Campuzano, M. Pedrero, B. Dalkiran, R. Barderas, R. Villalonga, E. Killiç, J.M. Pingarrón, Anal. Chem. 87 (2015) 2290.
[9] W. Muir, M.C. Barden, S.P. Collett, A.-D. Gorse, R. Monteiro, L. Yang, N.A. McDougall, S. Gould, N.J. Maeji, Anal. Biochem. 363 (2007) 97.
[10] H.W. Ooi, S.J. Cooper, C.-Y. Huang, D. Jennins, E. Chung, N.J. Maeji, A.K. Whittaker, Anal. Biochem. 456 (2014) 6.
[11] P. Wu, D.G. Castner, D.W. Grainger, J. Biomater. Sci. Polym. Ed. 19 (2008) 725.
[12] A.M. Wolf, D. Wolf, H. Rumpold, B. Enrich, H. Tilg, Biochem. Biophys. Res. Commun. 323 (2004) 630.
[13] H. Tilg, A.R. Moschen, Nat. Rev. Immunol. 6 (2006) 772.
[14] S. Thanakun, H. Watanabe, S. Thaweboon, Y. Izumi, Diabetol. Metab. Syndr. 6 (2014) 19.
[15] N. Brooks, K. Moore, R. Clark, M. Perfetti, C. Trent, T. Combs, Diabetes Obes. Metab. 9 (2007) 246–258.
[16] S.J. Koh, Y.J. Hyun, S.Y. Choi, J.S. Chae, J.Y. Kim, S. Park, C.-M. Ahn, Y. Jang, J.H. Lee, Clin. Chim. Acta 389 (2008) 45.
[17] A. Katsuki, M. Suematsu, E.C. Gabazza, S. Murashima, K. Nakatani, K. Togashi, Y. Yano, Y. Adachi, Y. Sumida, Diabetes Res. Clin. Pract. 73 (2008) 310.
[18] S. Matsui, T. Yasui, K. Keyama, A. Tani, T. Kato, H. Vemura, A. Kuwahara, T. Matsuzaki, M. Irahara, Clin. Chim. Acta 430 (2012) 104.
[19] I. Ojeda, J. López-Montero, M. Moreno-Guzman, B.C. Janegitz, A. González-Cortés, P. Yáñez-Sedeño, J.M. Pingarrón, Anal. Chim. Acta 743 (2012) 117.

Biographies

C. Arenas received his Chemistry Degree from Complutense University of Madrid in 2013. He is currently conducting experimental studies for his Ph.D. at Faculty of Chemistry in same university. His research interest includes the fabrication and application of nanomaterials and development of immunoassays.

E. Sánchez-Tirado received her Chemistry Degree from Complutense University of Madrid in 2014. In 2015 she finished the Science and Chemical Technology Master at the same University. Currently, her research interest includes the fabrication and application of electrochemical biosensors.

I. Ojeda received her Degree in Chemistry from Complutense University of Madrid in 2008 and obtained her Ph.D. in 2015 from the same University. Her research interest includes the fabrication and application of electrochemical immunosensors.

C.A. Gómez-Suárez received his Undergraduate Degree in Chemistry from Complutense University of Madrid in 2015. He is currently developing his career in Colombia.

A. González-Cortés is currently an associate professor at Analytical Department of Faculty of Chemistry, University Complutense of Madrid. She obtained her Ph.D. from the same University. Her research interest includes the application of nanomaterials in the preparation of electrochemical biosensor for the detection of bioactive substances.

R. Villalonga studied Chemistry at the University of Havana, where he graduated with Gold Diploma in 1993. Currently, he is a researcher at the University Complutense of Madrid. His research is focused on neoglycoenzymes, carbohydrate chemistry, drug delivery systems, biosensors and nanotechnology.

P. Yáñez-Sedeño is a full professor of Analytical Chemistry at the Complutense University of Madrid. Her research focuses on the development of electrochemical immunosensors for the determination of hormones and biomarker proteins related to obesity and aging.

J.M. Pingarrón is a full professor of Analytical Chemistry at the Complutense University of Madrid. His research interests focus on analytical electrochemistry, nanostructured electrochemical interfaces and electrochemical and piezoelectric sensors and biosensors.

Supplementary material

3.1. Optimization of the experimental variables

a) Effect of the incubation time with the Mix&Go polymer

10 µL of Mix&Go^{TM} solution were deposited onto the SPCE modified with 20 µL of rGO-CMC allowing incubation for 30 or 60 min. Thereafter, 5 µL of anti-APN 1/300 diluted in 25 mM MES of pH 5.0 were added, and the electrode was kept at room temperature for one hour under humid conditions. Then, 5 µL of a 5% BSA solution and 5 µL of 2 µg/mL APN solution (specific response), or 5 µL of 0.1 M PBS of pH 7.4 (unspecific response) were added and incubated for 40 min. Next, 5 µL of a solution containing 2 µg/mL biotin-anti-APN and 0.5 % BSA in 0.1 M PBS of pH 7.4 were drop casted and incubated for 20 min. Finally, 5 µL of 1:1000 diluted HRP-Strept solution prepared in the same buffer containing 0.5 % BSA, were added and allowed standing for 15 min. Figure S1 shows the amperometric responses obtained under the conditions described in section 2.4.3 after the addition of 5 mM H_2O_2 in the presence of 1 mM hydroquinone. As it can be seen, a similar behavior was found with both incubation times although a slightly higher specific-to-unspecific currents ratio occurred for 30 min. Therefore, this incubation time which also permitted a faster protocol was selected for further work.

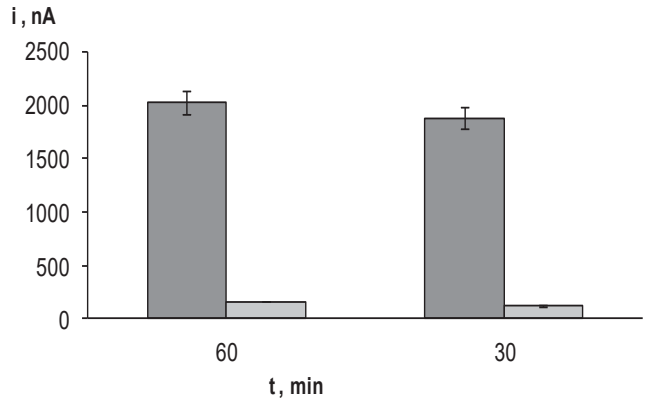

Figure S1. Effect of the incubation time of Mix&Go^{TM} polymer solution on the amperometric responses of the HRP-Strept-Biotin-anti-APN-APN-anti-APN-CMC-rGO/SPCE immunosensor: 2µg/mL APN (dark gray) and 0 µg/mL APN (light gray); E_{app} = -200 mV. See the text for more information. Results for triplicate analysis with error bars at ± s values.

b) Effect of the immobilized anti-APN loading

Under the experimental conditions described above, the optimum concentration of anti-APN for the immunosensor preparation was selected after evaluation of the specific and unspecific responses obtained using different antibody dilutions over the 1/37.5 to 1/450 range. The amperometric responses (Figure S2) exhibited the highest specific-to-unspecific current ratio for a 1/300 antibody dilution. Larger antibody concentrations gave rise to a decrease of the specific response probably due to a more pronounced hindering of the electrochemical reaction. Accordingly, the mentioned dilution was selected to construct the immunosensor.

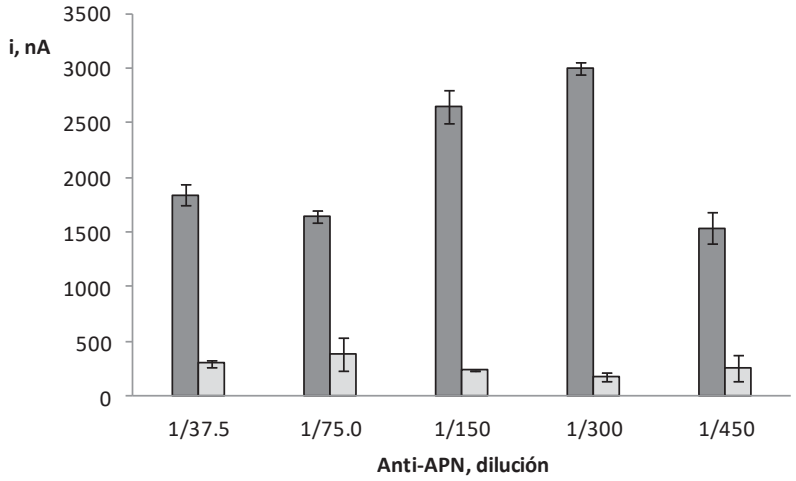

Figure S2. Effect of the immobilized anti-APN loading on the amperometric responses of the HRP-Strept-Biotin-anti-APN-APN-anti-APN-CMC-rGO/SPCE immunosensor: 2 μg/mL APN (dark gray) and 0 μg/mL APN (light gray). Other conditions as in Fig. 1

c*) Effect of pH on the immobilization of anti-APN*

As it can be seen in Figure S3, although small differences in the specific-to-unspecific ratio were observed between pH 5.0 and 5.5, it was slightly larger at pH 5.0 and, therefore, this pH value was selected to carry out the anti-APN immobilization.

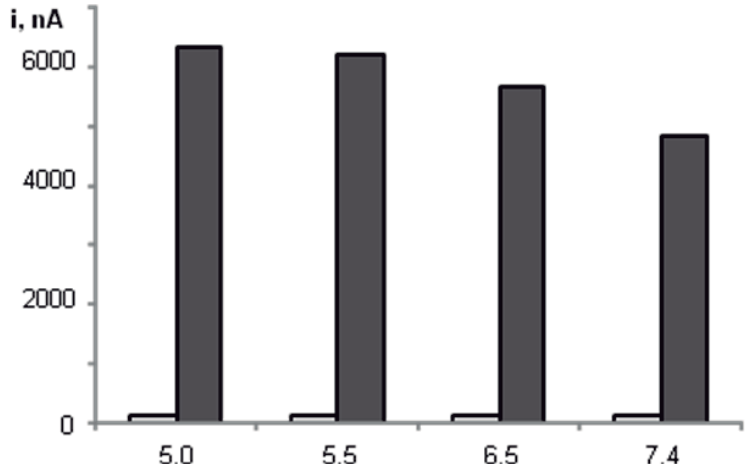

Figure S3. Effect of the pH value used in the anti-APN immobilization on the amperometric responses of the HRP-Strept-Biotin-anti-APN-APN-anti-APN-CMC-rGO/SPCE immunosensor: 10µg/mL APN (dark gray) and 0 µg/mL APN (light gray). Other conditions as in Fig. 1

d) Optimization of the blocking step

In order to minimize non-specific adsorptions of immunoreagents on the electrode surface, a blocking step of the unmodified free sites on the anti-APN-CMC-rGO/SPCE surface (unspecific responses) was accomplished. Optimization of this step included the nature of the blocking agent, its concentration, and the incubation time employed. 2% casein prepared in 0.1 M KOH and diluted in 0.1 M PBS pH 7.4, as well as 5% BSA and 50% semi-skimmed milk prepared in the same buffer solution were tested as the blocking agents. The protocol consisted of adding 5 µL of the blocking solution on the anti-APN-CMC-rGO/SPCE and allowing incubation for a pre-established time of 30 min. The obtained results are shown in Figure S4a. As it can be observed, the best blocking conditions, permitting lower unspecific and higher specific responses to be achieved corresponded to the use of the 5% BSA solution. Under these conditions, the specific-to-unspecific current ratio was around 15.

The effect of the presence or not of BSA in the secondary antibody (Biotin-anti-APN) and HRP-Strept solutions was also checked. Figure S4b shows as larger unspecific currents occurred when the reagents solutions did not contain BSA. Most likely, the addition of blocking agent only onto the anti-APN-CMC-rGO/SPCE was not sufficient to minimize in a large extent non-specific adsorptions produced onto the electrode surface. Therefore, the Biotin-anti.APN and HRP-Strept solutions were prepared containing 0.5 % BSA, as it was described in section 2.4.2.

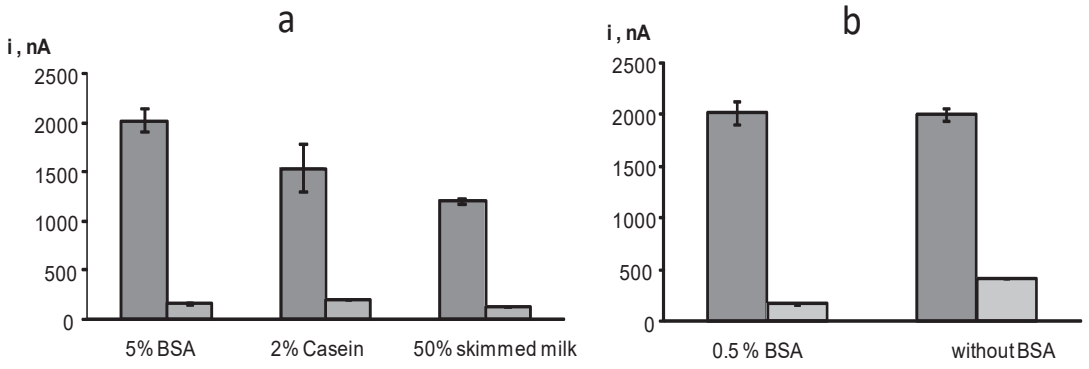

Figure S4. Effect of (a) the type of blocking agent; (b) the presence or not of BSA in the Biotin-anti-APN and HRP-Strept solutions, on the amperometric responses of the HRP-Strept-Biotin-anti-APN-APN-anti-APN-CMC-rGO/SPCE immunosensor: 2 μg/mL APN (dark gray) and 0 μg/mL APN (light gray). Other conditions as in Fig. 1

e) Effect of the concentration of Biotin-anti-APN onto APN-anti-APN-CMC-rGO/SPCE, and the time for incubation

The concentration of Biotin-anti-APN was optimized by comparing the specific and unspecific responses obtained with different immunosensors prepared using biotinylated antibody concentrations in the 1 to 4 μg/mL range. Figure S5 shows as the specific responses increased with the Biotin-anti-APN concentration, as a consequence of the ability to incorporate larger HRP-Strept loadings. However, higher unspecific currents were also found. Therefore, taking into account the largest specific-to-unspecific current ratio, 2 μg/mL Biotin-anti-APN were selected for further work. Under these conditions, such a ratio was approximately 15, with the current value from unspecific responses representing only about 5% of the immunosensor responses for a 2 μg/mL APN concentration.

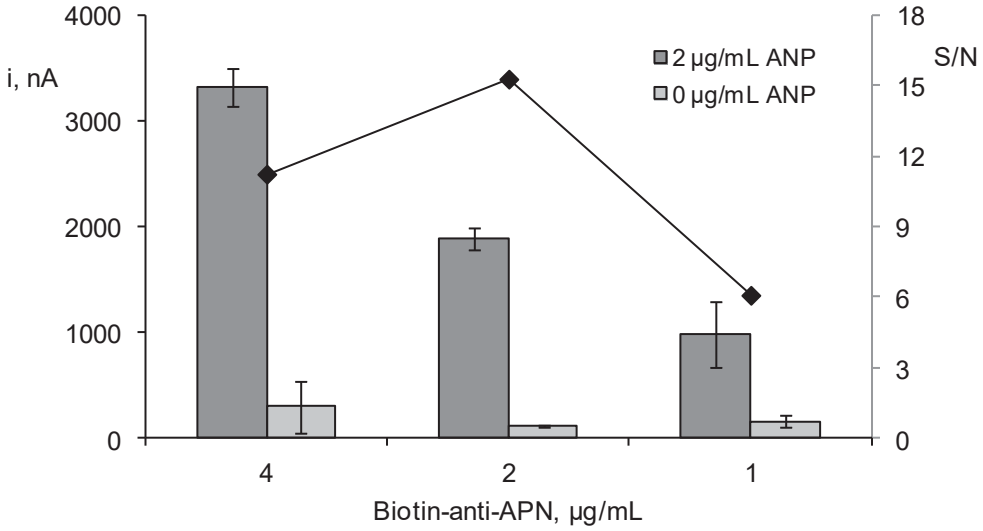

Figure S5. Effect of the Biotin-anti-APN concentration on the amperometric responses of the HRP-Strept-Biotin-anti-APN-APN-anti-APN-CMC-rGO/SPCE immunosensor: 2µg/mL APN (dark gray) and 0 µg/mL APN (light gray). Other conditions as in Fig. 1

f) Effect of the HRP-Strept concentration

Figure S6 shows the results obtained with immunosensors constructed using HRP-Strept solutions prepared for different dilution factors over the 1/500 and 1/2000 range. The largest difference between the currents measured in the presence or in the absence of APN was obtained for a 1/1000 dilution and, therefore, this parameter was selected for further work.

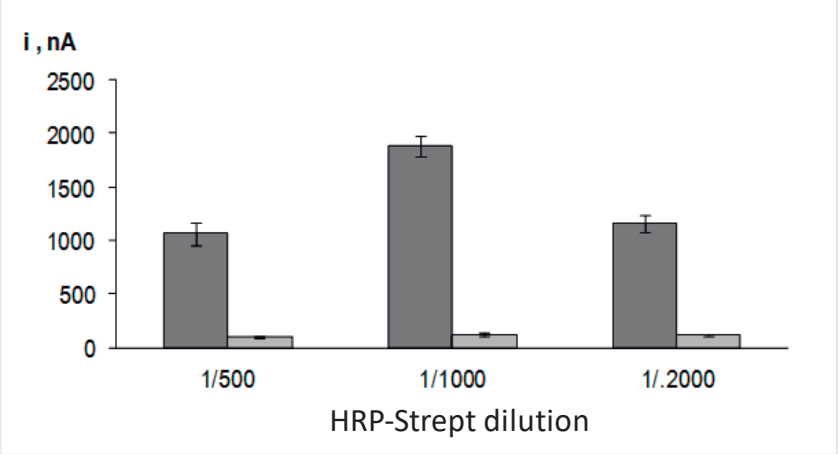

Figure S6. Effect of the HRP-Strept dilution factor on the amperometric responses of the HRP-Strept-Biotin-anti-APN-APN-anti-APN-CMC-rGO/SPCE immunosensor: 2 µg/mL APN (dark gray) and 0 µg/mL APN (light gray). Other conditions as in Fig. 1

g) Effect of the APN incubation time

This variable was optimized by depositing the antigen onto anti-APN-CMC-rGO/SPCEs and allowing incubation for 20, 40 or 60 minutes before proceeding with the further steps. Figure S7 shows as the longer incubation times provided the larger specific-to-unspecific current ratio. As this value was rather similar for 40 and 60 min, the former value was selected for the preparation of the immunosensor in order to shorten the whole procedure.

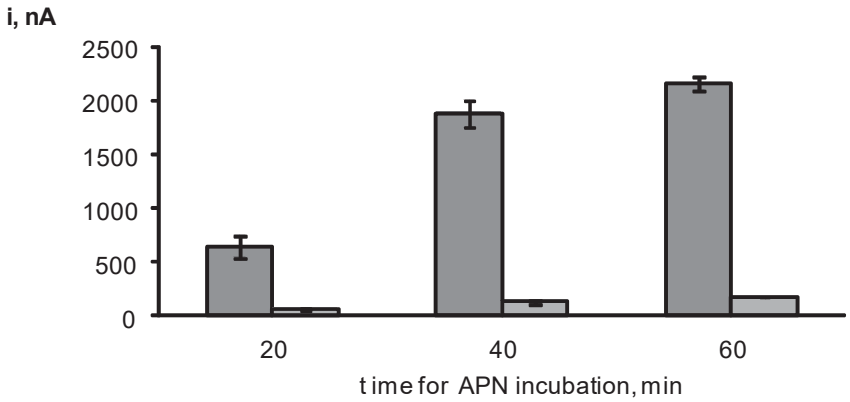

Figure S7. Effect of the APN incubation time on the amperometric responses of the HRP-Strept-Biotin-anti-APN-APN-anti-APN-CMC-rGO/SPCE immunosensor: 2 µg/mL APN (dark gray) and 0 µg/mL APN (light gray). Other conditions as in Fig. 1

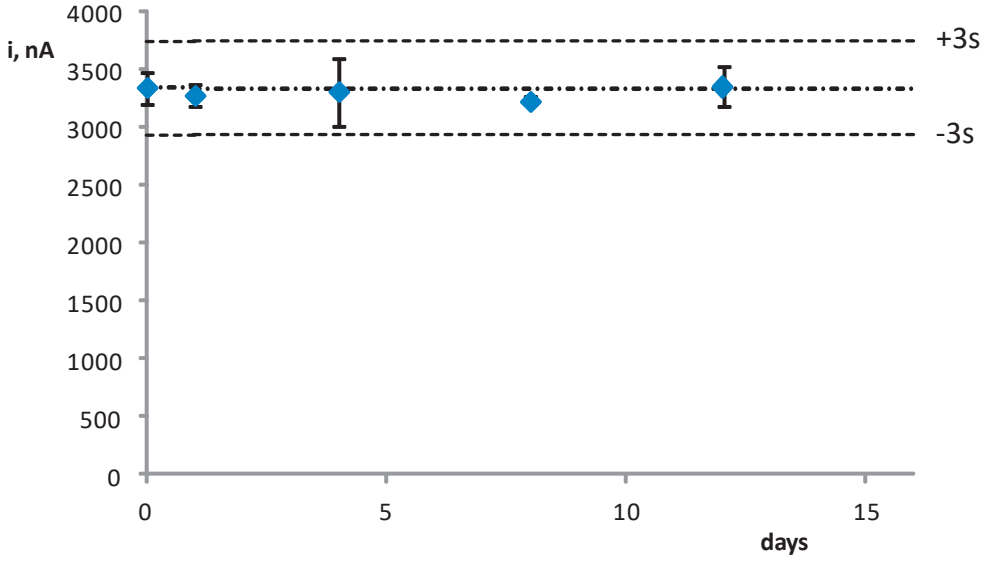

Figure S8. Control chart constructed to evaluate the storage stability of anti-APN-CMC-rGO/SPCE bioelectrodes. Each point corresponds to the mean value of three successive measurements in the presence of 7.5 µg/mL APN

Analyst 141 (2016) 5730-5737

Carbon nanotubes functionalized by click chemistry as scaffolds for the preparation of electrochemical immunosensors. Application to the determination of TGF-beta 1 cytokine

Volume 141 | Number 20 | 21 October 2016 | Pages 5663–5902

Analyst

www.rsc.org/analyst

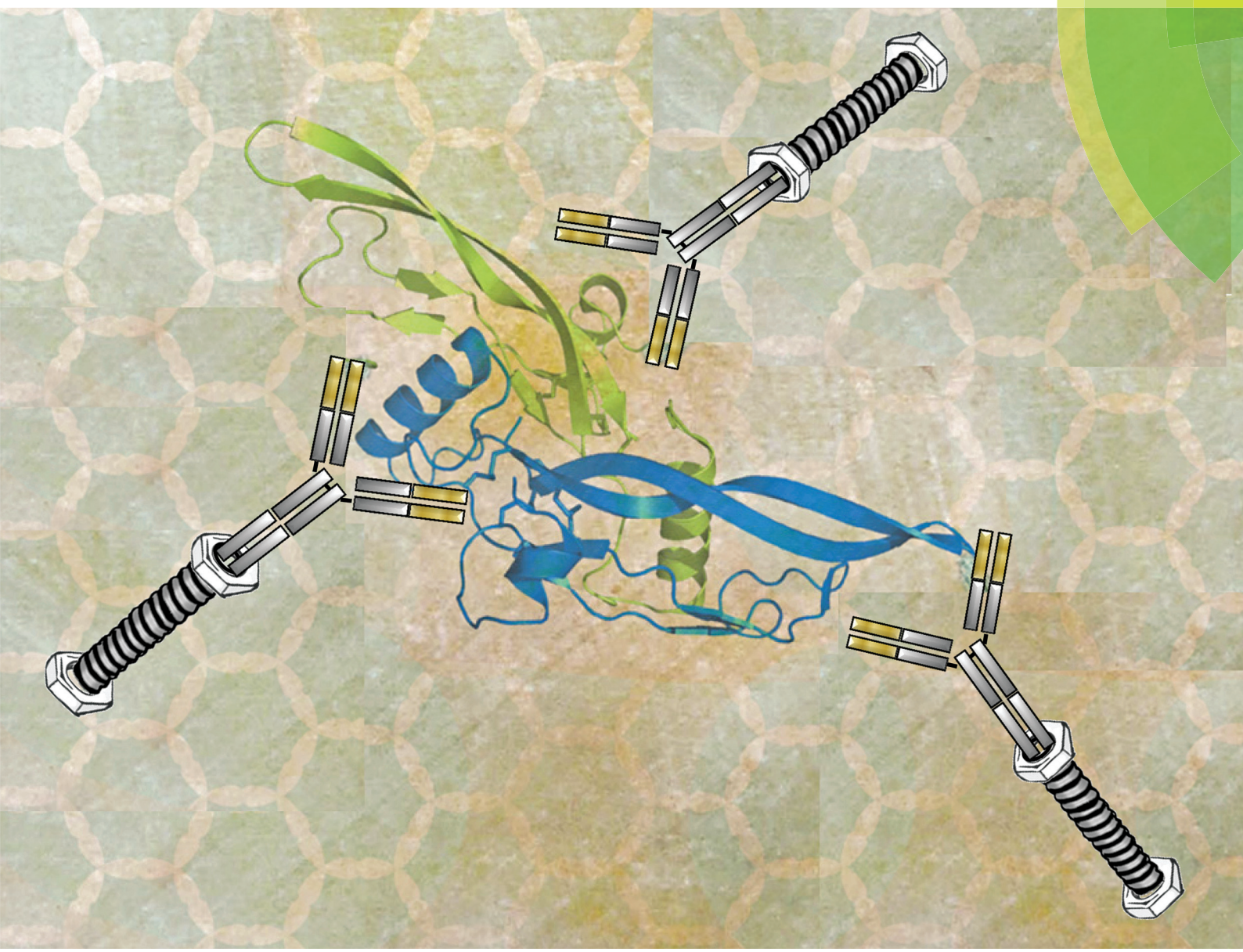

ISSN 0003-2654

ROYAL SOCIETY OF CHEMISTRY

PAPER

Paloma Yáñez-Sedeño *et al.*

Carbon nanotubes functionalized by click chemistry as scaffolds for the preparation of electrochemical immunosensors. Application to the determination of TGF-beta 1 cytokine

175 YEARS

Analyst

PAPER

Cite this: *Analyst*, 2016, **141**, 5730

Carbon nanotubes functionalized by click chemistry as scaffolds for the preparation of electrochemical immunosensors. Application to the determination of TGF-beta 1 cytokine†

E. Sánchez-Tirado, A. González-Cortés, P. Yáñez-Sedeño* and J. M. Pingarrón

An electrochemical immunosensor for the determination of the multifunctional Transforming Growth Factor β1 (TGF-β1) cytokine has been prepared using multi-walled carbon nanotube (MWCNT)-modified screen-printed carbon electrodes. MWCNTs were functionalized by means of copper(I) catalyzed azide–alkyne cycloaddition ("click" chemistry) as an efficient strategy for the covalent immobilization of immunoreagents without altering their configurations and preserving their biological activity. Alkyne-functionalized IgGs were also prepared and used to assemble IgG-alkyne–azide–MWCNT conjugates used as scaffolds for the immunosensor preparation. After a blocking step with casein, anti-TGF was immobilized and the target cytokine was sandwiched with biotinylated anti-TGF labeled with poly-HRP-labeled streptavidin. The affinity reaction was monitored amperometrically at −0.20 V using the hydroquinone (HQ)/H_2O_2 system. The calibration plot for TGF-β1 exhibited a range of linearity (r^2 = 0.995) extending between 5 and 200 pg mL^{-1} which is suitable for the determination of the target cytokine in human serum. A limit of detection of 1.3 pg mL^{-1} was achieved. The analytical performance of the immunosensor can be advantageously compared with that claimed for ELISA kits. The immunosensor was applied to the analysis of spiked human serum samples at different concentration levels with excellent recoveries.

Received 22nd April 2016,
Accepted 27th June 2016

DOI: 10.1039/c6an00941g

www.rsc.org/analyst

1. Introduction

Recently, copper(I) catalyzed azide–alkyne cycloaddition ("click" chemistry) has emerged as a powerful tool for functionalization of different materials as well as an efficient strategy for immobilization of biomolecules. This high interest is due to the high yields, no by-products, and moderate reaction conditions of this environmentally friendly process that can be applied in aqueous medium and under physiological conditions.[1] The methodology, involving azide and alkyne complementary functions, can be used for the functionalization of electrode surfaces[2] which can be used as platforms where biomolecules can be covalently coupled to different substrates without altering their configurations and preserving their biological activity.

Furthermore, carbon nanotubes (CNTs) have demonstrated largely the ability to promote the electron transfer reaction of a large number of molecules[3] thus making CNTs an attractive material for the development of electrochemical sensors and biosensors. A large number of enzyme biosensors using CNT-modified electrodes as convenient scaffolds have been described in the literature.[4] However, CNT-modified electrode based immunosensors have been reported to a much smaller extent. This is probably because biomolecule immobilization methods on this type of modified electrodes rely mostly on direct adsorption or covalent approaches which can reduce the stability of immunoreagents and the reproducibility of bioelectrodes.[5] In the efforts made to find a method for achieving stable and oriented immobilization of antigens or antibodies onto CNTs, "click" synthesis represents a promising strategy. However, despite the high interest in this methodology, only one electrochemical immunosensor has been reported so far using the Cu(I)-catalyzed azide–alkyne cycloaddition (CuAAC) reaction to prepare CNT-based platforms for immobilization of immunoreagents. Alkyne-IgG was coupled on single-walled carbon nanotubes (SWCNTs) functionalized with azide groups

Department of Analytical Chemistry, Faculty of Chemistry, University Complutense of Madrid, 28040-Madrid, Spain. E-mail: yseo@quim.ucm.es

†Electronic supplementary information (ESI) available. See DOI: 10.1039/c6an00941g

This journal is © The Royal Society of Chemistry 2016

and the bioconjugate was cast onto a glassy carbon surface to develop a competitive electrochemical immunoassay for the determination of anti-IgG as the target compound with HRP as an enzyme label.[6]

On the other hand, there is also recent growing interest in the determination of cytokines[7] due to their demonstrated relationship with inflammation or disease progression. Among cytokines, the multifunctional TGF-β1 (Transforming Growth Factor β1) is involved in various immune and inflammatory diseases,[8] and is considered as a good biomarker of liver fibrosis, bladder carcinoma, or renal diseases. TGF-β1 concentrations ranging between 0.1 and 25 ng mL^{-1} in plasma have been reported for healthy individuals,[9] while circulating levels of this cytokine have been shown to be increased in patients suffering from various types of diseases such as various cancers[10,11] or autoimmune disorders,[12] and severely depressed in advanced atherosclerosis.[13]

The current method to determine this protein is by ELISA tests. There is a variety of commercial kits using colorimetric detection and sandwich-type immunoassay configurations with peroxidase-labeled or biotinylated anti-TGF-β1 detection antibodies. The range in which TGF-β1 can be determined is between several tens to thousands of pg mL^{-1} with minimum detectable concentrations of a few pg mL^{-1}. However, the time required for this type of assay is rather long usually lasting over four hours. Regarding immunosensors, only one very recent impedimetric immunosensor for the determination of TGF-β1 in human serum has appeared in the literature. A self-assembled monolayer of polyethylene glycol (PEG) coated onto interdigitated electrodes was used for the covalent immobilization of antibodies. A linear impedance *vs.* log [TGF-β1] ranging between 1 and 1000 ng mL^{-1} with a detection limit of 0.570 ng mL^{-1} was reported.[14] However, this sensitivity is not sufficient for applications in clinical samples containing low TGF-β1 concentrations.

In this work, multi-walled carbon nanotubes (MWCNTs) were used to prepare scaffolds as electrode modifiers for the construction of a TGF-β1 immunosensor involving the CuAAC reaction to synthesize alkyne–azide conjugates. MWCNTs were selected for such a purpose due to their well-known excellent conducting and electrocatalytic properties.[15] The steps involved in the oxidation of carbon nanotubes and functionalization with an azide group as well as alkyne-functionalization of IgG and preparation of IgG-alkyne–azide–MWCNT conjugates were optimized. In addition, variables involved in the preparation and performance of the immunosensor were also addressed and optimized. Under the optimized conditions, TGF-β1 could be determined with the developed immunosensor with a high sensitivity and low detection limit exhibiting suitability for the analysis of clinical samples.

2. Experimental

2.1. Reagents and solutions

An anti-mouse IgG (Fc specific) from Sigma (SAB3700848) was used as a primary antibody. The capture antibody was a mouse anti-TGF, reconstituted with 500 μL of 0.1 M phosphate buffer solution of pH 7.4 (PBS) up to a 240 μg mL^{-1} concentration. A chicken biotinylated antibody (Biotin-anti-TGF) reconstituted up to a 18 μg mL^{-1} concentration with 1 mL of Reagent Diluent 1 (R&D Systems) was also used. Both anti-TGF antibodies and human TGF-β1 were the same as those used in the DuoSet® ELISA Development System (DY240-05) from R&D Systems. HRP-labeled streptavidin (Roche) and poly-HRP-Strept (65R-S105PHRP) (Fitzgerald) solutions were prepared in 0.1 M PBS of pH 7.4. Buffer solutions used were 0.1 M phosphate buffer solution (PBS) of pH 7.4; 10 mM PBS of pH 7.0; 0.1 M PBS and 0.15 M NaCl of pH 7.2 (coupling buffer), and 25 mM 2-(*N*-morpholino)ethanesulfonic acid (MES) buffer of pH 6.5. Reagent Diluent 1 and Washing Buffer from R&D Systems included in the Duoset® Ancillary Reagent Kit 1 (DY007) were also used. Multi-walled carbon nanotubes (MWCNTs, PD30L5-20) were from NanoLabs. 1% (w/v) casein solution (Blocker™ Casein, Thermo Fisher) in 0.1 M PBS of pH 7 was used as the blocking agent. 1-Ethyl-3-(3-dimethylaminopropyl)carbodiimide (EDC) and *N*-hydroxysulfo-succinimide (NHSS) were from Acros. *N*,*N*′-Dicyclohexylcarbodiimide (DCC) and *N*-hydroxysuccinimide (NHS) were from Sigma. Other reagents used were 11-azide-3,6,9-trioxaundecan-1-amine (Aldrich), and ethynyl hydrazide (Chem Space). All other reagents and solvents used were of analytical grade. De-ionized water was obtained from a Millipore Milli-Q purification system (18.2 MΩ cm). The analyzed samples were a lyophilized human serum from clotted whole blood (Sigma, S2257) spiked with TGF-β1 at different concentrations, and two real serum samples from one healthy (SG609-2, BBI Solutions) and one hypercholesterolemic (SG376-2, BBI Solutions) female.

2.2. Apparatus and electrodes

Amperometric measurements were performed with an INBEA potentiostat using the IbGraph software. Screen-printed carbon electrodes (SPCEs, 110 DRP, ϕ 4 mm) from DropSens (Oviedo, Spain) were used as working electrodes. These electrodes are provided with a silver pseudo-reference electrode and a carbon counter electrode. Incubation steps were carried out at 25 °C using an Optic Ivymen System constant temperature incubator shaker (Comecta S.A.). Electrochemical impedance spectroscopy was carried out with a μAutolab type III potentiostat (Ecochemie) controlled by FRA2 software. A Crison Basic 20+ pHmeter, an Elmasonic S-60 ultrasonic bath (Elma), and a Vortex homogenizator from Velp Scientifica were also employed.

2.3. Procedures

Azide-functionalized MWCNTs and alkyne-functionalized IgG were prepared by following the procedures described in the ESI† (Procedures S1–S3) and are schematized in Fig. S1 and S2,† respectively.

2.3.1. Preparation of the electrochemical immunosensor. Fig. 1 shows schematically the steps involved in the preparation of the amperometric immunosensor for TGF-β1. Step 1

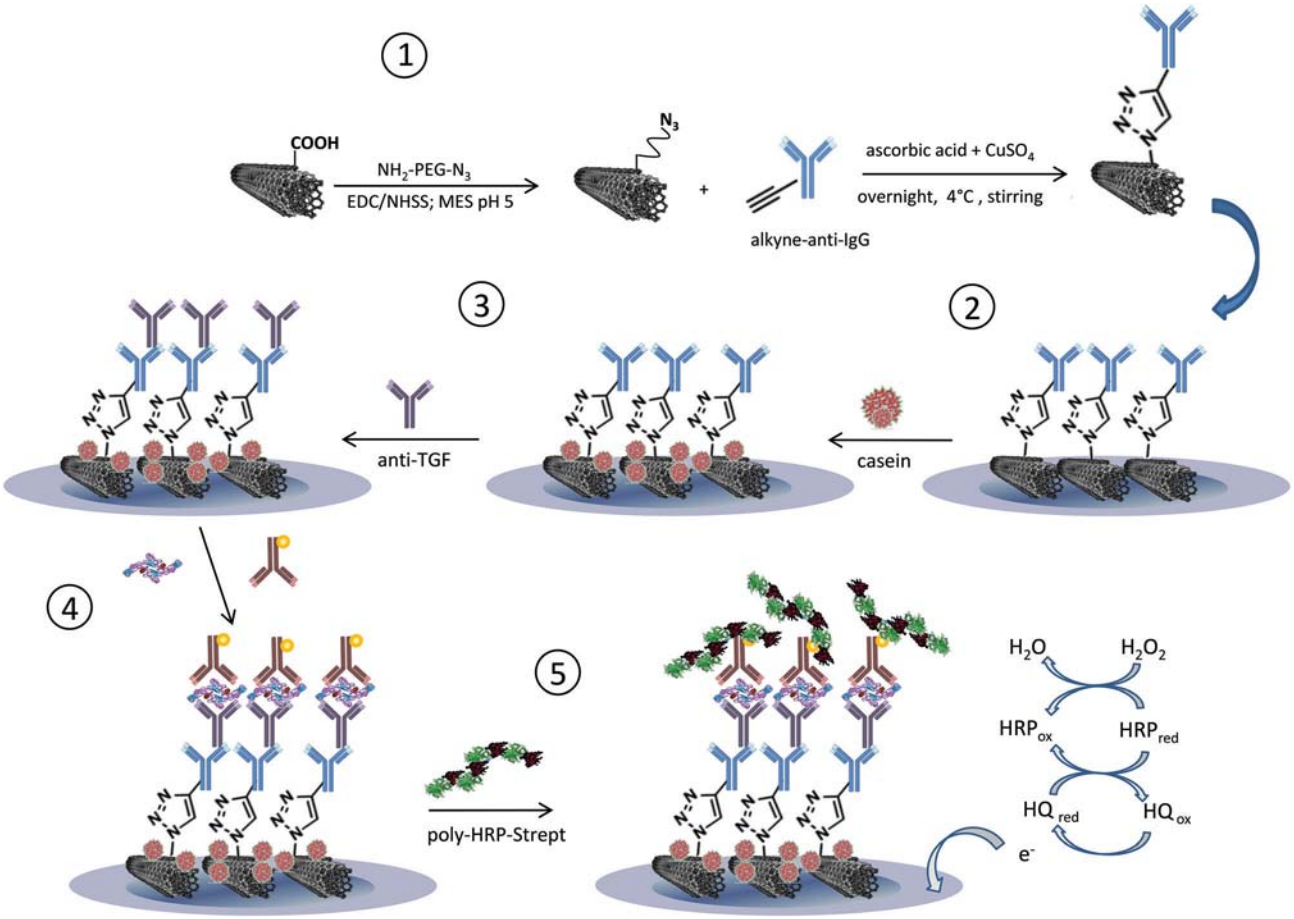

Fig. 1 Schematic display of the different steps involved in the preparation and functioning of the poly-HRP-Strept–Biotin-anti-TGF–TGFβ1–anti-TGF–IgG–MWCNT/SPCE immunosensor.

depicts the preparation of IgG-alkyne–azide–MWCNT conjugates by mixing 67.5 μL of a 1/100 diluted alkyne-functionalized-IgG solution with 45 μL of 5 mM ascorbic acid and 45 μL of 5 mM copper sulfate. Then, 157.5 μL of a 0.5 mg mL^{-1} azide-functionalized-MWCNT dispersion were added and magnetically stirred at 4 °C overnight. Step 2 involves 5 μL dropping of the IgG-alkyne–azide–MWCNT conjugate dispersion onto the SPCE surface and allowing it to dry, and a further blocking step by addition of 5 μL of 1% casein solution in 0.1 M PBS of pH 7.4 and allowing incubation for 30 min. Step 3 involved 5 μL addition of a 10 μg mL^{-1} anti-TGF solution and incubation for 60 min. Thereafter, 5 μL of a TGF-β1 standard solution (or the sample), and 5 μL of a 1 μg mL^{-1} Biotin-anti-TGF were added (step 4) allowing incubation for 60 min. Finally, step 5 involved labeling with 5 μL of a 1/500 diluted poly-HRP-Strept in 0.1 M PBS of pH 7.4 incubating for 20 min.

2.3.2. Determination of TGF-β1. Determination of TGF-β1 was accomplished by dropping 45 μL of a 1 mM hydroquinone (HQ) solution in 0.5 M PBS of pH 6.0 onto the surface of the poly-HRP-Strept–Biotin-anti-TGF–TGF-β1–anti-TGF–IgG–MWCNT/SPCE immunosensor horizontally positioned. A detection potential of −0.20 V was applied. Once the background current was stabilized (aprox. 100 s), 5 μL of a 50 mM H_2O_2 solution were added and allowed to stand for 200 s. The oxidation of hydrogen peroxide is catalyzed by peroxidase. The oxidized form of peroxidase oxidizes hydroquinone, and the product of the oxidation is reduced electrochemically at the electrode. The steady state current corresponding to the electrochemical reduction of benzoquinone was used as the analytical readout.

TGF-β1 determination was performed by applying this procedure to both serum samples spiked at 25, 75 and 125 pg mL^{-1} protein levels, which were 100 times diluted with PBS, and real serum samples from female individuals. The measured steady-state currents were interpolated into the linear calibration plot constructed with TGF-β1 standard solutions. In addition, the results obtained for the real samples were compared with those provided by a commercial DuoSet® ELISA Development System (DY240-05) kit.

3. Results and discussion

As is described in section 2.3.1 and depicted in Fig. 1, azide-functionalyzed MWCNTs and alkyne-functionalized IgG were

 This journal is © The Royal Society of Chemistry 2016

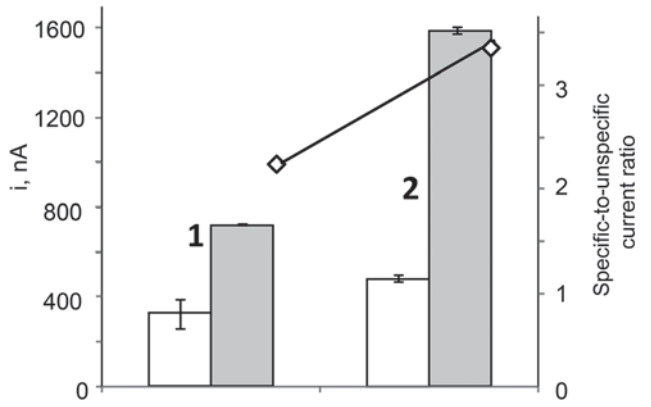

Fig. 2 Effect of the protocol applied for IgG-alkyne functionalization on the amperometric response measured with the poly-HRP-Strept–Biotin-anti-TGF–TGF-β1–anti-TGF–IgG–MWCNT/SPCE using succinimidyl-3-propionate (1) or sodium periodate (2). 5 μL 10 μg mL^{-1} IgG-alkyne–azide–MWCNTs; 5 μL casein, 30 min; 5 μL 10 μg mL^{-1} anti-TGF, 60 min; 0 (white) or 200 (grey) pg mL^{-1} TGF-β1; 5 μL 1 μg mL^{-1} Biotin-anti-TGF, 60 min; 5 μL 1/500 poly-HRP-Strept, 20 min.

synthesized and used to prepare IgG-alkyne–azide–MWCNT conjugates by Cu(I) catalyzed azide–alkyne-cycloaddition (CuAAC). The ESI† (Procedure S1) describes the employed method to prepare azide–MWCNTs by covalent immobilization of 11-azide-3,6,9-trioxaundecan-1-amine onto oxidized MWCNTs. Fig. S3 in the ESI† shows IR absorption spectra obtained for azide-functionalized carbon nanotubes as well as for a commercial azide. A characteristic band at 2106 cm^{-1} corresponding to the stretching vibration of the –N3 group appeared in both cases indicating the successful functionalization of MWCNTs.

Furthermore, alkyne-IgGs were prepared using two different protocols (Procedures S2 and S3) involving the use of succinimidyl-3-propiolate[16] or sodium periodate,[17] respectively. These protocols were compared by testing the responses obtained with TGF-β1 immunosensors prepared according to procedure 2.3.1 and using each alkyne-IgG derivative. Fig. 2 shows the amperometric measurements obtained for 0 (unspecific) and 200 pg mL^{-1} TGF-β1 with the immunosensors constructed with alkyne-IgG prepared by both methods. As can be seen, the specific-to-unspecific current ratio was about 25% larger when periodate was used to get alkyne-IgG. This finding is in agreement with the claimed properties of this reagent able to oxidize 1,2-diols of carbohydrates existing in the Fc region of antibodies thus leading to the oriented modification of IgG. Conversely, this oriented modification is not produced when succinimidyl-3-propiolate is used.[17] Accordingly, the protocol involving the use of periodate for the preparation of alkyne-functionalized IgG was selected for further work. Fig. S3 in the ESI† also shows the IR absorption spectrum obtained after the click reaction of the azide group in IgG-alkyne–azide–MWCNTs. As can be seen, the band at 2106 cm^{-1} did not appear in this case suggesting the successful binding of alkyne–anti-IgG.

3.1. Optimization of the variables involved in the preparation and performance of the immunosensor

Once IgG-alkyne–azide–MWCNT conjugates were prepared according to the procedure described in section 2.3.1, an aliquot of this conjugate dispersion was dropped onto the SPCE to construct the scaffolds employed for immobilization of the specific anti-TGF-β1 antibodies. The different variables affecting the performance of the developed immunosensor were optimized. These optimization studies involved the evaluation of: (a) the IgG-alkyne–azide–MWCNT loading on the SPCE; (b) the type of blocking agent; (c) the type of enzymatic labeling of the detection antibody; (d) the concentration of poly-HRP-Strept; (e) the anti-TGF loading on the IgG-alkyne–azide–MWCNT/SPCE; (f) the Biotin-anti-TGF loading on the TGF β1–anti-TGF–IgG-alkyne–azide–MWCNT/SPCE. Details on these optimization studies are given in the ESI (Fig. S4–S7†).

Electrochemical impedance spectroscopy (EIS) was employed to monitor the steps involved in the electrode modification. Fig. 3 shows the Nyquist plots recorded at the SPCE, azide–MWCNT/SPCE, IgG-alkyne–azide–MWCNT/SPCE, and anti-TGF–IgG-alkyne–azide–MWCNT/SPCE, using 5 mM $Fe(CN)_6^{3-/4-}$ as the redox probe in 0.1 M PBS of pH 7.4, as well as the equivalent circuits used to fit the spectra. Spectra 1, 2 and 3 fitted well to a Randles circuit whereas spectrum 4 fitted better to the equivalent circuit depicted on the right since some parts of the electrode are coated by the antibody while others remain exposed to the solution. The nesting parallel RC circuits mean that there is a film with defects such as pinholes or with a non-uniform thickness throughout the substrate.[18] As expected, the charge transfer resistance at the bare SPCE (curve 1) is notably higher (R_{CT} = 1247 ohm) than that measured at the azide–MWCNT/SPCE (curve 2, R_{CT} = 240 ohm) due to the well-known electron transfer promotion observed at carbon nanotube-modified electrodes. Furthermore, the resistance increased to a value of 658 ohm when the IgG-alkyne–azide–MWCNT conjugate was deposited onto the SPCE surface (curve 3), as a consequence of the isolating effect provoked by the biomolecules. Subsequent immobilization of the capture antibody led to a further resistance increase (curve 4) (R_{CT} = 865 ohm), due to the lower conductivity of the resulting biosurface. These results confirmed the suitability of the procedure used for the modification of the electrode involving immobilization of anti-TGF antibodies on IgG-alkyne–azide–MWCNTs.

3.2. Analytical figures of merit of the immunosensor

Fig. 4 shows the calibration plot for TGF-β1 constructed by amperometry at −0.20 V with the poly-HRP-Strept–Biotin-anti-TGF–TGF-β1–anti-TGF–IgG–MWCNT/SPCE immunosensor together with some typical amperometric responses recorded for different TGF-β1 concentrations. The range of linearity (r^2 = 0.995) extended between 5 and 200 pg mL^{-1} according to the equation Δi, nA = 5.60 [TGF-β1], pg mL^{-1} + 32.5. In this equation, Δi is the current obtained by subtracting the background current measured in the absence of an antigen from the amperometric response of the immunosensor.[19] Interest-

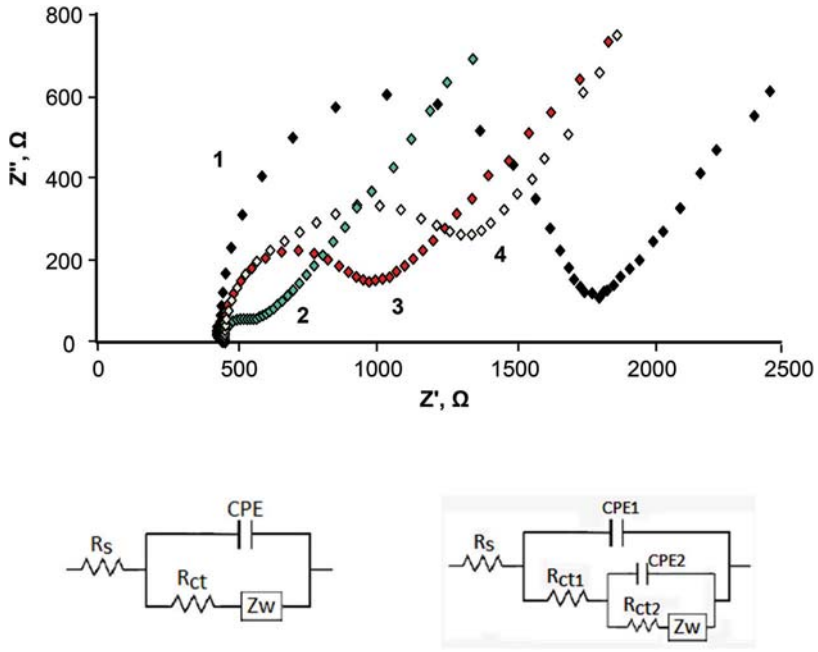

Fig. 3 Nyquist plots recorded at the SPCE (1), azide–MWCNT/SPCE (2), IgG-alkyne–azide–MWCNT/SPCE (3), and anti-TGF-IgG-alkyne–azide–MWCNT/SPCE (4), and equivalent circuits using 5 mM $Fe(CN)_6^{3-/4-}$ as the redox probe in 0.1 M PBS of pH 7.4.

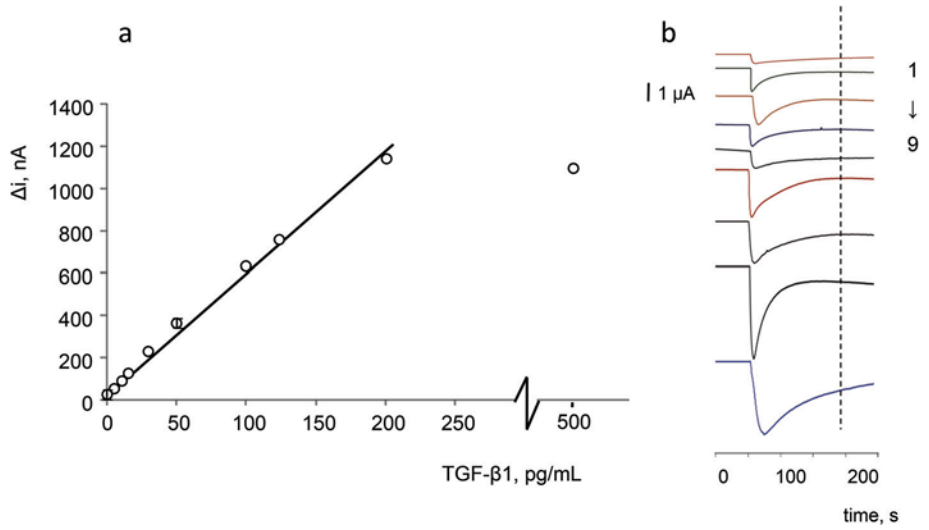

Fig. 4 Calibration plot and typical amperometric responses for TGF-β1 recorded with the poly-HRP-Strept–Biotin-anti-TGF–TGF-β1–anti-TGF–IgG–MWCNT/SPCE: (a) 0 pg mL^{-1}; (b) 5 pg mL^{-1}; (c) 10 pg mL^{-1}; (d) 15 pg mL^{-1}; (e) 30 pg mL^{-1}; (f) 50 pg mL^{-1}; (g) 100 pg mL^{-1}; (h) 125 pg mL^{-1}; (i) 200 pg mL^{-1} TFG-β1. See the text for more information.

ingly, this range is suitable for the determination of the target cytokine in human serum since the concentration levels found in healthy individuals are comprised between 0.1 and 25 ng mL^{-1}.[9]

The limit of detection, 1.3 pg mL^{-1}, was calculated according to the $3s_b$ criterion, where s_b was estimated as the standard deviation (n = 10) for the blank (measurements in the absence of TGF β1) in concentration units (pg mL^{-1}). Moreover, the limit of determination was calculated as $10s_b$ and the value was 4.3 pg mL^{-1}. When these analytical figures of merit are compared with data provided for commercial ELISA kits using similar immunoreagents, some noticeable differences are apparent. ELISA kits claim for dynamic ranges usually covering from several tens to thousands of pg mL^{-1} with minimum detectable concentrations of a few pg mL^{-1}. However, these parameters are calculated mostly from nonlinear logarithmic ranges and the precision levels are around 10% or higher. It is important to note that the criteria used to calculate the LOD

 This journal is © The Royal Society of Chemistry 2016

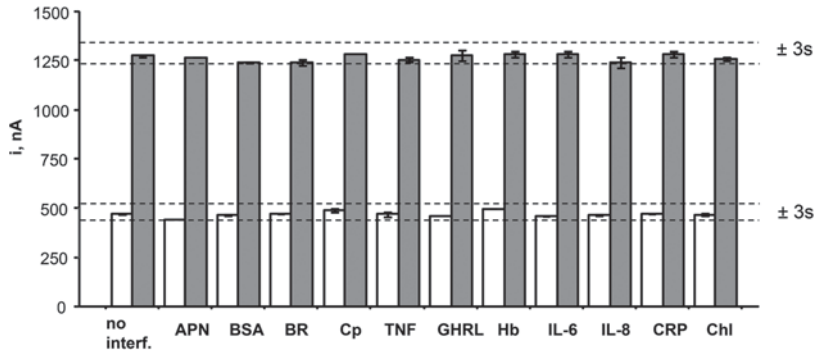

Fig. 5 Amperometric responses measured with the poly-HRP-Strept–Biotin-anti-TGF–TGF-β1–anti-TGF–IgG–MWCNT/SPCE immunosensor for 0 (white) and 125 (grey) pg mL^{-1} TGF-β1 in the presence of 20 μg mL^{-1} adiponectin (APN), 5 μg mL^{-1} BSA, 190 ng mL^{-1} bilirubin (BR), 500 μg mL^{-1} ceruloplasmin (CP), 100 pg mL^{-1} tumor necrosis factor alpha (TNF), 500 pg mL^{-1} ghrelin (GHRL), 50 μg mL^{-1} hemoglobin (Hb), 50 μg mL^{-1} interleukin 6 (IL-6), 30 pg mL^{-1} interleukin 8 (IL-8), 1 μg mL^{-1} C-reactive protein (CRP), and 20 μg mL^{-1} cholesterol (Chl).

values for these kits are rarely given in the commercial protocols. Moreover, the time lasted for the assay is remarkably longer with ELISA kits extending even over 4 h *versus* 1 h 20 min required for the immunosensor counting, in both cases, because of the immobilization of capture antibody. Therefore, it could be concluded that the analytical performance of the developed immunosensor, covering a wide linear range of TGF-β1 concentrations within the clinically relevant interval, improved, in general terms, the performance claimed for ELISA kits. On the other hand, when the comparison is made *versus* the reported impedimetric immunosensor,[14] the reported LOD was 0.570 ng mL^{-1} in this latter case, which is more than four hundred times higher than that calculated with the developed immunosensor.

The reproducibility of the amperometric measurements was tested for both 0 and 125 pg mL^{-1} TGF-β1 with five different immunosensors prepared on the same day. Relative standard deviations values, RSD, of 1.5 and 2.7%, respectively, were obtained. Furthermore, RSD values of 1.9 and 2.5% were obtained using five different immunosensors prepared in different days. Thus, these results demonstrated the good accuracy of the amperometric measurements and indicated that the proposed method for the immunosensor preparation is reliable and reproducible.

The storage capability of the anti-TGF–IgG–MWCNT/SPCE bioelectrode was also tested. In order to do that, different immunosensors were prepared on the same day and stored at 8 °C in a humid environment with 20 μL of Reagent Diluent 1. Then the immunosensors were used to measure 125 pg mL^{-1} TGF-β1 on different days according to the procedure described in sections 2.3.1 and 2.3.2. A control chart was constructed (Fig. S7†) by setting ±3s as control limits, where s is the standard deviation of the measurements (n = 10) carried out on the first day. The immunosensor responses remained within the control limits for at least 40 days (no longer storage times were tested) demonstrating a great stability of the prepared anti-TGF–IgG–MWCNT/SPCE.

Regarding the selectivity of the immunosensor, it is important to note that anti-TGF antibodies were the same as those used in the DuoSet® ELISA Development System (DY240-05) from R&D Systems (section 2.1). These antibodies exhibited a high selectivity toward other kinds of TGFs, with cross-reactivity factors of 0.15, 0.96 and 1.8%, for TGFβ2, TGFβ3, and TGFβ5, respectively. Moreover, the selectivity of the capture antibody was also evaluated by measuring the amperometric responses in the absence and in the presence of other proteins such as adiponectin (APN), bovine serum albumin (BSA), bilirubin (BR), ceruloplasmin (Cp), tumoral necrosis factor alpha (TNF), ghrelin (GHRL), hemoglobin (Hb), interleukin-8 (IL-6), interleukin-6 (IL-8), C-reactive protein (CRP), as well as cholesterol (Chl). All of them were checked at concentrations that can be found in the serum of healthy individuals. Fig. 5 shows clearly that there were no significant differences between the currents measured in the absence or in the presence of these compounds, thus demonstrating the practical specificity of the immunosensor for the determination of TGF-β1.

3.3. Determination of TGF-β1 in human serum

The possible existence of matrix effects in human serum was firstly evaluated. Fig. 6 compares the amperometric measurements recorded with the poly-HRP-Strept–Biotin-anti-TGF–TGFβ1–anti-TGF–IgG-MWCNT/SPCE immunosensor in 0.1 M

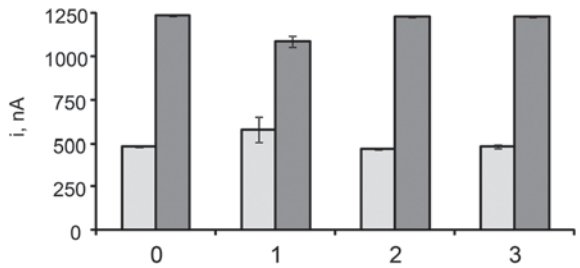

Fig. 6 Amperometric responses obtained with the poly-HRP-Strept–Biotin-anti-TGF–TGF-β1–anti-TGF–IgG–MWCNT/SPCE for 0 (light grey) and 125 pg mL^{-1} TGF-β1 (dark grey) in 0.1 M PBS of pH 7.4 (0), and in human serum diluted with 0.1 M PBS pH 7.4 at the 1/10 (1); 1/50 (2) and 1/100 (3) ratios.

PBS of pH 7.4 and in human serum containing no TGF-β1 or spiked with 125 pg mL^{-1} TGF-β1 (final concentration) upon dilution with 0.1 M PBS of pH 7.4 at different ratios. As can be deduced, measurements at a 1/10 serum dilution ratio (bars 1) showed a slight increase in the mean current value (n = 3) for the blank (light grey), together with a slight decrease of the mean current value for 125 pg mL^{-1} TGF-β1 (dark grey), with respect to the responses obtained in 0.1 M PBS (bars 0). These small differences could be attributed to a weak matrix effect provoked by the serum components. However, it is clear that no apparent matrix effect occurred from a 1/50 sample dilution ratio (bars 2). Taking into account the high sensitivity of the developed method and with the aim of ensuring the complete removal of any matrix effect, a 1/100 dilution ratio was selected to accomplish the protocol for the analysis of human serum. Under these conditions, a comparison of the calculated slope values of the calibration plots constructed with TGF-β1 standard solutions in 0.1 M PBS and in serum samples spiked with TGF-β1, at concentrations ranging between 0 and 125 pg mL^{-1}, was carried out. The slope value of the linear calibration graph obtained for spiked serum samples was 5.57 ± 0.01 nA mL pg^{-1} which is not statistically different from the slope of the calibration plot constructed in 0.1 M PBS with TGF-β1 standard solutions (5.60 nA mL pg^{-1}), thus demonstrating the complete removal of matrix effects. Accordingly, the determination of TGF-β1 in serum could be accomplished by interpolation of the current measured with the immunosensor in 1/100 diluted samples into the calibration plot prepared with TGF-β1 standard solutions. No further sample preparation was needed. Table 1 summarizes the results obtained in the analysis of both spiked serum and real serum samples from female individuals. Excellent recoveries ranging between 98 ± 1 and 101 ± 4% were found in serum spiked with 25, 75 and 125 pg mL^{-1} TFG-β1. In addition, the results obtained with sera from one healthy and one hypercholesterolemic female were compared with those provided by using the DuoSet® ELISA Development System (DY240-05). As can be seen in Table 1, mean TFG-β1 concentrations of 1.38 ± 0.05 ng mL^{-1} and 2.11 ± 0.06 ng mL^{-1} were found with the immunosensor (n = 8) for the healthy and hypercholesterolic patients, respectively. These mean values are in excellent agreement with those provided by the ELISA kit. Therefore, these results demonstrated clearly the suitability of the approach to determine low TGF-β1 concentrations in complex biological samples.

Table 1 Determination of TGF-β1 in human serum with the poly-HRP-Strept–Biotin-anti-TGF–TGF-β1–anti-TGF–IgG–MWCNT/SPCE

Spiked serum	TGF-β1, pg mL^{-1}	TGF-β1 found, pg mL^{-1}	Recovery, %
	25	25 ± 2	100 ± 9
	75	76 ± 3	101 ± 4
	125	123 ± 1	98 ± 1
Real serum		Immunosensor, ng mL^{-1}	ELISA[a], ng mL^{-1}
(SG609-2, BBI solutions)[b]		1.38 ± 0.05	1.40 ± 0.02
(SG376-2, BBI solutions)[c]		2.11 ± 0.06	2.10 ± 0.04

[a] Mean value ± ts (n = 8, α = 0.05). [b] From a healthy female. [c] From a hypercholesterolemic female.

4. Conclusions

A novel amperometric immunosensor for the cytokine TGF-β1 has been developed in this work. The immunosensor preparation strategy involves building up of electrode scaffolds composed of MWCNTs functionalized by copper(I) catalyzed azide–alkyne cycloaddition for binding of alkyne-functionalized IgGs and formation of IgG-alkyne–azide–MWCNT conjugates. This strategy allows oriented immobilization of capture antibodies preserving their biological activity. A sandwich-type configuration using poly-HRP-streptavidin labeling to achieve signal amplification led to the preparation of immunosensors exhibiting an excellent analytical performance in terms of sensitivity, clinically relevant linear range, reproducibility, storage stability and selectivity. The achieved analytical characteristics improve, in general, the performance claimed for ELISA kits and the reported impedimetric immunosensor. Moreover, the immunosensor shows an excellent suitability for the analysis of human serum with a minimal sample treatment consisting of only a 1/100 dilution with 0.1 M PBS of pH 7.4.

Acknowledgements

Financial support of Spanish Ministerio de Economía y Competitividad, Research Projects CTQ2015-70023-R and CTQ2015-71955-REDT, and the NANOAVANSENS Program from Comunidad de Madrid (S2013/MT-3029) is gratefully acknowledged.

References

1 H. C. Kolb, M. G. Finn and K. B. Sharpless, *Angew. Chem., Int. Ed.*, 2001, **40**, 2004.
2 A. Cernat, M. Tertiş, C. Cristea and R. Săndulescu, *Int. J. Electrochem. Sci.*, 2015, **10**, 6324.
3 A. T. Lawal, *Mater. Res. Bull.*, 2016, **73**, 308.
4 F. Kong and Y. F. Hu, *Anal. Bioanal. Chem.*, 2012, **403**, 7.
5 S. Puertas, M. G. Villa, E. Mendoza, C. Jiménez-Jorquera, J. de la Fuente, C. Fernández-Sánchez and V. Grazú, *Biosens. Bioelectron.*, 2013, **43**, 274.
6 H. Qi, C. Ling, R. Huang, X. Qiu, L. Shangguan, Q. Gao and C. Zhang, *Electrochim. Acta*, 2012, **63**, 76.
7 G. Liu, M. Qi, M. R. Hutchinson, G. Yang and E. M. Goldys, *Biosens. Bioelectron.*, 2016, **79**, 810.
8 M. V. Tsapenko, R. E. Nwoko, T. M. Borland, N. V. Voskoboev, A. Pflueger, A. D. Rule and J. C. Lieske, *Clin. Biochem.*, 2013, **46**, 1430.
9 D. J. Grainger, D. E. Mosedale and J. C. Metcalfe, *Cytokine Growth Factor Rev.*, 2000, **11**, 133.

This journal is © The Royal Society of Chemistry 2016

10 C. Wickenhauser, A. Hillienhof, K. Jungheim, J. Lorenzen, H. Ruskowski, M. L. Hansmann, J. Thiele and R. Fischer, *Leukemia*, 1995, **9**, 310.
11 V. Ivanovic, A. Melman, B. Davis-Joseph, M. Valcic and J. Geliebter, *Nat. Med.*, 1995, **1**, 282.
12 A. Pfeiffer, K. Middelberg-Bisping, C. Drewes and H. Schatz, *Diabetes Care*, 1996, **19**, 1113.
13 Z. Matharu, D. Patel, Y. Gao, A. Haque, Q. Zhou and A. Revzin, *Anal. Chem.*, 2014, **86**, 8865.
14 Y. Yao, J. Bao, Y. Lu, D. Zhang, S. Luo, X. Cheng, Q. Zhang, S. Li and Q. Liu, *Sens. Actuators, B*, 2016, **222**, 127.
15 L. Agüí, P. Yáñez-Sedeño and J. M. Pingarrón, *Anal. Chim. Acta*, 2008, **622**, 11.
16 J. Chao, W.-Y. Huang, J. Wang, S.-J. Xiao, Y.-C. Tang and J.-N. Liu, *Biomacromolecules*, 2009, **10**, 877.
17 H. T. Le, J. G. Jang, J. Y. Park, C. W. Lim and T. W. Kim, *Anal. Biochem.*, 2013, **435**, 68.
18 L. Bardini, *EIS 101 An Introduction to Electrochemical Impedance Spectrocopy*, 2015, pp. 21–23, DOI: 10.13140/RG.2.1.2248.5600.
19 Z.-H. Yang, Y. Zhuo, R. Yuan and Y.-Q. Chai, *Biosens. Bioelectron.*, 2016, **78**, 321.

SUPPLEMENTARY INFORMATION

1. Experimental procedures

Procedure S1. Preparation of azide-functionalized MWCNTs

Firstly, MWCNTs were carboxylated. 25 mg of MWCNTs were suspended in 85 mL of deionized water and ultrasonically stirred for one hour. Then, 16 mL of 65% w/w nitric acid were added and the mixture was kept under reflux for one hour. Once cooled at room temperature, the solid was centrifuged at 4000 rcf for 10 minutes. Finally, the resulting cMWCNTs were washed with deionized water until washing liquids reached pH 7, and dried under nitrogen stream. Thereafter, carboxyl groups were activated; 20 mg cMWCNTs were suspended in 2.8 mL of 25 mM MES buffer, pH 6.5, containing 21.4 mg EDC and 23.8 mg NHSS, and magnetically stirred for two hours in the dark. For the preparation of azide-functionalized-MWCNTs, 4.5 μL of 11-azide-3,6,9-trioxaun-decan-1-amine were added, and the mixture was magnetically stirred for 48 h in the dark. Then, the product was centrifuged at 4000 rcf for 10 minutes, and sequentally washed with 10 mM PBS of pH 7.0 and deionized water. Finally, the product was dried at 37 ºC.

Procedure S2. Preparation of alkyne-functionalized IgG using succinimidyl-3-propiolate

In this step, the method described by Qi[1] was applied with slight modifications (Figure S1). Succinimidyl-3-propiolate was synthesized[2] by dropping 10 mL of a solution containing 1.14 g N,N′-dicyclohexylcarbodiimide (DCC) onto another solution containing 0.39 g of propiolic acid and 0.64 g of N-hydroxysuccinimide (NHS) in

30 mL of ethyl acetate. The resulting solution was magnetically stirred at 4 ºC for 8 h. Next, the solution was filtered through a Büchner funnel and then, the solvent was removed using a rotary evaporator. The obtained residue was dissolved in 15 mL ethyl acetate and the resulting solution was transferred to a separatory funnel and sequentally washed by shaking 2 min each with 15 mL of a NaCl saturated aqueous solution (40 % w/w), 15 mL of a NH_4Cl saturated aqueous solution (60% w/w), and 15 mL of de-ionized water. After this, water traces from the organic solution were removed by addition of a small quantity of solid sodium sulfate and, once filtered, the solvent was eliminated from the solution using a rotary evaporator. The resulting product was recrystallized by dissolving repeadtely in the minimum volume of ethyl acetate, at 20ºC. Finally, the solvent in the last solution was evaporated at 37ºC in a rotary evaporator, and the obtained solid was stored in a vial at 8ºC until used. The succinimidyl-3-propiolate was identified by NMR.

From the as obtained succinimidyl-3-propiolate, a 1 mg/mL solution was prepared in 250 mM carbonate buffer of pH 9.0. An aliquot of 250 µL from this solution was then mixed with 125 µL of a 2 mg/mL anti-rabbit-IgG solution and diluted with the same carbonate buffer up to 1 mL. The resulting solution was maintained for 24 h at 4 ºC under continuous stirring. Thereafter, the solution was filtered through an Amicon® Ultra 10 K centrifuge filter by centrifugation at 1400 rcf and 8 ºC for 10 min. Five washing steps were then applied using each time 500 µL of 10 mM PBS of pH 7.0 at 8ºC, and centrifuge 10 min at 14,000 rcf, followed by turning the filter and centrifuge again 10 min at 1000 rcf. Finally, the obtained product was dissolved in 125 µL of 10 mM PBS of pH 7.0.

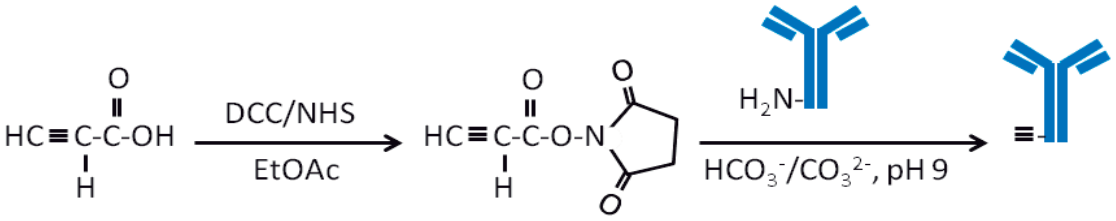

Figure S1. Preparation of alkyne-functionalized IgG using succinimidyl-3-propiolate

Procedure S3. Preparation of alkyne-functionalized IgG using sodium peryodate

The method described by Le[3] was applied (Figure S2). Briefly, 50 µL of a 20 mM sodium peryodate solution prepared in 0.1 M sodium acetate buffer (pH 5.5) were mixed with 800 µL of a 2 mg/mL anti–rabbit–IgG solution and the resulting solution was maintained in an ice bath and in the dark for 30 min. Next, the mixture was filtered through an Amicon® Ultra 10 K centrifuge filter by centrifugation at 14,000 rcf and 4 ºC for 15 min. Three washing steps were then applied using each time 500 µL of Coupling Buffer at 4 ºC, and centrifuge 15 min at 14000 rcf, followed by turning the filter and centrifuge 2 min at 1000 rcf. Finally, the resulting product was incubated for 2 h at 25 ºC with 500 µL of Coupling Buffer containing 8.8 mg of ethynyl hydrazide. Once filtered through another Amicon® Ultra 10 K centrifuge filter by centrifugation at 14,000 rcf and 4ºC for 15 min, five washing steps with 500 µL of Coupling Buffer were applied. Next, a last washing with 0.1 M PBS of pH 7.4 at 4ºC was performed, and centrifuge 15 min at 14,000 rcf, followed by turning the filter and centrifuge 2 min at 1000 rcf. Finally, the obtained product was disolved in 800 µL of 10 mM PBS of pH 7.0.

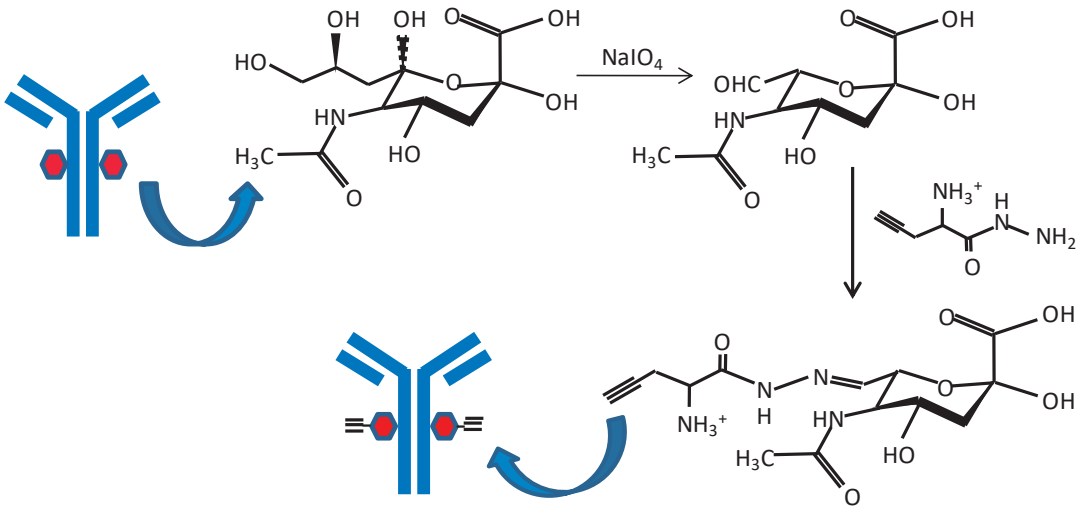

Figure S2. Preparation of alkyl-functionalized IgG using sodium peryodate

2. Characterization of the "click" synthesis by IR spectrophotometry

The IR absorption spectra obtained for the characterization of azide-functionalized-MWCNTs and the alkyne-anti-IgG binding are depicted in Figure S3.

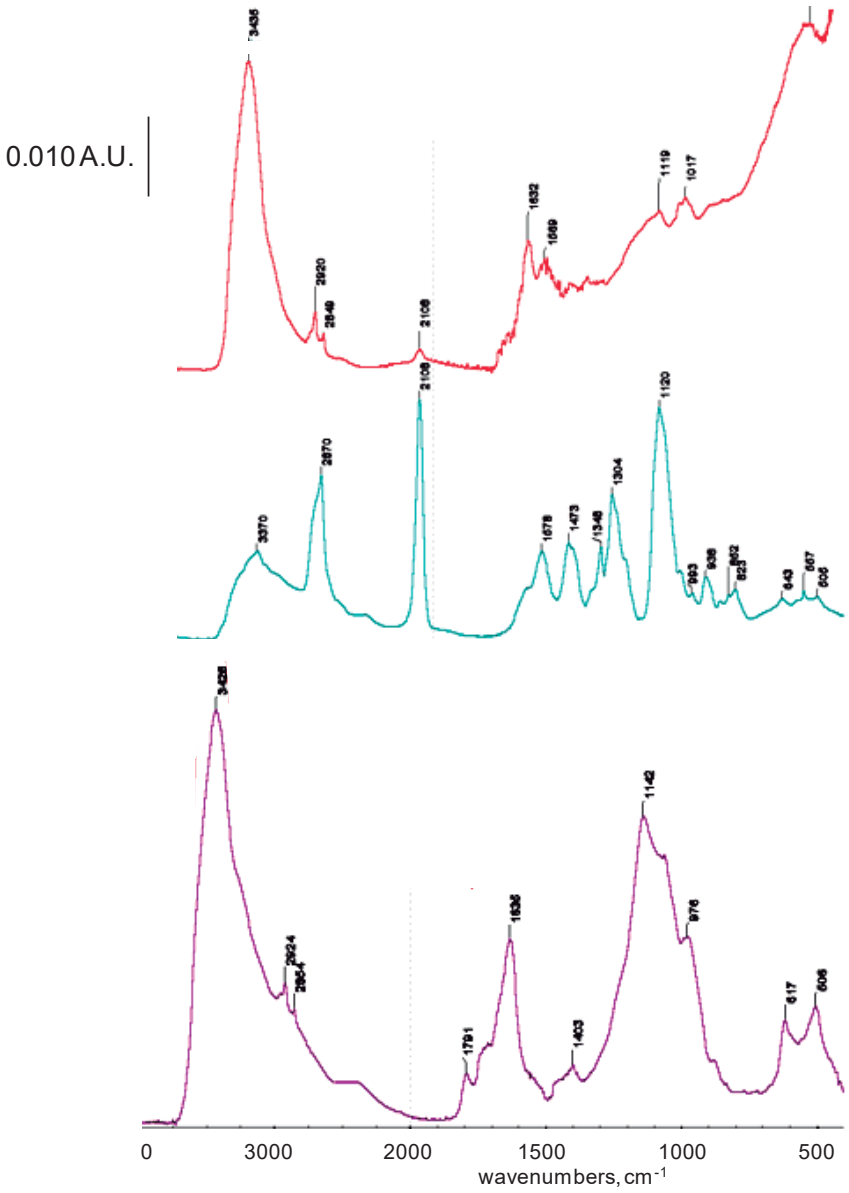

Figure S3. IR spectra of azide-MWCNTs (red), commercial azide (blue), and IgG-alkyne-azide-MWCNTs (purple).

3. Optimization of the variables involved in the preparation and performance of the immunosensor

a) Effect of the IgG-alkyne-azide-MWCNTs loading on the SPCE

The influence of the IgG-alkyne-azide-MWCNTs conjugate loading on the SPCE surface was evaluated by checking the amperometric responses obtained with different immunosensors prepared with conjugate contents of 2.5, 5.0, or 10.0 μg/mL for 0 (unspecific) and 100 pg/mL TGF-β1. The conjugate contents corresponded to the IgG concentration used for alkyne-functionalization and further conjugation with 0.25 mg/mL azide-MWCNTs. The immunosensors were prepared (Section 2.3.1) by sequential addition of the following solutions (5 μL each): IgG-alkyne-azide-MWCNTs, casein, 10 μg/mL anti-TGF, 1 μg/mL Biotin-anti-TGF, and 1/500 diluted poly-HRP-Strept. The obtained results are displayed in Figure S4a, showing that the largest specific-to-unspecific current ratio was obtained for 5 μg/mL conjugate. Therefore, this value was selected for the preparation of the immunosensor.

b) Effect of the type of blocking agent

Three different substances commonly used as blocking agents were tested to minimize unspecific adsorptions onto IgG-alkyne-azide-MWCNTs/SPCE after anti-TGF immobilization. Blockers solutions prepared at the typical concentrations used in the fabrication of immunosensors: 25 % milk powder, 1 % casein and 5% BSA, in 0.1 M PBS of pH 7.4, were evaluated with the results shown in Figure S4b. Best specific-to-unspecific current ratio was obtained using casein as blocking agent solutions. 60 min incubation time was shown to be sufficient for an effective blocking.

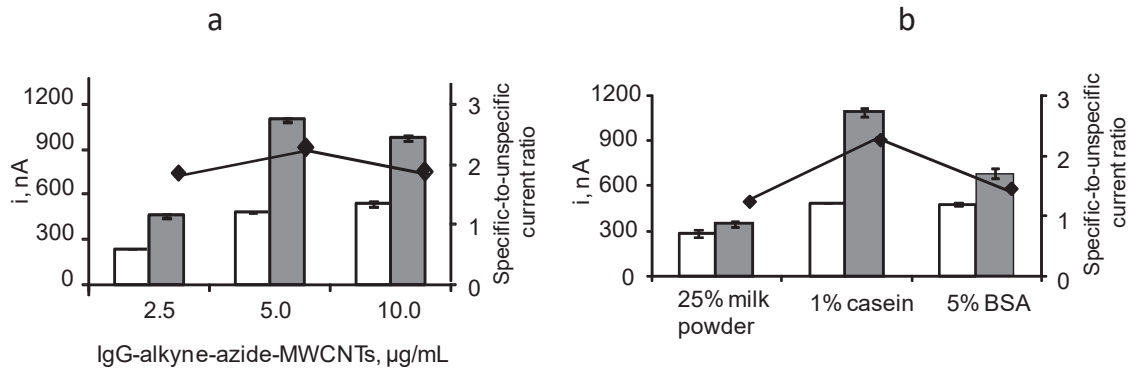

Figure S4. a) Effect of the IgG-alkyne-azide-MWCNTs loading on the SPCE: 5 µL IgG-alkyne-azide-MWCNTs; 5 µL 1% casein, 30 min. b) Effect of the type of blocking agent: 5 µL blocking agent; 5 µL 5 µg/mL IgG-alkyne-azide-MWCNTs. 0 (white) or 100 (dark grey) pg/mL TGF-β1; 5 µL 10 µg/mL anti-TGF, 60 min; 5µL 1 µg/mL Biotin-anti-TGF, 60 min; 5 µL 1/500 diluted poly-HRP-Strept, 20 min.

c) Effect of the type of enzymatic labeling of the detection antibody

Peroxidase-streptavidin polymer (poly-HRP-Strept) has been used as an efficient labeling tool to achieve electrochemical signal amplification in particular when compared with responses obtained with conventional HRP-Strept conjugates[4]. This comparison is shown in Figure S5a for Biotin-anti-TGF-TGF-β1-anti-TGF-IgG-alkyne-azide-MWCNTs/SPCE immunosensors using HRP-Strept or poly-HRP-Stept as enzyme labels. As expected, remarkably larger currents were measured for TGF-β1 when poly-HRP-Stept was employed as label because of the multiple HRP molecules in the polymer available to be involved in the biocatalysis of the enzyme substrate.

d) Effect of the poly-HRP-Strept concentration.

Figure S5b shows the dependence of the measured current with the poly-HRP-Strept dilution factor over the 1/250 to 1/2000 range. The specific response for 100 pg/mL TGF-β1 decreased slightly with the dilution factor while the best specific-to-unspecific current ratio was obtained for a 1/500 poly-HRP-Strept dilution and, therefore, this value was selected for further work. Furthermore, an incubation time of 20 min was enough to get an effective binding with the biotinylated secondary antibody.

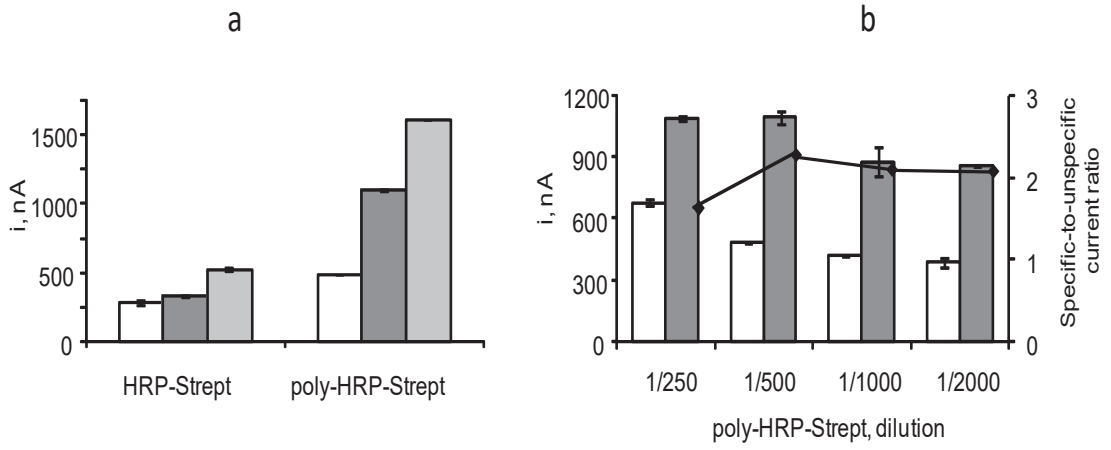

Figure S5. a) Effect of the type of enzymatic labeling of the detection antibody: 0 (white), 100 (dark grey) or 200 (light grey) pg/mL TGF–β1; 5 µL 1/2000 diluted HRP-Strept or 1/500 poly-HRP-Strept, 20 min incubation time. b) Effect of the poly-HRP-Strept concentration: 0 (white) or 100 (dark grey) pg/mL TGF–β1; 5 µL poly-HRP-Strept, 20 min. 5 µL 5 µg/mL IgG-alkyne-azide-MWCNTs; 5 µL 1% casein, 30 min; 5 µL 10 µg/mL anti-TGF, 60 min; 5 µL 1 µg/mL Biotin-anti-TGF, 60 min.

e) Effect of the anti-TGF loading on IgG-alkyne-azide-MWCNTs/SPCE

The anti-TGF loading was optimized by measuring the specific and unspecific responses with capture antibody concentrations ranging between 5 and 20 μg/mL. Figure S6a shows as the largest specific-to-unspecific current ratio was obtained for 10 μg/mL. The decrease and further stabilization observed for specific responses at higher antibody concentrations are attributed to probable reaching of the saturation level. Accordingly, 10 μg/mL anti-TGF was selected to construct the immunosensor. Regarding the incubation time for this step, 60 min were selected as an optimal value.

f) Effect of the Biotin-anti-TGF loading on TGF β1-anti-TGF- IgG-alkyne-azide-MWCNTs/SPCE

The electrochemical responses measured with different immunosensors prepared with Biotin-anti-TGF concentrations ranging between 0.5 and 10 μg/mL were also evaluated. Figure S6b shows as the measured current increased with increasing the Biotin-anti-TGF concentration between 0.5 and 1 μg/mL. Larger concentrations produced smaller responses suggesting saturation of the antibodies binding sites. Accordingly, 1 μg/mL was chosen as the conjugate concentration for further work. Regarding the incubation time for this step, a period of 60 min was shown be enough to allow binding of all biotinylated antibodies to TGF-β1 antigen.

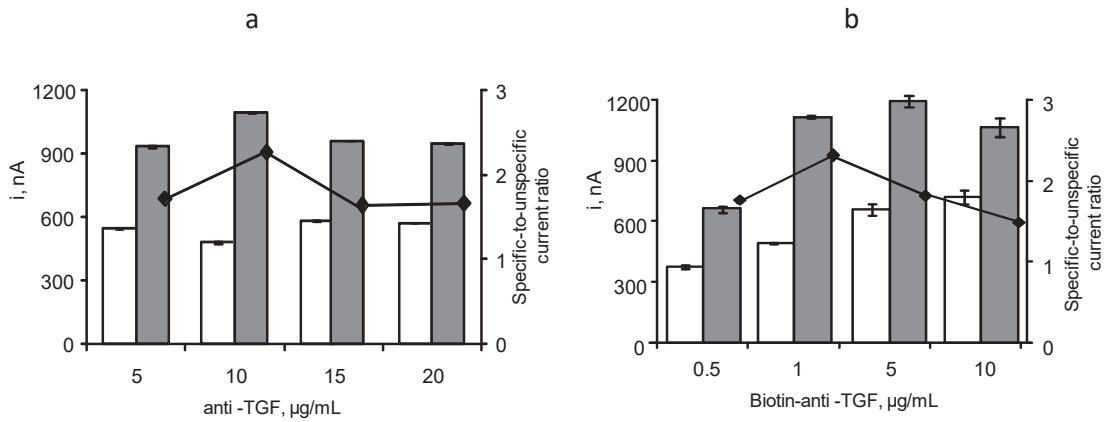

Figure S6. a) Effect of the anti-TGF loading on IgG-alkyne-azide-MWCNTs/SPCE: 5 µL anti-TGF, 60 min; 0 (white) or 100 (dark grey) pg/mL TGF–β1; 5 µL 1 µg/mL Biotin-anti-TGF, 60 min. b) Effect of the Biotin-anti-TGF loading on TGF β1-anti-TGF- IgG-alkyne-azide-MWCNTs/SPCE: 5 µL 10 µg/mL anti-TGF, 60 min; 0 (white) or 100 (dark grey) pg/mL TGF–β1; 5 µL Biotin-anti-TGF, 60 min. 5 µL 5 µg/mL IgG-alkyne-azide-MWCNTs; 5 µL 1% casein, 30 min; 5 µL 1/500 diluted poly-HRP-Strept, 20 min.

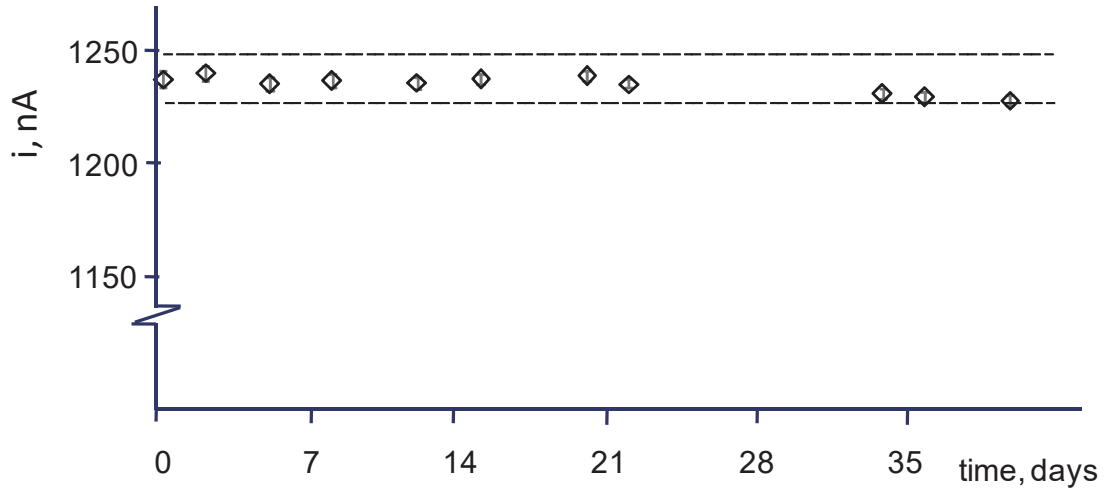

Figure S7. Control chart constructed to evaluate the storage stability of anti-TGF-IgG-alkyne-azide-MWCNTs/SPCE conjugates. Each point corresponds to the mean value of three successive measurements for 125 pg/mL TGF-β1.

REFERENCES

1 H. Qi, C. Ling, R. Huang, X. Qiu, L. Shangguan, Q. Gao and C. Zhang, *Electrochim. Acta*, 2012, **63**, 76.

2 J. Chao, W.-Y. Huang, J. Wang, S.-J. Xiao, Y.-C. Tang and J.-N. Liu, *Biomacromol.*, 2009, **10**, 877.

3 H.T. Le, J.G. Jang, J.Y. Park, C.W. Lim and T.W. Kim, *Anal. Biochem*. 2013, **435**, 68.

4 I. Ojeda, M. Moreno-Guzmán, A. González-Cortés, P. Yáñez-Sedeño, J.M. Pingarrón, *Anal. Bioanal. Chem*., 2014, **406**, 6363.

Talanta 211(2020) 120761

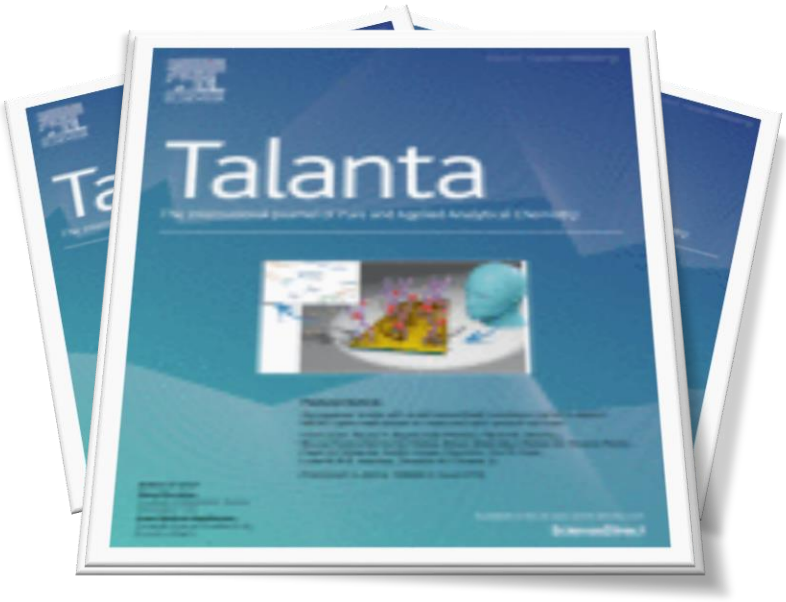

Electrochemical immunosensor for the determination of the cytokine interferon gamma (IFN-gamma) in saliva

Talanta 211 (2020) 120761

Contents lists available at ScienceDirect

Talanta

journal homepage: www.elsevier.com/locate/talanta

Electrochemical immunosensor for the determination of the cytokine interferon gamma (IFN-γ) in saliva

E. Sánchez-Tirado, A. González-Cortés**, P. Yáñez-Sedeño*, J.M. Pingarrón

Department of Analytical Chemistry, Faculty of Chemistry, Universidad Complutense de Madrid, 28040, Madrid, Spain

ARTICLE INFO

Keywords:
Interferon gamma
IFN-γ
Electrochemical immunosensor
Aryl diazonium salt
Grafting
Saliva

ABSTRACT

A simple, fast and sensitive amperometric immunosensing method for the determination of the clinically relevant cytokine interferon gamma (IFN-γ) in saliva complying the requirements demanded for this kind of sample is reported. The target analyte was sandwiched between a specific capture antibody covalently immobilized on a screen-printed electrode functionalized by the diazonium salt grafting of *p*-aminobenzoic acid, and a biotinylated detector antibody labeled with a streptavidin-horseradish peroxidase conjugate. The amperometric responses measured at - 0.20 V vs Ag pseudo-reference electrode upon addition of hydrogen peroxide in the presence of hydroquinone as the redox mediator allowed a calibration plot with a linear range between 2.5 and 2000 pg mL^{-1} and a low limit of detection (1.6 pg mL^{-1}) to be obtained. In addition, a good selectivity against other non-target proteins was achieved. The developed method was validated by analyzing a WHO 1st International Standard for IFN-γ. In addition, the immunosensor was used for the determination of the endogenous IFN-γ in saliva with results in excellent agreement with those obtained by a commercial ELISA kit.

1. Introduction

Human IFN-γ is a potent multifunctional cytokine primarily secreted by natural killer T cells as part of the innate immune response to intracellular pathogens. Originally characterized by its antiviral activities, IFN-γ also exerts anti-proliferative, immunoregulatory, and proinflammatory activities, and plays a central role in the progression of a variety of inflammatory and autoimmune diseases. For instance, increased IFN-γ production is associated with rheumatoid arthritis [1] and multiple sclerosis [2]. Therefore, because of this relevance, the development of sensitive, rapid and accurate methods for the determination of IFN-γ is crucial for monitoring the progress of these diseases. Among the available methods, ELISA kits for IFN-γ are usually employed in clinical practice providing suitable sensitivity for application to serum samples where concentrations of IFN-γ at the level of ng mL^{-1} [3] are expected. Typically, such immunoassays involve sandwich-type configurations with horseradish peroxidase (HRP)-labeled secondary antibodies and colorimetric detection. Logarithmic calibration plots with linear ranges between tens and thousands pg mL^{-1} IFN-γ and minimum detectable dose (MDD), calculated as the concentration corresponding to the mean response of the zero standard + 2s, of various units of pg mL^{-1}, are claimed. An important drawback of ELISA methods is the long time required for the immunoassay, extending from 3 h [https://www.thermofisher.com/elisa/product/IFN-gamma-Human-ELISA-Kit/EHIFNG]to4.5h[https://www.rndsystems.com/products/human-ifn-gamma-quantikine-elisa-kit_dif50].

Electrochemical affinity biosensors for IFN-γ have also been reported. Aptasensors with different detection strategies [4–11], which were applied to serum [7,8] and cell culture [6,9], exhibit linear ranges for the calibration plots in the ng mL^{-1} range [7,10], with limits of detection ranging between few pg mL^{-1} [8] and ng mL^{-1} [4,5]. Regarding electrochemical immunosensors, few papers have been found in the literature. However, these immunosensors exhibit, in general, a higher sensitivity than aptasensors, with linear calibration plots in the pg mL^{-1} range and LOD values of few pg mL^{-1} [12] or even lower [3,13,14], and have been applied to the analysis of serum samples. Label-free approaches [12] using electrochemical impedance spectroscopy (EIS), or sandwich-type configurations using CdS NPs as label tags and stripping voltammetry of dissolved nanoparticles [13,14] have been reported.

As it can be realized, there is a relatively high number of methods involving affinity interactions for the determination of IFN-γ in serum. However, there are no methods for the determination of this analyte in saliva, despite the variation of cytokine levels in this fluid is considered a helpful tool in the diagnosis and treatment of inflammatory or immune diseases and particularly in the case of oral diseases [15]. The analysis of saliva has already demonstrated a high potential diagnostic

* Corresponding author.
** Corresponding author.
E-mail address: yseo@quim.ucm.es (P. Yáñez-Sedeño).

https://doi.org/10.1016/j.talanta.2020.120761
Received 12 October 2019; Received in revised form 15 January 2020; Accepted 17 January 2020
Available online 17 January 2020
0039-9140/ © 2020 Elsevier B.V. All rights reserved.

value with the distinctive advantage over other clinical samples that it can be repeatedly collected noninvasively [16] thus providing a cost-effective approach for disease monitoring and screening of large populations [17].

The concentration of IFN-γ in saliva of healthy individuals is around various units of pg mL^{-1}, which makes it necessary to develop sensitive methods for this type of sample. With this objective, we report in this work a simple and reliable electrochemical immunosensor for the determination of IFN-γ, which comply with the clinical requirements of sensitivity and accuracy demanded for application to saliva. The rational design of the immunosensor involves the immobilization of capture antibodies onto a disposable screen-printed carbon electrode (SPCE) functionalized by grafting of the diazonium salt of *p*-aminobenzoic (*p*-ABA). A sandwich-type immunoassay was implemented using biotin-anti-IFN and conjugation with peroxidase-labeled streptavidin (HRP-Strept). Amperometric measurements were carried out upon adding hydrogen peroxide solution to the electrode surface in the presence of hydroquinone (HQ) as the redox mediator. The developed method was validated by application to a WHO 1st International Standard for IFN-γ (National Institute for Biological Standards and Control, NIBSC), and the analytical usefulness of the immunosensor was demonstrated by analyzing real saliva samples from volunteers with results in excellent agreement with those obtained by using a commercial ELISA kit.

2. Experimental

2.1. Apparatus and electrodes

Screen-printed carbon electrodes (SPCEs, 110 DRP, DropSens-Metrohm) consisting of a 4-mm ∅ working electrode, a silver pseudo-reference electrode and a carbon counter electrode, were used as platforms for the preparation of the immunosensor. A PGSTAT 101 potentiostat from Autolab controlled by Nova 1.6 electrochemical software (EcoChemie B·V.) was employed for grafting of *p*-ABA onto SPCEs. EIS measurements were carried out using an Autolab type III potentiostat controlled by the FRA2 software (EcoChemie). Amperometric measurements were made with a CHI 1030B potentiostat (CH Instruments) controlled by CHI 1030B software. An Elmasonic Se60 (Elma) ultrasonic bath, a Vortex homogenizer (Velp Scientifica) and a Crison Basic 20+ pHmeter were also used. All electrochemical experiments were performed at room temperature.

2.2. Reagents and buffer solutions

Human anti–IFN–γ capture antibody (anti-IFN), human biotinylated anti–IFN–γ antibody (biotin-anti-IFN), and human IFN-γ were from R&D Systems. All these reagents were included in the DuoSet ELISA (Cat. No. DY285B, from R&D Systems, https://www.rndsystems.com). Human IFN-γ capture antibody was reconstituted with 250 μL of 0.01 M phosphate buffer saline solution (PBS) of pH 7.4 containing 137 mM NaCl, 2.7 mM KCl, 8.1 mM Na_2HPO_4 and 1.5 mM KH_2PO_4. Anti-IFN solutions were prepared by appropriate dilution with 25 mM 2-(N-morpholino) ethanesulfonic acid (MES, from GERBU Biotechnik GmbH, https://www.gerbu.de) buffer solution of pH 5.0. Biotinylated anti-human IFN-γ was reconstituted with 500 μL of 0.01 M PBS solution of pH 7.4 supplemented with 1% (w/v) bovine serum albumin (BSA, GERBU Biotechnik GmbH, https://www.gerbu.de). IFN-γ standard solutions were prepared in the same medium.

Sodium nitrite (Panreac) and *p*-aminobenzoic acid (*p*-ABA, Acros) were used to modify SPCEs by electrochemical grafting of diazonium salt. Moreover, 1-ethyl-3-(3-dimethylamino-propyl) carbodiimide (EDC, Acros Organics) and N–hydroxy-sulfosuccinimide (sulfo-NHS, Sigma-Aldrich) were also used as activation agents for carboxyl groups confined at the electrode surface. For this purpose, 100 mM EDC and sulfo-NHS solutions, each in 25 mM MES buffer solution of pH 5, were used. HRP-Strept (Roche) solutions were prepared in PBS of pH 7.4 supplemented with 1% bovine serum albumin (BSA). The blocking agent was a commercial 2% (w/v) BSA solution prepared in 0.01 M PBS. 0.05 M $K_3Fe(CN)_6$ and $K_4Fe(CN)_6$ (Sigma) solutions were prepared in 0.01 M PB of pH 7.4. Hydrogen peroxide (Aldrich, 30% (w/w)) and hydroquinone (HQ, Sigma) were also employed. Transforming growth factor-β (TGF-β1), tumor necrosis factor alfa (TNF-α), interleukin 1 beta (IL-1β) and receptor activator for nuclear factor κ B (RANKL) from R&D Systems, BSA from Gerbu human immunoglobulin G (IgG), hemoglobin, glucose, ascorbic acid and uric acid, all from Sigma, interleukin 6 (IL-6) and interleukin 8 (IL-8) from Abcam, https://www.abcam.com. were tested as potential interfering compounds. All other chemicals used were of analytical reagent grade. All solutions were prepared with deionized water obtained from a Milli-pore Milli-Q purification system (18.2 MΩ cm at 25 °C).

A WHO 1st International Standard for IFN-γ (National Institute for Biological Standards and Control, NIBSC, code: 87/586), containing 12.5 ng mL^{-1} IFN-γ was used as a reference material for validation of the developed method. Moreover, saliva samples from volunteers obtained and pre-treated as described in section 2.3.3 were analyzed.

2.3. Procedures

2.3.1. Preparation of HRP-strept-biotin-anti–IFN–IFN-γ-anti-IFN/SPCE immunosensor

In a first step, SPCEs were modified by electrochemical grafting of *p*-ABA diazonium salt. To do that, 20 mg of *p*-ABA were dissolved in 2 mL 1 M HCl and cooled with ice. The diazonium salt was synthesized by adding 2 mM $NaNO_2$ aqueous solution dropwise to this solution (38 μL for each 200 μL) upon constant stirring. Next, 40 μL of the resulting solution were casted onto the SPCE and ten successive cyclic voltammetric scans were carried out between 0.0 and −1.0 V (υ = 200 mV s^{-1}). The as prepared modified electrodes were washed thoroughly with water and allowed drying in air (this process takes less than 1 min). Thereafter, the electrode surface confined carboxyl groups were activated by adding 10 μL of EDC/sulfo-NHS (0.1 M each) prepared in MES buffer solution of pH 5.0 and allowing incubation for 30 min at 25 °C in a humidified chamber. After rinsing with water, 5 μL of a 15 μg mL^{-1} anti-IFN solution prepared in MES buffer of pH 5.0 were added and left to react for 1 h. Next, the electrodes were rinsed with water and blocking of the remaining active sites was made by adding 10 μL of a 1% BSA solution in PBS, allowing incubation for 30 min. Thereafter, 5 μL of standard IFN-γ solutions or the samples were placed onto the electrode surface and incubated for 60 min. Then, 5 μL of biotin-anti–IFN–γ solution (1.25 μg mL^{-1}) were dropped onto the resulting electrode and incubated for 45 min followed by the addition of 5 μL of HRP-Strept solution (1/500 diluted in PBS pH 7.4) and incubating for 20 min. Washings with PBS were included between these steps and the immunosensor was kept with a drop of a 0.05 M PB solution of pH 6.0 until the measurements were made.

2.3.2. Amperometric measurements

Amperometric measurements were performed by adding 45 μL of a 1 mM HQ solution in 0.05 M PBS of pH 6.0 onto the surface of the immunosensor horizontally positioned. A detection potential of −200 mV vs Ag pseudo-reference electrode was applied and, once the background current was stabilized, (around 50 s), 5 μL of 50 mM H_2O_2 solution were added and allowed standing for 200 s to complete the enzyme reaction. The steady state current corresponding to the electrochemical reduction of benzoquinone was used as the analytical readout.

2.3.3. Samples analysis

Glass ampoules containing lyophilized samples of a biological reference standard for IFN-γ (NIBSC, code: 87/586) were stored at −20 °C. According to the instructions provided by the supplier, the

solid from each ampoule was reconstituted in 0.5 mL of sterile distilled water. Then, the ampoule was rinsed with 0.4 mL of the same water and diluted up to a volume of 1.0 mL to obtain a final aqueous solution containing the cytokine at a 250 IU/mL (12.5 ng mL^{-1}) concentration. The determination of IFN-γ was performed after a 1000-fold dilution with PBS by applying the procedure described in Section 2.3.2. The measured currents were interpolated into the linear portion of the calibration plot constructed with IFN-γ standard solutions.

Saliva from volunteers was collected in the morning. Volunteers were asked not to eat, brush their teeth, or use mouth rinse at least 2 h before sample collection. A Salivette® collection device (Sarstedt) was used. Briefly, once rinsed the mouth thoroughly with water, a cotton swab was inserted into the mouth and chewed for 1 min. Then, the swap saturated with saliva was inserted into the vial, sealed with the cap and centrifuged for 10 min at 3000 rpm. The determination was carried out immediately by applying the procedure described in Section 2.3.2 to 5 μL of undiluted saliva. Similarly to that stated above, the amperometric responses were interpolated into the calibration plot constructed with standard solutions.

3. Results and discussion

Fig. 1 shows a scheme of the steps involved in the preparation of the HRP-Strept-biotin-anti–IFN–IFN-γ-anti–IFN–Phe/SPCE immunosensor as well as the reactions involved in the amperometric detection. The proposed strategy takes advantage of the good performance of grafted electrochemical scaffolds for covalent immobilization of biomolecules. As it is known [18], modification of carbon electrodes through free radical grafting allows the formation of compact and stable organic monolayers with specific functionalities. In this case, the electrochemical reduction of *p*-ABA diazonium salt onto SPCEs provided a dense layer of surface confined carboxylic moieties on which the capture antibody was immobilized by covalent binding once they were activated with the EDC/sulfo-NHS system. As it can be seen in step 1, the diazonium salt was synthesized by diazotization reaction followed by cyclic voltammetry. The experimental conditions used in this step were those previously optimized and reported [19]. Upon covalent immobilization of the capture antibody (step 2), the remaining free active sites were blocked with BSA (step 3). After addition of the target IFN-γ, a sandwich type immunoassay was implemented involving biotin-anti-IFN and HRP-Strept (step 4). The affinity reaction was amperometrically monitored by adding H_2O_2 in the presence of HQ as the redox mediator (step 5).

3.1. Optimization of the experimental variables involved in the preparation of the immunosensor

The effect of the different variables involved in the preparation of the immunosensor for IFN-γ on the amperometric responses was tested. The checked variables included: a) the anti-IFN antibody loading onto Phe-SPCE and the corresponding incubation time; b) the type and concentration of blocking agent; c) the biotin-anti-IFN loading onto IFN-γ-anti–IFN–Phe-SPCE and the incubation time; and d) the concentration of HRP-Strept. A larger ratio between the currents measured in the presence or in absence of the target cytokine (specific-to-unspecific current ratio) was taken as the selection criterion for each tested variable. The results of the optimization studies are shown in Fig. 2 and summarized in Table 1.

Fig. 2a shows the effect of the capture antibody loading on the immunosensor response. In the experiments, 5 μL of 5–20 μg mL^{-1} anti-IFN solutions were incubated onto the grafted SPCE once the carboxylic groups were activated with the EDC/sulfo-NHSS solution and allowing 60 min for incubation. A larger specific-to-unspecific current ratio (S/N) was obtained for 15 μg mL^{-1} antibody, this value being selected for the preparation of the immunosensor. The lower specific current observed for larger antibody concentrations can be attributed to the steric hindrance for the antigen recognition when large amounts of the capture antibody are immobilized [20]. Using the selected loading,

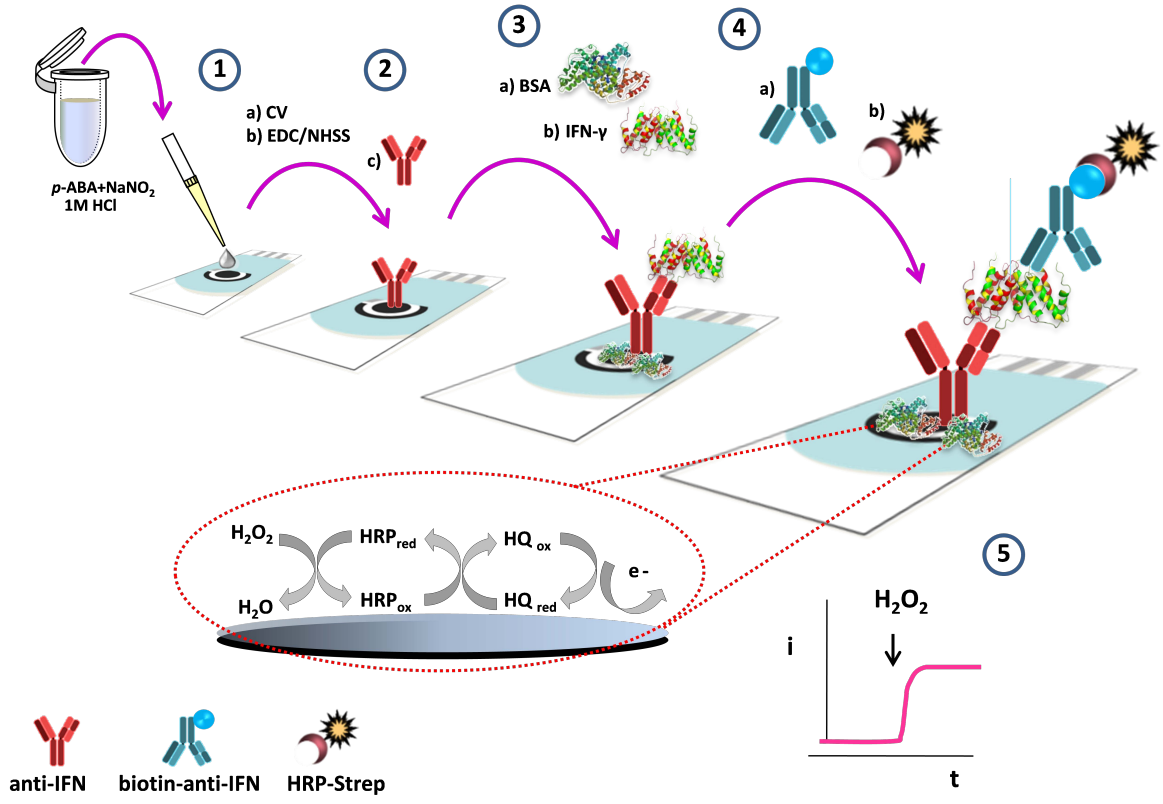

Fig. 1. Schematic picture of the steps involved in the preparation of the electrochemical immunosensor for the determination of IFN-γ. See the text for more information.

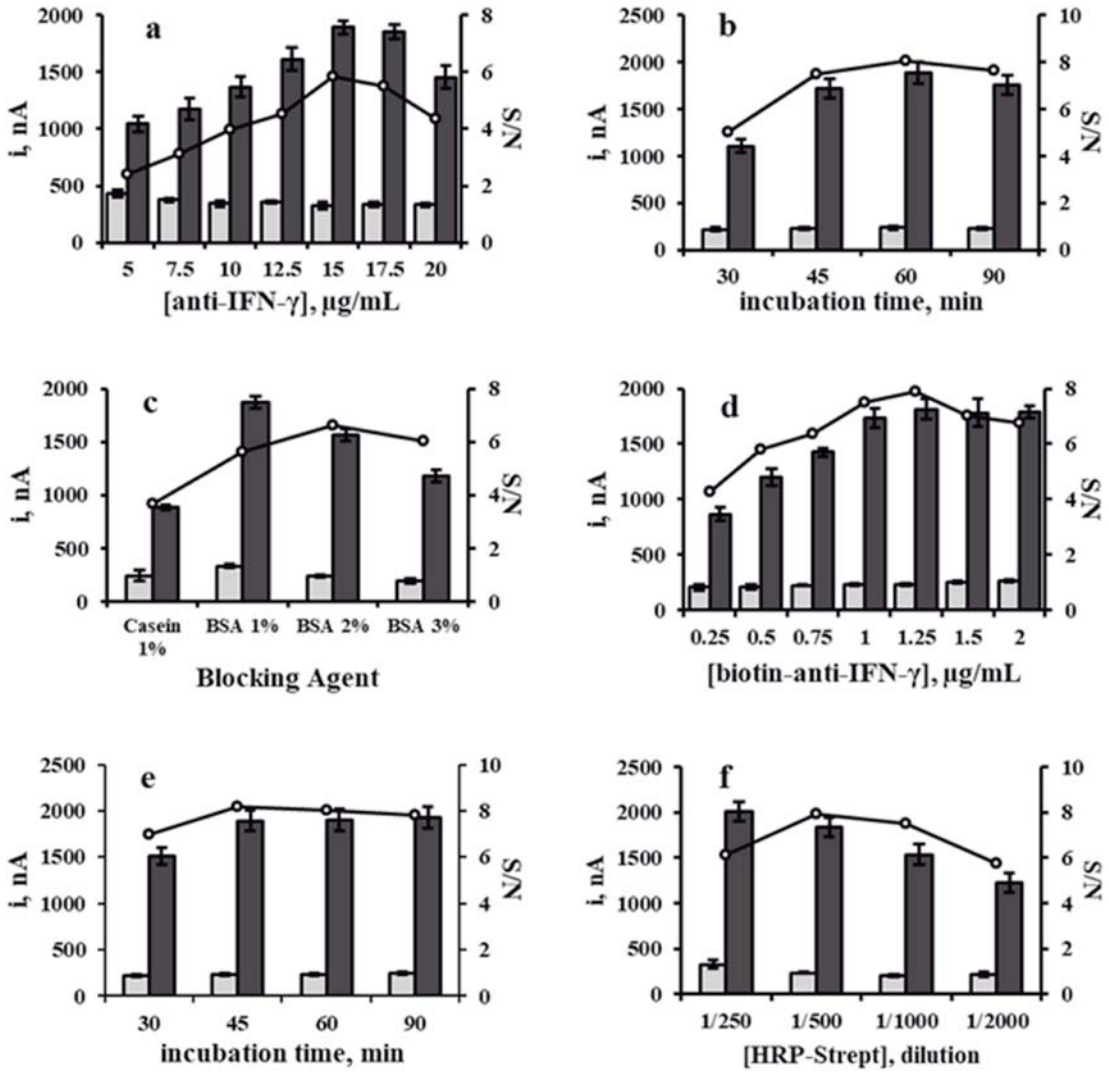

Fig. 2. Amperometric responses measured with the HRP-Strept-biotin-anti–IFN–IFN-γ-anti–IFN–Phe-SPCE immunosensors in the absence (light grey) and in the presence of 1.0 ng mL^{-1} IFN-γ (dark grey) as a function of: the anti-IFN loading (5–20 μg mL^{-1}) (a); the anti-IFN incubation time (30–90 min) (b); the type and concentration of blocking agent (1–3% (w/v)) (c); the biotin-anti-IFN loading (0.25–2 μg mL^{-1}) (d); the biotin-anti-IFN incubation time (e); and the HRP-Strept conjugate dilution factor (1/2000–1/250) (f). Error bars estimated as triple of the standard deviation (n = 3).

Table 1
Optimization of the experimental variables involved in the preparation of an amperometric immunosensor for IFN-γ.

Variable	Tested range (or compound)	Selected value
[anti-IFN], μg/mL	5–20	15
t_{inc} anti-IFN, min	30–90	60
blocking agent	casein, BSA	BSA
[BSA], % (w/v)	1–3	2
[biotin-anti-IFN], μg/mL	0.25–2	1.25
t_{inc} biotin-anti-IFN, min	30–90	45
HRP-Strept, dilution	1/250–1/2000	1/500

optimization of the anti-IFN incubation time in the 30–90 min range led us to choose 60 min for further work (Fig. 2b).

Blocking of the free active sites on the electrode surface was carried out by testing casein and BSA solutions as blocking agents due to their well-recognized ability to minimize. Fig. 2c shows that larger S/N ratios were achieved using 2% (w/v) BSA. 30 min incubation was shown to be sufficient for an effective blocking.

The effect of the biotin-anti-IFN concentration was evaluated over the 0.25–2.0 μg mL^{-1} range. Fig. 2d shows as the specific current increased with the biotinylated detector antibody concentration up to 1.25 μg mL^{-1} and levelled off for larger concentrations. Since the S/N current ratio exhibited also a larger value for this concentration, it this selected for further work. Regarding the effect of the incubation time with the biotin-anti-IFN solution, Fig. 2e shows that a larger S/N ratio was achieved for 45 min which was selected for the immunosensor preparation.

The effect of HRP-Strept dilution on the response of the immunosensor was checked by preparing different immunosensors using the previously optimized experimental conditions and ranging the dilution factor between January 2000 and 1/250. The results displayed in Fig. 2f led us to select a 1/500 dilution for the construction of the immunosensor.

3.2. Characterization studies by electrochemical impedance spectroscopy

Once the experimental variables were optimized, the different steps involved in the immunosensor preparation were characterized by EIS using 2 mM $Fe(CN)_6^{4-/3-}$ prepared in 0.05 M PB of pH 7.4 as the redox probe. The corresponding Nyquist plots and the equivalent circuits are displayed in Fig. 3a and b. As expected, modification of the bare SPCE with *p*-ABA diazonium salt provoked a large increase in the electron

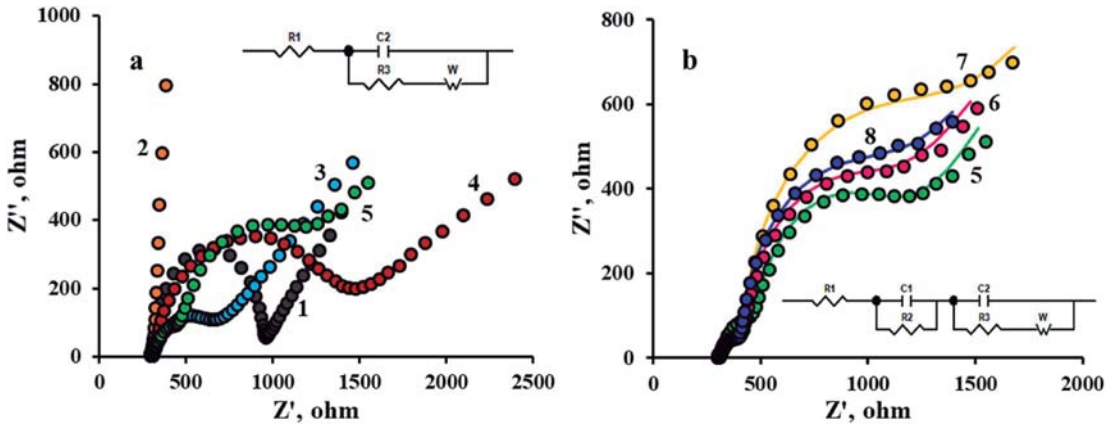

Fig. 3. Nyquist plots recorded in a 2 mM $Fe(CN)_6^{3-/4-}$ 0.1 M PB solution of pH 7.4 and equivalent circuits for: bare SPCE (1); *p*-ABA-SPCE (2); *p*-ABA-SPCE activated with EDC/sulfo-NHS (3); anti–IFN–Phe-SPCE (4); anti–IFN–Phe-SPCE blocked with BSA (5); IFN-γ-anti–IFN–Phe-SPCE (6); biotin-anti–IFN–γ–IFN–anti–IFN–Phe-SPCE (7); HRP-Strept-biotin-anti–IFN–IFN-γ-anti–IFN–Phe-SPCE (8). 1 ng mL^{-1} IFN-γ; range of frequencies, 10^5–0.040 Hz; open circuit. Lines in Fig. 2B were obtained by fitting the experimental data to the equivalent circuit displayed using Zview impedance software.

transfer resistance, Rct, from 646 to 4187 Ω, due to the electrostatic repulsion between the anionic redox probe and the negatively charged carboxylate groups present on the electrode surface at the working pH. Activation with EDC/sulfo-NHS gave rise to a dramatic decrease in the Rct value (497 Ω) because of the neutralization of the surface confined -COO^- groups upon reaction with the carbodiimide/succinimide system. As expected, a further significant increase in Rct occurred upon anti-IFN immobilization (1143 Ω), which is attributed to the partially insulating barrier on the electrode surface produced by the presence of the antibody. It is worth mentioning that subsequent incubation of the anti-–IFN–Phe-SPCE bioelectrode in the BSA blocking solution provided a Nyquist diagram showing two different semicircles (Fig. 3b), which is due to the presence of two differentiated layers on the electrode surface. Consequently, this status should be defined by an equivalent circuit at least constituted by two RC semi-circuits. The resistance, R_{ct2}, corresponding to the second semicircle of the Nyquist plot, described the electron transfer through the immobilized substances including BSA, the biotinylated detector antibody, the antigen and HRP-Strept. As it can be seen, the represented R1 (R2C1) (C2 [R3W1]) circuit fitted well with the experimental results as demonstrated by the overlapping of the experimental points in the Nyquist plots in Fig. 2B with the respective lines obtained using the Zview impedance software [21]. As expected, the resistance of the second semicircle increased after incubation with the antigen solution. Further increase occurred after incubation with the biotinylated detector antibody solution due to the blocking effect of both proteins toward the interfacial electron transfer and also to the repulsion between biotin (dissociated at the working pH) and the negatively charged redox probe in solution. However, a remarkable decrease was observed upon incubation with the HRP-Strept solution, probably because of the partial neutralization of the biotin negative charges as a consequence of the interaction with streptavidin [22].

3.3. Analytical figures of merit of the immunosensor

Fig. 4a displays the calibration plot for IFN-γ standard solutions constructed with the developed immunosensor under the optimized working conditions. Error bars were calculated from measurements carried out with three different immunosensors prepared in the same manner. Some typical recorded amperograms are also displayed in Fig. 4b. The steady state current vs. logarithm of IFN-γ concentration plot followed the adjusted equation i, nA = (591 ± 12) log [IFN-γ], pg/mL + (121 ± 25) (r^2 = 0.997) with a range of linearity extending between 2.5 and 2000 pg mL^{-1} IFN-γ. This range covers almost three orders of magnitude and is adequate for the determination of IFN-γ according to the expected concentrations in serum [3] and saliva [16]. Importantly, the cut-off concentration for LTBI (latent tuberculosis infection) in serum has been reported to be 15 pg mL^{-1} [23]. The obtained LOD value, 1.6 pg mL^{-1}, was calculated according to the 3 × s_b criterion, where s_b was estimated as the standard deviation, expressed in concentration units, calculated from ten amperometric responses of the immunosensors prepared in the absence of IFN-γ. The limit of quantification, calculated as 10 × s_b was LOQ = 5.3 pg mL^{-1}.

When these analytical figures of merit are compared with those claimed for commercial ELISA kits using similar immunoreagents, some noticeable differences are apparent. The dynamic range (non-linear) of the calibration plot reported for the Duo Set ELISA kit from R&D Systems (Cat. No. DY285B) is narrower, encompassing from 15.6 to 1000 pg mL^{-1} IFN-γ, and no LOD or MDD value is provided (https://resourcesrndsystems.com/pdfs/datasheets/dy285.pdf.). In addition, the required sample volume is 100 μL, twenty times larger than that needed with the immunosensor, and the assay time takes over 4 h 40 min, which is remarkably longer than the time taken with the immunosensor, 2 h 30 min (counting in both cases since the immobilization of the capture antibody). However, it must be said that the ELISA method can be performed in a 96 well plate at the same time. On the other hand, when the comparison is made with respect to other reported electrochemical immunosensors, the conclusions are not so clear since they use different strategies (label-free or sandwich-type with signal amplification) and transduction techniques (SWASV, DPV, or EIS). However, we can say that, in general, the range of linearity exhibited by the developed immunosensor is among the widest ones, and the achieved LOD value among the lowest ones. For example, the sandwich-type immunosensor reported by Wang et al. [13] involving the immobilization of the capture antibody onto magnetic particles, the use of CdS NPs/AuNPs as carrier tags for detector antibodies, and stripping voltammetry for the dissolved cadmium, provides a calibration plot with a non-linear dynamic range extending only over 0.4 and 40 pg mL^{-1}. In addition, it requires a much larger sample volume (100 μL). Regarding the LOD, the value achieved with our design is slightly lower than that obtained by Ruecha et al. (3.4 pg mL^{-1}) using a label-free impedimetric immunosensor where the capture antibody was immobilized onto a PANI/graphene screen-printed paper electrode. However, our LOD is notably larger than that reported by Zhang et al. (0.048 pg mL^{-1}) [3] using HRP-dAb-AuNPs tags for signal amplification. Nevertheless, the assay time is much longer, 4 h, and the required sample volume is four times larger.

The reproducibility of the amperometric measurements was tested by recording the responses in the absence and in the presence of 1 ng mL^{-1} IFN-γ with five different immunosensors prepared in the

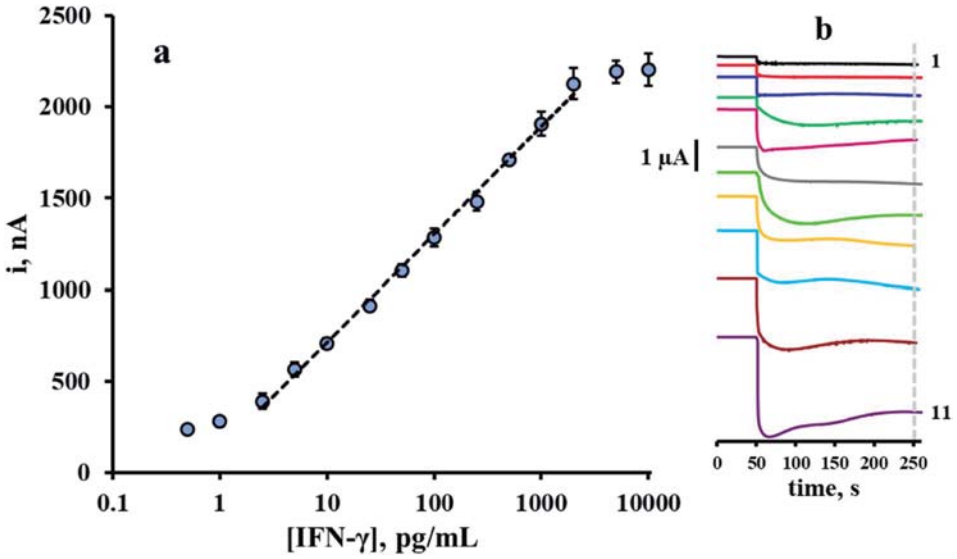

Fig. 4. A) Calibration plot constructed for IFN-γ with the HRP-Strept-biotin-anti–IFN–IFN-γ-anti–IFN–Phe-SPCE amperometric immunosensor. Error bars were estimated as triple of the standard deviation of measurements (n = 3). B) - Amperograms recorded with the immunosensor for different IFN-γ concentrations in pg mL^{-1}: (1) 0; (2) 2.5; (3) 5; (4) 10; (5) 25; (6) 50; (7) 100; (8) 250; (9) 500; (10) 1000; (11) 2000 pg mL^{-1}.

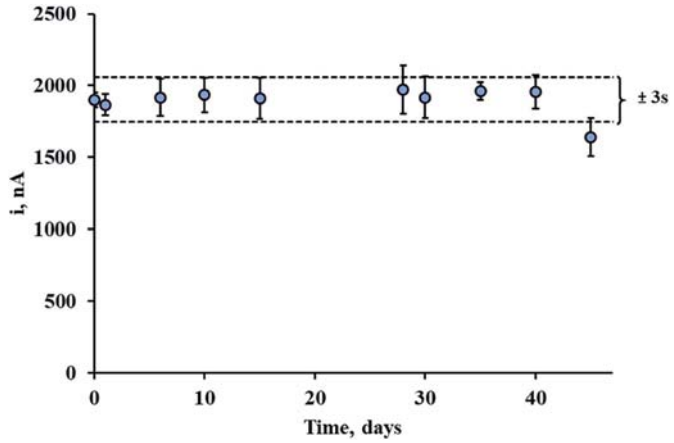

Fig. 5. Control chart constructed for checking the storage stability of the anti–IFN–Phe/SPCEs. Amperometric measurements corresponded to those recorded for 1 ng mL^{-1} IFN-γ. Error bars estimated as triple of the standard deviation (n = 3).

same manner and on the same day. The relative standard deviation (RSD) values were 1.4 and 1.8%, respectively. Furthermore, RSD values of 2.1 and 2.6% were found for measurements made with five different immunosensors prepared in different days in the absence and in the presence of the same concentration of IFN-γ, respectively. These RSD values show well the suitability and reproducibility of the protocols involved in the immunosensor preparation and in the amperometric transduction. The storage stability of the prepared anti–IFN–Phe-SPCEs conjugates was tested by preparing different immunosensing platforms on the same day and storing them dry at −20 °C. The stored biosensors were used to measure 1 ng mL^{-1} IFN-γ on different days. Fig. 5 shows the control chart constructed by setting the average current measured with 10 different immunosensors prepared the first working day as the central value, and the upper and lower limits of control at ± 3 × SD of this central value. As it can be observed, the amperometric responses remained inside the control limits for 40 days, thus showing the excellent storage stability of the prepared anti–IFN–Phe-SPCE immunosensing platforms.

3.4. Selectivity

The potential interference caused by the presence of other proteins on the amperometric quantification of IFN-γ with the developed immunosensor was checked by recording the responses for 0 and 1 ng mL^{-1} IFN-γ in the absence and in the presence of the following non-target compounds: 7 µg mL^{-1} ascorbic acid (AA), 5 mg mL^{-1} bovine serum albumin (BSA), 1 mg mL^{-1} glucose (Glu), 5 mg mL^{-1} hemoglobin (HB), 5 mg mL^{-1} human immunoglobulin G (IgG), 50 pg mL^{-1} interleukin 1 beta (IL–1β), 300 pg mL^{-1} interleukin 6 (IL–6), 300 pg mL^{-1} interleukin 8 (IL–8), 100 pg mL^{-1} receptor activator of nuclear factor kappa-B ligand (RANKL), 50 pg mL^{-1} transforming growth factor β1 (TGF-β1), 200 pg mL^{-1} tumoral necrosis factor alpha (TNF-α) and 100 µg mL^{-1} uric acid (UA). These

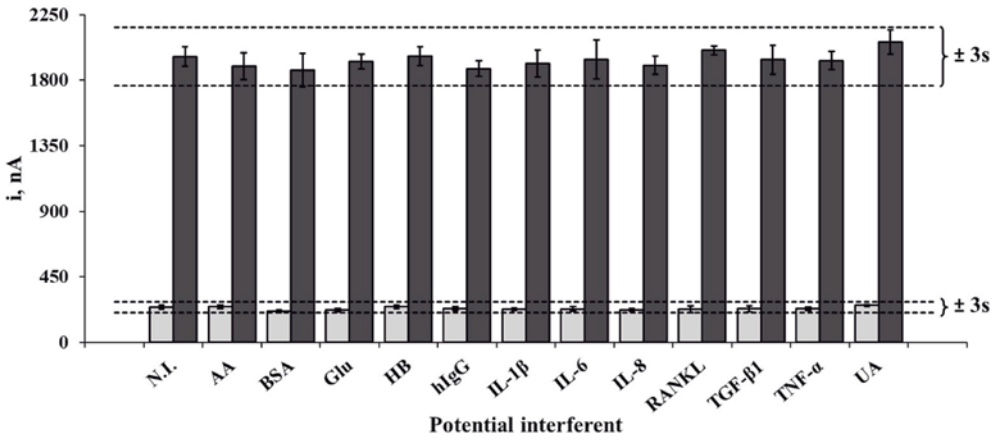

Fig. 6. Amperometric responses measured with HRP-Strept-biotin-anti–IFN–IFN-γ-anti–IFN–Phe-SPCE immunosensors for 0 (light grey) and 1 (dark grey) ng mL^{-1} IFN-γ standards in the absence and in the presence of 7 µg mL^{-1} AA, 5 mg mL^{-1} BSA, 1 mg mL^{-1} Glu, 5 mg mL^{-1} HB, 5 mg mL^{-1} human IgG, 50 pg mL^{-1} IL–1β, 300 pg mL^{-1} IL–6, 300 pg mL^{-1} IL–8, 100 pg mL^{-1} RANKL, 50 pg mL^{-1} TGF-β1, 200 pg mL^{-1} TNF-α, and 100 µg mL^{-1} UA. See the text for more information.

Table 2
Determination of IFN-g in a reference material and in saliva samples using the HRP-Strept-biotin-anti–IFN–IFN-γ-anti–IFN–Phe/SPCE immunosensor.

Biological International Standard			Student *t*-test
Sample	**Immunosensor (n = 9), pg/mL**	**ELISA (n = 6), pg/mL**	
NIBSC 87/586	12.5 ± 0.2	12.3 ± 0.5	t_{exp} = *1.732;* t_{tab} = *2.160*
Saliva			*Student t-test*
Sample	**Immunosensor (n = 6), pg/mL**	**ELISA (n = 3), pg/mL**	
1 (non-smoker)	8.4 ± 0.3	8.2 ± 0.4	t_{exp} = *1.822;* t_{tab} = *2.365*
2 (non-smoker)	7.3 ± 0.2	7.1 ± 0.3	t_{exp} = *1.774;* t_{tab} = *2.365*
3 (smoker)	7.6 ± 0.2	7.5 ± 0.3	t_{exp} = *1.477;* t_{tab} = *2.365*
4 (non-smoker)	7.2 ± 0.3	7.2 ± 0.5	t_{exp} = *1.443;* t_{tab} = *2.365*

concentrations are those expected according to the literature in healthy individuals. The results summarized in Fig. 6 allowed us to conclude that no significant interference was produced by any of the potential interfering biomolecule tested.

3.5. Determination of IFN-γ in a biological international standard and in saliva

Validation of the HRP-Strept-biotin-anti–IFN–IFN-γ-anti–IFN–Phe/SPCE immunosensor was performed by analyzing a Biological International Standard (BIS) for IFN-γ containing a 12.5 ng mL^{-1} IFN-γ certified concentration. In addition, the endogenous concentration of IFN-γ was quantified in saliva samples collected from four volunteers following the procedure described in Section 2.3.3. The potential occurrence of matrix effects was evaluated in both types of sample by statistically comparing the slope values of the calibration plots constructed by successive additions of IFN-γ standard aliquots to the samples (BIS, and Saliva 1,2,3 and 4) with the slope value of the calibration graph obtained using IFN-γ standard solutions in PBS. The corresponding regression equations were:

BIS: i, nA = (590 ± 12) log [IFN-γ], pg mL^{-1} + (121 ± 25)
Saliva 1: i, nA = (571 ± 16) log [IFN-γ], pg mL^{-1} + (125 ± 20)
Saliva 2: i, nA = (628 ± 24) log [IFN-γ], pg mL^{-1} + (56 ± 29)
Saliva 3: i, nA = (630 ± 29) log [IFN-γ], pg mL^{-1} + (56 ± 35)
Saliva 4: i, nA = (656 ± 47) log [IFN-γ], pg mL^{-1} + (17 ± 58)

The application of the Student t-test by comparing with the equation calculated with standard solutions, i, nA = (591 ± 12) log [IFN-γ], pg/mL + (121 ± 25), provided t_{exp} values 0.186 (BIS) and 0.993, 1.398, 1.277 and 1.352 for saliva samples 1 to 4, respectively. These t_{exp} values were, in all cases, lower than the tabulated one, t_{tab} = 2.228 for α = 0.05 and n = 10. Therefore, the determination of IFN-γ in BIS and saliva can be performed directly by interpolation of the amperometric current measured with the immunosensor for an aliquot of the undiluted sample, into the calibration plot constructed with standard solutions. The concentrations found in the analysis of BIS and saliva from two smoker and two non-smoker individuals are shown in Table 2. In addition, they are compared with the results provided by the commercial ELISA kit DuoSet ELISA, R&D Systems, Cat. No. DY285B. As it can be seen, an excellent agreement was found with the certified material as well as with the results obtained by the ELISA method. It is worth mentioning that the IFN-γ concentrations found in saliva also agree with the mean concentration value of 6.41 ± 2.53 pg mL^{-1} reported in the literature for saliva of healthy individuals [16]. It is important to remark that the immunosensor can be applied to the clinical determination of this cytokine without sample treatment and in a total assay time of approximately half the time required using the ELISA kit involving the same immunoreagents.

4. Conclusions

A disposable amperometric immunosensor using SPCEs as electrochemical platform and diazonium salt grafting of *p*-aminobenzoic acid for the covalent immobilization of the capture antibody was prepared for the determination of interferon gamma (IFN-γ). The implemented sandwich-type immunoassay, involving a biotin-labeled detector antibody and HRP-streptavidin conjugate, allows obtaining a calibration plot for IFN-γ with a wider linear range and a much shorter assay time and a remarkably smaller sample volume than the corresponding analytical characteristics claimed for ELISA methodology. A LOD value of 1.6 pg mL^{-1} was achieved which is adequate for the determination of IFN-γ in clinical samples. The immunosensor was employed for the determination of the biomarker in saliva with no sample treatment and results in good agreement with those obtained by using a commercial ELISA kit. The analytical performance exhibited by this new amperometric immunosensor of simple operation including disposability, as well as the possibility of using pocket-size electrochemical instrumentation makes it an attractive alternative for the development of automated POC systems for on-site determination of salivary IFN-γ.

Declaration of competing interest

The authors declare that they have no known competing financial interests or personal relationships that could have appeared to influence the work reported in this paper.

Acknowledgements

The financial support of the CTQ2015-64402-C2-1-R (Spanish Ministerio de Economía y Competitividad) and RTI2018-096135-B-I00 (Spanish Ministerio de Ciencia, Innovación y Universidades) Research Projects and the TRANSNANOAVANSENS-CM Program from the Comunidad de Madrid (Grant S2018/NMT-4349) are gratefully acknowledged.

References

[1] A. Bucht, P. Larsson, L. Weisbrot, C. Thorne, P. Pisa, G. Smedegaard, E. Keystone, A. Grönberg, Expression of interferon-gamma (IFN-γ), IL-10, IL-12 and transforming growth factor-beta (TGF-β) mRNA in synovial fluid cells from patients in the early and late phases of rheumatoid arthritis (RA), Clin. Exp. Immunol. 103–3 (1996) 357–367 https://doi: 10.1111/j.1365-2249.1996.tb08288.x.
[2] M. Truchetet, N.C. Brembilla, E. Montanari, Y. Allanore, C. Chizzolini, Increased frequency of circulating Th22 in addition to Th17 and Th2 lymphocytes in systemic sclerosis: association with interstitial lung disease, Arthritis Res. Ther. 13 (2011) R166, https://doi.org/10.1186/ar3486.
[3] Y. Zhang, B. Zhang, X. Ye, Y. Yan, L. Huang, Z. Jiang, S. Tan, X. Cai, Electrochemical immunosensor for interferon-γ based on disposable ITO detector and HRP-antibody-conjugated nano gold as signal tag, Mater. Sci. Eng. C 59 (2016) 577–584.
[4] Y. Liu, N. Tuleouva, E. Ramanculov, A. Revzin, Aptamer-based electrochemical biosensor for interferon gamma detection, Anal. Chem. 82 (2010) 8131–8136, https://doi.org/10.1021/ac101409t.
[5] H.X. Zhang, B.Y. Jiang, Y. Xiang, Y.Q. Chai, R. Yuan, Label-free and amplified electrochemical detection of cytokine based on hairpin aptamer and catalytic DNAzyme, Analyst 137 (2012) 1020–1023, https://doi.org/10.1039/

C2AN15962G.
[6] J. Xia, D. Song, Z. Wang, F. Zhang, M. Yang, R. Gui, L. Xia, S. Bi, Y. Xia, Y. Li, L. Xia, Single electrode biosensor for simultaneous determination of interferon gamma and lysozyme, Biosens. Bioelectron. 68 (2015) 55–61, https://doi.org/10.1016/j.bios.2014.12.045.
[7] Y. Chen, T.S. Pui, P. Kongsuphol, K.C. Tang, S.K. Arya, Aptamer-based array electrodes for quantitative interferon-γ detection, Biosens. Bioelectron. 53 (2014) 257–262, https://doi.org/10.1016/j.bios.2013.09.046.
[8] C. Liu, G. Xiang, D. Jiang, L. Liu, F. Liu, F. Luo, X. Pu, An electrochemical aptasensor detection of IFN-γ using graphene and a dual signal amplification strategy based on the exonuclease-mediated surface-initiated enzymatic polymerization, Analyst 140 (2015) 7784–7791 10.1039/C5AN01591J.
[9] G.P. Yan, Y.H. Wang, X.X. He, K.M. Wang, J.Q. Liu, Y.D. Du, A highly sensitive label-free electrochemical aptasensor for interferon-gamma detection based on graphene controlled assembly and nuclease cleavage-assisted target recycling amplification, Biosens. Bioelectron. 44 (2013) 57–63, https://doi.org/10.1016/j.bios.2013.01.010.
[10] S. Ding, C. Mosher, X.Y. Lee, S.R. Das, A.A. Cargill, X. Tang, B. Chen, E.S. McLamore, C. Gomes, J.M. Hostetter, J.C. Claussen, Rapid and label-free detection of interferon gamma via an electrochemical aptasensor comprising a ternary surface monolayer on a gold interdigitated electrode array, ACS Sens. 2 (2017) 210–217 https://doi:10.1021/acssensors.6b00581.
[11] J. Zhao, C. Chen, L. Zhang, J. Jiang, R. Yu, An electrochemical aptasensor based on hybridization chain reaction with enzyme-signal amplification for interferon-gamma detection, Biosens. Bioelectron. 36 (2012) 129–134, https://doi.org/10.1016/j.bios.2012.04.013.
[12] N. Ruecha, K. Shin, O. Chailapakul, N. Rodthongkum, Label-free paper-based electrochemical impedance immunosensor for human interferon gamma detection, Sens. Actuators, B 279 (2019) 298, https://doi.org/10.1016/j.snb.2018.10.024.
[13] Y. Wang, G.H. Mazurek, E.C. Alocilja, Measurement of interferon gamma concentration using an electrochemical immunosensor, J. Electrochem. Soc. 163 (2016) B140–B145 https://doi: 10.1149/2.0271605jes.
[14] H.X. Huang, J. Li, S.S. Shi, Y.Q. Yan, M.Y. Zhang, P.C. Wang, G.C. Zeng, Z.Y. Jiang, Detection of interferon-gamma for latent tuberculosis diagnosis using an immunosensor based on CdS quantum dots coupled to magnetic beads as labels, Int. J. Electrochem. Sci. 10 (2015) 2580–2593.
[15] E. Kaufman, I.B. Lamster, The diagnostic applications of saliva— a review, Crit. Rev. Oral Biol. Med. 13 (2002) 197–212, https://doi.org/10.1177/154411130201300209.
[16] N.A. Ghallab, N. El-Wakeel, O.G. Shaker, Levels of salivary IFN-gamma, TNF-alfa, and TNF receptor-2 as prognostic markers in (erosive) oral lichen planus, Mediat. Inflamm. (2010) 847632, https://doi.org/10.1155/2010/847632.
[17] S. Campuzano, P. Yáñez-Sedeño, J.M. Pingarrón, Electrochemical bioaffinity sensors for salivary biomarkers detection, TrAC Trends Anal. Chem. (Reference Ed.) 86 (2017) 14–24.
[18] P. Yáñez-Sedeño, S. Campuzano, J.M. Pingarrón, Integrated affinity biosensing platforms on screen-printed electrodes electrografted with diazonium salts, Sensors 18 (2018) 675, https://doi.org/10.3390/s18020675.
[19] M. Moreno-Guzmán, A. González-Cortés, P. Yáñez-Sedeño, J.M. Pingarrón, Multiplexed ultrasensitive determination of adrenocorticotropin and cortisol hormones at a dual electrochemical immunosensor, Electroanalysis 24 (2012) 1100–1108, https://doi.org/10.1002/elan.201200070.
[20] J. Eletxigerra, S. Martinez-Perdiguero, R. Merino, V. Barderas, R. Ruiz-Valdepeñas Montiel, J.M. Villalonga, J.M. Pingarrón, S. Campuzano, Estrogen receptor α determination in serum, cell lysates and breast cancer cells using an amperometric magnetoimmunosensing platform, Sens. Biosensing Res. 7 (2016) 71–76.
[21] A. Baraket, M. Lee, N. Zine, N. Yaakoubi, M.G. Trivella, A. Elaissari, M. Sigaud, N. Jaffrezic-Renault, A. Errachid, A flexible label-free biosensor sensitive and selective to TNF-α: application for chronic heart failure, Sensors & Transducers 27 (2014) 15–21.
[22] E. Sánchez-Tirado, A. González-Cortés, P. Yáñez-Sedeño, J.M. Pingarrón, Magnetic multiwalled carbon nanotubes as nanocarrier tags for sensitive determination of fetuin in saliva, Biosens. Bioelectron. 113 (2018) 88–94.
[23] J.H. Kim, Y.W. Chang, E. Bok, H.J. Kim, H. Lee, S.N. Cho, J.S. Shin, K.H. Yoo, Detection of IFN-γ for latent tuberculosis diagnosis using an anodized aluminum oxide-based capacitive sensor, Biosens. Bioelectron. 51 (2014) 366–370.

Analytica Chimica Acta 959 (2017) 66-73

Electrochemical immunosensor for simultaneous determination of interleukin-1 beta and tumor necrosis factor alpha in serum and saliva using dual screen printed electrodes modified with functionalized double-walled carbon nanotubes

Analytica Chimica Acta 959 (2017) 66–73

Contents lists available at ScienceDirect

Analytica Chimica Acta

journal homepage: www.elsevier.com/locate/aca

Electrochemical immunosensor for simultaneous determination of interleukin-1 beta and tumor necrosis factor alpha in serum and saliva using dual screen printed electrodes modified with functionalized double–walled carbon nanotubes

E. Sánchez-Tirado [a], C. Salvo [a], A. González-Cortés [a], P. Yáñez-Sedeño [a, *], F. Langa [b], J.M. Pingarrón [a]

[a] Department of Analytical Chemistry, Faculty of Chemistry, University Complutense of Madrid, Ciudad Universitaria s/n, 28040, Madrid, Spain
[b] Instituto de Nanociencia, Nanotecnología y Materiales Moleculares (INAMOL), Universidad de Castilla-La Mancha, 45071, Toledo, Spain

HIGHLIGHTS

- Electrochemical immunosensor for simultaneous determination of IL-β1 and TNF-α cytokines.
- Oriented immobilization of capture antibodies and signal amplification.
- Improved analytical performance with respect to previous approaches and ELISA methods.
- Application to human serum and saliva.

GRAPHICAL ABSTRACT

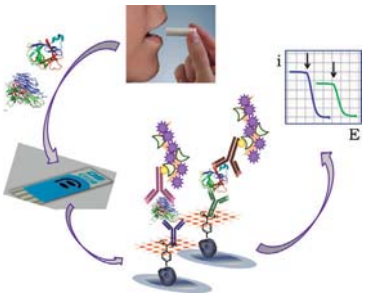

ARTICLE INFO

Article history:
Received 18 November 2016
Received in revised form
21 December 2016
Accepted 23 December 2016
Available online 2 January 2017

Keywords:
Interleukin-1 beta
Tumor necrosis factor-alpha
Electrochemical immunosensor
Multiplex
Double-walled carbon nanotubes
Saliva

ABSTRACT

Dual screen-printed carbon electrodes modified with 4-carboxyphenyl-functionalized double-walled carbon nanotubes (HOOC-Phe-DWCNTs/SPCEs) have been used as scaffolds for the preparation of electrochemical immunosensors for the simultaneous determination of the cytokines Interleukin-1β (IL-1β) and factor necrosis tumor α (TNF-α). IL-1β. Capture antibodies were immobilized onto HOOC-Phe-DWCNTs/SPCEs in an oriented form making using the commercial polymeric coating Mix&Go™. Sandwich type immunoassays with amperometric signal amplification through the use of poly-HRP-streptavidin conjugates and H_2O_2 as HRP substrate and hydroquinone as redox mediator were implemented. Upon optimization of the experimental variables affecting the immunosensor performance, the dual immunosensor allows ranges of linearity extending between 0.5 and 100 pg/mL and from 1 to 200 pg/mL for IL-1β and TNF-α, respectively, these ranges being adequate for the determination of the cytokines in clinical samples. The achieved limits of detection were 0.38 pg/mL (IL-1β) and 0.85 pg/mL (TNF-α). In addition, the dual immunosensor exhibits excellent reproducibility of the measurements, storage stability of the anti-IL-Phe-DWCNTs/SPCE and anti-TNF-Phe-DWCNTs/SPCE conjugates, and selectivity as well as negligible cross-talking. The dual immunosensor was applied to the simultaneous determination of IL-1β and TNF-α in human serum spiked at clinically relevant concentration levels and in real saliva samples.

© 2017 Elsevier B.V. All rights reserved.

* Corresponding author.
E-mail address: yseo@quim.ucm.es (P. Yáñez-Sedeño).

http://dx.doi.org/10.1016/j.aca.2016.12.034
0003-2670/© 2017 Elsevier B.V. All rights reserved.

1. Introduction

Cytokine detection is important for prognosis and diagnosis of different diseases related with inflammation, immunology, atherosclerosis and cancer [1]. However, monitoring of these proteins show some challenges related to their low concentration ranges in biological samples [2], which makes it difficult obtaining accurate and reliable analytical results. Moreover, as cytokines are known to work in concert to operate on the network of effectors [1] efficient analytical strategies should be implemented in the form of multiplexed detection [3]. It is well known that multianalyte approaches provide more information for each single sample and lead to faster and low-cost assays.

In this paper, we report the construction and analytical performance of an electrochemical platform for the simultaneous detection of two important cytokines: Interleukin-1β (IL-1β) and factor necrosis tumor α (TNF-α). IL-1β is a pro-inflammatory cytokine produced by a variety of cells including pancreatic cells, adipocytes or macrophages. Similar to other cytokines, the determination of IL-1β is relevant for monitoring inflammatory and immune processes, but it is also significant in some specific cases. For instance, elevation of the IL-1β concentration is a typical reaction of the brain to acute injury and it can be found in a number of chronic neurodegenerative diseases such as Alzheimer [4]. In addition, high glucose concentrations induce the pancreatic expression of IL-1β leading to alteration of insulin secretion, as well as a decrease in cellular proliferation and apoptosis of pancreatic beta cells. On the other hand, the role of TNF-α is critical in many diseases including rheumatoid arthritis [5] or cancer [6].

Biological activities of IL-1β and TNF-α, have been reported to be synergistic and overlapping [7]. For instance, both proteins exert an important inhibitory function on erythropoiesis blunting the endogenous production of EPO, and might play a role in the pathogenesis of anemia of chronic disorders or that of cancer patients which respond to recombinant EPO [8]. Moreover, increased IL-1β and TNF-α levels in vitreous humor and serum of patients with proliferative diabetic retinopathy has also been described [9]. Elevated levels of various cytokines, including IL-1β and TNF-α, have also been identified in the circulation of traumatic brain injury (TBI) patients within hours of injury [10]. Interestingly, both proteins can be used as biomarkers to predict side effects of cancer therapy such as inflammatory oral mucositis [11]. In addition, determination of salivary contents of both cytokines in patients with leukoplakia and oral cancer has a great interest [12] and very recently they have also been considered as novel biomarkers for the detection of periodontal diseases [13].

Due to the normal levels of IL-1β and TNF-α in biological fluids are in the concentration range of few pg/mL, sufficient sensitivity is a requirement for the developed analytical methods. Therefore, enhancement in sensitivity has been a common issue for the previously reported electrochemical immunosensors. As Table 1 shows [14–30], the number of sensors described for TNF-α is relatively high whereas those for IL-β1 are very scarce. Diverse electrode modifiers [15,16], signal amplifiers [16,17] and a variety of electrochemical techniques [18,19] have been employed to attain the required detection limits. Regarding the simultaneous determination of these cytokines, only three electrochemical immunoassay configurations have been reported (Table 1). An ultrasensitive microfluidic array was developed for TNF-α, IL-6, IL-1β, and C-reactive protein to assess oral mucositis risk in cancer patients. Magnetic beads were used to capture the analytes from serum and detected with a sensor array coated with gold nanoparticles and antibodies [11]. A fully integrated BioMEMS was also developed to simultaneously detect various interleukins (IL-1, IL-10, and IL-6) [3].

Table 1
Electrochemical immunosensors reported in the literature for the determination of IL-1β and TNF-α

Biomarker	Immunosensor	Technique	L.R., pg/mL	LOD, pg/mL	Assay time[a]	Sample	Ref.
TNFα	SiO_2-PGMA-QDs-anti-TNF- TNFα -anti-TNF-poly(*o*-ABA)/AuE	SWV	$10–10^6$	3	90 min	–	[14]
TNFα	AuNPs/PSA-AP-anti-TNF-TNFα-anti-TNF/PANI/PAA/GCE	DPV	20–20000	10	2 h 50 min	Spiked serum	[15]
TNFα	PB-CeO_2-anti-TNF-TNFα-anti-TNF-AuNPs/CNTs/GCE	amperom.	5–5000	2	2 h 30 min	Spiked serum	[16]
TNFα	AP/PS-anti-TNF-TNFα-anti-TNF-AuNPs/hydrogel + Chit/GCE	SWV	1–10000	0.5	2 h 30 min	Spiked serum	[17]
TNFα	GOx/GNR-anti-TNF-TNFα-anti-TNF-AuNPs/Fc-FF/PDDA/GCE	SWV	5–10000	5	2 h 30 min	Spiked serum	[18]
TNFα	TNFα-anti-TNF-poly(*o*-ABA)/SPCE	EIS	up to 100	5	2 h	Spiked serum	[19]
TNFα	HRP-anti-TNF-TNFα-anti-TNF-poly(*o*-ABA)/SPCE	DPV	up to 50	3.2	3 h	Spiked serum	[19]
TNFα, IL-12	Ab-16-MHDA-AuNPs/AuE	EIS	–	60; 3.4	30 min	–	[20]
TNFα	AP-Strept-Biotin-anti-TNF-TNFα-anti-TNF-MBs-Prot G/SPCE	DPV	up to 5000	44	2 h 40 min	Spiked serum	[21]
TNFα	TNFα-anti-TNF-PGMA-PFMMA-AuE	CV	$1–10^6$	3.9	2 h 30 min	–	[22]
TNFα	TNFα-anti-TNF-Nafion/K-Chit-GA/GCE	CV	20–34000	10	60 min + blocking	Spiked serum	[23]
TNFα	TNFα -anti-TNF-DSP-Au micro-array	EIS	1–10	1	1 h 15 min	Cell culture	[24]
IL-1, IL-6, IL-10	Ab-Au mcroelectrode (BioMEMS).	EIS	1–15	–	–	–	[3]
TNFα	HRP-Strept-Biotin-anti-TNF-TNFα-anti-TNF-MBs-COOH/SPCE	amperom.	$5 - 5 \times 10^6$	2	3 h 10 min	Spiked serum	[25]
TNFα	TNFα-anti-TNF-MBs-COOH/CSGM	EIS	1–1000	1	1 h 25 min	Spiked serum	[26]
TNFα	TNFα-anti-TNF-Ag@Pt/ MWCNTs/Chit/SPCE	DPV	6–60	1.6	>8 h	Spiked serum	[27]
TNFα	anti-TNF/IL/C_{60}-MWCNTs/SPCE	DPV	5–75	2	>8 h	Spiked serum	[34]
TNFα	AP-Strept-Biotin-anti-TNF-TNFα-anti-TNF-poly(*p*-ABA)-SPCE	DPV	3250–50000	4100	3 h 10 min	Spiked serum	[29]
TNFα, IL-6, IL-1β, CRP	HRP-MBs-Ab1- Ag -Ab2-GSH-AuNPs/PDDA/SPCE (microfluidic array)	amperom.	0.04–22 (IL) 0.01–12 (TNF)	0.04 (IL) 0.01 (TNF)	2 h 22 min	Spiked and real serum	[11]
TNFα	AP-IgG-anti-TNF-TNFα-anti-TNF (affibody®) -MBs-COOH/SPCE	DPV	76–5000	38	3 h 30 min	Spiked serum	[30]
IL-1β TNFα,	poly-HRP-Strept-Biotin-anti-TNF-TNFα-anti-TNF-HOOC-Phe-DWCNTs/SPCE	amperom.	0.5–100 (IL) 1 - 200 (TNF)	0.38 (IL) 0.85 (TNF)	2 h 30 min	Spiked serum, saliva	This work

Ab, antibody; AuE, gold electrode; AP, alkaline phosphatase; AuNPs, gold nanoparticles; Chit, chitosan; CNTs, carbon nanotubes; CSGM, comb structured gold microelectrode array; DPV, differential pulse voltammetry; DSP, dithiobis-succinimidylpropionate; EIS, electrochemical impedance spectroscopy; Fc, ferrocene; FF, diphenylalanine; GCE, glassy carbon electrode; GA, glutaraldehyde; GNR, gold nanorod; GOx, glucose oxidase; IL-12, interleukin-12; K-Chit-GA, $K_3[Fe(CN)_6]$-chitosan-glutaraldehyde; MBs, magnetic beads; 16-MHDA,16-mercaptohexadecanoic acid; *o*-ABA, *ortho*-aminobenzoic acid; *p*-ABA,para-aminobenzoic acid; PAA, poly(acrylic acid); PANI, polyaniline; PB, Prussian Blue; PDDA, polydiallyldimethylammonium; PFMMA, polyferrocenemethylmethacrylate; PGMA, polyglycidylmethacrylate; PS, polyethylene sphere; PSA, poly(styrene-co-acrylic acid); QDs, quantum dots; SPCE, screen-printed carbon electrode; SWV, square wave voltammetry.

[a] Counted once the antibody was immobilized.

Electrochemical impedance spectroscopy was also used to determine TNF-α and IL-12 with limits of detection of 60 and 3.4 pg/mL, respectively, by conjugation of antibodies to gold nanoparticles through self-assembled monolayers of 16-mercaptohexadecanoic acid [20]. It is worth to mention that commercial ELISA kits for the single determination of IL-1β or TNF-α are available but they are characterized by the long assay times required and the relatively large sample volumes.

The immunosensor described in this work for the simultaneous determination of IL-β1 and TNF-α involves the use of dual screen-printed carbon electrodes (SPCEs) modified with 4-carboxyphenyl-functionalized double-walled carbon nanotubes (HOOC-Phe-DWCNTs) as electrochemical scaffolds for immobilization of the specific anti-IL-1β and anti-TNF-α antibodies. As it is known, DWCNTs possess several beneficial properties with respect to MWCNTs for the preparation of electrochemical biosensors such as improved lifetimes and high stability under chemical, mechanical and thermal treatments [31]. Moreover, DWCNTs provide better electrochemical behavior than SWCNTs enhancing electron transfer and allowing significant overpotential reduction for various species. Furthermore, they show a higher reactivity, probably as a consequence of the larger number of lattice defects in DWCNTs [32]. Furthermore, upon chemical modification of DWCNTs, the outer cylinder acts as a protective sheath that preserves the electronic properties of the inner tube. Therefore, covalent sidewall chemistry can be performed onto DWCNTs without loss of the intrinsic properties [33].

Capture antibodies were immobilized onto HOOC-Phe-DWCNTs/SPCEs in an oriented form making using the commercial polymeric coating Mix&Go™. This polymer contains several metallic complexes with a high efficiency to bind proteins [34]. Sandwich type immunoassays with signal amplification through the use of poly-HRP-streptavidin conjugates were performed for each cytokine. This simple and relatively low cost immunosensor configuration allowed the development of a sensitive method for the simultaneous determination of IL-β1 and TNF-α exhibiting improved overall analytical performance with respect to previously reported data. In addition and in order to demonstrate the analytical usefulness of the developed methodology, the dual immunosensor was applied to the determination of both proteins in human serum and saliva.

2. Experimental

2.1. Reagents and solutions

Mouse TNFα capture antibody (anti-TNF), biotinylated goat TNFα detection antibody (biotin–anti–TNF), mouse IL1β capture antibody (anti-IL), and biotinylated goat ILβ1 detection antibody (biotin-anti-IL) were used. These immunoreagents as well as human TNFα and ILβ1 proteins were those included in the DuoSet® ELISA Development Systems DY201-05 (ILβ1), and DY210–05 (TNFα) from R&D Systems. Solutions of the respective capture antibodies at a concentration level of 240 μg/mL were prepared by dissolving the product in 500 μL PBS. Working solutions were prepared by dilution into a 25 mM buffer solution of *2*–(*N*–morpholino) ethanesulfonic acid (MES, Gerbu) of pH 5.0. Solutions of the respective detection antibodies at 18 μg/mL (TNFα) or 12 μg/mL (ILβ1) concentrations were prepared by dissolving the product in 1 mL PBS and 1% BSA. Phosphate buffer saline solution (PBS) consisted of a 137 mM NaCl, 2.7 mM KCl, 8.1 mM Na_2HPO_4, and 1.5 mM KH_2PO_4 solution of pH 7.4.

Streptavidin labeled with horseradish peroxidase (HRP-Strept, Roche), poly-HRP-Strept (85-R200) conjugate (Fitzerald), poly-HRP–Strept (S2438) conjugate (Sigma), and HRP–Strept–AuNPs (Nanovex Biotechnologies) were tested. Solutions from each conjugate at the working concentration were prepared in PBS. Double-walled carbon nanotubes functionalized with *p*–aminobenzoic acid (HOOC-Phe-DWCNTs) were provided by Instituto de Nanociencia, Nanotecnología y Materiales Moleculares (INAMOL) de la Universidad de Castilla La Mancha (Toledo), Mix&Go™ polymer was from Anteo Diagnostics. Hydroquinone (HQ) and hydrogen peroxide (30%, w/v) were from Sigma. Bovine serum albumin (BSA) was from GERBU Biotechnik, GmbH. Blocker® Casein in PBS was from Thermo Fisher. Adiponectin (APN, Abcam), ceruloplasmin (Cp, Abcam), ghrelin (GHRL, Anaspec) bovine serum albumin (BSA, Gerbu), cholesterol (Chol, Sigma), transforming growth factor β1 (TGF β1, R&D Systems), hemoglobin (Hb, Sigma), C-reactive protein (CRP, Fitzgerald), interleukin 6 (IL-6, Abcam), interleukin 8 (IL-8, Abcam), bilirubin (BIL, Aldrich), and leptin (Lep, R&D Systems) were tested as potential interfering compounds. Deionized water was from a Millipore Milli-Q purification system (18.2MΩ cm at 25 °C).

2.2. Apparatus and electrodes

All electrochemical measurements were carried out with a potenciostat from INBEA Biosensores S.L. equipped with the IbGraph software. Screen-printed carbon electrodes (SPCEs, 110 DRP, ϕ 4 mm), and dual SPCEs (C 1110 DRP) consisted of two elliptic carbon working electrodes with surface area of 5.6 mm^2, were from DropSens (Oviedo, Spain). These electrodes include a carbon counter electrode and a silver pseudo-reference electrode. An Elmasonic S–60 (Elma) ultrasonic bath, a Gyrozen 416 centrifuge (Controltechnica Instruments), and a Vortex homogenizator (Velp Scientifica) were also used. pH measurements were performed using a Crison Basic 20+ pH–meter. All experiments were performed at room temperature.

2.3. Samples

The samples analyzed were lyophilized human serum (S2257, Sigma) spiked with 2.5, 5 and 7.5 pg/mL IL-1β and 5, 10 and 15 pg/mL TNF-α, and saliva samples obtained from two lab researcher (male smoker and female nonsmoker volunteers) and collected using a Salivette® collection device (Sarstedt).

2.4. Procedures

2.4.1. Preparation of the immunosensors

A homogeneous dispersion of HOOC–Phe–DWCNTs was prepared by suspending 1 mg of the product in 2 mL distilled water, addition of 27.4 μL of Tween® 20, and ultrasonic stirring for 60 min. Thereafter, modification of the electrodes was made by casting 0.5 μL of the HOOC–Phe–DWCNTs dispersion onto the electrode surface and allowing drying under IR radiation. This procedure was repeated until a total dispersion volume of 1.5 μL was deposited. Next, 2.5 μL of Mix&Go solution were added and incubated for 60 min. Thereafter, the modified electrode was rinsed with water and allowed drying. This washing was accomplished after each electrode modification once incubation was made. Then, the corresponding capture antibody (anti–IL or anti-TNF) was immobilized by casting 2.5 μL of 4 μg/mL solution of each antibody and incubating for 60 min. Blocking with 2.5 μL of a 2% BSA solution in PBS for 30 min was then made to minimize unspecific interactions. Thereafter, 2.5 μL of the antigen (IL-β1 and/or TNF-α) standard solution or the sample were added and incubated for 60 min. Next, 2.5 μL of 0.5 μg/mL biotinylated antibody solution (Biotin–anti–IL or Biotin-anti-TNF) were added and incubated for 45 min. Finally, 2.5 μL of a 1/500 diluted poly–HRP–Strept solution were dropped

on the modified electrode allowing incubation for 15 min.

2.4.2. Simultaneous determination of IL-β1 and TNF-α

The determination of both cytokines was accomplished by dropping 45 μL of a 1 mM HQ solution onto the surfaces of the dual SPCE immunosensor horizontally positioned and applying a detection potential of −0.20 V. Once the background current was stabilized (approx.100 s), 5 mL of a 50 mM H_2O_2 solution was added and allowed standing for 200 s. The steady state current corresponding to the electrochemical reduction of benzoquinone was used as the analytical readout.

2.4.3. Samples analysis

Lyophilized serum was firstly reconstituted by dissolving 370 mg in 5 mL of deionized water mixing with gentle stirring. Then, the serum was spiked with 2.5, 5 or 7.5 pg/mL IL-1β and 5, 10 or 15 pg/mL TNF-α, and the determination of both proteins was performed by application of the procedures 2.4.1 and 2.4.2. and interpolation of the amperometric responses in the respective calibration plot constructed with standard solutions.

Regarding saliva, samples were collected from the volunteers after rinsing the mouth thoroughly with water and chewing a cotton swab for 5 min. Then, the swap saturated with saliva was inserted into a vial, sealed with the cap and centrifuged for 10 min at 3000 × g. The determination was performed immediately by applying the procedure described above using 5-μL aliquots of the undiluted sample.

3. Results and discussion

The methodologies employed in this work involved the immobilization of capture antibodies onto SPCEs modified with 4-carboxyphenyl-functionalized double-walled carbon nanotubes (HOOC-Phe-DWCNTs) and application of sandwich type immunoassays for each cytokine with signal amplification through the use of poly-HRP-streptavidin conjugates. These strategies took advantage of: i) the well-known enhancement of electron transfer processes occurring on DWCNTs-modified electrode surfaces, ii) the high availability of surface confined carboxyl groups onto HOOC-Phe-DWCNTs, iii) the oriented immobilization of antibodies by means of Mix&Go polymer, and iv) the amplification of the electrochemical responses with poly-HRP-Strept.

The protocols used for the preparation of the dual immunosensor are described in the Experimental section and schematically displayed in Fig. 1. Once Mix&Go was dropped onto each surface of HOOC-Phe-DWCNTs-modified dual SPCE, anti-IL and anti-TNF antibodies were immobilized and a subsequent blocking step of the remaining active free sites on the electrode surfaces was carried out. Then, sandwich type assays involving the target cytokines and biotinylated detector antibodies were accomplished. A further conjugation with poly-HRP-Strept allowed the amperometric determination of IL-1β and TNF-α to be performed using H_2O_2 as HRP substrate and hydroquinone (HQ) as the redox mediator.

3.1. Optimization of the experimental variables involved in the preparation of the dual immunosensor

Variables involved in the preparation of the dual immunosensor for the simultaneous determination of IL-1β and TNF-α were optimized. These studies were performed individually for each cytokine using single modified-SPCEs and included: a) the antibody (anti-IL or anti-TNF) loading onto HOOC-Phe-DWCNTs/SPCE and the time for incubation; b) the Biotin-antibody loading onto IL-1β-anti-IL-Phe-DWCNTs/SPCE or TNF-α-anti-TNF-Phe-DWCNTs/SPCE and the time for incubation; c) the blocking step, and d) the type of enzyme label and the loading of poly-HRP-Strept onto Biotin-anti-IL-IL1β-anti-IL-Phe-DWCNTs/SPCE or Biotin-anti-TNF-TNF-α-anti-TNF-Phe-DWCNTs/SPCE. Other variables involved in the preparation of the modified electrodes such as the loading of HOOC-Phe-DWCNTs onto SPCE and the loading of Mix&Go onto HOOC-Phe-

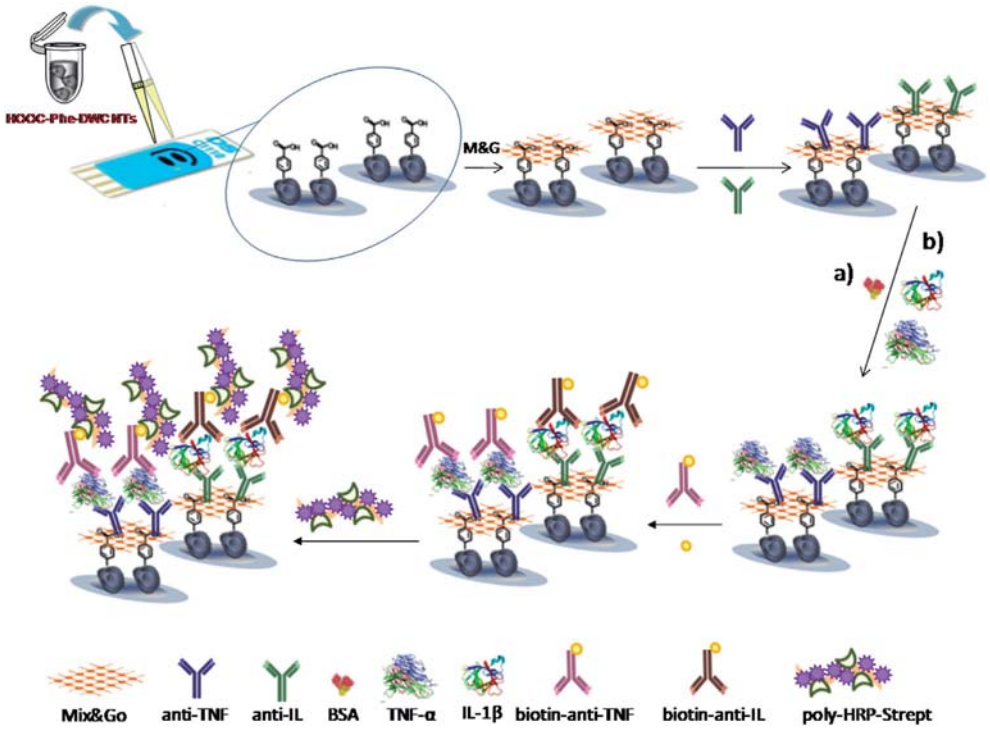

Fig. 1. Schematic display of the different steps involved in the preparation of the dual electrochemical immunosensor for multiplexed determination of IL-1β and TNF-α cytokines.

DWCNTs/SPCE, as well as those implied in the electrochemical detection such as the detection potential value or the concentration of H_2O_2 and HQ were the same than those employed in previous papers [35,36]. Details on these optimization studies are provided in Supplementary material and Figs. S1-S4 and summarized in Table 2.

3.2. Analytical characteristics of the dual immunosensor

The calibration plots for IL-1β and TNF-α constructed with the dual immunosensor under the optimized working conditions are shown in Fig. 2. Error bars were calculated from the measurements carried out with three different dual immunosensors for each concentration. The steady state current vs. IL-1β concentration (Fig. 2a) followed the adjusted equation I, nA = (624 ± 15) log C, pg/mL + 393 ± 18 (r^2 = 0.996), with a range of linearity extending between 0.5 and 100 pg/mL IL-1β. Fig. 2b displays the calibration plot for TNF-α with an equation I, nA = (746 ± 16) log C, pg/mL + (245 ± 22) (r^2 = 0.999), with a range of linearity from 1 to 200 pg/mL. It is worth to mention that these ranges, covering two orders of magnitude, are adequate for the determination of the cytokines in clinical samples taking into account the expected concentrations at the level of few pg/mL [19]. The achieved limits of detection were 0.38 pg/mL (IL-1β) and 0.85 pg/mL (TNF-α) and were calculated by using the $3s_b$ criterion, where s_b was estimated as the standard deviation expressed in concentration units (n = 10) of the measured currents for the blank (0 pg/mL IL-1β or TNF-α).

When these analytical characteristics are compared with those reported for other electrochemical immunosensors (Table 1), it can be concluded that the developed methodology can be ranked among the most sensitive exhibiting low detection limits and linear ranges covering low concentration ranges. It should also be remarked that this excellent analytical performance is accompanied by a relatively short time of analysis. In fact, the whole experimental procedure, once the capture antibodies are immobilized, took 2 h 30 min. This period is much shorter than that required when commercial ELISA kits for IL-1β or TNF-α are employed. For example, the assays with the DuoSet® ELISA from R&D Systems [www.rndsystems.com] last 4 h 40 min.

The reproducibility of the measurements was tested with different dual immunosensors prepared on the same day and on different days, and in the absence or in the presence of 50 pg/mL IL-1β or 100 pg/mL TNF-α. The relative standard deviation (RSD) values obtained were 0.6 and 2.7% (IL-1β) (n = 4), and 0.3 and 0.7% (TNF-α) (n = 5), respectively, for the assays performed on the same day, and 0.8% and 3.7% (IL-1β) (n = 4), and 0.5 and 0.7% (TNF-α) (n = 5) respectively, for the measurements made on different days. These results indicated the good level of precision achieved in the fabrication and functioning of the developed dual electrochemical immunosensing platform.

In addition, the storage stability of the anti-IL-Phe-DWCNTs/SPCE and anti-TNF-Phe-DWCNTs/SPCE conjugates, once they were blocked with 2% BSA, was tested under storage at −20 °C in a dry environment. Several bioconjugates were prepared on the same day, stored, and used to construct on different days, poly-HRP-Strept - Biotin - anti - IL - IL1β - anti - IL - Phe - DWCNTs/SPCE and poly - HRP-Strept-Biotin-anti-TNF-TNF-α-anti-TNF-Phe-DWCNTs/SPCE dual immunosensors. The amperometric currents measured for 50 pg/mL IL-1β and 100 pg/mL TNF-α solutions (Fig. S5) remained within the control limits set by ± 3 times the standard deviation of the measurements (n = 3) carried out on the first day, during at least 40 days. This excellent storage stability suggests the possibility of preparing a set of anti-IL-Phe-DWCNTs/SPCE and anti-TNF-Phe-DWCNTs/SPCE conjugates and storing them under the above mentioned conditions until their use for the preparation of the immunosensors was requested.

3.3. Selectivity studies

The effect of potential interfering compounds that may be present together with the target cytokines in biological samples on the electrochemical responses obtained with the dual immunosensors was studied. As the used antibodies exhibit demonstrated specificity for IL-1β or TNF-α against other cytokines such as IL-1α, or TNF-β, TNF-RI and TNF-TII, respectively, the compounds tested were: adiponectin (APN), bovine serum albumin (BSA), cholesterol (Chol), C-reactive protein (CRP), hemoglobin (Hb), interleukin 6 (IL-6), interleukin-8 (IL-8), transforming growth factor β1 (TGF-β1), bilirubin (BIL), ceruloplasmin (Cp), ghrelin (GHRL) and leptin (LEP). Fig. 3 shows a comparison of the amperometric responses obtained with the dual immunosensor for 0 and 10 pg/mL IL-1β or TNF-α in absence and in the presence of each tested compound at their normal concentration levels in human serum. As it is clearly shows, no significant effect on the dual electrochemical immunosensor response was apparent in the presence of any non-target compound, thus demonstrating the excellent selectivity of the proposed configuration for simultaneous IL-1β and TNF-α determination.

Moreover, the possible cross-talking between the adjacent working modified SPCEs in the dual configuration and reaction products was evaluated by comparing the amperometric responses recorded at the poly-HRP-Strept-Biotin-anti-IL-IL1β-anti-IL-Phe-DWCNTs/SPCE where 10 pg/mL TNF-α were deposited, and at the poly-HRP-Strept-Biotin-anti-TNF-TNF-α-anti-TNF-Phe-DWCNTs/SPCE with 25 pg/mL IL-1β, with those obtained for 0 or 25 pg/mL IL-β1 and 10 pg/mL TNF-α, respectively. Fig. 4 shows clearly that no significant differences in the amperometric responses of immunosensors exist in the absence of the non-target antigen, thus demonstrating that no appreciable cross-talking occurred with the developed dual immunosensor.

3.4. Simultaneous determination of IL-1β and TNF-α in spiked serum and saliva

The developed dual immunosensor was applied to the simultaneous determination of IL-1β and TGF-β in human serum spiked at clinically relevant concentration levels [37,38] and in real saliva samples. Regarding serum, the possible existence of matrix effects was initially evaluated by constructing a calibration plot in the

Table 2
Optimization of the experimental variables affecting the performance of poly-HRP-Strept-Biotin-anti-IL-IL-1β-anti-IL-Phe-DWCNTs/SPCE and poly-HRP-Strept-Biotin-anti-TNF-TNF-α-anti-TNF-Phe-DWCNTs/SPCE immunosensors.

Variable	Tested	Selected
Capture antibody (Ab), μg/mL	2-8 (IL-1β); 1-5 (TNF-α)	6 (IL-1β); 4 (TNF-α)
Incubation time for Ab, min	30-90 (IL-1β); 30-60 (TNF-α)	60
Biotinylated antibody (Biotin-Ab), μg/mL	0.25–1 (IL-1β); 0.25–0.75 (TNF-α)	0.5
Incubation time for Biotin-Ab), min	30–90	60
Blocking agent type	1%BSA, 2%BSA, casein, milk powder	2% BSA
HRP- Strept label type	HRP-Strept, HRP-Strept-AuNPs, poly-HRP-Strept (F), poly-HRP-Strept (S)	poly-HRP-Strept (F),
poly-HRP-Strept, dilution	1/500 - 1/1000 (IL-β1) 1/250 - 1/2000 (TNF-α)	1/500

(F) Fitzgeral; (S) Sigma.

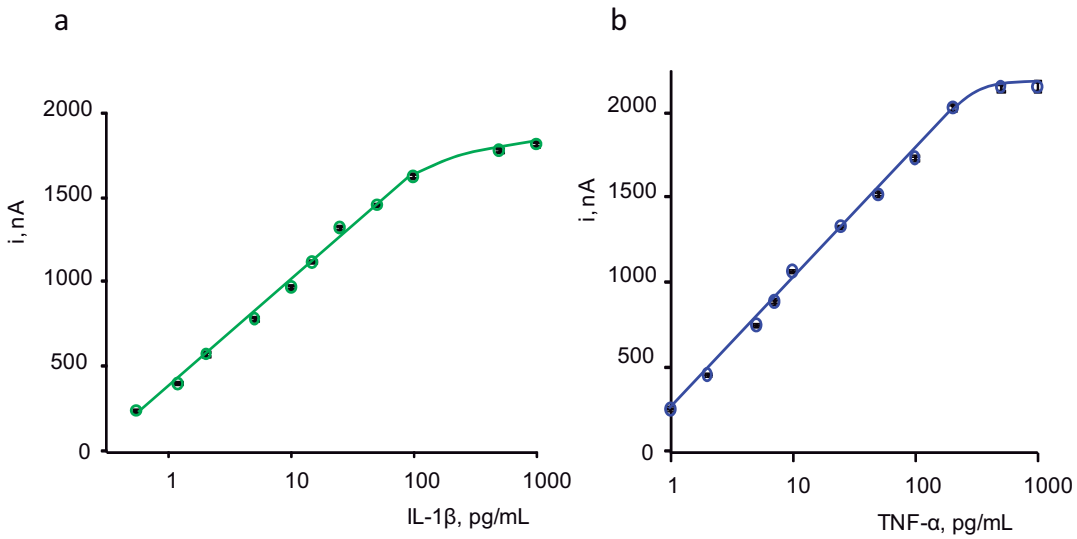

Fig. 2. Calibration plots for IL-1β (green) and TNF-α (blue) obtained with the dual poly-HRP-Strept-Biotin-anti-IL-IL1β-anti-IL-Phe-DWCNTs/SPCE and poly-HRP-Strept-Biotin-anti-TNF-TNF-α-anti-TNF-Phe-DWCNTs/SPCE immunosensor. See text for other conditions. (For interpretation of the references to colour in this figure legend, the reader is referred to the web version of this article.)

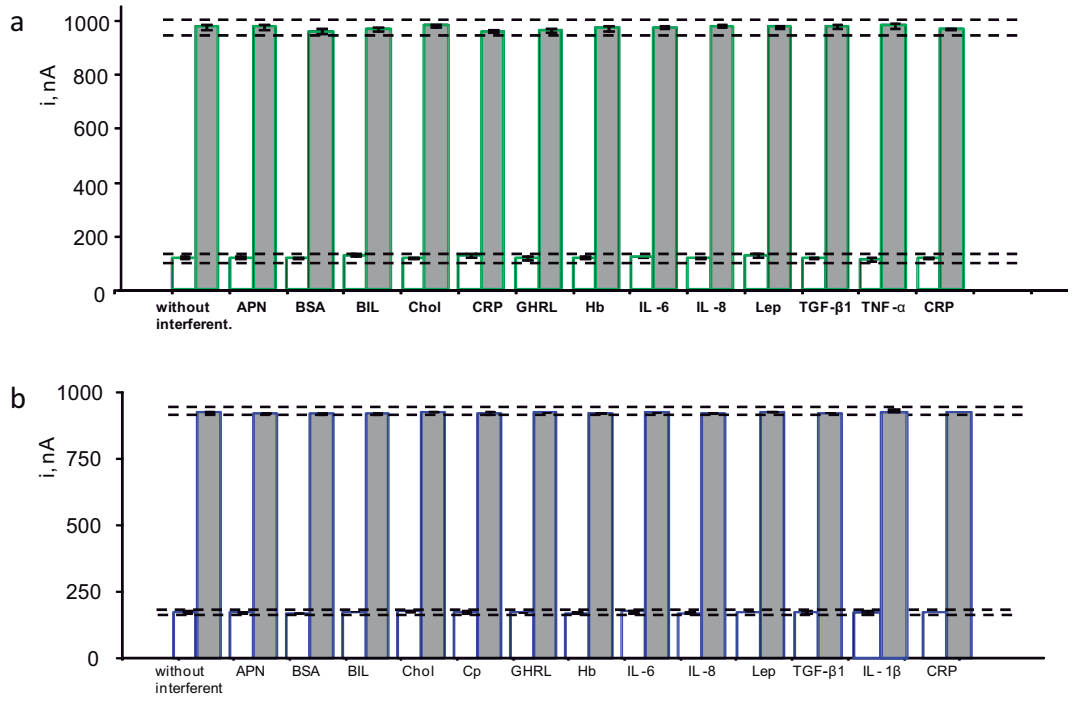

Fig. 3. Effect of the presence of 20 μg/mL APN, 5 mg/mL BSA, 190 ng/mL bilirubin (BIL), 20 μg/mL Chol, 500 μg/mL ceruloplasmin (Cp), 500 pg/mL ghrelin (GHRL), 50 μg/mL Hb, 50 pg/mL IL-6, 30 pg/mL IL–8, 5 ng/mL leptin (Lep), 500 pg/mL TGF–β1, 100 pg/mL TNF–α (a) or 50 pg/mL IL–1β (b), 1 μg/mL CRP on the amperometric responses obtained for 0 (white) and 10 (grey) pg/mL IL-1β (a) or TNF-α (b) at the dual electrochemical immunosensor. See the text for more information.

sample (lyophilized serum from Sigma) which was spiked with IL-1β over the 2.5–7.5 pg/mL, and with TNF-α over the 5–15 pg/mL concentration ranges, respectively. The equations obtained for the respective calibration graphs were I, nA = (597 ± 6) log C, pg/mL + (400 ± 4), (r^2 = 0.9998), and I, nA= (766.3 ± 0.2) logC, pg/mL + (237.8 ± 0.2), (r^2 = 0.9999) for IL-1β and TNF-α, respectively. The comparison of the slope values with those calculated for the calibration plots constructed with standard solutions by applying the Student's *t*-test showed t_{exp} values 1.655 (IL-1β) and 1.231 (TNF-α) lower than that tabulated t, 2.306, therefore indicating that no statistically significant differences existed between the slopes values for both types of calibration plots. Therefore, the determination of IL-1β and TNF-α could be carried out by interpolation of the current values measured for the serum samples into the calibration plots constructed with the standard solutions. Table 3 summarizes the results obtained by triplicate analysis of samples spiked at three different concentration levels: 2.5, 5.0 and 7.5 pg/mL IL-1β and 5. 10 and 15 pg/mL TNF-α. As it can be seen, recoveries ranged between 98 and 104%, indicating the reliability of the approach to determine low IL-1β and TNF-α concentrations in

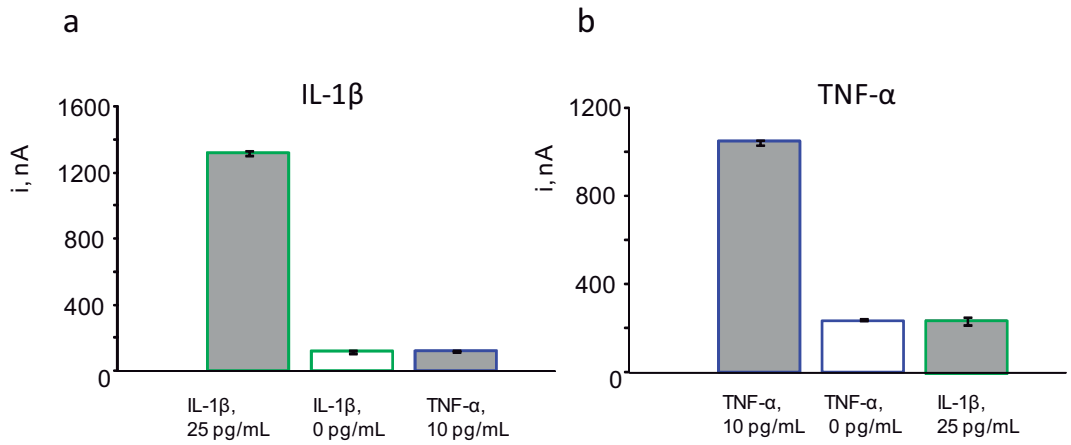

Fig. 4. Amperometric responses recorded with the dual immunosensor at poly-HRP-Strept-Biotin-anti-IL-IL1β-anti-IL-Phe-DWCNTs/SPCE for 25 or 0 pg/mL IL-1β (green), or 10 pg/mL TNF-α (blue) (a), and at poly-HRP-Strept-Biotin-anti-TNF-TNF-α-anti-TNF-Phe-DWCNTs/SPCE for with 10 or 0 pg/mL TNF-α (blue), or 25 pg/mL IL-1β (green) (b). See the text for more information. (For interpretation of the references to colour in this figure legend, the reader is referred to the web version of this article.)

serum following a simple working protocol.

Furthermore, two different saliva samples corresponding to a male smoker and a female nonsmoker volunteers were analyzed to determine the endogenous content of both IL-1β and TNF-α. Considering the complexity of saliva, we also evaluated the potential occurrence of matrix effect. A calibration plot was constructed by adding known cytokine concentrations between 0.5 and 50 pg/mL for IL-1β and 2 and 40 pg/mL for TNF-α to saliva from both patients. The respective slope values of the linear ranges (630 ± 14 and 627 ± 5 for IL-1β; 745 ± 37 and 758 ± 5 for TNF-α) were statistically compared with those calculated from the calibration graphs with IL-1β or TNF-α standards. (624 ± 15 and 746 ± 16 nA per decade of concentration). No significant difference for a 95% confidence interval (t_{exp} = 0.27 and 0.17 (IL-1β) and 0.10 and 0.67 (TNF-α) were lower than t_{tab} = 2.201). Accordingly, the determination of IL-1β and TNF-α in saliva was accomplished by interpolation of the measured current in the samples into the calibration plot constructed with standard solutions. Table 4 summarizes the results obtained in the analysis of saliva. Interestingly, the found values re consistent with those reported using other approaches and, as expected, no significant differences in salivary concentrations of the cytokines are apparent between smoker and non smoker individuals.

In addition, the results were compared with those obtained using the DuoSet® ELISA Development Systems DY201-05 (IL1β), and DY210–05 (TNFα) from R&D Systems. The ELISA protocols were similar for both cytokines and, briefly, involved incubating the capture antibody solution into the wells overnight at room temperature, followed by washing and blocking with BSA for a minimum of 1 h. Then, 100 μL of the sample or standards per well were added and incubated 2 h at room temperature. After washing, 100 μL of the detection antibody (biotinylated antibody) were added to each well and incubated 2 h at room temperature. Once washed, 100 μL of the HRP-Strept solution were added to each well leaving for 20 min at room temperature, and color development was achieved by the addition of TMB substrate solution. Finally, after 20 min, an acid "stop solution" was added, and the absorbance was measured at 450 nM. As it can be deduced from Table 4, the results obtained are consistent with those provided by the immunosensor. Indeed, the concentration values found by both methods were statistically compared by means of the Student's *t*-test. The t_{exp} values, 0.30 and 0.15 for IL-1β and 0.55 and 0.30 for TNF-α, were lower than the tabulated t value (2.16) and, therefore, no significant differences were found between both methodologies at a significance level of 0.05. These results demonstrate clearly the usefulness of the developed immunosensor to determine simultaneously IL-1β and TNF-α at clinically relevant concentrations in biological fluids such as serum or saliva.

Table 3
Simultaneous determination of IL-1β and TNF-α in spiked serum with the dual immunosensor.

IL-1β, pg/mL	IL-1β found[a], pg/mL	Recovery, %
2.5	2.5 ± 0.2	99 ± 8
5.0	4.9 ± 0.4	98 ± 6
7.5	7.3 ± 0.5	98 ± 8
TNF-α, pg/mL	TNF-α found[a], pg/mL	Recovery, %
5	5.1 ± 0.2	102 ± 7
10	10.2 ± 0.6	102 ± 5
15	15.7 ± 0.9	104 ± 6

[a] Mean value ± ts/√n.

Table 4
Simultaneous determination of IL-1β and TNF-α in saliva with the dual immunosensor.

	Immunosensor*	ELISA**
	IL-1β, pg/mL	IL-1β, pg/mL
Male smoker	52 ± 1	51.8 ± 0.5
Female nonsmoker	46.5 ± 0.5	46.5 ± 0.4
	TNF-α, pg/mL	TNF-α, pg/mL
Male smoker	13.3 ± 0.5	13.5 ± 0.9
Female nonsmoker	11.2 ± 0.3	11.3 ± 0.7

Mean value ± ts/√n (*n = 8; **n = 4).

4. Conclusions

An electrochemical dual platform for the simultaneous determination of IL-β1 and TNF-α cytokines is reported in this work. The platform profits the benefits inherent to electrode modification with 4-carboxyphenyl-functionalized double-walled carbon nanotubes where specific anti-IL-1β and anti-TNF-α antibodies were immobilized in an oriented manner using the commercial polymeric coating Mix&Go™. Sandwich type immunoassays with signal amplification by means of poly-HRP-streptavidin conjugates

allowed the development of a sensitive method for the simultaneous determination of IL-β1 and TNF-α with improved analytical performance with respect to previously reported approaches and commercial ELISA kits. The dual immunosensor was successfully applied to the determination of both cytokines at clinically relevant concentrations in biological fluids such as serum or saliva. In this context, an important point to be remarked is the simultaneous assay takes about 2 h 30 min once the capture antibodies were immobilized. Conversely, ELISAs require 4 h 40 min for each determination. Moreover, the reagents consumption is much lower in the method using the dual immunosensor since it only requires 2.5 μL each time while 100 μL of the same reagents are needed in the ELISA protocol.

Acknowledgments

Financial support of Spanish Ministerio de Economía y Competitividad, Research Projects CTQ2015-70023-R, and CTQ2015-71955-REDT, and NANOAVANSENS Program from Comunidad de Madrid (S2013/MT-3029), is gratefully acknowledged.

Appendix A. Supplementary data

Supplementary data related to this article can be found at http://dx.doi.org/10.1016/j.aca.2016.12.034.

References

[1] G. Liu, M. Qi, M.R. Hutchinson, G.Yang, E.M. Goldys, Recent advances in cytokine detection by immunosensing, Biosens. Bioelectron. 79 (2016) 810–821.
[2] J. Whicher, S. Evans, Cytokines in disease, Clin. Chem. 36 (1990) 1269–1281.
[3] A. Baraket, M. Lee, N. Zine, M.G. Trivella, M. Zabala, J. Bausells, M. Sigaud, N. Jaffrezic-Renault, A. Errachid, A fully integrated electrochemical bioMEMS fabrication process for cytokine detection: application for heart failure, Proc. Eng. 87 (2014) 377–379.
[4] S.S. Shaftel, W.S.T. Griffin, M.K. ÓBanion, The role of interleukin-1 in neuroinflammation and Alzheimer disease: an evolving perspective, J. Neuroinflam. 5 (2008) 7.
[5] M. Feldmann, F.M. Brennan, R.N. Maini, Role of cytokines in rheumatoid arthritis, Annu. Rev. Immunol. 14 (1996) 397–440.
[6] M.A. Palladino, F.R. Bahjat, E.A. Theodorakis, L.L. Moldawer, Anti-TNF-[alpha] therapies: the next generation, Nat. Rev. Drug Discov. 2 (2003) 736–746.
[7] K. Last-Barney, C.A. Homon, R.B. Faanes, V.J. Merluzzi, Synergistic and overlapping activities of tumor necrosis factor alpha and IL-1, J. Immunol. 141 (1988) 527–530.
[8] P. Musto, R. Matera, M.M. Minervini, C. Checchia-de Ambrosio, C. Bodenizza, A. Falcone, M. Carotenuto, Low serum levels of tumor necrosis factor and interleukin-1 beta in myelodysplastic syndromes responsive to recombinant erythropoietin, Haematologica 79 (1994) 265–268.
[9] N. Demircan, B.G. Safran, M. Soylu, M.M. Ozcan, S. Sizmaz, Determination of vitreous interleukin-1 (IL-1) and tumour necrosis factor (TNF) levels in proliferative diabetic retinopathy, Eye 20 (2006) 1366–1369.
[10] A.P. Di Battista, S.G. Rhind, M.G. Hutchison, S. Hassan, M.Y. Shiu, K. Inaba, J. Topolovec-Vranic, A.C. Neto, S.B. Rizoli, A.J. Baker, Inflammatory cytokine and chemokine profiles are associated with patient outcome and the hyperadrenergic state following acute brain injury, J. Neuroinflamm. 13 (2016) 40.
[11] C.E. Krause, B.A. Otieno, G.W. Bishop, G. Phadke, L. Choquette, R.V. Lalla, D.E. Peterson, J.F. Rusling, Ultrasensitive microfluidic array for serum proinflammatory cytokines and C-reactive protein to assess oral mucositis risk in cancer patients, Anal. Bioanal. Chem. 407 (2015) 7239–7243.
[12] V. Brailo, V. Vucicevic-Boras, J. Lukac, D. Biocina-Lukenda, I. Zilic-Alajbeg, A. Milenovic, M. Balija, Salivary and serum interleukin 1 beta, interleukin 6 and tumor necrosis factor alpha in patients with leukoplakia and oral cancer, Med. Oral Patol. Oral Cir. Bucal 17 (2012) 10–15.
[13] F.I. Fernandes Gomes, M.G. Brito Aragão, F.C. Barroso Barbosa, M. Marques Bezerra, V.de P. Teixeira Pinto, H. Vasconcelos Chaves, Inflammatory cytokines Interleukin-1β and tumour necrosis factor-α - novel biomarkers for the detection of periodontal diseases: a literature review, J. Oral Maxillofac. Res. 7 (2016) e2.
[14] L. Yuan, X. Hua, Y. Wu, X. Pan, S. Liu, Polymer-functionalized silica nanosphere labels for ultrasensitive detection of tumor necrosis factor-alpha, Anal. Chem. 83 (83) (2011) 6800–6809.
[15] Z. Yin, Y. Liu, L.-P. Jiang, J.-J. Zhu, Electrochemical immunosensor of tumor necrosis factor alpha based on alkaline phosphatase functionalized nanospheres, Biosens. Bioelectron. 26 (2011) 1890–1894.
[16] T. Li, Z. Si, L. Hu, H. Qia, M. Yang, Prussian Blue-functionalized ceria nanoparticles as label for ultrasensitive detection of tumor necrosis factor alpha, Sens. Actuators B 171– 172 (2012) 1060–1065.
[17] Y. Hou, T. Li, H. Huang, H. Quan, X. Miao, M. Yang, Electrochemical immunosensor for the detection of tumor necrosis factor alpha based on hydrogel prepared from ferrocene modified amino acid, Sens. Actuators B 182 (2013) 605–609.
[18] Z. Sun, L. Deng, H. Gan, R. Shen, M. Yang, Y. Zhang, Sensitive immunosensor for tumor necrosis factor alpha based on dual signal amplification of ferrocene modified self-assembled peptide nanowire and glucose oxidase functionalized gold nanorod, Biosens. Bioelectron. 39 (2013) 215–219.
[19] M. Mazloum-Ardakani, L. Hosseinzadeh, Z. Taleat, Two kinds of electrochemical immunoassays for the tumor necrosis factor α in human serum using screen-printed graphite electrodes modified with poly(anthranilic acid), Microchim. Acta 181 (2014) 917–924.
[20] J.T. La Belle, U.K. Demirok, D.R. Patelc, C.B. Cook, Development of a novel single sensor multiplexed marker assay, Analyst 136 (2011) 1496–1501.
[21] F. Bettazzi, L. Enayati, I. Campos Sánchez, R. Motaghed, M. Mascini, I. Palchetti, Electrochemical bioassay for the detection of TNF-a using magnetic beads and disposable screen-printed array of electrodes, Bioanalysis 5 (2013) 11–19.
[22] L. Yuan, W. Wei, S.Q. Liu, Label-free electrochemical immunosensors based on surface-initiated atom radical polymerization, Biosens. Bioelectron. 38 (2012) 79–85.
[23] S. Weng, M. Chen, C. Zhao, A. Liu, L. Lin, Q. Liu, J. Lin, X. Lin, Label-free electrochemical immunosensor based on $K_3[Fe(CN)_6]$ as signal for facile and sensitive determination of tumor necrosis factor-alpha, Sens. Actuators B 184 (2013) 1–7.
[24] T.S. Pui, P. Kongsuphol, S.K. Arya, T. Bansal, Detection of tumor necrosis factor (TNF-alpha) in cell culture medium with label free electrochemical impedance spectroscopy, Sens. Actuators B 181 (2013) 494–500.
[25] U. Eletxigerra, J. Martínez-Perdiguero, S. Merino, R. Villalonga, J.M. Pingarrón, S. Campuzano, Amperometric magnetoimmunoassay for the direct detection of tumor necrosis factor alpha biomarker in human serum, Anal. Chim. Acta 838 (2014) 37–44.
[26] P. Kongsuphol, H.H. Ng, J.P. Pursey, S.K. Arya, C.C. Wong, E. Stulz, M.K. Park, EIS-based biosensor for ultra-sensitive detection of TNF-α from non-diluted human serum, Biosens. Bioelectron. 61 (2014) 274–279.
[27] M. Mazloum-Ardakani, L. Hosseinzadeh, Highly-sensitive label-free immunosensor for tumor necrosis factor a based on Ag@Pt core–shell nanoparticles supported on MW CNTs as an efficient electrocatalyst nanocomposite, RSC Adv. 5 (2015) 70781–70786.
[28] M. Mazloum-Ardakani, L. Hosseinzadeh, A. Khoshroo, Label-free electrochemical immunosensor for detection of tumor necrosis factor α based on fullerene-functionalized carbon nanotubes/ionic liquid, J. Electroanal. Chem. 757 (2015) 58–64.
[29] U. Eletxigerra, J. Martinez-Perdiguero, S. Merino, Disposable microfluidic immuno-biochip for rapid electrochemical detection of tumor necrosis factor alpha biomarker, Sens. Actuators B 221 (2015) 1406–1411.
[30] G. Baydemir, F. Bettazzi, I. Palchetti, D. Voccia, Strategies for the development of an electrochemical bioassay for TNF- alpha detection by using a non-immunoglobulin bioreceptor, Talanta 151 (2016) 141–147.
[31] A.A. Green, M.C. Hersam, Properties and application of double-walled carbon nanotubes sorted by outer-wall electronic type, ACS Nano 5 (2011) 1459–1467.
[32] M. Pumera, Electrochemical properties of double wall carbon nanotube electrodes, Nanoscale Res. Lett. 2 (2007) 87–93.
[33] E. Moore, B.S. Flavel, A.V. Ellis, J.G. Shapter, Comparison of double-walled with single-walled carbon nanotube electrodes by electrochemistry, Carbon 49 (2011) 2639–2647.
[34] H.W. Ooi, S.J. Cooper, C.-Y. Huang, D. Jennins, E. Chung, N.J. Maeji, A.K. Whittaker, Coordination complexes as molecular glue for immobilization of antibodies on cyclic olefin copolymer surfaces, Anal. Biochem. 456 (2014) 6–13.
[35] M. Eguílaz, M. Moreno-Guzmán, S. Campuzano, A. González-Cortés, P. Yáñez-Sedeño, J.M. Pingarrón, An electrochemical immunosensor for testosterone using functionalized magnetic beads and screen-printed carbon electrodes, Biosens. Bioelectron. 26 (2010) 517–522.
[36] I. Ojeda, M. Moreno-Guzmán, A. González-Cortés, P. Yáñez-Sedeño, J.M. Pingarrón, Electrochemical magnetoimmunosensor for the ultrasensitive determination of interleukin-6 in saliva and urine using poly-HRP streptavidin conjugates as labels for signal amplification, Anal. Bioanal. Chem. 406 (2014) 6363–6371.
[37] Y. Dogan, S. Akarsu, B. Ustundag, E. Yilmaz, M.K. Gurgoze, Serum IL-1β, IL-2 and IL-6 in insulin-dependent diabetic children, Mediat. Inflamm. (2006) 1–6.
[38] O. Arica, M. Aral, S. Sasmaz, P. Ciragil, Serum levels of TNF-α, IFN-γ, IL-6, IL-8, IL-12, IL-17 and IL-18 in patients with active psoriasis and correlation with disease severity, Mediat. Inflamm. (2005) 273–279.

Supplementary information

Electrochemical immunosensor for simultaneous determination of interleukin-1 beta and tumor necrosis factor alpha in serum and saliva using dual screen printed electrodes modified with functionalized double–walled carbon nanotubes

E. Sánchez-Tirado, C. Salvo, A. González-Cortés, P. Yáñez-Sedeño*,

F. Langa[1], J.M. Pingarrón

Department of Analytical Chemistry, Faculty of Chemistry, University Complutense of Madrid, Ciudad Universitaria s/n, 28040-Madrid, Spain; [1]Instituto de Nanociencia, Nanotecnología y Materiales Moleculares (INAMOL), Universidad de Castilla-La Mancha, 45071-Toledo, Spain

*Corresponding author

Contents

S1.1. Effect of the antibodies loading and the time for incubation.

The influence of the amount of anti-IL or anti-TNF antibodies immobilized onto HOOC-Phe-DWCNTs/SPCEs using Mix&Go polymer was evaluated by checking the amperometric responses obtained with different immunosensors for 0 (unspecific) and 50 pg/mL IL-1β or TNF-α. The immunosensors preparation involved deposition of 5 µL of anti-IL or anti-TNF solutions prepared in the 2- 8 µg/mL or 1-5 µg/mL concentration range, respectively, and applying the procedure described in sections 2.4.1 and 2.4.2 with 0.5 µg/mL Biotin-anti-IL or Biotin-anti-TNF and 5 µg/mL of 1/2000 diluted poly-HRP-Strept. Figure S1a shows as the measured current values for IL-1β reached a maximum value for anti-IL loadings between 4 and 6 µg/mL. Regarding TNF-α, current values increased with anti-IL loading up to 4 µg/mL and slightly decreased for larger loading. Furthermore, the mentioned concentrations also provided the maximum specific to unspecific current ratios. Therefore, 6 µg/mL anti-IL and 4 µg/mL anti-TNF were selected for the preparation of the immunosensors. The time elapsed in incubation of anti-IL or anti-TNF was also optimized over the 30 to 90 min (IL-1β) and 30 to 60 (TNF-α) ranges. Results shown in Figure S1b and S1d indicated that an incubation time of 60 min was adequate for the preparation of both immunosensors.

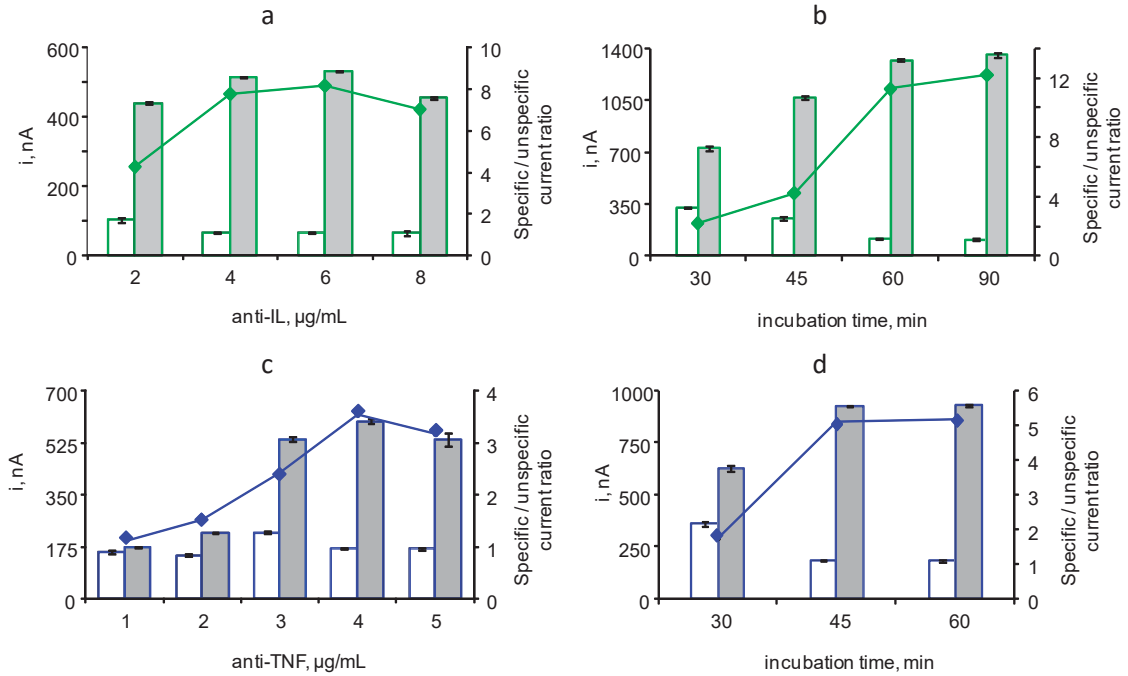

Figure S1. Effect of the antibodies loading (a) and (c) and incubation time (b) and (d) on the amperometric responses provided by the immunosensors constructed for the determination of IL-1β and TNF-α. Operational conditions: 3 µL COOH-Phe-DWCNTs; 5 µL Mix&Go, 60 min; 5 µL anti-IL (a) or anti-TNF (c),

60 min; 5 μL 2% BSA, 30 min; 5 μL 0 pg/mL IL-1β or TNF-α (white), and 50 pg/mL IL-1β or TNF-α (grey), 60 min; 5 μL 0.5 μg/mL Biotin-anti-IL (a) or Biotin-anti-TNF (c), 60 min; 5 μL 1/2000 diluted HRP-Strept, 20 min; 5 μL 6 μg/mL anti-IL (b) or 4 μg/mL anti-TNF (d); 5 μL 2% BSA, 30 min; 5 μL 0 pg/mL IL-1β or TNF-α (white), 25 pg/mL IL-1β (grey) or 10 μg/mL TNF-α (grey), 60 min; 5 μL 0.5 μg/mL Biotin-anti-IL (c) or Biotin-anti-TNF (d), 60 min; 5 μL 1/500 diluted poly-HRP-Strept (b) or 1/1000 diluted poly-HRP-Strept (d), 15 min.

S1.2. Effect of the biotinylated antibodies loading and the time for incubation.

In order to optimize the concentrations of Biotin-anti-IL and Biotin-anti-TNF, different immunosensors were prepared by incubating for 60 min IL-1β-anti-IL-Phe-DWCNTs/SPCE or TNF-α-anti-TNF-Phe-DWCNTs/SPCE, prepared in the absence (white) or in the presence of 250 pg/mL (IL-1β) (grey) (a) and in the absence (white) or 50 pg/mL (TNF-α) (grey) (c), in 0.25-1.0 μg/mL Biotin-anti-IL or 0.25-0.75 μg/mL Biotin-anti-TNF solutions. As it can be seen in Figure S2, specific and unspecific currents increased slightly for both cytokines in the tested concentration ranges showing the largest specific-to-unspecific current ratios at a 0.5 μg/mL concentration of each biotinylated antibody, which, accordingly, were selected for further work. Moreover, the effect of the incubation time in Biotin-anti-IL (b) or Biotin-anti-TNF (d) solutions was also evaluated over the 30 to 90 min interval by testing the amperometric responses obtained with the respective immunosensor in the absence of IL-1β or TNF-α (white), or in the presence of 25 pg/mL IL-1β or 10 pg/mL TNF-α (grey). In both cases, the largest specific-to-unspecific current ratio was obtained at 60 min and, therefore, this time was selected as the incubation time in this step.

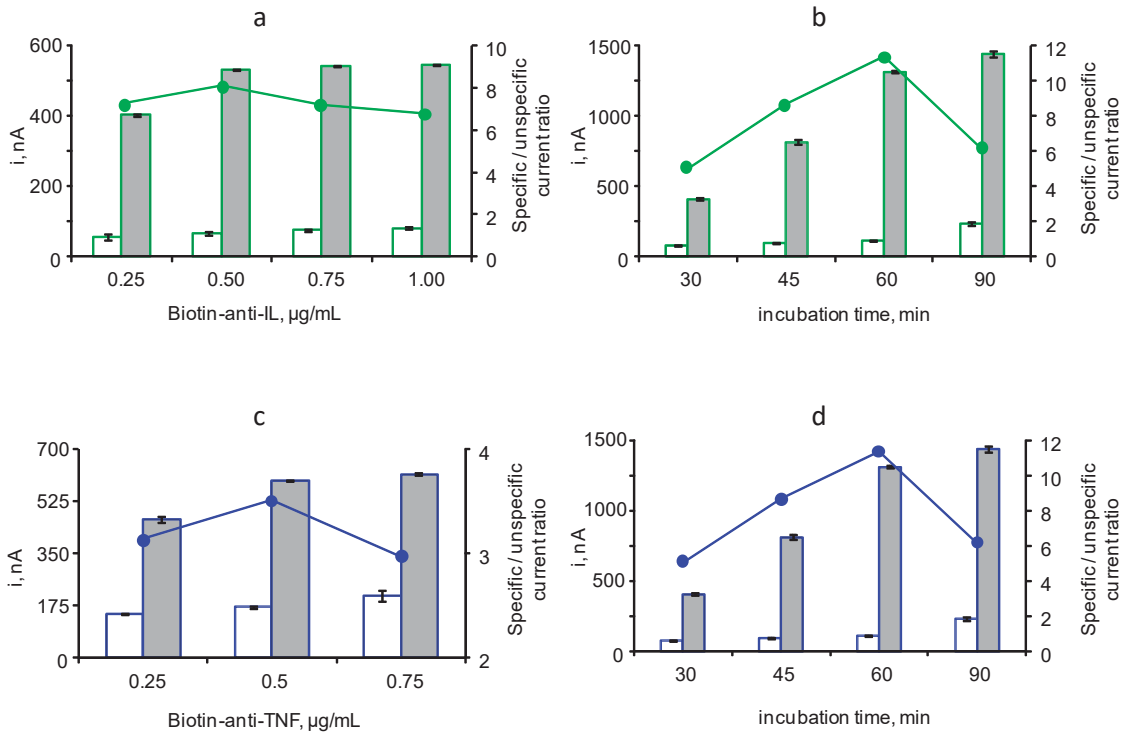

Figure S2. Effect of the biotinylated antibodies loading (a) and (c) and the incubation time (b) and (d) on the amperometric responses provided by the immunosensors constructed for the determination of IL-1β and TNF-α. 3 µL COOH-Phe-DWCNTs; 5 µL Mix&Go, 60 min; 5 µL 6 µg/mL anti-IL (a) or 4 µg/mL anti-TNF (c), 60 min; 5 µL 2% BSA, 30 min; 5 µL 0 pg/mL IL-1β or TNF-α (white), 250 pg/mL IL-1β or 50 pg/mL TNF-α (grey), 60 min; 5 µL Biotin-anti-IL (a) or Biotin-anti-TNF (c), 60 min; 5 µL 1/2000 diluted HRP-Strept, 20 min; 5 µL 6 µg/mL anti-IL (b) or 4 µg/mL anti-TNF (d); 5 µL 2% BSA, 30 min; 5 µL 0 pg/mL IL-1β or TNF-α (white), 25 pg/mL IL-1β or 10 µg/mL TNF-α (grey), 60 min; 5 µL 0.5 µg/mL Biotin-anti-IL (c) or Biotin-anti-TNF (d); 5 µL 1/500 diluted poly-HRP-Strept (b) or 1/1000 diluted poly-HRP-Strept (d), 15 min.

S1.3. Optimization of the blocking step.

In order to minimize unspecific adsorptions of immunoreagents on the electrode surface, various blocking strategies were evaluated. Various suitable reagents for this purpose (1% BSA, 2% BSA, casein, and powder milk) were tested. The protocol consisted of adding 5 µL of each blocking solution onto the anti-IL-Phe-DWCNTs/SPCE or the anti-TNF-Phe-DWCNTs/SPCE allowing incubation for a pre-established time of 30 min. Then, each immunosensor was prepared in the absence or in the presence of 6 µg/mL anti-IL or 4 µg/mL anti-TNF. The results shown in Figure S3a revealed a similar behaviour for IL-1β immunosensors using BSA or

casein, whereas in the case of TNF-α (Figure S3b), the largest specific-to-unspecific current ratio was obtained using 2% BSA. Therefore, this was selected as the blocking agent for further work. Moreover, 60 min incubation was selected as it was considered sufficient to effectively minimize unspecific adsorptions.

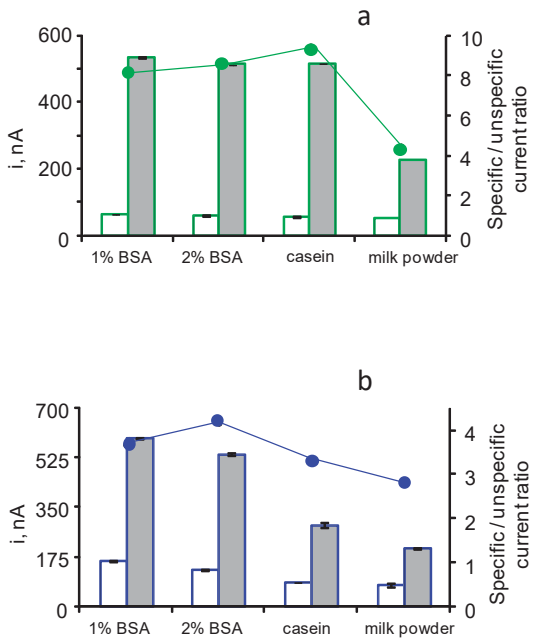

Figure S3. Optimization of the blocking step in the preparation of immunosensors for IL-1β (a) and TNF-α (b); 3 µL COOH–Phe–DWCNTs; 5 µL Mix&Go, 60 min; 5 µL 6 µg/mL anti-IL (a) or 4 µg/mL anti-TNF (b), 60 min; 5 µL blocking agent, 30 min; 5 µL 0 (white) or 250 (grey) pg/mL IL-1β (a), 0 (white) or 250 (grey) pg/mL TNF-α (b), 60 min; 5 µL 0.5 µg/mL Biotin-anti-IL (a) or Biotin-anti-TNF (b), 60 min; 5 µL 1/2000 HRP–Strept, 20 min.

S1.4.Optimization of the type and concentration of the HRP-label

The effect of different HRP-labels on the response of the immunosensors for IL-1β and TNF-α was also studied. Figure S3 a and c show the results obtained by using HRP-Strept , HRP–Strept–AuNPs, and two poly-HRP-Strept conjugates designed by (F) (from Fitzgerald) and (S) (from Sigma). As it was expected, HRP-Strept polymers provided a much bigger specific current in both cases because the more elevated concentration of enzymes in the label and, subsequently, the higher number of enzymes per antigen. As it can also seen, poly-HRP-Strept (F) provided the highest current and the best specific-to-unspecific current ratio, and thus, it was selected for further work.

Regarding the effect of the poly-HRP-Strept (F) dilution, Figure S4 b and d show a similar behavior for the specific currents with both immunosensors, exhibiting a decrease as the concentration of the enzyme label was lower. However, the specific-to-unspecific current ratio remained practically constant over the whole studied range of dilution factors for IL-1β immunosensors whereas slightly increased up to a 1/1000 dilution for the TNF-α immunosensors. These results led us to select 1/500 dilution of poly-HRP-Strept (F) for the preparation of IL-1β and TNF-α immunosensors.

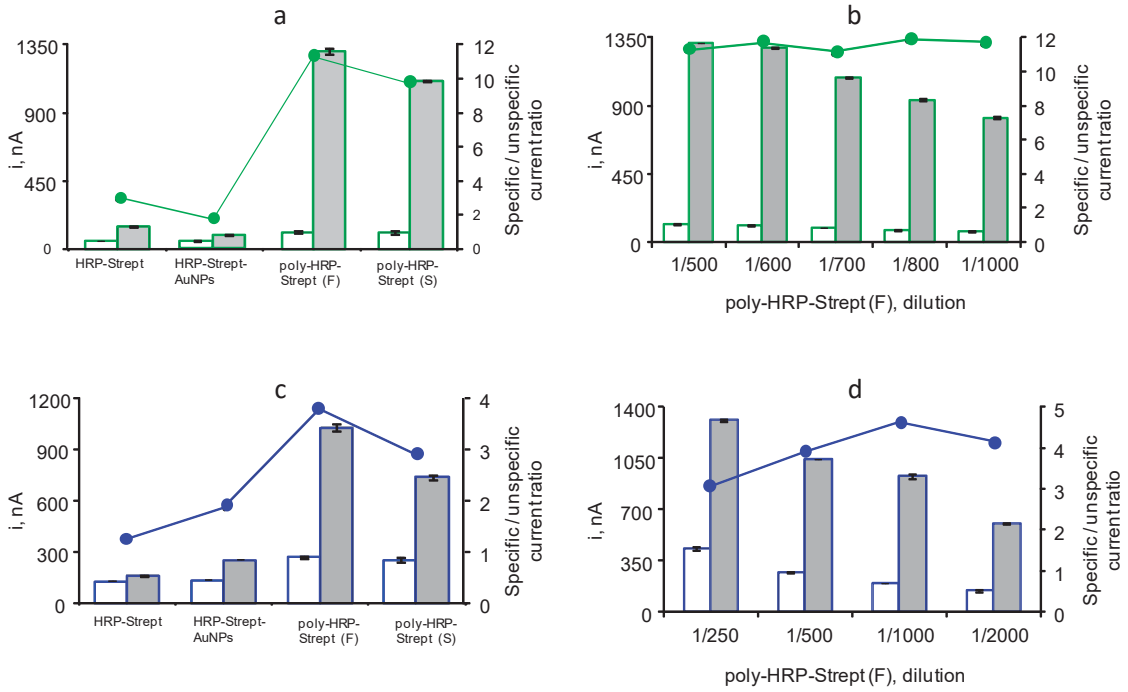

Figure S4. Optimization of the type (a,c) and concentration (b,d) of the HRP-label in the preparation of immunosensors for IL-1β (a, b) and TNF-α (c, d); 3 µL COOH–Phe–DWCNTs; 5 µL Mix&Go, 60 min; 5 µL 6 µg/mL anti-IL (a, b) or 4 µg/mL anti-TNF (c, d), 60 min; 5 µL blocking agent, 30 min; 5 µL 0 (white) or 25 (grey) pg/mL IL-1β (a, c), 0 (white) or 10 (grey) pg/mL TNF-α (c, d), 60 min; 5 µL 0.5 µg/mL Biotin-anti-IL (a, b) or Biotin-anti-TNF (c, d), 60 min; 5 µL poly-HRP–Strept (F) (b, d), 20 min.

1.5. Storage stability of the immunosensor

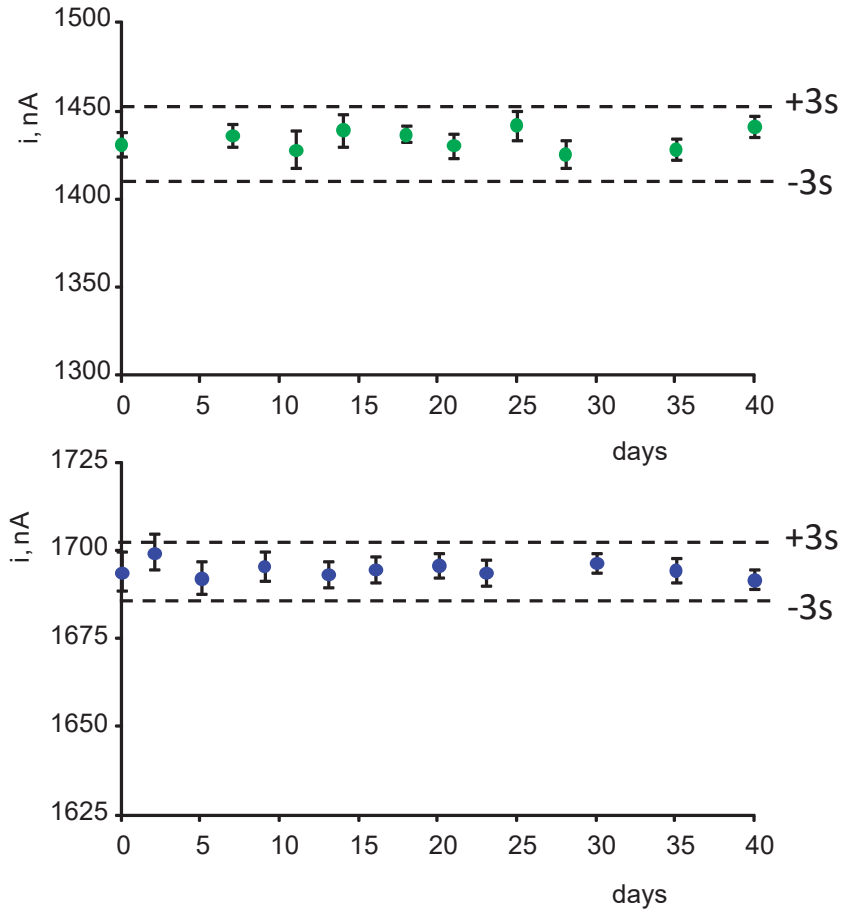

Figure S5. Control charts constructed to evaluate the storage stability of anti-IL-Phe-DWCNTs/SPCE and anti-TNF-Phe-DWCNTs/SPCE conjugates. Each point corresponded to the mean value of three successive measurements for 50 pg/mL IL-1β (green) or 100 pg/mL TNF-α (blue).

Biosensors and Bioelectronics 98 (2017) 240–247

Viologen-functionalized single-walled carbon nanotubes as carrier nanotags for electrochemical immunosensing. Application to TGF-beta 1 cytokine

Biosensors and Bioelectronics 98 (2017) 240–247

Contents lists available at ScienceDirect

Biosensors and Bioelectronics

journal homepage: www.elsevier.com/locate/bios

Viologen-functionalized single-walled carbon nanotubes as carrier nanotags for electrochemical immunosensing. Application to TGF-β1 cytokine

Esther Sánchez-Tirado[a], Luis M. Arellano[a,b], Araceli González-Cortés[a], Paloma Yáñez-Sedeño[a,*], Fernando Langa[a,b,*], José M. Pingarrón[a]

[a] Department of Analytical Chemistry, Faculty of Chemistry, University Complutense of Madrid, Ciudad Universitaria s/n, 28040 Madrid, Spain
[b] Instituto de Nanociencia, Nanotecnología y Materiales Moleculares (INAMOL), Universidad de Castilla-La Mancha, 45071 Toledo, Spain

ARTICLE INFO

Keywords:
Viologen
Transforming growth factor β1
Cytokine
Saliva
Electrochemical immunosensor

ABSTRACT

Viologen-SWCNT hybrids are synthesized by aryl-diazonium chemistry in the presence of isoamyl nitrite followed by condensation reaction of the resulting HOOC-Phe-SWCNT with 1-(3-aminoethyl)-4,4′-bipyridinium bromine and N-alkylation with 2-bromoethylamine. The V-Phe-SWCNT hybrids were characterized by using different spectroscopic techniques (FT-IR, Raman, UV–vis), TGA and Kaiser test. Viologen-SWCNTs were used for the preparation of an electrochemical immunosensor for the determination of the transforming growth factor β1 (TGF-β1) cytokine considered as a reliable biomarker in several human diseases. The methodology involved preparation of V-Phe-SWCNT(-HRP)-anti-TGF conjugates by covalent linkage of HRP and anti-TGF onto V-Phe-SWCNT hybrids. Biotinylated anti-TGF antibodies were immobilized onto 4-carboxyphenyl-functionalized SPCEs modified with streptavidin and a sandwich type immunoassay was implemented for TGF-β1 with signal amplification using V-Phe-SWCNT(-HRP)-anti-TGF conjugates as carrier tags. The analytical characteristics exhibited by the as prepared immunosensor (range of linearity between 2.5 and 1000 pg mL^{-1} TGF-β1; detection limit of 0.95 pg mL^{-1}) improve notably those reported with other previous immunosensors or ELISA kits. A great selectivity against other proteins was also found. The prepared immunosensor was validated by determining TGF-β1 in real saliva samples. Minimal sample treatment was required and the obtained results were in excellent agreement with those obtained by using a commercial ELISA kit.

1. Introduction

Viologens are 4,4´-bipyridine derivatives which exhibit reversible electrochemical responses at negative potentials corresponding to their three possible oxidation states, $V^{2+} \leftrightarrow V^{+\cdot} \leftrightarrow V^{o}$. The first reaction constitutes the basis for application of viologens as electron acceptors and electron transfer mediators to various proteins (Chen et al., 2009). The reversible redox behavior promotes the electron exchange between electrodes and proteins with the subsequent decrease in the ohmic overpotential (Lee et al., 2016). Taking advantage of this behavior, various electrochemical biosensors based on the use of viologens have been described. However, due to the solubility of viologen cations in aqueous solution and their high toxicity, immobilization on electrode surfaces using different strategies and materials is usually performed (Lee et al., 2016) (Ghica et al., 2005). An illustrative example of strategy not involving physical entrapment of viologen is the modification of a GCE based on the amino radical oxidation with subsequent formation of a carbon-nitrogen linkage on the electrode for the preparation of a hydrogen peroxide biosensor with horseradish peroxidase and gold nanoparticles (Jia et al., 2008). Another interesting approach relies on modification of a gold electrode with a self-assembled monolayer of thiol-functionalized viologen which was used to design a biosensor involving direct electron transfer of hemoglobin for the detection of H_2O_2 (Kafi et al., 2007).

Configurations using viologens have been implemented in the development of electrochemical immunosensors. A label-free design for the detection of α-fetoprotein was reported using gold nanoparticles functionalized by covalent surface capping with 1,1′-bis-(2-mercapto)-4,4′-bipyridinium dibromide (Liang et al., 2009). A platform for the construction of multi-array electrochemical immunosensors was prepared by immobilization of biotinylated viologen on modified polypyrrole-streptavidin films. In this strategy, the change in the electrochemical response of the redox molecule corresponding to the two electrons reduction of di-cationic to neutral viologen was monitored

* Corresponding authors.
E-mail addresses: yseo@quim.ucm.es (P. Yáñez-Sedeño), Fernando.Langa@uclm.es (F. Langa).

http://dx.doi.org/10.1016/j.bios.2017.06.063
Received 12 April 2017; Received in revised form 19 June 2017; Accepted 30 June 2017
Available online 01 July 2017
0956-5663/ © 2017 Elsevier B.V. All rights reserved.

after the antibody-antigen interaction (Miodek et al., 2016). The direct impedimetric detection of an anti-cholera toxin antibody was performed by using electropolymerized biotinylated poly(pyrrole-viologen) film as scaffold for the development of reagentless immunosensors (Gondran et al., 2010). The selective detection of α-fetoprotein (AFP) was performed by using an electrochemical immunosensor prepared by covalent immobilization of polyamidoamine (PAMAM) dendrimer-encapsulated AuNPs on a gold electrode followed by sequential immobilization of ethyleneamine-viologen as the redox marker and AFP antibody (Kavosi et al., 2014). Regarding DNA sensors, an interesting strategy involved a conjugate integrating an anthracene chromophore and a viologen moiety in the same molecular skeleton for discrimination between non-hybridized and hybridized surface-immobilized DNA (Conoci et al., 2014).

Viologens have been immobilized on materials such as graphene oxide (Park et al., 2012), conductive polymers (Gadgil et al., 2013), dendrimers (Kavosi et al., 2014) and carbon nanotubes (CNTs). Immobilization methods on CNTs included drop casting of viologen solution and electrochemical treatment by cyclic voltammetry (Swetha et al., 2012) (Lee et al., 2016), preparation of multilayers assembled through electrostatic interactions (Wang et al., 2008), and formation of composites (Wang et al., 2009).

Few examples of covalent attachment of viologens on CNTs have been described so far. Synthesis of an asymmetrically substituted viologen covalently anchored to SWCNTs through an ester linkage by reacting chlorinated purified SWCNTs with *N*-methyl-*N´*-(6-hydroxyhexyl)-4,4´-bipyridine was reported (Alvaro et al., 2005). More recently, Liu et al., 2013 linked covalently an electroactive organic electrolyte of viologen on MWCNTs through a diazonium coupling process to form layer-by-layer (LBL) multi-layers with poly(sodium-p-styrenesulfonate) at interfaces. A couple of redox waves in the potential range of −0.3 to −0.7 V vs. Ag/AgCl, corresponding to the electron transfer process of MWCNT-PhV^{2+} ↔ MWCNT-$PhV^{+\bullet}$ was observed.

Transforming growth factor β1 (TGF-β1) is a cytokine belonging to the structurally related group of multifunctional TGF-βs which regulates a variety of biological processes. In particular, TGF-β1 is involved in immune and inflammatory responses (Tsapenko et al., 2013) and is considered as a good biomarker of bladder carcinoma, liver fibrosis, or renal diseases. Normal levels of this protein are in the 0.1–25 ng/mL range in plasma of healthy individuals (Grainger et al., 2000). However, noticeable increases in circulating TGF-β1 can be found in patients suffering various types of cancer (Wickenhauser et al., 1995) or autoimmune disorders (Pfeiffer et al., 1996). Methods for the determination of this cytokine comprise immunoassays with ELISA kits involving sandwich type configurations and peroxidase-labeled or biotinylated immunoreagents. Regarding electrochemical immunosensors, very few methods can be found in the literature. An impedimetric design for the determination of TGF-β1 in serum was reported involving the preparation of a self-assembled monolayer of polyethylene glycol coated onto interdigitated electrodes. Covalent immobilization of antibodies allowed TGF-β1 determination in a linear range between 1 and 1000 ng/mL with a detection limit of 0.570 ng/mL (Yao et al., 2016). CNTs functionalized by click chemistry were used as scaffolds for the preparation of an electrochemical immunosensor for TGF-β1 determination in serum (Sánchez-Tirado et al., 2016). MWCNTs were functionalized by means of copper(I) catalyzed azide–alkyne cycloaddition followed by conjugation of an alkyne-functionalized IgG and assembling IgG-alkyne–azide–MWCNT conjugates for immobilization of antibodies. Once the target cytokine was sandwiched with biotinylated anti-TGF labeled with poly(HRP-Strept) conjugates, the affinity reaction was monitored amperometrically at −0.20 V using the hydroquinone/H_2O_2 system. The calibration plot for TGF-β1 exhibited a range of linearity extending between 5 and 200 pg mL^{-1}, and the limit of detection was 1.3 pg mL^{-1}. Recently, our group also developed an amperometric immunosensor for TGF-β1 using carboxylic acid-functionalized magnetic microparticles supported onto screen-printed carbon electrodes (SPCEs) to immobilize covalently the specific antibodies by means of Mix & Go polymer. A sandwich-type scheme was prepared with anti-TGF-biotin and conjugation with poly(HRP-Strept) for signal amplification. Amperometric measurements as described above provided a calibration plot with a linear range between 15 and 3000 pg mL^{-1} and a LOD value of 10 pg mL^{-1}. This configuration was validated by analyzing spiked urine at different TGF-β1 pg/mL concentration levels (Sánchez-Tirado et al., 2017). Moreover, an aptasensor for TGF-β1 involving aptamer-modified Au electrodes integrated with microfluidics was reported. Thiolated aptamers labeled with methylene blue were self-assembled on gold surfaces. The linear range covered up to 250 ng/mL with a detection limit of 1 ng/mL. This device was used to monitor TGF-β1 release from hepatic cells (Matharu et al., 2014).

This work reports a novel method for the preparation of viologen-SWCNT hybrids (V-Phe-SWCNTs) through aryl-diazonium chemistry in the presence of isoamyl nitrite followed by simple condensation reaction of the resulting HOOC-Phe-SWCNT with 1-(3-aminoethyl)-4,4′-bipyridinium bromine and N-alkylation with 2-bromoethylamine. The as prepared V-Phe-SWCNTs are used as carrier tags for signal amplification in the construction of an amperometric immunosensor for TGF-β1. Anti-TGF antibodies and HRP were immobilized on the synthesized V-Phe-SWCNT hybrids, and the target cytokine was sandwiched with V-Phe-SWCNT(-HRP)-anti-TGF conjugates and biotinylated antibodies immobilized onto SPCEs modified with streptavidin. The implementation of a sandwich type immunoassay allowed improved analytical characteristics to be obtained in terms of wider linear dynamic range of response and lower detection limit than those reported with other immunosensors and ELISA kits. In addition, a great selectivity against other proteins and ascorbic and uric acid was also found. The developed immunosensor was validated by determining TGF-β1 in real saliva samples with minimal sample treatment, and providing results in excellent agreement with those obtained by using a commercial ELISA kit.

2. Experimental

2.1. Reagents and solutions

All commercial solvents and reagents used for the synthesis of V-Phe-SWCNTs were employed without further purification. HiPco SWCNTs were purchased from NanoIntegris (www.nanointegris.com), with a diameter between 0.8–1.2 nm and length 100–1000 nm. Chicken biotinylated antibody (anti-TGF-Biotin), human TGF–β1, and mouse antibody (anti-TGF) were from R & D Systems. These reagents were included in the Duo Sets ELISA Development System (DY240-05). Horseradish peroxidase (HRP), streptavidin, hydrogen peroxide, hydroquinone, and terephthalic acid were from Sigma. 1–ethyl–3–(3–dimethylaminopropyl)carbodiimide(EDC),*N*–hydroxysulfosuccinimide (NHSS), and 4-aminobenzoic acid (4-ABA) were from Across. Sodium nitrite from Panreac was also used. Anti-TGF-Biotin solutions were prepared in Reagent Diluent 1 from Duoset® Ancillary Reagent Kit 1 (R & D Systems, DY007). Anti-TGF solutions were prepared in 0.1 M phosphate buffer solution of pH 7.4. This buffer solution was also used for preparing 0.5 mM solutions of D-biotin (Gerbu) used as blocking agent. 25 mM MES buffer solution of pH 5.0 prepared from 2–(N–morpholine) ethanosulfonic acid (Gerbu) was also used. Adiponectin (APN), tumor necrosis factor alfa (TNF–α) and interleukin 1 beta (IL–1β) from R & D Systems, cortisol and human inmunoglobulin G (IgG) from Sigma,interleukin 6 (IL–6) and interleukin 8 (IL–8) from Abcam, and bovine serum albumin (BSA, Gerbu) were tested as potential interfering compounds. Deionized water was obtained from a Millipore Milli-Q purification system (18.2 M Ω cm at 25 °C).

2.2. Apparatus and electrodes

Nuclear magnetic resonance 1 H and 13 C were recorded using Bruker Innova 400 MHz. Absorption spectra (UV–vis) were performed on Shimadzu UV 3600 spectrophotometer. The thermogravimetric analysis was performed on a Mettler Toledo TGA/DSC Linea Excellent under inert atmosphere of nitrogen with a rate of 10 °C/min, and the weight changes were recorded as a function of temperature. Raman measurements were carried out with a Renishaw inVia Reflex Confocal Raman Microscope at room temperature using laser excitation of 785 nm. Measurements were taken with 10 s of exposure times at varying numbers of accumulations. The laser spot was focused on the sample surface using a long working distance 100x objective. Raman spectra were collected on numerous spots on the sample and recorded with a Peltier cooled CCD camera. The sample was measured on glass without any sample preparation. The intensity ratio ID/IG was obtained by taking the peak intensities following any baseline corrections. FTIR spectrum were obtained on Avatar 370 Thermo Nicolet spectrophotometer using KBr pellets.

The following instruments were utilized for the preparation and functioning of the immunosensor: An INBEA potentiostat provided with the Ib Graph software was used for the amperometric measurements; electrochemical impedance spectroscopy was carried out with a μAutolab type III potentiostat (Ecochemie) controlled by FRA2 software. Screen-printed carbon electrodes (SPCEs, 110 DRP, ϕ 4 mm) purchased from DropSens (Oviedo, Spain) were used as working electrodes. These electrodes were provided with a silver pseudo-reference electrode and a carbon counter electrode. A Crison Basic 20+ pHmeter, an Elmasonic S-60 ultrasonic bath (Elma), an MPW-65R centrifuge from MPW Med. Instruments, a Vortex homogenizer and a magnetic stirrer, both from Velp Scientifica, were also employed.

2.3. Procedures

2.3.1. Functionalization of SWCNT

The preparation of viologen-SWCNT hybrid (V-Phe-SWCNT) was performed in three steps:

1. Synthesis of 1-(3-aminoethyl)-4,4′-bipyridinium bromine: A solution of 4,4′-bipyridine (500 mg, 3.2 mmol) and 2-bromoethylamine (71.4 mg, 0.32 mmol) in acetonitrile (10 mL) was refluxed for 1.5 h. After cooling, the precipitate was filtered and re-dissolved in hot DMF to remove the di-alkylated salt by filtration. In order to get the mono-alkylated product as a white solid, diethyl ether was added. Yield: 59%. ^{1}H NMR (400 MHz, D_2O); δ: 9.08 (d, J = 6.3 Hz, 2 H), 8.80 (d, 2 H), 8.52 (d, J = 6.3 Hz, 2 H), 7.95 (d, J = 6.3 Hz, 2 H), 5.06 (t, J = 6.5 Hz, 2 H), 3.78 (t, J = 6.5 Hz, 2 H).^{13}C NMR (100 MHz, D_2O); δ: 155.11, 149.91, 145.35, 142.31, 126.62, 122.54, 57.63, 39.11.
2. Synthesis of HOOC-SWCNT: A suspension of pristine-SWCNT (20 mg) in *N*-methyl-2-pyrrolidone (40 mL) was sonicated for 10 min, then 4-aminobenzoic acid (457 mg, 3.33 mmol, and isoamyl nitrite (0.54 mL, 3.98 mmol) were added. The mixture was stirred under argon atmosphere at 70 °C for 24 h. After cooling, the crude was filtered through PTFE membrane (Millipore 0.1 μm pore) and washed subsequently with NMP, MeOH and CH_2Cl_2, until the filtrate was clear, to obtain the carbon-based material as a black solid (23 mg).
3. Synthesis of viologen-SWCNT hybrid (V-Phe-SWCNT): SWCNT-Phe-COOH (8 mg) were dispersed in DMF anhydrous (20 mL) *N*,*N*′-dicyclohexylcarbodiimide (DCC) (21.9 mg, 0.11 mmol), hydroxybenzotriazole (HOBt) (14.4 mg, 0.11 mmol), and 1-(3-aminoethyl)-4,4′-bipyridinium bromine (16 mg, 0.08 mmol) were added to the mixture under argon atmosphere. The suspension was sonicated for 10 min and heated at 60 °C for 3 days. The solid was separated by filtration through a PFTE membrane (Millipore 0.1 μm pore) and washed several times with hot DMF, MeOH and CH_2Cl_2. Thereafter, the solid was re-dissolved in DMF, and 2-bromoethylamine (16 mg, 0.08 mmol) was added. The reaction mixture was heated at 120 °C for 24 h, and then filtered on a PFTE membrane (Millipore 0.1 μm pore). Finally, the solid was washed with DMF, MeOH and CH_2Cl_2 to get the V-Phe-SWCNTs (9.4 mg).

2.3.2. Preparation of V-Phe-SWCNT(-HRP)-anti-TGF conjugate

To obtain 100 μL of V-Phe-SWCNT(-HRP)-anti-TGF, 50 μL of a 200 mM EDC/NHSS solution prepared in 25 mM MES of pH 5.0 were mixed with 50 μL of 4 mg mL^{-1} terephthalic acid, and 100 μL of each 40 μg mL^{-1} HRP, 4 μg mL^{-1} anti–TGF. and 0.5 mg mL^{-1} aqueous V–SWCNT suspension. The mixture was incubated under magnetic stirring in the dark for 3 h. Once centrifuged at 8 °C and 14,000 rpm for 10 min, supernatant was retired and two washing steps with 500 μL of 0.1 M PBS of pH 7.4 were performed. Finally, the obtained conjugate was suspended in 100 μL of PBS.

2.3.3. Preparation of V-Phe-SWCNT(-HRP)-anti-TGF-TGF-β1-anti-TGF-Biotin-Strept/ SPCEs

In a first step, SPCEs were modified by grafting of a 4-ABA diazonium salt on the electrode surface. In order to do that, 20 mg of 4-ABA were dissolved in 2 mL of 1 M HCl and cooled with ice. Then, the diazonium salt was prepared by adding 2 mM $NaNO_2$ aqueous solution dropwise to this solution (38 μL for each 200 μL) with constant stirring. Next, 40 μL of the resulting solution was casted onto the SPCE and ten successive cyclic voltammetric scans between 0.0 and −1.0 V (ν=200 mV s^{-1}) were carried out. The modified electrodes were washed thoroughly with water and dried at room temperature. Dried ABA-g-SPCEs were activated by dropping 5 μL of EDC/NHSS (0.1 M each) prepared in MES buffer solution of pH 5.0 and allowed 30 min to stand. After rinsing with water, 5 μL of a 200 μg mL^{-1} streptavidin solution prepared in MES buffer of pH 5.0 were added and left to react for 1 h. Next, the electrodes were rinsed with water and dried. Immobilization of biotinylated antibody was further performed by adding 5 μL of a 7.5 μg mL^{-1} anti-TGF-Biotin prepared in Reagent Diluent 1 from Duoset® Ancillary Reagent Kit 1 (R & D Systems, DY007) on the modified electrode and left to stand for 60 min. Then, a blocking step was made by adding 5 μL of a 0.5 mg mL^{-1} biotin and left to incubate 30 min. Thereafter, 5 μL of standard TGF–β1 solutions or the samples were placed onto the electrode surface and incubated for 60 min. After washing with water and drying, 5 μL of V–SWCNT(-HRP)-anti-TGF were dropped onto the electrode and incubated for 60 min. Finally, the immunosensor was washed again and maintained with a drop of a 0.05 M PBS solution of pH 6.0 until the measurements were made.

2.3.4. Amperometric measurements

Amperometric measurements were performed by adding 45 μL of 0.5 M PBS of pH 6.0 to the immunosensor surface and applying a potential of −300 mV. Once the background current was stabilized, (around 100 s), 5 μL of 50 mM H_2O_2 were added and allowed standing for 200 s to complete the enzyme reaction.

2.3.5. Analysis of saliva

Saliva samples were obtained from volunteers and collected using a Salivette® collection device (Sarstedt). Briefly, once rinsed the mouth thoroughly with water, a cotton swab was inserted into the mouth and chewed for 1 min. Then, the swap saturated with saliva was inserted into the vial, sealed with the cap and centrifuged for 10 min at 3000 rpm. The determination was performed immediately by applying the procedure described above to 5 μL of undiluted saliva and interpolation of the amperometric response in the calibration plot constructed with standard solutions.

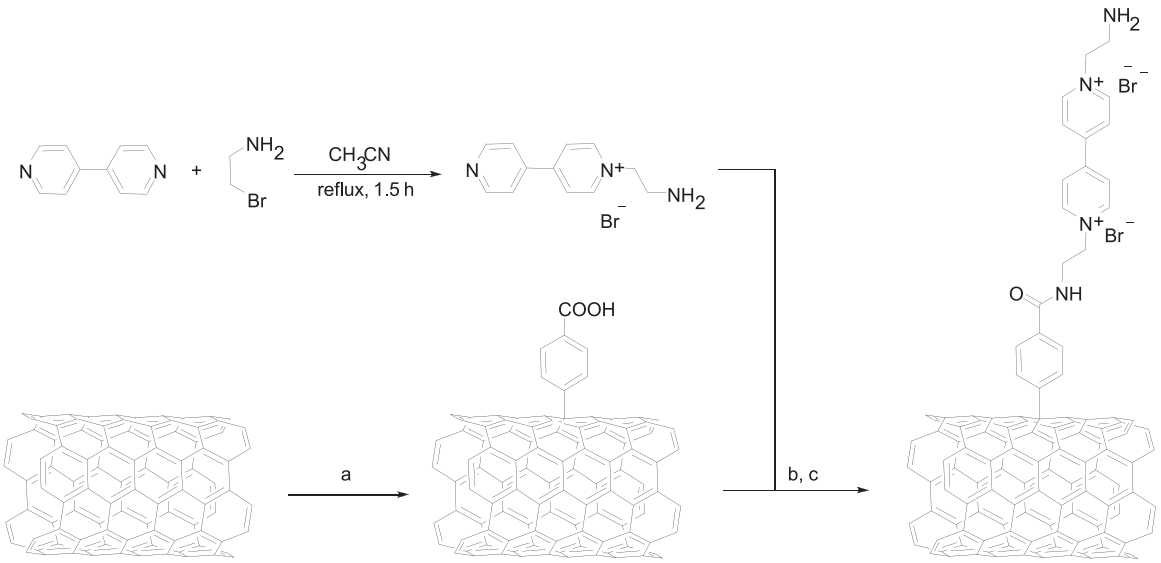

Scheme 1. Scheme showing the steps for the synthesis of V-Phe-SWCNTs. Reagents and conditions: (a) 4-aminobenzoic acid, isoamylnitrite, NMP, 70 °C for 24 h; (b) *1*-(3-aminoethyl)-4,4′-bipyridinium bromine, DCC, HOBt, at 60 °C, 3 days; (c) 2-bromoethylamine, DMF, 120 °C, 24 h.

3. Results and discussion

The synthesis of V-Phe-SWCNT hybrids was accomplished by following the procedure described in the Experimental section according with the Scheme 1. Briefly, careful mono-alkylation of viologen with 2-bromoethylamine in stoichiometric conditions afforded 1-(3-aminoethyl)-4,4′-bipyridinium bromine; functionalization of SWCNT was based on well-known aryl-diazonium chemistry in the presence of isoamyl nitrite (Palacin et al., 2009) followed by simple condensation reaction of the resulting HOOC-Phe-SWCNT with 1-(3-aminoethyl)-4,4′-bipyridinium bromine.

The V-Phe-SWCNT hybrids were characterized by using different spectroscopic techniques (FT-IR, Raman, UV–vis spectroscopies), TGA and Kaiser test. Details on this characterization are given in the Supplementary Material.

The functionalization degree of SWCNT hybrids and the amount of groups anchored to the nanotubes were quantified by TGA. Samples were heated over a temperature range of 40–1000 °C at a scanning rate of 10 °C/min under nitrogen atmosphere. At 600 °C, the thermogram shown in Fig. S1 shows a weight loss of 10.3% for *pristine*-SWCNT, 24.4% for HOOC-Phe-SWCNT and 43.6% for V-Phe-SWCNT. The corrected weight loss due to the functional groups on CNTs was estimated to be 14% for HOOC-Phe-SWCNT and 33.3% for V-Phe-SWCNT. Consequently, the number of phenyl acid functional groups in SWCNT was estimated as 1 per 50 carbon atoms, and with the same calculation, the number of viologen groups attached to the sidewall is approximately 1 per 114 carbon atoms.

Raman spectra (Fig. 1) of *pristine*-SWCNT showed the characteristics bands, a disorder mode (D-Band) with low intensity at 1292 cm^{-1} and a tangential mode (G-Band) at 1595 cm^{-1}(I_D/I_G =0.09). After functionalization, the intensity of the D-Band (I_D/I_G =0.54) increased (associated with the transformation of the sp^2 to sp^3 carbons), which indicated the incorporation of organic moiety on the surface of the CNT. Fig. S2(A) shows the radial breathing mode of the CNT (RBM zone) before and after Tour reaction. The reduction of the tubes intensity also confirms the incorporation of the different species on the wall. Furthermore, the G^+-Band is sensitive to charge transfer, as shown at Fig. S2(B), the G-Band is up-shifted by 2 cm^{-1} in the V-Phe-SWCNT as compared to *pristine*-SWCNT due to the p-doping (Straub et al., 2014) (Voggu et al., 2008). This result confirmed that the electron-acceptor viologen was attached on the skeleton of SWCNT.

FT-IR spectroscopy provided important information about the

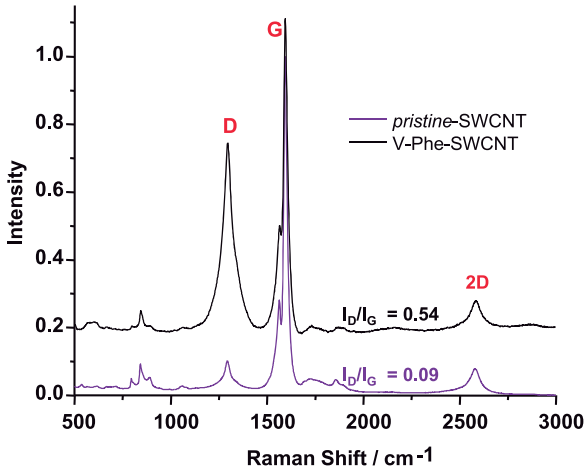

Fig. 1. Raman spectra (785 nm excitation) of *pristine*-SWCNT and V-Phe-SWCNT. The relative degree of functionalization was calculated by dividing the intensity of the D-Band by the G-Band.

covalent linkage of the viologen on the surface of SWCNT (Fig. S3). Comparing with *pristine*-SWCNT, V-Phe-SWCNT showed the characteristic bands of the skeletal in-plane vibrations of graphitic domains at 1554 cm^{-1}, the aliphatic C-H stretching mode at 2919 $cm^{-1}$and aromatic C-H nearby 3005 cm^{-1}. Furthermore, the appearance of strong peaks attributed to the viologen units were clearly observed at 3450 cm^{-1} (2x N-H vibrations), and 1095 cm^{-1} (C-N bond). In addition, a new peak at 1642 cm^{-1} was observed which can be assigned to an amide carbonyl stretching mode indicating the chemical attachment of the viologen on the SWCNT wall. In agreement with Raman and FT-IR information, UV–vis spectra of the V-Phe-SWCNT hybrid (Fig. S4) revealed the presence of the viologen unit by the appearance of a peak at 382 nm conversely to that observed with the *pristine*-SWCNT. The presence of primary amine on the V-Phe-SWCNT hybrid was determined by using the Kaiser test (Tuci et al., 2012).

3.1. Preparation of the V-Phe-SWCNT(-HRP)-anti-TGF-TGF-β1-anti-TGF-Biotin-Strept/ SPCE immunosensor

The methodology employed for the preparation of the immunosensor involved the following steps: a) preparation of V-Phe-SWCNT(-

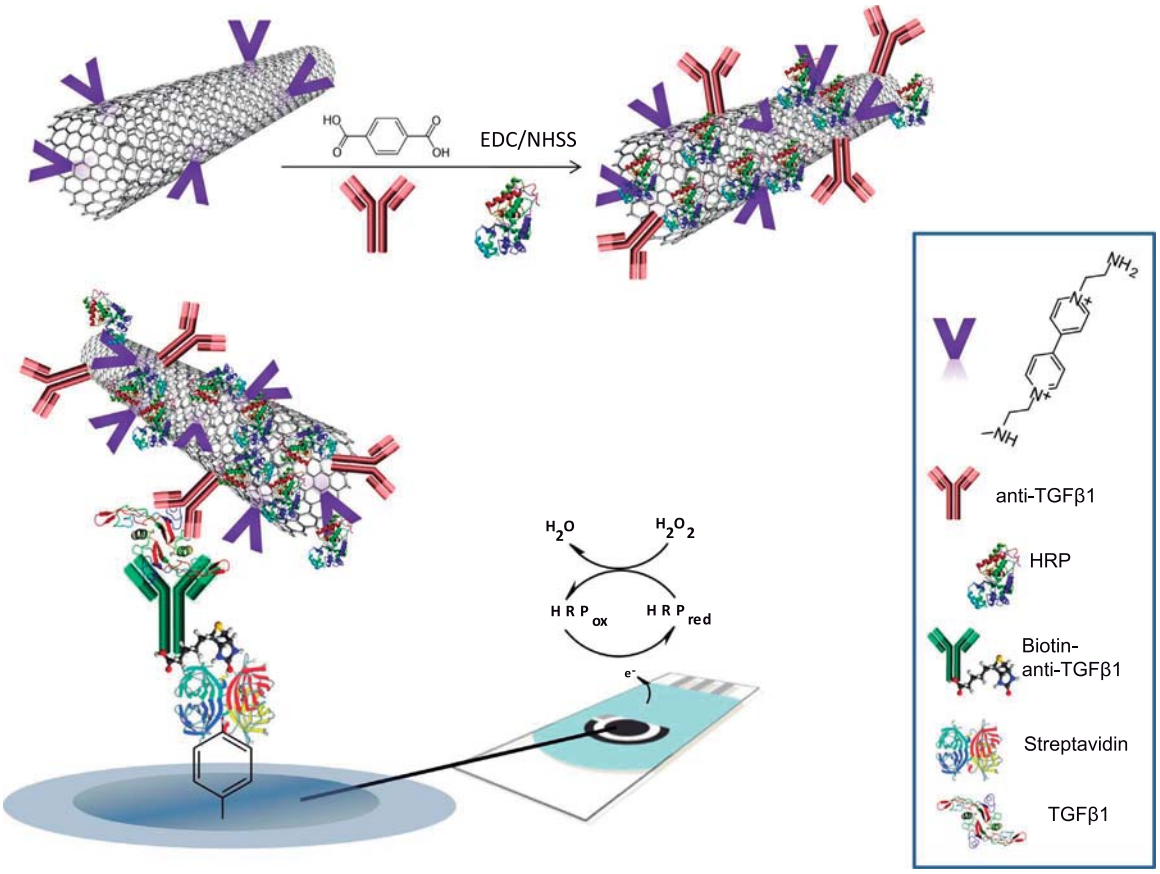

Fig. 2. Schematic display of the different steps involved in the construction of an amperometric immunosensor for TGF-β1 using V-Phe-SWCNT hybrids.

HRP)-anti-TGF conjugates by covalent linkage of HRP and anti-TGF onto V-Phe-SWCNT hybrids; b) construction of the immunosensing platform by immobilizing biotinylated antibodies onto 4-carboxyphenyl-functionalized SPCEs modified with covalently bonded streptavidin; c) implementation of a sandwich type immunoassay for TGF-β1 with signal amplification through the use of V-Phe-SWCNT(-HRP)-anti-TGF conjugates as carrier tags. The protocols used were described in the Experimental section, and Fig. 2 shows schematically these steps and the reaction providing the electrochemical response. The proposed strategy took advantage of both the good performance of grafted electrochemical scaffolds for covalent immobilization of immunoreagents, and the amplification of the electrochemical responses with V-Phe-SWCNT(-HRP)-anti-TGF conjugates. Modification of carbon electrodes through free radical grafting is known to provide compact and stable monolayers with specific functionalities. In the followed method, the electrochemical reduction of diazonium salt of 4-ABA onto SPCEs was performed followed by streptavidin immobilization by means of EDC/NHSS chemistry. The experimental conditions used in this step were those optimized previously (Moreno-Guzmán et al., 2012).

Regarding V-Phe-SWCNT(-HRP)-anti-TGF conjugates used as signals amplification tags, they were prepared by covalent immobilization of HRP and anti-TGF on the V-Phe-SWCNTs. In order to attain the maximum number of biomolecules immobilized on the nanotubes conjugate, covalent attachment to carboxylic groups at HOOC-Phe-SWCNTs was performed after activation with EDC/NHSS system and, furthermore, terephthalic acid was used as carbonyl-terminated linker for covalently immobilization onto amino groups of viologen moiety (Rahim Ruslinda et al., 2013).

Characterization of V-Phe-SWCNT(-HRP)-anti-TGF by UV–vis and FT-IR spectroscopies was also made with the results showed in the Supplementary Material (Fig. S5). Absorption spectra of V-Phe-SWCNT(-HRP)-anti-TGF shows the band at 266 nm corresponding to the presence of the antibody (see Fig. S5A), which confirmed the successful formation of the hybrid. Regarding FT-IR spectrum of V-Phe-SWCNT-HRP-anti-TGF (Fig. S5B) it showed a broader band for the characteristic O-H bending vibration at 3429 cm^{-1}, besides to new bands in the fingerprint region, which confirmed the antibody attachment, while the characteristic bands of V-SWCNT-Phe were maintained. In addition, V-Phe-SWCNT(-HRP)-anti-TGF displayed new bands at 803 cm^{-1}, around 656 cm^{-1} and 478 cm^{-1}, which are associated with the bound of antibody.

Fig. 3 shows cyclic voltammograms recorded in the 0.0 to −0.8 V potential range (vs. Ag pseudo-reference electrode) at V-Phe-SWCNT/GCE (curves 1 and 3) and V-Phe-SWCNT-HRP/GCE (curves 2 and 4) for solutions prepared in absence and in the presence of H_2O_2. As expected, the V-Phe-SWCNT-HRP/SPCE provided more sensitive response to the reduction of H_2O_2 which can be attributed to the role of V-Phe-SWCNT as mediator of the HRP catalytic reaction (Dong et al., 1997). This behavior is in agreement with that reported by Jia[5] for the electrochemical reduction of H_2O_2 at a glassy carbon electrode modified with gold nanoparticles-N,N′-bis(3-aminopropyl-4,4′-bipyridinium) tetrabromide (AuNPs/ BAPV/GCE) in the absence and in the presence of HRP. The following reaction scheme was suggested for the electrocatalytic process (Quan et al., 2010).

According with the cyclic voltammograms, a detection potential of − 0.3 V was selected for the amperometric measurements of H_2O_2 reduction and the subsequent determination of TGF-β1. Although the cathodic current increases as the potential is more negative, the above value was chosen to avoid potential interferences from electroactive substances present in real samples.

The variables involved in the preparation of the immunosensor for TGF-β1 were optimized. The effect on the electrochemical responses of the following parameters were tested: a) the loadings of HRP and anti-TGF antibody onto V-Phe-SWCNT; b) the streptavidin loading onto

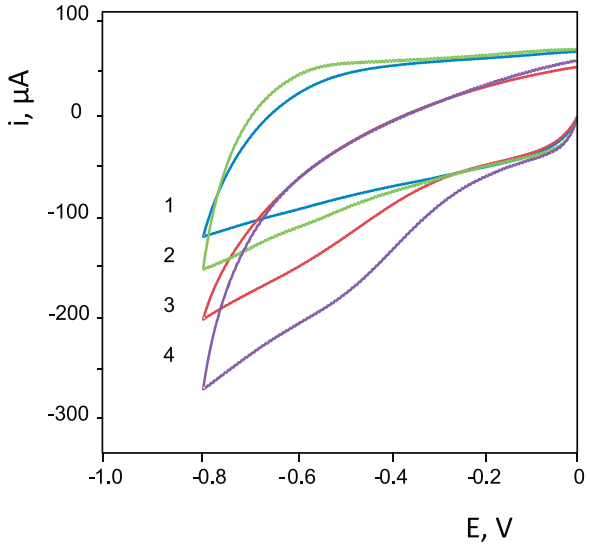

Fig. 3. Cyclic voltammograms recorded in 0.1 M phosphate buffer solution (voltammograms 1 and 2) containing 0.044 mM H_2O_2 (voltammograms 3 and 4) at: (1) V-Phe-SWCNT/GCE (voltammograms 1 and 3) and V-Phe-SWCNT-HRP/GCE (voltammograms 2 and 4).

SPCEs and c) the biotinylated antibody loading onto Strept-SPCEs. Other variables involved in the preparation of the modified electrodes such as the experimental conditions for grafting of SPCEs with 4-ABA diazonium salt or the amount of EDC/NHSS for covalent immobilization of biomolecules were optimized previously (Moreno-Guzmán et al., 2012). Details on these optimization studies are provided in Supplementary Material and Figs. S6 and S7.

3.2. Analytical characteristics of the immunosensor

Fig. 4 shows the calibration plot for TGF-β1 constructed with the developed immunosensor under the optimized working conditions. Error bars were calculated from measurements carried out with three different immunosensors in each case. In addition, some typical recorded amperograms used for the construction of the calibration graph are also displayed. The steady state current vs. logarithm of TGF-β1 concentration follows the adjusted equation i, nA = (332 ± 9) log [TGF-β1], pg mL^{-1} - (99 ± 18) (r^2=0.996) with a range of linearity extending between 2.5 and 1000 pg mL^{-1} TGF-β1. This range covers almost three orders of magnitude and is adequate for the determination of the cytokine in clinical samples taking into account the expected concentrations, at ng mL^{-1} level, in plasma (Grainger et al., 2000). The limit of detection, 0.95 pg mL^{-1}, was calculated according to the 3 s_b criterion, where s_b was estimated as the standard deviation, expressed in concentration units, of 10 blank current measurements (0 ng mL^{-1} TGF-β1). These analytical characteristics improve notably those reported with other previous immunosensors. For example, the lowest concentration in the calibration plot, 2.5 pg mL^{-1}, is six times lower and the limit of detection ten times lower than the corresponding values reported for immunosensors constructed using carboxylated magnetic beads (Sánchez-Tirado et al., 2017). Moreover, the immunosensor described in this work provides a calibration plot covering a wider linear range of concentrations (extending up to almost an order of magnitude larger) with a slope 60 times higher and a slightly lower limit of detection than the values achieved with an immunosensor prepared through click chemistry (Sánchez-Tirado et al., 2016). The developed immunosensor also exhibits a LOD value remarkably smaller than those provided with the aptasensor (1 ng mL^{-1}) (Matharu et al., 2014) and the impedimetric immunosensor (0.570 ng mL^{-1}) (Yao et al., 2016). Most importantly, the analytical characteristics achieved with the proposed immunosensor also improve those claimed for the commercial ELISA kits. For example, Duo Sets ELISA Development System (DY240-05) from R & D Systems (www.rndsystems. com/products/human-tgf-beta-1-duoset-elisa_-dy240) provides a calibration graph with a linear absorbance vs log [TGF-β1] ranging between 31 and 1000 pg mL^{-1}, and requires an assay time of 5 h 20 min which is remarkably longer than the time needed for preparing and using the developed electrochemical immunosensor (2 h 30 min). In both cases, the assay time was counted since the capture antibody was immobilized.

The reproducibility of the amperometric responses obtained with different immunosensors was evaluated by preparing sets of immunosensors both on the same day and on different days using a new anti-TGF-Biotin-Strept/SPCE in each case. Relative standard deviation (RSD) values of 3.4% and 3.1% (n=5) were calculated for the assays performed on the same day in the absence and in the presence of 125 pg mL^{-1} TGF-β1, respectively. In addition, RSD values of 6.5% and 7.2% (n=5) were obtained, respectively, for the measurements made on different days. These results reveal the good level of precision achieved in the fabrication and functioning of the developed immunosensor. Moreover, the storage ability of anti-TGF-Biotin-Strept/SPCE conjugates was also tested. Different anti-TGF-Biotin-Strept/SPCEs were prepared on the same day, stored under humidity conditions at 4 °C, and employed to prepare immunosensors to measure 125 pg mL^{-1} TGF- β1 on different days. The results obtained (not shown) indicated that the immunosensor responses remained within the control limits at ± 3 s, were s was the standard deviation of the measurements

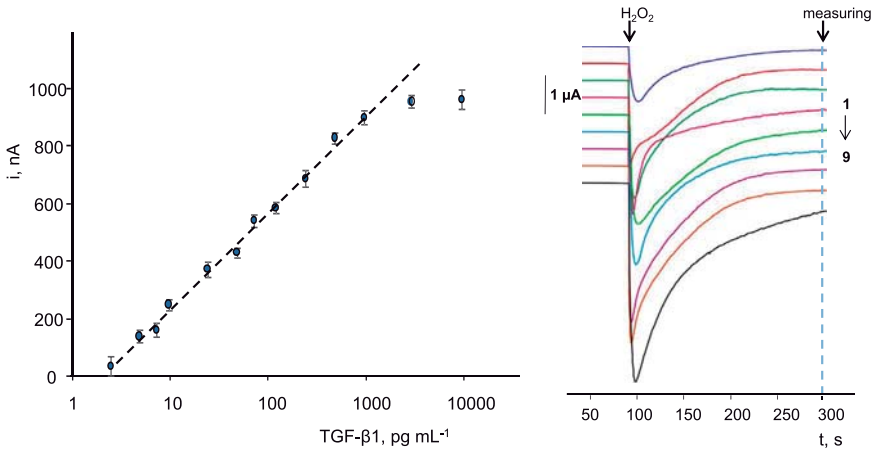

Fig. 4. Calibration plot (left) and amperograms recorded (right) for the amperometric determination of TGF-β1 with the V-Phe-SWCNT(-HRP)-anti-TGF-TGF-β1- anti-TGF-Biotin-Strept/SPCE immunosensor; TGF-β1, µg mL^{-1}: 5 (1); 7.5 (2); 10 (3); 25 (4); 50 (5); 75 (6); 125 (7); 250 (8); 500 (9).

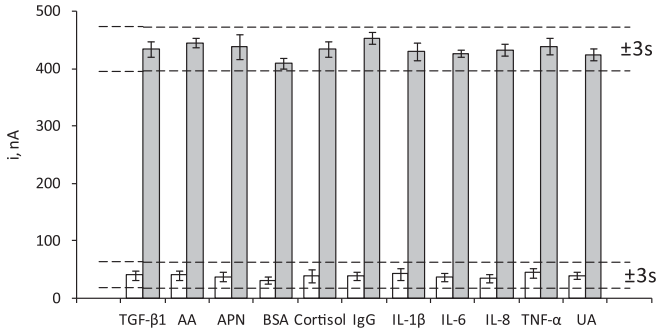

Fig. 5. Amperometric responses measured with V-Phe-SWCNT(-HRP)-anti-TGF-TGF-β1-anti-TGF-Biotin-Strept/SPCE immunosensors for 0 (white) and 50 (grey) pg mL^{-1} TGF-β1 standards in the absence and in the presence of 370 μg mL^{-1} ascorbic acid (AA), 5 pg mL^{-1} adiponectin (APN), 50 ng mL^{-1} bovine serum albumin (BSA), 12 ng mL^{-1} cortisol, 50 ng mL^{-1} immunoglobulin G (IgG), 50 pg mL^{-1} interleukin 1 beta (IL-1β), 50 pg mL^{-1} interleukin 6 (IL-6), 250 pg mL^{-1} interleukin 8 (IL-8), 10 pg mL^{-1} tumoral necrosis factor alpha (TNF-α) and 50 μg mL^{-1} uric acid (UA).

Table 1
Determination of TGF-β1 in real saliva samples.

TGF–β1 Saliva	Immunosensor (*n* = 5), pg/mL	ELISA (*n* = 4), pg/mL
smoker	27.6 ± 0.2	27.3 ± 0.2
smoker	26.4 ± 0.5	26.3 ± 0.1
non-smoker	21.2 ± 0.6	21.2 ± 0.1
non-smoker	22.8 ± 0.3	22.7 ± 0.5

(n=10) carried out on the first working day, for at least 30 days (no longer storage times were tested) demonstrating the excellent stability of the anti-TGF-Biotin-Strept/SPCE conjugates. In addition, the stability of V-Phe-SWCNT(-HRP)-anti-TGF conjugates was also checked by measuring 125 pg mL^{-1} TGF- β1 on different days with immunosensors constructed with different V-Phe-SWCNT(-HRP)-anti-TGF conjugates prepared on the same day, and stored in phosphate buffer solution of pH 7.4, at 8 °C. The immunosensor responses remained within the control limits at ± 3 s for at least 14 days.

A great selectivity against other proteins was also found. Fig. 5 displays the immunosensor amperometric responses in the absence and in the presence of 50 pg mL^{-1} TGF-β1, and in the presence of 5 pg mL^{-1} adiponectin (APN), 50 ng mL^{-1} bovine serum albumin (BSA), 12 ng mL^{-1} cortisol, 50 ng mL^{-1} human immunoglobulin G (IgG), 50 pg mL^{-1} interleukin 1 beta (IL–1β), 50 pg mL^{-1} interleukin 6 (IL–6), 250 pg mL^{-1} interleukin 8 (IL–8), and 10 pg mL^{-1} tumoral necrosis factor alpha (TNF–α). These concentrations are those expected according to the literature in healthy individuals. As it is clearly seen in Fig. 5, no significant interference was apparent for any potential interfering biomolecule. Interestingly, the moderate detection potential used (–300 mV) prevents the interference from electroactive species usually present in biological samples such as ascorbic (AA) and uric (UA) acids.

3.3. Determination of TGF-β1 in saliva

The usefulness of the immunosensor for the determination of low TGF-β1 concentrations in real samples was evaluated by analyzing saliva following the procedure described in Section 2.3.5. Saliva from four volunteers were analyzed. Firstly, the possible existence of matrix effects was tested by comparing the slopes value of the calibration plot constructed by successive addition of aliquots of TGF-β1 standards to the sample with that measured with the calibration graph prepared with analyte standard solutions. The application of the Student *t*-test provided t_{exp} values 0.969, 0.615, 0.254 and 0.221 lower than the tabulated one, t_{tab} = 2.179 for α = 0.05 and n=5. Therefore, the determination of TGF-β1 in saliva can be performed directly by interpolation of the amperometric current measured with the immunosensor for an aliquot of the undiluted sample, into the calibration plot constructed with standard solutions. The concentrations found in the analysis of the real samples (for two smoker and two non-smoker individuals) were compared with the results provided with a commercial ELISA kit (Table 1). As it can be seen, there is an excellent agreement between the results obtained by both methods. TGF-β1 concentration values of 24 pg mL^{-1} and 25 pg mL^{-1} TGF-β1 have been reported in the literature in saliva of healthy individuals (Yousefzadeh et al., 2006; Brand et al., 2014). Therefore, the values calculated with the immunosensor are also in good agreement with reported data. All these results demonstrated the usefulness of the developed immunosensor for the analysis of TGF-β1at low concentration levels in saliva with minimal sample treatment.

4. Conclusions

Viologen-SWCNTs hybrids, prepared using a novel method by aryldiazonium chemistry in the presence of isoamylnitrite followed by condensation of the resulting HOOC-Phe-SWCNT with 1-(3-aminoethyl)-4,4′-bipyridinium bromine and N-alkylation with 2-bromoethylamine, have been used as carrier tags for signal amplification in the construction of an amperometric immunosensor for TGF-β1. The implementation of a sandwich type immunoassay allowed improved analytical characteristic to be obtained in terms of wider linear dynamic range of response and lower detection limit than those reported with other previous immunosensors and those claimed for ELISA kits. In addition, a great selectivity against other proteins and ascorbic and uric acid was also found. The developed immunosensor was applied to the determination of TGF-β1 in saliva samples with minimal sample treatment and with results in excellent agreement with those obtained by using a commercial ELISA kit.

Acknowledgement

The financial support of projects CTQ2015-70023-R and CTQ2016-79189-R (Spanish Ministry of Economy and Competitivity Research Projects), S2013/MT-3029 (NANOAVANSENS Program from the Comunidad de Madrid) and PEII-2014-014-P (Junta de Comunidades de Castilla-La Mancha) are gratefully acknowledged.

Appendix A. Supporting information

Supplementary data associated with this article can be found in the online version at doi:10.1016/j.bios.2017.06.063.

References

Alvaro, M., Aprile, C., Atienzar, P., Garcia, H., 2005. J. Phys. Chem. B 109, 7692–7697.
Brand, H.S., Ligtenberg, A.J.M., Veerman, E.C.I., 2014. Saliva and wound healing, In: ed. p. 56; Ligtenberg, A.J.M., Veerman, E.C.I. (Eds.) Saliva: Secretion and functions, Monogr. Oral Sci, Vol 24, Karger, Basel, p.56.
Chen, G.P., Wang, X., Liu, A.-R., Quan, D.J., 2009. Mater. Sci. Eng. C. 29, 925–929.
Conoci, S., Mascali, A., Pappalardo, F., 2014. RSC Adv. 4, 2845–2850.
Dong, S., Li, J., 1997. Bioelectrochem. Bioenerg. 42, 7–13.
Gadgil, B., Damlin, P., Aaritalo, T., Kankare, J., Kvarnström, C., 2013. Electrochim. Acta 97, 378–385.
Ghica, M.E., Brett, C.M.A., 2005. Anal. Chim. Acta 532, 145–151.
Gondran, C., Orio, M., Rigal, D., Galland, B., Bouffier, L., Gulon, T., Cosnier, S., 2010. Electrochem. Commun. 12, 311–314.
Grainger, D.J., Mosedale, D.E., Metcalfe, J.C., 2000. 11, 133–145.
Jia, J., 2008. Microchim. Acta 163, 237–241.
Kafi, A.K.M., Lee, D.Y., Park, S.-H., Soo Kwon, Y., 2007. Microchem. J. 85, 308–313.
Kavosi, B., Hallaj, R., Teymourian, H., Salimi, A., 2014. Biosens. Bioelectron. 59, 389–396.
Lee, D., Kim, Y.H., Park, S., 2016. J. Electrochem. Soc. 163, G93–G98.
Liang, W., Yi, W., Li, S., Yuan, R., Chen, A., Chen, S., Xiang, G., Hu, C., 2009. Clin. Biochem 42, 1524–1530.

Liu, J., Chen, M., Qian, D.J., 2013. Colloids Surf., A 436, 953–960.
Matharu, Z., Patel, D., Gao, Y., Haque, A., Zhou, Q., Revzin, A., 2014. Anal. Chem. 86, 8865–8872.
Miodek, A., Anh, H.Q., Sauriat-Dorizon, H., Korri-Youssoufi, H., 2016. Electroanalysis 28, 1–10.
Moreno-Guzmán, M., Ojeda, I., Villalonga, R., González-Cortés, A., Yáñez-Sedeño, P., Pingarrón, J.M., 2012. Biosens. Bioelectron. 35, 82–86.
Palacin, T., Le Khanh, H., Jousselme, B., Jegou, P., Filoramo, A., Ehli, C., Guldi, D., Campidelli, S., 2009. J. Am. Chem. Soc. 131, 15394–15402.
Park, J.H., Xue, H., Jung, J.K., Ryu, K., 2012. Korean J. Chem. Eng. 29, 1409–1412.
Pfeiffer, A., Middelberg-Bisping, K., Drewes, C., Schatz, H., 1996. Diabetes Care 19, 1113–1117.
Quan, D., Nagarale, R.K., Shina, W., 2010. Electroanalysis 22, 2389–2398.
Rahim Ruslinda, A., Tanabe, K., Ibori, S., Wang, X., Kawarada, H., 2013. Biosens. Bioelectron. 40, 277–282.
Sánchez-Tirado, E., González-Cortés, A., Yáñez-Sedeño, P., Pingarrón, J.M., 2016. Analyst 141, 5730–5737.
Sánchez-Tirado, E., Martínez-García, G., González-Cortés, A., Yáñez-Sedeño, P., Pingarrón, J.M., 2017. Biosens. Bioelectron. 88, 9–14.
Straub, V., Gallego, A., de la Torre, G., Chamberlain, T.W., Khlobystov, A.N., Torres, T., Guldi, D.M., 2014. Faraday Discuss. 173, 233–256.
Swetha, P., Kumar, A.S., 2012. ECS Electrochem. Lett. 1, H1–H3.
Tsapenko, M.V., Nwoko, R.E., Borland, T.M., Voskoboev, N.V., Pflueger, A., Rule, A.D., Lieske, J.C., 2013. Clin. Biochem. 46, 1430–1435.
Tuci, G., Vinattieri, C.M., Luconi, L., Ceppatelli, M., Cicchi, S., Brandi, A., Filippi, J., Melucci, M., Giambastiani, G., 2012. Chem. Eur. J. 18, 8454–8463.
Voggu, R., Rout, C.S., Franklin, A.D., Fisher, T.S., Rao, C.N.R., 2008. J. Phys. Chem. C. 34, 13053–13056.
Wang, X., Huang, H.X., Liu, A.R., Liu, B., Chen, M., Qian, D.J., 2008. Thin Solid Films 516, 3244–3250.
Wang, X., Liu, B., Chen, M., Qian, D., 2009. J. Nanosci. Nanotechnol. 9, 1441–1444.
Wickenhauser, C., Hillienhof, A., Jungheim, K., Lorenzen, J., Ruskowski, H., Hansmann, M., Thiele, J., Fischer, R., 1995. Leukemia 9, 310–315.
Yao, Y., Bao, J., Lu, Y., Zhang, D., Luo, S., Cheng, X., Zhang, Q., Li, S., Liu, Q., 2016. Sens. Actuators B 222, 127–132.
Yousefzadeh, G., Larijani, B., Mohammadirad, A., Heshmat, R., Dehghan, G., Rahimi, R., Abdollahi, M., 2006. Ann. NY Acad. Sci. 1091, 142–150.

SUPPLEMENTARY MATERIAL

Viologen-functionalized single-walled carbon nanotubes as carrier nanotags for electrochemical immunosensing

E. Sánchez-Tirado, L.M. Arellano[1], A. González-Cortés, P. Yáñez-Sedeño*,

F. Langa* [1], J.M. Pingarrón

Department of Analytical Chemistry, Faculty of Chemistry, University Complutense of Madrid, Ciudad Universitaria s/n, 28040-Madrid, Spain; [1]Instituto de Nanociencia, Nanotecnología y Materiales Moleculares (INAMOL), Universidad de Castilla-La Mancha, 45071-Toledo, Spain

1. Characterization of V-Phe-SWCNT hybrids

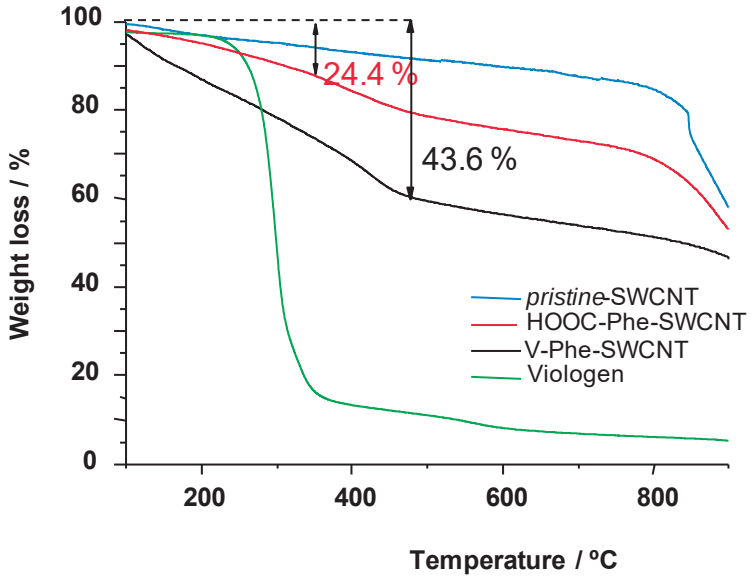

Figure S1. TGA profiles of *pristine*-SWCNTs (blue), HOOC-Phe-SWCNTs (red), V-Phe-SWCNTs (black) and viologen (green).

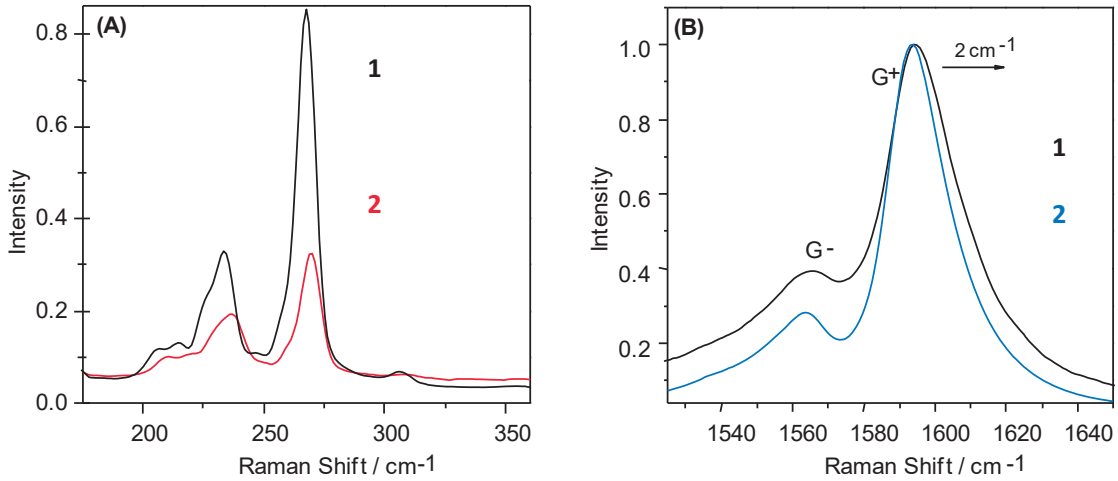

Figure S2. (A) Comparative Raman spectra from RBM zone (785 nm excitation): (1) before and (2) after functionalization; (B) G-band region (785 nm excitation): (1) V-Phe-SWCNT; (2) *pristine*-SWCNT

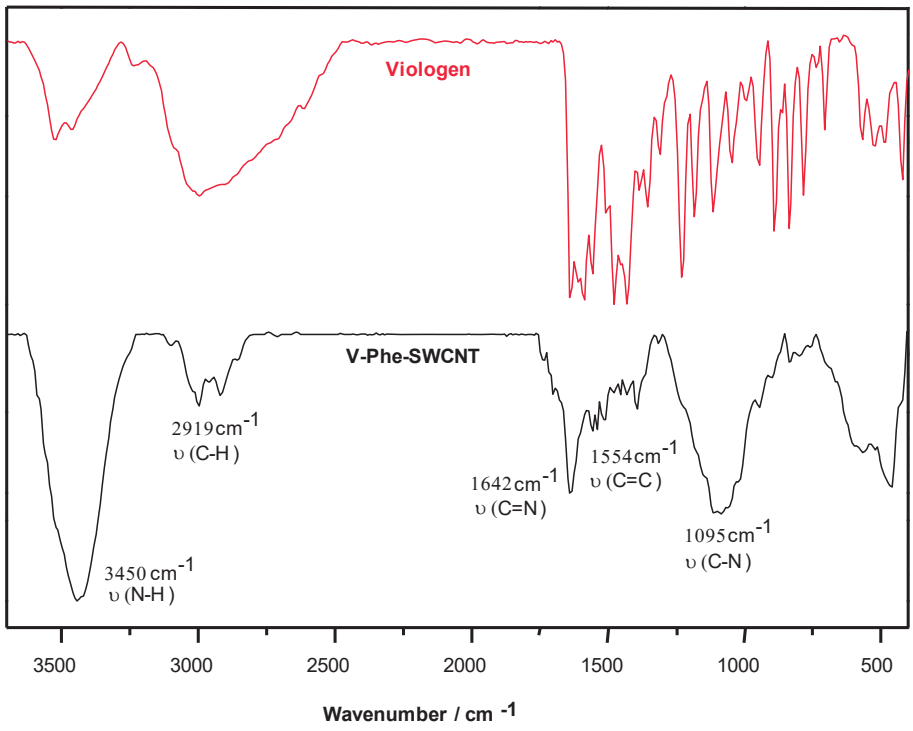

Figure S3. FT-IR of viologen (red) and V-Phe-SWCNT (black).

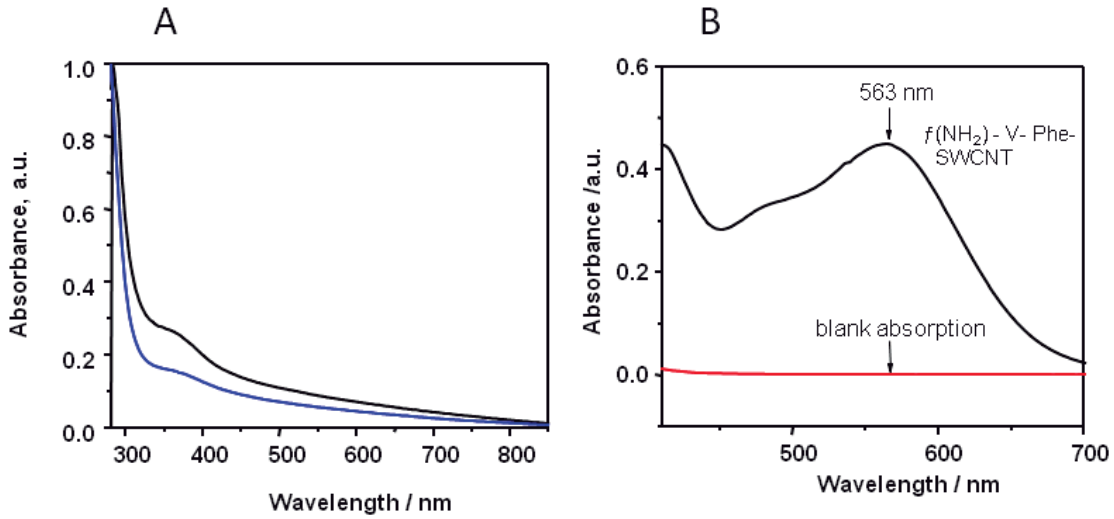

Figure S4. A) UV-vis (solvent NMP) of V-Phe-SWCNT hybrid (black) and 1-(3-aminoethyl)-4,4'-bipyridinium bromine (blue). B) Kaiser test measurement of V-Phe-SWCNT-V hybrid.

2. Characterization of V-Phe-SWCNT(-HRP)-anti-TGF

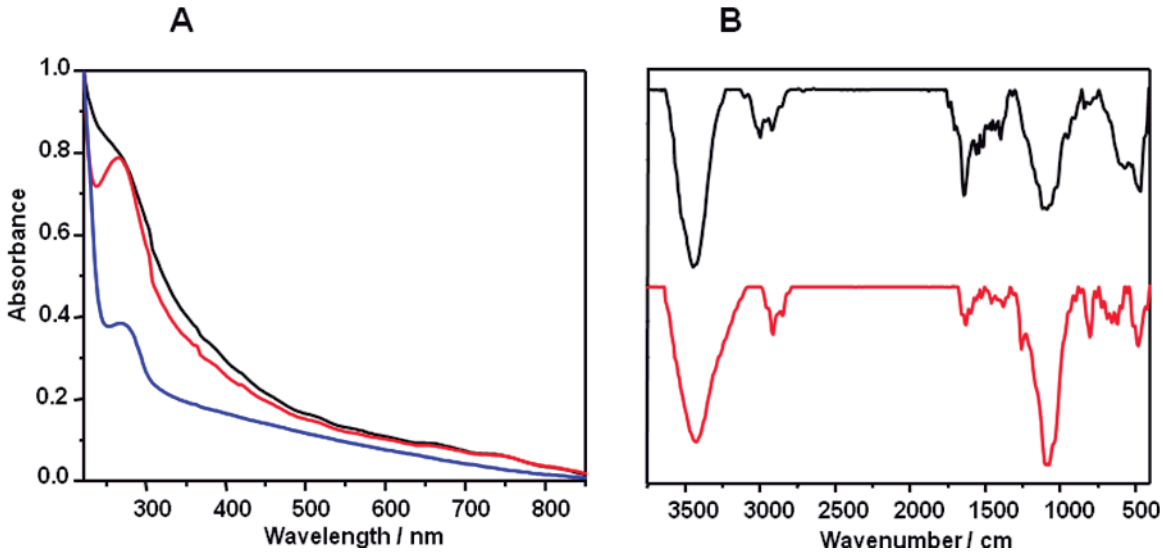

Figure S5. A) Absorption spectra in H2O of: V-Phe-SWCNT (black), V-SWCNT-Phe-HRP (red) and V-Phe-SWCNT(-HRP)-anti-TGF (blue). B) FT-IR spectra of V-Phe-SWCNT (black) and V-Phe-SWCNT-HRP-anti-TGF (red).

2. Optimization of the experimental variables involved in the preparation of the immunosensor

2.1.Effect of the HRP and anti-TGF antibody loadings on V-Phe-SWCNTs

As described in the Experimental section and with the aim of implementing a simpler and faster protocol, the immobilization of HRP and anti-TGF onto the previously synthesized V-Phe-SWCNT was performed in a single step by incubating them in a solution containing both biomolecules. An incubation period of 3 h was found to be adequate to obtain V-Phe-SWCNT(-HRP)-anti-TGF conjugates able to provide suitable immunosensor responses. The influence of HRP loading on the V-Phe-SWCNTs was evaluated using solutions containing 2.5, 5, 10, and 20 μg mL^{-1} HRP and a constant anti-TFG concentration of 2 μg mL^{-1}. The respective amperometric responses were measured with V-Phe-SWCNT(-HRP)-anti-TGF-TGF-β-anti-TGF-Biotin-Strept-SPCE immunosensors prepared using 5 μL of a 200 μg mL^{-1} Strept solution and 5 μL of a 5 μg mL^{-1} anti-TGF-Biotin solution. Moreover, blocking of the remaining sites for binding on the electrode surface was accomplished with 5 μL of a 0.5 mg mL^{-1} Biotin solution. Amperometric measurements were carried out at -300 mV vs Ag pseudo-reference electrode upon addition of 5 μL of 50 mM H_2O_2 for 0 (white, unspecific response) and 125 pg mL^{-1} TGF-β1 (grey, specific response). The obtained results are displayed in Figure 6a As expected, the measured current values for both the specific and unspecific responses increased with increasing HRP concentration in the whole tested range. However, the largest specific to unspecific current ratio (S/N) was obtained for 10 μg mL^{-1} HRP and therefore, this concentration was selected for the preparation of the immunosensors.

Regarding the loading of anti-TGF immobilized onto V-Phe-SWCNTs, solutions containing 10 μg mL^{-1} HRP and 1, 2 or 3 μg mL^{-1} anti-TGF were checked by measuring the responses of various immunosensors (at the same conditions mentioned above) prepared with 5 μL of a 200 μg mL^{-1} Strept solution and 5 μL of a 7.5 μg mL^{-1} anti-TGF-Biotin solution. Figure 6b shows as larger S/N ratio was obtained for a 2 μg mL^{-1} anti-TGF concentration.

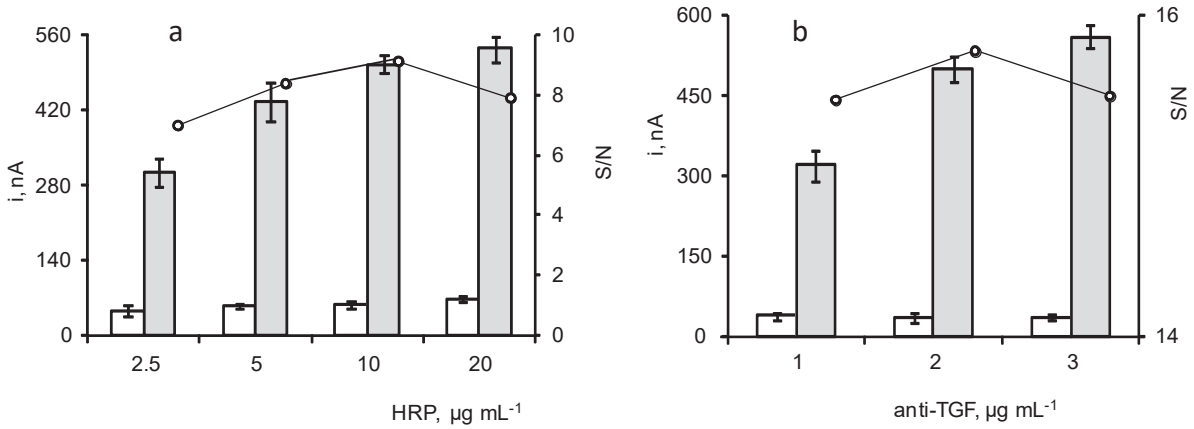

Figure S6. Effect of the (a) HRP (a) and anti-TGF (b) concentration used to prepare the V-Phe-SWCNT-based immunosensor. V-Phe-SWCNT(-HRP)-anti-TGF prepared with (a) 2.5, 5, 10 or 20 µg mL^{-1} HRP and 2 µg mL^{-1} anti-TGF; (b) 10 µg mL^{-1} HRP and 1, 2 or 3 µg mL^{-1} anti-TGF; SPCE prepared with 5 µL 200 µg mL^{-1} Strept solution, 5 µL of 5 µg mL^{-1} (a) or 7.5 µg mL^{-1} (b) anti-TGF-Biotin solution, and 5 µL of 0.5 mg mL^{-1} Biotin solution; 0 (white) and 125 (grey) pg mL^{-1} TGF-β1; 5 µL of 50 mM H_2O_2. E_{det} = -300 mV vs Ag pseudo-reference electrode

2.2. Effect of the streptavidin loading on SPCEs and anti-TGF-Biotin loading on Strept-SPCEs.

The influence of the streptavidin loading on the amperometric response of the resulting immunosensors was studied by immobilizing different amounts of this protein on the 4-ABA activated SPCEs over the 100 and 300 µg mL^{-1} concentration range. Then, different immunosensors were prepared with 5 µL of 7.5 µg mL^{-1} anti-TGF-Biotin solution, and 5 µL of a 0.5 mg mL^{-1} Biotin blocking solution. V-Phe-SWCNT(-HRP)-anti-TGF conjugates were prepared with 10 µg mL^{-1} HRP and 2 µg mL^{-1} anti-TGF. Solutions containing 0 (white) and 125 (grey) pg mL^{-1} TGF-β1 were measured after addition of 5 µL of 50 mM H_2O_2. As Figure 7a shows, the largest current value for the specific response and the best specific-to-unspecific current ratio were obtained for a Strept concentration of 200 µg mL^{-1}, which was selected for further work. Using these conditions, the anti-TGF-Biotin loading was also optimized. Figure 7b shows as the measured current remained practically constant from a conjugate concentration of 7.5 µg mL^{-1}. Moreover, the highest specific-to-unspecific current ratio was also obtained for this value, and therefore, it was selected for further work.

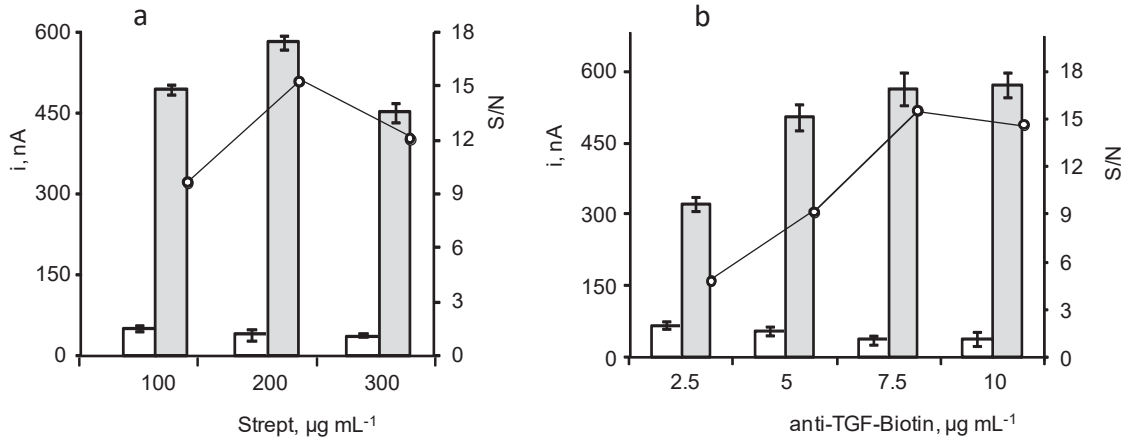

Figure S7. Effect of the streptavidin loading on SPCEs (a) and the anti-TGF-Biotin loading on Strept-SPCEs (b) on the amperometric responses of the V-Phe-SWCNT-based immunosensor. V-Phe-SWCNT(-HRP)-anti-TGF prepared with 10 µg mL^{-1} HRP and 2 µg mL^{-1} anti-TGF; SPCEs prepared with (a) 5 µL of 0, 100, 200 or 300 µg mL^{-1} Strept solutions and 5 µL of a 7.5 µg mL^{-1} anti-TGF-Biotin solution, and (b) 200 µg mL^{-1} Strept solutions and 5 µL of 2.5, 5, 7.5 or 10 µg mL^{-1} anti-TGF-Biotin solution; 0 (white) and 125 (grey) pg mL^{-1} TGF-β1; 5 µL of 50 mM H_2O_2. E_{det} = -300 mV vs Ag pseudo-reference electrode

Biosensors and Bioelectronics 113 (2018) 88–94

Magnetic multiwalled carbon nanotubes as nanocarrier tags for sensitive determination of fetuin in saliva

Biosensors and Bioelectronics 113 (2018) 88–94

Contents lists available at ScienceDirect

Biosensors and Bioelectronics

journal homepage: www.elsevier.com/locate/bios

Magnetic multiwalled carbon nanotubes as nanocarrier tags for sensitive determination of fetuin in saliva

Esther Sánchez-Tirado, Araceli González-Cortés, Paloma Yáñez-Sedeño*, José M. Pingarrón

Department of Analytical Chemistry, Faculty of Chemistry, University Complutense of Madrid, 28040 Madrid, Spain

ARTICLE INFO

Keywords:
Fetuin
Electrochemical immunosensor
Magnetic carbon nanotubes
Saliva

ABSTRACT

This paper reports the development and performance of an electrochemical immunosensor using magnetic multiwalled carbon nanotubes (*m*-MWCNTs) as nanocarrier tags for the determination of human fetuin A (HFA), a relevant biomarker of obesity, insulin resistance, and type-2 diabetes as well as for pancreatic and liver cancers and inflammatory processes. Screen-printed carbon electrodes were grafted with *p*-aminobezoic acid and streptavidin was covalently immobilized on the electrode surface. A biotinylated capture antibody was immobilized through streptavidin-biotin interaction and a sandwich assay configuration was implemented using *m*-MWCNTs conjugated with HRP and anti-HFA antibodies as the detection label. The determination of HFA was accomplished by measuring the current produced by the electrochemical reduction of benzoquinone at −200 mV upon addition of H_2O_2 as HRP substrate. The prepared *m*-MWCNTs were characterized by SEM, TEM, XRD and EDS. All the steps involved in the immunosensor preparation were monitored by electrochemical impedance spectroscopy and cyclic voltammetry. A linear calibration plot for HFA was found between 20 and 2000 pg/mL with a LOD value of 16 pg/mL. This performance is notably better than that reported for an ELISA kit and a chronoimpedimetric immunosensor. The favorable contribution of *m*-MWCNTs in comparison with MWCNTs without incorporated magnetic particles to this excellent analytical performance is also highlighted. The immunosensor selectivity against other proteins and potentially interfering compounds was excellent. In addition, the usefulness of the immunosensor was demonstrated by the analysis of HFA in saliva with minimal sample treatment.

1. Introduction

Human Fetuin A (HFA), also known as α2-Heremans-Schmid glycoprotein (AHSG), is encoded by the AHSG gene on chromosome 3. Plasmatic HFA is a 59 kDa disulfide bond-linked two chain polypeptide consisting of two N-terminal cystatin domains and a smaller C-terminal domain (Dziegielewska et al., 1990). HFA is considered as a candidate biomarker of obesity, insulin resistance, and type-2 diabetes. High HFA serum concentrations have been observed in individuals with fatty or swollen liver (Yilmaz et al., 2010) related with increased risk of type-2 diabetes (Dabrowska et al., 2015). The relevance of HFA as a new potential biomarker for pancreatic and liver cancers and in metastasis of tumor cells (Sakwe et al., 2010) (Yi et al., 2009) as well as to differentiate prostate cancer and benign prostatic hyperplasia (Silva et al., 2016) has been also claimed.

In addition, the synthesis of HFA is down-regulated during injury and inflammation (Choi, 2016) and plays an important role in blood vessel calcification (Schinke et al., 1996). As HFA acts as a potent inhibitor of calcium-phosphate precipitation and the calcification process, its levels are also related with dental calculus which is the first response in the inflammation of tooth supportive tissues (Doğan et al., 2016). Therefore, the relationship between HFA and the periodontal disease makes the determination of HFA in saliva relevant.

Due to the clinical importance of HFA, assays using different bioreagents for HFA detection have emerged. Table S1 in the Supplementary material summarizes the characteristics of commercially available ELISA kits involving sandwich-type configurations, peroxidase-labeled immunoreagents and colorimetric detection through the TMB/H_2O_2 system. For instance, the Quantikine Human Fetuin A Immunoassay (https://www.rndsystems.com/products/human-fetuin-a-quantikine-elisa-kit_dfta00) is a 4.5-h solid-phase colorimetric ELISA that provides a calibration plot in the 7.8–500 ng/mL range and a minimum detectable dose (MDD), defined as the concentration corresponding to the mean absorbance of zero standard replicates (n = 20) + 2 s, of 0.62 ng/mL.

In the case of electrochemical biosensors, the strong interaction of

* Corresponding author.
E-mail address: yseo@quim.ucm.es (P. Yáñez-Sedeño).

https://doi.org/10.1016/j.bios.2018.04.056
Received 25 February 2018; Received in revised form 26 April 2018; Accepted 26 April 2018
Available online 30 April 2018
0956-5663/ © 2018 Elsevier B.V. All rights reserved.

HFA glycoprotein with specific lectins has been explored (Table S1). Specifically, Bertok et al. (2013a, 2013b) developed an impedimetric biosensor involving the *Sambucus nigra* lectin and a mixed SAM of 11-mercaptoundecanoic acid and 6-mercaptohexanol. Biorecognition of fetuin was accomplished through carboxyl group activation and lectin adhesion. Electrochemical impedance spectroscopy (EIS) was used as transduction technique. The same authors developed a more sensitive biosensor where a linker layer of amino-terminated alkanethiol was assembled on a gold electrode for further incorporation of gold nanoparticles The limit of detection achieved was 0.5 ± 0.1 aM (Bertok et al., 2013a, 2013b).

Nagaraj et al. (2010) developed another lectin-based biosensor for the label-free detection of HFA. They used a silicon chip with a row of gold electrodes and relied on the impedance variations upon HFA binding to lectins. The limit of detection was 1 pg/mL. Moreover, a label-free electrochemical biosensor using *Cratyliamollis lectin* (Cramoll 1,4), assembled carboxylated carbon nanotubes and poly-L-lysine film was also proposed using square-wave voltammetry. A limit of detection of 0.017 μg/mL was achieved (Silva et al., 2016) (Table S1).

It is well known that the advantageous analytical capabilities of electrochemical immunosensors become more evident when using nanomaterials which can increase the loading of electrochemically detectable species as well as catalyze the electrochemical reaction enhancing the electrochemical signal (Ding et al., 2013). Carbon nanomaterials can be utilized in different amplification routes in electrochemical biosensing which mainly imply their use as electrode materials, redox mediators or carriers for signaling elements (Yáñez-Sedeño et al., 2017). Very recently, a fullerene-PAMAM(G5) composite was used for the preparation of a chronoimpedimetric immunosensor for HFA showing a 5–400 ng/mL linear range with a LOD of 1.44 ng/mL (Uygun et al., 2018).

Apart from this article, to our knowledge, there are no other configurations reported for electrochemical immunosensors for HFA. Here, we describe the development and performance of an electrochemical immunosensor using magnetic multiwalled carbon nanotubes (*m*-MWCNTs) as nanocarrier tags for the determination of HFA in the 20–1000 pg/mL with a LOD of 16 pg/mL. Screen-printed carbon electrodes were modified by grafting with *p*-aminobezoic acid and, upon activation of the surface-confined carboxylic groups, streptavidin was covalently immobilized and, after conjugation with biotin-anti-HFA capture antibody, a sandwich scheme was prepared using m-MWCNTs (-HRP)-anti-HFA conjugates as the detection label. The excellent biosensor performance allowed the determination of HFA in saliva at clinical levels.

2. Experimental

2.1. Reagents and solutions

The antibodies used and the HFA protein were those included in the DuoSet®ELISA Development System from R&D Systems (DY1184). A goat biotinylated anti-HFA antibody was used as the capture antibody. Biotin-anti-HFA 36 μg/mL solutions in phosphate buffer of pH 7.4 were also used. Detection antibody was a mouse anti-HFA dissolved in the same buffer solution. Aqueous streptavidin (Strept, Sigma) solutions were firstly prepared and diluted with 25 mM *2*–(*N*–morpholine)ethanesulfonic (MES) (Gerbu) of pH 5.0. Lithium perchlorate (Sigma), *p*-aminobenzoic acid (*p*ABA, Acros), and absolute ethanol (VWR Chemicals) were used for the grafting protocol. Covalent immobilization of capture antibody was carried out with 1–ethyl–3–(3–dimethylaminopropyl) carbodiimide (EDC) and sodium *N*–hydroxysulfosuccinimide (NHSS) (Acros). D-biotin (Gerbu) was used as the blocking agent. Solutions were prepared in phosphate buffer of pH 7.4.

Ascorbic acid (AA, Fluka), uric acid (UA, Sigma), bovine serum albumin (BSA, Gerbu), cortisol (CL), creatinine (CR), estradiol (E2) and human immunoglobulin G (IgG), all from Sigma, interleukin-1 beta (IL–1β), transforming growth factor beta 1 (TGF-β1), and tumor necrosis factor alpha (TNF-α), all from R&D Systems, interleukin-6 (IL–6) and interleukin-8 (IL–8) from Abcam, were checked as potential interferents. Hydrogen peroxide (Aldrich, 30% (w/w)) and hydroquinone (HQ, Sigma) were also used.

Other buffer solutions used were: 0.01 M phosphate buffer saline (PBS) of pH 7.4 prepared by dissolving Na_2HPO_4 (Scharlau) and KH_2PO_4 (Merck) in 137 mM NaCl (Labkem) and 2.7 mM KCl (Probus) aqueous solution. 0.1 M and 0.01 M PBS of pH 7.0 prepared by dissolving Na_2HPO_4 and NaH_2PO_4 (Labkem) in 150 mM NaCl aqueous solution; 0.1 M PBST of pH 7.0 prepared by adding 5 μL of Tween® 20–10 mL of 0.1 M PBS of pH 7.0, and 0.05 M phosphate buffer (PB) of pH 6.0 prepared by dissolving 2.180 g of K_2HPO_4 in distilled water and adjusting the pH value.

All reagents used were of analytical grade. Deionized water (18.2 MΩ cm at 25 °C) was obtained from a Millipore Milli–Q purification system.

2.2. Apparatus and electrodes

Amperometric measurements were done with an INBEA Biosensores potentiostat equipped with the Ib-Graph software. Impedimetric and voltammetric measurements were performed with a μAutolab type III potentiostat controlled by FRA2 and GPES 4.7 (EcoChemie) softwares, respectively. A Crison Basic 20 + pHmeter, an ultrasonic bath Elmasonic S–60 (Elma), a Vortex (Velp Scientifica) stirrer, and a Dynal MPC–S 120.20 (Dynal BiotechASA) magnetic separator, were also used. Characterization by SEM, EDX, TEM and XRD were performed using a FESEM (Field Emission Scanning Electron Microscope): JEOL JSM 7600F, a TEM: JEOL JEM 1400, and a difractometer PAMalytical model X´Pert MPD.

Screen printed carbon electrodes (SPCEs, 110 DRP, ϕ4 mm) were from DropSens (Oviedo, Spain). These electrodes were provided with a carbon counter electrode and a silver pseudo-reference electrode.

2.3. Procedures

2.3.1. Preparation of the modified SPCEs

The screen-printed carbon electrodes were modified by immersion in an ethanolic *p*-ABA solution containing $LiClO_4$ and making three successive cyclic voltammograms between 0.0 and 0.6 V at 30 mV/s. Then, the modified electrodes were washed with deionized water and let dry at air. The grafted surface carboxylic groups were activated by dropping 10 μL of a 100 mM each EDC/NHSS solution prepared in 25 mM MES buffer of pH 5.0, and allowing incubation for 30 min. Once the electrodes were washed and dried again, modification with streptavidin was performed by casting 5 μL of a 600 μg/mL Strept solution prepared in the same buffer solution and incubating for 60 min.

2.3.2. Preparation of magnetic MWCNTs

25 mg of MWCNTs were dispersed in 85 mL of Milli–Q water by ultrasonic stirring for one hour. Then, 16 mL of concentrated nitric acid were added and refluxed for 24 h. The resulting dispersion was centrifuged at 4000 rpm for 10 min at room temperature. The carboxylated MWCNTs were washed with Milli–Q water up to washing water reached pH 7.0 and let dry under nitrogen stream. Magnetization of the resulting HOOC-MWCNTs was performed by suspending 19.4 mg in 10 mL of water, adding 13.1 mg of $FeCl_3{\cdot}6H_2O$ and 5.9 mg of $FeCl_2{\cdot}4H_2O$ and adjusting the pH value at 10–11 with a 25% aqueous ammonia solution by applying ultrasonic stirring for 30 min under nitrogen atmosphere. The resulting dispersion was maintained at 80 °C under magnetic stirring and nitrogen atmosphere for 60 min. Finally, once cold at room temperature, the resulting *m*-MWCNTs were washed with water up to neutral pH and dried at 37 °C.

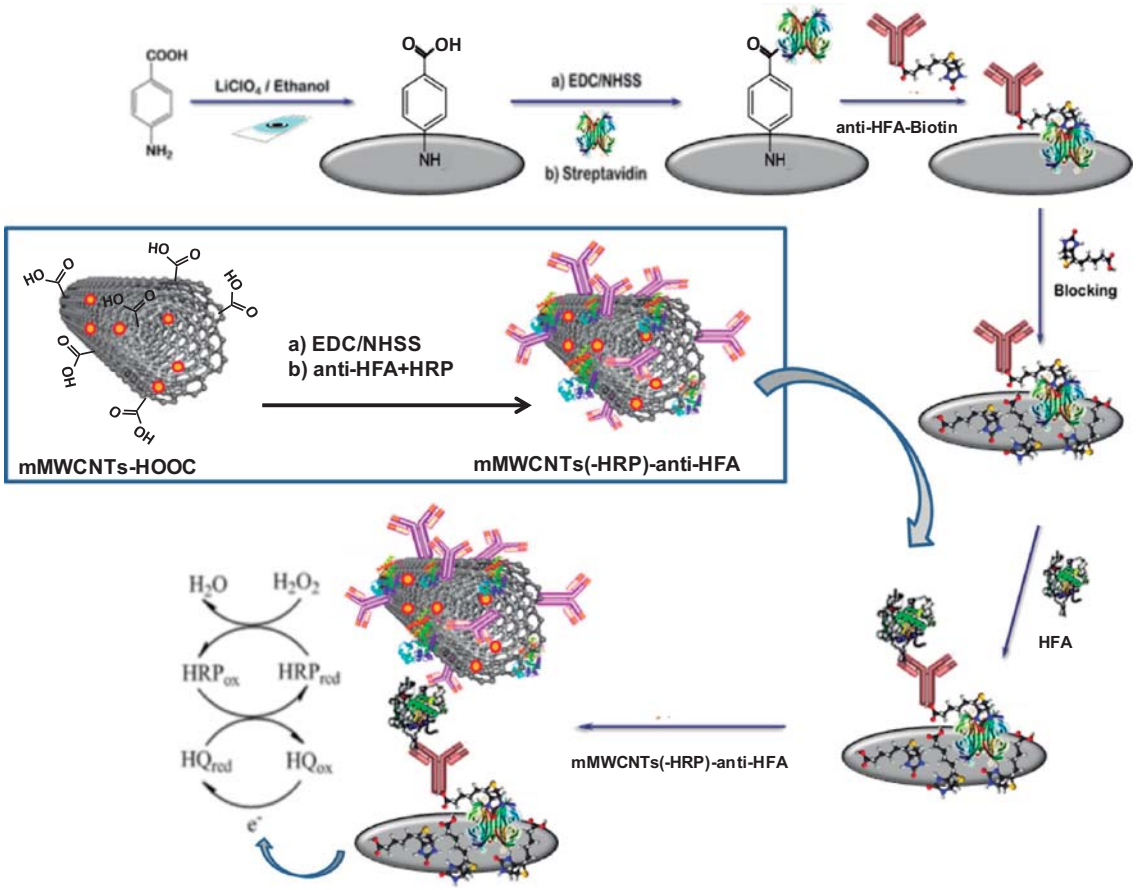

Fig. 1. Schematic display of the different steps involved in the construction of the amperometric immunosensor for HFA involving *p*-ABA grafting onto SPCEs and covalent immobilization of Strept followed by Biotin-anti-HFA conjugation and sandwich assay with *m*-MWCNTs(-HRP)-anti-HFA.

2.3.3. Preparation of m-MWCNTs(-HRP)-anti-HFA conjugates

A dispersion was prepared with 1.5 mg of *m*-MWCNTs in 2 mL of 100 mM PBS of pH 7.0 with ultrasonic stirring for 30 min. Next, 1 mL of a solution composed of 400 mM EDC and 100 mM NHSS in the same buffer was added and incubated in the dark with magnetic stirring for 6 h. The resulting suspension was centrifuged at 14,000 rpm and room temperature during 5 min and, thereafter, 1 mL of a solution containing 5 μg/mL of detection antibody (anti–HFA) and 1 mg/mL of HRP in 100 mM PBS of pH 7.0 was added. After an incubation period of 24 h under magnetic stirring, the conjugates were washed three times with 10 mM PBS of pH 7.0, and the residue was re-dispersed in 1 mL of 100 mM PBST of pH 7.0.

2.3.4. Preparation of anti-HFA-Biotin-Strept-Phe-SPCE immunosensor

Grafted SPCEs (Procedure 2.3.1) were treated with 5 μL of a 100 mM each EDC/NHSS solution in 25 mM MES buffer of pH 5.0 and incubated for 30 min. Then, the modified electrode was washed with water and let dry. Immobilization of Strept was performed by dropping 5 μL of a 600 μg/mL solution in the same buffer and incubation for 60 min. Once the Strept-Phe-SPCEs were washed with water and dried, the biotinylated capture antibody (Biotin–anti–HFA) was immobilized by depositing 5 μL of a 7 μg/mL solution in 0.01 M PBS of pH 7.4 and incubated for 60 min. A blocking step was implemented by adding 5 μL of a 1.5 mg/mL Biotin solution and incubation for 30 min.

2.3.5. Determination of HFA

After a washing and drying step, 5 μL of antigen solution (or the sample) were added and incubated for 60 min onto the resulting anti-HFA-Biotin-Strept-Phe-SPCE immunosensor. Thereafter, 5 μL of the *m*-MWCNTs (–HRP)–anti–HFA conjugate were added and, after 60 min, the bioelectrodes were washed with water and then stored until use by addition of a drop of 50 mM phosphate buffer solution of pH 6.0. The determination of HFA was accomplished by dropping 45 μL of a 1 mM HQ solution prepared in 0.5 M phosphate buffer solution of pH 6.0 onto the surface of the horizontally postioned *m*-MWCNTs(-HRP)-anti-HFA-HFA-anti-HFA-Biotin-Strept-Phe-SPCE immunosensor and by applying a potential of −200 mV. Once the background current was stabilized (100 s approximately), 5 μL of a 50 mM H_2O_2 solution prepared in the same buffer were added and allowed to incubate for 200 s. Then, the current produced by the electrochemical reduction of benzoquinone was measured.

2.3.6. Analysis of HFA in saliva

Saliva samples were obtained from volunteers and collected using a Salivette® collection device (Sarstedt). Briefly, once rinsed the mouth thoroughly with water, a cotton swab was inserted into the mouth and chewed for 1 min. Then, the swap saturated with saliva was inserted into the vial, sealed with the cap and centrifuged for 10 min at 3000 rpm. After this, 10-μL sample aliquots were diluted with 990 μL of 0.01 PBS of pH 7.4. The determination was performed immediately by applying the procedure described above to 5 μL of diluted saliva, and interpolation of the amperometric response into the calibration plot constructed with standard solutions.

3. Results and discussion

As described in Procedure 2.3.2, *m*-MWCNTs were prepared by acidic oxidation of MWCNTs followed by incorporation of magnetic particles according with the method of Zhang et al. (2014) with slight modifications. Briefly, this procedure consisted of the treatment of carboxylated MWCNTs with $FeCl_3{\cdot}6H_2O$ and $FeCl_2{\cdot}4H_2O$ in ammonia solution at 80 °C under nitrogen atmosphere. Thereafter (Fig. 1 inset),

anti-HFA and HRP were covalently immobilized onto the prepared *m*-MWCNTs through EDC-NHSS chemistry (Akter et al., 2016). Fig. 1 also shows schematically the different steps involved in the preparation of the *m*-MWCNTs(-HRP)-anti-HFA-HFA-anti-HFA-Biotin-Strept-Phe-SPCE immunosensor. As it was described in the Experimental section, the SPCE surface was functionalized by grafting of *p*-ABA cation radical followed by covalent immobilization of streptavidin. The biotinylated capture antibody, anti-HFA-Biotin, was immobilized trough streptavidin-biotin interaction and a sandwich assay configuration was implemented with *m*-MWCNTs(-HRP)-anti-HFA.

The determination of HFA was accomplished by measuring the current produced by the electrochemical reduction of benzoquinone at − 200 mV upon addition of H_2O_2 as HRP substrate.

Magnetic MWCNTs (*m*-MWCNTs) were characterized by scanning electron microscopy (SEM), transmission electron microscopy (TEM), X-Ray diffraction (XRD) and energy-dispersive X-Ray spectroscopy (EDS). As it can be seen in Fig. 2a and b, as well as in the photograph showing MWCNTs and *m*-MWCNTs upon applying an external magnet, Fe_3O_4 particles were attached to the walls of MWCNTs. X-Ray diffraction recordings of *m*-MWCNTs and MWCNTs are shown in Fig. 2c. It can be observed the peaks corresponding to the structure of MWCNTs (red response) also appearing in that of *m*-MWCNTs (blue response), together with other peaks that can be attributed to the different types of common iron oxides (Kim et al., 2010) (Gong et al., 2009). Peaks appearing at 2θ = 30.2°; 35.7°; 43.3° and 57.2° can be assigned to magnetite (Mn, Fe_3O_4) or maghemite (Mh, γ-Fe_2O_3). Other peaks appearing at 2θ = 53.9° and 62.8° can be related to the presence of the non-magnetic (Hm, α-Fe_2O_3). Moreover, chemical analysis using EDS (Fig. 2d) demonstrated the presence of Fe, O and C in the *m*-MWCNTs.

The room-temperature magnetization hysteresis loop of *m*-MWCNTs was obtained using a vibrating sample magnetometer and compared with those of HOOC-MWCNTs and pure Fe_3O_4 particles prepared under the same reaction conditions. The results shown in Fig. S2 (Supplementary material) demonstrated the superparamagnetic behavior of *m*-MWCNTs, with a saturation magnetization of 9.89 emu/g, which, as expected, was significantly lower than that of Fe_3O_4 particles (62.12 emu/g) owing to the presence of carbon nanotubes.

3.1. Optimization of the experimental variables

The different variables affecting the preparation of *m*-MWCNTs (-HRP)-anti-HFA conjugate, anti-HFA-Biotin-Strept-Phe-SPCE, and the performance of the resulting *m*-MWCNTs(-HRP)-anti-HFA-HFA-anti-HFA-Biotin-Strept-Phe-SPCE immunosensor were evaluated and optimized. The largest ratio between the currents measured with the as prepared immunosensor in the presence (S), at a 250 pg/mL concentration level, or in the absence (N) of the target compound was taken as the selection criterion for each tested variable. The optimization studies involved evaluation of: a) loadings of HRP and anti-HFA onto *m*-MWCNTs; b) loading of streptavidin covalently linked to *p*-ABA-modified SPCE; c) anti-HFA-Biotin loading onto Strept-Phe-SPCE; d) concentration of blocking agent. The results of these tests are discussed in the Supplementary material (Figs. S2-S4). Moreover, the experimental conditions used for SPCE modification by grafting from the electrochemically generated *p*-ABA cation radical and covalent bond of streptavidin were optimized previously (Ojeda et al., 2012). Similarly, the detection potential of − 200 mV was also previously selected for the same catalytic system (Eguílaz et al., 2010).

All the steps involved in the immunosensor preparation were monitored by electrochemical impedance spectroscopy and cyclic voltammetry using 2 mM $Fe(CN)_6^{4-/3-}$ as the redox probe in 0.1 M phosphate buffer solution of pH 7.4. Fig. 3a shows as modification of the SPCE with *p*-ABA gave rise to a large increase in the electron transfer resistance, R_{CT}, varying from 376 to 1885 Ω as a consequence of the electrostatic repulsion between the redox probe and the negatively charged carboxylate groups. After activation with EDC/NHSS and immobilization of streptavidin, the R_{CT} value dramatically decreased (R_{CT} = 957 Ω), while showed a further increase after conjugation with anti-HFA-Biotin (R_{CT} = 1513 Ω) due to the partially insulating barrier on the electrode surface produced by the presence of proteins. The blocking of the remaining unreacted sites with biotin produced a larger R_{CT} value of 1711 Ω in agreement with the expected decrease in the electrode conductivity at a quasi-passivated surface. Surprisingly, further conjugation of HFA antigen provoked a decrease in the charge transfer resistance, R_{CT} = 1497 Ω. A possible explanation of this behavior relies with incorporation of biotin, which is dissociated at the working pH value, and provokes a high increase in R_{CT} due to charge repulsion. The subsequent incorporation of the antigen led the charge transfer resistance to values similar that measured before the blocking step. In addition, lower R_{CT} (1184 Ω) was observed for the *m*-MWCNTs (-HRP)-anti-HFA-HFA-anti-HFA-Biotin-Strept-Phe-SPCE immunosensor probably as a consequence of the high conductivity inherent to the modified carbon nanotubes.

Similar changes and conclusions were apparent from CV especially in the early stages of immunosensor preparation. The voltammogram corresponding to the bare SPCE (curve 1) shows the characteristic oxidation and reduction peaks of the redox pair at potential values of + 0.27 and − 0.06 V, respectively, while the anodic and cathodic currents exhibited approximately the same magnitude (130 μA). Modification of SPCE by grafting with *p*-ABA (curve 2) caused a decrease in the peak currents and a larger separation of peak potentials which is most likely due to the electrostatic repulsion between the redox probe and the dissociated carboxyl groups on the electrode surface. When streptavidin is linked (curve 3), the corresponding voltammogram shows a behavior more similar that of the unmodified electrode, probably due to the lower effect of charge repulsion. Successive incorporation of the other immunoreagents provoked slight variations in the CVs towards a less reversible behavior, as a consequence of the presence of insulating layers of increasing thickness on the electrode surface.

3.2. Analytical characteristics for HFA determination

Under the optimized working conditions, a calibration plot for HFA (Fig. 4) was constructed over the 10–5000 pg/mL concentration range. A linear range between 20 and 2000 pg/mL was found (r^2 = 0.995) which fitted to the equation: i, μA = 2.17 ± 0.07 log [HFA, pg/mL] − 2.22 ± 0.4. A mandatory comparison is the calibration plot constructed using MWCNTs(-HRP)-anti-HFA as the carrier tag, i.e., without magnetic particles incorporated to the nanotubes. In this latter case, a calibration graph with a lower slope value (1.21 ± 0.05 μA per decade of concentration) was obtained over the same dynamic range (r^2 = 0.997). The higher sensitivity achieved with the magnetic nanoparticles highlights their favorable contribution to enhance conductivity and ability of carbon nanotubes for biomolecules adsorption. According with Zhang et al. (2014), *m*-MWCNTs used as labels of anti-HFA secondary antibodies offer a large specific surface area and promote electron transfer between the solution and the electrode. The improved analytical performance can also be partially attributable to the magnetic particles weak pseudo-peroxidase activity. Nevertheless, the enzymatic catalysis by HRP of the hydrogen peroxide reaction is much more important, as it can be deduced from the much smaller slope value, m = 0.102 ± 0.02 μA per decade of concentration, of the calibration graph in the same range of HFA concentrations constructed with the immunosensor using *m*-MWCNTs-anti-HFA label without HRP enzyme. This biosensor showed also a poorer linearity (r^2 = 0.95). To highlight the relevant effect for signal amplification provided by the use of *m*-MWCNTs(-HRP)-anti-HFA label, the results obtained with the as prepared *m*-MWCNTs(-HRP)-anti-HFA-HFA immunosensor were compared with those achieved with a HRP-IgG-anti-HFA-HFA-anti-HFA-Biotin-Strept-Phe-SPCE immunosensor. Fig. S5 in Supplementary material shows as the current measured for 250 pg/mL HFA was

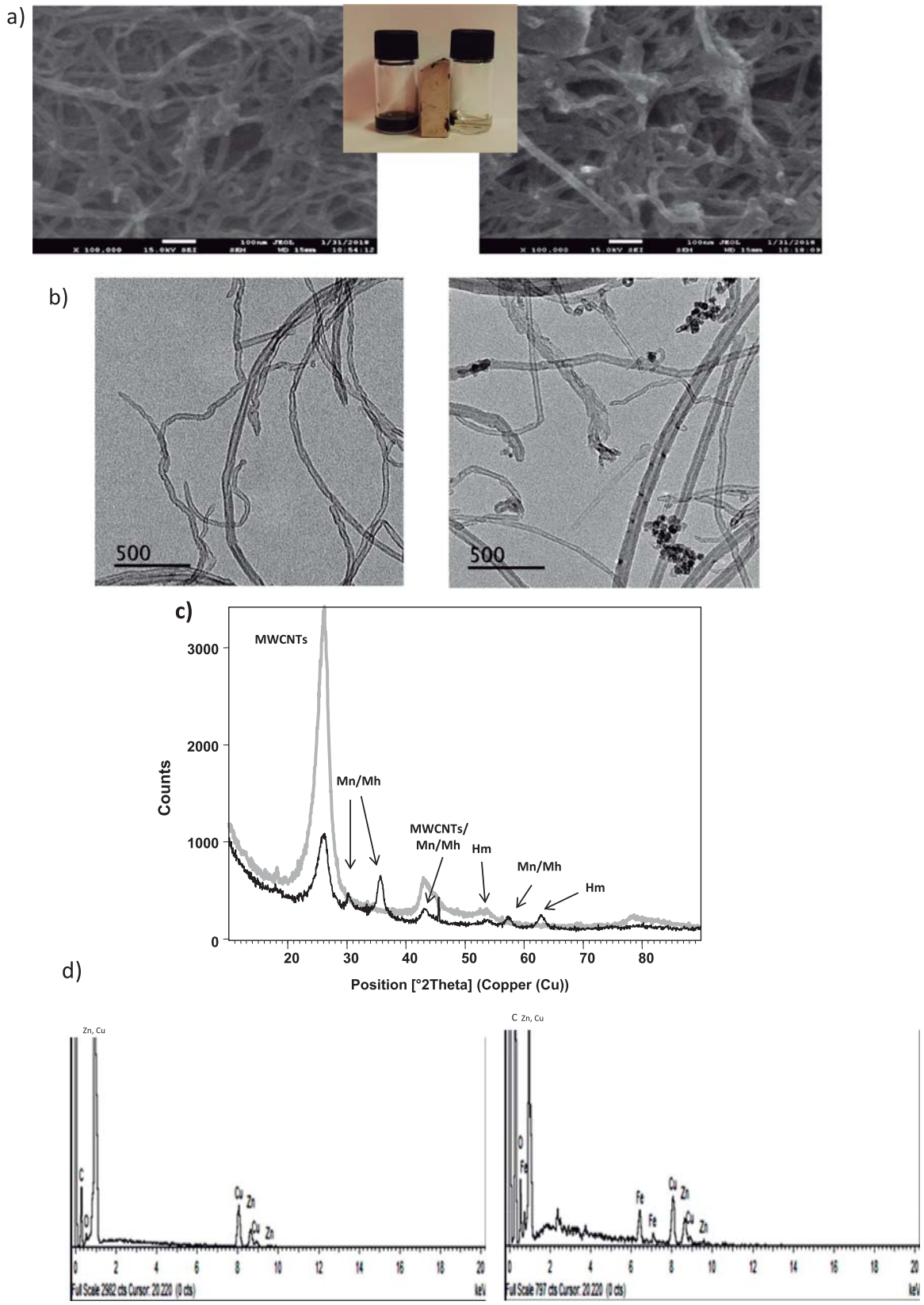

Fig. 2. Scanning electron microscopy (SEM) and photograph showing MWCNTs and *m*-MWCNTs with an external magnet (a); transmission electron microscopy (TEM) (b); X-Ray diffraction (XRD) (c) and energy dispersion spectrum (EDS) (d) of HOOC-MWCNTs (a, b, d-left; c-gray),and *m*-MWCNTs (a, b, d-right; c-black).

approximately three times larger using *m*-MWCNTs(-HRP)-anti-HFA conjugate as the carrier tag. Moreover, despite the higher current achieved for HFA detection, the unspecific signals represented only less than 13 per cent of such magnitude, thus providing a high S/N ratio.

The linear range of the calibration plot (20–2000 pg/mL) covers much lower HFA concentrations and in a wider interval than those

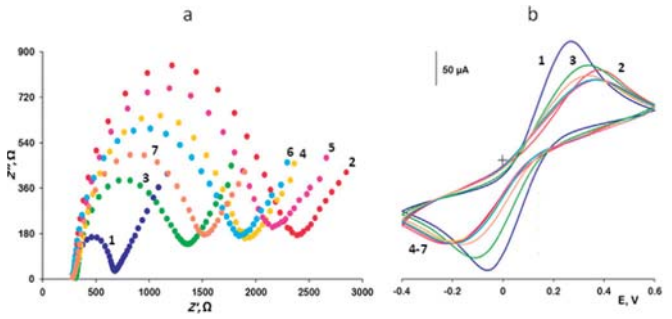

Fig. 3. Nyquist plots (a) and cyclic voltammograms (b) recorded in a 2 mM Fe $(CN)_6^{3-/4-}$ 0.1 M phosphate buffer solution of pH 7.4 for bare SPCE (1); *p*-ABA-SPCE (2); Strept-Phe-SPCE (3); anti-HFA-Biotin-Strept-Phe-SPCE (4); blocking with Biotin (5); HFA-anti-HFA-Biotin-Strept-Phe-SPCE (6); *m*-MWCNTs(-HRP)-anti-HFA-HFA-anti-HFA-Biotin-Strept-Phe-SPCE (7); 250 pg/mL HFA; range of frequencies, 10^5–0.040 Hz; open circuit (a); 50 mV/s (b).

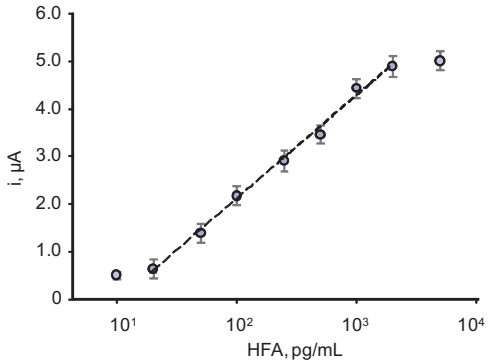

Fig. 4. Calibration plot for HFA constructed with the *m*MWCNTs(-HRP)-anti-HFA-HFA-anti-HFA-Biotin-Strept-Phe-SPCE immunosensor.

claimed for the ELISA kit (https://www.rndsystems.com/products/human-fetuin-a-quantikine-elisa-kit_dfta00), 7.8–500 ng/mL HFA, as well as the comparison is made against the electrochemical immunosensor reported by Silva et al. (2016), 0.5–25 µg/mL. The limit of detection achieved with our immunosensor design was calculated according with the $3\,s_b/m$ criterion, where s_b was estimated as the standard deviation, expressed in concentration units, for 10 blank current measurements (0 pg/mL HFA). The obtained LOD value, 16 pg/mL, is notably better (more than 10^3 times lower) than that reported in (Silva et al., 2016), 0.017 µg/mL, and the minimum detectable dose (MDD) of the ELISA kit, 0.62 ng/mL.

The reproducibility of the measurements performed with the developed immunosensor was evaluated. Amperometric measurements for 0 and 250 pg/mL HFA were made with five different immunosensors prepared simultaneously for each HFA concentration. The calculated RSD values were 6.7% and 7.4%, respectively. Moreover, measurements were also carried out with five immunosensors prepared in five different days. In this case, the RSD values were 7.2% and 7.5% for the same concentration levels, respectively. On the other hand, the storage stability of anti-HFA-Biotin-Strept-Phe-SPCEs was evaluated by preparing the same day various immunosensors which were used for measuring the amperometric responses of 250 pg/mL HFA in different days, once the blocking reagent and the *m*-MWCNTs(-HRP)-anti-HFA conjugate were added. Between measurements, the bioelectrodes were stored at − 20 °C in dry ambient. The results obtained (Fig. S6a) revealed that the initial immunosensor response was maintained within the limits of control set by ± 3 times the standard deviation of the measurements (n = 3) carried out on the first day, during 40 days after the immunosensor preparation thus showing an excellent storage stability.

In addition, the stability of the *m*-MWCNTs(-HRP)-anti-HFA conjugates was also checked by preparing an amount of them and keeping in the refrigerator at 4 °C. A new immunosensor was prepared each working day with a different conjugate and used to measure the current corresponding to 250 pg/mL HFA. The results shown in Fig. S6b confirmed a storage stability of the conjugates for at least 30 days after their preparation.

3.3. Selectivity

Various proteins (bovine serum albumin (BSA), interleukin 1 beta (IL-1β), interleukin 6 (IL-6), interleukin 8 (IL-8), human immunoglobulin G (IgG), tumor necrosis factor alpha (TNF–α), and transforming growth factor beta 1 (TGF–β1)), as well as other compounds potentially present in samples containing HFA, such as creatinine (CR), ascorbic acid (AA), uric acid (UA), cortisol (CL), and estradiol (E2) were tested as potential interfering substances for the determination of HFA with the developed immunosensor. The evaluation of the selectivity was accomplished by comparing the immunosensor responses for 0 and 250 pg/mL HFA in the absence and in the presence of each tested compound at a concentration corresponding approximately to the normal level in the undiluted saliva samples, except BSA, which was tested at a higher concentration. Fig. 5 shows that not significantly different currents were measured in all cases with the current mean values within the ± 2 × standard deviation range of the current measured in the absence of interferent.

3.4. Determination of HFA in saliva

The usefulness of the immunosensor in the analysis of real samples was tested by analyzing saliva from two smoker and non-smoker-volunteers. This type of sample was chosen because, as indicated in the Introduction section, HFA plays an important role in the detection of dental inflammatory processes (Doğan al, 2016). In addition, saliva is increasingly recognized as an attractive fluid for diagnostics since it allows a non-invasive cost-efficient sample collection method among other advantages (Campuzano et al., 2017). With the aim of minimizing the possible matrix effects and to fit the HFA concentration in the samples within the obtained range of linearity, various saliva dilution factors using 0.01 M PBS of pH 7.4 were assayed. As it is shown below, these requirements were achieved by applying a 100-fold dilution to the sample.

Under these conditions, the possible existence of matrix effects was tested by comparing the slope value of the calibration plots constructed by successive addition of HFA standard aliquots to the diluted samples, with

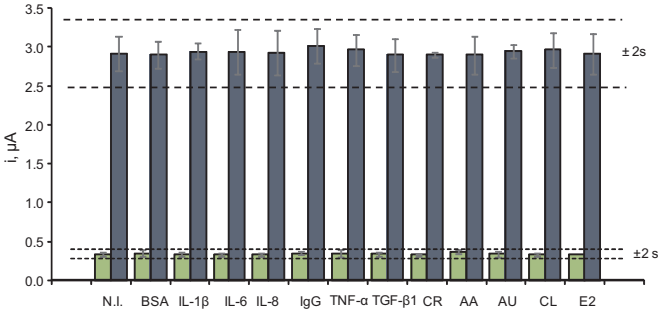

Fig. 5. Effect of the presence of 5 mg/mL bovine serum albumin (BSA), 50 pg/mL interleukin 1 beta (IL–1β), 50 pg/mL interleukin 6 (IL–6), 250 pg/mL interleukin 8 (IL–8), 16 µg/mL human immunoglobulin G (IgG), 200 pg/mL tumor necrosis factor alfa (TNF–α), 500 pg/mL transforming growth factor beta 1 (TGF–β1), 10 pg/mL creatinine (CR), 370 µg/mL ascorbic acid (AA), 50 µg/mL uric acid (UA), 12 ng/mL cortisol (CL), and 200 pg/mL estradiol (E2) on the amperometric responses obtained for 0 (■) or 250 (■) pg/mL HFA at the *m*MWCNTs(-HRP)-anti-HFA-HFA-anti-HFA-Biotin-Strept-Phe-SPCE immunosensor.

the slope of the calibration graph prepared with buffered HFA standard solutions (Fig. 4). Slope values of 2.16 ± 0.03 and 2.17 ± 0.03 μA per decade of concentration were found in non-smoker and smoker saliva, respectively, which were very similar to that of the calibration graph constructed with HFA standards, 2.17 ± 0.07 μA per decade of concentration. The application of the Student *t*-test provided t_{exp} values much lower than the tabulated one, t_{tab} = 2.262 for $\alpha = 0.05$ and n = 9. Therefore, the determination of HFA in saliva could be performed directly by interpolation of the amperometric current measured with the immunosensor for an aliquot of the 100-fold diluted sample into the calibration plot constructed with standard solutions. Fig. S7 (Supplementary Material) displays the calibration plot obtained with the saliva samples overlapped with that constructed from standard HFA solutions in PB buffer showing the coincidence between them.

The concentrations found in the analysis of the saliva samples were 44.6 ± 0.5 and 43.0 ± 0.2 ng/mL for the smoker and non-smoker individuals (n = 5) showing, as expected, that no important differences are apparent in the absence of inflammatory disease. These results were compared with those obtained using the commercial ELISA kit, 44.8 ± 0.8 ng/mL and 42.9 ± 0.6 ng/mL (n = 4), respectively. As it is obvious, an excellent agreement between the results obtained by both methods was apparent, what is also in agreement with that reported in the literature for saliva of healthy individuals, 41 ng/mL (Doğan al, 2016). All these results demonstrated the usefulness of the developed immunosensor for the analysis of HFA at low concentration levels in saliva with minimal sample treatment.

4. Conclusions

This paper reports the first amperometric immunosensor for the determination of the biomarker HFA. The designed strategy involved SPCEs grafted with *p*-aminobezoic acid for covalent binding of streptavidin, and a sandwich configuration with biotinylated capture antibody and magnetic MWCNTs conjugated with HRP and anti-HFA antibodies as the detection label. The use of this signal amplification approach provides important analytical advantages in terms of wider linear dynamic concentration range and sensitivity with respect to commercial ELISA kits as well as to the only electrochemical immunosensor (chronoimpedimetric) reported so far for HFA. Importantly, the developed immunosensor can be used to determine HFA in saliva with minimal sample treatment. Other relevant advantages of the developed immunosensor are the great reproducibility of the measurements, both with immunosensors prepared on the same day and on different days, and the excellent storage stability and selectivity. This immunosensing strategy can be easily extended to the electrochemical determination of other biomarkers since the disposable electrode surface modification protocol and the use of magnetic multiwalled carbon nanotubes as nanocarrier tags can be viewed as general working approaches to design other electrochemical immunoplatforms.

Acknowledgement

The financial support of projects CTQ2015-70023-R (Spanish Ministry of Economy and Competitivity Research Projects), and S2013/MT-3029 (NANOAVANSENS Program from the Comunidad de Madrid) are gratefully acknowledged.

Appendix A. Supporting information

Supplementary data associated with this article can be found in the online version at http://dx.doi.org/10.1016/j.bios.2018.04.056.

References

Akter, R., Jeong, B., Choi, J.-S., Rahman, Md.A., 2016. Biosens. Bioelectron. 80, 123–130.
Bertok, T., Sediva, A., Katrlik, J., Gemeiner, P., Mikula, M., Nosko, M., Tkac, J., 2013a. Talanta 108, 11–18.
Bertok, T., Gemeiner, P., Mikula, M., Gemeiner, P., Tkat, J., 2013b. Microchim. Acta 180, 151–159.
Campuzano, S., Yáñez-Sedeño, P., Pingarrón, J.M., 2017. TrAC Trends Anal. Chem. 86, 14–24.
Choi, K.M., 2016. Endocrinol. Metab. 31, 1–6.
Dabrowska, A.M., Taracha, J.S. Wojtysiak-Duma, B., Dumac, D. 2015. Biomedical Papers of the Medical Faculty of the University Palacky, Olomouc, Czech Republic, 159, pp. 352–359.
Ding, L., Bond, A.M., Zhai, J., Zhang, J., 2013. Anal. Chim. Acta 797, 1–12.
Doğan, G.E., Demír, T., Laloğlu, E., Sağlam, E., Aksoy, H., Yildirim, A., Akçay, F., 2016. Braz. Oral. Res. 30, e129.
Dziegielewska, K.M., Brown, W.M., Casey, S.-J., Christie, D.L., Foreman, R.C., Hill, R.M., Saunders, N.R., 1990. J. Biol. Chem. 265, 4354–4357.
Eguílaz, M., Moreno-Guzmán, M., Campuzano, S., González-Cortés, A., Yáñez-Sedeño, P., Pingarrón, J.M., 2010. Biosens. Bioelectron. 26, 517–522.
Gong, J.-L., Wang, B., Zeng, G.-M., Yang, C.P., Niu, C.-G., Niu, Q.-Y., Zhou, Y., Liang, W.-J., 2009. J. Hazard. Mater. 164, 1517–1522.
Kim, I.T., Nunnery, G.A., Jacob, K., Schwartz, J., Liu, X., Tannenbaum, R., 2010. J. Phys. Chem. 114, 6944–6951.
Nagaraj, V.J., Aithal, S., Eaton, S., Bothara, M., Wiktor, P., 2010. Nanomedicine 5, 369–378.
Ojeda, I., López-Montero, J., Moreno-Guzmán, M., Janegitz, B.C., González-Cortés, A., Yáñez-Sedeño, P., Pingarrón, J.M., 2012. Anal. Chim. Acta 743, 117–124.
Sakwe, A.M., Koumangoye, R., Goodwin, S.J., Ochieng, J., 2010. J. Biol. Chem. 285, 41827–41835.
Schinke, T., Amendt, C., Trindl, A., Pöschke, O., Müller-Esterl, W., Jahnen-Dechent, W., 1996. J. Biol. Chem. 23, 20789–20796.
Silva, P.M.S., Lima, A.L.R., Silva, B.V.M., Coelho, L.C.B.B., Dutra, R.F., Correia, M.T.S., 2016. Biosens. Bioelectron. 85, 171–177.
Uygun, Z.O., Şahin, Ç., Yılmaz, M., Akçay, Y., Akdemir, A., Sağın, F., 2018. Anal. Biochem. 542, 11–15.
Yáñez-Sedeño, P., Campuzano, S., Pingarrón, J.M., 2017. J. Carbon Res. 2017 (3), 3. http://dx.doi.org/10.3390/ c3010003.
Yi, J.K., Chang, J.W., Han, W., Lee, J.W., Ko, E., Kim, D.H., Bae, J., Yu, J., Lee, C., Yu, M., Noh, D., 2009. Cancer Epidemiol. Biomark. Prev. 18, 1357–1364.
Yilmaz, Y., Yonal, O., Kurt, R., Ari, F., Oral, A.Y., Celikel, C.A., Korkmaz, S., Ulukaya, E., Ozdogan, O., Imeryuz, N., Avsar, E., Kalayci, C., 2010. Ann. Clin. Biochem. 47, 549–553.
Zhang, Q., Chen, X., Tu, F., Yao, C., 2014. Biosens. Bioelectron. 59, 377–383.

SUPPLEMENTARY MATERIAL

MAGNETIC MULTIWALLED CARBON NANOTUBES AS NANOCARRIER TAGS FOR SENSITIVE DETERMINATION OF FETUIN

Esther Sánchez-Tirado, Araceli González-Cortés, Paloma Yáñez-Sedeño*,
José M. Pingarrón

Department of Analytical Chemistry, Faculty of Chemistry, University Complutense of Madrid, 28040-Madrid. Spain *Corresponding author: E-mail yseo@quim.ucm.es

CONTENTS

Table 1. Comparison of the performance of ELISA kits, electrochemical biosensors involving lectin, impedimetric immunosensor and the amperometric immunosensor reported in this work for the determination of HFA

Technique	Method/Configuration	Analytical characteristics	Reference
ELISA	Sandwich-type configuration prepared with HFA-anti-HFA onto precoated wells and detector anti-HFA followed by color development.	Dynamic range: 7.8 - 500 ng/mL MDD: 0.62 ng/mL Assay time: 4 h 30 min	https://www.rndsystems.com/products/human-fetuin-a-quantikine-elisa-kit_dfta00
ELISA	Sandwich-type configuration prepared with HFA-anti-HFA onto precoated wells and Biotin-anti-HFA followed by HRP-Strept. Colorimetric detection with TMB/H_2O_2	Dynamic range: 0.205 - 50 ng/mL LLD: 0.2 ng/mL Assay time: 5h 30 min	http://www.thermofisher.com/order/catalog/product/EHAHSG
ELISA	Sandwich-type configuration prepared with HFA-anti-HFA onto precoated wells and Biotin-anti-HFA followed by HRP-Avidin. Colorimetric detection with TMB/H_2O_2	Dynamic range: 0.781 – 50 ng/mL Sensitivity: 0.32 ng/mL (not defined) Assay time: 2h 45 min	https://www.lsbio.com/elisakits/manualpdf/ls-f5287.pdf
ELISA	Sandwich-type configuration prepared with HFA-anti-HFA onto precoated wells and Biotin-anti-HFA followed by HRP-Avidin. Colorimetric detection with TMB/H_2O_2	Dynamic range: 0.312 - 20 ng/mL Sensitivity: 30 pg/mL (not defined) Assay time: 3h 50 min	http://www.abcam.com/ps/products/119/ab119594/documents/ab119594
EIS, lectin-based biosensor	Lectin covalently immobilized on a mixed SAMof 11-MUA and 6-MH onto AuNPs/ AAT/AuE. PVA used as a blocking agent. Detection by measurement of R_{CT}	Dynamic range: 1.0 aM – 10 pM LOD: 0.5 aM (S/N=3)	Bertok et al., 2013
EIS, lectin-based biosensor	Lectin covalently immobilized on a mixed SAMof 11-MUA and 6-MH onto AuE. PVA used as a blocking agent. Detection by measurement of R_{CT}	Dynamic range: 1.0 fM – 10 nM LOD: 0.33 fM (S/N=3)	Bertok et al., 2013a
SWV, lectin-based biosensor	Label-free configuration. Gly/Cramoll-HOOC-CNT/PLL/GCE. Voltammetric detection of $Fe(CN)_6^{3-/4-}$	Dynamic range: 0.5 – 25 µg/mL LOD: 0.017 µg/mL (S/N=3) Applied to serum samples	Silva et al., 2016
EIS, lectin-based biosensor	Biotinylated lectin immobilized on a Strept-DSP-AuE. Casein used as a blocking agent. Detection by measurement of R_{CT}	Dynamic range: 0.001 –10 ng/mL LOD: 1pg/mL Applied to normal and cancerous cells	Nagaraj et al., 2010
EIS, immunosensor	Anti-HFA-GA/PAMAM-NH_2 (G5)/ C60/4-ATP/AuSPE. Detection by measurement of ΔR_{CT} / min.	Dynamic range: 5.0 – 400 ng/mL LOD: 1.44 ng/mL (S/N=3) Applied to serum samples	Uygun et al., 2018
Amperometry immunosensor	Sandwich.type configuration prepared with Biotin-anti-HFA onto Strept/SPCE followed by addition of HFA and *m*-MWCNTs(-HRP)-anti-HFA. Detection with H_2O_2/HQ.	Dynamic range: 20 - 2000 pg/mL LOD: 16 pg/mL (S/N=3) Applied to saliva samples. Assay time: 2 h	This work

Key: AAT, aminoalkanethiol; AuNPs, gold nanoparticles; CNT, carbon nanotubes; Cramoll, *Cratylia mollis* lectin; DSP, dithiobis succinimidyl propionate; EIS, electrochemical impedance spectroscopy; GCE, glassy carbon electrode; Gly, glycine; HQ, hydroquinone; LLD, lower limit of detection; LOD, detection limit; MDD, minimum detectable dose; 6-MH, 6-mercaptohexanol; 11-MUA, 11-mercapto undecanoic acid; PLL. poly(L-lysine); PVA, poly(vinyl alcohol); SAM, self-assembled monolayer; SWV, square-wave voltammetry;TMB, 3,3',5,5'-tetra-methylbenzidine.

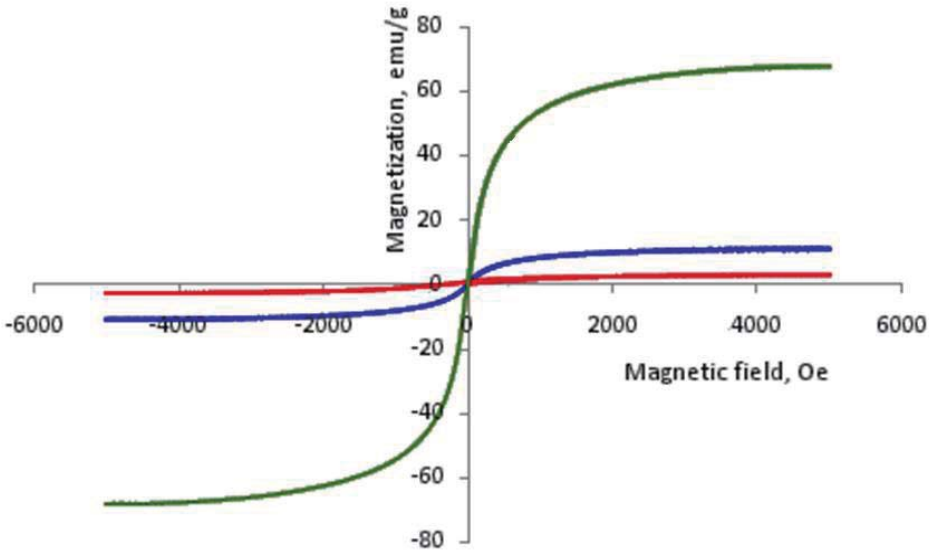

Figure S1. Magnetization curves of *m*-MWCNTs (blue), Fe_3O_4 (black) and MWCNTs (red) at room temperature.

2. Optimization of experimental variables

The different variables affecting the preparation of *m*-MWCNTs(-HRP)-anti-HFA conjugate, anti-HFA-Biotin-Strept-Phe-SPCE, and the performance of the resulting *m*-MWCNTs(-HRP) - anti - HFA - HFA - anti - HFA - Biotin - Strept - Phe - SPCE immunosensor were optimized. The largest ratio between the currents measured with the as prepared immunosensor in the presence (S) or in absence (N) of the target compound was taken as the selection criterion for each tested variable. The optimization studies involved evaluation of (a) loadings of HRP and anti-HFA onto *m*-MWCNTs; (b) loading of streptavidin covalently linked to *p*ABA-modified SPCE; c) anti-HFA-Biotin loading onto Strept-Phe-SPCE, and (d) concentration of the blocking agent.

Figure S2a shows the results obtained in the study of the effect of HRP loadings onto the *m*-MWCNTs on the amperometric response of different immunosensors prepared from SPCEs modified with 5 µL each of 7 µg/mL anti-HFA-Biotin, 1.5 mg/mL biotin, and 0 (green) or 250 (blue) pg/mL HFA that were sandwiched with 5 µL of *m*-MWCNTs(-HRP)-anti-HFA nanocarriers prepared with HRP loadings in the 1 - 2.5 mg/mL range and 5 µg/mL anti-HFA. As it can be seen, only small changes in the specific current occurred with HRP concentration, whereas the unspecific responses increased slightly. Therefore, the largest S/N ratio was obtained for a 1.0 mg/mL HRP concentration. Figure S2b shows the effect of the anti-HFA loading over the 2.5 to

10 µg/mL range and a constant 1 mg/mL HRP concentration. Larger S/N ratio was attained for a 5 µg/mL antibody concentration.

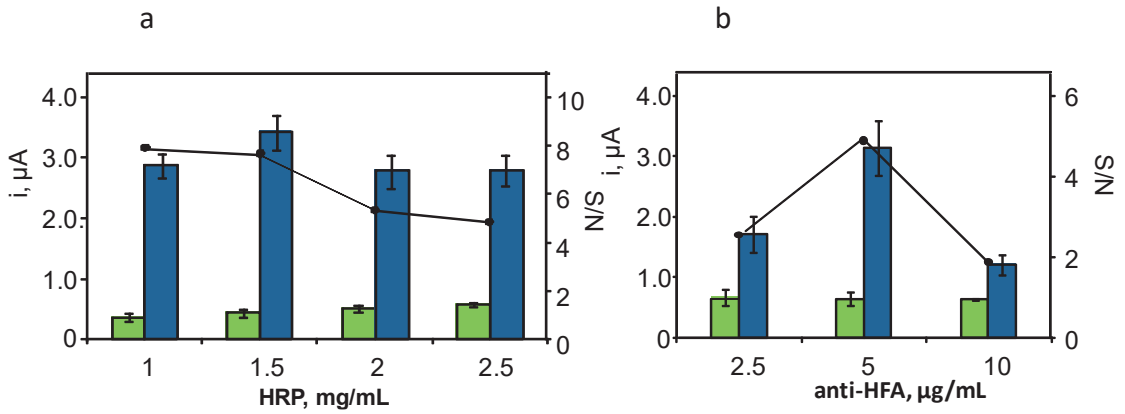

Figure S2. Effect of the HRP (a) and anti-HFA (b) loadings onto the *m*-MWCNTs on the amperometric responses obtained with immunosensors prepared with SPCE modified with 5 µL each 7 µg/mL anti-HFA-Biotin, 1.5 mg/mL biotin, 0 (green) or 250 (blue) pg/mL HFA, and 5 µL of *m*-MWCNTs(-HRP)-anti-HFA; 5 µg/mL anti-HFA (a), 1 mg/mL HRP (b).

The concentration of streptavidin immobilized covalently on the *p*-ABA-grafted SPCE was optimized by comparing the measurements obtained with immunosensors prepared with streptavidin loadings ranging between 200 and 800 µg/mL. Figure S3a shows as the specific responses increased with streptavidin concentration up to 600 µg/mL and decreased for larger concentration, probably due to a higher electron transfer resistance at the electrode surface in the presence of an excess of streptavidin. Therefore, a concentration of 600 µg/mL streptavidin was selected for further work. The optimal incubation time of streptavidin onto *p*-ABA-grafted SPCE was found to be 60 min. Under these experimental conditions, the effect of anti-HFA-Biotin loading on the immunosensor response was checked over the 5-12 µg/mL range (Figure S3b). As it can be seen, the specific current increased with biotinylated antibody concentration up to 7 µg/mL showing a significant decrease for larger loadings. Moreover, 60 min was selected as the optimum time for incubation of anti-HFA-Biotin onto Strept-Phe SPCE.

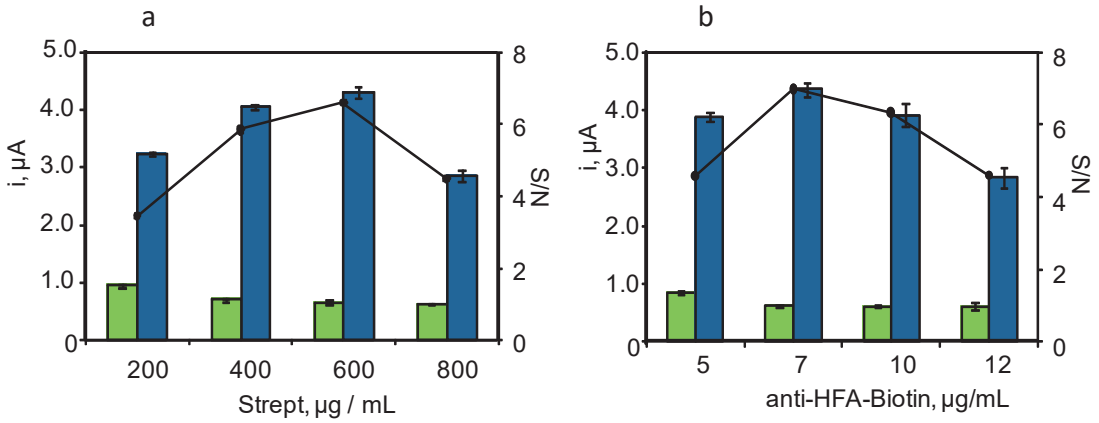

Figure S3. Effect of the streptavidin loading onto *p*-ABA-modified SPCE(a), and anti-HFA-Biotin loading onto Strept-Phe-SPCE (b) on the amperometric responses obtained with immunosensors prepared with:5 µL 200 - 800 µg/mL streptavidin and 7 µg/mL anti-HFA-Biotin (a); 600 µg/mL streptavidin and 5 - 12 anti-HFA-Biotin (b); 1.5 mg/mL biotin, 0 (green) or 250 (blue) pg/mL HFA, and 5 µL of *m*-MWCNTs(-HRP)-anti-HFA prepared with 1 mg/mL HRP and 5 µg/mL anti-HFA.

Blocking of the remaining activated unreacted sites on the electrode surface to avoid non-specific adsorption of the enzyme labeled conjugate was accomplished. Biotin was selected as the blocking agent to avoid unspecific adsorptions with the remaining sites of streptavidin. Thus, immunosensors prepared under the above optimized conditions were incubated with different concentrations of biotin over the 0.5 to 2 mg/mL range. A blocking solution consisting of 0.5 mg/mL biotin prepared in 0.1 % BSA was also tested. Figure S4 shows as both specific and unspecific responses decreased when increasing the biotin concentration, probably due to the increase in the thickness of the insulating layer on the electrode surface. In addition, the presence of BSA did not improve the S/N ratio. Thus, a 1.5 mg/mL biotin concentration was selected for further work. In this case, an incubation time of 30 min was sufficient to achieve an adequate blocking.

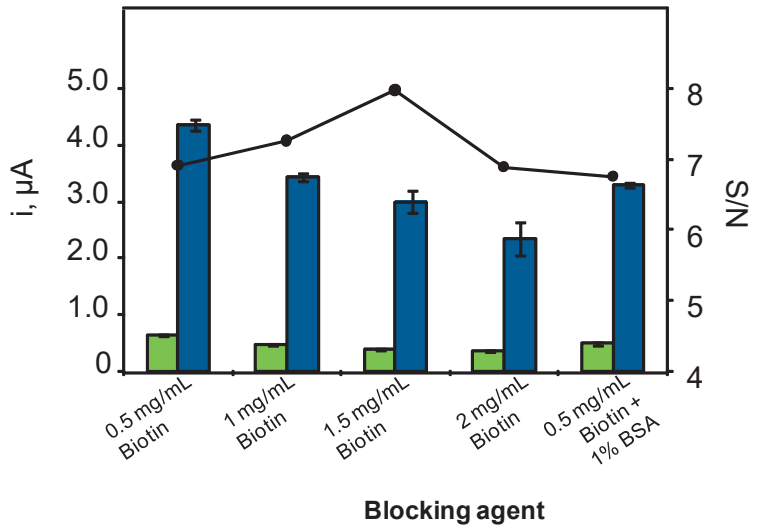

Figure S4. Effect of blocking solution on the amperometric responses obtained with immunosensors prepared with5 µL 600 µg/mL streptavidin, 7 µg/mL anti-HFA-Biotin, 0.5 - 2 mg/mL biotin and 0.5 mg/mL biotin + 1% BSA; 0 (green) or 250 (blue) pg/mL HFA, and 5 µL of *m*-MWCNTs (-HRP)-anti-HFA prepared with 1 mg/mL HRP and 5 µg/mL anti-HFA.

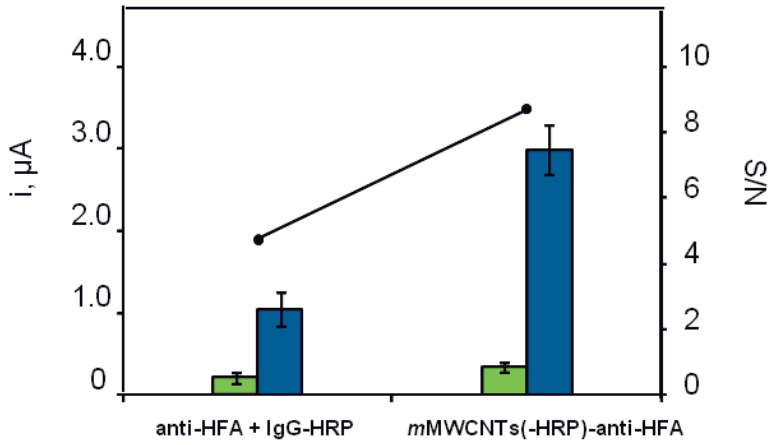

Figure S5. Comparison of the electrochemical responses of *m*-MWCNTs(-HRP)-anti-HFA-HFA-anti-HFA-Biotin-Strept-Phe-SPCE and HRP-IgG-anti-HFA-HFA-anti-HFA-Biotin-Strept-Phe-SPCE immunosensors

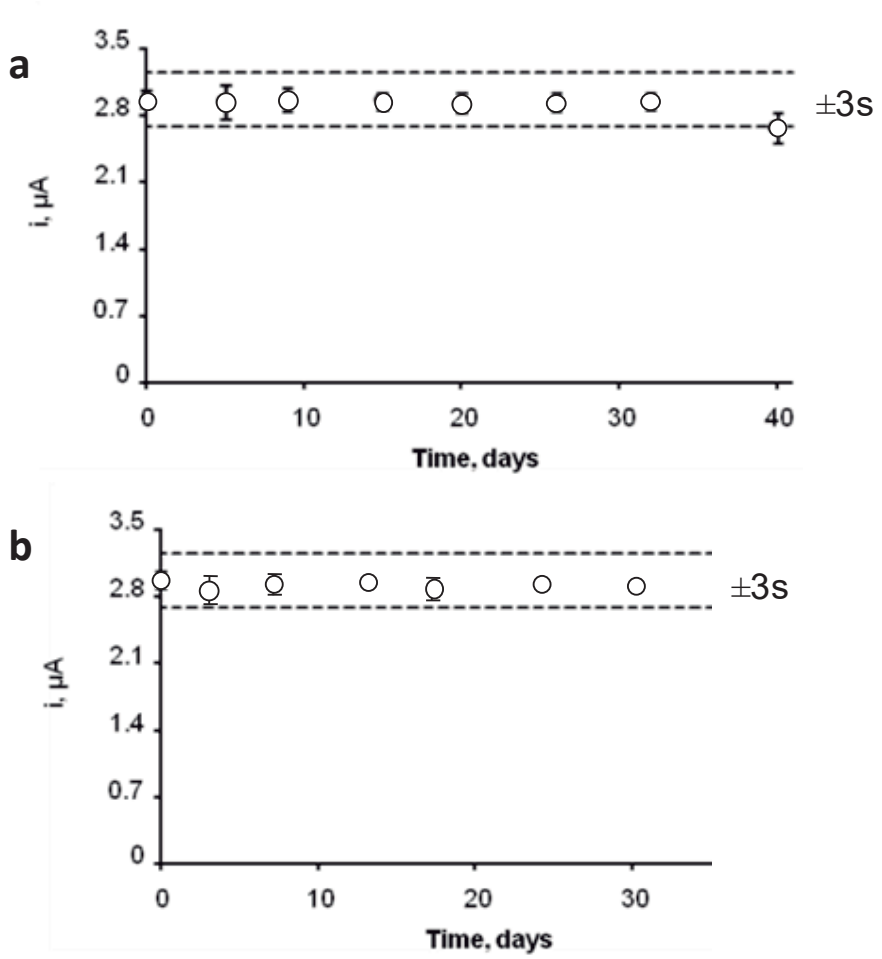

Figure S6. Control chart constructed to check the storage stability of (a) anti-HFA-Biotin-Strept-Phe-SPCE bioelectrodes upon storage at -20 ºC in dry ambient, and (b) *m*MWCNTs(-HRP)-anti-HFA conjugates upon storage at 4 ºC in dry ambient The central value was set as the average amperometric current for ten measurements of different solutions of 250 pg/mL HFA. Upper and lower limits of control were set as three times the standard deviation of these measurements.

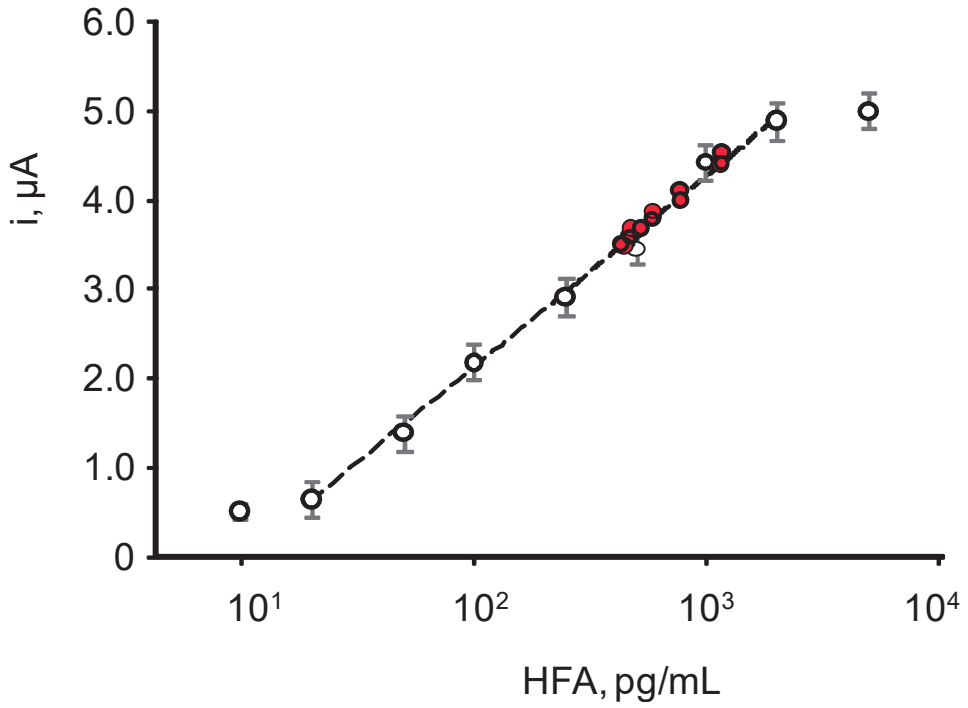

Figure S7. Comparison of the calibration plots constructed with the *m*-MWCNTs (-HRP)-anti-HFA-HFA-anti-HFA-Biotin-Strept-Phe-SPCE immunosensor for HFA in saliva (twelve red points) and buffered 0.01 M PBS of pH 7.4 solutions (white points).

9

Glosario de Abreviaturas

A

AA: ácido ascórbico

Ab: anticuerpo

Ab*: anticuerpo marcado

ACh: acetilcolina

AChE-ISO: isoprostano marcado con acetilcolinesterasa

Ag: antígeno

Ag*: antígeno marcado

alkyne-IgG: inmunoglobulina G etinilada

AMPK: proteína quinasa activada por monofosfato de adenosina

anti-APN: anticuerpo frente a adiponectina

anti-CD105: anticuerpo frente a endoglina

anti-HFA: anticuerpo frente a fetuina A humana

anti-IFN: anticuerpo frente a interferón gamma

anti-IL: anticuerpo frente a interleucina 1 beta

anti-ISO: anticuerpo frente a 8-isoprostano

anti-mouse-IgG: anticuerpo IgG Fc específico de ratón

anti-TGF: anticuerpo frente a factor de crecimiento transformante beta 1

anti-TNF: anticuerpo frente al factor de necrosis tumoral alfa

APN: adiponectina

APTES: (*3*-aminopropil)trietoxisilano

AU: ácido úrico

azida-MWCNT: nanotubo de carbono de pared múltiple funcionalizada con *11*-azido-*3,6,9*-trioxaundecan-*1*-amina

B

BIL: bilirrubina

Biotin-Ab: anticuerpo marcado con biotina

Biotin-anti-APN: anticuerpo frente a adiponectina marcado con biotina

Biotin-anti-CD105: anticuerpo frente a endoglina marcado con biotina

Biotin-anti-HFA: anticuerpo frente a fetuina A humana marcado con biotina

Biotin-anti-IFN: anticuerpo frente a interferón gamma marcado con biotina

Biotin-anti-IL: anticuerpo frente a interleucina 1 beta marcado con biotina

Biotin-anti-TGF: anticuerpo frente a factor de crecimiento transformante beta 1 marcado con biotina

Biotin-anti-TNF: anticuerpo frente a factor de necrosis tumoral alfa marcado con biotina

BOSS: Estudio de Biomarcadores de Estrés Oxidativo (Biomarkers of Oxidative Stress Strudy)

BSA: albúmina de suero bovino

C

cAb: anticuerpo de captura

Cad17R: receptor de cadherina-17

CB: disolución reguladora carbonato

CD105: endoglina

Chol: colesterol

CL: cortisol

CMC-rGO: nanomaterial híbrido de óxido de grafeno reducido y carboximetilcelulosa

CNH: nanocuerno de carbono

CNT: nanotubo de carbono

Cp: ceruloplasmina

CP: polímero conductor

CR: creatinina

CRP: proteína C reactiva

CuAAC: cicloadición *1,3*-dipolar azida-alquino catalizada por cobre (I)

CV: voltamperometría cíclica

D

dAb*: anticuerpo de detección marcado

DCC: *N, N'*-diciclohexil carbodiimida

DMF: *N,N'*-dimetilformamida

DNA: ácido desoxirribonucleico

DTNB: ácido *5,5'*-ditiobis-(*2*-nitrobenzoico) o reactivo de Ellman

DWCNT: nanotubo de carbono de pared doble

E

E-Cad: E-cadherina

EDC: *N*-(*3*-dimetilaminopropil)-*N'*-etilcarbodiimida

EIS: espectroscopia de impedancia electroquímica

ELISA: ensayo por inmunoabsorción ligado a enzimas (Enzyme-Linked ImmunoSorbent Assay)

ErbB2: proteína recombinante HER2

E2: estradiol

F

Fab: región variable del anticuerpo donde se produce la unión al antígeno

Fc: región constante del anticuerpo que determina su actividad biológica

FGFR4: receptor de factor de crecimiento de fibroblastos 4

FTIR: especrometría infrarroja por Transformada de Fourier

G

GHRL: grelina

Glu: glucosa

GO: óxido de grafeno

H

HB hemoglobina

HDL: lipoproteína de alta densidad

HFA: fetuina A humana

HOBt: hidroxibenzotiazol

HOOC-CNH: nanocuerno de carbono carboxilado

HOOC-MWCNT: nanotubo de carbono de pared múltiple carboxilado

HOOC-mMWCNT: nanotubo de carbono de pared múltiple magnético carboxilado

HOOC-Phe-DWCNT: nanotubo de carbono de pared múltiple funcionalizado con el grupo funcional *4*-carboxifenilo

HQ: hidroquinona

HRP: enzima peroxidasa de rábano

HRP-Ab: anticuerpo marcado con peroxidasa de rábano

HRP-Av: avidina marcada con la enzima peroxidasa de rábano

HRP-IgG: inmunoglobulina G marcada con peroxidasa de rábano

HRP-ISO: 8-isoprostano marcado con la enzima peroxidasa de rábano

HRP-Strept: estreptavidina marcada con la enzima peroxidasa de rábano

I

IFN: familia de interferones

IFN-α: interferón alfa

IFN-β: interferón beta

IFN-γ: interferón gamma

IgG: inmunoglobulina G

IgG-MWCNT: nanotubos de carbono de pared doble funcionalizados con inmunoglobulina G etinilada

IL: familia de interleucinas

IL-1: interleucina 1

IL-1β: interleucina 1 beta

IL-6: interleucina 6

IL-8: interleucina 8

ISO o **8-ISO-PGF2α**: 8-isoprostano

L

LDL: lipoproteína de baja densidad

M

MES: ácido *2*-(*N*-morfolino)etanosulfónico

mRNA: RNA mensajero

MWCNT: nanotubo de carbono de pared múltiple

mMWCNT: nanotubo de carbono de pared múltiple magnético

N

NIH: Instituto Nacional de Salud (National Institute of Heath)

NK cells: células *natural killer*

NHS: *N*-hidroxisuccinimida

NHSS: *N*-hidroxisulfosuccinimida

NMP: *N*-metil-*2*-pirrolidona

P

p53: proteína recombinante p53 humana de longitud completa

***p*-ABA**: ácido *p*-aminobenzoico

***p*-ABA-DWCNT**: nanotubos de carbono de pared doble funcionalizados con ácido *p*-aminobenzoico

PB: disolución reguladora fosfato

PBS: disolución reguladora fosfato salino

PBST: disolución reguladora fosfato salino suplementada con Tween® 20

PPA: ácido *1H*-pirrol-*1*-propiónico

pPPA: ácido poli(pirrolpropiónico)

pPY: poli(pirrol)

poli-HRP-Strept o **poly-HRP-Strept**: polímero de estreptavidina y peroxidasa de rábano

R

RANKL: ligando de receptor activador para el factor nuclear kappaB

R_{CT}: resistencia a la transferencia de carga

rGO: óxido de grafeno reducido

RNA: ácido ribonucleico

RNS: especies reactivas de nitrógeno (Reactive Nitrogen Species)

ROS: especies reactivas de oxígeno (Reactive Oxygen Species)

S

SPCE: electrodo serigrafiado de carbono

SWCNT: nanotubo de carbono de pared simple

T

TGF: familia de factores de crecimiento transformante

TGF-β: familia de factores de crecimiento transformante beta

TGF-β1: factor de crecimiento transformante beta 1

TIR: receptor de interleucina 1 de tipo Toll

TLR: receptor de tipo Toll

TMB: *3,3',5,5'*-tetrametilbencidina

TNF: familia de factores de necrosis tumoral

TNF-α: factor de necrosis tumoral alfa

V

V: aminoviológeno

V-Phe-SWCNT: nanotubo de carbono de pared simple con aminoviológeno

V-Phe-SWCNT(-HRP)-anti-TGF: conjugado aminoviológeno-nanotubos de carbono de pared simple-anticuerpo-peroxidasa de rábano

W

WHO: Organización Mundial de la Salud (World Health Organization)

1

11-β-HSD1: 11β-hidroxiesteroide deshidrogenasa